

**ELECTROCHEMISTRY
AND
CORROSION SCIENCE**

NESTOR PEREZ

Kluwer Academic Publishers

ELECTROCHEMISTRY AND CORROSION SCIENCE

This page intentionally left blank

ELECTROCHEMISTRY AND CORROSION SCIENCE

by

Nestor Perez

*Department of Mechanical Engineering
University of Puerto Rico*

KLUWER ACADEMIC PUBLISHERS

NEW YORK, BOSTON, DORDRECHT, LONDON, MOSCOW

eBook ISBN: 1-4020-7860-9
Print ISBN: 1-4020-7744-0

©2004 Kluwer Academic Publishers
New York, Boston, Dordrecht, London, Moscow

Print ©2004 Kluwer Academic Publishers
Boston

All rights reserved

No part of this eBook may be reproduced or transmitted in any form or by any means, electronic, mechanical, recording, or otherwise, without written consent from the Publisher

Created in the United States of America

Visit Kluwer Online at: <http://kluweronline.com>
and Kluwer's eBookstore at: <http://ebooks.kluweronline.com>

Contents

Preface	ix
Dedication	xiii
CHAPTERS:	
1 FORMS OF CORROSION	1
1.1 INTRODUCTION	1
1.2 CLASSIFICATION OF CORROSION	3
1.2.1 GENERAL CORROSION	3
1.2.2 LOCALIZED CORROSION	3
1.3 ATMOSPHERIC CORROSION	4
1.4 GALVANIC CORROSION	7
1.4.1 MICROSTRUCTURAL EFFECTS	12
1.5 PITTING CORROSION	16
1.6 CREVICE CORROSION	18
1.7 CORROSION-INDUCED SPALLING	19
1.8 STRESS CORROSION CRACKING	20
1.9 NONMETALLIC MATERIALS	24
1.10 SUMMARY	25
1.11 REFERENCES	25
2 ELECTROCHEMISTRY	27
2.1 INTRODUCTION	27
2.2 ELECTRICAL POLES	28
2.3 ELECTROCHEMICAL CELLS	31
2.3.1 OPEN-CIRCUIT CONDITION	38
2.3.2 CLOSED-CIRCUIT CONDITION	39
2.3.3 APPLICATION OF GALVANIC CELLS	40
2.4 THERMODYNAMICS	41
2.5 STANDARD ELECTRIC POTENTIAL	53
2.6 POURBAIX DIAGRAMS	56
2.6.1 DIAGRAM FOR WATER AND OXYGEN	56
2.6.2 POURBAIX DIAGRAM FOR A METAL M	59

2.7	ELECTRICAL DOUBLE LAYER	61
2.8	DEGREE OF DISSOCIATION	64
2.9	SUMMARY	67
2.10	PROBLEMS/QUESTIONS	68
2.11	REFERENCES	70
3	KINETICS OF ACTIVATION POLARIZATION	71
3.1	INTRODUCTION	71
3.2	ENERGY DISTRIBUTION	72
3.3	POLARIZATION	80
3.4	ACTIVATION POLARIZATION	81
3.5	POLARIZATION METHODS	83
3.5.1	LINEAR POLARIZATION	83
3.5.2	TAFEL EXTRAPOLATION	85
3.6	CORROSION RATE	90
3.7	IMPEDANCE SPECTROSCOPY	97
3.8	CHARACTERIZATION OF ELECTROLYTES	105
3.9	ELECTROLYTE CONDUCTIVITY	109
3.10	SUMMARY	113
3.11	PROBLEMS/QUESTIONS	113
3.12	REFERENCES	118
4	KINETICS OF CONCENTRATION POLARIZATION	121
4.1	INTRODUCTION	121
4.2	MASS TRANSFER MODES	121
4.3	MIGRATION MOLAR FLUX	125
4.4	FICK'S LAWS OF DIFFUSION	126
4.4.1	DIFFUSION IN A RECTANGULAR ELEMENT	127
4.4.2	DIFFUSION IN A CYLINDRICAL ELEMENT	129
4.4.3	SOLUTION OF FICK'S SECOND LAW EQUATION	129
4.4.4	STATIONARY BOUNDARIES	138
4.5	DIFFUSION AND MIGRATION	140
4.6	REVERSIBLE CONCENTRATION CELL	141
4.7	LIMITING CURRENT DENSITY	142
4.8	GALVANOSTATIC POLARIZATION	147
4.9	A.C. POLARIZATION	148
4.10	SUMMARY	149
4.11	PROBLEMS/QUESTIONS	149
4.12	REFERENCES	153
5	MIXED POTENTIAL THEORY	155
5.1	INTRODUCTION	155
5.2	MIXED-ELECTRODE POTENTIAL	155
5.3	INTERPRETATION OF POLARIZATION	159
5.4	PREDETERMINED CORROSION RATE	161
5.5	POLARIZATION OF A GALVANIC CELL	163

5.6	EFFECT OF SURFACE AREA	165
5.7	SUMMARY	165
5.8	REFERENCES	165
6	CORROSIVITY AND PASSIVITY	167
6.1	INTRODUCTION	167
6.2	INSTRUMENTATION	167
6.2.1	TREE-ELECTRODE SYSTEM	170
6.3	POLARIZATION CURVES	172
6.4	CYCLIC POLARIZATION CURVES	177
6.5	PASSIVE OXIDE FILM	178
6.6	KINETICS OF PASSIVATION	179
6.7	MECHANISM OF PASSIVATION	184
6.8	SUMMARY	185
6.9	PROBLEMS	186
6.10	REFERENCES	187
7	ELECTROMETALLURGY	189
7.1	INTRODUCTION	189
7.2	ELECTROWINNING	192
7.3	MATHEMATICS OF ELECTROWINNING	198
7.3.1	FARADAY'S LAW OF ELECTROLYSIS	198
7.3.2	PRODUCTION RATE	200
7.3.3	ECONOMY	205
7.3.4	ELECTROWINNING OF ZINC	206
7.4	ELECTROREFINING	208
7.5	ELECTROPLATING	209
7.6	MOLTEN SALT ELECTROLYSIS	211
7.6.1	CURRENT EFFICIENCY MODEL	213
7.6.2	MAGNETOHYDRODYNAMIC FLOW	215
7.7	MOVING BOUNDARY DIFFUSION	219
7.8	DIFFUSION AND MIGRATION	222
7.9	MASS TRANSFER BY CONVECTION	223
7.9.1	STATIONARY PLANAR ELECTRODES	223
7.9.2	ROTATING-DISK ELECTRODE	231
7.10	LIMITING CURRENT DENSITY	233
7.11	SUMMARY	237
7.12	PROBLEMS	238
7.13	REFERENCES	243
8	CATHODIC PROTECTION	247
8.1	INTRODUCTION	247
8.2	ELECTROCHEMICAL PRINCIPLES	248
8.3	CATHODIC PROTECTION CRITERIA	252
8.4	IMPRESSED CURRENT TECHNIQUE	255
8.5	STRAY CURRENT TECHNIQUE	260

8.6	POTENTIAL ATTENUATION	262
8.7	EQUIVALENT CIRCUIT	270
8.8	MASS TRANSFER IN A CREVICE	272
8.9	CREVICE GROWTH RATE	275
8.10	DESIGN FORMULAE	276
8.11	DESIGNING PRESSURE VESSELS	283
8.12	SUMMARY	290
8.13	PROBLEMS/QUESTIONS	291
8.14	REFERENCES	292
9	ANODIC PROTECTION	295
9.1	INTRODUCTION	295
9.2	DESIGN CRITERIA	295
9.3	RELEVANT DATA	298
9.4	SUMMARY	300
9.5	REFERENCES	300
10	HIGH-TEMPERATURE CORROSION	301
10.1	INTRODUCTION	301
10.2	THERMODYNAMICS OF OXIDES	302
10.3	POINT DEFECTS IN OXIDES	312
10.4	KINETICS OF CORROSION IN GASES	315
10.4.1	PILLING-BEDWORTH RATIO	316
10.4.2	MATHEMATICS OF OXIDATION	318
10.5	IONIC CONDUCTIVITY	322
10.6	WAGNER THEORY OF OXIDATION	327
10.7	EXPERIMENTAL DATA	331
10.8	SUMMARY	336
10.9	PROBLEMS	337
10.10	REFERENCES	338
A	SOLUTION OF FICK'S SECOND LAW	339
A.1	FIRST BOUNDARY CONDITIONS	340
A.2	SECOND BOUNDARY CONDITIONS	341
A.3	THIRD BOUNDARY CONDITIONS	341
B	CRYSTAL STRUCTURES	343
C	CONVERSION TABLES	345
D	GLOSSARY	349
	INDEX	353

Preface

The purpose of this book is to introduce mathematical and engineering approximation schemes for describing the thermodynamics and kinetics of electrochemical systems, which are the essence of corrosion science. The text in each chapter is easy to follow by giving clear definitions and explanations of theoretical concepts, and full detail of derivation of formulae. Mathematics is kept simple so that the student does not have a stumbling block for understanding the physical meaning of electrochemical processes, as related to the complex subject of corrosion. Hence, understanding and learning the corrosion behavior and metal recovery can be achieved when the principles or theoretical background is succinctly described with the aid of pictures, figures, graphs and schematic models, followed by derivation of equations to quantify relevant parameters. Eventually, the reader's learning process may be enhanced by deriving mathematical models from principles of physical events followed by concrete examples containing clear concepts and ideas.

Example problems are included to illustrate the ease application of electrochemical concepts and mathematics for solving complex corrosion problems in an easy and succinct manner.

The book has been written to suit the needs of Metallurgical and Mechanical Engineering senior/graduate students, and professional engineers for understanding Corrosion Science and Corrosion Engineering. Some Mechanical Engineering students comply with their particular curriculum requirement without taking a corrosion course, which is essential in their professional careers.

Chapter 1 includes definitions of different corrosion mechanisms that are classified as general corrosion and localized corrosion. A full description and detailed scientific approach of each corrosion mechanism under the above classification is not included since books on this topic are available in the literature.

Chapter 2 is devoted to concepts and principles of thermodynamics of electrochemical systems. An overview of thermodynamics of phases in solution and the concept of charged particles are succinctly described as they relate to electrical potential (voltage) difference between the solution and a metal surface.

Chapter 3 and 4 deal with the kinetics of activation and concentration polarization of electrochemical systems, respectively. The electrochemical reaction kinetics is essential for determining the rate of corrosion (rate of dissolution) of a metal M or an alloy X immersed in an aggressive and destructive chemical solution, containing positively and negatively charged ions (atoms that have lost or gained electrons).

Chapter 5 is concentrated on a mixed activation polarization and concentration polarization theory. Entire polarization curves are analyzed in order to determine the change in potential of a metal immersed in an electrolyte during oxidation and reduction.

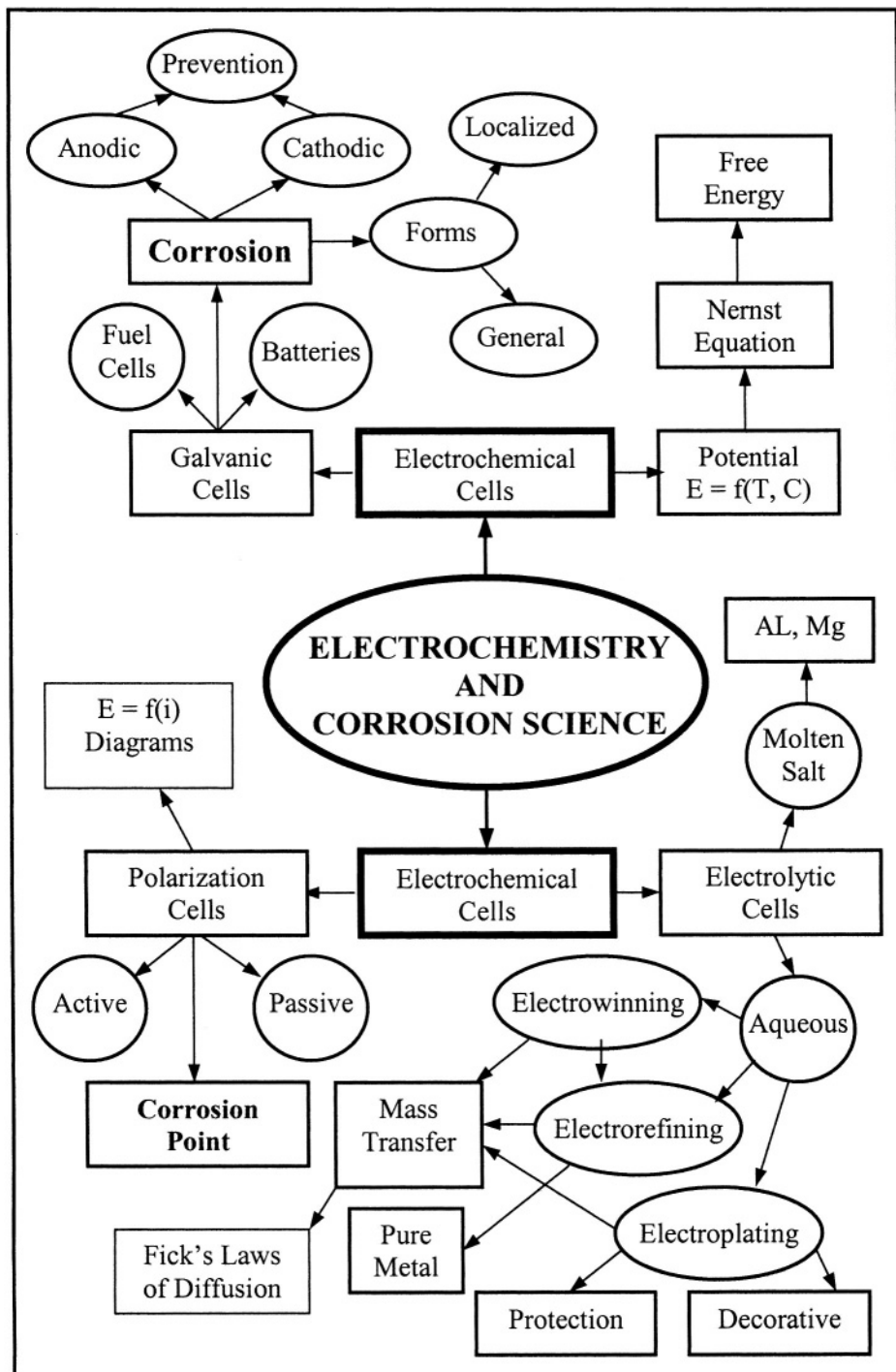
Chapter 6 deals with the degree of corrosivity of electrolytes for dissolving metals and the ability of metals immersed in these electrolytes to passivate or protect from further dissolution. Thus, passivity due to a current flow by external or natural means is studied in this chapter.

Chapter 7 is devoted to Electrometallurgy of Production of Metals. This topic includes principles electrochemical which are essential in recovering metals and precious metals (gold, silver, platinum) for metal oxides (minerals) in acid solutions.

Chapter 8 and 9 provide schemes for designing against corrosion through cathode protection and anodic protection, respectively. These chapters include procedures for protecting large engineering structures using current flow and coating (phenolic paints).

Chapter 10 deals with high temperature corrosion, in which the thermodynamics and kinetics of metal oxidation are included. The Pilling Bedworth Ratio and Wagner's parabolic rate constant theories are defined as related to formation of metal oxide scales, which are classified as protective or nonprotective.

The content in this book can be summarized as shown in the flowchart given below. A solution manual is available for educators or teachers upon the consent of the book publisher.



This page intentionally left blank

PREFACE

Dedication

My wife Neida

My daughters Jennifer and Roxie

My son Christopher

This page intentionally left blank

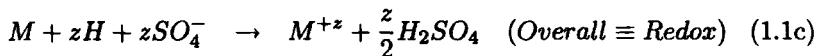
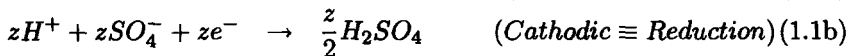
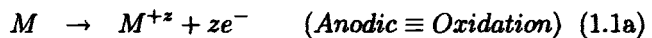
Chapter 1

FORMS OF CORROSION

1.1 INTRODUCTION

This introductory section includes basic definitions related to chemical and electrochemical reactions in the forward (f) and reverse (r) directions. The word **Corrosion** stands for material or metal deterioration or surface damage in an aggressive environment. Corrosion is a chemical or electrochemical oxidation process, in which the metal transfers electrons to the environment and undergoes a valence change from zero to a positive value z . The environment may be a liquid, gas or hybrid soil-liquid. These environments are called electrolytes since they have their own conductivity for electron transfer.

An electrolyte is analogous to a conductive solution, which contains positively and negatively charged ions called cations and anions, respectively. An ion is an atom that has lost or gained one or more outer electron (s) and carries an electrical charge. Thus, the corrosion process which can be chemical in nature or electrochemical due to a current flow, requires at least two reactions that must occur in a particular corrosive environment. These reactions are classified as anodic and cathodic reactions and are defined below for a metal M immersed in sulfuric acid (H_2SO_4) solution as an example. Hence, metal oxidation occurs through an anodic reaction and reduction is through a cathodic reaction as shown below



where M = Metal

H^{+} = Hydrogen cation

Z = Valence or oxidation state

M^{+z} = Metal cation

SO_4^{-} = Sulfate anion

The interpretation of the above equations indicate that an anodic reaction, which is equivalent to what is known as oxidation, loses ze^- metal electrons and the cathodic reaction accepts or gains ze^- electrons for reducing pertinent ions. Consequently, both anodic and cathodic reactions are coupled in a corrosion process. Adding eqs. (1.1a) and (1.1b) yields eq. (1.1c). Thus, REDOX (RED = reduction and OX = oxidation) is the resultant reaction equation, eq. (1.1c), and represents the overall reaction at equilibrium where the anodic and cathodic reaction rates are equal. Observe that the anodic reaction is also referred to as an oxidation reaction since it has lost ze^- electrons, which has been gained by the cathodic reaction for producing sulfuric acid (H_2SO_4). Thus, a cathodic reaction is equivalent to a reduction reaction. Furthermore, The arrows in eq. (1.1) indicate the reaction directions as written and they represent irreversible reactions. On the other hand, a reversible reaction is represented with an equal sign. Thus, the metal reaction can proceed to the right for oxidation or to the left for reduction as indicated by eq. (1.2)



This expression means that the reaction proceeds from left to right or vice versa under specific chemical or electrochemical conditions. The concepts of metal oxidation and metal reduction or electrodeposition are schematically shown in Figure 1.1. The dark thick line on the metal electrode is a representation of metal deposition as a result of metal ion reduction and metal oxidation is shown on the left-hand side of the electrode.

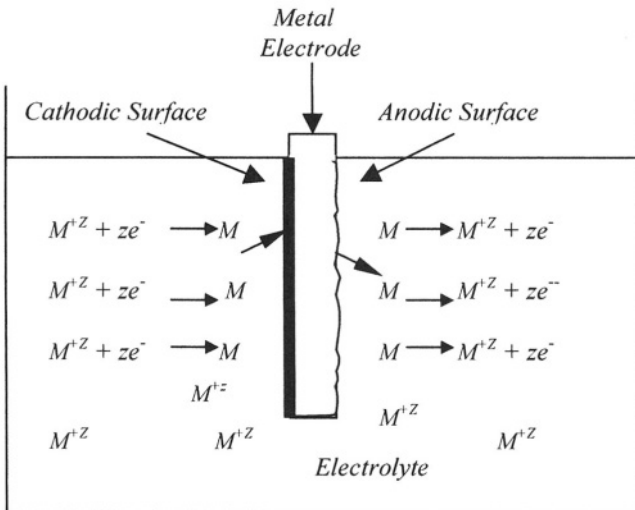


Figure 1.1 Schematic electrochemical cell.

1.2 CLASSIFICATION OF CORROSION

There is not a unique classification of the types of corrosion, but the following classification is adapted hereafter.

1.2.1 GENERAL CORROSION

This is the case when the exposed metal/alloy surface area is entirely corroded in an environment such as a liquid electrolyte (chemical solution, liquid metal), gaseous electrolyte (air, CO_2 , SO_2 , etc.), or a hybrid electrolyte (solid and water, biological organisms, etc.). Some types of general corrosion and their description are given below [8].

Atmospheric Corrosion on steel tanks, steel containers, **Zn** parts, *Al* plates, etc..

Galvanic Corrosion between dissimilar metal/alloys or microstructural phases (pearlitic steels, α - β copper alloys, α - β lead alloys).

High-Temperature Corrosion on carburized steels that forms a porous scale of several iron oxide phases.

Liquid-Metal Corrosion on stainless steel exposed to a sodium chloride (*NaCl*) environment.

Molten-Salt Corrosion on stainless steels due to molten fluorides (*LiF*, *BeF₂*, etc.).

Biological Corrosion on steel, *Cu* – alloys, *Zn* – alloys in seawater.

Stray-Current Corrosion on a pipeline near a railroad.

1.2.2 LOCALIZED CORROSION

This term implies that specific parts of an exposed surface area corrodes in a suitable electrolyte. This form of corrosion is more difficult to control than general corrosion. Localized corrosion can be classified as [9]

Crevice Corrosion which is associated with a stagnant electrolyte such as dirt, corrosion product, sand, etc. It occurs on a metal/alloy surface holes, underneath a gasket, lap joints under bolts, under rivet heads.

Filiform Corrosion is basically a special type of crevice corrosion, which occurs under a protective film. It is common on food and beverage cans being exposed to the atmosphere.

Pitting Corrosion is an extremely localized corrosion mechanism that causes destructive pits.

Oral Corrosion occurs on dental alloys exposed to saliva.

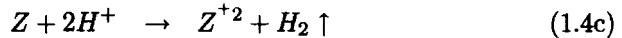
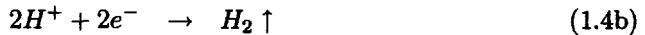
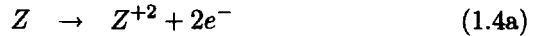
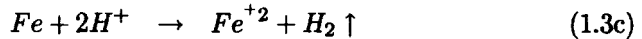
Biological Corrosion due to fouling organisms non-uniformly adhered on steel in marine environments.

Selective Leaching Corrosion is a metal removal process from the base alloy matrix, such as dezincification (**Zn** is removed) in *Cu* – *Zn* alloys and graphitization (*Fe* is removed) in cast irons.

1.3 ATMOSPHERIC CORROSION

This is a uniform and general attack, in which the entire metal surface area exposed to the corrosive environment is converted into its oxide form, provided that the metallic material has a uniform microstructure.

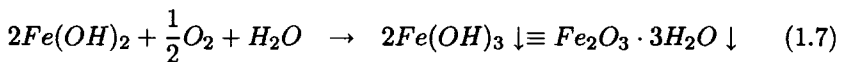
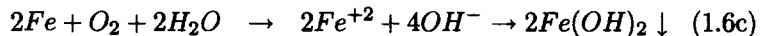
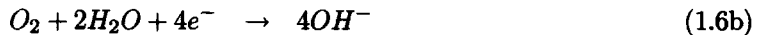
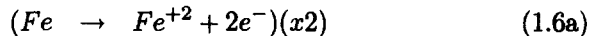
Aqueous corrosion of iron (*Fe*) in H_2SO_4 solution and of *Zn* in diluted H_2SO_4 solution are examples of uniform attack since *Fe* and *Zn* can dissolve (oxidize) at a uniform rate according to the following anodic and cathodic reactions, respectively.



where $H_2 \uparrow$ is hydrogen gas. The cathodic reaction is the common hydrogen evolution process. In fact, the aggressiveness of a solution to cause a metal to oxidize can be altered by additions of water, which is an amphoteric compound because it can act as an acid or base due to its dissociation as indicated below

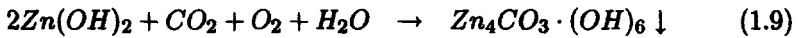
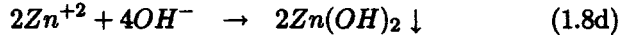
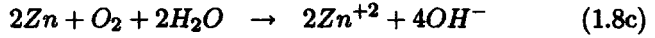
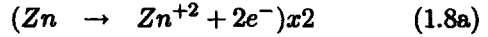


Atmospheric corrosion of a steel structure is also a common example of uniform corrosion, which is manifested as a brown-color corrosion layer on the exposed steel surface. This layer is a ferric hydroxide compound known as **Rust**. The formation of **Brown Rust** is as follows

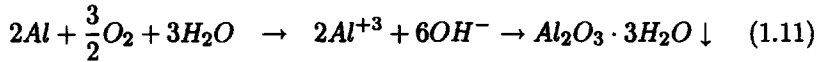


where $(x2)$ = Multiplying factor for balancing the number of electrons
 $2Fe(OH)_2$ = Ferrous hydroxide (unstable compound)
 $2Fe(OH)_3$ = Ferric hydroxide (with Fe^{+3} cations)
 $Fe_2O_3 \cdot 3H_2O$ = Hydrated Ferric hydroxide
 \downarrow = The compound precipitates as a solid

In addition, **Zn** can uniformly corrode forming a White Rust according to the following reactions [1-3,12]



In fact, the compound $Zn_4CO_3 \cdot (OH)_6$ or $ZnCO_3 \cdot 3Zn(OH)_2$ is zinc carbonate or white rust or wet-storage stain (porous). Atmospheric corrosion of aluminum is due to a passive oxide film formation instead of a porous layer. The gray/black-color film may form as follows



In general, the oxidation process can be deduced using a proper Pourbaix diagram, as schematically shown in Figure 1.2. This diagram is a plot of electric potential of a metal as a function of pH of water at 25°C [4].

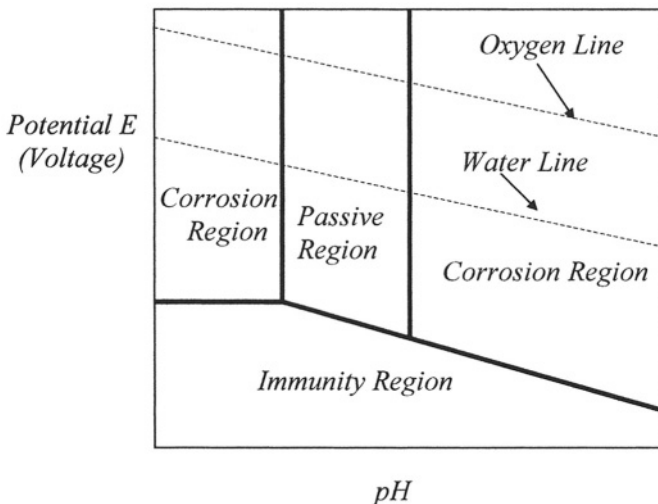


Figure 1.2 Schematic Pourbaix diagram for a hypothetical metal.

This type of diagram indicates the possible electrochemical process on a metal surface if the potential and the pH of the electrochemical systems are known or estimated. In fact, corrosion rates can not be determined from a Pourbaix diagrams. The diagram includes regions identified as corrosion where a metal oxidizes, passive region where a metal is protected by a stable oxide film being adhered on the metal surface, and immunity where corrosion or passivation are suppressed.

Furthermore, the **prevention of uniform corrosion** can be accomplished by selecting an adequate 1) material having a uniform microstructure, 2) coating or paint, 3) inhibitor(s) for retarding or suppressing corrosion. These are classified as adsorption-type hydrogen-evolution poisons, scavengers, oxidizers, and vapor-phase[5], and 4) cathodic protection, which is an electrochemical process for suppressing corrosion in large steel structures. Figures 1.3 and 1.4 show atmospheric uniform corrosion on typical structures. Both the steel bridge structures and the pipeline were exposed to air by the ocean. Notice how the steel structures were subjected to chemical reactions, which proceeded uniformly over the exposed metal surface area.



Figure 1.3 Uniform corrosion (atmospheric attack) of a steel bridge.

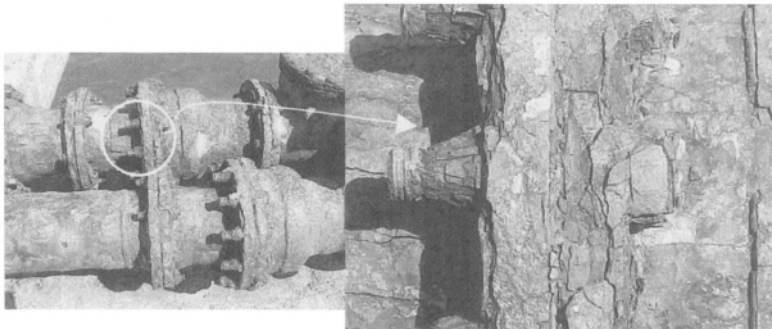


Figure 1.4 Uniform corrosion (atmospheric attack) of a pipeline located on a concrete pier above the ocean water.

1.4 GALVANIC CORROSION

Galvanic corrosion is either a chemical or an electrochemical corrosion. The latter is due to a potential difference between two different metals connected through a circuit for current flow to occur from more active metal (more negative potential) to the more noble metal (more positive potential).

Galvanic coupling is a galvanic cell in which the anode is the less corrosion resistant metal than the cathode. Figure 1.5 shows atmospheric galvanic corrosion of a steel bolt-hexagonal nut holding a coated steel plate and electrical control steel box attached to a painted steel electrical post. Both corroded bolt-nut and the steel box are the anodes having very small surface areas, while the coated steel plate and the steel post have very large cathodic surface areas. Corrosion rate can be defined in terms of current density, such as $i = I/A$ where I is the current and A is the surface area. Therefore, the smaller A the larger i . This is an area effect on galvanic coupling. Thus, the driving force for corrosion or current flow is the potential (voltage) E between the anode and cathode. Subsequently, Ohm's law, $E = IR = iAR$, is applicable. Here, R is the galvanic cell resistance.

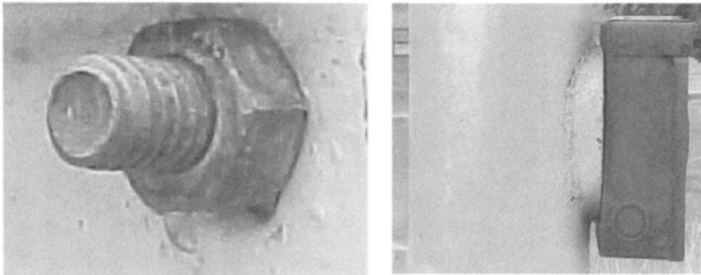


Figure 1.5 Galvanic corrosion (atmospheric attack) of a a) steel bolt/nut and b) steel sheet box attached to a painted steel electrical post.

In addition, galvanic corrosion can be predicted by using the electromotive force (emf) or standard potential series for metal reduction listed in Table 2.1. These reactions are reversible. The standard metal potential is measured against the standard hydrogen electrode (SHE), which is a reference electrode having an arbitrary standard potential equals to zero. Details on types of reference electrodes are included in chapter 2.

In selecting two metals or two alloys for a galvanic coupling, both metals should have similar potentials or be close to each other in the series in order to suppress galvanic corrosion. For example, $Fe - Cr$ or $Cu - Sn$ (bronze) couplings develop a very small potential differences since they are close to each other in their respective standard potential series. The given data in Table 2.1 is very appealing in designing against galvanic corrosion of pure metals. The closer the standard potentials of two metals the weaker the galvanic effect; otherwise, the galvanic effect is enhanced.

Eventually, galvanic coupling can be used for cathodic protection purposes. In fact, in coupling two different metals the metal with the lowest standard potential acts as the anode and its standard potential sign is changed. Figure 1.6 shows two galvanic coupling cases, in which copper and zinc can be in the form of sheets or electroplated coatings. Recall that iron (Fe) is the base metal for steel; therefore, Fe is to be protected against corrosion. Therefore, Fe is the anode for Cu and the cathode for Zn couplings. In the latter case, Zn becomes a sacrificial anode, which is the principle of coupling for galvanized steel sheets and pipes. On the other hand, if Cu coating breaks down, steel is then exposed to an electrolyte and becomes the anode, and therefore, it oxidizes. These two cases are schematically shown in Figure 1.6. A detailed analysis of galvanic cells will be dealt with in Chapter 2.

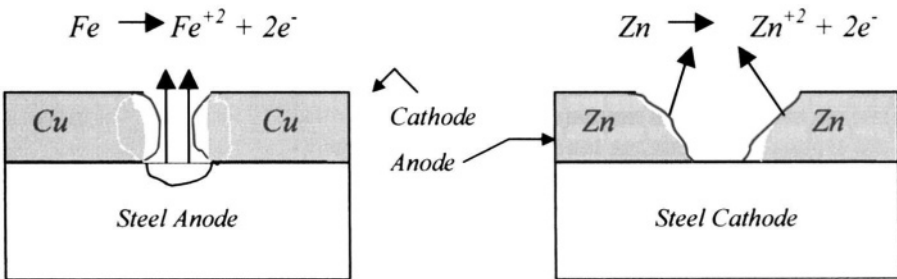
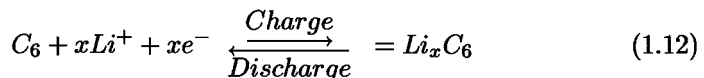


Figure 1.6 Schematic galvanic couplings [5].

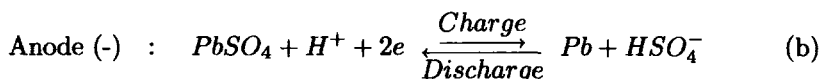
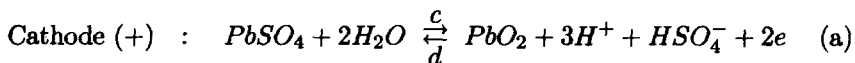
Other types of galvanic coupling are batteries and fuel cells. Both are electrochemical power sources in which chemical energy is converted into electrochemical energy through controlled redox electrochemical reactions [6]. Subsequently, these electrochemical devices represent the beneficial application of galvanic corrosion. Among the reactions that occur in batteries, high hydrogen evolution is desirable. Reference [6] includes details of several types of batteries and fuel cells which are briefly described below.

Lithium Ambient-Temperature Batteries (LAMBS): These are high energy density devices, in which the Li anode is passivated. The solid cathode can be made of $LiCuO$, $LiMnO_2$, LiV_2O_5 , or $LiBi_2Pb_2O_5$. Some LABS use liquid cathodes, such as $LiSO_2$ [7]. For negative cathodes made of carbon (graphite or coke) in lithium-ion batteries, the reaction on this electrode is

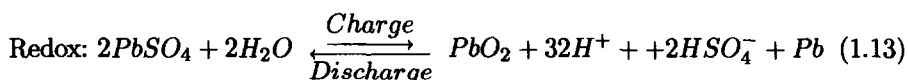


The reduction reaction is for charging and the oxidation is for discharging processes of the lithium-ion cells. Detail analysis of these cells, including side reactions can be found elsewhere [13-15].

Lead-Acid Battery: The basic operation of a lead-acid ($Pb - H_2SO_4$) battery is based on groups of positive and negative plates immersed in an electrolyte that consists of diluted sulfuric (H_2SO_4) acid and water. Hence, the mechanism of this type of battery is based on the electron-balanced anodic (-) and cathodic (+) reactions. Hence, the ideal electrode reactions are reversed during charging (\xrightarrow{c}) and discharging (\xleftarrow{d})



The redox reaction in lead-acid batteries is the sum of the above half-cell reaction



According to the above half-cells, the anode is pure lead (Pb) and the cathode is lead dioxide (PbO_2). In addition, both electrodes dissolve in the electrolyte during discharge, forming lead sulfate ($PbSO_4$). However, when the battery is charged, reverse reactions occur. Thus, this reversible electrochemical cycle can last for a prolong time, but in practice batteries have a finite lifetime due to the lead sulfate build-up acting as an insulation barrier.

Most automotive batteries have lead-calcium grids for maintenance-free and have a life time from 1 to 5 years; however, longer battery life is possible. Generally, a lead-acid battery is used as a 12 - volt electrochemical device, which consists of six 2 - volt cells connected in series. The average activity and density of the sulfuric acid solution are in the order of $4.5 \text{ mol/l} = 4.5 \times 10^{-3} \text{ mol/cm}^3 = 432 \text{ g/l}$ and 1.25 g/cm^3 at $20^\circ C$, respectively.

If the battery is overcharged, then electrolysis (dissociation) of water occurs leading to hydrogen evolution at the cathodes and oxygen evolution at the anodes. In general, batteries can store and supply energy because of the interactions between the electrodes submerged in the electrolyte.

Dry-Cell Battery: This is a common galvanic cell which contains a moist ammonium chloride electrolyte. An schematic battery is shown in Figure 1.7. The zinc casing and the solid carbon in contact with the electrolyte (electric conductor) develop a potential difference, which in turn, produces an electron flow when the zinc and carbon are electrically connected. Consequently, the zinc eventually corrodes galvanically since it provides the electrons to the electrolyte for generating reduction reactions. The electrolyte (moist paste) carries the current from the zinc anode to the carbon cathode.

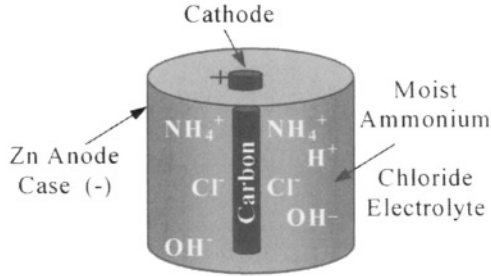
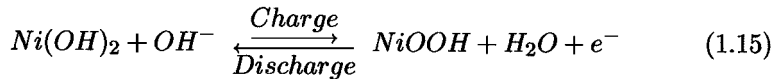
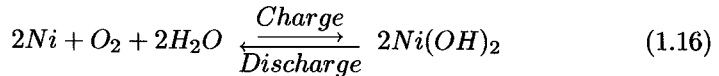


Figure 1.7 Two-dimensional view of a schematic dry-cell battery [5].

Sintered Nickel Electrode in Alkaline Batteries: These batteries are galvanic devices containing a porous *Ni* matrix that holds the active (anodic) materials. The following reaction is reversed upon discharging [16-17]

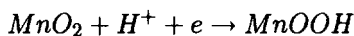


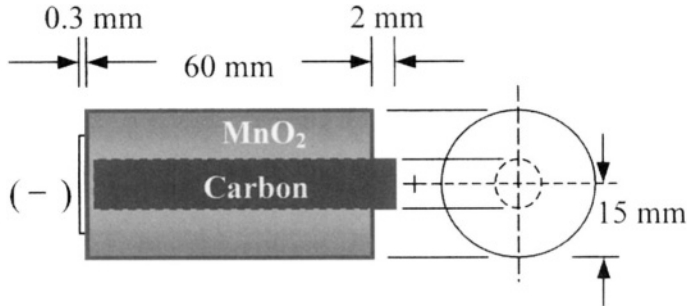
In addition, corrosion of the *Ni* electrode may occur under unfavorable conditions, leading to loss of electrical continuity due to the following reaction



Other side reactions must be taken into account for characterizing nickel-hydrogen cells. Details on this matter can be found elsewhere [14-17]. The subject of galvanic corrosion is discussed in Chapter 5 using polarization curves. For purpose of clarity, the driving force for current flow through a moist electrolyte and electrochemical corrosion is the potential (voltage) difference between the anode and the cathode electrodes. With this in mind, an example usually helps the reader to understand the simple mathematics and parameters involved in determining the magnitude of the available driving force needed to operate a simple battery for a time t . In fact, a battery is simply an electrochemical device used as a energy storage. Thus, the reader is briefly introduced to the concepts of electric charge (Q), the Faraday's constant (F) and valence (z).

Example 1.1 Calculate a) the mass and number of moles of a zinc battery (**Zn**) casing, b) the mass and number of moles of the manganese dioxide (**MnO₂**) in the electrolyte if the battery has a stored energy of **36 kJ/V** and a power of 3 Watts. c) Find the time it takes to consume the stored energy if the battery operates at a current of 2 A and the potential (voltage). The thickness of the cell is $x = 1 \text{ mm}$. Other dimensions, such as length (L) and radius (r), are indicated below. The discharging reaction is



**Solution:**

The stored energy needs to be converted into units of coulombs. Hence,
 $Q = 36 \text{ kJ/V} = 36,000 \text{ A}\cdot\text{s} = 36,000 \text{ Coulombs}$

The area and volume are

$$A_s = 2\pi Lr = (2\pi)(6 \text{ cm})(1.5 \text{ cm}) = 56.55 \text{ cm}^2$$

$$V = xA_s = (0.1 \text{ cm})(5.6549 \text{ cm}^2) = 5.65 \text{ cm}^3$$

a) The mass and the moles of Zn are

$$m_{Zn} = V\rho = (5.65 \text{ cm}^3)(7.14 \text{ g/cm}^3) = 40.34 \text{ g}$$

$$X_{Zn} = \frac{m_{Zn}}{A_{w,Zn}} = \frac{40.34 \text{ g}}{65.37 \text{ g/mol}} = 0.62 \text{ mol}$$

b) The moles and the mass of MnO_2 are

$$X_{MnO_2} = \frac{Q}{zF} = \frac{36,000 \text{ A}\cdot\text{s}}{(1)(96,500 \text{ A}\cdot\text{s/mol})}$$

$$X_{MnO_2} = 0.37 \text{ mol}$$

$$M_{MnO_2} = X_{MnO_2}A_{w,MnO_2} = (0.37 \text{ mol})(86.94 \text{ g/mol})$$

$$M_{MnO_2} = 32.17 \text{ g}$$

c) The time for discharging the stored energy and the potential are

$$t = \frac{Q}{I} = \frac{36,000 \text{ A}\cdot\text{s}}{2 \text{ A}} = 5 \text{ hours}$$

$$E = P/I = (3 \text{ V}\cdot\text{A}) / (2 \text{ A}) = 1.5 \text{ V}$$

1.4.1 MICROSTRUCTURAL EFFECTS

A mechanically deformed metal or alloy can experience galvanic corrosion due to differences in atomic plane distortion and a high dislocation density. In general, dislocations are line defects in crystals. Figure 1.8a shows a mechanically worked steel nail indicating localized anodes. The tip and the head of the nail act as stress cells for oxidation of iron to take place, provided that the nail is exposed to an aggressive environment. These two parts of the nail are examples of strain hardening, but are susceptible to corrode galvanically due to the localized crystal defects and the presence of mainly compressive residual stresses induced by the mechanical deformation process. Furthermore, the nail shank act as the cathode and the tip/head-shank form galvanic cells in a corrosive environment.

In addition, improper heat treatment can cause nonuniform microstructure and therefore, galvanic-phase corrosion is enhanced in corrosive media. In a crystalline metal, galvanic coupling can occur between grains and grain boundaries. Figure 1.8b shows a schematic microstructure of a metal subjected to corrosion along the grain boundaries, as in the case of a typical polished and etched microstructure. This type of corrosion can be referred to as grain-boundary corrosion because the grain boundaries act as anodes due to their atomic mismatch and possible segregation of impurities.

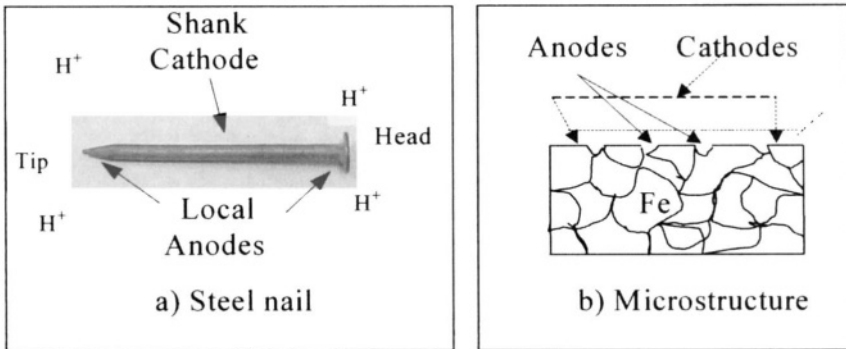


Figure 1.8 Localized galvanic cells. a) Stress cells and b) microcells.

Galvanic corrosion can occur in a polycrystalline alloys, such as pearlitic steels, due to differences in microstructural phases. This leads to galvanic-phase coupling or galvanic microcells between ferrite ($\alpha\text{-Fe}$) and cementite (Fe_3C) since each phase has different electrode potentials and atomic structure. Therefore, distinct localized anodic and cathodic microstructural areas develop due to microstructural inhomogeneities, which act as micro-electrochemical cells in the presence of a corrosive medium (electrolyte). This is an electrochemical action known as galvanic corrosion, which is mainly a metallic surface deterioration.

This form of corrosion is not always detrimental or fatal to metals. For instance, revealing the microstructure of pearlitic steels with a mild acid can be

accomplished due to the formation of galvanic microcells. In this case, pearlite consists of ferrite and cementite and when it is etched with a mild acid, which is the electrolyte, galvanic microcells between ferrite (*cathode*) and cementite (*anode*) are generated. Consequently, pearlite is revealed as dark cementite and white ferrite.

In addition, if a zinc is immersed in hydrochloric acid HCl (reagent) at room temperature and it spontaneously reacts in this strong corrosive environment. Figure 1.9 shows a galvanized steel nail was immersed in such as solution. Notice that nail is covered with hydrogen bubbles. This is an example of hydrogen evolution that occurs in acid solutions. Thus, HCl acid solution acts as an oxidizer and the corrosion rate of zinc is increased very rapidly. The initial chemical reactions for the case shown in Figure 1.9 are similar to eq. (1.14) with the exception of the source of the hydrogen ions. In general, the following reactions take place on the surface of the galvanized steel nail surface during oxidation

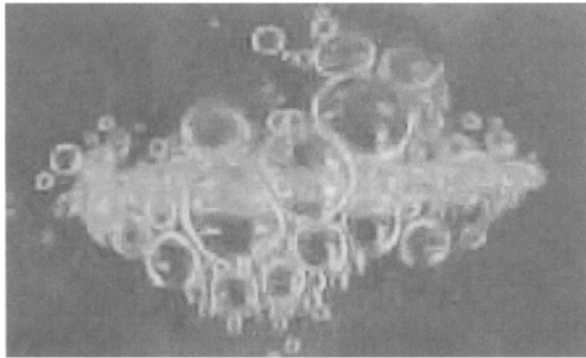
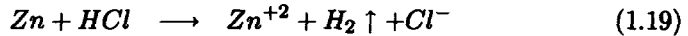


Figure 1.9 A galvanized steel nail reacting in concentrated HCl acid solution.

Furthermore, solid surfaces, such as automobile underbody parts, in contact with a mixture of mud, soil and salt can deteriorate due to galvanic corrosion. In this case, the mixture is a stagnant electrolyte that causes the least galvanic action when compared with agitated electrolytes. In fact, agitation and temperature gradients can accelerate the galvanic action due to a higher current density and consequently, galvanic corrosion is manifested as metal dissolution. If the corroding metal part is under the influence of a tensile stress, then it may become weak and may fail due to reduction in cross-sectional area.

Furthermore, the microstructure of crystalline solids is composed of grains, which are surrounded by grain boundaries. A single grain is composed of a regular and repeated array of atoms, which in turn, form the atomic structure. The most common crystal lattices in engineering materials are the body-centered cubic (BCC), face-centered cubic (FCC) and hexagonal close-packed (HCP). For instance, Figure 1.10 shows the BCC crystal structure encountered in engineering metallic materials, such as chromium, iron, carbon steels, molybdenum and the like. On the other hand, brass and the 300-series stainless steels have an FCC crystal structure. Other crystal structures can be found in any book on Physical Metallurgy and Materials Science. The closed-packed spheres in Figure 1.10 represent an atomic arrangement having unit cells, which repeat themselves forming the lattice crystal structure. Each atom is bounded to its neighbors and each atom has its nucleus surrounded by electrons. The outer atoms forming the electrode surface exposed to a corrosive medium become electron-deficient and are detached from the lattice and form part of the medium, such as an aqueous electrolyte or react with atoms from the medium to form a surface corrosion product. The corrosion rate in terms of current density or penetration per time is the kinetic parameter that must be determined experimentally. Chapter 3 includes details on how to determined this parameter.

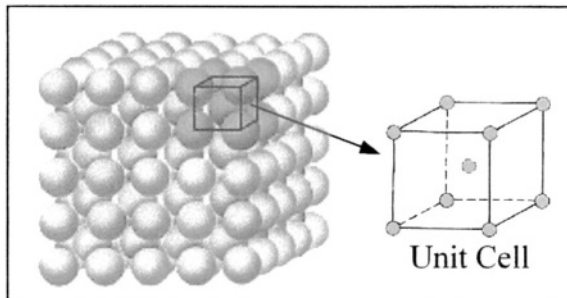


Figure 1.10 Closed packed body-centered cubic crystal structure [18]

The grain boundaries in crystalline solids represent high-energy areas due to the atomic mismatch and therefore, they are considered microstructural defects, which corrode more rapidly than the grain surfaces. Figure 1.11 illustrates two microstructures of AISI 304 stainless steel being annealed at 1000°C for 0.5 hours and 24 hours at 1100°C for a rapidly solidified and consolidated $Ni_{53}Mo_{35}B_9Fe_2$ alloy (RSA). Figure 1.12a shows the grain boundaries as dark lines because of the severe chemical attack using an Aqua Regia etching solution (80% HCl + 20% HNO_3). Figure 1.12b shows crystalline particles embedded in an Ni-Mo matrix after being etched with Marble's reagent. Denote that the RSA alloy does not have visible grain boundaries, but it is clear that the severe chemical attack occurred along the matrix-particle interfaces due to localized galvanic cells [19]. These interfaces appear as bright areas due to optical effects.

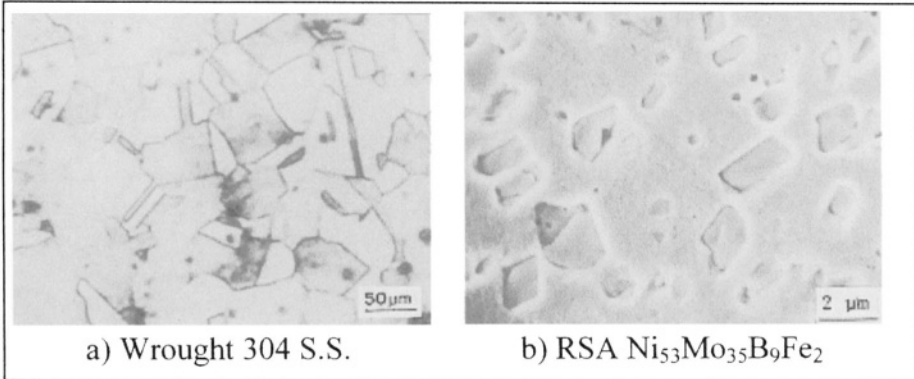


Figure 1.11 Photomicrograph revealing the microstructure of annealed a) AISI stainless steel 304 at 200x and b) rapidly solidified alloy (RSA) $Ni_{53}Mo_{35}B_9Fe_2$ at 5,000x [19]

Another metallurgical aspect to consider is the dislocation network encounter in plastically deformed alloys. In general, dislocations are linear defect, which can act as high energy lines and consequently, they are susceptible to corrode as rapidly as grain boundaries in a corrosive medium. Figure 1.12 illustrates dislocation networks in an AISI 304 stainless steel and in RSA $Ni_{53}Mo_{35}B_9Fe_2$. The relevant pretreatment conditions can be found elsewhere [19].

With respect to Figure 1.12b, there is a clear grain boundary shown as a dark horizontal line across the upper part of the TEM photomicrograph. The small white areas surrounded by dislocations are called sub-grains, which are crystal having an FCC structure for both alloys.

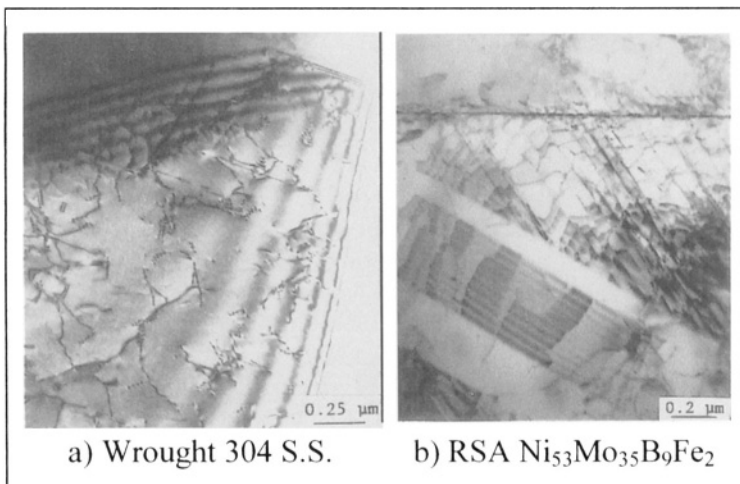


Figure 1.12 Bright field TEM photomicrographs showing dislocations networks [19].

1.5 PITTING CORROSION

This form of corrosion is extremely localized and it manifests itself as holes on a metal surface. The initial formation of pits is difficult to detect due to the small size, but it requires a prolonged time for visual detection. Figure 1.13 shows a scanning electron microscope (SEM) photomicrograph of a 2195 Al-Li alloy (Weldalite 049 trade name) containing pits with an average diameter of approximately $4 \mu\text{m}$. Also included in Figure 1.13 is the model for pitting mechanism. Pitting corrosion may occur due to breakdown of a protective film (passive oxide film or organic coating). This form of corrosion can be found on aluminum and its alloys and automobile chromium-plated bumpers or body coated (painted) parts due to film/coating breakdown at isolated surface sites. Pits vary in shape, but are very small surface holes due to the extremely localized anodic reaction sites.

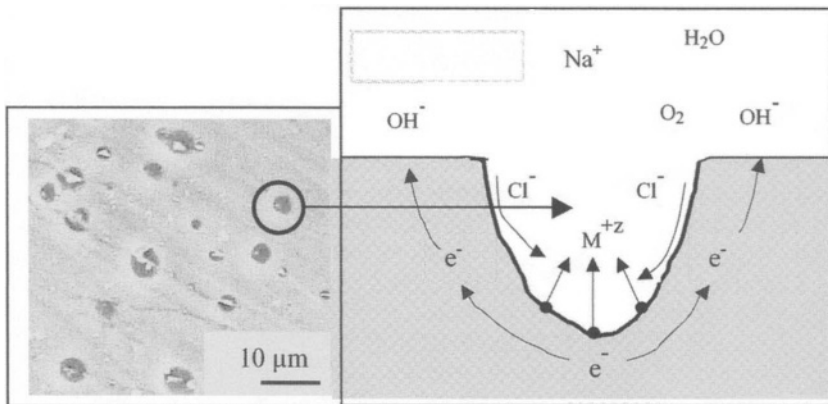
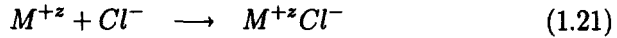
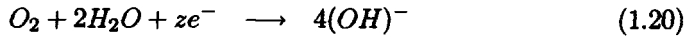
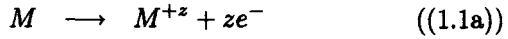


Figure 1.13 a) Localized corrosion on 2195 Al-Li alloy after a potentiodynamic polarization run in 3.5% NaCl. The alloy was aged at 190C for 0.5h. SEM photomicrograph taken at a magnification of 2,000x. b) Pitting mechanism.

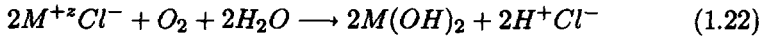
The appearance of pits on a metal surface is not very appealing, but they can be harmless if perforation does not occur. The initiation of pits occurs at localized sites on a metal surface defects, which may be due to coating failure, mechanical discontinuities or microstructural phase heterogeneities such as secondary phases. Besides the prolonged time needed for pit formation or pit growth, it is assumed that many anodic and cathodic reactions take place at localized sites. Both rates of anodic and cathodic reactions are slow; however, the reactions continue inward in the direction of gravity in most cases. This suggests that the bottom of pits are rich in metal M^{+z} ions due to the large number of anodic reactions.

In a water-base electrolyte containing chlorine Cl^- ions and oxygen molecules (O_2), the Cl^- ions migrate towards the bottom of the pits and O_2 molecules react with water molecules on the metal surface [5]. Therefore, metal

chloride $M^{+z}Cl^-$ and hydroxyl ions $(OH)^-$ are produced. This is a oxidation process known as metal dissolution. Prior to the formation of $M^{+z}Cl^-$ aqueous compound is produced, the initial governing reactions are as follows:



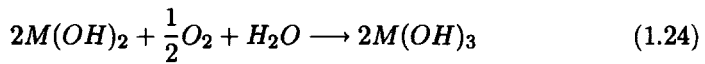
Subsequently, $M^{+z}Cl^-$ is hydrolyzed by water molecules. Hence,



where H^+Cl^- is the free hydrochloric acid that forms at the bottom of the pits increasing the acidity at these locations. This implies that the hydrogen ion concentration $[H^+]$ in *mol/liter* is increased and the degree of acidity can be defined by

$$pH = -\log [H^+] \quad (1.23)$$

The metal hydroxide $2M(OH)_2$ compound is unstable and therefore, it reacts with oxygen and water to form the final corrosion product. Hence,



Typical examples of specific formation of $M(OH)_3$ type corrosion product are given below

$$M(OH)_3 = \begin{cases} Fe(OH)_3 \text{ for steel pits} \\ Al(OH)_3 \text{ for aluminum hydroxide pits} \\ Cr(OH)_3 \text{ for chromium hydroxide pits} \end{cases} \quad (1.25)$$

Should pitting occur, a heterogeneous mechanism for metal dissolution defines a localized attack that may involve metal penetration in thin structural sections. In the case of massive structural sections, pitting is usually of little significance. On the other hand, surface fatigue failures due to pitting mechanism are well documented in the literature. Hence, pitting develops with surface microcracks.

Furthermore, pitting depth (d) can be define by the following empirical equation

$$d = \lambda t^n \quad (1.26)$$

where $\lambda, n =$ Constants
 $t =$ Time

1.6 CREVICE CORROSION

Relatively low temperature electrochemical oxidation of a metal may occur as a sequence of localized anodic reactions according to eq. (1.1a) in a sheltered crevice surface-containing a stagnant electrolyte (water, grease-sand mixture or other insoluble substance). Figure 1.11 shows a schematic rivet-plate joint, in which the sheltered metal surface (joint inner surface) was in contact with a suitable electrolyte. The mechanism of crevice corrosion is electrochemical in nature and it is also illustrated in Figure 1.14. It requires a prolong time to start the metal oxidation process, but it may be accelerated afterwards [5].

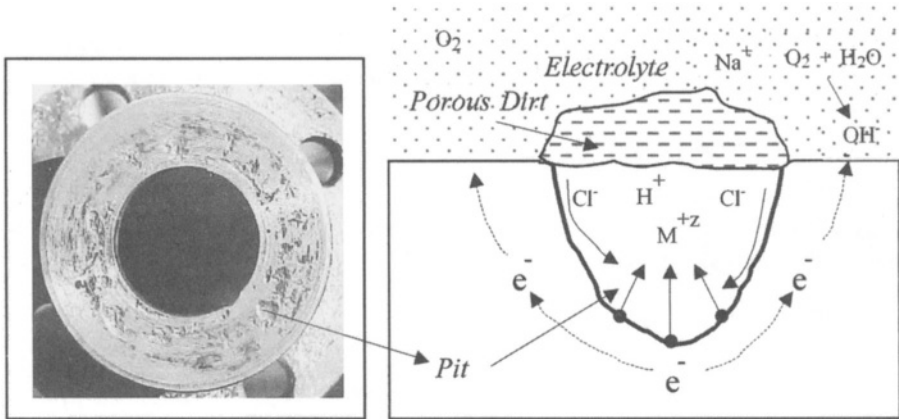


Figure 1.14 Crevice corrosion. a) Stainless steel flange and b) mechanism [5].

Crevice corrosion is similar to pitting corrosion after its initiation stage in a stagnant electrolyte. This form of corrosion initiates due to changes in local chemistry such as depletion of oxygen in the crevice, increase in pH with increasing hydrogen concentration $[H^+]$, and increase of chlorine Cl^- ions. Oxygen depletion implies that cathodic reaction for oxygen reduction cannot be sustained within the crevice area and consequently, metal dissolution occurs. The problem of crevice corrosion can be eliminated or reduced using proper sealants and protective coatings

This is a case for illustrating the effects of nonmetallic materials (gasket, rubber, concrete, wood, plastic and the like) in contact with a surface metal or alloy exposed to an electrolyte (stagnant water). For instance, as Fontana [5] pointed out, crevice attack can cut a stainless steel sheet by placing a stretched rubber band around it in seawater. Thus, metal dissolution occurs in the area of contact between the alloy and rubber band.

1.7 CORROSION-INDUCED SPALLING

Figure 1.15 shows a spalling-induced corrosion of a steel frame, which was initially protected by an organic coating (paint). Notice that spalling is a separation of the surface coating. This particular case is another atmospheric-related corrosion phenomenon. Spalling can also occur on metal oxides and refractory materials due to thermal cycling.

Spalling is a unique defect that represents local disruption of the original protective coating. Figure 1.15 illustrates a severe case of spalling since the organic coating became detached over the central area of the steel structure. This type of defect normally takes a prolong time to manifest its deleterious effects. Thus, corrosion-induced spalling may be attributable to the generation of molecular hydrogen, which is known as hydrogen evolution beneath the organic coating. The pertinent reaction for hydrogen evolution is given by eq. (1.4b).

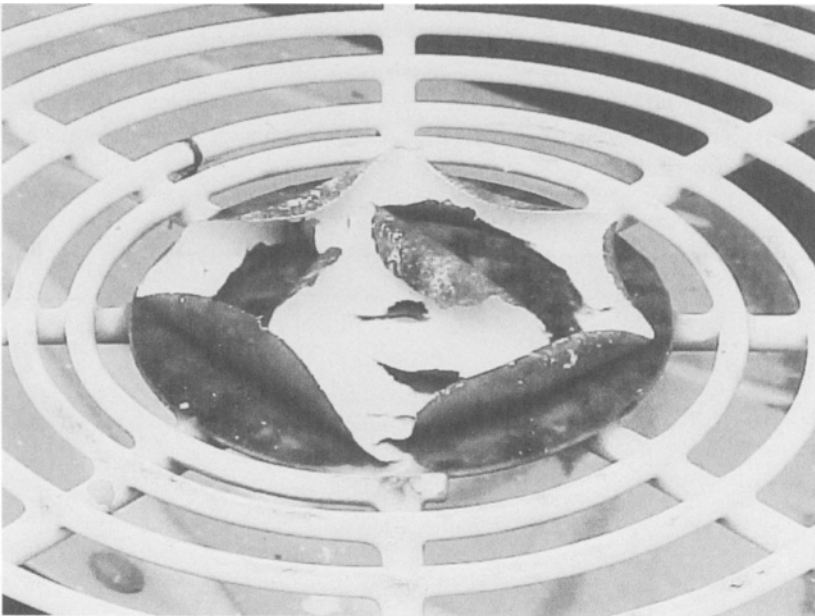


Figure 1.15 Corrosion-induced spalling of coating.

Furthermore, spalling is a common defect in concrete pavements that may become hazardous to roadway users. It occurs due to high compressive stresses in the concrete when cracks and joints are not properly closed or repaired. In fact, spalling tends to grow under repeated thermal stresses caused by traffic loadings. In addition, concrete bridges may fail due to spalling and cracking.

1.8 STRESS CORROSION CRACKING

Structural parts subjected to a combination of a tensile stress and a corrosive environment may prematurely fail at a stress below the yield strength. This phenomenon is known as environmentally induced cracking (EIC), which is divided into the following categories: stress-corrosion cracking (SCC), hydrogen-induced cracking (HIC) and corrosion-fatigue cracking (CFC). These three categories can develop under the influence of an applied potential related to polarization diagram. The former is extensively discussed in Chapter 3 and 4. The EIC phenomenon has been studied for decades, but more research needs to be done in order to have a better understanding of corrosion. Since literature is abundant on this subject, it is convenient to include in this section a brief discussion on SCC and HIC.

It is known that SCC occurs under slow strain-rate (SSR) and (CL) only if the tensile strain rate or the applied potential is within a narrow and yet, critical range; otherwise metals and alloys would appear to be immune to SCC either due to film repair at low strain rates or mechanical failure at high strain rates [20]. Figure 1.16 shows Parkins' classical stress-strain curves [21] for assessing SCC susceptibility of carbon steel in two different environments at relatively high temperature using the slow strain-rate (SSR) technique. Obviously, the specimen exhibited SCC in hot sodium nitrate since the stress-strain curve shows approximately 4% total elongation as compared to nearly 25% elongation in the inert environment.

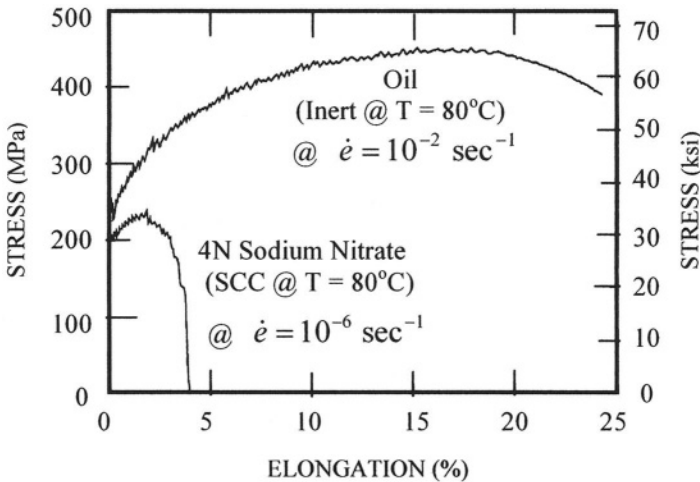


Figure 1.16 Stress-strain curves for carbon steel in hot oil and hot sodium nitrate [20]

In order to assess SCC in details, there must exist a lower and an upper bound of strain rate at a constant applied potential and a potential range at

constant strain rate for ductile materials. This is schematically illustrated in Figure 1.17 after Kim and Wilde [22]. In this figure, the dashed rectangular shape indicated the range of strain rate and range of potential for activation of SCC cracks. The critical SCC state is illustrated as the minimum ductility. Also indicated in Figure 1.17 is the HIC continuous curve for brittle materials.

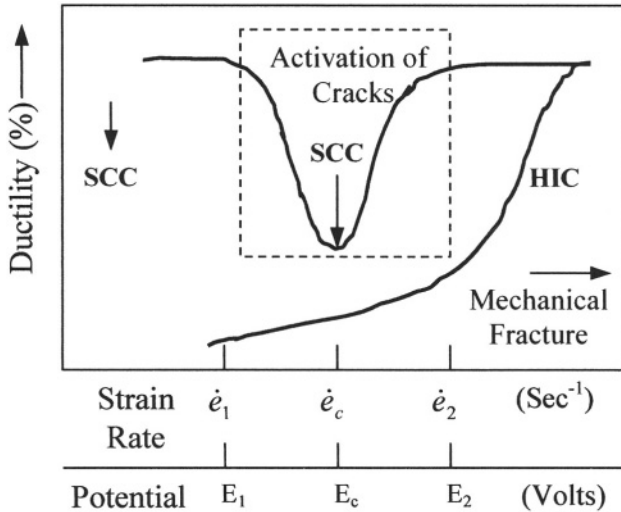


Figure 1.17 Schematic effect of strain rate on ductility using a slow strain rate testing method [22].

Experimental verification of Kim and Wilde SCC curve is shown in Figure 1.18 for a rapidly solidified alloy (RSA) and ingot metallurgy (IM) AISI 304 stainless steels under tension testing using smooth round specimens in 0.10N H_2SO_4 solution at room temperature [19]. These steels have the same chemical composition, but they were produced using different technologies. Their initial microstructural condition were cold rolled as indicated in Figure 1.18. Ductility is characterized reduction in cross-sectional area (RA). The IM 304 steel exhibited maximum SCC at zero potential, while the RSA 304 apparently was degraded due to HIC since RA decreases continuously as the potential decreases. In addition, Figure 1.18 includes the steels polarization curves for comparison purposes. Polarization is discussed in details in Chapter 3 through 5.

Figure 1.19 shows typical secondary cracks on the specimen gage length. Only half of the fractured specimen is shown since the other half exhibited similar cracking morphology. These cracks are typically developed in ductile materials susceptible to SCC. This type of specimen fracture is attributable to SCC, which is corroborated by the drop-off in ductility and the formation of secondary cracks. Therefore, the combination of an applied stress and applied potential in a corrosive environment degrade the material mechanical properties,

specifically due to the deterioration of the specimen surface. As shown in Figure 1.19, the visible secondary cracks are related to the dispersed and localized anodic cells, which may act as such due to machining defects, metallurgical secondary phases, microstructural defects and the like.

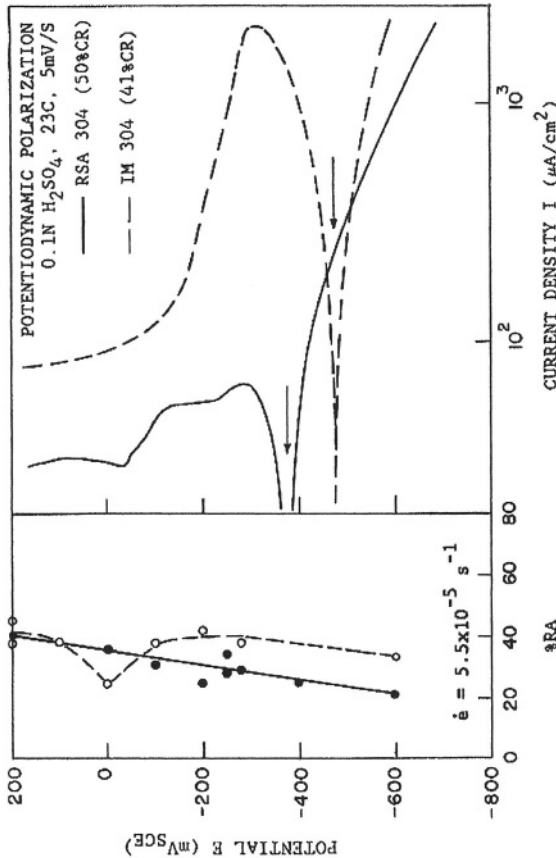


Figure 1.18 Influence the slow strain rate technique and the applied potential on the ductility of 41% cold rolled and annealed AISI 304 S.S. at 1000°C for 24 hours. The applied strain rate was $5.5 \times 10^{-5} \text{ sec}^{-1}$ [19].

In addition, the fracture surface appear perpendicular to the longitudinal direction of the specimen, indicating a brittle fracture at a macroscale. Therefore, SCC is a brittle fracture mechanism at relatively low tensile stress. This implies that the main crack growth occurs perpendicular to the applied tensile load transgranularly, intergranularly or a combination of these mechanisms. Intergranular crack growth appears to be the most common metallurgical failure during SCC and cracking is primarily by mechanical fracture at the crack tip,

where anodic dissolution may occur as a secondary mechanism of the overall SCC process.

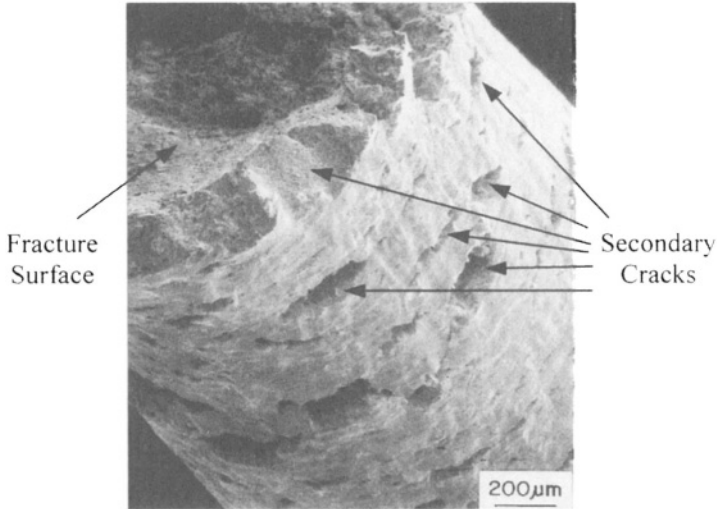


Figure 1.19 SEM fractograph of annealed AISI 304 stainless steel at 1000°C for 24 hours. The specimen was tension tested in 0.10N H_2SO_4 at 23°C at $5.5 \times 10^{-5} \text{ sec}^{-1}$ and $E = 0 \text{ mV}$ [19].

There are similarities in CFC and SCC with respect to the brittle fracture surface mode in a corrosive medium and mechanically, both have a tensile stress component that influences crack opening. The cyclic stress range for CFC is a dynamic process that induces crack initiation on the surface of the metallic component. If the component is exposed to a corrosive solution, then the combination of the cyclic stress and environment accelerate cracking and reduce fatigue life.

The primary characteristic of HIC is the brittle mechanical fracture caused by diffusion of atomic hydrogen into the material because hydrogen is very small and has the capability of migrating through the crystal lattice. The detrimental effects of atomic hydrogen diffusion on mechanical properties is schematically shown Figures 1.17 and 1.18 by a continuous decrease in ductility (as well as in strength as illustrated in Figure 1.16). This particular mechanism is also known in the literature as hydrogen embrittlement (HE) and it is a form of an irreversible hydrogen damage. If hydrogen atoms within the lattice defects, such as voids, react to form molecular hydrogen, and these molecules form babbles, then the metallurgical damage is called blistering.

In addition, failure analysis is normally conducted on tested specimens for further characterization of the effects of EIC.

1.9 NONMETALLIC MATERIALS

CERAMICS. These are brittle and corrosion resistant compounds made out of metallic and nonmetallic elements. Some examples of ceramics are Al_2O_3 (alumina), SiC (silicon carbide), MgO (magnesia), Fe_3O_4 (magnetite), and ZrO (zirconia). Other ceramics are made of basic ceramics and are known as bricks, clay, concrete, porcelain and the like. On the other hand, **refractories** are ceramics that withstand very high temperatures prior to melting, such as NbC (niobium carbide) @ $3615^\circ C$ and MgO @ $2852^\circ C$. In addition, ceramics are immune to corrosion by almost all environments. Those which are not dissolve by chemical oxidation.

POLYMERS. These type of nonmetallic materials are very common in today's society. A polymer is an organic compound, which means "poly" \equiv many and "meres" \equiv parts and consists of repeated long-chain molecular structure bounded by covalent bonds [10-11]. Natural polymers are known as proteins, silks, deoxyribonucleic (DNA) among many others. On the other hand, synthetic polymers, such as nylon (polyamides), polyvinyl chloride (PVC), polyacrylonitrile (PAN), polyethylene, epoxy and many more are known as **plastics**, which are so important in nowadays society due to their vast and broad domestic and industrial applications. However, polymers are susceptible to degradation in natural and synthetic environments, such as high temperatures (thermal degradation), moisture, radiation, ultraviolet light and mechanical agents. Degradation of polymers in natural environments is known as weathering due to the effect of ultraviolet radiation from the sunlight, moisture, and temperature. Some oxidation agents of polymers can be found elsewhere [11]. In addition, degradation or damage of polymers can be classified as 1) oxidation damage according to the oxidation reaction $R \longrightarrow R^+ + e^-$ due to high-energy ionization radiation (radiolysis), such as electron beams, γ - **radiation**, and x - **rays** and 2) swelling caused by moisture and oxygen [11]. Furthermore, the polymer R loses one electron leading to a degradation known a depolymerization.

WOODS. These are organic in nature and corrosion resistant in water and diluted acids. Woods consist of cellulose fibers surrounded by lignin. The cellulose fibers are strong and yet, flexible, whereas the lignin is stiffer. Some woods can dissolve in strong acids and diluted alkalies [5]. However, the wood texture and properties play an important role in the material selection scheme for making violins, guitar, pianos, furniture, and houses.

1.10 SUMMARY

The forms of corrosion encounter in diverse engineering structures have a common oxidation mechanism represented by an anodic reaction, such as $M \rightarrow M^{+z} + ze^{-}$, eq. (1.1a). Thus, corrosion may be due to chemical or electrochemical reactions. One common corrosion process is the formation of ferric hydroxide, $Fe(OH)_3$, as indicated by the sequence of reactions given by eq. (1.7). Therefore, corrosion is classified as a localized or general oxidation process. It manifests its natural or forced behavior in various forms from atmospheric corrosion of steel structures to oral corrosion on dental alloys due to the effect of saliva and food.

In fact, the most common forms of corrosion are atmospheric and galvanic. Normally, a coating is applied on a structure to prevent or suppress oxidation since it is a cost effective method. However, most coatings are synthetic polymers which oxidize in several environments leading to spalling-induced corrosion as shown in Figure 1.13. Ceramics, on the other hand, are made or formed by a combination of metallic and nonmetallic elements. Their unique characteristics for being corrosion and high temperature resistant materials do not exclude them from the corrosion schemes. Some strong acids are the cause of ceramic oxidation. The oxidation of polymers is represented by a molecular anodic reaction of the form $R \rightarrow R^{+} + e^{-}$. This implies that the polymer R loses one electron leading to a degradation known as depolymerization. In addition, woods also degrade in strong acids and alkalies.

1.11 REFERENCES

[1] P. Morriset, Zinc el Alliages, "Zinc and Zinc Alloys," in Corrosion: Metal-Environment Reactions, third edition, Edited by L.L. Shreir, R.A. Jarman, and G.T. Burstein, Butterworth-Heinemann, 20(1959)15.

[2] A.R.L. Chivers and F.C. Porter, "Zinc and Zinc Alloys" in Corrosion: Metal/Environment Reactions, third edition, Edited by L.L. Shreir, R.A. Jarman, and G.T. Burstein, Butterworth-Heinemann, (1994) 4:172.

[3] C.H. Dale Nevison, "Corrosion of Zinc" Corrosion, Vol. 13, Ninth edition, ASM international, (1987)756.

[4] J.C. Bailey, F.C. Porter, A.W. Pearson and R.A. Jarman, "Aluminum and Aluminum Alloys," in Corrosion: Metal /Environment Reactions, third edition, Edited by L.L. Shreir, R.A. Jarman, and G.T. Burstein, Butterworth-Heinemann, (1994) 4.15.

[5] M.G. Fontana, "Corrosion Engineering," McGraw-Hill Book Company, (1986) 282,41.

[6] "Corrosion in Batteries and Fuel-cell Power Sources," in Corrosion, Vol. 13, Ninth edition, ASM International, (1987)1317.

[7] J.P. Gabano, "Lithium Battery Systems: An overview," in Lithium Batteries, edited by J.P. Gabano, Academic Press, (1983)1-12.

- [8] S.L. Pohlman, “*General Corrosion*,” in *Corrosion*, Vol. 13, Ninth edition, ASM International, (1987) 80
- [9] S.C. Dexter, “*Localized Corrosion*,” in *Corrosion*, Vol. 13, ASM International, (1987) 104.
- [10] A. Kumar and R.K. Gupta, “*Fundamentals of Polymers*,” The McGraw-Hill Companies, Inc., New York, (1998).
- [11] J.R. Fried, “*Polymer Science and Technology*,” Prentice Hall, Inc., New Jersey, (1995).
- [12] C. Leygraf and T. Graedel, “*Atmospheric Corrosion*,” Wiley-Interscience A John Wiley & Sons, Inc., Publication, New York, (2000) 330-333.
- [13] P. Arora and R.E. White, and M. Doyle, *J. Electrochem. Soc.*, Vol. 145, No. 10, (1998) 3647-3667.
- [14] P. Arora, M. Doyle, and R.E. White, *J. Electrochem. Soc.*, 146 (10) (1999) 3543-3553.
- [15] P. Arora, B.N. Popov, and R.E. White, *J. Electrochem. Soc.*, Vol. 145, No. 3, (1998) 807-814.
- [16] P. De Vidts, J. Delgado, B. Wu, D. See, K. Kosanovich, and R.E. White, *J. Electrochem. Soc.*, Vol. 145, No. 11, (1998) 3874-3883.
- [17] B. Wu and R.E. White, *J. Electrochem. Soc.*, 148 (6) (2001) 3A5985-A609.
- [18] W.G. Moffat, G.W. Pearsall and J. Wulff, “*The Structure and Properties of Materials*,” Vol. I, Structure, (1984) 51 as reported by W.D. Callister, “*Materials Science and Engineering: An Introduction*,” Six Edition, John Wiley & Sons, Inc., (2002) 33
- [19] N. Perez, Ph.D. Dissertation, (1990)
- [20] R.N. Parkins, F. Mazza, J.J. Royuela and J.C. Scully, *Br. Corrosion Journal*, 7 (1972) 154
- [21] R.N. Parkins, “*Stress Corrosion Cracking - The Slow Strain Rate Technique*,” ASTM STP 665, (1979) 5
- [22] C.D. Kim and B.E. Wilde, ASTM STP 665, (1979) 97

Chapter 2

ELECTROCHEMISTRY

2.1 INTRODUCTION

The goal of this chapter is to elucidate the fundamental characteristics and technological significance of electrochemical cells. A comprehensive review on the subject is excluded since the intention hereafter is to describe the principles of electrochemistry, which should provide the reader with relevant key definitions and concepts on metal reduction and metal oxidation in galvanic couplings. Thus, the principles of anodic protection and cathodic protection become uncomplicated or unproblematic to understand and comprehend suitable applications of electrochemistry for preventing localized corrosion and general corrosion on metallic structures. In general, electrochemistry deals with the chemical response of an electrode/electrolyte system to an electrical stimulation and the electrochemical behavior of species (ions) can be assessed, including concentration, kinetics, and reaction mechanisms.

Electrochemical galvanic cells involve electron transfer from a metal (electrode) surface to a environment (electrolyte). This metal is treated as the anode due to its ability to oxidize by losing electrons and becoming electron-deficient atoms called cations. On the other hand, the metal receiving or gaining electrons is the cathode since its cations in solution reduce or deposit on the cathode surface as atoms. Therefore, an electric field must exist in the electrolyte due to the presence of charge particles represented by ions [1]. If an electrochemical cell produces energy it is known as a galvanic cell and if it consumes energy it is an electrolytic cell. Nonetheless, an electrochemical process is treated as an electroanalytical technique associated with electricity and chemistry so that electrical quantities are measured in order to quantify chemical changes in a cell. Chemical measurements normally involve heterogeneous bulk solutions and electrochemical processes are analyzed according to the ionic interactions at the electrode-electrolyte interface.

The applications of electrochemistry is broad. Simply stated, metal ions can be reduced into atoms on an electrode surface by chemical and electrochemical

processes. The former process does not involve any current flow to drive a redox reaction, but the latter does. Eventually, metal reduction starts at a nanoscale forming atom agglomerates or nanoparticles [13-16] and it may proceed to a microscale as in thick film formation or macroscale as in electrowinning technology for recovering, say, copper from solution. Nowadays, nanotechnology is gaining acceptance in the scientific community.

2.2 ELECTRICAL POLES

Assume that electrical conductors, such as aqueous solutions containing charged particles known as ions, exists in a static electrochemical system and that there exists an infinitesimal current flow. Thus, an electric field strength vector \vec{E} at a point P in space and an inner electric potential ϕ of the system are defined below, respectively [1]

$$\vec{E} = \vec{F}/Q \quad (2.1a)$$

$$\phi = \lim_{Q \rightarrow 0} \frac{W}{Q} \quad (2.1b)$$

where \vec{F} = Electric force vector (N)
 Q = Electric charge (C = Coulomb)
 W = Electric work (J)

In fact, Q depends on the type of ions, which are treated hereafter as poles, and it is related to **Faraday's constant** F . Both F and Q are defined by

$$F = q_e N_A \simeq 96,500 \text{ C/mol} \quad (2.1c)$$

$$Q = zFX_i \quad (2.1d)$$

where q_e = Electron charge = $(1.6022 \times 10^{-19} \text{ C/ions})$
 N_A = Avogadro's number = $(6.02213 \times 10^{23} \text{ ions/mol})$
 X_i = Mole fraction (mol)
 z = Valence or oxidation number
 $\text{C/mol} = \text{A} \cdot \text{s/mol} = \text{J/mol} \cdot \text{V}$

The Cartesian electric field strength components in a three-dimensional scheme are defined as follows

$$\begin{bmatrix} E_x \\ E_y \\ E_z \end{bmatrix} = -\nabla\phi = - \begin{bmatrix} \partial\phi/\partial x \\ \partial\phi/\partial y \\ \partial\phi/\partial z \end{bmatrix} \quad (2.2a)$$

$$\begin{bmatrix} E_x \\ E_y \\ E_z \end{bmatrix} = \lambda Q \begin{bmatrix} x^{-2} \\ y^{-2} \\ z^{-2} \end{bmatrix} \quad (2.2b)$$

where $\epsilon_o = 8.854 \times 10^{-12} \frac{C}{Nm^2}$ = Permittivity of vacuum
 $\lambda = 1/(4\pi\epsilon_o) = 9 \times 10^9 \frac{Nm^2}{C^2}$

MONOPOLE: Let ϕ be defined at a point P in space around a charge Q^+ in an electrical monopole $Q^+ - P$ path shown in Figure 2.1a. Integrating eq. (2.2a) yields the inner electric potential in the x-direction

$$\phi_x = \int_0^r E_x dx = \frac{\lambda Q}{r} \quad (2.3)$$

Equation (2.3) gives the definition of the monopole potential due to a point charge Q . This is a simple definition of an internal potential between two points located at a relatively short distance. Otherwise, $\phi \rightarrow 0$ as $r \rightarrow \infty$. On the other hand, when $\phi \rightarrow \infty$ as $r \rightarrow 0$ an electric potential “singularity” can be established for ϕ in the order of r^{-1} as predicted by eq. (2.3).

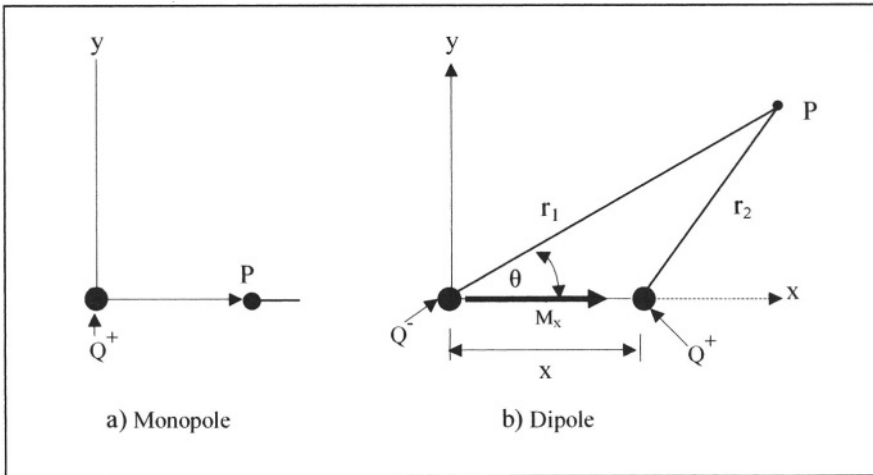


Figure 2.1 Schematic electrical poles in aqueous phase.

Consider an electrolyte or a metal as a single electrical conductor phase in equilibrium. In this case, current flow does not occur and the electric field at all points in the phase is zero. In fact, a non-infinitesimal current is an irreversible process since heat is generated by the current flowing in the phase [1]. At equilibrium, eq. (2.2b) gives $E_x = E_y = E_z = 0$, which means that the electric potential ϕ is constant in the bulk phase so that $\phi \neq 0$ and the current is $I = 0$.

This can be analyzed by using eq. (2.2a) since $\partial\phi/\partial x = 0$, but $\int \partial\phi = 0$ gives $\phi + C = 0$ where $C = \text{constant}$; therefore, $\phi \neq 0$, which implies that it is a net electrical charge being uniformly distributed over the surface of the phase; otherwise, the repulsive force of like charges will not allow diffusion (motion) of charges to the phase surface [1].

DIPOLE: Consider the charge couple shown in Figure 2.1b, in which the negative and positive charges are separated by a distance $x \ll r_i$, making an electrical dipole for which the electrical dipole moment has a magnitude of $M_x = xQ$. Suppose that the charged particles and the point P in space make **1) a right triangle Q^-PQ^+** . Thus, an extension of the single charge case described by eq. (2.3) can provide the internal electric potential ϕ . Using eq. (2.3) along with $M_x = xQ$ yields

$$\phi = \int_0^r E_x dx = \int_0^r E \cos \theta dx = \int_0^r \frac{\lambda Q \cos \theta}{r^2} dx \quad (2.4)$$

$$\phi = \frac{\lambda M_x \cos \theta}{r^2} \quad \text{for } r \gg x \quad (2.5)$$

2) If Q^-PQ^+ make an **oblique triangle**, then the electric potential is

$$\phi = \int_{r_2}^{r_1} E dr = \int_{r_2}^{r_1} \frac{\lambda Q}{r^2} dr = \lambda Q \left(\frac{1}{r_2} - \frac{1}{r_1} \right) \quad (a)$$

$$\phi = \lambda Q \left[\frac{r_1^2 - r_2^2}{r_1 r_2 (r_1 + r_2)} \right] \quad (b)$$

Using the law of cosines and assuming that $r_i \gg x$ yields

$$r_2 = r_1^2 + x^2 - 2xr_1 \cos \theta \quad (c)$$

$$r_2 \approx r_1^2 - 2xr_1 \cos \theta \quad \text{since } r_i \gg x \quad (d)$$

$$r_1^2 - r_2^2 \approx 2xr_1 \cos \theta \quad (e)$$

Substituting eq. (e) and $M_x = xQ$ into (b) gives

$$\phi \approx \lambda M_x \left[\frac{2 \cos \theta}{r_2 (r_1 + r_2)} \right] \quad (f)$$

Now, letting $r \approx r_1 \approx r_2$ in eq. (f) the electric potential becomes [1]

$$\phi \approx \frac{\lambda M_x \cos \theta}{r^2} \quad \text{for } r \gg x \quad (2.5)$$

The electric potential ϕ "singularity" is in the order of r^{-2} since $\phi \rightarrow \infty$ as $r \rightarrow 0$. Thus, the electric field strength according to eqs. (2.3) and (2.5) are, respectively

$$E_x = -\frac{\partial\phi}{\partial r} = \frac{\lambda Q}{r^2} \quad (\text{Monopole}) \quad (2.6a)$$

$$E_\theta = -\frac{\partial\phi}{\partial r} = \frac{2\lambda M_x \cos\theta}{r^3} \quad (\text{Dipole}) \quad (2.6b)$$

Notice that the E “singularity” is in the order of r^{-2} for the monopole and r^{-3} for the dipole cases. This brief introduction of the source of the electric field strength of a phase is for the reader to notice that a phase has been treated as an electrically neutral thermodynamic system, which is not the case for a heterogeneous electrochemical cell. In addition, this section serves the purpose of comparison with the proceeding electrochemical treatment.

Example 2.1 Let an electrolyte contain a net charge due to 10^{-11} moles of nickel cations (Ni^{+2}). Calculate the surface electric potential ϕ at a distance of 7 cm from the solid electrode-electrolyte interface in the x -direction. Will this calculated potential value differ from the electric potential difference ($\Delta\phi$) between electrodes? Explain.

Solution:

from eq. (2.1d),

$$Q = x_i(zF) = (10^{-11} \text{ mol})(2)(96,500 \text{ C/mol}) = 1.93 \times 10^{-6} \text{ C}$$

But,

$$\lambda = 1/(4\pi\epsilon_0) = 9 \times 10^9 \frac{\text{Nm}^2}{\text{C}^2}$$

$$r = 0.05 \text{ m}$$

Thus, inserting these values into eq. (2.3) gives the electric potential

$$\phi = \lambda Q/r \simeq 0.25 \times 10^6 \text{ V} \quad \left(\frac{\text{Nm}}{\text{C}} = \frac{\text{Nm}}{\text{J/V}} = \frac{\text{JV}}{\text{J}} = \text{V} \right)$$

This large amount of volts does not represent a typical difference in electric potential between electrodes of a practical electrochemical system. Normally, a few volts are needed to operate a simple electrochemical system. Conclusively, $\phi \gg \Delta\phi$.

2.3 ELECTROCHEMICAL CELLS

First of all, corrosion is basically an electrochemical process that involves ionic interactions leading to metal dissolution or surface deterioration. Thus, the theory of corrosion requires thorough understanding of the electrochemical events

within a particular metal-electrolyte system for mitigating corrosion. This dictates that the driving force for electrochemical events must be known in order to classify the type of electrochemical cells to be characterized either to recover metals from solution (see Chapter 7) or prevent corrosion (Chapter 8).

In general, electrochemical cells have four basic components called

- The **electrolyte** is an electrical conductive fluid or moist soil.
- The **anode electrode** is a metal in contact with the electrolyte allowing anodic reactions to take place.
- The **cathode electrode** is a metal in contact with the electrolyte allowing reduction reactions to occur on the surface.
- The **power supply** which is connected to the anode and cathode electrodes, providing the potential to the electrochemical system for reduction reactions (electrolysis) or current through the anode to protect the cathode from corrosion.

Furthermore, an electrochemical system can be classified according to the schematic cells depicted in Figure 2.2. The electrochemical cells are described below.

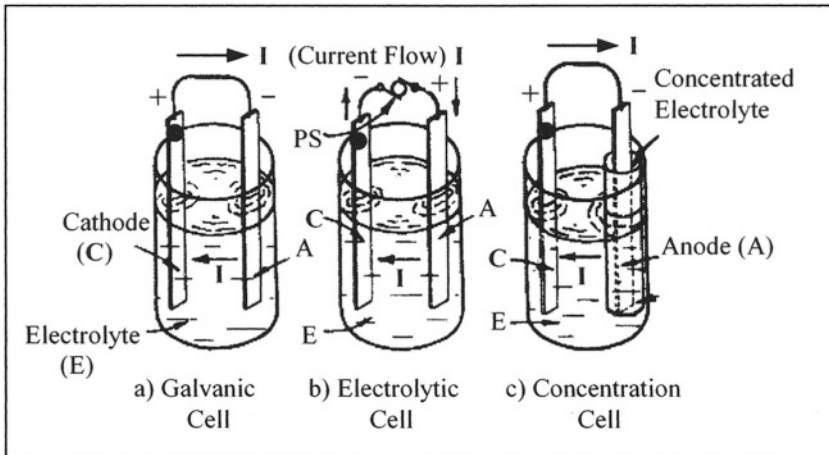


Figure 2.2 Type of electrochemical cells. PS = Power supply [20].

1) **Galvanic cell**, which is a bimetallic cell since it has different metallic electrodes, but current flows clockwise as indicated in Figure 2.2a by the arrows. This electrochemical event produces electric energy from the stored chemical energy in the metallic anode. Consequently, current flows from the cathode to the anode through the metallic circuit and electric power, $P = EI$, is

produced. Faraday's law of electrolysis is obeyed for forming electrochemical reaction reactions under the principles of electrochemical stoichiometry so that the redox reaction occurs spontaneously without the aid of an external power supply. The subject of electrolysis will be dealt with in Chapter 7.

2) **Electrolytic Cell**, in which current flows clockwise as shown in Figure 2.2b, but the source of power is external. The cell has bimetallic or mono-metallic electrodes. This cell consumes power, $P = EI$, and the cell reactions are driven in the reverse direction as opposed to galvanic ; that is, the galvanic spontaneous reactions are driven backwards. This is possible if the applied potential is greater than the galvanic potential. This type of cell is very useful in the electrometallurgy field for recovering metals from oxide ores by electroplating the metal ions on cathodes. Hence, if current flows, then the principles of electrochemical stoichiometry is used for producing electrochemical reactions through the process of electrolysis and metal ions are deposited on a cathode surface. Electrolysis stands for an electrochemical process in which the redox reaction is forced (non-spontaneous) to occur by passing a direct current (dc) through the electrolyte. Therefore, $E_{\text{electrolytic}} > E_{\text{galvanic}}$, but the measurable cell potential difference in an electrolytic or galvanic cell can be influence by the Ohm's potential ($E = IR$) drop. Table 2.1 lists comparison between galvanic and electrolytic cells.

Table 2.1 Comparison of electrochemical cells

Galvanic Cell	Electrolytic Cell
Produces Chemical Energy	Provides Electrical Energy
Chemical \rightarrow Electrical energy	Electrical \rightarrow Chemical energy
$\Delta G^\circ < 0$ and $E^\circ > 0$	$\Delta G^\circ > 0$ and $E^\circ < 0$
Spontaneous Redox Reaction	Forced Redox Reaction
Positive Cathode	Negative Cathode
Negative Anode	Positive Anode
Dry Batteries	Electroplating, Cathodic Protection

3) **Concentration Cell**, which has mono-metallic electrodes, but the anode is immersed in a concentrated region of the electrolyte as shown in Figure 2.2c. This cell has the electrodes made of the same metal and it is similar to a galvanic with respect to the electrode polarity and current flow direction. The electrodes are immersed in a nonhomogeneous electrolyte, but the anode is within the concentrated portion of the electrolyte where the concentration of species j is $C_j(\text{anode}) > C_j(\text{cathode})$.

Figure 2.3 shows two galvanic cells indicating metal dissolution at the anode (left electrode) and the direction of current flow. Figure 2.3a shows metals M_1 and M_2 as the anode and cathode, respectively. Both are immersed in their own sulfate-base electrolyte. Each $M_1 - M_1SO_4(aq)$ and $M_2 - M_2SO_4(aq)$

constitute what is known as anodic half-cell and cathodic half-cell, respectively. Subsequently, the electrochemical galvanic cell is composed of these two half-cells if current flows as shown in Figure 2.3a. On the other hand, Figure 2.3b shows a chemical galvanic cell due to the lack of current flow, but electron flow occurs from the anode to the cathode through the wires.

Recall that $M_1SO_4(aq)$ and $M_2SO_4(aq)$ are in their ionic state in solution (aqueous). Both metals are externally connected to a electrical circuit in order to measure the potential difference between them. In other words, the circuit is used to measure the galvanic cell potential by a voltmeter (V). This measurable cell potential is current/resistance dependent. If current ceases to flow, then the cell potential is known as the open-circuit potential or standard potential (E°), which are illustrated in Figure 2.2 for pure metal reduction. The standard potential is also known as the electromotive force (emf) under equilibrium conditions: unit activity, $25^\circ C$, and 1 atm (101 kPa) pressure.

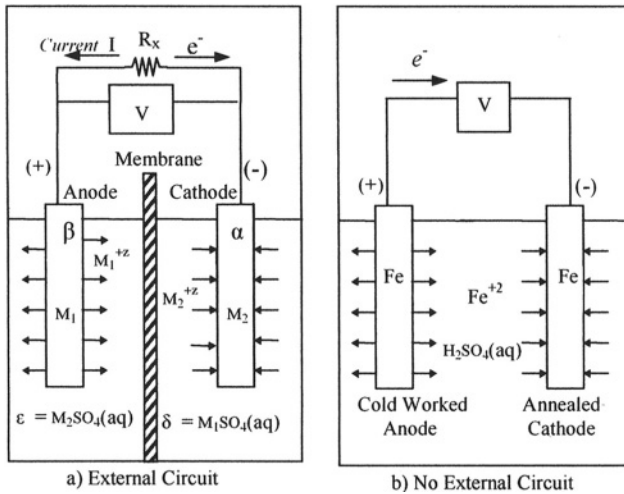


Figure 2.3 a) Electrochemical galvanic cell and b) Galvanic chemical cell.

Figure 2.3b, on the other hand, shows an iron (Fe) galvanic cell composed of a cold worked electrode (anode) and an annealed electrode (cathode). The former electrode becomes the anode due to a high microstructural defects, such as dislocation density, and internal (residual) stresses introduced during the cold working (plastic deformation) process. The latter electrode is stress relieved during annealing and the dislocation density is nearly zero or eliminated.

The assessment of Fe-base couplings to form galvanic cells can be elucidated using two cases. According to the galvanic series in Figure 2.2, Fe is located between copper (Cu) and zinc (Zn). Suppose that a steel plate is coated with Zn and another with Cu . Consequently, Fe is the anode for Cu and the cathode for Zn couplings. In the latter case, Zn becomes a sacrificial anode, which is the principle of coupling for galvanized steel sheets and pipes.

On the other hand, if *Cu* coating breaks down, steel is then exposed to an electrolyte and becomes the anode, and therefore, it oxidizes. These two cases are schematically shown in Figure 1.6. The cell potential of each coupling case is determined by adding the standard potentials, but the sign of $E_{Fe}^{\circ} = +0.44 \text{ V}$ and $E_{Zn}^{\circ} = +0.763 \text{ V}$ are reversed since they act as anodes. Recall that Figure 2.2 illustrates standard potentials for reduction reactions. Hence,

- a) *Fe* – *Cu* coupling: $E_{cell}^{\circ} = E_{Fe}^{\circ} + E_{Cu}^{\circ} = +0.44 \text{ V} + 0.337 \text{ V} = 0.777 \text{ V}$
 b) *Fe* – *Zn* coupling: $E_{cell}^{\circ} = E_{Fe}^{\circ} + E_{Zn}^{\circ} = -0.44 \text{ V} + 0.763 \text{ V} = 0.323 \text{ V}$

The above standard state (Table 2.2) conforms to the convention adopted by the International Union of Pure and Applied Chemistry (IUPAC), which requires that all tabulated electromotive force (emf) or standard electrode potential values (E°) be so with respect to the standard hydrogen electrode (SHE) for reduction reactions of pure metals, such as $M^{+z} + ze^{-} = M$. In addition, Table 2.3 illustrates standard potentials for some compounds.

Table 2.2 Standard potential for metal reduction [5-6].

	Reduction Reaction	E° (V_{SHE})	
Noble	$Au^{+3} + 3e^{-} = Au$	+1.498	
	$O_2 + 4H^{+} + 4e^{-} = 2H_2O$	+1.229	
↑	$Pt^{+2} + 2e^{-} = Pt$	+1.200	
	$Pd^{+2} + 2e^{-} = Pd$	+0.987	
	$Ag^{+} + e^{-} = Ag$	+0.799	
	$Cu^{+2} + 2e^{-} = Cu$	0.337	
	$Re^{+3} + 3e^{-} = Re$	0.300	
	↓	$2H^{+} + 2e^{-} = H_2$	0.000
		$Fe^{+3} + 3e^{-} = Fe$	-0.036
		$Pb^{+2} + 2e^{-} = Pb$	-0.126
		$Sn^{+2} + 2e^{-} = Sn$	-0.136
		$Ni^{+2} + 2e^{-} = Ni$	-0.250
		$Co^{+2} + 2e^{-} = Co$	-0.277
		$Cd^{+2} + 2e^{-} = Cd$	-0.403
		$Fe^{+2} + 2e^{-} = Fe$	-0.440
		$Cr^{+3} + 3e^{-} = Cr$	-0.744
		$Zn^{+2} + 2e^{-} = Zn$	-0.763
		$Ti^{+2} + 2e^{-} = Ti$	-1.630
		$Al^{+3} + 3e^{-} = Al$	-1.662
		$Mg^{+2} + 3e^{-} = Mg$	-2.363
$Na^{+} + e^{-} = Na$		-2.714	
↓		$K^{+} + e^{-} = K$	-2.925
		Active	$Li^{+} + e^{-} = Li$

Thus, *Cu* atoms coat the *Zn* rod or sediment to the bottom of the beaker. Eventually, this redox (overall) reaction produces chemical energy, which is dissipated as heat. This, then is a source of chemical energy that can be converted to useful work by adequately designing a device called electrochemical cell as schematically shown in Figure 2.3a and 2.4. In fact, this cell is assumed to contain charged species, but at least one electrically charged specie cannot penetrate all the phases of the system, and a difference in electric potential will be developed between phases.

Table 2.3 Standard potentials for compounds [6].

	Reduction Reaction	E° (V_{SHE})
Anodic ↑	$O_3 + 2H^+ + 2e^- = O_2 + H_2O$	+2.070
	$H_2O_2 + 2H^+ + 2e^- = 2H_2O$	+1.776
	$MnO_2 + 4H^+ + 4e^- = Mn^{+2} + 2H_2O$	+1.230
	$O_2 + 4H^+ + 4e^- = 2H_2O$	+1.229
	$AuCl_4^- + 3e^- = Au + 4Cl^-$	0.994
	$TiO_2 + 4H^+ + 4e^- = Ti + 2H_2O$	0.860
	$NiO_2 + 2H_2O + 2e^- = Ni(OH)_2 + 2(OH^-)$	0.760
	$Ag_2SO_4 + 2e^- = 2Ag + SO_4^{-2}$	0.653
	$AgNO_2 + e^- = Ag + NO_2^-$	0.590
	$O_2 + 2H_2O + 4e^- = 4(OH^-)$	0.401
	$Ag_2O + H_2O + 2e^- = 2Ag + 2(OH^-)$	0.342
	$AgCl + e^- = Ag + Cl^-$	0.222
	$Pt(OH)_2 + 2e^- = Pt + 2(OH^-)$	0.40
	$Pd(OH)_2 + 2e^- = Pd + 2(OH^-)$	0.100
	↓	$2H^+ + 2e^- = H_2$
$AgCN + e^- = Ag + CN^-$		-0.020
$WO_2 + 4H^+ + 4e^- = W + 2H_2O$		-0.120
$Cu(OH)_2 + 2e^- = Cu + 2(OH^-)$		-0.224
$PbSO_4 + 2e^- = Pb + SO_4^{-2}$		-0.359
$Ni(OH)_2 + 2e^- = Ni + 2(OH^-)$		-0.660
$Co(OH)_2 + 2e^- = Co + 2(OH^-)$		-0.730
$Fe(OH)_3 + 3e^- = Fe + 3(OH^-)$		-0.771
$2H_2O + 2e^- = H_2 + 2(OH^-)$		-0.828
$Fe(OH)_2 + 2e^- = Fe + 2(OH^-)$		-0.877
Cathodic	$Mn(OH)_2 + 2e^- = Mn + 2(OH^-)$	-1.470

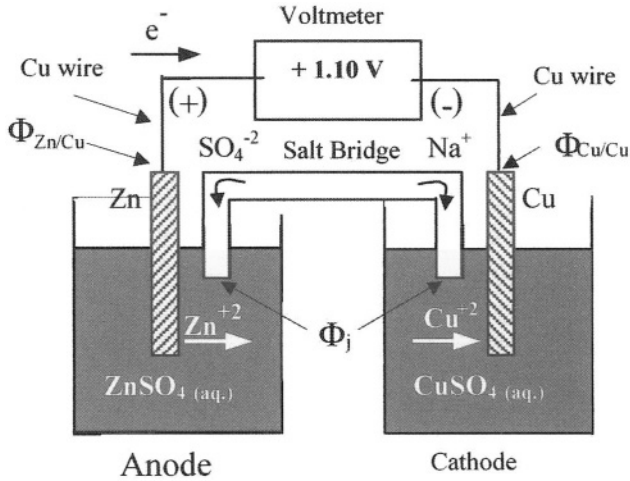


Figure 2.4 The Zn/Cu galvanic (voltaic) cell.

Furthermore, either Figure 2.3a or 2.4 can be used as the point of departure for developing the thermodynamics of electrochemical systems, which is referred to as electrochemical cells containing phases that are electrical conductors, which are known as electrolytes. Thus, electrolytes are needed for the proper development of a potential difference. In a conventional electrochemical cell set up, the cathode is the most positive electrode kept on the right hand side and the anode is the most negative electrode [2]. Thus, electron flow occurs from left to right through the terminals in the above Figures 2.3 and 2.4, which are schematic representations of galvanic cells or voltaic cells.

In general, an electrochemical cell can be used to drive or be driven by an external electrical system or device, such as an incandescent light or motor-generator, respectively. A motor-generator can drive or be driven by an electrochemical cell, depending on the cell potential or on the applied potential, respectively.

With regard to Figure 2.4, $\Phi_{Zn/Cu}$ and $\Phi_{Cu/Cu}$ are contact potentials and Φ_j is the liquid junction potential. The measurable standard cell potential for Figure 2.4 is a measure of interfacial potentials

$$E_{cell}^{\circ} = (E_{Zn}^{\circ} + E_{Cu}^{\circ}) + [\Phi_{Zn/Cu} + \Phi_{Cu/Cu} + \Phi_j] \quad (2.7a)$$

In real cases, nonstandard conditions exist and the cell potential can be predicted by

$$E_{cell} = E_{cell}^{\circ} + [E_{Nernst} - E_{Ohmic} - \eta] \quad (2.7b)$$

where E_{Nernst} , E_{Ohmic} and η are potential terms for correcting the standard potential expression, eq. (2.7a). These terms will be dealt with in a later section.

The system shown in Figure 2.4 is a galvanic cell known as a voltaic cell, which consists of two different solids called anodic **Zn** electrode and cathodic **Cu** electrode. In summary, this electrochemical coupling has several events which can be described as follows:

1) Zinc (**Zn**) is immersed in aqueous zinc sulfate [$\text{ZnSO}_4(\text{aq})$] so that $\text{Zn} - \text{ZnSO}_4(\text{aq})$ becomes the anodic half-cell. Similarly, copper in copper sulfate, $\text{Cu} - \text{CuSO}_4(\text{aq})$, is the cathodic half-cell.

2) $\text{Zn} - \text{Cu}$ cell \equiv $\text{Zn} - \text{ZnSO}_4(\text{aq})$ half cell + $\text{Cu} - \text{CuSO}_4(\text{aq})$ half cell.

3) $\text{ZnSO}_4(\text{aq})$ and $\text{CuSO}_4(\text{aq})$ are solutions known as electrolytes, which are phases like **Zn** and **Cu** electrodes and are electrical conductors as well.

4) **Cu** wire is used to connect the **Zn** and **Cu** electrodes so that no potential difference develops between the wires, which are called terminals.

5) The salt bridge or porous membrane is used to connect both electrolytes and allow the migration of ions to maintain electrical neutrality of the cell.

6) If a salt bridge is not used, both half-cells become isolated and electrical neutrality is lost since the **Zn** electrode becomes more positive as Zn^{+2} cations are produced and the **Cu** electrode becomes more negative as Cu^{+2} are removed from solution and deposited as **Cu** atoms on the electrode surface. Thus, the Zn^{+2} cations (positively charged particle) and sulfate SO_4^{-2} anions (negatively charged) migrate through the salt bridge in the opposite direction.

7) The terminals are connected to a voltmeter to complete the well-known electrochemical galvanic cell circuit.

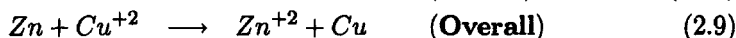
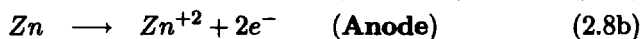
8) The galvanic cell (like a battery) converts chemical energy to electrical energy due to electron flow from the anode to the cathode through the terminals.

9) The voltmeter is used to measure the potential difference between the **Zn** and **Cu** electrodes at equilibrium.

2.3.1 OPEN-CIRCUIT CONDITION

This is the case when the voltmeter is removed leaving an open-circuit. A summary of events are outlined below for Figure 2.4.

1) Due to instability of the galvanic cell, Cu^{+2} cations diffuse into the $\text{ZnSO}_4(\text{aq})$ solution through the salt bridge. Diffusion is slow, but Cu^{+2} ions will come in contact with the **Zn** electrode. Consequently, the zinc anode oxidizes and the copper cations reduce to form atoms as shown below. The redox reaction results by adding both the anodic and cathodic reactions



2) A spontaneous redox reaction occurs without electron flow. Eventually, the **Zn** electrode will go into solution or simply dissolves.

3) The redox reaction indicates that **Zn** oxidizes in **ZnSO₄(aq)** solution and **Cu** reduces in **CuSO₄(aq)** solution. Eventually, the cell would be destroyed.

4) In order to avoid destruction of the cell, just connect a resistor like a voltmeter to the terminals. This will keep **Cu⁺²** cations away from the **ZnSO₄(aq)** solution due to the electric field force in the **CuSO₄(aq)** solution.

2.3.2 CLOSED-CIRCUIT CONDITION

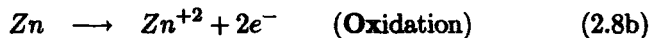
This is the case when a voltmeter (resistor) is connected to the galvanic cell for operation purposes, so that the potential difference between the **Zn** and **Cu** electrodes is measured as $E_{cell}^{\circ} = +1.10 \text{ V}$. What happens when the cell is operating, say, at standard condition ($P = 1 \text{ atm.}$, $T = 25^{\circ}\text{C}$, 1 mol/liter)?

1) The **Cu – Zn** junction potential $\Phi_{Zn/Cu}$ is lower than the **Cu – Cu** junction $\Phi_{Cu/Cu}$. Since $\Phi_{Zn/Cu} < \Phi_{Cu/Cu}$ electrons will flow from the lowest electric potential reservoir (anodic half-cell) to the highest reservoir (cathodic half-cell) through the external wires or terminals.

2) The electrical work is $W = Q\Delta\phi = QE_{cell} > 0$ for electron flow to occur as negative charges. Here, $\Delta\phi$ is the cell potential difference.

3) If $W > 0$, then positive charges flow from low to high potential reservoirs (from **Cu** to **Zn** electrodes).

4) Consequently, the following reactions occur



The electrons (e^{-}) arriving at the **CuSO₄(aq)** electrolyte combine with **Cu⁺²** cations in solution and deposit as **Cu** atoms on the **Cu** electrode surface. This **Cu** deposition is called electroplating.

5) An electric potential difference is developed since **CuSO₄(aq)** electrolyte becomes depleted of **Cu⁺²** cations and **ZnSO₄(aq)** electrolyte becomes enriched with **Zn⁺²** cations.

6) Once $\Delta\phi = E_{cell}$ is developed, positive ions flow through the solution from **Zn** to **Cu** electrodes, provided that the half-cells are separated by a porous membrane or salt bridge (Figure 2.3). According to Ohm's Law, the change in inner potential is $\Delta\phi = IR$.

7) The salt bridge is filled with an agar gel (polysaccharide agar or polymer gel) and concentrated aqueous salt (**NaCl** or **KCl**) solution in order to maintain electrical neutrality between the half cells (Figure 2.3). The gel allows diffusion of ions, but eliminates convective currents [1].

8) The maximum potential difference and the corresponding cell diagram (Figure 2.5) for Figure 2.4 are given below

$$E_{cell} = (E_{Zn}^{\circ} + E_{Cu}^{\circ}) + [\Phi_{Zn/Cu} + \Phi_{Cu/Cu} + \Phi_j] \quad (2.7a)$$

$$E_{cell} \approx E_{Zn}^{\circ} + E_{Cu}^{\circ} \approx 1.10 V_{SHE} \quad (2.7b)$$

since $[\Phi_{Zn/Cu} + \Phi_{Cu/Cu} + \Phi_j] \approx 0$.

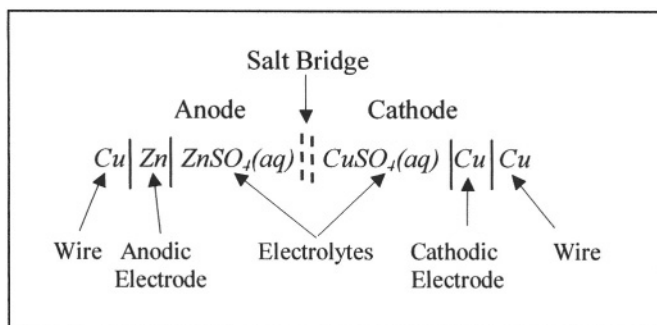


Figure 2.5 Galvanic cell diagram for Figure 2.4.

Vertical lines represent phase boundaries. A salt bridge is symbolized by two vertical lines and has two liquid junctions of insignificant potentials.

Now that an electrochemical galvanic cell has been described in details, it is convenient at this moment to expand the thermodynamic of electrochemistry in terms of chemical energy, which in turn, will be converted to electrical energy. The subsequent analytical procedure leads to the derivation of the Nernst equation, which is suitable for determining the cell electric potential when ion activities are less than unity as nonstandard conditions.

2.3.3 APPLICATION OF GALVANIC CELLS

The $Zn - Cu$ electrochemical galvanic cell being described so far (Figure 2.3) is a chemical energy source capable of producing 1.10 volts, which is a relatively low energy output. This energy source capacity can be enhanced by connecting several cells in series. A common application of galvanic cells is in the production of batteries for flashlights, radios, automobiles and so on. For instance, the production of lead-sulfuric acid ($Pb - H_2SO_4$) automobile batteries include lead anodes and lead oxide cathodes immersed in sulfuric acid solution. A brief description of these type of batteries is included in Chapter 1, section 1.4. Furthermore, a single $Pb - H_2SO_4$ galvanic cell produces 2 volts, but six (6) cells coupled in series produce 12 volts. If the cell is coupled in parallel, the total potential is 2 volts, but the total current is 6 times that of a single cell. The lifetime of these $Pb - H_2SO_4$ automobile batteries can be prolonged by supplying an external current provided by an alternator. In this case, the oxidation

and reduction reactions are reversed and the battery is maintained charged for some time. Table 2.4 lists alloy galvanic series.

Table 2.4 Galvanic series of metal and alloys in sea water [7].

Noble ↑	Zinc (Zn)
	Low carbon steels
	Alloy steels
	Cast iron
	Stainless steels
	α-brass
	Aluminum brass
	Red brass
	Copper (Cu)
	Aluminum bronze
	Cu – Ni alloys
	Nickel (Ni)
	Inconel
	Monel
	Hastelloy C
↓ Active	Titanium

2.4 THERMODYNAMICS

Using Figure 2.3a as the basic cell, the thermodynamics involved is treated below in a general case. Remove the salt bridge and treat each cell as isolated systems. Let metal M rod be the α phase being immersed in an aqueous solution (electrolyte), which is the ϵ phase (MSO_4). Let z^+ and z^- be the valence of the cations (M^{z^+}) and the anions ($X^{-z^-} = SO_4^{-2}$). Let ϕ^α be the electric potential of the metallic α phase and ϕ^ϵ the electric potential of the ϵ phase. Once the α phase is in contact with the ϵ phase, an exchange of charged particles between α and ϵ phases causes a change in the total energy of the system, which consists of the negatively charged α phase as electrons are discharged into the electrolyte. The altered total energy is due to the change in electrostatic potential energy of the phases involved, specifically at the metal-electrolyte interface where a strong electric field exists and a double layer of charged particles disturbs the charge on the interface. This double layer is a normal balance (equal number) of positive and negative ions, which diffuse to the interface causing such as disturbance in energy [4]. Eventually, the system will reach the state of equilibrium within the electrolyte.

The entropy change (dS), the electrical energy change (dE), and the change of charge (dq) for a α - ϵ coupling, in which α is the metallic phase and ϵ is the electrolyte phase are, respectively

$$dS = dS^\alpha + dS^\epsilon \quad (2.10)$$

$$T^\alpha dS^\alpha = dU^\alpha + P^\alpha dV^\alpha - [(\mu^\alpha d\eta^\alpha)_M + (\mu^\alpha d\eta^\alpha)_e] \quad (2.11)$$

$$T^\epsilon dS^\epsilon = dU^\epsilon + P^\epsilon dV^\epsilon - (\mu^\epsilon d\eta^\epsilon)_{M+z} \quad (2.12)$$

$$dE = dU^\alpha + dU^\epsilon + \phi^\alpha dq^\alpha + \phi^\epsilon dq^\epsilon \quad (2.13)$$

$$dq = dq^\alpha + dq^\epsilon = z_e F (d\eta^\alpha)_e + z F (d\eta^\epsilon)_{M+z} \quad (2.14)$$

where μ = Chemical potential

P = Pressure

U = Internal energy

V = Volume

S = Entropy

T = Temperature

q_e = Electron charge

η = Number of moles

ϕ = Electric potential

F = Faraday's constant

For an isolated $\alpha - \epsilon$ thermodynamic system, the following constraints can be used to develop equilibrium conditions and the Gibbs free energy change (ΔG) [3]

$$(d\eta^\alpha)_{M+z} = -(d\eta^\alpha)_M \quad (a)$$

$$dV^\epsilon = -dV^\alpha \quad (b)$$

$$dV = 0 \quad (c)$$

$$dE = 0 \quad (d)$$

$$dq = 0 \quad (e)$$

Hence, combining eq. (e) and (2.14) and the resultant expression with eq. (a) yields

$$(d\eta^\alpha)_e = +(d\eta^\epsilon)_e \quad \text{since } z_e = -1 \quad (f)$$

$$(d\eta^\alpha)_e = -z (d\eta^\epsilon)_M \quad \text{since } z \geq 1 \quad (g)$$

The physical interpretation of these constraints, eqs. (f) and (g), and eq. (2.14) implies that adding $(d\eta^\alpha)_e$ and $(d\eta^\epsilon)_{M+z}$ moles to the α phase and the ϵ phase, respectively, the change in electron charges becomes [3]

$$dq^\alpha = -F (d\eta^\alpha)_e \quad (h)$$

$$dq^\epsilon = +zF (d\eta^\epsilon)_{M+z} \quad (i)$$

Substituting eqs. (a) and (f) into (2.14) and (2.14) into (2.13) yields

$$dU^\alpha + dU^\epsilon + zF (\phi^\alpha - \phi^\epsilon) (d\eta^\alpha)_M = 0 \quad (j)$$

$$dU^\epsilon = - [dU^\alpha + zF(\phi^\alpha - \phi^\epsilon)(d\eta^\alpha)_M] \quad (k)$$

Substituting eqs.(a) through (k) into (2.11) and (2.12) and the resultant expressions into (2.10), and subsequently, collecting terms yields the entropy change of the $\alpha - \epsilon$ system

$$dS = \left[\frac{1}{T^\alpha} - \frac{1}{T^\epsilon} \right] dU^\alpha + \left[\frac{P^\alpha}{T^\alpha} - \frac{P^\epsilon}{T^\epsilon} \right] dV^\alpha \quad (2.15)$$

$$+ \left[-\frac{(\mu^\alpha)_M}{T^\alpha} + \frac{z(\mu^\alpha)_e}{T^\alpha} - \frac{(\mu^\epsilon)_{M+z}}{T^\epsilon} + \frac{(zF)(\phi^\epsilon - \phi^\alpha)}{T^\epsilon} \right] (d\eta^\alpha)_M$$

At equilibrium, $dS = 0$ and the following is deduced from eq. (2.15) [3]

1) For thermal equilibrium,

$$\left[\frac{1}{T^\alpha} - \frac{1}{T^\epsilon} \right] = 0 \text{ since } T^\alpha = T^\epsilon \quad (2.16)$$

2) For mechanical equilibrium,

$$\left[\frac{P^\alpha}{T^\alpha} - \frac{P^\epsilon}{T^\epsilon} \right] = 0 \text{ since } P^\alpha = P^\epsilon \quad (2.17)$$

3) For electrochemical equilibrium, $T^\alpha = T^\epsilon$ and

$$(\mu^\alpha)_M - [z(\mu^\alpha)_e - (\mu^\epsilon)_{M+z}] + zF(\phi^\alpha - \phi^\epsilon) = 0 \quad (2.18)$$

$$(\mu^\alpha)_M - [z(\mu^\alpha)_e - (\mu^\epsilon)_{M+z}] = -zF(\phi^\alpha - \phi^\epsilon) \quad (2.19)$$

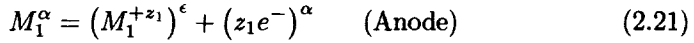
$$\Delta G^\alpha = (\mu^\alpha)_M - [z(\mu^\alpha)_e - (\mu^\epsilon)_{M+z}] \quad (2.20a)$$

$$\Delta G^\alpha = -zF(\phi^\alpha - \phi^\epsilon) \quad (2.20b)$$

Thus, $(\mu^\alpha)_M - [z(\mu^\alpha)_e - (\mu^\epsilon)_{M+z}]$ is the affinity for $M^\alpha = (M^{+z})^\epsilon + (ze^-)^\epsilon$ and ΔG^α is the Gibbs free energy change for the α - ϵ system.

In addition, the potential difference $(\phi^\alpha - \phi^\epsilon)$ between two phases in a half-cell at equilibrium cannot be measured. Instead, two electrodes are connected as shown in Figure 2.3a to measure the electric potential difference between the electrodes. This can be done by connecting, say, β - δ system to the previous α - ϵ system using a salt bridge or porous membrane. Thus, the electric potential difference between the β and α electrodes is $E = (\phi^\alpha - \phi^\beta)$. Recall that the salt bridge is a glass tube filled with an electrolyte that allows charge transfer between the cell electrolytes without disturbing the equilibrium state.

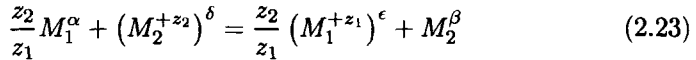
Apply the generalized expression given by eq. (2.19) to the galvanic cell shown in Figure 2.3a. Thus, the anodic and cathodic reactions and their respective energy change expressions are, respectively



$$\Delta G^\alpha = -z_1 F (\phi^\alpha - \phi^\epsilon) \quad (\text{Anode}) \quad (\text{a})$$

$$\Delta G^\beta = -z_2 F (\phi^\delta - \phi^\beta) \quad (\text{Cathode}) \quad (\text{b})$$

In order to balance the number of electrons in eqs. (2.21) and (2.22), multiply eq. (2.21), as well as eq. (a), by z_2/z_1 and add them up to get the redox reaction and its energy change as



$$\Delta G = \frac{z_2}{z_1} \Delta G^\alpha + \Delta G^\beta \quad (\text{a})$$

$$\Delta G = -z_2 F (\phi^\alpha - \phi^\beta) \quad (\text{b})$$

$$\Delta G = -z_2 F E \quad (2.24)$$

where $(z_1 e^-)^\alpha = (z_2 e^-)^\beta$, $(\mu^\beta)_e = (\mu^\alpha)_e$, $\phi^\epsilon = \phi^\delta$ and $E = (\phi^\alpha - \phi^\beta)$.

In general, the equilibrium and no-equilibrium energy change expressions are, respectively

$$\Delta G^\circ = -z F E^\circ \quad (2.25)$$

$$\Delta G = -z F E \quad (2.26)$$

Using the argument for deriving eq. (2.19), the standard Gibbs free energy change can be defined in a general form as

$$\Delta G = \sum \nu_i \mu_i = \left(\sum \nu_i \mu_i \right)_{\text{product}} - \left(\sum \nu_i \mu_i \right)_{\text{reactants}} \quad (2.27)$$

where ν_i = Number of ions or molecules in an reaction
 i = Specie involved in the reaction

Combining eqs. (2.26) and (2.27) yields the standard electric potential in terms of standard chemical potential

$$E = -\frac{\sum \nu_i \mu_i}{z F} \quad (2.28)$$

Table 2.5 illustrates standard chemical potentials for some metals, ions, and molecules. A more complete data can be found in Pourbaix work [18-19]. Applying eq. (2.28) to the redox reaction given eq. (2.23) yields

$$E = -\frac{1}{z_2 F} \left\{ \left[\frac{z_2}{z_1} (\mu_{M_1^{+z_1}})^\epsilon + (\mu_{M_2})^\beta \right] - \left[\frac{z_2}{z_1} (\mu_{M_1})^\alpha + (\mu_{M_2^{+z_2}})^\delta \right] \right\} \quad (2.28a)$$

Table 2.5 Standard chemical potentials [18].

Name	μ° (kJ/mol)	Name	μ° (kJ/mol)
Al	0	Cu	0
Al ₂ O ₃	-1576.41	CuO	-127.19
Al(OH) ₃	-1137.63	Cu(OH) ₂	-356.90
Al ⁺³	-481.16	CuSO ₄	-661.91
AlO ₂ ⁻	-839.77	Cu ⁺²	+64.98
Cr	0	Fe	0
Cr(OH) ₂	-587.85	Fe(OH) ₂	-483.54
Cr(OH) ₃	-900.82	Fe(OH) ₃	-694.54
Cr ⁺³	-215.48	FeSO ₄	-829.69
CrO ₂ ⁻	-835.93	Fe ⁺²	-84.94
H ₂ (g)	0	Fe ⁺³	-10.59
H ⁺	0	Zn	0
OH ⁻	-157.30	Zn(OH) ₂	-559.09
H ₂ O	-237.19	Zn ⁺²	-147.21

Example 2.2 Let's apply the above generalized procedure to the galvanic cell shown in Figure 2.4. Assume that the cell is in equilibrium and that the cell phases are $M_1^\alpha = Zn^\alpha$ with $z_1 = +2$, $\epsilon = ZnSO_4(aq)$, $M_2^\beta = Cu^\beta$ with $z_2 = +2$, and $\delta = CuSO_4(aq)$. Will the redox reaction occur?

Solution:

Using eqs. (2.23) and (2.24) along with $E^\circ = E_{Zn}^\circ + E_{Cu}^\circ = 0.763 \text{ V} + 0.337 \text{ V} = 1.10 \text{ V}$ (Figure 2.4) and $z_1 = z_2 = z = 2$ yields

$$\begin{aligned} Zn^\alpha + (Cu^{+2})^\delta &= (Zn^{+2})^\epsilon + Cu^\beta \\ \Delta G^\circ &= -zFE^\circ = (2)(96.50 \text{ kJ/mol V})(1.10 \text{ V}) \\ \Delta G^\circ &= -212.30 \text{ kJ/mol} \end{aligned}$$

Therefore, the redox reaction occurs spontaneously as written since $\Delta G^\circ < 0$.

Example 2.3 Let the anodic phases be $M_1^\alpha = Cr^\alpha$ with $z_1 = +3$ and $\epsilon = CrSO_4(aq)$, whereas the cathodic phases are $M_2^\beta = Cu^{+2}$ with $z_2 = +2$,

and $\delta = \text{CuSO}_4(\text{aq})$. a) Determine the redox reaction using eq. (2.23) and b) calculate the Gibbs free energy change. Will the redox reaction occur?

Solution:

a) From, eq. (2.23),

$$\begin{aligned}\frac{2}{3}\text{Cr}^\beta + (\text{Cu}^{+2})^\epsilon &= \frac{2}{3}(\text{Cr}^{+3})^\delta + \text{Cu}^\alpha \\ \text{Cr}^\beta + \frac{3}{2}(\text{Cu}^{+2})^\epsilon &= (\text{Cr}^{+3})^\delta + \frac{3}{2}\text{Cu}^\alpha \\ 2\text{Cr}^\beta + 3(\text{Cu}^{+2})^\epsilon &= 2(\text{Cr}^{+3})^\delta + 3\text{Cu}^\alpha\end{aligned}$$

b) According to Figure 2.3a, the cell potential is

$$E^\circ = E_{\text{Cr}/\text{Cr}^{+2}}^\circ + E_{\text{Cu}^{+2}/\text{Cu}}^\circ = 0.774 \text{ V} + 0.337 \text{ V} = 1.08 \text{ V}$$

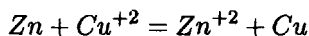
and from eq. (2.24), the standard free energy change is

$$\begin{aligned}\Delta G^\circ &= -z_2 F E^\circ = (2)(96.50 \text{ kJ/mol V})(1.08 \text{ V}) \\ \Delta G^\circ &= -208.44 \text{ kJ/mol}\end{aligned}$$

Therefore, the redox reaction occurs spontaneously as written since $\Delta G^\circ < 0$.

Example 2.4 Use the data given in Table 2.5 to determine the half-cells and the redox standard potentials for the galvanic cell shown in Figure 2.4. Compare the results with the data given in Table 2.2.

Solution:



From eq. (2.28) and Table 2.5,

$$\begin{aligned}E_{\text{Cu}^{+2}/\text{Cu}}^\circ &= -\frac{(\nu\mu^\circ)_{\text{Cu}} - (\nu\mu^\circ)_{\text{Cu}}^{+2}}{zF} \\ E_{\text{Cu}^{+2}/\text{Cu}}^\circ &= -\left[\frac{(1)(0) - (1)(+64.98 \text{ kJ/mol})}{(2)(96.50 \text{ kJ/mol} \cdot \text{V})}\right] = +0.337 \text{ V} \\ E_{\text{Zn}/\text{Zn}^{+2}}^\circ &= -\frac{(\nu\mu^\circ)_{\text{Zn}^{+2}} - (\nu\mu^\circ)_{\text{Zn}}}{zF} \\ E_{\text{Zn}/\text{Zn}^{+2}}^\circ &= -\left[\frac{(1)(-147.21 \text{ kJ/mol}) - (1)(0)}{(2)(96.50 \text{ kJ/mol} \cdot \text{V})}\right] = +0.763 \text{ V}\end{aligned}$$

These results are exactly the same as given in Table 2.2. Thus, eq. (2.7b) yields the standard cell potential

$$E^{\circ} = E_{\text{Cu}^{+2}/\text{Cu}}^{\circ} + E_{\text{Zn}/\text{Zn}^{+2}}^{\circ} = +1.10 \text{ V}$$

In addition, the activity a_j of a specie j for a redox reaction can be determined by considering the change in free energy

$$dG = -SdT + V_j dP \quad (2.29)$$

For an isothermal ($T = \text{constant}$) and isometric ($V_j = \text{constant}$) system, eq. (2.29) yields

$$\int_{\Delta G_j^{\circ}}^{\Delta G_j} dG = V_j \int_{P_o}^P dP \quad (a)$$

$$G_j - G_j^{\circ} = V_j (P - P_o) \quad (b)$$

or

$$\exp \left[\frac{\Delta G_j - \Delta G_j^{\circ}}{RT} \right] = \exp \left[\frac{V_j (P - P_o)}{RT} \right] \quad (c)$$

where $P = \text{Pressure}$

$P_o = \text{Standard pressure} = 1 \text{ atm,}$

$R = 8.314510 \text{ J mol}^{-1} \text{ K}^{-1}$ (Universal gas constant)

$T = \text{Absolute temperature } (^{\circ}\text{K})$

Thus, the activity $a_j = [j]$ is defined as

$$a_j = \exp \left[\frac{G_j - G_j^{\circ}}{RT} \right] = \exp \left[\frac{V_j (P - P_o)}{RT} \right] \quad (2.29a)$$

At standard conditions, $T = 25^{\circ}\text{C}$, $P = P_o = 1 \text{ atm}$ and $a_j = 1 \text{ mol/l}$. Table 2.6 illustrates some important definitions, which are needed to solve electrochemical problems.

Table 2.6 Some useful definitions for solving electrochemical problems.

$a_i = [j] = \gamma_j x_j$ (Henry's law) $C_j = a_j A_{w,j}$ $a_j = \text{Activity (mol/l)}$ $a_j = 1 \text{ mol/l}$ for solids and molecules $C_j = \text{Concentration (g/l)}$ $V_j = \text{Molar volume (l)}$ $P_j = \text{Pressure (MPa)}$	$a_j = P_j/P_o$ $\gamma_j = \text{Activity coefficient}$ $A_w = \text{Atomic weight (g/mol)}$ $X_j = \text{Mole fraction}$ $P_o = 1 \text{ atm} = 101 \text{ kPa}$
Dissociation of water: $H_2O = H^+ + OH^-$ $K_w = [H^+][OH^-] = 10^{-14}$ $pH = -\log[H^+]$ $pH = 14 + \log[OH^-]$	

Now, the equilibrium constant K for eq. (2.23) can be defined in terms of activities as follows:

$$K = \frac{\sum a_{\text{Product}}}{\sum a_{\text{Reactants}}} = \frac{\sum [\text{Product}]}{\sum [\text{Reactants}]} \quad (2.30a)$$

$$K = \frac{[(M_1^{+z_1})^\epsilon]^{z_2/z_1} \cdot [M_2^\beta]}{[M_1^\alpha]^{z_2/z_1} \cdot [(M_2^{+z_2})^\delta]} \quad (2.30b)$$

Using eqs. (2.29a) and (2.30a) for a redox reaction yields

$$K = \exp\left(\frac{\Delta G - \Delta G^\circ}{RT}\right) \quad (2.30c)$$

Solving eq. (2.30c) for the no-equilibrium energy change ΔG gives

$$\Delta G = \Delta G^\circ + RT \ln(K) \quad (2.31a)$$

At standard conditions, $\Delta G = 0$ and eq. (2.31a) becomes

$$\Delta G^\circ = -RT \ln(K) \quad (2.31b)$$

Thus, the equilibrium constant K can be determined from measurements of the electric potential (E°) or chemical potential (μ°).

Substituting eqs. (2.25) and (2.26) into (2.31a) yields the **Nernst Equation** for calculating the nonequilibrium electric potential (E) of an electrochemical cell. Hence,

$$E = E^\circ - \frac{RT}{zF} \ln(K) \quad (2.32)$$

The interpretation of the Nernst equation suggests that the current resulting from the change of oxidation state of the metals M_1 and M_2^{+z} is known

as **Faradaic current**, which is a measure of the rate of redox reaction. The term zF in eq. (2.32) stands for the number of coulombs needed for reacting 1 mol of an electroactive specie. Therefore, eq. (2.32) embodies the Faraday's law of electrolysis since the redox reaction involves electron transfer between phases having different electric potential. For instance, electrochemical equilibrium is achieved if current flow ceases in a reversible galvanic cell (Figure 2.3). Despite that the Nernst equation is derived assuming thermodynamic equilibrium of a reversible cell, K in eq. (2.32) is not exactly the same as the chemical equilibrium constant due to a current flow. The Nernst equation gives the open-circuit potential difference (emf) for a reversible galvanic cell and excludes liquid junction potentials [see eq. (2.7a)], which are always present, but small in magnitude. For example, the liquid junction potential difference for the cell in Figure 2.4 is $\phi_j = \phi_{CuSO_4(aq)} - \phi_{ZnSO_4(aq)} \approx 0$, but it is not completely eliminated after a salt bridge is connected.

From a macroscale, the Nernst equation is graphically depicted in Figure 2.6, which elucidates a simple calculus plot. The intercept is just the standard potential (E°) at $25^\circ C$ and the slope, $b = -RT/zF$, is the energy/charge ratio.

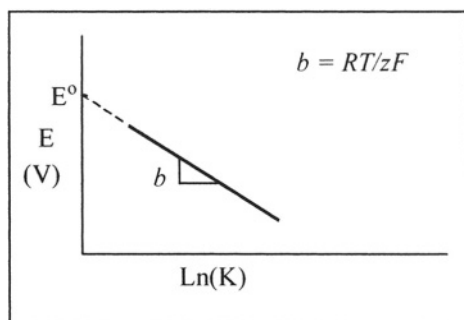


Figure 2.6 Nernst plot.

Example 2.5 Apply the preceding procedure to the galvanic cell shown in Figure 2.4 or to the cell diagram in Figure 2.5 at a temperature of $25^\circ C$ for determining a simplified expression for the equilibrium constant K and the Nernst cell potential E .

Solution:

From eq. (2.30b),

$$K = \frac{[Cu][Zn^{+2}]}{[Cu^{+2}][Zn]} = \frac{[Zn^{+2}]}{[Cu^{+2}]}$$

since $[Cu] = [Zn] = a$ (solids) = a (molecules) = 1 mol/liter. Thus, the cell potential defined by eq. (2.32) along with $z_1 = z_2 = z = 2$ and $E = E^\circ = 1.10 V$ (Figure 2.4) becomes

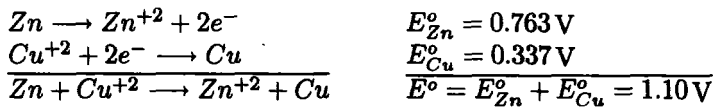
$$E = E^\circ - \frac{RT}{zF} \ln \frac{[Zn^{+2}]}{[Cu^{+2}]}$$

$$E = E^\circ - \frac{2.303RT}{zF} \log \frac{[Zn^{+2}]}{[Cu^{+2}]}$$

$$E = 1.10 \text{ V} - (0.0296 \text{ V}) \log \frac{[Zn^{+2}]}{[Cu^{+2}]}$$

Example 2.6 Derive the Nernst equation, eq. (2.32), using the anodic and cathodic reactions for Figure 2.4.

Solution:



Then,

$$E = E_{Zn} + E_{Cu} \tag{a}$$

$$E = \left[E_{Zn}^\circ - \frac{RT}{zF} \ln \frac{[Zn^{+2}]}{[Zn]} \right] + \left[E_{Cu}^\circ - \frac{RT}{zF} \ln \frac{[Cu]}{[Cu^{+2}]} \right] \tag{b}$$

$$E = (E_{Zn}^\circ + E_{Cu}^\circ) + \frac{RT}{zF} (\ln [Cu^{+2}] - \ln [Zn^{+2}]) \tag{c}$$

$$E = E^\circ + \frac{RT}{zF} \ln \frac{[Cu^{+2}]}{[Zn^{+2}]} \tag{d}$$

Example 2.7 The application of eq. (2.32) is suitable for determining the activity of Cu^{+2} ions when the $Zn - ZnSO_4(aq)$ anodic half-cell is mechanically kept replenished so that $a_{Zn^{+2}} = [Zn^{+2}] = 1 \text{ mol/l}$. If current ceases to flow in the galvanic cell shown in Figure 2-4, calculate the activity and the concentration of copper ions $[Cu^{+2}]$ in g/l at 25°C .

Solution:

From eq. (2.32) and Example 2.5,

$$E = E^\circ + \frac{RT}{zF} \ln \frac{[Cu^{+2}]}{[Zn^{+2}]} = 1.10 \text{ V} + (0.0296 \text{ V}) \log [Cu^{+2}] = 0$$

Solving for $a_{Cu^{+2}}$ yields

$$a_{Cu^{+2}} = [Cu^{+2}] = 6.20 \times 10^{-38} \text{ mol/l}$$

From Table 2.6, the concentration of Cu^{+2} is

$$\begin{aligned} C_{Cu^{+2}} &= (a_{Cu^{+2}})(A_w) = (6.20 \times 10^{-38} \text{ mol/l})(63.55 \text{ g/mol}) \\ C_{Cu^{+2}} &= 3.95 \times 10^{-36} \text{ g/l} \end{aligned}$$

which is very low.

An electrochemical cell can be used to measure the entropy change (ΔS) and the enthalpy change (ΔH) of a reversible reaction. This can be accomplished by measurements of the Nernst potential (E) as a function of temperature. At constant pressure, the free energy change (ΔG), ΔS and ΔH are defined by

$$\Delta G = -zFE \quad (2.26)$$

$$\Delta S = -\left(\frac{\partial \Delta G}{\partial T}\right)_p \quad (2.33)$$

$$\Delta H = \Delta G + T\Delta S \quad (2.34)$$

Differentiating eq. (2.26) with respect to the temperature T yields

$$\left(\frac{\partial \Delta G}{\partial T}\right)_p = -zF\left(\frac{\partial E}{\partial T}\right)_p \quad (2.35)$$

Then, the entropy change becomes

$$\Delta S = zF\left(\frac{\partial E}{\partial T}\right)_p \quad (2.35)$$

The reversible thermal energy (heat) is defined by

$$Q = -T\Delta S = -zFE - \Delta H \quad (2.36)$$

Substituting eqs. (2.33) and (2.26) into (2.34) yields

$$\Delta H = zF\left[T\left(\frac{\partial E}{\partial T}\right)_p - E\right] \quad (2.37)$$

The heat capacity at constant pressure (P) is defined by

$$C_p = T\left(\frac{\partial S}{\partial T}\right)_p \quad (2.38)$$

From eq. (2.35),

$$C_p = zFT \left(\frac{\partial^2 E}{\partial T^2} \right)_p \quad (2.39)$$

Using an electrochemical cell to measure the cell potential, eq. (2.32), as a function of temperature at constant pressure leads to curve fitting an empirical function, usually a polynomial. One particular polynomial is of the form [5]

$$E = a + b(T - T_o) + c(T - T_o)^2 + d(T - T_o)^3 \quad (2.40)$$

$$\frac{\partial E}{\partial T} = b + 2c(T - T_o) + 3d(T - T_o)^2 \quad (2.41)$$

$$\frac{\partial^2 E}{\partial T^2} = 2c + 6d(T - T_o) \quad (2.42)$$

where T_o = Reference temperature (K)
 a, b, c, d = Curve fitting coefficients

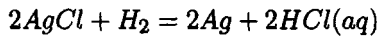
Now, the above thermodynamic state functions can be defined in terms of temperature. Thus,

$$\Delta G = -zF [a + b(T - T_o) + c(T - T_o)^2 + d(T - T_o)^3] \quad (2.43)$$

$$\Delta S = zF [b + 2c(T - T_o) + 3d(T - T_o)^2] \quad (2.44)$$

$$C_p = zFT \cdot [2c + 6d(T - T_o)] \quad (2.45)$$

Example 2.8 Levine [5] applied eq. (2.40) as continuous function in the closed temperature interval [0°C, 90°C] or [273.15 K, 363.15 K] for plating silver (Ag) from silver chloride (AgCl) according to the following redox (overall) reaction



The curve fitting coefficients at $P = 1$ atm and $T_o = 273.15$ K are

$$\begin{aligned} a &= 0.2366 \text{ V} & b &= -4.8564 \times 10^{-4} \text{ V / K} \\ c &= -3.4205 \times 10^{-6} \text{ V / K}^2 & d &= 5.8690 \times 10^{-9} \text{ V / K}^3 \end{aligned}$$

Calculate a) E° , ΔG° , ΔS° , ΔH° , Q , and C_p° at $T = 25^\circ\text{C}$ and b) use the Rolle's theorem to determine if the functions $E = f(T)$ and $\Delta G = (T)$ are differentiable in the open temperature interval [273.15 K, 363.15K].

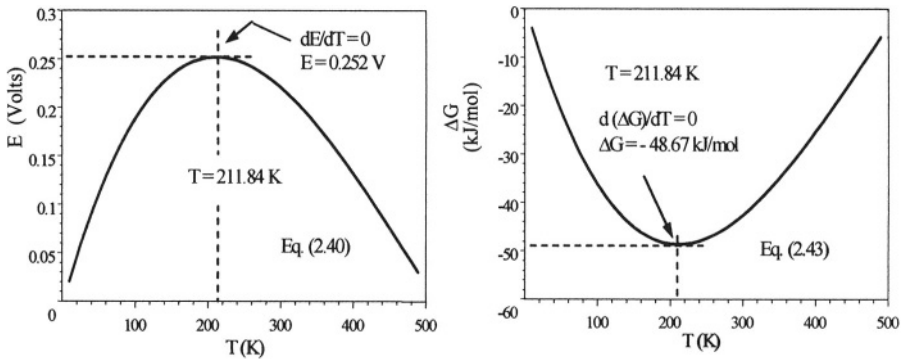
Solution:

a) If $T = 25\text{ }^{\circ}\text{C} = 298.15\text{ K}$, $(T - T_o) = 25\text{ K}$, $z = 2$ and $F = 96,500\text{ C/mol} = 96,500\text{ J/mol V}$, then the following results

$$\begin{aligned} \text{From eq. (2.40),} & \quad E^{\circ} = 0.222\text{ V} \\ \text{From eq. (2.43),} & \quad \Delta G^{\circ} = -42,926\text{ J/mol} < 0 \\ \text{From eq. (2.44),} & \quad \Delta S^{\circ} = -124.61\text{ J/mol}\cdot\text{K} < 0 \\ \text{From eq. (2.37),} & \quad \Delta H^{\circ} = -80,000\text{ J/mol} < 0 \\ \text{From eq. (2.86),} & \quad Q_{\text{irrev}} = -37,152.47\text{ J/mol} < 0 \\ \text{From eq. (2.45),} & \quad C_P^{\circ} = 343\text{ J/mol}\cdot\text{K} \end{aligned}$$

These results indicate that Ag can be plated at $T = 25\text{ }^{\circ}\text{C}$ since $E^{\circ} > 0$, $\Delta G^{\circ} < 0$, $\Delta S^{\circ} < 0$, $\Delta H^{\circ} < 0$, and $Q_{\text{rev.}} < 0$. Notice that the calculated value for $E^{\circ} = 0.222\text{ V}$ matches with the value given in Table 2.3.

b) The required plots, $E = f(T)$ and $\Delta G = f(T)$ are shown below as per eq. (2.40) and (2.43), respectively. According to Rolle's theorem the derivatives are $\partial E/\partial T = 0$ and $\partial \Delta G/\partial T = 0$ and, $E = 0.252\text{ V}$ and $\Delta G = -48.67\text{ kJ/mol}$ at $T = 211.84\text{ K}$. The condition $E(a) = E(b)$ and $\Delta G(c) = \Delta G(d)$ are met in the open interval $[273.15\text{ K}, 363.15\text{ K}]$. For instance, $E(100) = E(343.36) = 0.19\text{ V}$ and $\Delta G(100) = \Delta G(343.36) = -36.22\text{ kJ/mol}$. Therefore, both functions are continuous and differentiable.



Example 2.8b

2.5 STANDARD ELECTRIC POTENTIAL

In this section, a procedure to carry out measurements of the electromotive force (emf) is described. This emf is known as the standard potential (E°) already introduced in Table 2.2. The standard hydrogen electrode (SHE) is used as the reference electrode in conducting these measurements. In general, a reference electrode one selects to measure E° of a metal has to be reversible since classical

thermodynamics applies to all reversible processes. The SHE cell diagram for the potential E_M^o measurement is shown in Figure 2.7 and the schematic cell is shown in Figure 2.8.

Nonetheless, the *SHE* is a gas electrode that consists of a platinum foil suspended in sulfuric acid solution having H^+ unit activity ($a_{H^+} = 1 \text{ mol/l}$) at 1 atm and 25 °C. In order to maintain $a_{H^+} = 1 \text{ mol/l}$ purified hydrogen (H_2) gas is injected into the anodic half-cell in order to remove any dissolved oxygen. The platinum foil is an inert material in this solution and it allows the hydrogen molecules to oxidize, providing the electrons needed by the metal M^{+z} ions to be reduced on the cathode surface. The concentration of M^{+z} ions are also kept at unit activity. By convention, the standard hydrogen electrode potential is zero; $E_H^o = 0$.

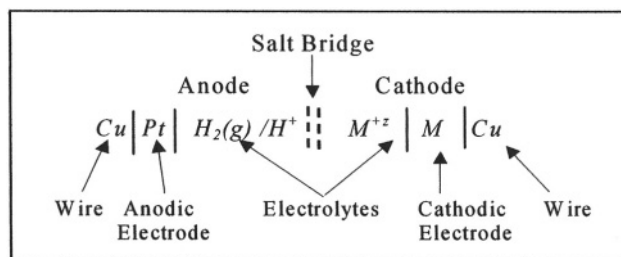


Figure 2.7 Metal/SHE standard cell diagram.

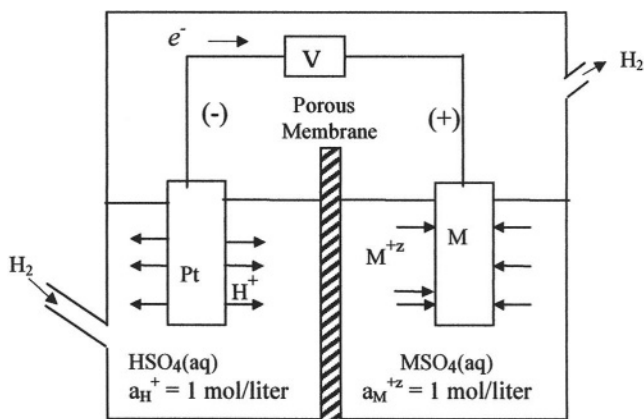


Figure 2.8 Schematic metal/SHE cell.

In addition, Table 2.7 lists some conversion of potential vs. SHE and half-cell reactions for secondary reference electrodes used for measuring corrosion potentials of metals and alloys in specific applications.

Table 2.7 Secondary reference electrode potentials [5].

Name	Half-cell reaction	$E(V)$ vs. SHE
Mercury Sulfate	$HgSO_4 + 2e^- = 2Hg + SO_4^{2-}$	0.615
Copper Sulfate	$CuSO_4 + 2e^- = 2Cu + SO_4^{2-}$	0.318
Saturated Colomel	$Hg_2Cl_2 + 2e^- = 2Hg + 2Cl^-$	0.241
Silver Chloride	$AgCl + e^- = Ag + Cl^-$	0.222
Standard Hydrogen	$2H^+ + 2e^- = H_2$	0.000

Example 2.9 If the potential of a metal M with respect to the saturated colomel electrode (SCE) is -0.541 V, convert this measured potential to SHE potential.

Solution:

If $E = -0.541$ V_{SCE}, then $E = E_{measured} + E_{Table 2.7}$

$$E = (-0.541 + 0.241) V_{SHE} = -0.30 V_{SHE}$$

As can be seen in Figure 2.8, the metal M is coupled with the platinum (Pt) electrode and the electric potential of M at the surface is measured against the SHE . Recall that this potential is the resultant of several interfacial potentials described by eq. (2.7a). The junction potentials of the Pt and M electrodes are small, equal, and apposite so that they cancel out. The liquid junction potential is also small and negligible. The cell potential is also known as the **interfacial cell potential**, which depends on the chemical potential of the species (ions) in solution at equilibrium and it is predicted by eq. (2.28). The electrons flow toward the cathodic electrode M , where the metal cations M^{+z} gain these electrons and enter the electrode lattice. This is a reduction process that strongly depends on the chemical potential of the M^{+z} cations.

The spontaneous redox reaction in Figure 2.8 is



and the standard cell potential using Table 2.5 is

$$E_{M^{+z}/M}^{\circ} = \frac{1}{zF} \left\{ \begin{array}{l} [(1)\mu_M^{\circ} + (2)\mu_{H^+}^{\circ}] \\ - [(1)\mu_M^{\circ} + (1)\mu_{H_2}^{\circ}] \end{array} \right\} \quad (\text{b})$$

$$E_{M^{+z}/M}^{\circ} = \frac{\mu_{M^{+z}}^{\circ}}{zF} \quad \text{since } \mu_M^{\circ} = \mu_{H^+}^{\circ} = \mu_{H_2}^{\circ} = 0 \quad (\text{c})$$

For instance, if $M^{+z} = Cu^{+2}$, then

$$E_{Cu^{+2}/Cu}^{\circ} = \frac{+64.98 \text{ kJ/mol}}{(2)(96.50 \text{ kJ/mol} \cdot V)} = +0.337 \text{ V} \quad (\text{e})$$

This is exactly the result given in Table 2.2.

2.6 POURBAIX DIAGRAMS

Potential-pH plots are known as Pourbaix diagrams since they were first made by Pourbaix in 1938. A compilation of these diagrams is available in the *Atlas of Electrochemical Equilibria in Aqueous Solutions* [9]. In practice, Pourbaix diagrams are suitable for studies of corrosion, electrowinning, electroplating, hydrometallurgy, electrolysis, electrical cells, and water treatment since they are electrochemical maps indicating the domain of stability of ions, oxides and hydroxides [9]. This map provides the oxidizing power in an electrochemical field measured as potential and the acidity and alkalinity of species measured as pH. Thus, any reaction involving hydroxyl (OH^-) ions should be written in terms of H^+ ion concentration, which in turn is converted into pH. The conversion factor is given in Table 2.6. Besides the possible reactions that may occur in an electrochemical system, a simplified Pourbaix diagram gives important areas for designing and analyzing electrochemical systems. These areas are known as corrosion, passivation, and immunity. However, a Pourbaix diagram does not include corrosion rate, which is essential in kinetic studies.

2.6.1 DIAGRAM FOR WATER AND OXYGEN

The construction of the E-pH Pourbaix diagram for water and oxygen is straightforward. Consider the hydrogen evolution reaction at standard conditions ($T = 25^\circ\text{C}$, $P_o = 1 \text{ atm}$)



for which the equilibrium constant is

$$K = \frac{a_{H_2}}{a_{H^+}} = \frac{[H_2]}{[H^+]^2} = \frac{P_{H_2}/P_o}{[H^+]^2} \quad (a)$$

$$\log [K] = \log (P_{H_2}) - 2 \log [H^+] \quad (b)$$

From eq. (2.32), the Nernst equation gives the hydrogen potential as

$$E_H = E_{H^+/H_2}^o - \frac{2.303RT}{zF} \log [K] \quad (c)$$

$$E_H = \frac{b}{2} [2pH - \log (P_{H_2})] \quad (2.47)$$

where $b = \text{slope} = -2.303RT/F = -0.0592\text{V}$, $Z = 2$, $E_{H^+/H_2}^o = 0$, and $pH = -\log [H^+]$.

Figure 2.9 shows the plot for eq. (2.47) labeled H_2 .

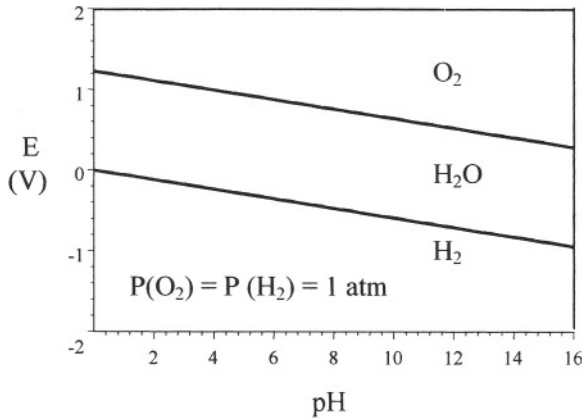


Figure 2.9 Pourbaix diagram form water and oxygen

For oxygen in an acid solution,



where

$$K = \frac{[H_2O]^2}{[O_2][H^+]^4} = \frac{1}{[P_{O_2}/P_o][H^+]^4} \tag{b}$$

$$\log [K] = -\log (P_{O_2}) - 4 \log [H^+] \tag{c}$$

$$\log [K] = -\log (P_{O_2}) + 4pH \tag{d}$$

Using eq. (2.32) along with $Z = 4$ yields

$$E_{O_2} = E_{O_2}^\circ - \frac{2.303RT}{zF} \log [K] \tag{e}$$

$$E_{O_2} = 1.229 \text{ V} + \frac{b}{4} [4pH - \log (P_{O_2})] \tag{2.48}$$

Plotting eq. (2.48) yields a straight line as shown in Figure 2.9. Notice that the slope $b = -0.0592 \text{ V}$ does not change if P_{H_2} and P_{O_2} change. Usually, these straight lines are superimposed on a metal $M - H_2O$ diagram for comparison purposes.

Analysis of Figure 2.9:

@ $P_{H_2} < 1 \text{ atm}$, water is unstable and decomposes to hydrogen gas H_2 . Thus, $H_2O + 2e^- = H_2 + 2(OH^-)$

@ $P_{H_2} = 1 \text{ atm}$, eq. (2.47) becomes $E_H = -0.0592 (pH)$ and establishes the limit of predominance between H_2O and H_2 , but H_2 predominates.

@ $P_{H_2} > 1 \text{ atm}$, water is stable

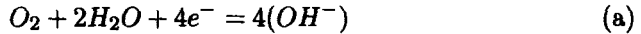
@ $P_{O_2} < 1 \text{ atm}$, water is stable

@ $P_{O_2} = 1 \text{ atm}$, eq. (2.48) becomes $E_{O_2} = 1.229 \text{ V} - 0.0592 \text{ V} (pH)$ and it establishes the limit of predominance between O_2 and H_2O , but O_2 predominates.

@ $P_{O_2} > 1 \text{ atm}$, O_2 predominates.

Example 2.10 Drive eq. (2.48) for an alkaline solution and compute the E_H and E_{O_2} for a $pH = 10$ under standard conditions.

Solution:



from which

$$K = \frac{[OH^-]^4}{[O_2]} = \frac{[OH^-]^4}{P_{O_2}/P_o} \quad (\text{b})$$

$$\log(K) = 4 \log [OH^-] - \log(P_{O_2}) \quad (\text{c})$$

From Table 2.6,

$$pH = 14 + \log [OH^-] \quad (\text{d})$$

Then, eq. (c) becomes

$$\log(K) = 4(pH - 14) - \log(P_{O_2}) \quad (\text{e})$$

From eq. (2.32) with $b = -2.303RT/F = -0.0592 \text{ V}$ and $Z = 4$, E_{O_2} becomes

$$E_{O_2} = E_{O_2}^\circ - \frac{2.303RT}{zF} \log(K) \quad (\text{f})$$

$$E_{O_2} = 0.401 \text{ V} + \frac{b}{4} [4(pH - 14) - \log(P_{O_2})] \quad (\text{g})$$

$$E_{O_2} = 1.229 \text{ V} + \frac{b}{4} [4pH - \log(P_{O_2})] \quad (\text{2.48})$$

It can be concluded that eq. (2.48) gives the same result if either acid or alkaline solution is selected.

2.6.2 POURBAIX DIAGRAM FOR A METAL M

Below is a brief description on how to construct a Pourbaix diagram for a metal $M - H_2O$ electrochemical system. Figure 2.10 shows a schematic and yet, simple $M - H_2O$ Pourbaix diagram, which includes the water and oxygen lines for comparison purposes. The construction of the diagram consists of determining the potential E for lines 1 and 3 using the Nernst equation, and the pH for lines 2 and 4 using known equilibrium constant K . The range of metal ion concentration can be $10^{-6} \text{ mol/l} \leq a(M^{+z}) \leq 1 \text{ mol/l}$, but $a(M^{+z}) = 10^{-6} \text{ mol/l}$ is chosen hereafter in order to simplify the procedure for constructing the diagram. Otherwise, several vertical and incline lines would be generated. If $a(M^{+z}) = 1 \text{ mol/l}$, the electrochemical corrosion process is unrealistic [5]. The procedure is as follows

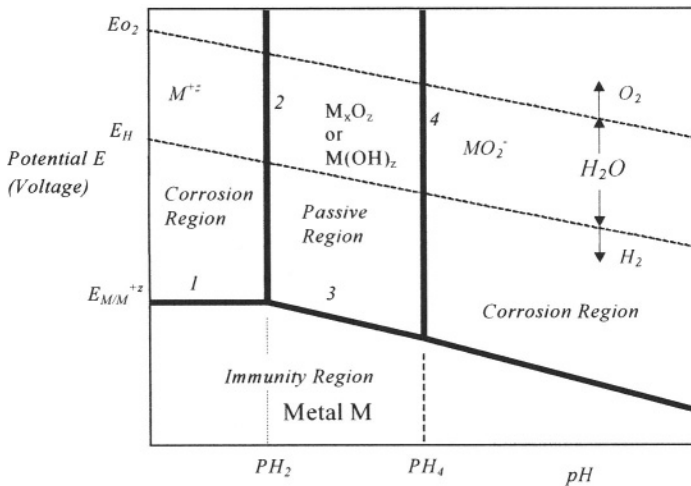


Figure 2.10 Schematic Pourbaix diagram for a metal M, water and oxygen.

1) Horizontal Line 1:



$$K = \frac{[M^{+z}]}{[M]} = [M^{+z}] \tag{b}$$

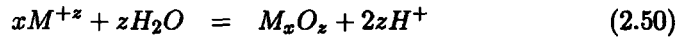
This reaction involves electron transfer only. Thus, the Nernst equation, eq. (2.32), with $[M^{+z}] = 10^{-6} \text{ mol/l}$ and $T = 298 \text{ K}$ becomes

$$E_1 = E_{M/M^{+z}}^{\circ} - \frac{2.303RT}{zF} \log [M^{+z}] \tag{c}$$

$$E_1 = E_{M/M^{+z}}^{\circ} - \frac{0.3552}{z} \tag{2.49}$$

The value for the standard potential $E_{M/M^{+z}}^{\circ}$ is given in Table 2.2, provided that the metal M is known. Thus, eq. (2.49) plots a horizontal line shown in Figure 2.10 as line 1.

2) Vertical Line 2:



$$K = \frac{[H^+]^{2z}}{[M^{+z}]^x} \quad (a)$$

This reaction involves a fixed hydrogen concentration only, the equilibrium constant K for this reaction must be known so that

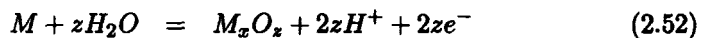
$$\log(K) = 2z \log[H^+] - x \log[M^{+z}] \quad (b)$$

$$\log(K) = -2z(pH_2) - 6x \quad (c)$$

$$pH_2 = -\frac{1}{2z} [\log(K) + 6x] \quad (2.51)$$

Therefore, a straight line is drawn starting at $E_1 - pH_2$ point. This is shown in Figure 2.10 as line 2. It should be mentioned that the metal oxide M_xO_z can be replaced by a metal hydroxide $M(OH)_2$ or $M(OH)_3$ depending on the chosen metal. Thus, eq. (2.50) should be balanced accordingly. Hence,

3) Incline Line 3:

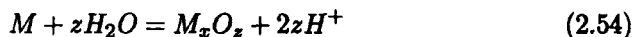


$$K = [H^+]^{2z} \quad (a)$$

Notice that this reaction involves both hydrogen and electron transfer. Then, the Nernst equation becomes

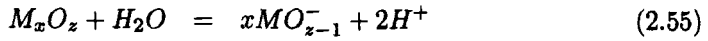
$$E_3 = E_{M/M_xO_z}^{\circ} - 0.0592(pH) \quad (2.53)$$

The standard potential $E_{M/M_xO_z}^{\circ}$ must be known. In Figure 2.10, Line 2 and line 3 intersect at a pH value given by eq. (2.51). Above this pH, a passivation process takes place on the metal surface according to the following reaction



where M_xO_z is a passive film compound. This reaction is reversed below the pH given by eq. (2.52).

4) Vertical Line 4:



$$K = a(H^+)^2 a(MO_{z-1}^-)^x \quad (a)$$

Letting $[MO_{z-1}^-] = 10^{-6} \text{ mol/l}$ in eq. (a) yields

$$\log(K) = 2 \log a(H^+) + x \log a(MO_{z-1}^-) \quad (b)$$

$$\log(K) = -2(pH_4) - 6x \quad (c)$$

Solving for pH gives

$$pH_4 = -0.5[6x + \log(K)] \quad (2.56)$$

Subsequently, a vertical line 4 is drawn at this pH_4 value.

2.7 ELECTRICAL DOUBLE LAYER

When a metal M is immersed in a suitable electrolyte, initially its atoms oxidize at a relatively high rate, and subsequently, the oxidation (dissolution) process gradually ceases and eventually stops due to a negative charge build-up on the metal surface. Thus, the dynamic equilibrium is attained, provided that no other complex electrochemical reactions take place. In this process, metal atoms are removed from their lattice sites to ionize as cations (M^{+x}) into the electrolyte, forming a negatively charge metal surface. If polar water (H_2O) molecules and hydrogen cations (H^+) are in the electrolyte, they are attracted by the negatively charged metal surface to form an ionic structure (layer), which prevent other ions from the bulk solution to be part of it. This structure is a complex ionic arrangement in an electric field and has a limited thickness. Eventually, metal dissolution ceases if there is no external current flow, but it proceeds until the ionic structure is dense enough to protect and prevent the metal from reacting any further until equilibrium is reached. With respect to the the metal-layer-bulk within which there must exists an electric potential decay. The ionic structure is known in the literature as the electrical double-layer (*EDL*). This *EDL* seems to limit the continuous electrochemical reactions at the metal surface due to the lack of charge transfer.

One finds in the literature [10-12] different models for explaining the interfacial structure of the electrical double layer. This layer is referred to as the Helmholtz layer which behaves like a charged capacitor. Figure 2.11 shows an schematic electrical double-layer model.

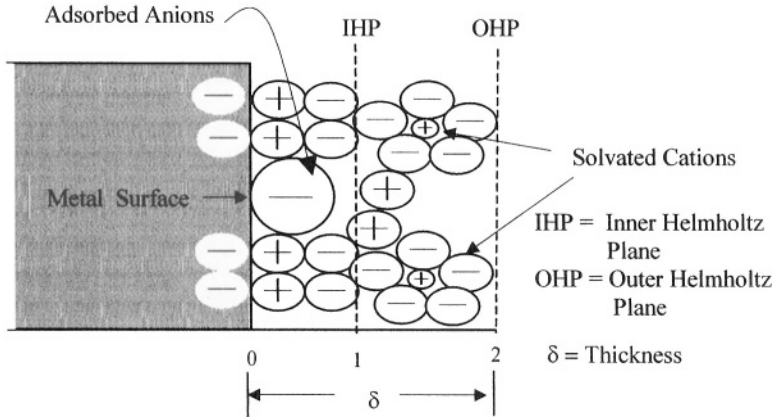


Figure 2.11 Schematic electrical double layer.

This model indicates that some negatively charge ions are adsorbed on the metal electrode surface and polar water covers the rest of this surface, forming a protective layer. The positively charged hydrogen is in contact with the negatively charge metal surface. Thus, one can conclude that

1) The **Inner Helmholtz Plane (IHP)** is an ionic layer that consists of adsorbed dipole H_2O molecules. The majority of the anions do not penetrate this layer, some do as indicated in Figure 2.11. The inner potential on the boundary of this ionic plane is ϕ_1 .

2) The **Outer Helmholtz Plane (OHP)** consists of a plane of adsorbed ions due to electrostatic forces in contact with a diffuse ionic layer at a inner potential ϕ_2 .

3) The **Diffuse Layer (DL)** is a thick layer located in a region of diffusely ions in contact with the OHP and the bulk of solution at a potential range of $\phi_1 < \phi_{Diffuse} < \phi_3$. Thus, the diffuse layer/bulk boundary is at $\phi_3 = \phi_b$.

The distribution of the inner electric potential ϕ in solution is shown in Figure 2.12 and defined by [4]

$$\phi(x) = \phi_o \exp(-\lambda x) \quad (2.57)$$

where $\lambda = \text{constant}$ and $x = \text{distance from the metal surface}$.

In fact, this mathematical model represents an electric potential decay since

$$\phi(x) = \phi_o \longrightarrow \phi_{\max} \text{ when } x \longrightarrow 0 \quad (\text{a})$$

$$\phi(x) = \phi_b \longrightarrow 0 \text{ when } x \longrightarrow \infty \quad (\text{b})$$

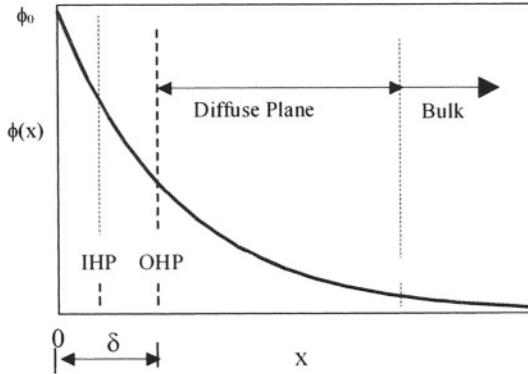


Figure 2.12 Schematic inner electrical potential distribution.

The concentration of the oxidized species, $C(x)$, may be predicted using the Nernst equation, eq. (2.32). In this case, the potential E is replaced by ϕ . Thus, for a species j the interfacial potential within the electrolyte is defined by

$$\phi(x) = -\frac{RT}{zF} \ln [K] \quad (2.58)$$

$$\phi(x) = -\frac{RT}{zF} \ln \left[\frac{C(x)}{C_o} \right] \quad (2.59)$$

where $K = C(x)/C_o$

K = Rate constant

$C(x)$ = Concentration (activity) at $x > 0$

C_o = Concentration (activity) at $x = 0$

Solving eq. (2.59) for $C(x)$ yields the concentration decay function, which is dependent on both interfacial potential $\phi(x)$ and temperature T

$$C(x) = C_o \exp \left[-\frac{zF\phi(x)}{RT} \right] \quad (2.60)$$

For small values of $\phi(x)$, eq. (2.60) can be linearized by expanding the exponential function using Taylor's series. Hence,

$$C(x) = C_o \left[1 - \frac{zF\phi(x)}{RT} \right] \quad (2.60a)$$

The resultant expression implies that there is a linear relationship between $C(x)$ and $\phi(x)$.

2.8 DEGREE OF DISSOCIATION

Since electrolytes transport charge in the solid, aqueous or vapor state, it is worthwhile mentioning that the degree of dissociation of a compound added to a solvent can be estimated by the degree of dissociation parameter α_1 . Electrolytes hereafter are treated as aqueous electrolytes (solutions) unless otherwise stated. In general, if $\alpha_1 < 1$, the solution is a weak electrolyte and if $\alpha_1 \geq 1$ the solution is a strong electrolyte since the compound being added to a solvent completely dissociates into ionic components, such as cations and anions.

Consider the following reaction for a salt M_xO_y dissolved in a solvent



where M is a metal and O is an oxide or hydroxide. The ionic components are metal M^{+z} cations and oxide or hydroxide O^{-z} anions.

The standard free energy change for chemical equilibrium and the equilibrium constant are, respectively

$$\Delta G^\circ = -RT \ln(K) \quad (2.62)$$

$$K = \frac{[M^{+z}]^x [O^{-z}]^y}{[M_xO_y]} \quad (2.63)$$

The activity or molar concentration a_i , the degree of dissociation α_1 , and the total molar activity $[C_T]$ are defined as follows [3]

$$[M^{+z}] = x\alpha_1 [C_T] \quad (2.64a)$$

$$[O^{-z}] = y\alpha_1 [C_T] \quad (2.64b)$$

$$[M_xO_y] = (1 - \alpha_1) [C_T] \quad (2.64c)$$

Substituting eq. (2.64) into (2.63) yields

$$K = (x^x y^y) \left[\frac{\alpha_1^{x+y} [C_T]^{x+y-1}}{1 - \alpha_1} \right] \quad (2.65)$$

If $\alpha_1 \ll 1$, then eq. (2.65) becomes

$$K = (x^x y^y) \left[\alpha_1^{x+y} [C_T]^{x+y-1} \right] \quad (2.66)$$

from which

$$\alpha_1 = (K x^{-x} y^{-y})^{1/(x+y)} [C_T]^{-1+1/(x+y)} \quad (2.67)$$

This expression indicates that the degree of dissociation increases with increasing concentration; that is, $\alpha_1 \uparrow$ as $[C_T] \uparrow$. Further, if $\alpha_1 \ll 1$, a hydroxyl ion activity $[OH^-]$ is related to a hydrogen ion activity $[H^+]$ through the dissociation of water. Hence, the dissociation constant for water is

$$K_w = \frac{[H^+][OH^-]}{[H_2O]} = [H^+][OH^-] = 10^{-14} \quad (2.68)$$

For a neutral solution, $[H^+] = [OH^-] = 10^{-7}$. Also, the acidity or alkalinity of a solution is defined by the pH

$$pH = -\log [H^+] \quad (2.69)$$

Hence,

$$[H^+] = 10^{-pH} \quad (2.70)$$

$$[OH^-] = K_w / [H^+] = 10^{-14} / 10^{pH} \quad (2.71)$$

This hydroxyl concentration may be used in the dissociation of a metal hydroxide compound, such as $Ag(OH)$. An example can make this procedure very clear.

Example 2.11 Determine the amount of silver hydroxide $Ag(OH)$ needed to make one liter of silver-containing electrolyte having a pH = 11.6 at 25°C and 1 atm. The dissociation constant of $Ag(OH)$ is 1.10×10^{-4} . The atomic weight of silver is 107.87 g/mol and the molecular weight of $[Ag(OH)]$ is 124.87 g/mol.

Solution:

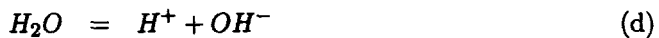
In this problem, the silver hydroxide is assumed to dissolve to an extent in pure water. The reactions of interest are



$$K = \frac{[Ag^+][OH^-]}{[Ag(OH)]} \quad (b)$$

$$K = [Ag^+][OH^-] = 1.10 \times 10^{-4} \quad (c)$$

and



$$K_w = \frac{[H^+][OH^-]}{[H_2O]} \quad (e)$$

$$K_w = [H^+][OH^-] = 10^{-14} \quad (f)$$

From eq. (2.70) and 2.71),

$$\begin{aligned}
 [H^+] &= 10^{-pH} = 10^{-11.6} = 2.51 \times 10^{-12} \text{ mol/l} \\
 [OH^-] &= K_w/a(H^+) = 10^{-14}/10^{-11.6} = 3.98 \times 10^{-3} \text{ mol/l} \\
 C_{H^+} &= (2.51 \times 10^{-12} \text{ mol/l}) (A_w)_{H^+} = (2.51 \times 10^{-12} \text{ mol/l}) (1 \text{ g/mol}) \\
 C_{H^+} &= 2.51 \times 10^{-12} \text{ g/l} \\
 C_{OH^-} &= (3.98 \times 10^{-3} \text{ mol/l}) (A_w)_{OH^-} = (3.98 \times 10^{-3} \text{ mol/l}) (17 \text{ g/mol}) \\
 C_{OH^-} &= 0.068 \text{ g/l}
 \end{aligned}$$

From eq. (2.66) with $x = y = 1$, the total silver concentration in solution is predicted by

$$[C_T] = K/\alpha_1^2 \quad (\text{g})$$

Solving for $[Ag^+]$ in eq. (c) yields

$$[Ag^+] = \frac{K}{[OH^-]} = \frac{K[H^+]}{K_w} = 2.76 \times 10^{-2} \text{ mol/l} \quad (\text{h})$$

From eq. (2.64b),

$$[OH^-] = \alpha_1 [C_T] \quad (\text{i})$$

$$\alpha_1 = \frac{[OH^-]}{[C_T]} \quad (\text{j})$$

Substituting eq. (j) into (g) gives

$$\begin{aligned}
 [C_T] &= \frac{[OH^-]^2}{K} = \frac{(3.98 \times 10^{-3} \text{ mol/l})^2}{1.10 \times 10^{-4}} = 0.144 \text{ mol/l} \\
 C_{Ag(OH)} &= [C_T] A_w = (0.144 \text{ mol/l}) (124.87 \text{ g/mol}) \\
 C_{Ag(OH)} &= 17.98 \text{ g/l}
 \end{aligned}$$

From eq. (j),

$$\alpha_1 = \frac{[OH^-]}{[C_T]} = \frac{3.98 \times 10^{-3} \text{ mol/l}}{0.144 \text{ mol/l}} = 0.03$$

which implies that the solution is a weak electrolyte since $\alpha_1 < 1$. The total weight of $Ag(OH)$ added to water solvent is

$$W = VC = (1 \text{ liter}) (17.98 \text{ g/liter}) = 17.98 \text{ grams}$$

Therefore, add 17.98 grams of solid $Ag(OH)$ to one liter of pure water, stir until a homogeneous electrolyte is attained. This electrolyte can be used for silver plating purposes.

2.9 SUMMARY

It has been shown that the potential difference of an electrochemical galvanic cell is $E = \phi^\beta - \phi^\alpha$, where both ϕ^β and ϕ^α are the inner surface potentials and the sum of the junction potentials was assumed to be very small. Thus, the repulsive forces of like charged particles (ions) in an electrical polypole system allow diffusion of these particles to the phase surfaces. This is a significant electrochemical process to convert chemical energy into electrical energy as in the case of a battery flash light. In principle, electrical energy can be converted into chemical energy as in the case of electrolysis of copper ion reduction where the cell potential is $E > |\phi^\beta - \phi^\alpha|$.

In addition, $E = \phi^\beta - \phi^\alpha$ can be predicted by the Nernst equation, eq. (2.32). If the standard hydrogen electrode (SHE) is coupled with a pure metal electrode, the standard metal electrode potential is $E_m = \phi_M^\beta - \phi_H^\alpha = \phi_M^\beta$ since $\phi_H^\alpha = 0$. Moreover, the inner surface potential is $\phi(x) = f(x)$, where x is the distance from the metal electrode surface. It is assumed that $\phi(x)$ decays linearly through the Helmholtz double layer ($0 \leq x \leq \delta$) and exponentially in the diffuse layer and bulk ($\delta \leq x \leq \infty$).

An electrochemical cell can be used to determine thermodynamic energy changes like the change in entropy (ΔS), change in enthalpy (ΔH), change in Gibbs free energy (ΔG), the heat capacity at constant pressure (C_p) and the reversible thermal energy (heat) Q .

Also, Pourbaix diagrams being electrochemical maps of ionic species can be constructed using electrochemical cells containing water as the solvent at a constant temperature. These diagrams are potential-pH plots that show areas known as corrosion, passivation, and immunity. In spite of the usefulness of these diagrams for characterizing electrochemical systems, kinetics parameters, such as corrosion rate, cannot be predicted from such diagrams.

Electrolytes can be classified as strong or weak solutions through the degree of dissociation parameter α_1 . Thus, if $\alpha_1 < 1$, then the electrolyte is weak; otherwise, strong if $\alpha_1 \geq 1$.

2.10 PROBLEMS/QUESTIONS

2.1 Define the galvanic electrode potential for the cell shown in Figure 2.4 using the interfacial potentials involved in the electrochemical process.

2.2 Describe what happens in the galvanic cell shown in Figure 2.4 when electrons leave the Cu terminal at the Cu-Zn interface.

2.3 Explain why an electrode potential difference occurs in Figure 2.4.

2.4 Why are Cu^{+2} cations electroplated on the Cu electrode surface in Figure 2.4?

2.5 Calculate the standard potential for the formation of ferric hydroxide $Fe(OH)_3$ (brown rust). [$E^\circ = 1.172 \text{ V}$].

2.6 Consider the following electrochemical cell $|Cu^{+2}, Cu| |H_2, H^+| Pt$ to calculate the maximum activity of copper ions Cu^{+2} in solution due to oxidation of a copper strip immersed in sulfuric acid H_2SO_4 at 25°C , 101 kPa and $pH = 2$. [Solution: $a_{Cu^{+2}} = [Cu^{+2}] = 4.04 \times 10^{-16} \text{ mol/l}$].

2.7 Consider a galvanic cell $|Zn| 0.10 \text{ M ZnSO}_4 || 0.10 \text{ M NiSO}_4 | Ni |$. Calculate the cell potential using the Nernst equation at 25°C . [Solution; $E^\circ = 0.513 \text{ V}$].

2.8 The dissociation of silver hydroxide, $AgOH$, is 1.10×10^{-4} at 25°C in an aqueous solution. a) Derive an expression for the degree of dissociation as a function of total activity $[C_T]$ and plot the resultant expression for $0 < [C_T] < 0.50 \text{ mol/l}$, b) calculate the degree of dissociation constant α_1 when the molar concentration is $[C_T] = 0.144 \text{ mol/l}$, and c) determine the Gibbs free energy change ΔG° . [Solutions: b) $\alpha_1 = 0.028$, $\Delta G^\circ \approx -22.58 \text{ kJ/mol}$].

2.9 Calculate a) the concentration of $AgOH$, Ag^+ and OH^- at 25°C and b) the pH if $[C_T] = 0.144 \text{ mol/l}$ and $\alpha_1 = 0.028$. [Solutions: a) $C_{OH^-} = 6.85 \times 10^{-2} \text{ g/l}$, $C_{Ag^+} = 0.43 \text{ g/l}$, $C_{AgOH} = 17.48 \text{ g/l}$ and b) $pH = 11.61$].

2.10 If an electrochemical copper reduction reaction at 25°C and 101 kPa occurs at an infinitely low current density calculate a) the Gibbs free energy change ΔG° as the driving force, b) the equilibrium constant K and c) the copper ion concentration $[Cu^{+2}]$ in g/l . [Solutions: a) $\Delta G^\circ \approx -65 \text{ kJ/mol}$, b) $K = 2.52 \times 10^{11}$, c) $C_{Cu^{+2}} = 2.52 \times 10^{-10} \text{ g/l}$].

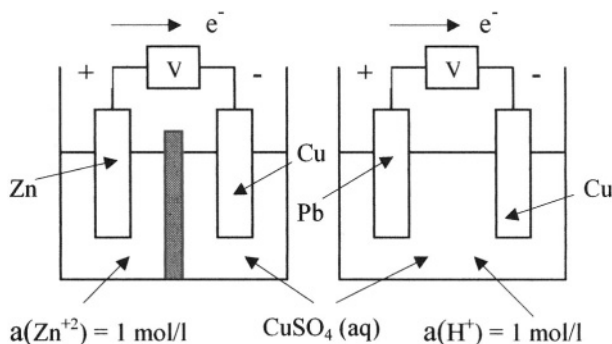
2.11 Use the electrochemical cell $|Cd| 0.05 \text{ M Cd}^{+2} || 0.25 \text{ M Cu}^{+2} | Cu |$ to calculate a) the temperature for an electric potential of 0.762 V_{SHE} , and b) ΔS , ΔG , ΔH , and Q . [Solutions: a) $T \approx 44^\circ\text{C}$ and b) $\Delta S = 13.38 \text{ J/(mol K)}$, $\Delta G \approx -147 \text{ kJ/mol}$, $\Delta H \approx -143 \text{ kJ/mol}$, $Q \approx -4.24 \text{ kJ/mol}$].

2.12 Pure copper and pure cobalt electrodes are separately immersed in solutions of their respective divalent ions, making up a galvanic cell that yields a cell potential of $0.65 V_{SHE}$. Calculate a) the cobalt activity if the activity of copper ions is 0.85 mol/l at 25°C and b) the change in entropy ΔS° and Gibbs free energy ΔG° . [Solutions: a) $[Co^{+2}] = 0.053 \text{ mol/l}$ and b) $\Delta S^\circ \simeq 23 \text{ J/mol K}$ and $\Delta G^\circ = -125.45 \text{ kJ/mol}$].

2.13 Show that the activities are $[M_1^{+2}] = [M_2^{+2}]$ in a galvanic cell, provided that the potentials is $E = E^\circ$.

2.14 Show that $\Delta S = -R \ln K$ in a galvanic cell at constant pressure.

2.15 Derive an expression for $\ln [Cu^{+2}] = f(T)$ for the given cells below. Assume that the current ceases to flow and that the cells are not replenished with fresh solutions. Plot the expressions for a temperature range of $0^\circ\text{C} \leq T \leq 60^\circ\text{C}$, and draw some suitable conclusions to explain the electrochemical behavior based on the resultant trend. [Solutions: a) $\ln [Cu^{+2}] = -2.55 \times 10^4/T$ and b) $\ln [Cu^{+2}] = -7.89 \times 10^3/T$].



2.16 Explain why care must be exercised in using the galvanic series illustrated in Table 2.2?

2.17 If zinc and copper rods are placed in salt water, a direct chemical reaction may slightly corrode zinc. Why?

2.18 Is the cell potential a surface potential? If so, why?

2.19 Prove eq. (2.59).

2.20 Assume a solution containing a concentrations of $[Cu^{+2}] \ll 1 \text{ mol/l}$ and $[H^+] = 1 \text{ mol/l}$ at 25°C . Determine the concentration of copper ions for hydrogen evolution to occur. [Solution: $[Cu^{+2}] \leq 3.97 \times 10^{-12} \text{ mol/l}$].

2.11 REFERENCES

- [1] I.N. Levine, “*Physical Chemistry*,” McGraw-Hill Book Company, New York, (1978) 350-396.
- [2] D.L. Reger, S.R. Goode, and E.E. Mercer, “*Chemistry: Principles & Practice*,” Second Ed., Saunders College Publishing, New York, (1997) 795.
- [3] R.T. Dehoff, “*Thermodynamics in Materials Science*,” McGraw-Hill Inc., New York, (1993) 458-484.
- [4] J.W. Evans and L.C. De Jonghe, “*The Production of Inorganic Materials*” Macmillan Publishing Company, New York, (1991) 1497-149.
- [5] D.A. Jones, “*Principles and Prevention of Corrosion*,” Macmillan Publishing Company, New York, (1992) 39-70.
- [6] G.F. Carter, “*Principles of Physical and Chemical Metallurgy*” American Society For Metals. Metals Park, Ohio 44073, (1979) 316-317.
- [7] A.L. Rouff, “*Materials Science*,” Prentice-Hall Inc., New Jersey, (1973) 697.
- [8] D.L. Piron, “*Potential versus pH (Pourbaix) Diagrams*,” in Corrosion Vol. 13, American Society For Metals, ASM Handbook, ninth edition, Metals Park, Ohio 44073, (1987).
- [9] M. Pourbaix, “*Atlas of Electrochemical Equilibria in Aqueous Solutions*,” NACE, Houston, Texas, (1974).
- [10] J. O’M Bockris, et al., Proc. Roy. Soc. A274 (1963) 55.
- [11] C.A. Barlow, Jr., “*The Electrical Double Layer*,” in Physical Chemistry: An Advanced Treatise, Vol. IXA/Electrochemistry, Edited by Henry Eyring, Academic Press, New York, (1970).
- [12] T. Erdey-Gruz, “*Kinetics of Electrode Processes*,” Wiley-Interscience, John Wiley & Sons Inc., New York, (1972) 442.
- [13] A. Corrias et al., Chem. Mater., 2 (1990) 363.
- [14] J. Yiping et al., J. Appl. Phys., 69 (1991).
- [15] G.N. Glavee et al., Inorg. Chem., 32 (1993) 474.
- [16] K. J. Klabunde and C. Mohs, in “*Chemistry of advanced Materials: an overview*,” Ed. by L.V. Interrante and M.J. Hampden-Smith, Wiley-VCH, New York, (1998) 271-316.
- [17] P.T. Taney, Jean-Remi Butruille, and T.J. Pinnvaia, in “*Chemistry of advanced Materials: an overview*,” Ed. by L.V. Interrante and M.J. Hampden-Smith, Wiley-VCH, New York, (1998) 329-379.
- [18] M. Pourbaix, “*Enthalpies Libres de Formations Standards*,” Cebelcor Report Technique, 87 (1960).
- [19] “*Corrosion*” Vol. 2, Corrosion Control, Edited by L.L. Sheir, R.A. Jarman, and G.T. Burstein, Butterworth-Heinemann, Boston, (1994) 21:12-21:24.
- [20] O.C. Mudd, Corrosion, Vol. 1, 1 (1945) 192-201.

Chapter 3

KINETICS OF ACTIVATION POLARIZATION

3.1 INTRODUCTION

Electrochemical reaction kinetics is essential in determining the rate of corrosion of a metal M exposed to a corrosive medium (electrolyte). On the other hand, thermodynamics predicts the possibility of corrosion, but it does not provide information on how slow or fast corrosion occurs. The kinetics of a reaction on a electrode surface depends on the electrode potential. Thus, a reaction rate strongly depends on the rate of electron flow to or from a metal-electrolyte interface. If the electrochemical system (electrode and electrolyte) is at equilibrium, then the net rate of reaction is zero. In comparison, reaction rates are governed by chemical kinetics, while corrosion rates are primarily governed by electrochemical kinetics.

Electrochemical kinetics of a corroding metal can be characterized by determining at least three polarization parameters, such as corrosion current density (i_{corr}), corrosion potential (E_{corr}), and Tafel slopes (β_a and/or β_c). Then the corrosion behavior can be disclosed by a polarization curve (E vs. $\log i$). Evaluation of these parameters leads to the determination of the polarization resistance (R_p) and the corrosion rate as i_{corr} , which is often converted into **Faradaic corrosion rate** C_R having units of mm/y . This is an accelerated electrochemical process for determining C_R that has an advantage over the C_R determined by weight loss since the latter is a time consuming process, which may lead to unsatisfactory results when C_R changes with time [13]. Instead, a polarization curve is readily obtained and it can offer a practical method for characterizing electrochemical kinetics parameters.

3.2 ENERGY DISTRIBUTION

For a polarized electrode under steady-state current flow, the generalized reaction given by eq. (1.2) can be used to derive the Butler-Volmer equation, which involves energy barriers known as activation energies. Only the activation energy change is used for the forward (ΔG_f) (reduction) and reverse (ΔG_r) (oxidation) reactions. For example, the hydrogen reaction, $2H^+ + 2e^- = H_2$ at equilibrium requires that the rate of discharge of H^+ ions in the forward direction (reduction) must be exactly equal to the rate of ionization of H_2 molecule in the reverse direction (oxidation). However, if deviation from the equilibrium state occurs, an overpotential develops and consequently, the electrochemical cell polarizes and the activation energies become dependent on the exchange current density (i_o). These energies are depicted in Figure 3.1 in which the **activation state** is at the maximum point (saddle point). This figure represents the Boltzmann or Maxwell-Boltzmann distribution law for the energy distribution of the reacting species (ions) [4,7]. This schematic energy distribution is for reversible electrodes. If these are polarized by an overpotential under steady-state conditions, the rate of reactions are not equal, $R_f \neq R_r$.

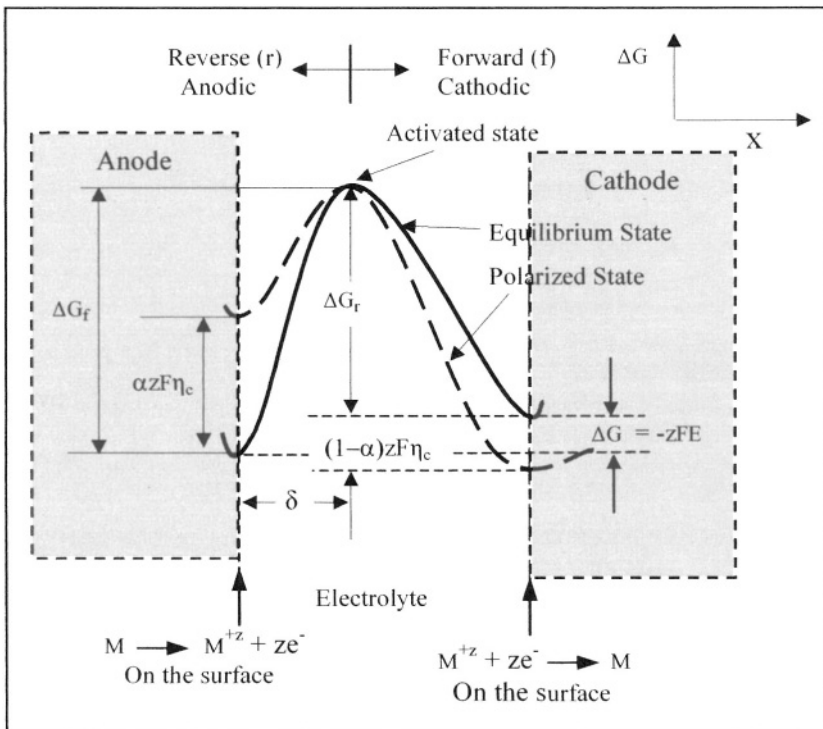


Figure 3.1 Schematic activation free energy distribution.

In general, the electrochemical and chemical rates of reactions due to either anodic or cathodic overpotentials can be predicted using both Faraday and Arrhenius equations, respectively

$$R_F = \frac{iA_{w,j}}{zF} \quad (3.1)$$

$$R_A = \gamma_a \exp\left(-\frac{\Delta G^*}{RT}\right) \quad (3.2)$$

where i = Applied current density (A/cm^2)

$A_{w,j}$ = Atomic weight of species j (g/mol)

$A_{w,alloy} = \sum f_j A_{w,j}/z_j$ in units of g/mol

z = Oxidation state or valence number

z_j = Valence number of element j

f_j = Weight fraction of element j

γ_a = Chemical reaction constant

ΔG^* = Activation energy or free energy change (J/mol)

At equilibrium, Faraday's and Arrhenius' rate equations become equal ($R_F = R_A$) and consequently, the current density becomes

$$i = \gamma_o \exp\left(-\frac{\Delta G^*}{RT}\right) \quad (3.3)$$

Here, the term $\gamma_o = zF\gamma_a/A_w$ may be defined as the electrochemical rate constant having unit of current density (A/cm^2). For a reversible electrode at equilibrium, the current density in eq. (3.3) becomes the exchange current density; that is, $i = i_o$. In addition, Table 3.1 gives typical experimental values for i_o .

Table 3.1 Exchange current density data at $25^\circ C$ [4].

Electrode	Electrolyte	Reaction	i_o (A/cm^2)
Al	2N H_2SO_4	$2H^+ + 2e^- = H_2$	1×10^{-10}
Au	1N HCl	$2H^+ + 2e^- = H_2$	1×10^{-6}
Cu	0.1N HCl	$2H^+ + 2e^- = H_2$	2×10^{-7}
Fe	2N H_2SO_4	$2H^+ + 2e^- = H_2$	1×10^{-6}
Ni	1N HCl	$2H^+ + 2e^- = H_2$	4×10^{-6}
Ni	05N $NiSO_4$	$Ni = Ni^{+2} + 2e^-$	1×10^{-6}
Pb	1N HCl	$2H^+ + 2e^- = H_2$	2×10^{-13}
Pt	1N HCl	$2H^+ + 2e^- = H_2$	1×10^{-3}
Pt	0.1N $NaOH$	$O_2 + 4H^+ + 4e^- = 2H_2O$	4×10^{-13}
Pd	06N HCl	$2H^+ + 2e^- = H_2$	2×10^{-4}
Sn	1N HCl	$2H^+ + 2e^- = H_2$	1×10^{-8}

On the other hand, if an electrode is polarized by an overpotential under steady-state conditions, then the rates of reactions are not equal ($R_F \neq R_A$) and consequently, the forward (cathodic) and reverse (anodic) current density components must be defined in terms of the free energy change ΔG^* deduced from Figure 3.1. Hence,

$$i_f = k'_f \exp \left[-\frac{\Delta G_f^*}{RT} \right] \quad (\text{Cathodic}) \quad (3.4)$$

$$i_r = k'_r \exp \left[-\frac{\Delta G_r^*}{RT} \right] \quad (\text{Anodic}) \quad (3.5)$$

$$\begin{aligned} \text{where } \Delta G_f^* &= \Delta G_f - \alpha z F \eta_c \\ \Delta G_r^* &= \Delta G_r + (1 - \alpha) z F \eta_a \\ \alpha &= \text{Symmetry coefficient} \end{aligned}$$

For a cathodic case, the net current and the overpotential are $i = i_f - i_r$ and η_c , respectively. Substituting eqs. (3.4) and (3.5) into this expression yields the net current density in a general form

$$\begin{aligned} i &= k'_f \exp \left(-\frac{\Delta G_f}{RT} \right) \exp \left(\frac{\alpha z F \eta}{RT} \right) \\ &\quad - k'_r \exp \left(-\frac{\Delta G_r}{RT} \right) \exp \left[-\frac{(1 - \alpha) z F \eta}{RT} \right] \end{aligned} \quad (3.6)$$

from which the exchange current density is deduced as

$$i_o = k'_f \exp \left(-\frac{\Delta G_f}{RT} \right) = k'_r \exp \left(-\frac{\Delta G_r}{RT} \right) \quad (3.7)$$

Substituting eq. (3.7) into (3.6) for one-step reaction yields the well-known **Butler-Volmer equation** for polarizing an electrode from the open-circuit potential E_o under steady-state conditions

$$i = i_o \left\{ \exp \left[\frac{\alpha z F \eta}{RT} \right]_f - \exp \left[-\frac{(1 - \alpha) z F \eta}{RT} \right]_r \right\} \quad (3.8)$$

$$\begin{aligned} \text{where } \eta &= E - E_o \\ E &= \text{Applied potential} \end{aligned}$$

It is clear that overpotential depends on the applied current density; therefore, $\eta = f(i)$. In addition, the exchange current density (i_o) can be defined as the rate of oxidation and reduction reactions at equilibrium. Specifically, i_o is the current density at which the rate of oxidation and rate of reduction are equal in a state of equilibrium. Thus, i_o is just the reversible reaction rate at equilibrium and it is a kinetic parameter, whereas ΔG is a thermodynamic parameter.

In fact, i_o is very sensitive to electrode surface condition and it is temperature-dependent as indicated by eq. (3.8). Thus, one can generalize the Arrhenius equation, eq. (3.2), for a series of electrochemical reactions as follows [47]

$$i_{o,T,l} = i_{o,T_o,l} \exp \left[-\frac{\Delta G^*}{RT} \left(\frac{1}{T} - \frac{1}{T_o} \right) \right] \quad (3.9)$$

where $i_{o,T,k}$ = Exchange current density at temperature T

$i_{o,T_o,k}$ = Reference exchange current density at temperature T_o

$l = 1, 2, 3, 4, \dots$ = Number of reactions.

This expression, eq. (3.8), is the general non-linear rate equation in terms of current density that most electrochemical cells obey under charge-transfer control. Thus, $\eta = \eta_a = (E - E^o) > 0$ and $\eta = \eta_c = (E - E^o) < 0$ are the anodic and cathodic overpotentials, respectively, which represent a deviation from the half-cell potential E^o , and E is the applied potential. In summary, the applied anodic current density is $i = i_a - i_o$ at $\eta_a > 0$ and the cathodic current density is $i = i_c - i_o$ at $\eta_c < 0$. At equilibrium conditions, the potential is $E = E^o$ and $\eta = 0$, and eq. (3.8) yields $i_a = i_c = i_o$. This implies that the rates of metal dissolution (oxidation) and deposition (reduction) are equal. However, a deviation from **equilibrium of the half-cells** is the normal case in real situations.

Furthermore, if one is interested in determining the total ionic molar flux J due to the mass transfer of a species j , then $i = zFJ$ and

$$J = \frac{i_o}{zF} \left\{ \exp \left[\frac{\alpha z F \eta}{RT} \right]_f - \exp \left[-\frac{(1 - \alpha) z F \eta}{RT} \right]_r \right\} \quad (3.10)$$

This ionic molar flux will be defined in details in Chapter 4. The reaction rate in terms of current density i given by eq. (3.8) is valid for one-step reaction. Hence, the controlling reaction may be part of a series of reaction steps, but the slowest reaction step is the rate-controlling. For any reaction, eq. (3.8) can be approximated by letting $x = \alpha z F \eta / RT$ and $y = (1 - \alpha) z F \eta / RT$. Expanding the exponential functions according to Taylor's series yields

$$\exp(x) = \sum_{k=0}^{\infty} \frac{x^k}{k!} \simeq 1 + x \quad (3.11)$$

$$\exp(-y) = \sum_{k=0}^{\infty} \frac{(-y)^k}{k!} \simeq 1 - y \quad (3.12)$$

Thus, eq. (3.8) can be expressed as a linear approximation when the overpotential is small in magnitude

$$i \simeq i_o [(1 + \alpha z F \eta / RT) - (1 - (1 - \alpha) z F \eta / RT)] \quad (3.13)$$

$$i \simeq i_o \left(\frac{z F \eta}{RT} \right) \quad (3.14)$$

Eq. (3.13) and (3.14) can be used for small values of overpotential like $\eta < 0.01 \text{ V}$ [7]. However, one can take a different approach to approximate the current density by considering the following inequality

$$\exp \left[\frac{\alpha z F \eta}{RT} \right]_f \gg \exp \left[-\frac{(1-\alpha) z F \eta}{RT} \right]_r \quad (3.15)$$

If this is the case, then eq. (3.8) yield

$$i = i_o \exp \left(\frac{\alpha z F \eta}{RT} \right) \quad (3.16)$$

Solving eq. (3.16) for the overpotential yields the **Tafel equation**

$$\eta = a + b \log(i) \quad (3.17)$$

where

$$a = -\frac{2.303RT}{\alpha z F} \log(i_o) \quad (3.18)$$

$$b = \frac{2.303RT}{\alpha z F} \quad (3.19)$$

In fact, eq. (3.17) yields a linear behavior when $\eta = f[\log(i)]$ for either an anodic polarization or cathodic polarization analysis. With regard to reaction rates, let R_f and R_r be the forward (reduction) and reverse (oxidation) reaction rates, respectively and let $K = K_f/K_r$ be the equilibrium constant. Thus,

$$\ln(K) = \ln(K_f) - \ln(K_r) \quad (a)$$

and from eq. (3.2),

$$\ln(K_f) = \ln(R_f) + \frac{\Delta G_f}{RT} \quad (b)$$

$$\ln(K_r) = \ln(R_r) + \frac{\Delta G_r}{RT} \quad (c)$$

Substituting eqs. (b) and (c) into (a) yields

$$\ln(K) = \ln(R_f) + \frac{A_f}{RT} + \ln(R_r) - \frac{A_r}{RT} \quad (d)$$

Differentiating eq. (d) with respect to the temperature T gives

$$\frac{d \ln(K)}{dT} = \frac{\Delta G_r}{RT^2} - \frac{\Delta G_f}{RT^2} = \frac{\Delta G^*}{RT^2} \quad (f)$$

Rearranging eq. (f) yields the activation energy [5]

$$\Delta G^* = RT^2 \cdot \frac{d \ln(K)}{dT} \quad (3.20)$$

In addition, Faraday's law of electrolysis describes the quantitative relationship for determining the rate of charge transfer in terms of current. Thus, the quantity of charge transferred (Q) at a time t is $Q = It$, and the quantity of moles for zF charge transfer is $N = Q/zF$. Now, the Faraday's weight loss or gain can be deduced by multiplying the number of moles, eq. (3.12b), by the atomic weight of metal M

$$W = NA_w = \frac{ItA_w}{zF} \quad (3.21)$$

Example 3.1 *Two identical zinc rods are exposed to HCl-base electrolyte. One rod is immersed at 25°C for 2 hours, while the other rod is at 50°C for 1 hour. Calculate the time of exposure of a third identical rod immersed the electrolyte at 30 °C.*

Solution:

The zinc oxidation reaction is $Zn \longrightarrow Zn^{+2} + 2e^-$ which requires an chemical activation energy to proceed in the written direction. The zinc rods are not polarized through an external circuit. Thus, the Arrhenius equation, eq. (3.2), yields

$$R_1 = 1/t_1 = \gamma_a \exp\left(-\frac{\Delta G^*}{RT_1}\right) \quad (a)$$

$$R_2 = 1/t_2 = \gamma_a \exp\left(-\frac{\Delta G^*}{RT_2}\right) \quad (b)$$

Dividing these equations gives

$$\frac{t_2}{t_1} = \exp\left[-\frac{\Delta G^*}{R} \left(\frac{1}{T_1} - \frac{1}{T_2}\right)\right] \quad (c)$$

Then, at $T_1 = 25^\circ\text{C} = 298\text{ K}$ and $t_1 = 2\text{ h}$ with $R = 8.314510\text{ J mol}^{-1}\text{ K}^{-1}$ and at $T_2 = 50^\circ\text{C} = 323\text{ K}$ and $t_2 = 1\text{ h}$ the reaction rates are

$$\begin{aligned} R_1 &= 1/t_1 = 0.50\text{ h}^{-1} \\ R_2 &= 1/t_2 = 1.00\text{ h}^{-1} \end{aligned}$$

Then, the activation energy becomes

$$\Delta G^* = -R \left(\frac{1}{T_1} - \frac{1}{T_2}\right)^{-1} \ln\left(\frac{t_2}{t_1}\right) \quad (d)$$

$$\Delta G^* = -8.314510 \text{ J mol}^{-1} \text{ K}^{-1} \left(\frac{1}{298 \text{ K}} - \frac{1}{323 \text{ K}} \right)^{-1} \ln \left(\frac{1 \text{ h}}{2 \text{ h}} \right)$$

$$\Delta G^* = 22,189.16 \text{ J/mol}$$

Substituting this energy into eq. (a) and solving for γ_a yields

$$\gamma_a = \frac{1}{2 \text{ h}} \exp \left[\frac{22,189.16 \text{ J/mol}}{(8.314510 \text{ J mol}^{-1} \text{ K}^{-1})(298 \text{ K})} \right] \quad (\text{e})$$

$$\gamma_a = 3,875.05 \text{ h}^{-1}$$

@, $T_3 = 30^\circ\text{C} = 303 \text{ K}$, the time and rate of reaction are, respectively

$$R_3 = 1/t_3 = \gamma_a \exp \left(-\frac{A_e}{RT_3} \right) \quad (\text{f})$$

$$t_3 = \frac{1}{\gamma_a} \exp \left(+\frac{A_e}{RT_3} \right) \quad (\text{g})$$

$$t_3 = \frac{1}{3,875.05 \text{ h}^{-1}} \exp \left[\frac{22,189.16 \text{ J/mol}}{(8.314510 \text{ J mol}^{-1} \text{ K}^{-1})(303 \text{ K})} \right]$$

$$t_3 = 1.73 \text{ h}$$

$$R_3 = 1/t_3 = 0.58 \text{ h}^{-1}$$

For comparison purposes, the reaction rates are

$$R_1 < R_3 < R_2$$

Example 3.2 Given the following data for a hypothetical metal undergoing chemical oxidation in a aqueous solution, a) plot the data (Arrhenius plot) and determine the activation energy from the plot and b) calculate the chemical rate at 308°C .

T (K)	R_A ($\times 10^{-2} \text{ h}^{-1}$)
298	50.01
300	50.26
305	50.88
310	51.48
315	52.08

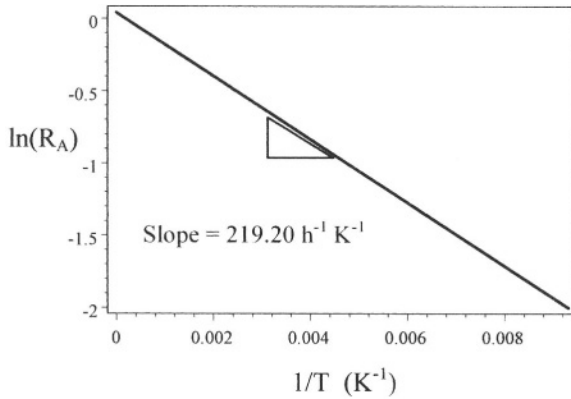
Solution:

a) Using eq. (3.2) to curve fit the given data yields the resultant curve fitting equation

$$\ln(R_A) = 4.3046 \times 10^{-2} h^{-1} - (219.20 h^{-1} K^{-1})/T$$

$$R_A = 1.044 \exp\left(-\frac{219.20}{T}\right)$$

where $\ln(\gamma_a) = 4.3046 \times 10^{-2} h^{-1}$ and the slope = $219.20 h^{-1} K^{-1}$. The required Arrhenius plot is shown below.



Example 3.2a

b) If $T = 308K$, then $\ln(R_A) = -0.66863$ and $R_A \approx 0.51 h^{-1}$

Example 3.3 Determine the atomic weight of $82Mg - 10Al - 8Zn$ alloy.

Solution:

The state of oxidation and the atomic weight of each element are

$$\begin{array}{lll} z_{Mg} = +2 & A_{w,Mg} = 24.31 \text{ g/mol} & f_{Mg} = 0.82 \\ z_{Al} = +3 & A_{w,Al} = 26.98 \text{ g/mol} & f_{Al} = 0.10 \\ z_{Zn} = +2 & A_{w,Zn} = 65.37 \text{ g/mol} & f_{Zn} = 0.08 \end{array}$$

The atomic weight of the alloy is

$$A_{w,alloy} = \sum \frac{f_i A_{w,i}}{z_i}$$

$$A_{w,alloy} = \frac{f_{Mg} A_{w,Mg} + f_{Al} A_{w,Al} + f_{Zn} A_{w,Zn}}{z_{Mg} + z_{Al} + z_{Zn}}$$

$$A_{w,alloy} = 13.48 \text{ g/mol}$$

3.3 POLARIZATION

This section partially treats the copious literature for supporting the mathematical models for characterizing the kinetics of charge transfer mechanism involved in an electrochemical system. Thus, electrode reactions are assumed to induce deviations from equilibrium due to the passage of an electrical current through an electrochemical cell causing a change in the working electrode (WE) potential. This electrochemical phenomenon is referred to as polarization. In this process, the deviation from equilibrium causes an electrical potential difference between the polarized and the equilibrium (unpolarized) electrode potential known as overpotential (η) [1].

Figure 3.2 shows a partial polarization diagram and related kinetic parameters. For instance, both Evans and Stern diagrams are superimposed in order for the reader to understand the significance of the electrochemical behavior of a polarized metal (M) electrode in a hydrogen-containing electrolyte.

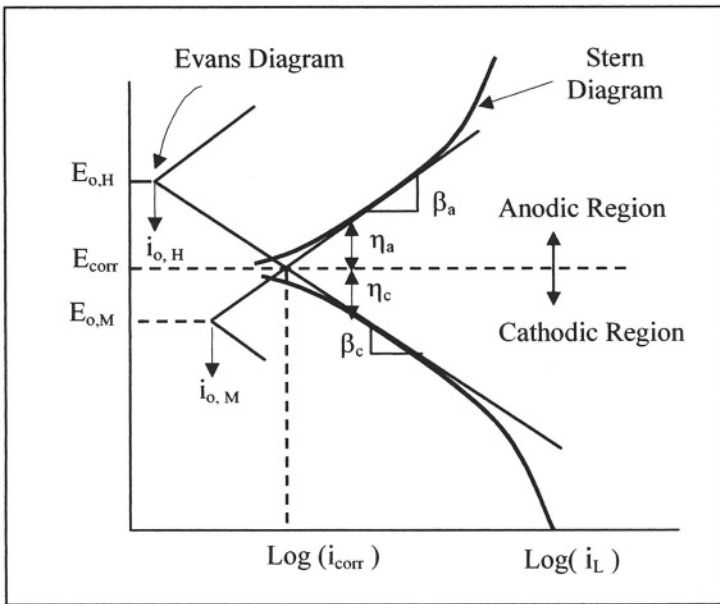


Figure 3.2 Schematic polarization curve showing Tafel extrapolation.

From Figure 3.2, $E_{o,H}$ and $E_{o,M}$ are the open-circuit potentials for hydrogen and metal M , respectively, $i_{o,H}$ $i_{o,M}$ are the exchange current densities, and i_L is the limiting current density.

For a reversible electrode, Evans diagram allows the determination of the corrosion point where both the hydrogen cathodic and the metal anodic line intercept. On the other hand, the irreversible electrochemical behavior denoted by the cathodic and anodic Stern diagram is also used for determining the corrosion point by simply extrapolating the linear portions of both curves until the

intercept as indicated in Figure 3.2. The latter diagram is a very common in electrochemical studies of pure metals and their alloys. Therefore, both Evans and Stern polarization diagrams provide the corrosion potential (E_{corr}) and the corrosion current density (i_{corr}). The other parameters illustrated in Figure 3.2 will become relevant as the electrochemical analysis advances in this chapter. With respect to the Stern diagram, this represents a polarization behavior that can be determined experimentally using potentiostatic and potentiodynamic methods, and it will be referred to as a polarization curve. Thus, a polarization curve is the result of polarizing from the corrosion potential anodically or cathodically and it is a very common experimental output in electrochemical studies on corroding electrodes.

Evaluation of corrosion behavior is normally done through a function that depends on kinetic parameters depicted in Figure 3.2. Hence, the current density function for polarizing an electrode irreversibly from the corrosion potential is similar to eq. (3.8). Hence,

$$i = i_{corr} \left\{ \exp \left[\frac{\alpha z F \eta}{RT} \right]_f - \exp \left[-\frac{(1 - \alpha) z F \eta}{RT} \right]_r \right\} \quad (3.22)$$

where $\eta = E - E_{corr}$

E = Applied potential (V)

β_a = Anodic polarization constant (Tafel anodic slope) (V)

β_c = Cathodic polarization constant (Tafel cathodic slope) (V)

Moreover, anodic polarization caused by an anodic overpotential $\eta_a = (E - E_{corr}) > 0$ is referred to as an electrochemical process in which a metal surface oxidizes (corrodes) by losing electrons. Consequently, the metal surface is positively charged due to the loss of electrons. This electrochemical polarization is quantified by η_a . On the other hand, cathodic polarization requires that electrons be supplied to the metal surface at an negative overpotential, $\eta_c = (E - E_{corr}) < 0$, which implies that $E < E_{corr}$.

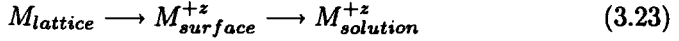
3.4 ACTIVATION POLARIZATION

In general, the activation polarization is basically an electrochemical phenomenon related to a charge-transfer mechanism, in which a particular reaction step controls the rate of electron flow from a metal surface undergoing oxidation. This is the case in which the rate of electron flow is controlled by the slowest step in the half-cell reactions [1-4].

Despite that eq. (3.22) is a generalized expression, it represents a measure of anodic polarization for corrosion studies and indicates that $\eta_a = 0$ for an unpolarized and $\eta_a \neq 0$ for a polarized electrode surface. For the latter case, the reaction rate for activation polarization depends on the charge-transfer overpotential as in metal oxidation due to electrons loss, the diffusion overpotential as in mass transport of ions, the reaction overpotential due to rate determining chemical reaction mechanism, the crystallization overpotential as in metal

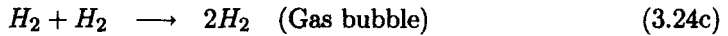
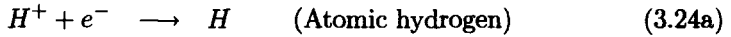
deposition in which atoms are incorporated into the electrode crystal surface lattice, and the Ohmic overpotential due to a resistance at the electrode/terminal junctions [2].

In general, the anodic metal undergoes a succession of reaction steps prior to dissolve in the electrolyte. This succession is hypothetically shown by the following idealized metal oxidation reactions during activation polarization



This succession indicates that the metal M loses $+z$ electrons on its surface and eventually the metal cation M^{+z} goes into solution. If the metal is silver undergoing oxidation, then the cation is just Ag^+ . For iron, the succession may be $Fe \rightarrow Fe^+ \rightarrow Fe^{+2} \rightarrow Fe^{+3}$.

For hydrogen evolution, Fontana's idealized model [1] for activation polarization is depicted in Figure 3.3 can be used to explain the succession of the reaction steps that may take place after the hydrogen cations are adsorbed (attached) on the electrode surface. Hence, the possible reaction steps are



Thus, only one step in eq. (3.23) and one in eq. (3.24) controls the charge transfer for activation polarization. For instance, the formation of hydrogen gas bubbles on the metal electrode surface is the last step in the succession of reactions and eventually, the bubbles move to the surface of the electrolyte where they burst.

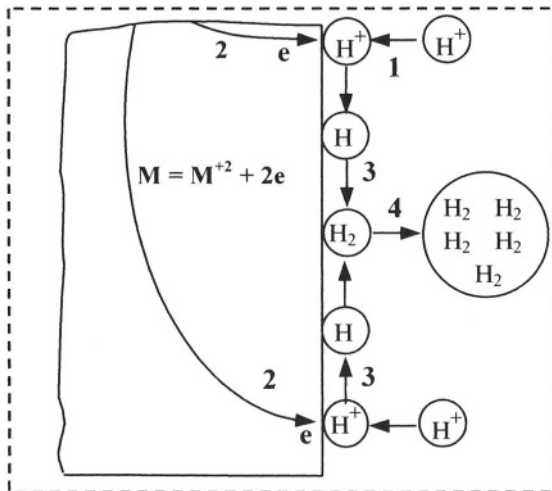


Figure 3.3 Activation polarization model after Fontana [1]

According to the model in Figure 3.3, the metal oxidation process can be represented by the following redox **stoichiometric reaction** $M + 2H^+ = M^{+z} + H_2$. On the other hand, if this reaction is reversed, then the metal M^{+z} cations in solution, specifically at the electrode/electrolyte interface, are deposited (plated) on the metal electrode. This is possible since electrons in the solution are supplied to the electrode surface. Thus, cathodic polarization occurs giving a negative overpotential, $\eta_c < 0$. In any event, anodic and cathodic reaction rates are assumed to be sufficiently slow.

3.5 POLARIZATION METHODS

The polarization resistance (R_p) of a metal/electrolyte system and the pitting or breakdown potential (E_b) can be determined using at least two-electrode system. Subsequently, the rate of metal dissolution or corrosion rate is calculated using a function of the form $i_{corr} = f(\beta, R_p) > i_o$. The methods are

- Linear Polarization (LP) as schematically shown in Figure 3.4 covers both anodic and cathodic portions of the potential E versus current density i curve for determining R_p .
- Tafel Extrapolation technique (TE) (Figure 3.2) takes into account the linear parts of the anodic and cathodic curves for determining R_p .
- Electrochemical Impedance Spectroscopy (EIS) as schematically shown in Figure 3.10 requires an alternating current (AC) and the output is a Nyquist plot for charge-transfer or diffusion control process, which can be used to determine R_p , which in turn, is inversely proportional to the corrosion current density i_{corr} .

Standard or recommended experimental procedures for measurements of R_p can be found in the American Society for Testing Materials ASTM G-59 and ASTM G-106 testing methods, and ASTM G-5 is for anodic potentiodynamic studies, are included in the annual Book of ASTM Standards Vol. 03.02.

3.5.1 LINEAR POLARIZATION

First of all, using eq. (3.8) under anodic and cathodic polarization individually, the Tafel slopes are derived by letting $\exp\left[\frac{\alpha z F \eta}{RT}\right]_f \gg \exp\left[-\frac{(1-\alpha)z F \eta}{RT}\right]$ for an anodic polarization analysis, where $i_a \gg |i_c|$ and $\eta_a \gg \eta_c$. On the other hand, $\exp\left[\frac{\alpha z F \eta}{RT}\right]_f \ll \exp\left[-\frac{(1-\alpha)z F \eta}{RT}\right]$ is for characterizing cathodic polarization when $|i_c| \gg i_a$ and $\eta_c \gg \eta_a$. Under these conditions, eq. (3.8) reduces to

$$i_a = i_o \exp \left[\frac{\alpha z F \eta_a}{RT} \right] \quad (\text{for } i_a \gg i_c, \eta_a \gg \eta_c) \quad (3.25a)$$

$$i_c = -i_o \exp \left[-\frac{(1-\alpha) z F \eta_c}{RT} \right] \quad (\text{for } i_c \gg i_a, \eta_c \gg \eta_a) \quad (3.25b)$$

Solving eqs. (3.25) for the overpotential yields

$$\eta_a = \beta_a \log \left(\frac{i_a}{i_o} \right) \quad (3.26a)$$

$$\eta_c = -\beta_c \log \left(\frac{i_c}{i_o} \right) \quad (3.26b)$$

where β_a and β_c are known as Tafel slopes of the anodic and cathodic reactions, respectively. These slopes are defined by

$$\beta_a = \frac{2.303RT}{\alpha z F} = \frac{(1-\alpha)\beta_c}{\alpha} \quad (3.27a)$$

$$\beta_c = \frac{2.303RT}{(1-\alpha)zF} = \frac{\alpha\beta_a}{(1-\alpha)} \quad (3.27b)$$

Additionally, if $\alpha = 0.5$, then $\beta_a = \beta_c$. Figure 3.4 shows a theoretical polarization curve for conducting polarization resistance measurements.

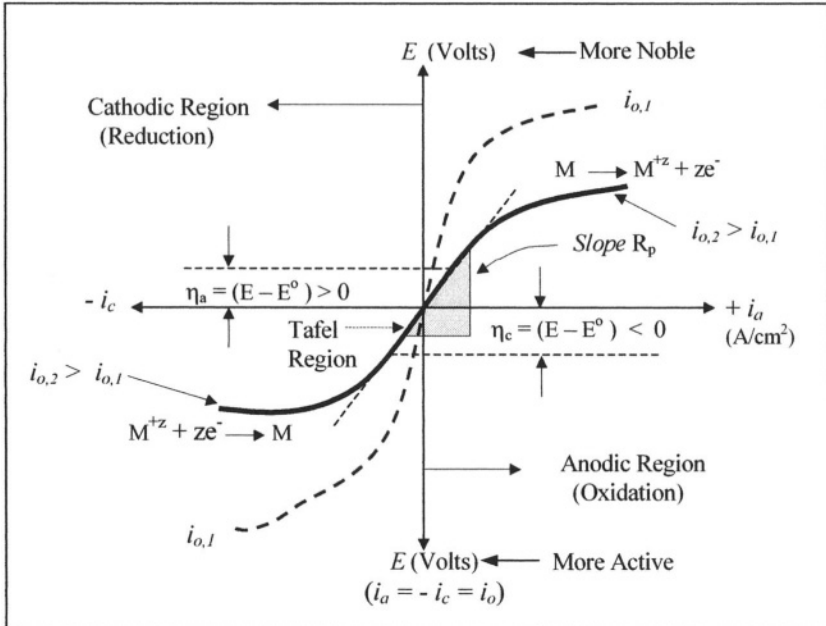


Figure 3.4 Schematic linear polarization curve.

The linear polarization is confined to a small magnitude of the overpotentials η_a and η_c , respectively, using linear coordinates. This technique allows the determination of i_{corr} using a potential range of ± 10 mV from the E_{corr} [3]. Prior to determining i_{corr} , the polarization resistance R_p is estimated from the linear slope of the curve (Figure 3.4) as

$$R_p = \frac{\Delta E}{\Delta i} = \frac{\eta}{\Delta i} \quad (3.28)$$

The corresponding corrosion current density depends on kinetic parameters since $i_{corr} = f(\beta, R_p)$. Thus, the simple linear relation that defines the corrosion current density is of the form

$$i_{corr} = \frac{\beta}{R_p} \quad (3.29)$$

where $\beta = f(\beta_a, \beta_c)$, and β_a and β_c are taken as positive kinetic parameters for determining i_{corr} of a corroding or oxidizing metallic material. Notice that eq. (3.29) predicts that the corrosion current density is very sensitive to changes in the polarization resistance. In fact, the magnitude of the polarization resistance is mainly controlled by the corrosion current density [1,46]. Hence,

$$\beta = \frac{\beta_a \beta_c}{2.303 (\beta_a + \beta_c)} \quad (3.30)$$

This constant β will be derived in the next section. In fact, this method requires knowledge of the Tafel anodic β_a and cathodic β_c slopes in order to calculate β , and subsequently predict i_{corr} using eq. (3.29). This i_{corr} expression is simple, but essential in corrosion measurements since i_{corr} can be converted to corrosion rate in units of mm/y , which are more convenient for engineering purposes after β and R_p are determined. finally, the values of these slopes are $\beta_a < 1$ volt and $\beta_c < 1$ volt, and $\beta < 1$ volt.

3.5.2 TAFEL EXTRAPOLATION

This method involves the determination of the Tafel slopes β_a and β_c as well as E_{corr} and i_{corr} from a single polarization curve as shown in Figure 3.2. This curve is known as the Stern diagram (non-linear polarization) based on eq. (3.22). The Evans diagram (linear polarization) is also included in order to show that both diagrams have a common $E_{corr} \cdot i_{corr}$ point. This figure illustrates a hypothetical electrochemical behavior of a metal M immersed in an electrolyte containing one type of oxidizer, such as H^+ ions.

For electrochemical systems containing several oxidizers, determining the corrosion point is more complex using the Evans diagram, but the Stern diagram would provided a similar polarization curve as shown in Figure 3.2, from which both E_{corr} and i_{corr} are easily determined by extrapolating the Tafel anodic and cathodic linear parts until they intersect as straight lines. Also included in Figure 3.2 are the exchange current densities, $i_{o,H}$ and $i_{o,M}$, and their

counterpart potentials, $E_{o,H}$ and $E_{o,M}$, for hydrogen evolution and metal oxidation, respectively. These potentials, $E_{o,H}$ and $E_{o,M}$, are known as open-circuit potentials. Furthermore, the limiting current density i_L for cathodic polarization is included as an additional information one can extract from a cathodic polarization curve. The latter term will be dealt with in Chapter 5.

Further analysis of Figure 3.2 yields the following summary:

- The solid curve can be obtained statically or dynamically.
- This non-linear curve is divided into two parts. If $E > E_{corr}$, the upper curve represents an anodic polarization behavior for oxidation of the metal M . On the contrary, if $E < E_{corr}$ the lower curve is a cathodic polarization for hydrogen reduction as molecular gas (hydrogen evolution). Both polarization cases deviate from the electrochemical equilibrium potential (E_{corr}) due to the generation of anodic and cathodic overpotentials, which are arbitrarily shown in Figure 3.2 as η_a and η_c , respectively.
- Both anodic and cathodic polarization curves exhibit small linear parts known as Tafel lines, which are used for determining the Tafel slopes β_a and β_c . These slopes can be determined using either the Evans or Stern diagram.
- Extrapolating the Tafel or Evans straight lines until they intersect define the $E_{corr} \cdot i_{corr}$ point.
- The disadvantage in using the Evans diagram is that the exchange current density (i_o), the open-circuit potential E_o (no external circuit is applied), and the Tafel slopes for the metal and hydrogen have to be known quantities prior to determining the $E_{corr} \cdot i_{corr}$ point.
- The advantage of the Stern diagram over the Evans diagram is that it can easily be obtained using the potentiodynamic polarization technique at a constant potential sweep (scan rate) and no prior knowledge of the above kinetics parameter is necessary for determining the $E_{corr} \cdot i_{corr}$ point. The resultant curve is known as a potentiodynamic polarization curve.
- In conclusion, E_{corr} and i_{corr} can be determined from an Evans diagram for an **unpolarized metal** since $i_{corr} = i_a = -i_c$ at $E = E_{corr}$. On the other hand, if the metal is **polarized**, then the Stern diagram can be used for determining E_{corr} , i_{corr} , β_a , and β_c . In addition, E_{corr} is a reversible potential also known as a mixed potential. Further analysis of the polarization phenomenon requires use of the Ohm's law. Hence, the cell and the inner potentials are defined by, respectively

$$E = E_{corr} - \eta_a - \eta_c - \phi_s = IR_x \quad (3.31)$$

$$\phi_s = IR_s \quad (3.32)$$

where I = Current (A)

R_x = External resistance (Ohm = V / A)

R_s = Solution resistance (Ohm = V / A)

ϕ_s = Internal potential (V)

Solving eq. (3.31) for I yields

$$I = \frac{E_{corr} - \eta_a - \eta_c - IR_s}{R_x} \quad (3.33)$$

The current in eq. (3.33) strongly depends on the magnitude of the external resistance. A slight decrease in R_x increases the current I . Hence, if $R_x \rightarrow 0$, then $I \rightarrow \infty$ and $I \rightarrow 0$ when $R_x \rightarrow \infty$. In addition, $IR_x \rightarrow 0$ as $E \rightarrow 0$.

With regard to eq. (3.32), ϕ_s can be neglected due to its small contribution to the cell potential. However, the electrolyte conductivity is of significance in determining the governing current expression. For instance, when $IR_x \gg IR_s$ the electrolyte has a high conductivity and if $IR_x \ll IR_s$ the electrolyte has a low conductivity. Hence, from eq. (3.33) the governing current expressions are

$$I = \frac{E_{corr} - \eta_a - \eta_c}{R_x} \quad \text{for } IR_x \gg IR_s \quad (3.34a)$$

$$I = \frac{E_{corr} - \eta_a - \eta_c}{R_s} \quad \text{for } IR_s \gg IR_x \quad (3.34b)$$

Nowadays, sophisticated instrumentation, such as a potentiostat/galvanostat is commercially available for conducting electrochemical experiments for characterizing the electrochemical behavior a metal or an alloy in a few minutes. Nevertheless, a polarization diagram or curve is a **potential control** technique. This curve can experimentally be obtained statically or dynamically. The latter approach requires a linear potential scan rate to be applied over a desired potential range in order to measure the current response.

On the other hand, a galvanostat can be used as the **current control** source for determining the potential response on a electrode surface. However, the potential control approach is common for characterizing electrochemical behavior of metallic materials. The potential can be applied uniformly or in a stepwise manner using a waveform. The former case generates a steady-state current response, while the latter provides a transient current response.

Further interpretation of the polarization curves can be extended using Pourbaix graphical work depicted in Figure 3.5 for pure iron (Fe). The resultant plots represent the functions $E = f(i)$ and $E \text{ vs. } f[\log(i)]$ for an electrolyte containing $C_{Fe^{+2}} = 0.01 \text{ g/l} = 1.79 \times 10^{-4} \text{ mol/l} = 1.49 \times 10^{-7} \text{ mol/cm}^3$ at $pH = 0$. Additionally, the reactions depicted in Figure 3.5 and some related kinetic parameters are listed in Table 3.2 for convenience. One important observation is that both anodic and cathodic Tafel slopes, β_a and β_c , respectively are equal numerically and consequently, Figure 3.5b has an inflection point at (i_{corr}, E_{corr}) . This electrochemical situation is mathematically predicted and discussed in the next section using a current density function for a mixed-potential system.

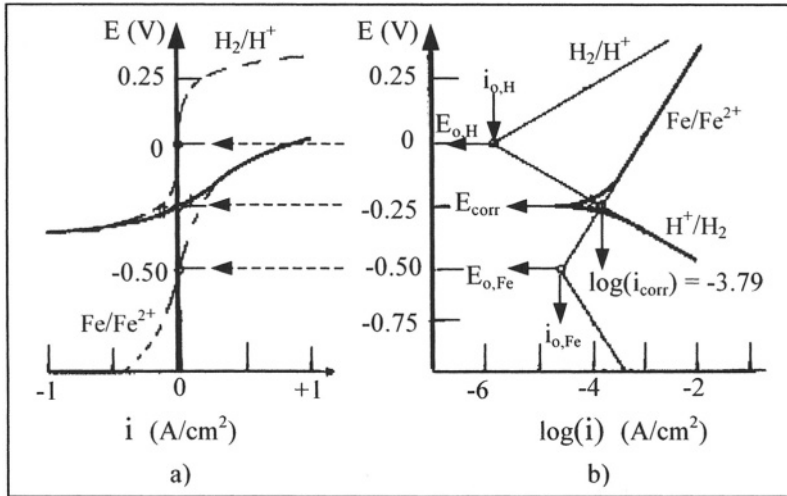


Figure 3.5 Corrosion of iron (0.01 g/l) with hydrogen evolution at $pH = 0$ [46].

Table 3.2 Kinetic parameters for Iron (0.01g/l) and hydrogen reactions at $pH = 0$ [46].

Parameters	$Fe = Fe^{+2} + 2e^-$	$2H^+ + 2e^- = H_2$
E^o (V_{SHE})	-0.50	0
i_o (A/cm^2)	3.16×10^{-5}	1.41×10^{-6}
β_a (V)	+0.328	+0.123
β_c (V)	-0.328	-0.123

In fact, Figure 3.5 compares both linear and extrapolation results for iron. The interpretation of this figure is based on complete activation control in the absence of diffusion and external current [46]. Thus, it can be deduced from this figure that

- the net current density ($i_{net} = i_a - i_c$) is zero at equilibrium, but the corrosion current density is $i_{corr} = 0.1622 \text{ mA/cm}^2$ at the corrosion potential, $E_{corr} = -0.25 \text{ V}_{SHE}$.
- The polarization curves are reversible in nature; however, if irreversibility occurs, the heavy line in Figure 3.5a would follow the vertical axis at a potential range $E_{o,c} \leq E \leq E_{o,a}$ when $i_{net} = 0$.
- The open-circuit potentials, $E_{o,H}$ and $E_{o,Fe}$, can be estimated using the Nernst equation.

One important fact is that the solution must be continuously stirred to keep a uniform concentration of the species in solution; otherwise, the concentration

at the electrodes become uneven and the open-circuit potential $E_{c,Fe}$ increases during oxidation and $E_{c,H}$ decreases during reduction. At equilibrium, the overpotential becomes $\eta = E - E_o = 0$ since the applied potential and the applied current density are $E = E_o$, and $i = i_o$, respectively. However, if $i > i_{o,Fe}$, the iron reaction is irreversible because it corrodes by liberating electrons.

Combining the Pourbaix diagram and the polarization curves for iron in water at $pH = 7$ yields interesting information on the electrochemical state as shown in Figure 3.6, which includes the hydrogen and oxygen lines for comparison [46]. Observe the correspondence of potential between both diagrams. For instance, the potential at point A, indicates that corrosion occurs along line CP, but at point B the potential suggests that passivation occurs and iron is protected anodically. Point P is a transitional potential at the critical current density. Any slight change in potential iron passivates at $E > E_p$ or corrodes at $E < E_p$. Also, if $E < E_c$ Pourbaix predicts immunity, but the polarization curve indicates that corrosion is possible.

Furthermore, the advantage of the Pourbaix diagram as shown in Figure 3.6a is that it predicts the electrochemical state for immunity, corrosion, and passivation, and it is related to the polarization curve shown in Figure 3.6b. However, only the polarization curve predicts the corrosion rate through the current density i_{corr} for metal oxidation and the passivation rate through the passive current density for metallic cation reduction to form an oxide protective film on the electrode surface. The passivation phenomenon is discussed in details in Chapter 6.

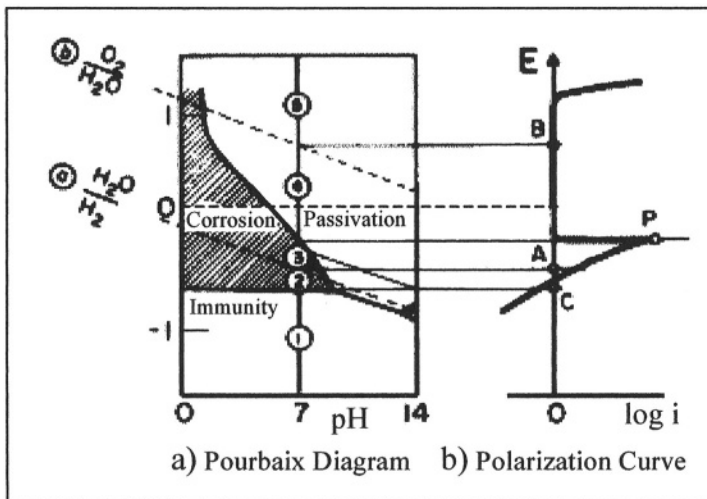


Figure 3.6 Comparison of Pourbaix diagram and polarization curve for iron in water at $pH = 7$ and $P = 101$ kPa [46].

3.6 CORROSION RATE

During corrosion (oxidation) process, both anodic and cathodic reaction rates are coupled together on the electrode surface at a specific current density known as i_{corr} . This is an electrochemical phenomenon which dictates that both reactions must occur on different sites on the metal/electrolyte interface. For a uniform process under steady state conditions, the current densities at equilibrium are related as $i_a = -i_c = i_{corr} @ E_{corr}$. Assume that corrosion is uniform and there is no oxide film deposited on the metal electrode surface; otherwise, complications would arise making matters very complex. The objective at this point is to determine both E_{corr} and i_{corr} either using the Tafel Extrapolation or Linear Polarization techniques. It is important to point out that i_{corr} cannot be measured at E_{corr} since $i_a = -i_c$ and current will not flow through an external current-measuring device [3].

When polarizing from the corrosion potential with respect to anodic or cathodic current density, the overpotential expressions given by eqs. (3.26a) and (3.26b) become

$$\eta_a = \beta_a \log \left(\frac{i_a}{i_{corr}} \right) \quad (3.35a)$$

$$\eta_c = -\beta_c \log \left(\frac{i_c}{i_{corr}} \right) \quad (3.35b)$$

Recall that $\eta_a = \Delta E = (E - E_{corr}) > 0$ and $\eta_c = \Delta E = (E - E_{corr}) < 0$ now represent the potential changes from the steady-state corrosion potential E_{corr} . Solving eqs. (3.35a) and (3.35b) for the anodic and cathodic current densities yields, respectively

$$i_a = i_{corr} \exp \left[\frac{2.303 (E - E_{corr})}{\beta_a} \right] \quad (3.36)$$

$$i_c = i_{corr} \exp \left[-\frac{2.303 (E - E_{corr})}{\beta_c} \right] \quad (3.37)$$

Assuming that the applied current density is $i = i_a - i_c$ and substituting eqs. (3.36) and (3.37) into this expression yields the **Butler-Volmer equation** that quantifies the kinetics of the electrochemical corrosion

$$i = i_{corr} \left\{ \exp \left[\frac{2.303 (E - E_{corr})}{\beta_a} \right] - \exp \left[-\frac{2.303 (E - E_{corr})}{\beta_c} \right] \right\} \quad (3.38)$$

This expression resembles eq. (3.22), but it is a convenient expression at this point since the inverse polarization resistance is easily obtainable by deriving eq. (3.38) with respect to the applied potential E . Thus,

$$\left(\frac{di}{dE} \right) = 2.303 i_{corr} \left\{ \begin{array}{l} \beta_a^{-1} \exp [2.303 (E - E_{corr}) / \beta_a] \\ -\beta_c^{-1} \exp [-2.303 (E - E_{corr}) / \beta_c] \end{array} \right\} \quad (3.39)$$

Further,

$$\left(\frac{d^2i}{dE^2}\right) = 5.3038i_{corr} \left\{ \begin{array}{l} \beta_a^{-2} \exp[2.303(E - E_{corr})/\beta_a] \\ -\beta_c^{-2} \exp[-2.303(E - E_{corr})/\beta_c] \end{array} \right\} \quad (3.40)$$

Let's set some conditions for eq. (3.40) such that

$$\left(\frac{d^2i}{dE^2}\right) \Rightarrow \left\{ \begin{array}{ll} < 0 & \text{for } E = E_{max} > E_{corr} \\ = 0 & \text{for an inflection point: } E = E_{corr} \\ > 0 & \text{for } E = E_{min} < E_{corr} \end{array} \right. \quad 3.41$$

Evaluating eq. (3.40) at the inflection point yields

$$\left(\frac{d^2i}{dE^2}\right)_{E=E_{corr}} = 5.3038i_{corr} (\beta_a^{-2} - \beta_c^{-2}) \quad (3.42)$$

which clearly indicates that the inflection point is achieved if and only if $\beta_a = \beta_c$. This condition was pointed out by Oldham and Mansfield [13] as the mathematical proof for the $E_{corr} \cdot i_{corr}$ point depicted in Figure 3.2.

Additionally, evaluating eq. (3.39) at $E = E_{corr}$ yields the polarization resistance

$$\left(\frac{di}{dE}\right)_{E=E_{corr}} = 2.303i_{corr} \left(\frac{\beta_a + \beta_c}{\beta_a\beta_c}\right) \quad (3.43)$$

$$R_p = \left(\frac{di}{dE}\right)_{E=E_{corr}}^{-1} \quad (3.44)$$

Thus,

$$R_p = \frac{\beta_a\beta_c}{2.303i_{corr}(\beta_a + \beta_c)} = \frac{\beta}{i_{corr}} \quad (3.45)$$

Here, β is the proportionality constant defined by (3.30). Notice that R_p is inversely proportional to i_{corr} as indicated by eq. (3.45) and depicted in Figure 3.7a, but it can be linearized as shown in Figure 3.7b. Thus,

$$\log(R_p) = \log(\beta) - \log(i_{corr}) \quad (3.46)$$

In general, a corroding metal is equivalent to a short-circuit cell or energy-producing system, in which energy dissipation occurs during the production of a corrosion product [3].

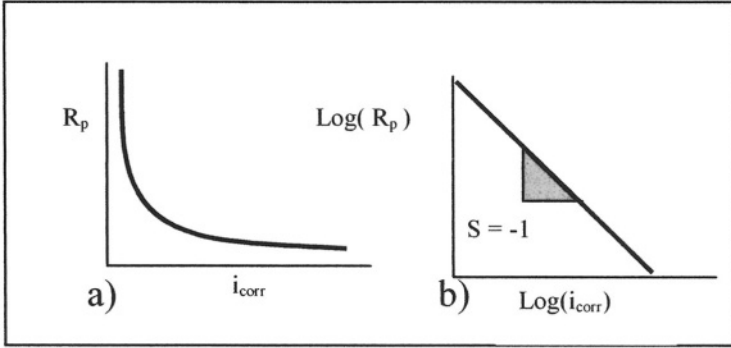


Figure 3.7 Non-linear and linear R_p plots.

Thus, metal oxidation is equivalent to metal corrosion. Now, dividing Faraday's rate of reaction, eq. (3.1), by the metal density ρ defines the corrosion rate (rate of metal dissolution) as

$$C_R = \frac{R_F}{\rho} \quad (3.47)$$

$$C_R = \frac{i_{corr} A_w}{zF\rho} \quad (3.48)$$

In addition, corrosion rate can be represented by the rate of weight loss [1] or rate of penetration [4], but eq. (3.48) is a mathematical model convenient for determining the metal dissolution in terms penetration per year in units of mm/y . These are common units to the engineers or designers.

Example 3.4 Calculate the corrosion rate C_R in units of mm/y , and the electrochemical rate constant in $\mu g/cm^2 \cdot s$, and $mol/cm^2 \cdot s$ for a low carbon steel plate ($1cm \times 1cm \times 4cm$) immersed in sea water. Given data: $I = 110 \mu A$ (current), $\rho = 7.87 g/cm^3$ and $A_w = 55.85 g/mol$.

Solution:

Since the carbon steel is basically iron (Fe), the oxidation reaction involved in this problem is $Fe \rightarrow Fe^{+2} + 2e^-$ with $z = 2$ and $F = 96,500 A \cdot s/mol$, and the exposed area is $A = 1cm \times 1cm = 1 cm^2$. Then, the current density is $i = I/A = 110 \times 10^{-6} \text{ amps}/1 cm^2$. Using eq. (3.48), the corrosion rate is

$$C_R = \frac{i A_w}{zF\rho} = \frac{(110 \times 10^{-6} A/cm^2) (55.85 g/mol)}{(2) (96,500 A \cdot s/mol) (7.87 g/cm^3)}$$

$$C_R = 4.04 \times 10^{-9} cm/s = 1.28 mm/y$$

From eq. (3.1), the electrochemical rate constant is

$$R_F = \frac{iA_w}{zF} = \frac{(110 \mu\text{A}/\text{cm}^2)(55.85 \text{ g/mol})}{(2)(96,500 \text{ A} \cdot \text{s/mol})}$$

$$R_F = 0.0318 \mu\text{g}/\text{cm}^2\text{s}$$

Eliminating the atomic weight in eq. (3.1) yields

$$R_F = \frac{i}{zF} = \frac{(110 \mu\text{A}/\text{cm}^2)}{(2)(96,500 \text{ A} \cdot \text{s/mol})}$$

$$R_F = 5.70 \times 10^{-10} \text{ mol}/(\text{cm}^2 \cdot \text{s})$$

Example 3.5 Assume that the rates of oxidation of Zn and reduction of H^+ are controlled by activation polarization. Use the data given below to a) plot the appropriate polarization curves and determine E_{corr} and i_{corr} from the plot. Calculate b) both E_{corr} and i_{corr} c) the corrosion rate C_R in mm/y , and the polarization resistance R_p in $\text{ohm} \cdot \text{cm}^2$. Data:

$\text{Zn} = \text{Zn} + 2e^- \implies$	$E_{\text{Zn}} = -0.80 \text{ V}$	$i_{o,\text{Zn}} = 10^{-7} \text{ A}/\text{cm}^2$
	$\beta_a = 0.10 \text{ V}$	$\rho = 7.14 \text{ g}/\text{cm}^3$
	$A_w = 65.37 \text{ g}/\text{mol}$	
$2\text{H}^+ + 2e^- = \text{H}_2 \implies$	$E_{\text{H}} = 0.10 \text{ V}$	$i_{o,\text{H}} = 10^{-10} \text{ A}/\text{cm}^2$
	$\beta_c = 0.10 \text{ V}$	

Solution:

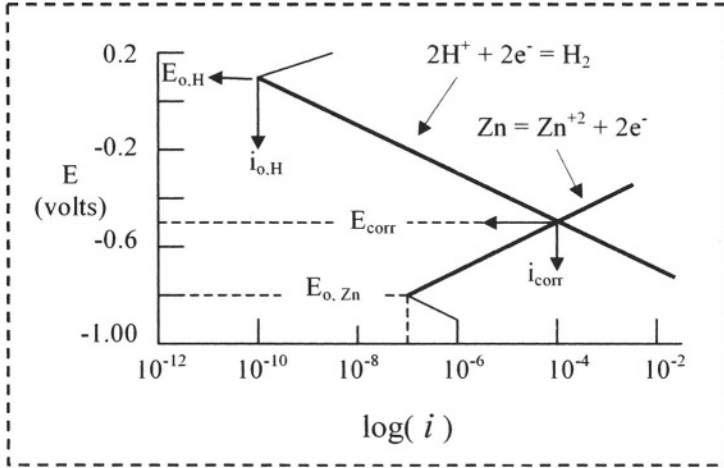
a) E vs. $\log(i)$ plot

1) Plot $(i_{o,\text{H}}, E_{\text{H}}) = (\log 10^{-10} \text{ A}/\text{cm}^2, 0.10 \text{ V})$

and $(i_{o,\text{Zn}}, E_{o,\text{Zn}}) = (\log 10^{-7} \text{ A}/\text{cm}^2, -0.80 \text{ V})$

2) Draw the hydrogen reduction and zinc oxidation lines with β_c and β_a slopes, respectively

3) The intercepting point defines the corrosion point as $(i_{\text{corr}}, E_{\text{corr}}) = (10^{-4} \text{ A}/\text{cm}^2, -0.50 \text{ V})$ for the unpolarized Zn metal. In addition, $i_{\text{corr}} = i_a = i_c$ at $E = E_{\text{corr}}$ and $E_{o,\text{Zn}}$ and $E_{o,\text{H}}$ are the open-circuit potentials, which can be determined using the Nernst equation, eq. (2.32).



Example 3.5

b) Using eqs. (3.26a) and (3.26b) with $i_a = i_c = i_{\text{corr}}$, $\eta_a = E - E_{o,\text{Zn}}$ and $\eta_c = E - E_{o,\text{H}}$ yields

$$E = E_{o,\text{Zn}} + \beta_a \log(i_{\text{corr}}/i_{o,\text{Zn}}) \quad (\text{a})$$

$$E = E_{o,\text{H}} - \beta_c \log(i_{\text{corr}}/i_{o,\text{H}}) \quad (\text{b})$$

Equating eqs. (c) and (d) and solving for i_{corr} yields the corrosion current density

$$\log i_{\text{corr}} = \frac{1}{\beta_a + \beta_c} [E_{o,\text{H}} - E_{o,\text{Zn}} + \beta_a \log i_{o,\text{Zn}} + \beta_c \log i_{o,\text{H}}] \quad (\text{c})$$

$$\log i_{\text{corr}} = \frac{0.1 + 0.8 + 0.1 \log 10^{-7} + 0.1 \log 10^{-10}}{0.2} = -4$$

$$i_{\text{corr}} = 10^{-4} \text{ A/cm}^2$$

Letting $E = E_{\text{corr}}$ and using eg. (a) or (b) gives $E_{\text{corr}} = -0.50 \text{ V}$

c) From eq. (3.48)

$$C_R = \frac{i_{\text{corr}} A_w}{zF\rho} = \frac{(10 \times 10^{-4} \text{ A/cm}^2) (65.37 \text{ g/mol})}{(2) (96,500 \text{ A} \cdot \text{s/mol}) (7.14 \text{ g/cm}^3)}$$

$$C_R = 1.50 \text{ mm/y}$$

d) From eq. (3.30),

$$\beta = \frac{\beta_a \beta_c}{2.303(\beta_a + \beta_c)}$$

$$\beta = \frac{(0.10 \text{ V})(0.10 \text{ V})}{2.303(0.10 \text{ V} + 0.10 \text{ V})} = 0.0217 \text{ V}$$

and from eq. (3.45),

$$R_p = \frac{\beta}{i_{\text{corr}}} = \frac{0.0217 \text{ V}}{10^{-4} \text{ A/cm}^2}$$

$$R_p = 217 \text{ ohm} \cdot \text{cm}^2$$

Example 3.6 A copper surface area, $A = 100 \text{ cm}^2$, is exposed to an acid solution. After 24 hours, the loss of copper due to corrosion (oxidation) is $15 \times 10^{-3} \text{ grams}$. Calculate a) the current density i in $\mu\text{A/cm}^2$, b) the corrosion rate C_R in mm/y , and c) the number of reactions per unit time. Use the data: $A_w = 63.54 \text{ g/mol}$, $\rho = 8.96 \text{ g/cm}^3$, $q_e = 1.6022 \times 10^{-19} \text{ C/reaction}$.

Solution:

First of all, the corrosion process of copper can be represented by the following anodic reaction:



where the valence is $Z = +2$. Thus,

a) According to Faraday's law the current density is

$$i = \frac{I}{A_s} = \frac{zFm}{A_s t A_w} \quad (3.49a)$$

$$i = \frac{(2)(96,500 \text{ A.s/mol})(15 \times 10^{-3} \text{ g})}{(100 \text{ cm}^2)(24 \times 3600 \text{ s})(63.54 \text{ g/mol})}$$

$$i = 5.27 \mu\text{A/cm}^2$$

b) From eq. (3.48),

$$C_R = \frac{i A_w}{z F \rho}$$

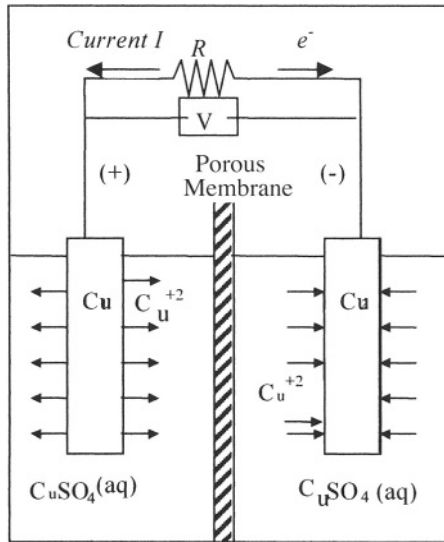
$$C_R = \frac{(5.27 \times 10^{-6} \text{ A/cm}^2)(63.54 \text{ g/mol})}{(2)(96,500 \text{ A.s/mol})(8.96 \text{ g/cm}^3)}$$

$$C_R = 0.06 \text{ mm/y}$$

c) Recall that $1\text{ C} = \text{A}\cdot\text{s}$ so that $q_e = 1.6022 \times 10^{-19}\text{ A}\cdot\text{s}/\text{reactions}$. Thus, the number of reactions per time in seconds is

$$\begin{aligned} r &= \frac{I}{Zq_e} = \frac{iA}{Zq_e} & (3.49b) \\ r &= \frac{(5.27 \times 10^{-6}\text{ A}/\text{cm}^2)(100\text{ cm}^2)}{(2)(1.6022 \times 10^{-19}\text{ A}\cdot\text{s}/\text{reactions})} \\ r &= 1.64 \times 10^{15}\text{ reactions}/\text{s} \end{aligned}$$

Example 3.7 An electrochemical cell shown below was used as a concentration cell in order to measure the current due to the difference in ionic concentration between the anodic half-cell and the cathodic-half cell. Determine the corrosion rate in terms of electrons/second and the number of anodic reactions/second if the measured current is $3.23 \times 10^{-7}\text{ }\mu\text{A} = 3.23 \times 10^{-7}\text{ C}/\text{s}$.



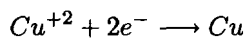
Example 3.7 Ionic concentration cell.

Solution:

The oxidation of copper (corrosion) is due to the following anodic reaction:



and the reduction of copper (electroplating) is due to cathodic reaction



Clearly, the oxidation state is $Z = 2$. Thus, the corrosion rates are

$$\begin{aligned} r &= \frac{I}{q_e} & (3.50a) \\ r &= \frac{3.23 \times 10^{-7} \text{ C/s}}{(1.6022 \times 10^{-19} \text{ C/electrons})} \\ r &= \approx 2 \times 10^{12} \text{ electrons/s} \end{aligned}$$

Also,

$$\begin{aligned} r &= \frac{I}{Zq_e} & (3.50b) \\ r &= \frac{3.23 \times 10^{-7} \text{ C/s}}{(2 \frac{\text{electrons}}{\text{reactions}}) (1.6022 \times 10^{-19} \text{ C/electrons})} \\ r &= 10^{12} \text{ reactions/s} \end{aligned}$$

3.7 IMPEDANCE SPECTROSCOPY

The electrochemical impedance spectroscopy (EIS) method is very useful in characterizing an electrode corrosion behavior. The electrode characterization includes the determination of the polarization resistance (R_p), corrosion rate (C_R), and electrochemical mechanism [1,4,6,19-28]. The usefulness of this method permits the analysis of the alternating current (AC) impedance data, which is based on modeling a corrosion process by an electrical circuit. Several review papers address the electrochemical impedance technique based on the AC circuit theory [22-24,29-30].

The EIS technique is based on a transient response of an equivalent circuit for an electrode/solution interface. The response can be analyzed by transfer functions due to an applied small-amplitude potential excitation at varying signals or sweep rates. In turn, the potential excitation yields current response and vice versa. In impedance methods, a sine-wave perturbation of small amplitude is employed on a corroding system being modeled as an equivalent circuit (Figure 3.8) for determining the corrosion mechanism and the polarization resistance. Thus, a complex transfer function takes the form

$$T = \frac{\text{Output}}{\text{Input}} \quad (\text{a})$$

The transfer functions depend on the angular frequency and are expressed as impedance $Z(\omega)$ and admittance $Y(\omega)$. It should be emphasized that $Z(\omega)$ is the frequency-dependent proportionality factor of the transfer function between the potential excitation and the current response. Thus, for a sinusoidal current

perturbation, the transfer function is the system impedance $[Z(\omega)]$ and for a sinusoidal potential perturbation, the transfer function is the system admittance $[Y(\omega)]$. Hence,

$$Z(\omega) = \frac{E(t)}{I(t)} = Z'(\omega) + jZ''(\omega) \quad (3.51a)$$

$$Y(\omega) = \frac{I(t)}{E(t)} = Y'(\omega) + jY''(\omega) \quad (3.51b)$$

where $E(t)$ = Time-dependent potential (V)

$I(t)$ = Time-dependent current (A)

$\omega = 2\pi f$ = Angular frequency (Hz)

f = Signal frequency (Hz)

$Z'(\omega), Y'(\omega)$ = Real parts

$Z''(\omega), Y''(\omega)$ = Imaginary parts

t = Time (s)

$j = \sqrt{-1}$ = Imaginary operator

$j^2 = -1$

In addition, Ohm's law can be viewed in two different current imposition cases as per ASTM G-106 standard testing method. Hence,

$$E = IR \quad \text{For DC, } f = 0 \text{ Hz} \quad (3.52)$$

$$E = I|Z(\omega)| \quad \text{For AC, } f \neq 0 \text{ Hz} \quad (3.53)$$

Here, $|Z(\omega)|$ is the magnitude of the impedance containing elements of an equivalent circuit, such as capacitors and inductors. Capacitors oppose or impede the current flow. In modeling an electrochemical system as an electrochemical circuit, a potential waveform is applied across the circuit and a current response to the frequency signal generates impedance data. Thus, the impedance data is related to a phase shift angle and a variation in potential and current amplitudes. This technique is a straightforward approach for analyzing the corrosion behavior of a metal [24]. Figure 3.8 shows two schematic electrochemical circuit models. For a charge-transfer control (Figure 3.8a), only the solution resistance (R_s), polarization resistance (R_p), and the capacitor (C_{dl}) are needed in a simple circuit. On the other hand, if the electrochemical system is diffusion-control (Figure 3.8b), a diffusion impedance (Z_D) is incorporated in the circuit.

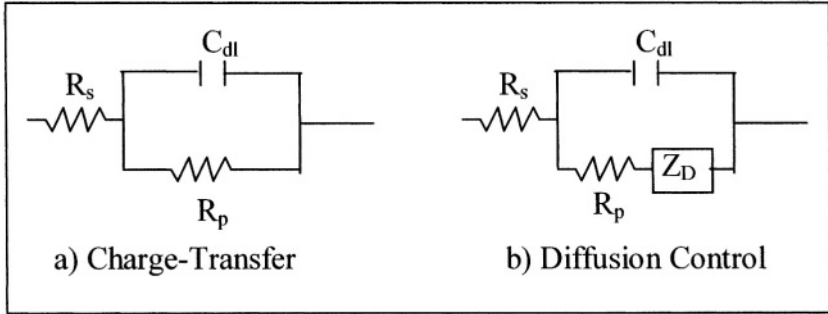


Figure 3.8 Schematic electrochemical circuits.

The potential excitation and its current response are schematically shown in Figure 3.9 as sinusoidal excitations. The electrochemical impedance spectroscopy method is conducted according to the ASTM G-106 standard practice, in which a range of small-amplitude sinusoidal potential perturbation is applied to the electrode/solution interface at discrete frequencies. These frequencies cause an out of phase current response with respect to the applied sinusoidal potential waveform.

If a sinusoidal potential excitation is applied to the electrode/solution interface, the potential, current and impedance can be predicted as per Barn and Faulkner mathematical models [6]. Thus,

$$E(t) = I(t) Z(\omega) = E_o \sin(\omega t) \tag{3.54}$$

$$I(t) = I_o \sin(\omega t + \theta) \tag{3.55}$$

where $E_o, I_o =$ Constants

$\theta =$ Phase shift angle between $E(t)$ and $I(t)$

$\omega = 2\pi f$ and $10 \text{ Hz} \leq f \leq 100 \text{ Hz}$ (intermediate)

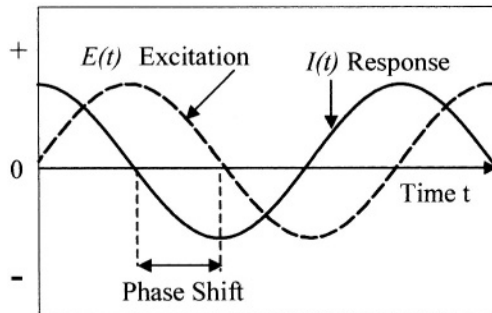


Figure 3.9 Schematic sinusoidal potential excitation.

The magnitude of $Z(\omega)$ and $Y(\omega)$ are

$$|Z(\omega)| = \sqrt{[Z(\omega)']^2 + [Z(\omega)'']^2} \quad (3.56)$$

$$|Y(\omega)| = \sqrt{[Y(\omega)']^2 + [Y(\omega)'']^2} \quad (3.57)$$

and the phase shift angle is defined as

$$\theta = \tan^{-1} [Z(\omega)'' / Z(\omega)'] \quad (3.58)$$

The fundamental characteristic of an AC signal in a simple electrochemical circuit (Figure 3.8a) is described by the impedance of the form [22,24]

$$Z(\omega) = \left[R_s + \frac{R_p}{1 - \omega^2 C^2 R_p^2} \right] - j \left[\frac{\omega C R_p^2}{1 - \omega^2 C^2 R_p^2} \right] \quad (3.59)$$

where C is the interfacial capacitance of a electrical double-layer at the electrode surface (*Farad/cm²*).

For low and high frequency amplitudes, eq. (3.59) yields

$$Z(\omega)_o = R_s + R_p \quad @ \quad \omega = 0 \quad (3.60)$$

$$Z(\omega)_\infty = R_s \quad @ \quad \omega = \infty \quad (3.61)$$

Combining eqs. (3.60) and (3.61) yields the polarization resistance as

$$R_p = Z(\omega)_o - R_s = Z(\omega)_o - Z(\omega)_\infty \quad (3.62)$$

which is the sought output in electrochemical impedance measurements. Equating eqs. (3.45a) and (3.62) yields the corrosion current density in terms of impedance

$$i_{corr} = \frac{\beta}{[Z(\omega)_o - Z(\omega)_\infty]} \quad (3.63)$$

Upon using Faraday's law, eq. (3.63) becomes

$$C_R = \frac{\beta A_w}{[Z(\omega)_o - Z(\omega)_\infty] Z F \rho} \quad (3.64)$$

Further analysis of eq. (3.59), together with eq. (3.52), yields the impedance equation of a circle [22]. Hence,

$$Y(\omega) = \frac{1}{Z(\omega)} = Y'(\omega) + jY''(\omega) \quad (3.65)$$

$$Y'(\omega) = \frac{R_s + R_p + (\omega C R_s R_p)^2}{(R_s + R_p)^2 + (\omega C R_s R_p)^2} \quad (3.66a)$$

$$Y''(\omega) = \frac{\omega C R_p^2}{(R_s + R_p)^2 + (\omega C R_s R_p)^2} \quad (3.66b)$$

and

$$Z'(\omega) = \frac{Y'(\omega)}{[Y'(\omega)]^2 + [Y''(\omega)]^2} \tag{3.67a}$$

$$Z''(\omega) = \frac{Y''(\omega)}{[Y'(\omega)]^2 + [Y''(\omega)]^2} \tag{3.67b}$$

Then, the equation of a circle for charge-control mechanism becomes [22]

$$\left[Z'(\omega) - \left(R_s + \frac{1}{2} R_p \right) \right]^2 + [Z''(\omega)]^2 = \left[\frac{1}{2} R_p \right]^2 \tag{3.68}$$

The locus of eq. (3.68) is schematically shown in Figure 3.10 with a radius of $R_p/2$. This figure is known as the **Nyquist plot**, from which the maximum phase shift angle and polarization resistance become

$$\tan(\theta) \simeq \frac{|Z(\omega)|}{R_p/2} \quad (\nabla abc) \tag{3.69}$$

$$R_p \simeq \frac{2|Z(\omega)|}{\tan(\theta)} \tag{3.70}$$

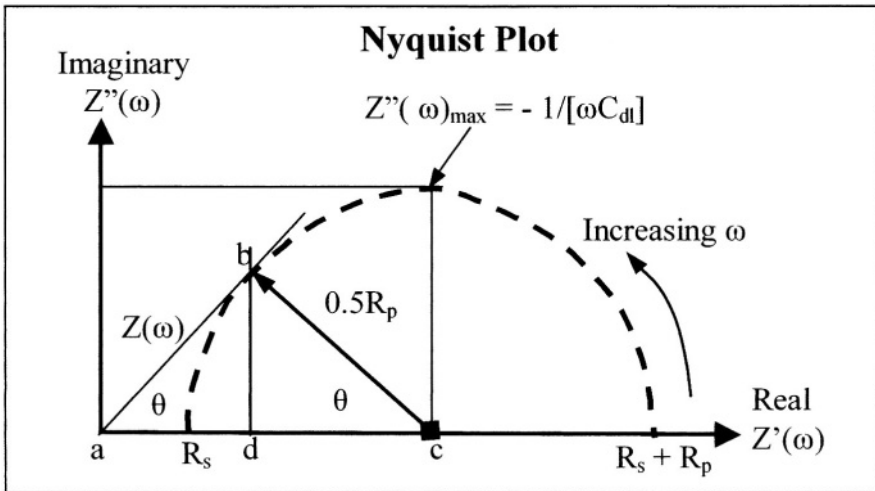


Figure 3.10 Ideal Nyquist plot of impedance for the electrochemical circuit shown in Figure 3.10a. Charge-control mechanism.

Figure 3.11 shows Nyquist plots of a AISI 1030 steel immersed in phosphoric acid (H_3PO_4) containing butanol and thiosemicarbonate (TSC) at room temperature. These data is for a charge-control mechanism with and without the

TSC inhibitor [26]. Notice from this Figure 3.11 that the Nyquist impedance semicircles increase with increasing content of the TSC inhibitor. This implies that the polarization resistance (R_p) also increases with additions of this inhibitor, which in turn, decreases the corrosion rate (C_R) as indicated in Table 3.3.

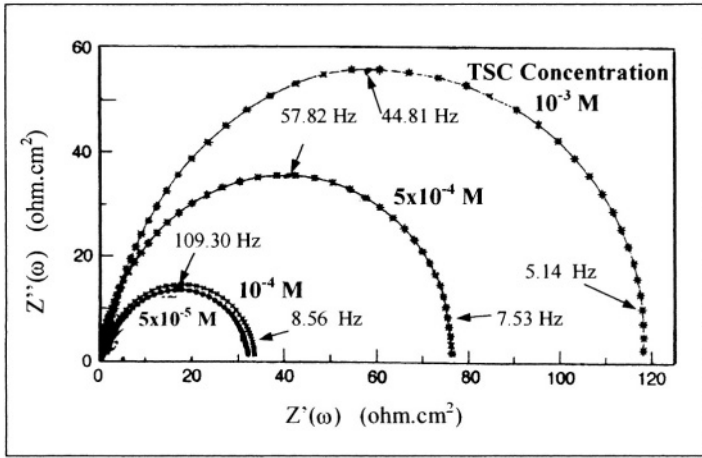


Figure 3.11 Experimental Nyquist plots for AISI 1030 steel in 35% H_3PO_4 + 6% butanol + TSC inhibitor at room temperature [26].

In addition, the double-layer capacitance (C_{dl}) can be calculated using the following expression [31]

$$C_{dl} = 1/[\omega R_p] \quad (3.71)$$

Table 3.3 gives relevant experimental data extracted from the complex Nyquist plot elucidated in Figure 3.11.

Table 3.3 Electrochemical impedance data for AISI 1030 steel [26].

TSC ($\times 10^{-4}$ M)	R_p (Ohm cm^2)	C_{dl} ($\mu F/cm^2$)	C_R (mm/y)
0	4.80	130.80	63.25
0.10	14.50	121.00	20.85
0.50	31.30	77.49	9.65
1.00	33.50	74.08	9.02
5.00	77.90	45.45	3.89
10.00	119.50	39.11	2.52

On the other hand, Figure 3.12 shows schematic **Bode plots** for the circuit in Figure 3.8a with three polarization resistance values. This type of plots show the effect of angular frequency on the impedance and phase shift angle.

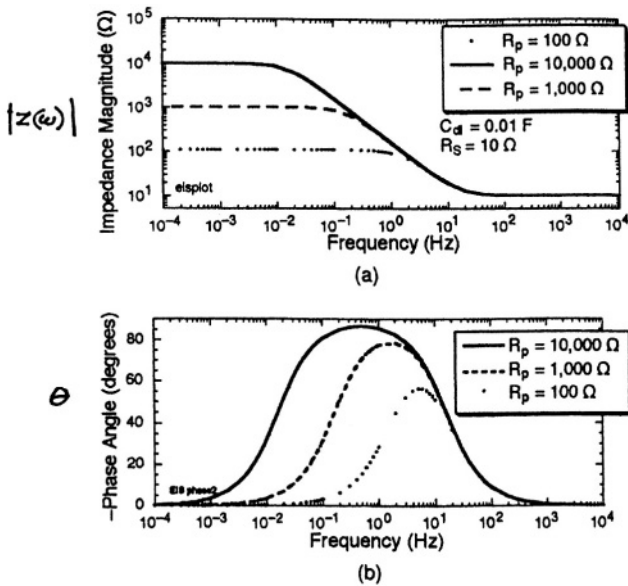


Figure 3.12 Hypothetical Bode plots using the equivalent circuit shown in Figure 3.10a. a) Impedance magnitude and b) phase angle [24].

When an electrochemical process is controlled by diffusion or film adsorption, the electrochemical system can be modeled using the ideal circuit shown in Figure 3.8b. In this case, a diffusion impedance (Z_D) is included in the circuit series and it is known as **Warburg impedance**. Notice that Z_D and R_p are connected in series. An ideal Nyquist-Warburg plot is shown in Figure 3.13

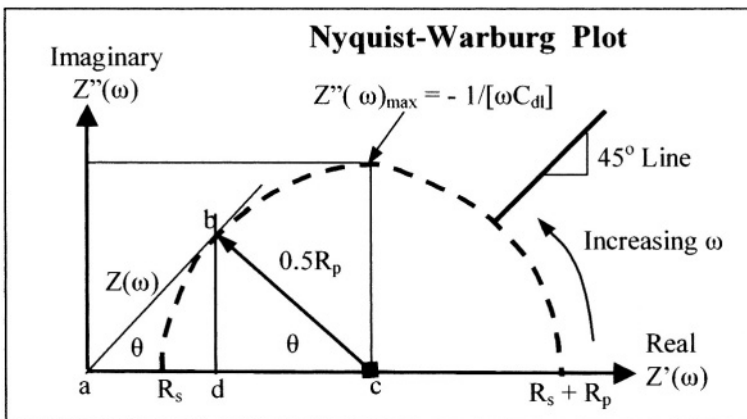


Figure 3.13 Schematic Nyquist-Warburg plot for diffusion control.

The interpretation of Figure 3.13 indicates that the 45° portion of the line corresponds to a low angular frequency range. In this case, the kinetics of the electrochemical system is limited by a diffusion-control process (concentration polarization). Also, extrapolating the semicircle (dashed curve) to intercept the real impedance axis $Z(\omega)'$ graphically defines the polarization resistance R_p . A particular case for using Z_D is when diffusion through a surface film is the rate-controlling of carbon steel immersed in concentrated sulfuric acid (H_2SO_4). Thus, iron (Fe) oxidizes and forms a $FeSO_4$ film [25].

Figure 3.14 shows an experimental Nyquist-Warburg plot for a precipitation hardening (aged) 2195 Al-Li alloy. Notice that the semicircle is depressed due to a diffusion process, which is confirmed by the 45° line. The polarization resistance for this alloy is $R_p = 140 \text{ ohm}$ in an aerated solution containing 3.5% $NaCl$ at $21.5^\circ C$.

The diffusion impedance expression due the formation of a thin oxide film is define by [31-32]

$$Z_D(\omega) = \sigma_w \omega^{-1/2} - j \sigma_w \omega^{-1/2} \coth \left[\delta \left(\frac{j\omega}{D} \right)^{1/2} \right] \quad (3.73)$$

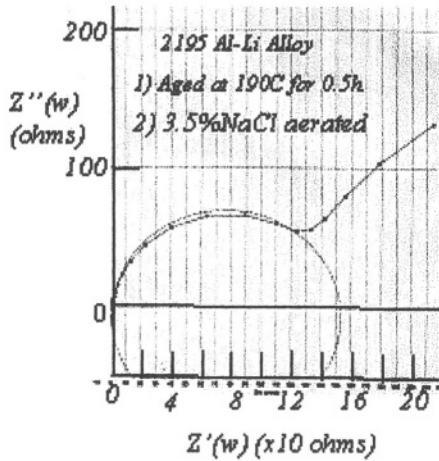


Figure 3.14 Nyquist-Warburg plot for Wledalite 2195 Al-Li alloy.

where $\sigma_w =$ Warburg impedance coefficient $= RT / (zFAC_x \sqrt{2D})$, $\delta =$ Thickness of the diffusion layer, $C_x =$ Concentration of the specie in the diffusion layer and $A =$ Exposed area.

For the 45° Warburg line in Figure 3.13, $Z_D(\omega)$ becomes

$$Z_D(\omega) = \sigma_w \omega^{-1/2} \left(1 - \frac{D}{\omega} \sqrt{\frac{\pi \delta_x}{4}} \right) \quad (3.74)$$

since $\delta \left(\frac{j\omega}{D}\right)^{1/2} = \pi/4$ and from which $j = (D/\omega) \sqrt{(\pi\delta_x)/4}$.

Furthermore, the impedance of a depressed Nyquist plot due to surface roughness, dielectric inhomogeneities and diffusion is defined as the Cole-Cole impedance formula [33-36]. Hence,

$$Z(\omega) = \frac{R_p}{1 + (jR_p C_x)^n} \quad \text{for } 0 < n < 1 \quad (3.75)$$

3.8 CHARACTERIZATION OF ELECTROLYTES

Assume that an electrolyte solution contains positively and negatively charged ions (particles) with valence equals to z^+ and z^- , respectively. If the solution has different type of ions, the number of cations (z^+) and anions (z^-) are, respectively

$$N^+ = \sum N_j^+ = \sum y_j^+ N_A \quad (3.76a)$$

$$N^- = \sum N_j^- = \sum y_j^- N_A \quad (3.76b)$$

where j = Represents species or ions of different valance
 y_j^+, y_j^- = Number of moles

Let an applied electrical field disturb the thermodynamical equilibrium so that the ions migrate a distance x from their initial position toward the electrode of opposite charge due to exerted electric forces on them as the charge carriers. Hence, an electrical mobility B_j generates in the solution. Consequently, the distance traveled by ions to the opposite charged electrode (Figure 3.15) is [5]

$$x_j^+ = v_j^+ dt \quad (3.77a)$$

$$x_j^- = v_j^- dt \quad (3.77b)$$

where v_j^+ = Velocity of cations (cm/s)
 v_j^- = Velocity of anions (cm/s)
 dt = Infinitesimal change of time (s)

The number of ions that travel distance x_j is

$$N^+ = \sum \frac{N_j^+ x_j^+}{L} \quad (3.78a)$$

$$N^- = \sum \frac{N_j^- x_j^-}{L} \quad (3.78b)$$

where L = Distance between electrodes (Figure 3.15).

Recall that electrical conduction is a mass transport phenomenon, in which electrons and ions carry the electric charge due to their particular mobility within the electrically charged system. Hence, the charge (Q) that passes through the cross-section of the electrolyte solution (conductor) at time dt is related to the rate of flow of charge referred to as the current (I). It should be mentioned that the electrons carry the current through the wires and electrodes, while the ions carry the current through the solution.

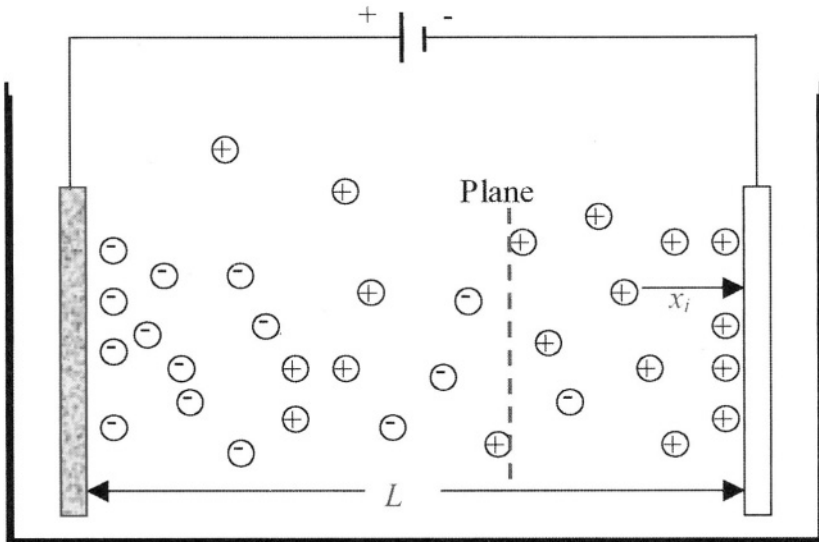


Figure 3.15 Schematic cell showing the ionic travel distance.

This phenomenon implies that electrochemical reactions occur at the electrode-solution interface by transferring electrons from or to the electrode. For instance, if $Cu^+ + 2e^- \rightleftharpoons Cu$ occurs, this means that one mole of Cu is deposited on the electrode surface while 2 moles of electrons flow through the circuit. This situation resembles an electrolysis process in which the cation valence is $z_{Cu}^+ = 2$ electrons. Nevertheless, if the current is kept constant, the charge (q) that flows through the circuit is

$$dq = Idt \quad (3.79)$$

The total charge crossing a plane parallel to the electrodes in time dt [5]

$$\frac{dq^+}{dt} = \frac{z_j^+ q_e v_j^+ N_j^+}{L} \quad (3.80a)$$

$$\frac{dq^-}{dt} = \frac{|z_j^-| q_e v_j^- N_j^-}{L} \quad (3.80b)$$

where $q_e = \text{Electron charge} = 1.602 \times 10^{-19} \text{ C}$.

In addition, the current I and density (i) are

$$I = \frac{dq}{dt} \quad (3.81)$$

$$i = \frac{1}{A} \frac{dq}{dt} \quad (3.82)$$

Combining eq. (3.80) and (3.82) yields

$$i^+ = \sum \frac{z_j^+ q_e v_j^+ N_j^+}{V} \quad (3.83a)$$

$$i^- = \sum \frac{|z_j^-| q_e v_j^- N_j^-}{V} \quad (3.83b)$$

where $V = AL = \text{Volume of the solution (cm}^3\text{)}$.

The concentration (activity) of ions is

$$C_j^+ = \frac{1}{V} \sum y_j^+ \quad (3.84a)$$

$$C_j^- = \frac{1}{V} \sum y_j^- \quad (3.84b)$$

Combining eqs. (3.10a), (3.76), (3.84) and (3.83) yields

$$i^+ = \sum z_j^+ F v_j^+ C_j^+ \quad (3.85a)$$

$$i^- = \sum z_j^- F v_j^- C_j^- \quad (3.85b)$$

The total current density becomes $i = i^+ + i^-$ as in electrolysis. Hence,

$$i = \sum z_j^+ F v_j^+ C_j^+ + \sum |z_j^-| F v_j^- C_j^- \quad (3.86)$$

The ionic velocity v_j for migration toward the electrode is small when compared with the random velocity v_r , based on the translational kinetic energy in the absence of an electrical field [5]. This is mathematically shown below

$$\frac{3}{2} kT = \frac{1}{2} m v_{r,j}^2 \quad (3.87)$$

From eqs. (3.85) and (3.87),

$$v_{r,j}^+ = \sqrt{\frac{3kT}{m_j^+}} \gg v_j^+ = \frac{i^+}{z_j^+ F v_j^+ C_j^+} \quad (3.88a)$$

$$v_{r,j}^- = \sqrt{\frac{3kT}{m_j^-}} \gg v_j^- = \frac{i^-}{z_j^- F v_j^- C_j^-} \quad (3.88b)$$

where m_j^\pm = Mass of cations (species).

In addition, electroneutrality is achieved when the rate of charge for cations and anions balance and this is represented by $dq^+/dt = dq^-/dt$. However, the "quality" of the electrolyte to act as an aqueous electrical conductor can be characterized by its conductivity parameter K_c . For a one-dimensional analysis, K_c is

$$K_c = i/F_x = 1/\rho_c \quad (3.89)$$

where K_c = Conductivity ($ohm^{-1} \cdot cm^{-1}$)

ρ_c = Resistivity ($ohm \cdot cm$)

$F_x = -d\phi/L \approx -\Delta\phi/L$ = Electrical force gradient (V/cm)

ϕ = Electrical potential at a point in the electrolyte solution (V)

Furthermore, the effectiveness of ion migration can be characterized by the ionic mobility (B_j) in the solution when an electrical force field acts on the ions. This implies that the ionic mobility is related to the electrolyte conductivity. This can be assessed by substituting eq. (3.86) into (3.89)

$$K_c = \frac{1}{F_x} \left(\sum z_j^+ F v_j^+ C_j^+ + \sum |z_j^-| F v_j^- C_j^- \right) \quad (3.90)$$

$$K_c = \sum z_j^+ F B_j^+ C_j^+ + \sum |z_j^-| F B_j^- C_j^- \quad (3.91)$$

since the ionic or electrical mobility is defined as

$$B_j = v_j/F_x \quad (3.92)$$

which has units of $cm^2/(V \cdot s) = mol \cdot cm^2/(J \cdot s)$. Normally, an electrochemical process is analyzed using a particular metal ion M^{+z} in solution. Assuming that this is the case, eq. (3.91) can be treated in a general form. Hence,

$$K_c = z_j F B_j C_j \quad (3.93)$$

Then, B_j and i become

$$B_j = \frac{K_c}{z_j F C_j} \quad (3.94)$$

$$i = z_j F v_j C_j \quad (3.95)$$

From this crude approximation, one can determine the diffusion coefficient or diffusivity of the metal cation M^{+z} as follows. Multiply both sides of eq. (3.94) by the Boltzmann constant k and the absolute temperature T so that

$$kTB_j = kT \frac{K_c}{zFC_j} \quad (3.96)$$

Notice that kTB_j is the Nernst-Einstein diffusion coefficient D , which is the rate of swept area of cations [45]. Hence, the **Nernst-Einstein equation** is

$$D = kTB_j \quad (3.97)$$

and

$$D = kT \left(\frac{K_c}{zFC_j} \right) \quad (3.98)$$

The subject of diffusion is well documented [37-45] and it is a manifestation of continuous atom or ion motion at random from position to a neighboring position in the atomic structure of solids (S), liquids (L), and gases (G). Thus, the diffusivity is related to the atomic jump frequency and jump distance. However, $D_L > D_s$ at a constant or the same temperature and diffusion in liquids differ from diffusion in solids since the geometry of atomic arrangement in liquids is not completely understood.

In addition, electrolytes and n-type semiconductors conduct current by transport of ions and electron, respectively. Both ions and electrons are the charge carriers for both sources. With regard to an electrolyte under the influence of an electrical field, it can be expected that ions drift through the bulk aqueous medium at a lower velocity than the electron velocity. However, the nature of the ions and their concentration influence both electrolyte conductivity K_c and ionic mobility B_j as predicted by eqs. (3.93) or (3.94). If a relatively low steady potential (voltage) is applied to electrodes, virtually current ceases to flow after the electrical double-layer capacitor C_{dl} is positively charged on the negative electrode surface and negatively charged on the opposite side at a distance δ from the electrode surface. The charged double-layer acts as an electrical capacitor, which breaks down as the applied potential is increased beyond a critical potential for current flow to resume motion across the electrode-electrolyte interface. In this case, metal oxidation occurs at the positive electrode, while reduction occurs at the negative electrode. Consequently, current flow causes energy dissipation as heat in the electrolyte since the ions must overcome frictional forces during their motion through the medium [42].

3.9 ELECTROLYTE CONDUCTIVITY

The influence of an electrical field on an electrolyte can also be characterized by measurements of the electrolyte electrical conductivity. In fact, electrolytes conduct current by the bulk ionic mass transport and charge carrier across the ionic

double-layer at the electrode surface. Consequently, K_c in eq. (3.96) strongly depends on the ionic concentration, temperature, and ionic mobilities. The application of an external potential along with an alternating current (AC) mode of frequency f causes current flow through the bulk electrolyte and charges the ionic double-layer (Figure 2.7) as a capacitor. If current flows, then dissipation of electrical energy arises as heat in the bulk electrolyte and electrical energy is stored in the double layer capacitor. The dissipation of energy is attributed to the frictional forces during ionic mobility caused by the inner potential (ϕ). Thus, ϕ is the driving force for Faradaic processes (e.g. reduction and oxidation reactions) and electrolyte Ohmic resistance [42].

The Wheatstone bridge shown in Figure 3.16 can be used to determine the electrolyte resistance (R_s). This is a classical technique reviewed by Braunstein-Robbins [42] who provided clear details on the current topic. Moreover, only one Wheatstone bridge case is briefly described hereafter.

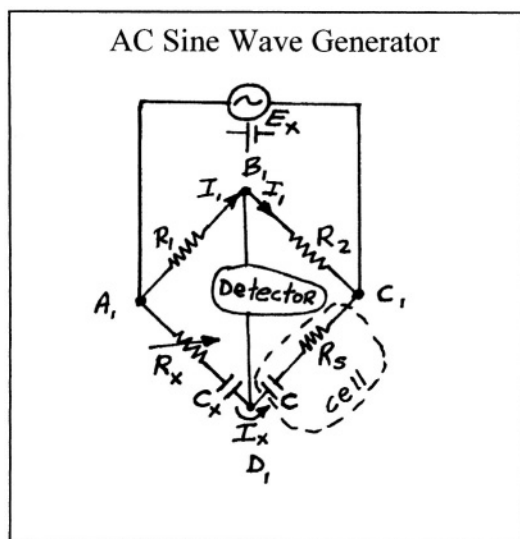


Figure 3.16 Wheatstone bridge with a series RC circuit [42].

The K_c expression given by eq. (3.89) is redefined as [43]

$$K_c = \frac{L}{A_e} \frac{1}{R_s} = \frac{\lambda}{R_s} \quad (3.99)$$

where $\lambda = L/A_e = \text{Cell constant (cm}^{-1}\text{)}$

$L = \text{Distance between electrodes (cm)}$

$A_e = \text{Cross-sectional area of the electrolytic conducting path (cm}^2\text{)}.$

According to Braunstein-Robbins [42], the Kholrausch method [43] can be used for evaluating K_c . In this method, the electrodes are electrolytically coated with colloidal platinum black in order to

- increase the electrode surface area
- reduce the polarization resistance that may develop and
- adsorb any gases produced during the cycle of the alternating current.

On the other hand, AC is used in order to avoid changes of electrolyte resistance due to changes in concentration of the electrolyte and buildup of electrolysis products at the electrode surfaces [5]. Subsequently, R_s is measured at potential frequency (f) by adjusting the resistance R_x so that the current and potential are in-phase, which require a variable external conductance (C_x). Also included in the Wheatstone bridge is the double-layer capacitor (C). Let's use two different balance conditions.

1) If the capacitance C_x and C are excluded, then for a pure resistance case the potential across points B_1D_1 is $E_{B_1D_1} = 0$ and the potential balance according to Ohm's law is

$$I_1 R_1 = I_x R_x \quad (a)$$

$$I_1 R_2 = I_x R_s \quad (b)$$

Eliminating I_1 from eqs. (a) and (b) yields

$$R_s = R_x R_2 / R_1 \quad (c)$$

Then, eq. (3.99) becomes

$$K_c = \frac{L}{A} \frac{1}{R_s} = \frac{\lambda R_1}{R_x R_2} \quad (3.100)$$

2) If the capacitance C_x and C are included, then the circuit is not a pure resistance case and the potential drop across points B_1D_1 is defined in terms of impedance. Hence,

$$Z(\omega)_s = Z'(\omega)_s + jZ''(\omega)_s = R_s - j\left(\frac{1}{\omega C}\right) \quad (3.101)$$

$$Z(\omega)_x = Z'(\omega)_x + jZ''(\omega)_x = R_x - j\left(\frac{1}{\omega C_x}\right) \quad (3.102)$$

This implies that $Z(\omega)_s = Z(\omega)_x$, $C = C_x$, and $R_s = R_x$. Inserting $Z'(\omega)_x$ and $Z''(\omega)_x$ into eq. (3.56) gives

$$|Z(\omega)_x| = \sqrt{R_x^2 + 1/(\omega C_x)^2} \quad (3.103)$$

Inserting eq. (3.103) into eq. (3.53) yields

$$E_x = I_x \sqrt{R_x^2 + 1/(\omega C_x)^2} \quad (3.104)$$

For an AC case with $f \neq 0$ Hz, eq. (3.99) becomes

$$K_c = \frac{\lambda}{|Z(\omega)_x|} \quad (3.105)$$

$$K_c = \lambda \left[R_x^2 + 1/(\omega C_x)^2 \right]^{-1/2} \quad (3.106)$$

The potential expression given by eq. (3.104) can also be derive using complex function [42]. Hence,

$$E = E_o e^{j\omega t} \quad (3.107)$$

$$I = I_o e^{j\omega t} \quad (3.108)$$

The charge (q) stored in the double-layer capacitor (C_x) is related to the potential drop (E_c) across the capacitor as indicated below

$$q = C_x E_c \quad (3.109)$$

$$E_c = E - IR_x \quad (3.110)$$

Combining eqs. (3.109), (3.110) and (3.81) yields

$$I = C_x \frac{dE}{dt} - R_x C_x \frac{dI}{dt} \quad (3.111)$$

Now, using the complex functions defined by eqs. (3.107) and (3.108) on (3.111) gives

$$I_o e^{j\omega t} = j\omega C_x e^{j\omega t} - j\omega R_x C_x e^{j\omega t} \quad (a)$$

Thus,

$$E_o = I_o \left[R_x - j \left(\frac{1}{\omega C_x} \right) \right] = I_o Z(\omega) \quad (b)$$

Letting $E_x = |E_o|$, $I_x = |I_o|$, and $Z(\omega)_x = |Z(\omega)| = \sqrt{R_x^2 + 1/(\omega C_x)^2}$ yields the applied potential

$$E_x = I_x \sqrt{R_x^2 + 1/(\omega C_x)^2} \quad (3.104)$$

3.10 SUMMARY

In determining the rate of corrosion of a metal M , one needs to know the kinetic parameters prior to computing it. Thus, the current density function $i = f(\eta, i_{\text{corr}}, \beta_a, \beta_c)$ allows the evaluation of the corrosion behavior under activation polarization at steady-state conditions. In order for polarization to occur on a metal surface, an overpotential $\eta \neq 0$ must develop in the electrochemical system and it is defined by the Tafel equation. Three electrochemical methods were described for determining i_{corr} . For instance, the linear polarization method is applied at a small potential range of $\Delta E \pm 10 \text{ mV}$ from the E_{corr} value. This method provides result for i_{corr} , R_p , β_a , and β_c . On the other hand, the extrapolation method generates anodic and cathodic curves near the corrosion potential. These curves normally a small part of linearization from which the Tafel slopes are determined and extrapolation of the linear lines converge at E_{corr} where i_{corr} is defined. The third method deals with impedance spectroscopy measurements (ISM). It is based on a transient current response to a potential excitation. This method allows the determination of the impedance $Z(\omega)$ as a measurement of the polarization resistance (R_p) and generates impedance data for modeling a corrosion process based on an electrochemical circuit containing resistances and capacitors. This impedance technique is based on AC circuit theory. The output of the impedance technique is a Nyquist plot for charge-transfer or Nyquist-Warburg plot for diffusion control.

Finally, mathematical models based on diffusion describe the generation of current density in a electrolyte solution in terms of ionic mobility and conductive capacity of the electrolyte. Hence, the Nernst-Einstein equation for diffusivity was determined.

3.11 PROBLEMS/QUESTIONS

3.1 What are the three conditions for galvanic corrosion to occur?

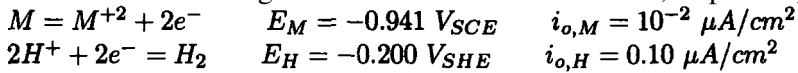
3.2 If the state of equilibrium of an electrochemical cell is disturbed by an applied current density i_x , then $i_a = -i_c = i_{\text{corr}}$ no longer holds. Let i_x be a cathodic current density and the slope of the corresponding polarization curve be $dE/d\log(i_x)$, which increases approaching the Tafel constant β_c . Determine a) the value of i_x when $i_c = 10^{-3} \text{ A/cm}^2$ and $i_a = 10^{-9} \text{ A/cm}^2$ and b) the value of β_c when $i_{\text{corr}} = 10^{-5} \text{ A/cm}^2$ and $\eta = -0.20 \text{ V}$. [Solutions: a) $i_x = 10^{-3} \text{ A/cm}^2$ and b) $\beta_c = 0.10 \text{ V}$].

3.3 According to the Stockholm Convention Cell $Fe | Fe^{+2} | H^+, H_2 | Pt$, the corrosion potential of iron (Fe) is -0.70 V_{SCE} at $pH = 4.4$ and 25°C in a deaerated (no oxygen is involved) acid solution. Calculate a) the corrosion rate in mm/y when

$$\begin{array}{ll} i_{o,H} = 10^{-6} \text{ A/cm}^2 & \beta_c = -0.10 \text{ V}_{SHE} \\ i_{o,Fe} = 10^{-8} \text{ A/cm}^2 & E_{Fe} = -0.50 \text{ V}_{SHE} \end{array}$$

b) the Tafel anodic slope β_a and c) draw the kinetic diagram E vs. $\log i$ [Solutions: a) $C_R = 1.16 \text{ mm/y}$, b) $\beta_a = 0.010 V_{SHE}$].

3.4 Let the following anodic and cathodic reactions be, respectively



where $i_{corr} = 10^2 \mu A/cm^2$ and $E_{corr} = -0.741 V_{SCE}$. a) Construct the corresponding kinetic diagram and b) determine both β_a and β_c from the diagram and from the definition of overpotential equations. [Solutions: b) $\beta_a = 0.05 V_{SHE}$ and $\beta_c = 0.10 V_{SHE}$].

3.5 A steel tank is hot dipped in a deaerated acid solution of $5 \times 10^{-4} \text{ mol/cm}^3$ molality zinc chloride ($ZnCl_2$) so that a 0.15-mm zinc coating is deposited on the steel surface. This process produces a galvanized steel tank. Calculate the time it takes for the zinc coating to corrode completely at a $pH = 4$. Data: $E_{Zn} = -0.8 V$, $i_{o,Zn} = 10 \mu A/cm^2$, $i_{o,H} = 10^{-3} \mu A/cm^2$, $\beta_a = 0.08 V$, $\beta_c = 0.12 V$, $T = 25^\circ C$. [Solution: $t \simeq 0.40 \text{ years}$].

3.6 Calculate the activity and the corrosion rate of iron (Fe) immersed in an aerated aqueous solution of $pH = 9$. The dissociation constant for ferrous hydroxide, $Fe(OH)_2$, is 1.64×10^{-14} . Given data:

$$\begin{array}{lll} i_{o,Fe} = 10^{-2} \mu A/cm^2 & E_{corr} = -0.30 V & \beta_a = 0.10 V \\ A_{w,Fe} = 55.85 \text{ g/mol} & \rho_{Fe} = 7.86 \text{ g/cm}^3 & \end{array}$$

[Solution: $[Fe^{+2}] = 1.64 \times 10^{-4} \text{ mol/l}$ and $C_R = 232 \mu m/y$].

3.7 Plot the anodic data given below and determine the polarization resistance (R_p) and the anodic Tafel slope (β_a) for a metal M . Use $\beta_c = 0.07 V$ and $i_{corr} = 0.019 A/cm^2$.

$M = M^{+2} + 2e^-$	$i (\mu A/cm^2)$	$E (V_{SHE})$
$2H^+ + 2e^- = H_2$	0.08	-0.32
	0.10	-0.30
	0.15	-0.25
	0.18	-0.22
	0.20	-0.20

[Solution: $R_p = 1 \text{ ohm} \cdot \text{cm}^2$ and $\beta_a = 0.12 V$].

3.8 Why does a pearlitic steel corrode rapidly in an acidic solution?

3.9 Why will the tip and the head of an iron nail behave as anodes relative to the shank? See Figure 1.10a.

3.10 It is known that the standard electrode potential (E°) for pure crystalline zinc is -0.763 V . Will this value change by cold working and impurities? Explain.

3.11 An electrolyte contains a very low activity ($8 \times 10^{-9}\text{ mol/l}$) of silver cations (Ag^+) and an unknown concentration of copper cations. If the cell potential difference between the copper anode and the silver cathode is -0.04 V , determine a) which cation will be reduced (electroplated) on the cathode and b) the concentration of $[\text{Cu}^{+2}]$ in g/l at 40°C . Neglect the effects of other ions that might react with silver. [Solution: a) Ag will be reduced and b) $[\text{Cu}^{+2}] = 60.19\text{ g/l}$].

3.12 Suppose that a cold worked copper electrode has $8,000\text{ J/mol}$ stored energy and it dissolves in an aqueous electrolyte. Calculate the overpotential.

3.13 What is the significant differences between the overpotential (η) and the Ohmic potential (E)?

3.14 If a sheet of zinc (Zn) is placed in hydrochloric acid (HCl), Zn goes into solution. Why?

3.15 Calculate the equilibrium constant at 25°C for the electrochemical cell shown in Figure 2.4. [Solution: $K = 1.64 \times 10^{37}$].

3.16 Show that $\Delta G = zF\beta_a \log(i_a/i_{corr})$ where the local potential E can be defined by the Nernst equation.

3.17 If an electrochemical cell operates at 10 amps , 25°C , and 101 kPa for 30 minutes, calculate a) the number of moles and b) the weight of copper would be produced. [Solution: a) $N = 0.093$ moles and b) $W = 5.93\text{ grams}$].

3.18 a) Derive the Arrhenius equation from the general definition of the activation energy of any rate reaction process and determine the Arrhenius constants if $r_1 = 10^{11}\text{ s}^{-1}$, $r_2 = 4r_1$, $T_1 = 200^\circ\text{K}$ and $T_2 = 400^\circ\text{K}$. b) Plot r vs. $1/T$ @ $200^\circ\text{K} \leq T \leq 400^\circ\text{K}$.

3.19 Plot the given conductivity data vs. the aqueous $\text{Cu}^{+2}\text{SO}_4^-$ concentration at 25°C and 1 atm . (The data was taken from Ref. [5]). Conduct a nonlinear regression analysis on these data and explain the resultant curve.

C (mol/cm^3) $\times 10^{-6}$	K_c ($\text{ohm}^{-1} \cdot \text{cm}^{-1}$) $\times 10^{-3}$
0	0
25.00	3.00
50.00	5.10
75.00	7.40
100.00	8.50
102.50	10.00
105.00	12.00
107.50	14.00
200.00	15.00
202.50	16.00

3.20 An electrochemical cell operates at a small overpotential and the corroding metal is exposed to a H^+ ion-containing electrolyte. Use the given data

$\eta = 0.005 \text{ V}$	$T = 25^\circ\text{C}$
$i = 3.895 \times 10^{-8} \text{ A}/\text{cm}^2$	$\rho = 7.14 \text{ g}/\text{cm}^3$
$i_o = 10^{-7} \text{ A}/\text{cm}^2$	$D = 10^{-5} \text{ cm}^2/\text{s}$
$C_R = 5.8277 \times 10^{-4} \text{ mm}/\text{y}$	

in order to determine a) the corroding metal by calculating the atomic weight A_w and determining its anodic reaction. Assume that there is a linear relationship between the current density and the overpotential. b) The activity of the corroding metal if $a_{H^+} = 1 \text{ mol}/\text{l}$, c) the free energy change ΔG . Will the reaction you have chosen occur?, d) the ionic velocity of the corroding metal. As a crude approximation, neglect the ionic velocity of other ions in solution, e) The ionic mobility B_e and f) electrolyte conductivity neglecting other ions present in the electrolyte. [Solution: b) $6.77 \times 10^{-4} \text{ mol}/\text{cm}^3$, d) $v_i \simeq 2.98 \times 10^{-10} \text{ cm}/\text{s}$].

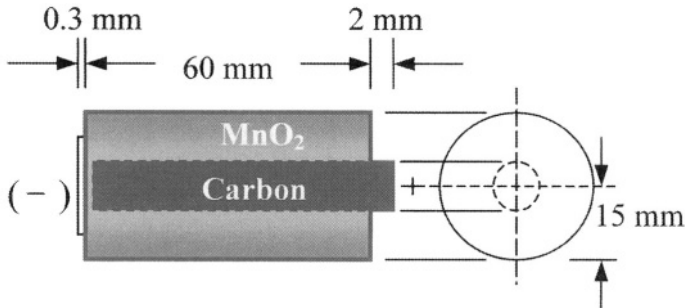
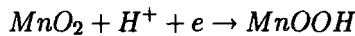
3.21 If an electrochemical copper reduction process is carried out at 5 amperes. for 20 minutes, determine a) the electric charge (amount of coulombs of electricity), b) the number of electrons if there are $1/(1.6022 \times 10^{-19}) = 6.24 \times 10^{18} \text{ electron}/\text{C}$, c) the number of moles, d) Faraday's weight reduced on a cathode, and the reduction rate (production rate in Chapter 7). Data: $A_w = 63.55 \text{ g}/\text{mol}$ and $T = 35^\circ\text{C}$. [Solutions: a) $Q = 6,000 \text{ C}$, b) $\simeq 4 \times 10^{22}$ electrons, c) $N = 0.0311 \text{ moles}$, d) $W = 1.98 \text{ g}$, and e) $P_R = 5.94 \text{ g}/\text{h}$].

3.22 Calculate the overpotential that causes hydrogen evolution on a flat platinum (*Pt*) electrode surface immersed in an acid solution, when the applied cathodic and exchange current densities are $6,000 \mu\text{A}/\text{cm}^2$ and $100 \mu\text{A}/\text{cm}^2$, respectively. Assume a symmetry factor of 0.50 at room temperature (25°C). [Solution: $\eta_c = -0.21 \text{ V}$].

3.23 Consider a discharge (chemical desorption) mechanism as the rate determining for $Ni^{+2} + 2e^- = Ni$ at $25^\circ C$ in a nickel battery. Calculate the cathodic Tafel slope per decade if the symmetry factor is 0.50, the exchange current density is constant, and the cathodic overpotential is $\eta_c < 0$. [Solution: $\beta_c = -0.06 V/decade$].

3.24 Plot the normalized current profile as a function of both symmetry factor (α) and overpotential; that is, $i/i_o = f(\alpha, \eta)$ when the oxidation state is defined is $z = 2$ and $\alpha = 0.35, 0.50$ and 0.75 at room temperature ($25^\circ C$). Explain the polarization behavior very succinctly.

3.25 Calculate the number of moles and mass of a) the battery zinc (Zn) casing and b) the manganese dioxide (MnO_2) in the electrolyte if the battery has a stored energy of $36 kJ/V$ and a power of $3 Watts$. Calculate c) the time it takes to consume the stored energy if the battery operates at a current of $2 A$ and d) the potential (voltage). The thickness of the cell casing is $x = 1 mm$ and other dimensions are indicated below. The discharging reaction is



[Solution: a) $40.34 g$ and $0.62 moles$, b) $0.37 moles$ and $32.17 g$, c) $5 h$ and $1.5 V$]

3.26 A plate of pure nickel (Ni) oxidizes in an electrochemical cell containing an acid solution at $25^\circ C$. The total surface area of the nickel plate is $100 cm^2$. If 2×10^{16} electrons per second are relieved on the plate surface, then calculate a) the corrosion rate in mm/y and b) the mass of nickel being lost in a year. [Solution: a) $C_R = 0.35 mm/y$ and b) $m = 31.15 g$].

3.27 Use the data listed in Table 3.3 to perform a least squares analysis and subsequently, determine the polarization proportionality constant β . Let the atomic weight and the density of the steel be $A_{w,steel} \simeq A_{w,Fe} = 55.85 g/mol$ and $\rho = 7.85 g/cm^3$, respectively. [Solution: $\beta = 0.03 V$].

3.28 Equal amounts of $CuSO_4$ and $NiSO_4$ are dissolved with water to make up an electrolyte. Hypothetically, the ion velocities and concentrations are

$$\begin{aligned} v_{Cu^{+2}} &= 0.22 \text{ cm/s} & C_{Ni^{+2}} &= 10^{-5} \text{ mol/cm}^3 \\ v_{SO_4^{-2}} &= 0.1 \text{ cm/s} & C_{SO_4^{-2}} &= 10^{-5} \text{ mol/cm}^3 \\ C_{Cu^{+2}} &= 10^{-5} \text{ mol/cm}^3 \end{aligned}$$

If the current density is 1 A/cm^2 , calculate the velocity of the nickel ions (Ni^{+2}). [Solution: 0.20 cm/s].

3.29 An electrochemical cell operates at 10 A , $R_x = 0.25 \text{ ohm}$, and $\omega = 50 \text{ Hz}$. Determine a) the electrolyte resistance (R_s), b) the potential E_x when the external resistance and the capacitance are $R_x = 0.25 \text{ ohm}$ and $C_x = 20 \text{ A.s/V}$ at $30^\circ C$ and c) the electrolyte conductivity K_c . The distance between electrodes is $L = 15 \text{ cm}$ and the effective electrode surface is $A = 8,000 \text{ cm}^2$. [Solution: a) $Z(\omega)_x = 0.25 \text{ ohm}$, b) $E_x = 2.5 \text{ V}$ and c) $K_c = 7.50 \times 10^{-3} \text{ ohm}^{-1} \cdot \text{cm}^{-1}$].

3.30 Determine and analyze the impedance profile by varying the angular frequency for fixed $R_x = 0.25 \text{ ohm}$ and $C_x = 20 \text{ A.s/V}$.

3.31 Assume that an electrolytic cell is used for recovering nickel from a solution containing 10^{-4} mol/cm^3 of Ni^{+2} at $35^\circ C$. The nickel ionic mobility and the electric-field strength are $B = 55 \times 10^{-5} \text{ cm}^2 V^{-1} s^{-1}$ and $F_x = 10 \text{ V/cm}$ [Taken from reference 5], respectively, calculate a) the ionic velocity (v), b) the solution electric conductivity (K_c) and the electric resistivity (ρ_c). [Solution: a) $v = 0.0055 \text{ cm/s}$, b) $K_c = 0.0106 \text{ ohm}^{-1} \cdot \text{cm}^{-1}$ and c) $\rho_c = 94.21 \text{ ohm} \cdot \text{cm}$].

3.32 It is known that current flows when there exists a gradient of electric potential ($d\phi/dx$) within an electric conductor, such as an electrolyte. Consider a current-carrying homogeneous conductor with constant cross-sectional area (A_c) so that the electric-field strength (E_x) is constant at every point in the conductor. Derive an expression for the current as a function of the gradient of electric potential. In this particular problem "x" stands for direction as well as length of the electric conductor. Start with the following current density definition $i = K_c E_x$, where K_c is the electric conductivity ($\text{ohm}^{-1} \cdot \text{cm}^{-1}$).

3.12 REFERENCES

[1] M.G. Fontana, "Corrosion Engineering," third edition, McGraw-Hill Book Company, New York, (1986).

[2] T.N. Andersen and H. Eyring, "Principles of Electrode Kinetics" in Physical Chemistry: An Advanced Treatise, Vol. IXA/Electrochemistry, Edited by Henry Eyring, Academic Press, Inc., (1970).

- [3] D.W. Shoesmith, "*Kinetics of Aqueous Corrosion*," in Corrosion, ASM Handbook, Vol. 13, American Society for Metals, Ninth edition, (1987).
- [4] D.A. Jones, "*Principles and Prevention of Corrosion*," Macmillan Publishing Company, New York, (1992).
- [5] I.N. Levine, "*Physical Chemistry*" McGraw-Hill Book Company, New York, (1978) 454-459, 498-500.
- [6] A.J. Bard and L.R. Faulkner, "*Electrochemical Methods*," John Wiley & Sons, New York, (1980) 316.
- [7] L.L. Shreir, "*Outline of Electrochemistry*," in Corrosion, Vol. 2, Corrosion Control, Edited by L.L. Shreir, R.A. Jarman, and G.T. Burstein, Butterworth-Heinemann, Boston, (1994).
- [8] U.R. Evans, J. Franklin Institute, 208 (52) (1929).
- [9] U.R. Evans, "*The Corrosion and Oxidation of Metals*," Arnold, London, (1961).
- [10] M. Stern, J. Electrochem. Soc., 104 (1957) 56.
- [11] M. Stern, J. Corrosion, 13 (1957) 755.
- [12] L.L. Shreir, "*Corrosion in Aqueous Solutions*" in Corrosion, , Vol. 1, Metal/Environment Reactions, Edited by L.L. Shreir, R.A. Jarman, and G.T. Burstein, Butterworth-Heinemann, Boston, (1994).
- [13] J.R. Scully, "*Electrochemical Methods of Corrosion Testing*," in Corrosion, Vol. 13, Laboratory Testing, ninth edition, ASM Inter. (1987) 213.
- [14] H.P. Hack, "*Evaluation of Galvanic Corrosion*," in Corrosion, Vol. 13, Ninth edition, ASM Inter., (1987) 236.
- [15] J.R. Maloy, J. Chem. Educ., 60 (1983) 285.
- [16] J. Wang, "*Analytical Electrochemistry*," Second edition, Wiley-VCH, Inc., (2000) 4-7.
- [17] J.W. Evans and L.C. De Jonghe, "*The Production of Inorganic Materials*" Macmillan Publishing Company, New York, (1991) 149.
- [18] T. Erdey-Cruz, "*Kinetics of Electrode Processes*" Wiley-Interscience, New York, (1972) 442.
- [19] D.D. McDonald, J. Electrochem. Soc., 125 (1978) 1443.
- [20] A.C. Makrides, Corrosion, Vol. 18, (Sept. 1962) 338.
- [21] A.C. Makrides, J. Electrochem. Soc., 107 (1960) 869.
- [22] F. Mansfeld, Corrosion, Vol. 36, 5 (1981) 301-307.
- [23] F. Mansfeld, Corrosion, Vol. 38, 11 (1982) 570.
- [24] J.R. Scully, Corrosion, Vol. 56, 2 (200) 1999.
- [25] J.H. Wang, F.I. Wei, and H.C. Shih, Corrosion, Vol. 52, 8 (1996) 600.
- [26] E. Khamis, M.A. Ameer, N.M. Al-Andis, and G. Al-Senani. Corrosion, Vol. 56, 2 (2000) 127.
- [27] P. Piereon, K.P. Bethune, W.H. Hartt, and P. Anathakrishnan, Corrosion, Vol. 56, 4 (2000) 350.
- [28] D.W. Law, S.G. Millard, and J.H. Bungey, Corrosion, Vol. 56, 1 (2000) 48.
- [29] D.D. McDonald and M.H. McKubre, in *Modern Aspects of Electrochemistry*, Edited by J. O'M. Bockris, B.E. Conway and R.E. White, Vol. 14, Plenum Press, New York, (1982) 61.

- [30] K. Hladky, L.M. Callow, and J.L. Dawson, Br. Corrosion Journal, Vol. 15, 1 (1980) 20.
- [31] O.C. Ho, D. Raistrick, and R.A. Huggins, Electrochem. Acta, 127 (1980) 343.
- [32] D.R. Franceschetti and J.R. McDonald, Electrochem. Acta, 129 (1982) 1754.
- [33] M.W. Kendig, E.T. Allen, and F. Mansfeld, J. Electrochem. Soc., 131 (1984) 935.
- [34] R. Delevie and L. Pospisil, J. Electroanal. Chem., 22 (1969) 277.
- [35] L. Nyikos and T. Pajkossy, Electrochem. Acta, 35 (1990) 1567.
- [36] K.S. Cole and R.H. Cole, J. Chem. Phys. 9 (1941) 341.
- [37] P.G. Shewmon, "*Diffusion in Solids*," McGraw-Hill, New York, (1963).
- [38] R.J. Weiss, "*Physics of Materials*," Hemisphere Publishing Corp., New York, (1990) 360-362.
- [39] A.G. Guy and J.J. Hren, "*Physical Metallurgy*" Third edition, Addison-Wesley Publishing Company, Reading, Massachusetts, (1974) 367-399.
- [40] C.A. Wert and R.M. Thompson, "Physics of Solids," Second edition, McGraw-Hill Book Company, New York, (1970) 54-73.
- [41] J. Crank, "*The Mathematics of Diffusion*," Second edition,, Oxford University Press, New York, (1990).
- [42] J. Braunstein and G.D. Robbins, J. Chem. Edu., Vol. 48, 1 (1971) 52-59.
- [43] F. Kohlrausch, Weid. Ann., 60 (1897) 315.
- [44] B. Wu and R.E. White, "*Modeling of a Nickel-Hydrogen Cell: Phase Reactions in the Nickel Active Material*," J. Electrochemical Soc., Vol. 148, No. 6 (June 2001) A595-A609.
- [45] G.H. Geiger and D.R. Poirier, "*Transport Phenomena in Metallurgy*" Addison-Wesley Publishing Company, Reading, Massachusetts, (1973) 434, 443, 449-451.
- [46] M. Pourbaix, "*Lectures of Electrochemical Corrosion*," Plenum Press, New York, (1973) 239-252.

Chapter 4

KINETICS OF CONCENTRATION POLARIZATION

4.1 INTRODUCTION

Whenever the concentration of a specie j like $[H^+]$ becomes the rate controlling, an electrochemical cell is cathodically polarized. This is attributed to the cathodic reactions due to ionic mass transfer [1]. In this case, the concentration of the specie j at the cathode electrode surface is lower than the bulk concentration ($C_s < C_b$) and therefore, the electrochemical process is controlled by the rate of mass transfer (flux) rather than charge transfer. In general, the mass transfer may be due to diffusion, migration of charged species under the influence of an electrical field, and convection due to fluid motion by stirring, rotation or vibration. In the latter case, the convective flux strongly depends on the velocity of the mass transfer and concentration of the species. Indiscriminating the source of the flux, steady-state or transient conditions must be taken into account in the analysis of an electrochemical process. Henceforth, an electrolyte means an electrolytic solution containing positively and negatively charged ions (species).

4.2 MASS TRANSFER MODES

Mass transfer of chemical or electrochemical specie j , known as ions can be a complex phenomenon because the solution (fluid) containing the ions may be strongly influenced by turbulent flow, and to a lesser extent to laminar flow, diffusion and an electrical field. For a stationary chemical or electrochemical system, such as a tank, pipe or battery, as observed by a stationary observer, under internal laminar flow the mass transfer is quantified by the molar or mass flux. For a one-dimensional treatment in the x-direction, the mass transfer

can be characterized as an idealized cylindrical or rectangular (parallelepiped) element of a solution. This is schematically shown in Figure 4.1 as a simplified model of a three-dimensional analysis. Thus, the molar flux J is a vector quantity perpendicular to a plane of species j [22].

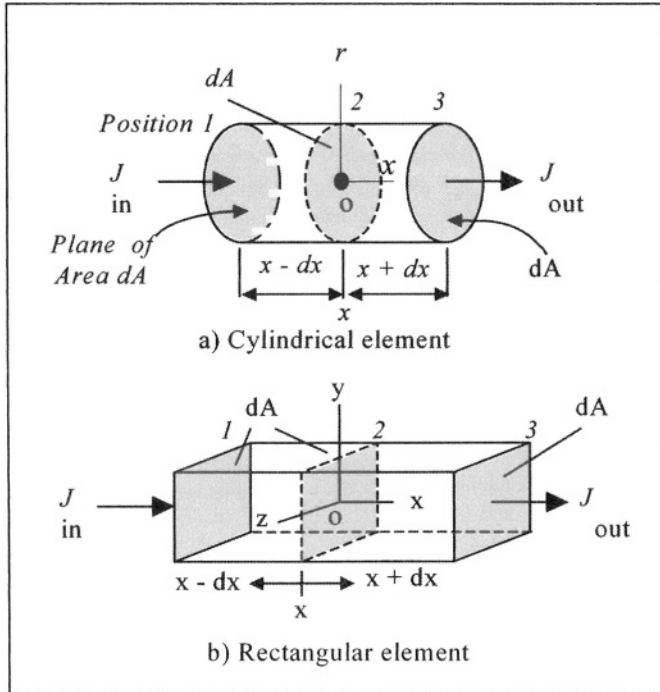


Figure 4.1 Volume elements for diffusion of a plane along the x-direction.

The model indicates that a plane of area dA containing species j moves in the x -direction from position 1 to position 2, and then to position 3. This motion is influenced by modes of mass transfer, such as **diffusion** due to a molar concentration gradient, **migration** due to an electrical field, natural or forced **convection** due to the kinematic velocity or a combination of these modes, mass transfer of species j can be quantified by the absolute value of the molar flux J or the mass flux J^* . Notice that J is perpendicular to the moving plane of species j and represents the absolute value of the vector molar flux \vec{J} . The total flux can be defined as

$$J = \sum J_j \quad (4.1a)$$

$$J^* = \sum J_j A_{w,j} \quad (4.1b)$$

where $A_{w,j}$ = Atomic weight of species j

In addition, J represents the number of moles of specie j that pass per unit time through a unit area. Thus, the units of J are $\text{mol}\cdot\text{cm}^{-2}\cdot\text{s}^{-1}$ and that of J^* are $\text{g}/\cdot\text{cm}^{-2}\cdot\text{s}^{-1}$. For a steady-state conditions and stationary x-axis, the concentration rate is $dC_j/dt = 0$ and the total molar flux is defined by the **Nernst-Plank equation** [16,19,21]

$$J = -D \frac{dC}{dx} - \frac{zFDC}{RT} \frac{d\phi}{dx} + Cv \quad (4.2)$$

$$J_d = -D \frac{dC}{dx} \quad (4.3)$$

$$J_m = -\frac{zFDC}{RT} \frac{d\phi}{dx} \quad (4.4)$$

$$J_c = Cv \quad (4.5)$$

where J_d = Diffusion molar flux due to dC/dx ($\text{mol}/\text{cm}^2 \cdot \text{s}$)

J_m = Migration molar flux due to $d\phi/dx$ ($\text{mol}/\text{cm}^2 \cdot \text{s}$)

J_c = Convective molar flux due to fluid motion ($\text{mol}/\text{cm}^2 \cdot \text{s}$)

dC/dx = Concentration gradient (mol/cm^4)

$d\phi/dx$ = Potential gradient (V/cm)

D = Diffusivity (Diffusion coefficient) (cm^2/s)

C = Ionic concentration (mol/cm^3 or mol/liter)

v = Hydrodynamic velocity (cm/s)

The physical interpretation of eq. (4.2) is schematically shown in Figure 4.2 after Maloy's modes of mass transfer [15]. The diffusivity for most ions is in the order of $D \approx 10^{-5} \text{ cm}^2/\text{s}$ [Ref. 7,16,21]. The diffusion molar flux J_d arises due to a concentration gradient of ions located at a distance x from the electrode surface. In general, diffusion is the process by which matter moves due to random particle (ion, atom or molecule) motion. On the other hand, migration molar flux J_m develops due to an electrical field, which causes a potential gradient in the solution. The convective molar flux J_c is caused by a moving or flowing solution (electrolyte) due to rotation, stirring or vibration.

In an electrical field, the rate of reaction process for metal reduction or oxidation is normally represented by the current density (i). Using eq. (3.21) the generalized Faraday's equation for the current density is

$$i = zF \frac{m}{A_w t A} \quad (4.6)$$

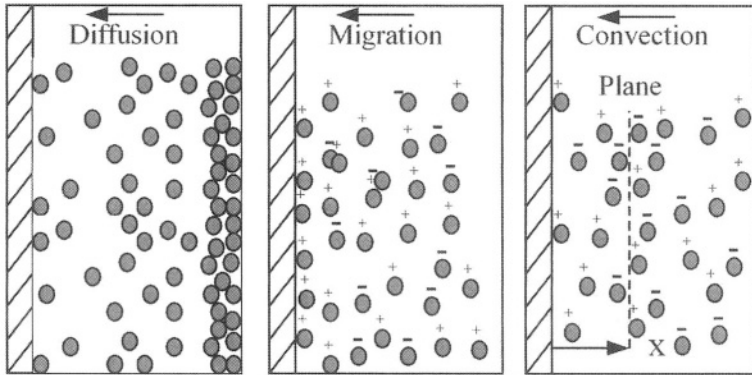


Figure 4.2 Modes of mass transport.

Notice that the term $m/(A_w t A)$ has units of $\text{mol}/(\text{cm}^2 \cdot \text{s})$ and represents the total molar flux. Thus,

$$J = \frac{m}{A_w t A} \quad (4.7)$$

For a one-dimensional analysis in the x-direction eq. (4.6) becomes

$$i = zFJ \quad (4.8)$$

Substituting eq. (4.2) into (4.8) yields what may be called the **Nernst-Planck-Faraday** (NPF) equation for the current density

$$i = zF [J_d + J_m + J_c] \quad (4.9)$$

Substituting eqs. (4.3) through (4.5) into ((4.9) yields the total current density for the above mass transfer modes

$$i = zF \left[-D \frac{dC}{dx} - \frac{zFDC}{RT} \frac{d\phi}{dx} + Cv \right] \quad (4.9a)$$

Usually, J_d and J_m are coupled in the operation of electrochemical cells. This is a coupled mass transfer process which is referred to as **Ambipolar Diffusion** [9] or binary system where the migration molar flux J_m evolves due to a chemical potential gradient $d\mu/dx$, which in turn, emerges as a result of a potential gradient $d\phi/dx$. However, other factors such as pressure gradient dP/dx , concentration gradient dC/dx , and temperature gradient dT/dx are neglected as contributing factors to the total value of J_m expression as defined by eq. (4.4).

4.3 MIGRATION MOLAR FLUX

The migration molar flux can be defined as [17]

$$J_m = -CB \frac{d\mu}{dx} \quad (4.10)$$

where $B = \text{Ionic mobility } [cm^2/V \cdot s = cm^2 \cdot mol / (J \cdot s)]$
 $d\mu/dx = \text{Chemical potential gradient } [J / (cm \cdot mol)]$

In addition, the terms dC/dx , dP/dx , and dT/dx are absent in eq. (4.10) as contributing gradients to the total migration flux. Therefore, eq. (4.10) represents an approximation model. However, $d\mu/dx$ strongly contributes to J_m and it can be defined as

$$\frac{d\mu}{dx} = zq_e \frac{d\phi}{dx} \quad (4.11)$$

where $q_e = 1.6022 \times 10^{-19} \text{ Coulomb } (= J/V)$. Substituting eq. (4.11) into (4.10) yields the migration molar flux in terms of potential gradient

$$J_m = -zq_e CB \frac{d\phi}{dx} \quad (4.12)$$

The mobility is defined as [5-6]

$$B = \frac{v}{F_x} \quad (4.13)$$

where $v = \text{Kinematic velocity of the flowing specie } j \text{ (cm/s)}$
 $F_x = \text{Electrical potential acting on the specie } j \text{ (V/cm)}$

A more convenient approach to derive B is by combining eqs. (4.4) and (4.12) along with eq. (2.1c). Thus,

$$B = \frac{DN_A}{RT} = \frac{D}{\kappa T} \quad (4.14)$$

where $T = \text{Absolute temperature}$
 $\kappa = R/N_A = 1.38 \times 10^{-23} \text{ J/K} = \text{Boltzmann constant}$
 $N_A = \text{Avogadro's number}$
 $R = 8.314 \text{ J/mol.K} = \text{Gas constants}$

Since $D \approx 10^{-5} \text{ cm}^2/\text{s}$ for most ions [7,16,21], the mobility becomes $B \approx 2.43 \times 10^{15} \text{ cm}^2/\text{J.s}$ at $T = 298\text{K}$. Solving eq. (4.14) for D yields the **Nernst-Einstein equation** [21]

$$D = B\kappa T \quad (4.15)$$

for a specie j being treated as a spherical particle. This equation can also be derived using chemical potential (see problem 4.24) [20].

4.4 FICK'S LAWS OF DIFFUSION

Diffusion can be defined as the process in which the transfer of matter is due to random motion. The mathematics of diffusion can be found in Crank's book [23], in which different diffusion processes are analyzed. Let's assume an isotropic and homogeneous medium in which the diffusivity D is constant and the rate of transfer of matter (ions, atom or molecules) is described by **Fick's first law of diffusion**. Despite that diffusion may be treated as a three-dimensional process, it may be assumed that it occurs in isotropic media.

In general, the conditions for steady-state ($\partial C/\partial t = 0$) and for transient-state ($\partial C/\partial t \neq 0$) are governed by Fick's laws of diffusion

$$J_i = -\sum_{i=1}^3 D_{ii} \frac{\partial C}{\partial x_i} \quad (\text{First law}) \quad (4.16)$$

$$\frac{\partial C}{\partial t} = \sum_{i=1}^3 D_{ij} \frac{\partial^2 C}{\partial x_{ij}^2} \quad (\text{Second law}) \quad (4.17)$$

where $\partial C/\partial t =$ Concentration rate ($\text{mol}/\text{cm}^3 \cdot \text{s}$)
 $i, j = 1, 2, 3$ which stand for $x_1 = x$, $x_2 = y$, and $x_3 = z$
 $\partial^2 C/\partial x_{ij}^2 = \partial^2 C/\partial x_{ji}^2$ and $D_{ij} = D_{ji}$. due to symmetry

Fick's laws are significant in measuring diffusivity in isotropic and anisotropic media. Confining a diffusion problem to a one-dimensional treatment suffices most approximations in diffusion. Hence, eqs. (4.16) and (4.17) can be simplified for diffusion flow along the x-direction in isotropic media

$$J_x = -D \frac{\partial C}{\partial x} \quad (\text{First law}) \quad (4.18)$$

$$\frac{\partial C}{\partial t} = D \frac{\partial^2 C}{\partial x^2} \quad (\text{Second law}) \quad (4.19)$$

These expressions imply that both the molar flux and concentration rate strongly depend on the concentration gradient along the x-direction only since $\partial C/\partial y = \partial C/\partial z = 0$, and that the diffusion flow is perpendicular to the moving plane of a solute (Figure 4.1). General solutions of Fick's second law equation can be found elsewhere [20-23] for a few relevant diffusion problems related to a two-component system, such as an electrode sheet immersed or suspended in a liquid solution.

Fick's first law is analog of Newton's law of viscosity, Ohm's law of electrical conduction, and Fourier's law of thermal conduction. Consider Einstein's assumption that spherical particles (ions) move through a continuous medium (solution) of viscosity η_v under **self-diffusion** conditions and that Stoke's drag or friction force F per unit length acts on these particles, and neglecting inter-atomic forces, then F_x , B and D can be predicted by [21]

$$F_x = 6\pi R_i \eta_v v \quad (4.20)$$

$$B = \frac{1}{6\pi R_i \eta_v} \quad (4.21)$$

$$D = \frac{\kappa T}{6\pi R_i \eta_v} \quad (4.22)$$

where R_i = Radius of spherical particles (cm)
 η_v = Viscosity ($J.s/cm^3$ or $g.s/cm^2$)

Furthermore, substituting eq. (4.3) into (4.8) yields the current density as a function of concentration gradient

$$i = zFD \frac{dC}{dx} \quad (4.23)$$

where $dC/dx > 0$ so that $i > 0$ and $J_d > 0$.

For small values of the overpotential η , and combining eqs. (3.16c) and (4.23), the exchange current density becomes

$$i_o = \frac{RTD}{\alpha\eta} \frac{dC}{dx} \quad (4.24)$$

The diffusivity or diffusion coefficient is defined using the Arrhenius type equation. Hence,

$$D = D_o \exp\left(-\frac{E^*}{RT}\right) \quad (4.25)$$

where D_o = Diffusion constant (cm^2/s)
 E^* = Activation energy (J/mol)

This diffusivity equation is similar to eq. (3.7) and its physical interpretation is given in section 3.3 along with Figure 3.2. Thus, there is no need to repeat that materials in this section.

4.4.1 DIFFUSION IN A RECTANGULAR ELEMENT

Fick's second law of diffusion is for a non-steady state or transient conditions in which $dC_j/dt \neq 0$. Using Crank's model [23] for the rectangular element shown in Figure 4.1 yields the fundamental differential equations for the rate of concentration. Consider the central plane as the reference point in the rectangular volume element and assume that the diffusing plane at position 2 moves along the x -direction at a distance $x - dx$ from position 1 and $x + dx$ to position 3. Thus, the rate of diffusion that enters the volume element at position 1 and leaves at position 3 is

$$R_x = dydz \left[J_x - \frac{\partial J_x}{\partial x} dx \right] - dydz \left[J_x + \frac{\partial J_x}{\partial x} dx \right] \quad (a)$$

$$R_x = -2dxdydz \frac{\partial J_x}{\partial x} = -2dV \frac{\partial J_x}{\partial x} \quad (4.26)$$

Similarly,

$$R_y = -2dxdydz \frac{\partial J_y}{\partial y} = -2dV \frac{\partial J_y}{\partial y} \quad (4.27)$$

$$R_z = -2dxdydz \frac{\partial J_z}{\partial z} = -2dV \frac{\partial J_z}{\partial z} \quad (4.28)$$

The concentration rate is defined as

$$\frac{\partial C}{\partial t} = \frac{1}{2dV} \sum R_i \quad (4.29)$$

$$\frac{\partial C}{\partial t} = -\frac{\partial J_x}{\partial x} - \frac{\partial J_y}{\partial y} - \frac{\partial J_z}{\partial z} \quad (4.30)$$

This expression is the equation of continuity for conservation of mass [27]. Using eqs. (4.16) and (4.30), with $D = \text{constant}$, yields **Fick's second law equation** in three dimensions

$$\frac{\partial C}{\partial t} = D \left[\frac{\partial^2 C}{\partial x^2} + \frac{\partial^2 C}{\partial y^2} + \frac{\partial^2 C}{\partial z^2} \right] \quad (4.31)$$

Again, one-dimensional diffusion suffices most analysis of isotropic medium. Note that "z" has been used as a coordinate in eqs. (4.28), (4.30) and (4.31). Hence, for diffusion in the x-direction, the concentration rate in eq. (4.31) becomes the most familiar **Fick's second law equation**

$$\frac{\partial C}{\partial t} = D \frac{\partial^2 C}{\partial x^2} \quad (4.19)$$

If D is not constant, then eq. (4.31) yields the concentration rate in the x-direction as

$$\frac{\partial C}{\partial t} = \frac{\partial}{\partial x} \left[D \frac{\partial C}{\partial x} \right] \quad (4.32)$$

$$\frac{\partial C}{\partial t} = \frac{\partial D}{\partial x} \frac{\partial C}{\partial x} + D \frac{\partial^2 C}{\partial x^2} \quad (4.33)$$

which is a difficult equation to solve since D has been treated as a variable that depends on x and t ; that is, $D = f(x, t)$. In fact, during a transient period, D and C are functions of position and time. Therefore, eq. (4.19) is the most used form of Fick's second law and it is the general diffusion expression for one-dimensional analysis under non-steady state condition.

4.4.2 DIFFUSION IN A CYLINDRICAL ELEMENT

The concentration rate equation follows by transformation of coordinates. Letting dr , $r d\theta$, and dz be the sides of a cylinder and

$$x = r \sin \theta \quad (\text{a})$$

$$y = r \cos \theta \quad (\text{b})$$

$$dV = r \theta dr dz \quad (\text{c})$$

the diffusion equation becomes [23]

$$\frac{\partial C}{\partial t} = \frac{1}{r} \left[\frac{\partial}{\partial r} \left(r D \frac{\partial C}{\partial r} \right) + \frac{\partial}{\partial \theta} \left(\frac{D}{r} \frac{\partial C}{\partial \theta} \right) + \frac{\partial}{\partial z} \left(r D \frac{\partial C}{\partial z} \right) \right] \quad (4.34)$$

For a **radial diffusion** in a large cylinder, eq. (4.34) gives

$$\frac{\partial C}{\partial t} = \frac{1}{r} \frac{\partial}{\partial r} \left(r D \frac{\partial C}{\partial r} \right) \quad (4.35)$$

For a steady-state condition eq. (4.35) reduces to

$$\frac{d}{dr} \left(r \frac{dC}{dr} \right) = 0 \quad (4.36)$$

The solution of these equations can be found elsewhere [23] for different diffusion cases.

4.4.3 SOLUTION OF FICK'S SECOND LAW EQUATION

For the **rectangular element** shown in Figure 4.1, the solution of eq. (4.19) is subjected to proper boundary conditions given in Appendix A for a particular case, which includes detailed analytical procedures for deriving two suitable solutions. From Appendix A, the normalized concentration expression for concentration polarization **case** ($C_\infty = C_b > C_o$) is

$$\frac{C_x - C_b}{C_o - C_b} = 1 - \operatorname{erf} \left(\frac{x}{\sqrt{4Dt}} \right) \quad \text{For } C_b > C_o \quad (4.37)$$

$$C_x = C_o + (C_b - C_o) \operatorname{erf} \left(\frac{x}{\sqrt{4Dt}} \right) \quad \text{For } C_b > C_o \quad (4.38)$$

and for activation polarization ($C_o > C_b = C_\infty$) is

$$\frac{C_x - C_o}{C_b - C_o} = \operatorname{erf} \left(\frac{x}{\sqrt{4Dt}} \right) \quad \text{For } C_o > C_b \quad (4.39)$$

$$C_x = C_o - (C_o - C_b) \operatorname{erf} \left(\frac{x}{\sqrt{4Dt}} \right) \quad \text{For } C_o > C_b \quad (4.40)$$

where C_b is the bulk concentration of a specie j and C_o is the concentration at the electrode surface. The error function $\operatorname{erf}\left(x/\sqrt{4Dt}\right)$ is an integral function that is solved numerically by series expansion such as [23]

$$\operatorname{erf}(y) = \frac{2}{\sqrt{\pi}} \int_0^y \exp(-y^2) dy \quad (4.41)$$

$$\operatorname{erf}(y) = \frac{2}{\sqrt{\pi}} \left(\frac{1}{0!} \frac{y}{1} - \frac{1}{1!} \frac{y^3}{3} + \frac{1}{2!} \frac{y^5}{5} - \frac{1}{3!} \frac{y^7}{7} + \dots \right) \quad (4.42)$$

$$\operatorname{erf}(y) = \frac{2}{\sqrt{\pi}} \sum_{n=1}^{\infty} \frac{(-1)^{n+1} y^{2n-1}}{(n-1)!(2n-1)} \quad (4.43)$$

and its complement function is defined by

$$\operatorname{erf}(y) + \operatorname{erf}c(y) = 1 \quad (4.44)$$

$$\operatorname{erf}c(y) = \frac{2}{\sqrt{\pi}} \int_y^{\infty} \exp(-y^2) dy \quad (4.45)$$

where $y = x/\sqrt{4Dt}$.

The error function is illustrated in Table 4.1 and Figure 4.3. Despite that the error function data is repeated, it is convenient to illustrate this function in a graphical form in order to show its profile.

Table 4.1 Values of the Error Function $\operatorname{erf}(y)$

y	$\operatorname{erf}(y)$	y	$\operatorname{erf}(y)$	y	$\operatorname{erf}(y)$
0	0	0.55	0.5633	1.30	0.9340
0.025	0.0282	0.60	0.6039	1.40	0.9523
0.05	0.0564	0.65	0.6420	1.50	0.9661
0.10	0.1125	0.70	0.6778	1.60	0.9763
0.15	0.1680	0.75	0.7112	1.70	0.9838
0.20	0.2227	0.80	0.7421	1.80	0.9891
0.25	0.2763	0.85	0.7707	1.90	0.9928
0.30	0.3286	0.90	0.7970	2.00	0.9953
0.35	0.3794	0.95	0.8209	2.10	0.9970
0.40	0.4284	1.00	0.8427	2.20	0.9981
0.45	0.4755	1.10	0.8802	2.30	0.9989
0.50	0.5205	1.20	0.9103	2.40	0.9993

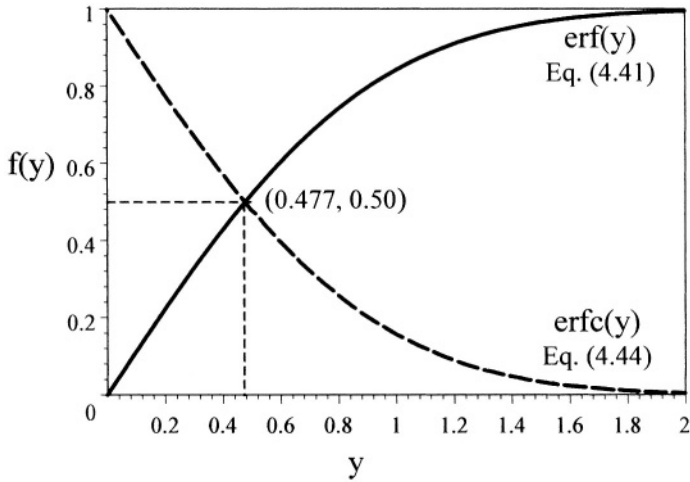


Figure 4.3 Error and complement function profiles.

The graphical application of eq. (4.37) is schematically shown in Figure 4.4. Note that the curves are displaced upwards with increasing time and downwards with increasing distance x . Furthermore, Eq. (4.38) is plotted in Figure 4.5 in which the diffusion layer δ increases as the curve is displaced to the right with increasing time t [7,16-18].

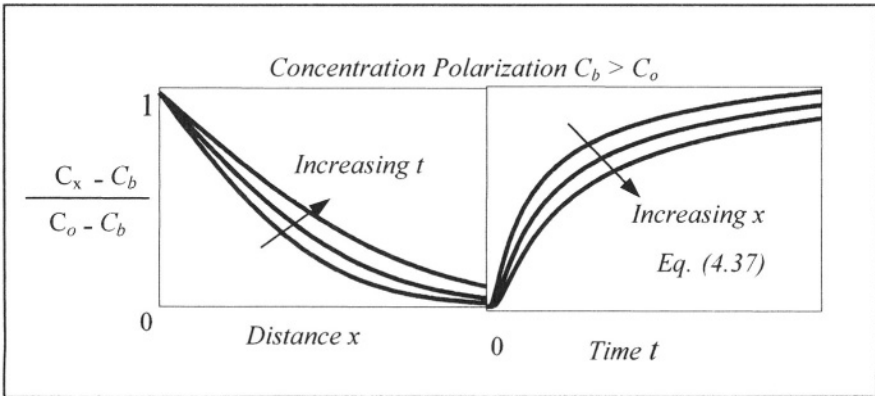


Figure 4.4 Normalized concentration for concentration polarization.

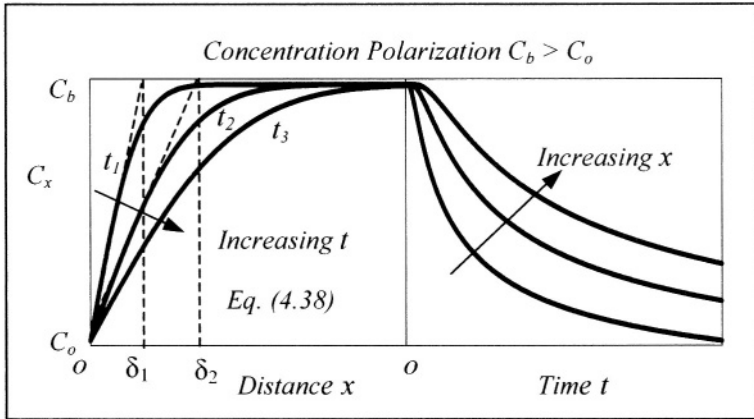


Fig 4.5 Schematic concentration profiles for concentration polarization.

In addition, the concentration gradient dC/dx for both concentration polarization and activation polarization can be determined from eqs. (4.38) and (4.40). Hence, for concentration polarization with $C = C_x$ yields

$$\frac{\partial C}{\partial x} = -(C_o - C_b) \frac{\partial}{\partial x} \left[\frac{2}{\sqrt{\pi}} \int_y^\infty \exp(-y^2) dy \right] \quad (4.46)$$

$$\frac{\partial C}{\partial x} = -\frac{(C_o - C_b)}{\sqrt{\pi Dt}} \exp\left(-\frac{x^2}{4Dt}\right) \quad \text{For } C_b > C_o \quad (4.47)$$

$$\left. \frac{\partial C}{\partial x} \right|_{x=0} = -\frac{(C_o - C_b)}{\sqrt{\pi Dt}} \approx +\frac{C_b}{\sqrt{\pi Dt}} \quad \text{For } C_b \gg C_o \quad (4.48)$$

For activation polarization ($C = C_x$),

$$\frac{\partial C}{\partial x} = -(C_o - C_b) \frac{\partial}{\partial x} \left[\frac{2}{\sqrt{\pi}} \int_y^\infty \exp(-y^2) dy \right] \quad (4.49)$$

$$\frac{\partial C}{\partial x} = -\frac{(C_o - C_b)}{\sqrt{\pi Dt}} \exp\left(-\frac{x^2}{4Dt}\right) \quad \text{For } C_o > C_b \quad (4.50)$$

$$\left. \frac{\partial C}{\partial x} \right|_{x=0} = -\frac{(C_o - C_b)}{\sqrt{\pi Dt}} \approx -\frac{C_o}{\sqrt{\pi Dt}} \quad \text{For } C_o \gg C_b \quad (4.51)$$

Substituting eq. (4.46) into (4.23) yields the **Cottrell equation** for the current density due to diffusion mass transfer [16,19]

$$i = \frac{zFDC_b}{\sqrt{\pi Dt}} = \frac{zFDC_b}{\delta} \quad (4.52)$$

$$\delta = \sqrt{\pi Dt} \quad (4.53)$$

where δ = Thickness of the diffusion double-layer. Experimentally, this parameter is $0.3 \text{ mm} \leq \delta \leq 0.5 \text{ mm}$ [30].

Let's use Fontana's classical model of concentration polarization [1] shown in Figure 4.6. This model suggests that the ionic concentration in the bulk of solution is higher than that on the electrode surface. Therefore, $C_b > C_o$ meaning that the diffusion direction of hydrogen cations is towards the electrode surface where anodic and cathodic reactions take place. Hence, the diffusion molar flux is determined by Fick's first law equation under steady-state conditions. It can be assumed that no other mass transfer phenomenon is present.

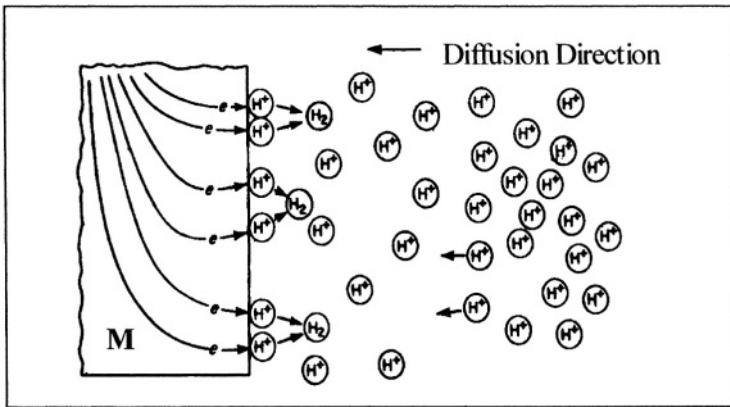


Figure 4.6 Schematic model for concentration polarization [1].

Assuming that all variables in eq. (4.52) are constant, except time t , one can predict the current density profile as a nonlinear behavior for a particular electrolyte. This is shown in Figure 4.7

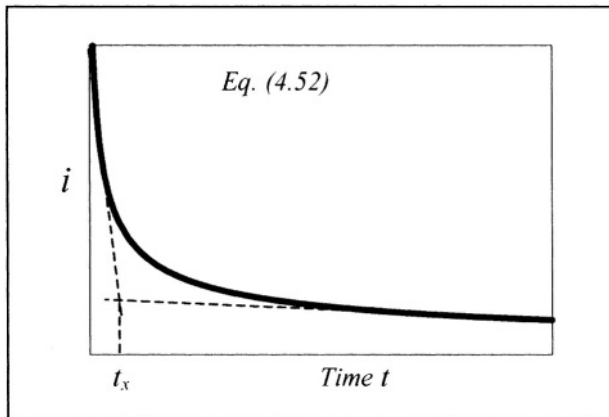


Figure 4.7 Schematic of nonlinear current density profile of Cottrell equation.

Linearization of eqs. (4.48) and (4.52) are shown in Figure 4.8. For a concentration gradient profile at the electrode surface, where the concentration gradient is $dC/dx = f(x = 0, t)$, the diffusivity D and the valence z can be determined from the slope of Figure 4.8a and 4.8b, respectively.

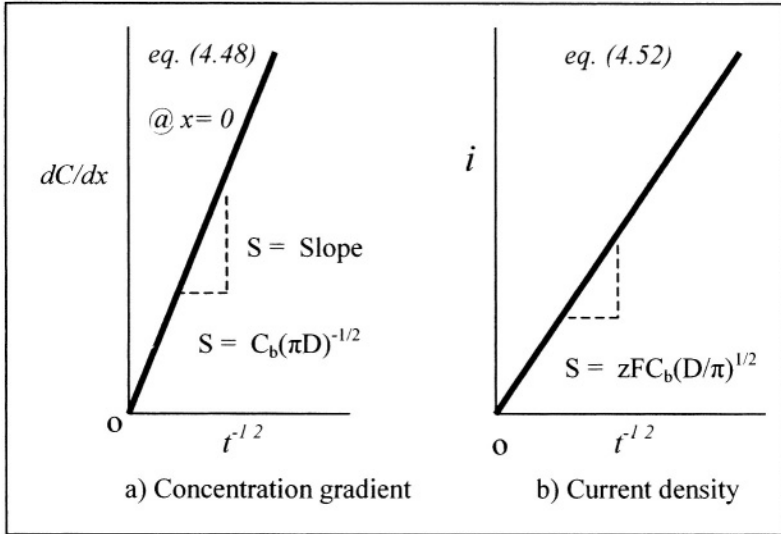


Figure 4.8 Schematic concentration gradient and current density at the electrode surface @ $x = 0$.

Furthermore, the area under the curve in Figure 4.7 represents the electrical charge per unit area. The definition of charge according is

$$q = \int i A_s dt \tag{4.54}$$

where A_s = Electrode surface area.

Inserting eq. (4.52) into (4.54) and solving the integral yields

$$q = \frac{2}{3} z F A C_b \sqrt{D/\pi} t^{3/2} \tag{4.55}$$

Now, substituting back eq. (4.52) into (4.55) gives

$$q = \frac{2}{3} A i t \tag{4.56}$$

Figure 4.9 illustrates ideal charge profiles as per eq. (4.55). The curves are displaced upwards with increasing original bulk concentration C_b .

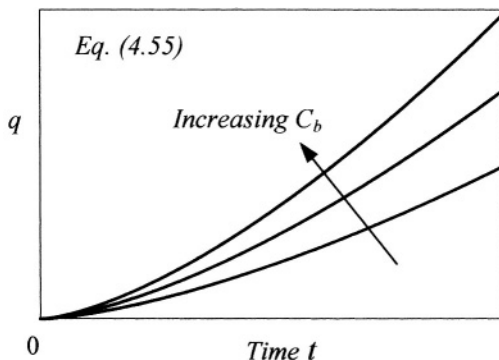


Figure 4.9 Schematic nonlinear profiles of the electrical charge q .

Example 4.1 Consider the application of Fick's second law to solve an activation polarization problem. An electrochemical cell contains a bulk concentration and an electrode surface concentration of copper ions Cu^{+2} equal to $4 \times 10^{-4} \text{ mol/cm}^3$ and 10^{-2} mol/cm^3 , respectively. If the diffusivity of copper ions is $1.5 \times 10^{-6} \text{ cm}^2/\text{s}$, calculate a) the concentration of Cu^{+2} ions at 0.12 mm from the electrode surface after 10 minutes and b) the time for a concentration of 10^{-3} mol/cm^3 of Cu^{+2} ions at 0.10 mm from the electrode surface.

Solution:

$$\text{Data: } D = 1.5 \times 10^{-6} \text{ cm}^2/\text{s} \quad C_b = 4 \times 10^{-4} \text{ mol/cm}^3 @ x = \infty \\ C_o = 10^{-2} \text{ mol/cm}^3 @ x = 0$$

$$\text{a) } C_x = ? @ x = 0.12 \text{ mm}, t = 10 \text{ min} = 600 \text{ s}$$

$$y = x/\sqrt{4Dt} = (0.012 \text{ cm})/\sqrt{(4)(1.5 \times 10^{-6} \text{ cm}^2/\text{s})(600 \text{ s})} = 0.20$$

From Table 4.1,

$$\text{erf}(y) = \text{erf}(0.20) = 0.22$$

From eq. (4.40) with $C_o > C_b$,

$$C_x = C_o - (C_o - C_b) \text{erf}\left(x/\sqrt{4Dt}\right) \\ C_x = 10^{-2} \text{ mol/cm}^3 - (10^{-2} \text{ mol/cm}^3 - 4 \times 10^{-4} \text{ mol/cm}^3)(0.22) \\ C_x = 7.89 \times 10^{-3} \text{ mol/cm}^3$$

$$\text{b) } t = ? @ C_x = 10^{-3} \text{ mol/cm}^3, x = 0.10 \text{ mm and from eq. (4.39)}$$

$$\begin{aligned} (C_x - C_o) / (C_b - C_o) &= \operatorname{erf} \left(x / \sqrt{4Dt} \right) \\ (C_x - C_o) / (C_b - C_o) &= (10^{-3} - 10^{-2}) / (4 \times 10^{-4} - 10^{-2}) \\ (C_x - C_o) / (C_b - C_o) &= 0.94 = \operatorname{erf} (y) \end{aligned}$$

From Table 4.1,

$$y = 1.33 = x / \sqrt{4Dt}$$

$$t = \frac{1}{4D} \left(\frac{x}{y} \right)^2 = \left\{ 1 / [(4) (1.5 \times 10^{-6} \text{ cm}^2/\text{s})] \right\} (0.010 \text{ cm} / 1.33)^2$$

$$t = 9.42 \text{ sec}$$

Example 4.2 Assume that two columns of ionic solutions are connected by a barrier, such as a diaphragm. If the barrier is suddenly removed at time $t = 0$, free diffusion takes place. Derive an expression for a) the concentration C_x at $x = 0$ and b) the molar flux J_x in the x -direction at $x = 0$ and c) C_x/C_o vs. $x/\sqrt{4Dt}$. Determine C_x/C_o from the plot at $x = 0$, and d) plot the molar flux J_x vs. time at $x = 0$. Given data: $D = 10^{-5} \text{ cm}^2/\text{s}$, $C_o = 10^{-4} \text{ mol}/\text{cm}^3$.

Solution:

a) From Appendix A,

$$y = x / \sqrt{4Dt}$$

$$\int_{C_o}^{C_x} dC = B \int_{-\infty}^{\infty} \exp(-y^2) dy$$

$$B = C_o / \sqrt{\pi}$$

$$\int_{C_o}^{C_x} dC = B \int_y^{\infty} \exp(-y^2) dy$$

$$C_x = (C_o / \sqrt{\pi}) (\sqrt{\pi} / 2) \operatorname{erf} c(y)$$

$$C_x = (C_o / 2) \operatorname{erf} c(y)$$

$$C_x = (C_o / 2) [1 - \operatorname{erf}(y)]$$

$$C_x = (C_o / 2) \left[1 - \operatorname{erf} \left(x / \sqrt{4Dt} \right) \right]$$

$$C_x = C_o / 2 \quad @ \quad x = 0$$

c) $C_x/C_o = 0.5 [1 - \operatorname{erf}(y)]$ where $y = x/\sqrt{4Dt}$

b) From part a),

$$C_x = (C_o / 2) \operatorname{erf} c(y)$$

$$C_x = -\frac{C_o}{2} \frac{2}{\sqrt{\pi}} \int_{\infty}^y \exp(-y^2) dy$$

$$y = x / \sqrt{4Dt}; \quad dy = dx / \sqrt{4Dt}$$

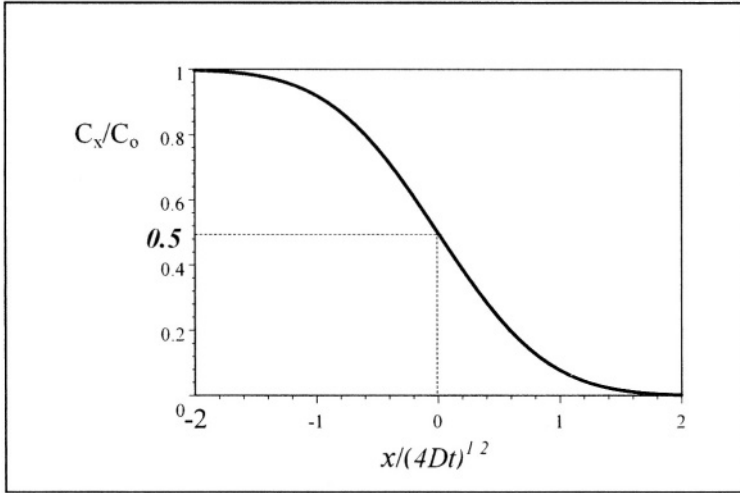
$$dC_x / dx = - \left(\frac{C_o}{\sqrt{4\pi Dt}} \right) \exp(-x^2 / 4Dt)$$

$$dC_x / dx = -C_o / \sqrt{4\pi Dt} \quad @ \quad x = 0$$

From eq. (4.3),

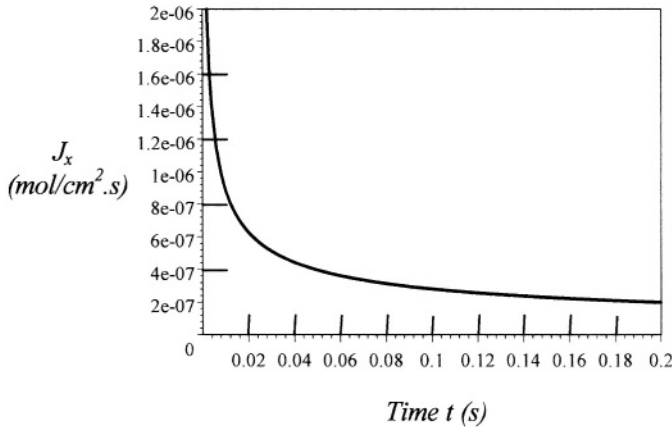
$$J_x = -D dC_x / dx$$

$$J_x = C_o \sqrt{D / 4\pi t} \quad @ \quad x = 0$$



Example 4.2c.

d) Note that the molar flux is very sensitive at very small periods of time.



Example 4.2d.

In comparison, species in gases and liquids are always in motion from one place to another, while in solids they oscillate around their lattice positions. Since diffusion in aqueous medium is the main subject in this section, the concentration of a specie j can be smoothed out by diffusion since the mass transfer occurs from the high to low concentration region as in cathodic processes under concentration polarization. Maintaining a continuous supply and removal of a

specie j in an electrolyte at a constant temperature, a steady-state is achieved and D can be experimentally determined since $\partial C/\partial t = 0$; otherwise, a non-steady state or transient diffusional process arises and the concentration rate becomes $\partial C/\partial t > 0$ [26].

In general, methodological sources for determining the diffusivity can be found elsewhere [20-21,23,26-28]. In order for the reader to have a better understanding on diffusion, simple and yet, important diffusion processes can be generalized by connecting a system A and a system B at the same temperature T and pressure P causes a mixture of species A and B until a uniform composition is achieved due to diffusion of A into B and vice versa. Then, the average composition of the mixture is $C = (C_A + C_B)/2$. For example, below are some common diffusion cases for mixing species A and B .

- Diffusion of gases, such as helium and argon to form a mixture in a closed vessel at T and P .
- Diffusion of liquids, such as water and alcohol, water and liquid soap.
- Diffusion in solids, such as a bar of Cu and a bar of Ni clamped together in a furnace at $1050^\circ C$.

4.4.4 STATIONARY BOUNDARIES

The open-ended capillary technique is used for determining the diffusivity of self-diffusing ions in dilute solutions [23,28]. The capillary shown in Figure 4.10 has stationary boundaries in the liquid medium and an open upper end where ions (solute) interactions take place due to diffusion.

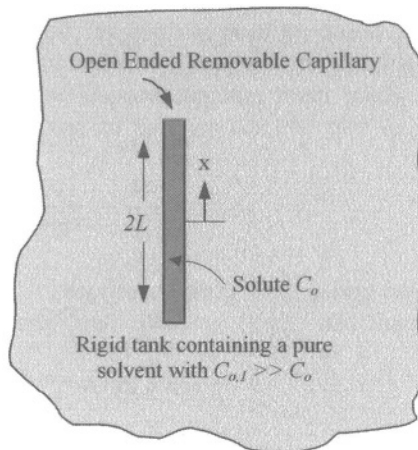


Figure 4.10 Open-ended capillary.

For non-steady state diffusion of ions contained in a volume capillary with known initial concentration C_o , the general concept for an experimental set-up

is schematically shown in Figure 4.10. The capillary is attached to other components for easy handling during immersion and withdrawing from the solution. The reader wishing to obtain design details of an apparatus should consult the work of Anderson and Saddington [29] and Kumar and Gupta [28].

In this technique, the ions or species j in the capillary and in the solvent diffuse through the open-ended space at an infinite time. After time t has elapsed, the capillary is removed from the system for determining the final concentration as $C = f(x, t)$ and the concentration ratio C/C_o is related to the diffusivity D . The solution to this diffusion problem is based on the boundary conditions given below

$$C = C_o \quad \text{@ } x = 0, t \geq 0 \quad \text{(a)}$$

$$\partial C / \partial x = 0 \quad \text{@ } x = 0, t \geq 0 \quad \text{(b)}$$

$$C = 0 \quad \text{@ } x = L, t \geq 0 \quad \text{(c)}$$

$$C = C_x \quad \text{@ } -L < x < L \quad \text{(d)}$$

Note that condition b) dictates that diffusion must not occur across the central plane at $x = 0$. The solution of eq. (4.19) is based on methods such as Laplace Transform and Separation of Variables. Using either method yields the solution of eq. (4.19) as normalized concentration [23]

$$\frac{C - C_o}{C_1 - C_o} = 1 - \frac{4}{\pi} \sum_{k=0}^{\infty} \frac{(-1)^n}{2n+1} \exp \left[-\frac{(2n+1)^2 \pi^2 Dt}{4L^2} \right] \cos \left[\frac{(2n+1) \pi x}{2L} \right] \quad (4.57)$$

If $C_1 = 0$ at $x = L$ then $t = 0$, and eq. (4.57) reduces to

$$\frac{C}{C_o} = \frac{4}{\pi} \sum_{n=0}^{\infty} \frac{(-1)^n}{2n+1} \exp \left[-\frac{(2n+1)^2 \pi^2 Dt}{4L^2} \right] \cos \left[\frac{(2n+1) \pi x}{2L} \right] \quad (4.58)$$

The accuracy of eq. (4.58) depends on the number of terms used to carry out the series. Assuming that one term in this series yields accurate enough results, then the diffusivity becomes

$$D = \frac{4L^2}{\pi t} \ln \left[\frac{\pi C_o}{4C} \sec \left(\frac{\pi x}{2L} \right) \right] \quad \text{For } C < C_o, t > 0 \quad (4.59)$$

Letting $x = L/2$ in eq. (4.59) yields

$$D = \frac{4L^2}{\pi t} \ln \left[\frac{\pi \sqrt{2} C_o}{4C} \right] \quad \text{@ } x = L/2, C < C_o, t > 0 \quad (4.60)$$

Consequently, $D = f(C_o/C)$ at $t > 0$ as previously assumed.

4.5 DIFFUSION AND MIGRATION

One important observation can be made with respect to the derived mathematical models for $C = f(x, t)$, $dC/dx = (x, t)$ and $i = f(t)$. All these variables decay with time at a fixed distance from the electrode surface since they are proportional to the inverse square root of time. The previous analytical approach is the outcome of a potential-control process for which the current response is measured at a particular temperature. As of now, this analytical work has been done for determining the current density response as expressed by eq. (4.23), which is the result of the concentration gradient that develops in the electrolyte due to kinetic mass transfer according to a simple reaction such as $M^{+z} + ze^- = M$, in which M^{+z} is reduced to metal M . Further analysis of the mass transfer in a aqueous electrolyte subjected to potential-control process suggests that the current density response, eq. (4.23), may solely be by diffusion. However, a potential-control electrochemical system generates an electrical field and it is apparent that both diffusion and migration molar fluxes are related to the concentration and potential gradients, respectively. The latter has a strong effect on the magnitude of the current density. Thus, the Nernst-Planck equation without the convective molar flux term may provide adequate results. If the electrical field is weak and the migration molar flux approaches zero ($J_m \rightarrow 0$), then the diffusion molar flux (J_d), as predicted by Fick's first law, is the controlling step for mass transfer under steady-state condition, in which the concentration rate is $\partial C/\partial t = 0$. On the other hand, if $\partial C/\partial t \neq 0$ it implies that diffusion molar flux is time-dependent and it is described by Fick's second law for a linear diffusion process.

With respect to a coupled diffusion and migration mass transfer case, eq. (4.2) reduces to

$$i = zF [J_d + J_m] = -zFD \frac{dC}{dx} - \frac{zFDC}{RT} \frac{d\phi}{dx} \quad (4.61)$$

Let $di/dx = 0$ so that (see Problem 4.21)

$$\frac{d^2\phi}{dx^2} + \frac{1}{\sqrt{\pi Dt}} \frac{d\phi}{dx} = 0 \quad (4.62)$$

Solving this ordinary differential equation gives a theoretical definition of the potential gradient as

$$\frac{d\phi}{dx} + \frac{\phi}{\sqrt{\pi Dt}} = 0 \quad (4.63)$$

If $d\phi/dx = 0$, the current density response i is solely controlled by diffusion at the electrode surface where $x = 0$. The solution of eq. (4.63) for $x = \delta$ is

$$\phi = \phi_o \exp\left(-\frac{x}{\sqrt{\pi Dt}}\right) = \phi_o \exp(-x/\delta) \quad (4.64)$$

which is similar to eq. (2.57) with $\phi_o = RT/zF$ (see Problem 4.23). Here, δ is the thickness of the electrical double-layer as defined by eq. (4.53). If $x = 0$,

then $\phi = \phi_o > 0$ at the electrode surface. The inner potential ϕ_o can be defined by the Nernst equation as indicated by eq. (2.59). If $dC/dx = 0$ in eq. (4.61), then the current density due to migration mass transfer becomes

$$i_m = \frac{zFDC_o}{\delta} = \frac{zFDC_o}{\sqrt{\pi Dt}} \quad \text{For } t > 0 \quad (4.64a)$$

and that for diffusion mass transfer is

$$i_d = \frac{zFDC_o}{\delta} = \frac{zFDC_o}{\sqrt{\pi Dt}} \quad \text{For } t > 0 \quad (4.64b)$$

Hence, for a coupled diffusion and migration case the total current density is defined as

$$i = i_m + i_d = \frac{2zFDC_o}{\sqrt{\pi Dt}} \quad \text{For } t > 0 \quad (4.64c)$$

4.6 REVERSIBLE CONCENTRATION CELL

For a reversible electrochemical cell, the overpotential for concentration polarization is defined by Nernst equation. Using eq. (2.32) with the constant $K = C_x/C_o$ and the cathodic overpotential as $\eta_c = E - E_o$ yields the cathodic overpotential in terms of concentration ratio

$$\eta_c = -\frac{RT}{zF} \ln \left[\frac{C_x}{C_o} \right] \quad (4.65)$$

which indicates that η_c becomes more negative as the concentration C_x increases. Here, $C_x = C(x) > 0$ and $C_x = C(\infty) = C_b$ as the limited concentration in the bulk. Evaluating eq. (4.64) at $x = \infty$ and $x = 0$ yields the overpotential as

$$\eta_c = \phi(\infty) - \phi(0) \quad (a)$$

$$\eta_c = \phi_o \exp(-\infty) - \phi_o \exp(-0) \quad (b)$$

$$\eta_c = -\phi \exp(x/\delta) \quad (4.66)$$

Recall that $\delta = \sqrt{\pi Dt}$.

Combining eqs. (4.65) and (4.66) yields the interfacial potential as

$$\phi = \frac{RT}{zF} \ln \left[\frac{C_x}{C_o} \right] \cdot \exp(-x/\delta) \quad (4.66a)$$

From eq. (4.65), the concentration for concentration (conc.) polarization becomes

$$C_x = C_o \exp \left(\frac{zF\eta_c}{RT} \right) \quad (\text{Conc. Polarization, } C_b > C_o) \quad (4.67)$$

and for activation (act.) polarization is

$$C_x = C_o \exp\left(-\frac{zF\eta_a}{RT}\right) \quad (\text{Act. Polarization, } C_b < C_o) \quad (4.68)$$

from which the activation overpotential is defined as

$$\eta_a = \frac{RT}{zF} \ln \left[\frac{C_o}{C_x} \right] \quad (4.69)$$

The concentration profile expressions, eqs. (4.67) and (4.68), are now determined as exponential functions, instead of the error function as previously treated in a diffusion process.

4.7 LIMITING CURRENT DENSITY

Assume that the mass transfer is due to diffusion and that the diffusion molar flux (J_x) is the chemical rate of the mass transfer under steady-state condition. Subsequently, the diffusion process can be described by Fick's first law. Thus, eq. (4.18) becomes

$$J_x = -D \frac{\Delta C}{\Delta x} = -D \left(\frac{C_x - C_o}{\delta} \right) \quad (4.70)$$

where $\Delta x = x - x_o = \delta = \sqrt{\pi Dt}$ since $x_o = 0$ at the electrode surface.

Combining eqs. (4.8) and (4.70) yields the cathodic current density for a steady-state condition $\Delta C < 0$

$$i_c = -\frac{zFD\Delta C}{\sqrt{\pi Dt}} \quad (4.71)$$

Recall that zF product is the number of coulombs required to convert 1 mole of metal to corrosion product. However, there must exist a limiting current density (i_L). Hence, eq. (4.71) becomes

$$i_L = \frac{zFDC_o}{\sqrt{\pi Dt}} \quad (4.72)$$

since $C_o = 0$ at a distance $x = 0$ (electrode surface).

Example 4.3 Use the data given in Example 4.1, part a, to calculate a) the concentration gradient at $x = 0$, J_x , i and δ and b) η_a and i_L @ $x = 0.12$ mm and $t = 10$ minutes.

Solution:

Data: $D = 1.5 \times 10^{-6}$ cm²/s; $C_o = 10^{-2}$ mol/cm³; $C_b = 4 \times 10^{-4}$ mol/cm³

$$C_x = 7.89 \times 10^{-3} \text{ mol/cm}^3 \text{ @ } x = 0.12 \text{ mm and } t = 10 \text{ min} = 600 \text{ s}$$

a) From eq. (4.51),

$$\partial C / \partial x = (C_b - C_o) / \sqrt{\pi D t}$$

$$\partial C / \partial x = -0.18 \text{ mol/cm}^4$$

From eq. (4.52),

$$i = z F D \Delta C / \sqrt{\pi D t}$$

$$i = 2.18 \times 10^{-3} \text{ A/cm}^2$$

From eq. (4.3),

$$J_d = -D \partial C / \partial x$$

$$J_d = 2.70 \times 10^{-7} \text{ mol/cm}^2 \cdot \text{s}$$

$$\delta = \sqrt{\pi D t}$$

$$\delta = 0.53 \text{ mm}$$

b) @ $x = 0.12 \text{ mm}$, $t = 600 \text{ s}$ and $T = 25^\circ \text{C} = 298 \text{K}$

From eq. (4.69),

$$\eta_a = \frac{RT}{zF} \ln \left[\frac{C_o}{C} \right]$$

$$\eta_a = 3.04 \text{ mV}$$

From eq. (4.72),

$$i_L = z F D C_x / \sqrt{\pi D t}$$

$$i_L = 4.31 \times 10^{-2} \text{ A/cm}^2 > i$$

Combining eqs. (4.71) and (4.72) yields the current density ratio as

$$\frac{i_c}{i_L} = \frac{\Delta C}{C} = \frac{C_x - C_o}{C_x} = 1 - \frac{C_o}{C_x} \quad (4.73)$$

Thus, the concentration ratio becomes

$$\frac{C_o}{C_x} = 1 - \frac{i_c}{i_L} \quad (4.74)$$

Substituting eq. (4.74) into (4.65) gives the overpotential for concentration polarization in terms of the limiting current density

$$\eta_{conc} = \frac{RT}{zF} \ln \left(1 - \frac{i_c}{i_L} \right) \quad (\text{For } i_L > i_c) \quad (4.75)$$

$$\eta_{conc} = \frac{2.303RT}{zF} \log \left(1 - \frac{i_c}{i_L} \right) \quad (4.76)$$

If $\eta_{conc} \rightarrow 0$, then eq. (4.75) becomes a linear approximation

$$\eta_{conc} = \frac{RT}{zF} \left(1 - \frac{i_c}{i_L} \right) \quad (4.77)$$

Recall that the overpotential for activation polarization is given by eq. (3.20), but it is renumbered here for convenience. Thus,

$$\eta_{act} = \beta_c \log \left(\frac{i_c}{i_o} \right) = -\frac{2.303RT}{(1-\alpha)zF} \log \left(\frac{i_c}{i_o} \right) \quad (4.78)$$

where $i_o = i_{corr}$. Now, the total cathodic overpotential for the assumed diffusion process is the sum of eqs. (4.76) and (4.78)

$$\eta_c = \eta_{conc} + \eta_{act} \quad (4.79)$$

$$\eta_c = \frac{2.303RT}{zF} \left[\log \left(1 - \frac{i_c}{i_L} \right) - \frac{1}{(1-\alpha)} \log \left(\frac{i_c}{i_o} \right) \right] \quad (4.80)$$

or

$$\eta_c = \frac{RT}{zF} \left[\ln \left(1 - \frac{i_c}{i_L} \right) - \frac{1}{(1-\alpha)} \ln \left(\frac{i_c}{i_o} \right) \right] \quad (4.81)$$

But, $\eta_c = E_c - E_o$ where E_c is the applied cathodic potential and $E_o = E_{corr}$ is the corrosion potential. Thus, eq. (4.81) becomes

$$E_c = E_o + \frac{2.303RT}{zF} \left[\log \left(1 - \frac{i_c}{i_L} \right) - \frac{1}{(1-\alpha)} \log \left(\frac{i_c}{i_o} \right) \right] \quad (4.82)$$

This equation gives a cathodic curve from i_{corr} to i_L as schematically shown in Figure 4.11 [3,6].

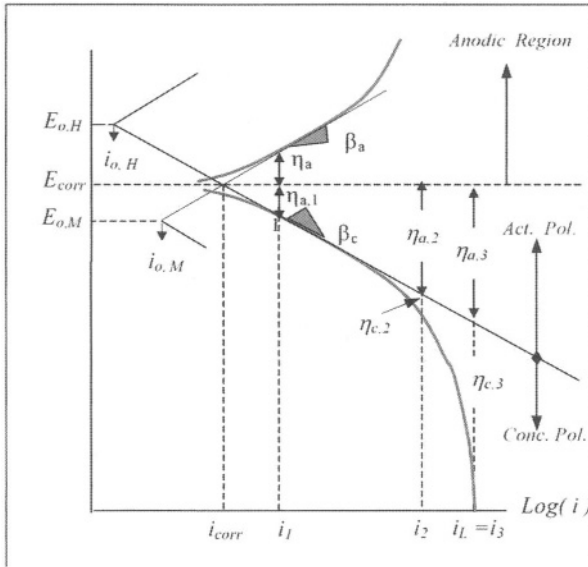


Figure 4.11 Schematic curves illustrating the activation polarization (Act. Pol.) and concentration polarization (Conc. Pol.) regions.

Notice from Figure 4.11 that

- A shift from (E_{corr}, i_{corr}) to point 1 gives the overpotential as $\eta = \eta_{a,1}$ and activation polarization controls the mass transfer.
- At point 2, $\eta = \eta_{a,2} + \eta_{c,2}$ and a mixed polarization exists, but $\eta_{a,2} > \eta_{c,2}$.
- At point 3, $\eta = \eta_{a,3} + \eta_{c,3}$ and a mixed polarization exists, but the current density at this point does not depend on potential and $i_3 = i_L$.
- According to eq. (4.82), a change in temperature shifts the cathodic polarization curve.

In determining the oxidation or reduction state, which is just the valence, one needs to know the Tafel slopes and symmetry factor defined by eqs. (3.21) and (3.22). However, the valence z can be estimated using the relationship for concentration polarization given by eq. (4.75) with $\eta_{conc} = E_c - E_{corr}$. Hence,

$$E_c = E_{corr} + \frac{RT}{zF} \ln \left(1 - \frac{i_c}{i_L} \right) \quad (4.83)$$

Plotting E_c vs $\ln(1 - i_c/i_L)$ gives a straight line as schematically shown in Figure 4.12. Extrapolating the straight line provides an intercept that corresponds to E_{corr} .

The slope of the straight line is

$$S_c = \frac{\Delta E}{\Delta \ln(1 - i_c/i_L)} = \frac{RT}{zF} \quad (4.84)$$

Solving eq. (4.84) for z yields an expression for approximating the oxidation state. Hence,

$$z = \frac{RT}{FS_c} \quad (4.85)$$

The slope can also be determined mathematically by taking the first derivative of eq. (4.83) with respect to the cathodic current density. Thus,

$$\frac{dE_c}{di_c} = -\frac{RT}{zF(i_c - i_L)} \quad (4.86)$$

$$S_c = \frac{dE_c}{di_c} = \frac{\Delta E_c}{\Delta i_c} \quad (4.87)$$

Then,

$$z = -\frac{RT}{S_c F(i_c - i_L)} \quad (4.88)$$

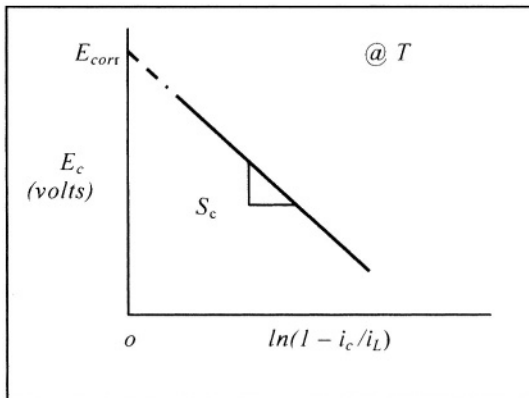


Figure 4.12 Linearization of eq. (4.83).

The preceding graphical approach is quite fundamental, but it is an essential element in electrochemistry. For instance, this linear approach is normally used in determining z for organic compounds in irreversible polarographic processes, which is a controlled-potential technique that requires a current response as a function of time for reducing species j [19]. The goal in this technique is to measure the limiting current $I_L = A_s i_L = f(t)$ where A is the surface area of the electrode. Hence, eq. (4.52) becomes

$$I_L = \frac{zFA_s DC_b}{\sqrt{\pi Dt}} \quad (4.89)$$

Furthermore, during cathodic processes, ions move towards the cathode, the bulk and surface concentration are related as $C_b > C_s$ and a limiting current density arises due to ion depletion in the bulk solution. From a hydrodynamic point of view, i_L increases with increasing the velocity and temperature of the solution. Thus, the rate of mass transfer under laminar flow can be converted to i_L using Faraday's law. In fact, the precise control of solution velocity and a stationary electrode or a rotating electrode in a quasi-stationary solution is difficult to achieved at high velocities. For instance, the classical **rotating-disk electrode** having a smooth surface is convenient for characterizing the effects of solution flow on corrosion reactions. According to Boden [24], the mathematical model for determining $i_L \simeq i_{corr}$ as a function of angular velocity is based on the Levich equation derived in Chapter 7, but after some rearrangement the final form of this equation, which is used to determine D , is [25]

$$i_L = 0.62zFC_b D^{2/3} K_v^{-1/6} \sqrt{\omega} \quad (4.90)$$

where r = Rotating-disk radius (cm)
 K_v = Kinematic viscosity (cm^2/s)
 ω = Angular velocity ($Hz = 1/s$)

A simple relationship for i_L is as follows

$$i_L = \varepsilon \sqrt{\omega} \quad (4.91)$$

$$\varepsilon = 0.62zFC_b D^{2/3} K_v^{-1/6} \quad (4.92)$$

In addition, eq. (4.91) suggests that the rotating smooth surface exposed to the solution is subjected to a transition from laminar to turbulent flow at a Reynolds number defined by [22]

$$Re = \frac{\omega r_t^2}{K_v} = \frac{\omega r_t^2 \rho}{\eta_v} \quad (4.93)$$

where r_t = Radius at which transition occurs (cm)
 η_v = Fluid viscosity ($g/cm.s$)
 ρ = Density of particles (ions) (g/cm^3)

The transitional radius is smaller than the disk radius ($r_t < r$). Also, knowing the number of revolutions per unit time (N) of a rotating disk, the angular velocity is easily computed as $\omega = 2\pi N$. Commercial instrumentation is nowadays available for conducting electrochemical experiments using a rotating electrode systems at a wide range of electrode speeds. The reader wishing to obtain detailed information on commercial equipment should use a World Wide Web (www) search engine.

4.8 GALVANOSTATIC POLARIZATION

Using the galvanostatic technique gives rise to a current across the cathode electrode and the potential response is measure prior to reaching steady-state. According to Erdey-Gruz [31], the boundary condition used for solving Fick's second law can be deduced from eq. (4.23). Hence,

$$D \frac{\partial C}{\partial x} = \frac{i}{zF} \quad \text{for } t > 0, \quad x = 0, \quad i = \text{constant} \quad (4.94)$$

Subsequently, the concentration equation as a function of time takes the following analytical form

$$C = C_o - \frac{2i}{zF} \sqrt{\frac{t}{\pi D}} \quad (4.95)$$

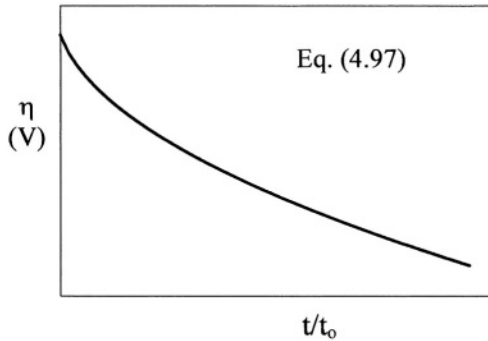
In addition, the transition diffusion time for $C = C_s = 0$ at $x = 0$ (electrode surface) is deduced from eq. (4.95) as

$$t_o = \frac{\pi D}{4} \left(\frac{zFC_o}{i} \right)^2 \quad (4.96)$$

Combining eqs.(4.95) and (4.96) yields the diffusion overpotential as a function of time as well as temperature

$$\eta = \frac{RT}{zF} \ln \left(1 - \sqrt{t/t_o} \right) \simeq \frac{RT}{zF} \left(1 - \sqrt{t/t_o} \right) \quad (4.97)$$

The interpretation of eq.(4.97) suggests that $\eta \rightarrow \infty$ when $t = t_o$ which is unrealistic. Instead, $\left(1 - \sqrt{t/t_o} \right) < 1$ so that $\eta < 0$ and another electrochemical process takes place when $t \rightarrow t_o$. The profile given by eq. (4.97) is shown in Figure 4.13.



4.9 A.C. POLARIZATION

An A.C. polarization is caused by an alternating current (A.C.), which in turn, affects the concentration periodically in the vicinity of the cathode electrode surface, but the charged double-layer is assumed to remain undisturbed [31]. Under these A.C. conditions, eq. (3.55) becomes

$$i = i_o \sin(\omega t) \quad (4.98)$$

Inserting this expression into eq. (4.23) gives the alternating concentration gradient

$$\frac{\partial C}{\partial x} = \frac{i_o}{zFD} \sin(\omega t) \quad (4.99)$$

According to Erdey-Gruz [31], the periodic concentration is defined as

$$C = C_o - \frac{i_o}{zF\sqrt{\omega D}} \exp\left(-x\sqrt{\frac{\omega}{2D}}\right) \cos\left(\omega t + \frac{\pi}{4} - x\sqrt{\frac{\omega}{2D}}\right) \quad (4.100)$$

Thus, the overpotential becomes

$$\eta = \frac{RT}{zF} \ln\left(\frac{C_s}{C_o}\right) \quad (4.101)$$

$$\eta = \frac{RT}{zF} \ln\left(1 + \frac{C_s - C_o}{C_o}\right) \quad (4.102)$$

$$\eta \simeq \frac{RT}{zF} \ln\left(\frac{C_s - C_o}{C_o}\right) \quad (4.103)$$

Combining eqs. (4.100) and (4.103) along with $C_s = 0$ at $x = 0$ yields the periodic overpotential for activation polarization defined by

$$\eta_{ac} = \frac{RTi_o}{(zF)^2 C_o \sqrt{\omega}} \sin\left(\omega t + \frac{\pi}{4}\right) \quad (4.104)$$

$$\eta_{ac} \simeq \frac{RTi_o}{(zF)^2 C_o \sqrt{\omega}} \left(\omega t + \frac{\pi}{4}\right) \quad \text{for } \left(\omega t + \frac{\pi}{4}\right) \rightarrow 0 \quad (4.105)$$

4.10 SUMMARY

The concentration of a specie j is lower at the electrode surface than in the bulk $C_b > C_o$. This is the opposite of activation polarization in which $C_b < C_o$. The kinetics of concentration polarization is a rate-controlling electrochemical process since the electrode is cathodically polarized. The mass transfer may be by diffusion, migration, convection or a combination of these modes. Thus, the Nernst-Planck equation can give reasonable results. However, if diffusion is the solely mechanism, Fick's first law states that the diffusion molar flux depends on the concentration gradient at a steady-state since the concentration rate is $dC/dt = 0$. On the other hand, Fick's second law of diffusion requires that $dC/dt \neq 0$, but it strongly depends on the concentration gradient $\partial^2 C/\partial x^2$ and time. The solution of Fick's second law depends on the type of diffusion problem and related boundary conditions, but the presented solution given in Appendix A is based on the error function of the Bell-Shaped Function $y = \exp(-x^2)$, and it predicts that the concentration of a specie j , the concentration gradient, and current density decay with time $t^{-1/2}$ at the electrode surface. Despite that the current density is a time-dependent parameter, it is influenced by the flux of specie j and it is restrictive to the limiting current density (i_L) as its maximum value. Therefore, the overpotential needed for concentration polarization depends on the current density ratio i_c/i_L as described by the Nernst equation as $\eta_c = f(i_c/i_L)$.

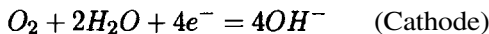
4.11 PROBLEMS/QUESTIONS

4.1 Why convective mass transfer is independent of concentration gradient $\partial C/\partial x$ in eq. (4.2)?

4.2 Use the information given in Example 4.2 to determine the concentration rate in the x-direction at 1 mm from the columns interface. Given data: $D = 10^{-5} \text{ cm}^2/\text{s}$, $C_o = 10^{-4} \text{ mol}/\text{cm}^3$ and $t = 10 \text{ sec}$. [Solution: $1.96 \times 10^{-16} \text{ mol}/(\text{cm}^3 \cdot \text{s})$].

4.3 What's the action of hydrogen on a steel blade exposed to an aqueous solution of hydrogen sulfide if the following reaction takes place $Fe + H_2S = FeS + 2H$? Assume that the steel blade gets damaged during service.

4.4 An aerated acid solution containing 10^{-2} mol/l of dissolved oxygen (O_2) moves at 2×10^{-4} cm/s in a stainless steel pipe when a critical current density of $10^3 \mu A/cm^2$ passivates the pipe. Calculate a) the thickness of the Helmholtz ionic structural layer (δ), b) the limiting current density (i_L) if the three modes of flux are equal in magnitude, and c) Will the pipe corrode under the current conditions? Why? or Why not? Data:



$D_{O_2} = 10^{-5} \text{ cm}^2/\text{s}$	$T = 25^\circ C$	$F = 96,500 \text{ A.s/mol}$
---	------------------	------------------------------

[Solutions: a) $\delta = 0.5 \text{ mm}$, b) $i_L = 2.32 \times 10^3 \mu A/cm^2$ and c) It will not].

4.5 a) Determine the oxygen concentration for Problem 4.4 that will promote corrosion of the stainless steel pipe. b) How long will it take for corrosion to occur? [Solutions: a) $C_b = 1.30 \times 10^{-2} \text{ mol/l}$ and b) $t = 1.34 \text{ min.}$].

4.6 Use the given data to calculate a) the diffusivity of copper ions in a cathodic process at $25^\circ C$ and b) the valence z . The original concentration in an acidic solution is 60 g/l . [Solution: a) $D = 10^{-5} \text{ cm}^2/\text{s}$ and b) $z = 2$].

t (sec)	i ($x10^{-2} \text{ A/cm}^2$)	$\partial C/\partial x$ ($x10^{-3} \text{ mol/cm}^4$)
0	0	0
5	0.1455	0.7531
10	0.1029	0.05325
15	0.0840	0.04350
20	0.0728	0.03766

4.7 It is desired to reduce copper, $Cu^{+2} + 2e^- = Cu$, at $35^\circ C$ from an electrolyte containing 60 g/l of Cu^{+2} ions. Calculate a) the total molar flux that arises from equal amounts of diffusion and migration mass transfer under steady-state conditions, b) the gradients dc/dx , $d\phi/dx$, and $d\mu/dx$, and c) approximate the thickness of the diffusion layer at the cathode electrode surface. Operate the electrowinning cell for 10 minutes and let the diffusivity for Cu^{+2} ions be $10^{-5} \text{ cm}^2/\text{s}$. [Solution: a) $J = 6.88 \times 10^{-8} \text{ mol/cm}^2 \cdot \text{s}$, b) $\partial C/\partial x|_{x=0} = 3.88 \times 10^{-3} \text{ mol/cm}^4$, $d\phi/dx = -4.83 \times 10^{-2} \text{ V/cm}$, $d\mu/dx = -1.55 \times 10^{-20} \text{ J/cm}$, and c) $\delta = 1.37 \text{ mm}$].

4.8 Show that $J_{x=0} = DC_o/\delta$.

4.9 Show that $dC/dx = C_b/\sqrt{\pi Dt}$.

4.10 Prove that the diffusivity D is constant in the Fick's second law, eq. (4.19).

4.11 Assume that the total molar flux of a specie j is due to diffusion and convection. The convective force acting on the specie is $F_x = - (1/N_A) (d\Delta G/dx)$, where N_A is Avogadro's number and $d\Delta G/dx$ is the molar free energy gradient. Recall that the volume fraction is equals to the mole fraction divided by molar concentration; that is, $V = X/C$. Based on this information, show that

$$\frac{dC}{dx} = C \left[\frac{d \ln (C/C_o)}{dx} \right]$$

where $J_d = J_c$, $K = C/C_o < 1$ and $C_o = \text{Constant (mol/l)}$.

4.12 Use the information given in Problem 4.11 to show that

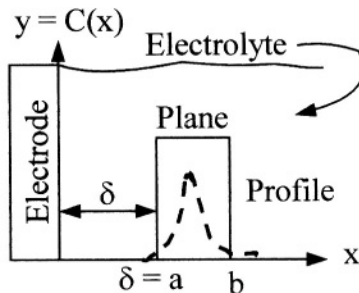
$$\frac{d\Delta G}{dx} = \frac{RT}{C} \frac{dC}{dx}$$

4.13 Use the information given in Problem 4.12 to show that

$$v_x = - \frac{D}{C} \frac{dC}{dx}$$

4.14 If the migration flux is neglected in eq. (4.2), approximate the total flux at low and high temperatures. Assume that $C_x \gg C_o$ at a distance x from an electrode surface.

4.15 Consider the concentration plane shown below. This is a transient electrochemical system having finite dimensions. Derive a solution for Fick's second law, $\partial C/\partial t = D\partial^2 C/\partial x^2$ when $a \leq x \leq b$.



4.16 Derive Fick's second law if the volume element in Figure 4.2 has a unit cross-sectional area and a thickness x .

4.17 What does Fick's first law mean in terms of atoms or ions of a single phase?

4.18 What will Fick's first law mean if D does not vary with x or C ?

4.19 Derive Fick's second law if the volume element in Figure 4.2 has a unit cross-sectional area and the diffusing plane is located between x and $x + dx$, where J_x is the entering molar flux at x and J_{x+dx} is that leaving at $x + dx$.

4.20 Find an expression for x when

$$\frac{C_x - C_b}{C_o - C_b} = 0.5205 = \operatorname{erf}\left(\frac{x}{\sqrt{4Dt}}\right)$$

4.21 Prove eq. (4.62).

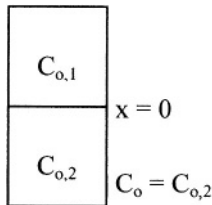
4.22 Show that $d\phi/dx = -7\phi_o/(19\sqrt{\pi Dt})$ in a coupled diffusion and migration mass transfer. let $x = \sqrt{\pi Dt}$.

4.23 For activation polarization, the concentration gradient is given by eq. (4.50). If $C_b \ll C_o$, then show that

$$\frac{C}{C_o} = \frac{1}{\sqrt{4\pi Dt}} \left(\frac{x^3}{12Dt} - x \right)$$

4.24 Derive the Nernst-Einstein equation (4.15) by converting eq. (2.31a) into chemical potential if only one ion participates in a reaction. The reaction constant is defined by $K = \gamma C$, where γ is the activity coefficient and C is the concentration. Let the molar diffusion and migration be equal in eq. (4.15).

4.25 Use exactly the same statement given in Example 4.2, but including the information on page 134 for determining the average concentration as the starting point in this problem. Let $C_{o,1}$ and $C_{o,2}$ be the original concentrations of columns 1 and 2, respectively.



4.26 This problem requires the determination of the total molar flux and current density profiles due to diffusion, migration and convection for the electrodeposition of nickel from an electrolyte containing $8 \times 10^{-4} \text{ mol/cm}^3$ of Ni^{+2} cations. The electrochemical cell has a continuous and direct fluid flow system of 20 cm/s at 35°C . The diffusivity of Ni^{+2} cations is $D = 1.44 \times 10^{-5} \text{ cm}^2/\text{s}$.
 a) Use $0 \leq t \leq 100$ seconds for $J_x = f(t, x = 0)$ at the electrode surface and

b) $0 \leq x \leq 10$ centimeters for $J_x = f(x, t = 10)$, and c) analyze the resultant profiles very succinctly and determine which molar flux dominates in this hypothetical electrodeposition process for Ni^{+2} cations from solution. Can this process achieve a steady-state?

4.27 a) Derive an expression for the concentration in g/l as a function of temperature T and distance x from an oxidizing pure copper electrode in an electrolyte under an electrostatic field. Use the chemical potential gradient, $d\mu/dx = -(zF) d\phi/dx$ with an electric potential decay. Let the free energy change be defined as $\Delta G = \Delta G_x @ x$ and $\Delta G = \Delta G_\infty @ x = \infty$. b) Plot the concentration C_x profile at two different temperatures. Let

$\phi_\infty = 0$	$\lambda = 0.2 \text{ cm}^{-1}$
$\phi_o = 8.314 \times 10^{-3} \text{ V}$	$0 \leq x \leq 3.8 \text{ cm}$
$T = 298^\circ \text{K}$ (curve)	$C_\infty = 1.57 \times 10^{-3} \text{ mol/l} = 0.1 \text{ g/l}$
$T = 318^\circ \text{K}$ (- - curve)	$F = 96,500 \text{ J/mol.V}$

4.28 Derive an expression for $i_L = f(C_x, T, v_x)$ and explain its physical significance with respect to concentration polarization and metal reduction. Use a schematic polarization diagram to support your explanation. When is the concentration polarization process discernible (apparent)?

4.12 REFERENCES

[1] M.G. Fontana, "Corrosion Engineering," Third edition, McGraw-Hill Book Company, New York, (1986).

[2] T.N. Andersen and H. Eyring, Chapter 3 "Principles of Electrode Kinetics," in *Physical Chemistry: An Advanced Treatise*, Vol. IXA/Electrochemistry, Edited by Henry Eyring, Academic Press Inc., (1970).

[3] D.W. Shoesmith, "Kinetics of Aqueous Corrosion," in *Corrosion*, ASM Handbook, Vol. 13, American Society for Metals International, Ninth edition, (1987).

[4] D.A. Jones, "Principles and Prevention of Corrosion," Macmillan Publishing Company, New York, (1992).

[5] I.N. Levine, "Physical Chemistry" McGraw-Hill Book Company, New York, (1978) 500.

[6] E.M. Purcell, "Electricity and Magnetism," Berkeley Physics Course, Vol. 2, McGraw-Hill Book Company, New York, (1965) 420.

[7] L.L. Shreir, "Outline of Electrochemistry," in *Corrosion* Vol. 2, Corrosion Control, Edited by L.L. Shreir, R.A. Jarman, and G.T. Burstein, Butterworth-Heinemann, Boston, USA, (1994).

[8] U.R. Evans, J. Franklin Institute, 208 (52) (1929).

[9] U.R. Evans, "The Corrosion and Oxidation of Metals" Arnold, London, UK, (1961).

[10] M. Stern, J. Electrochem. Soc., 104 (1957) 56.

- [11] M. Stern, *Corrosion*, 13 (1975) 755.
- [12] L.L. Shreir, "Corrosion in Aqueous Corrosion," in *Corrosion Vol. 1, Metal/Environment Reactions*, Edited by L.L. Shreir, R.A. Jarman, and G.T. Burstein, Butterworth-Heinemann, Boston, USA, (1994).
- [13] J.R. Scully, "Electrochemical Methods of Corrosion Testing" in *Corrosion, Vol. 13, Laboratory Testing*, American Society for Metals International., Ninth edition, ASM Inter. (1987) 213.
- [14] H.P. Hacks, "Evaluation of Galvanic Corrosion," in *Corrosion, Vol. 13, Ninth edition*, American Society for Metals International, ASM Inter., (1987) 236.
- [15] J.R. Maloy, *J. Chem. Educ.*, 60 (1983) 285.
- [16] J. Wang, "Analytical Electrochemistry," Wiley-VCH, Inc., (2000) 5.
- [17] J.W. Evans and L.C. De Jonghe, "The Production of Inorganic Materials," Macmillan Publishing Company, New York, (1991) 149, 186, 190.
- [18] T. Erdey-Cruz, "Kinetics of Electrode Processes" Wiley-Interscience, John Wiley & Sons Inc., New York, (1972) 442.
- [19] J. Wang, "Analytical Electrochemistry," Wiley-VCH, Inc., (1994) 32.
- [20] D.R. Gaskell, "An Introduction to Transport Phenomena in Materials Engineering," Macmillan Publishing Company, New York, (1992) 373-379, 483-89, 505.
- [21] G.H. Geiger and D.R. Poirier, "Transport Phenomena in Metallurgy," Addison-Wesley Publishing Company, Readings, Massachusetts, (1973) 449-459.
- [22] A. F. Mills, "Basic Heat and Mass Transport," second edition, Prentice-Hall Inc., (1999) 330, 758, 820-823.
- [23] J. Crank, "The Mathematics of Diffusion," second edition, Oxford University Press, (1975).
- [24] P.J. Boden, "Effect of Concentration, Velocity and Temperature," in *Corrosion: Metal/Environment Reactions*, third edition, Edited by L.L. Shreir, R.A. Jarman and G.T. Burstein, Butterworth-Heinemann, (1998) 2:3-2:30.
- [25] V.G. Levich, "Physicochemical Hydrodynamics," Prentice-Hall Inc., (1962).
- [26] T. Rosenquist, "Principles of Extractive Metallurgy," Second edition, McGraw-Hill Book, New York, Company, (1983) 106-107.
- [27] A.L. Rouff, "Materials Science," Prentice-Hall, Inc., New Jersey, (1973) 447.
- [28] A. Kumar and R.K. Gupta, "Fundamentals of Polymers," The McGraw-Hill Companies, Inc., New York, (1998) 411-421.
- [29] J.S. Anderson and K. Saddington, *J. Chem. Soc.*, (1949) s381-s386.
- [30] L.G. Twidwell, "Electrometallurgy," Unit Process in Extractive Metallurgy, NSF Project SED 75-04821, (1978).
- [31] T. Erdey-Cruz, "Kinetics of Electrode Processes," Wiley-Interscience a Division of John Wiley & Sons, Inc., New York, (1972) 127-131.

Chapter 5

MIXED POTENTIAL THEORY

5.1 INTRODUCTION

This chapter is confined to analyze the complex aqueous corrosion phenomenon using the principles of mixed-potential, which in turn is related to the mixed electrode electrochemical corrosion process. This theory has been introduced in Chapter 3 and 4 as oxidation and reduction electrochemical reactions. Basically, this Chapter is an extension of the principles of electrochemistry, in which partial reactions were introduced as half-cell reactions, and their related kinetics were related to activation and concentration polarization processes. The principles and concepts introduced in this chapter represent a unique and yet, simplified approach for understanding the electrochemical behavior of corrosion (oxidation) and reduction reactions in simple electrochemical systems.

Both Evans and Stern diagrams are included in order to compare and analyze simple and uncomplicated electrochemical systems. The concept of anodic control and cathodic control polarization is also introduced. In addition, the predetermined corrosion circuit is included in order to analyze corrosion using an electrochemical device containing an external circuit.

5.2 MIXED-ELECTRODE POTENTIAL

Electrochemical corrosion systems can be characterized using the kinetic parameters previously described as Tafel slopes, exchange and limiting current densities. However, the mixed potential theory requires a mixed electrode system. This is shown in Figure 5.1 for the classical pure zinc (**Zn**) electrode immersed in hydrochloric (*HCl*) acid solution [1,8-9]. This type of graphical representation of electrode potential and current density is known as Evans Diagram for representing the electrode kinetics of pure zinc.

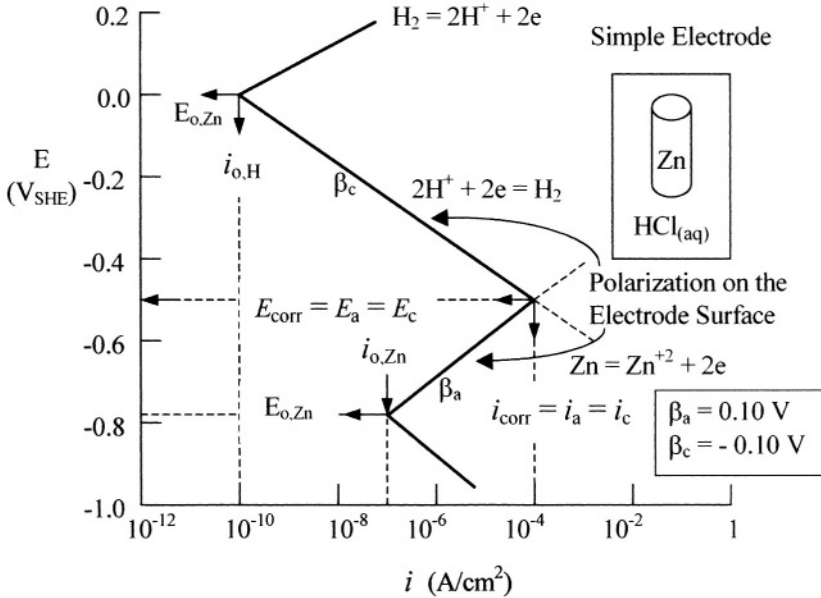


Figure 5.1 Evans Diagram for Zinc in HCl acid solution.

The Evans diagram requires anodic and cathodic straight lines and the corrosion potential (E_{corr}) and the corrosion current density (i_{corr}) point located where hydrogen reduction (H^+/H_2) line and zinc oxidation (Zn/Zn^{+2}) line converge. Furthermore, the exchange current densities (i_o) and the open-circuit potentials for hydrogen and zinc are necessary for completing the diagram as shown in Figure 5.1 for a simple Zn /electrolyte electrochemical system..

In fact, this type of potential-current density diagram can be developed for any solid material in contact with an electrolyte containing one or more oxidizing agents such as H^+ , Fe^{+2} , etc..As a result, the corrosion potential and the corrosion current density can be determined from the diagram (Figure 5.1).In addition, connecting the i_o and i_{corr} provides the shown straight lines, which are accompany by their respective overpotential equation. With regard to the $E_{corr} - i_{corr}$ point in Figure 5.1, the potentials and current densities are equal since this point represents electrochemical equilibrium.

On the other hand, Stern [10] used eq. (3.38) to draw anodic and cathodic nonlinear polarization curves, which provide a more realistic representation of the electrode kinetics of an electrochemical system. Evans (straight lines) and Stern (solid curves) graphical methods are illustrated in Figure 5.2 for a corroding hypothetical metal M immersed in an corrosive medium containing H^+ and F^{+2} oxidizers [6,13].

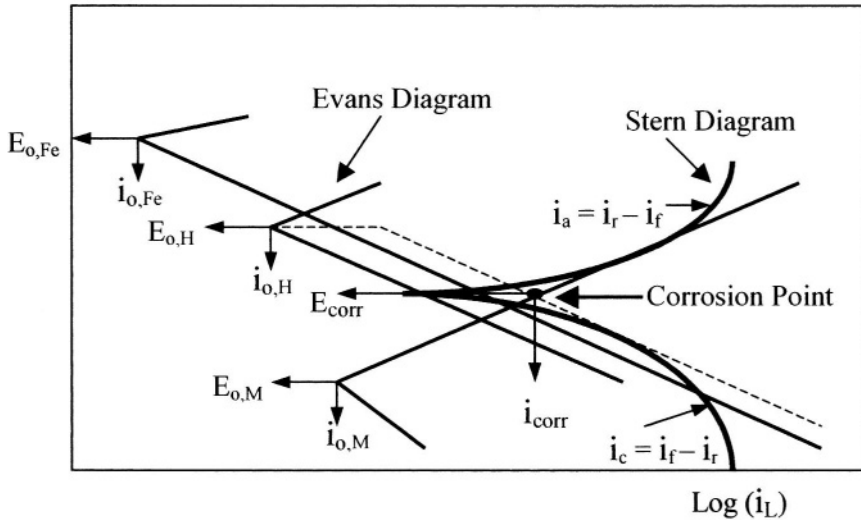


Figure 5.2 Comparison of polarization diagrams.

The addition of ferrous F^{+2} oxidizer to the electrolyte increases the corrosiveness of the electrolyte and requires an additional Evans diagram in order to determine the corrosion point of the metal M . In this particular case, the exchange current density, open-circuit potential and the Tafel slopes for each oxidizing agent and the metal is question must be known prior to construct the Evans diagram. This, then, is a disadvantage of this technique for determining E_{corr} and i_{corr} for the metal M .

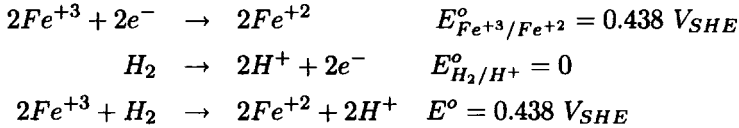
Furthermore, using the potentiostatic or potentiodynamic technique is very useful in determining the polarization curve near the corrosion point. However, the latter technique is a faster approach for obtaining even an entire polarization curve from a low potential at the limiting current density to a high potential for oxygen evolution. This dynamic approach is quite advantageous in obtaining a complete polarization curve in a few minutes.

Analysis of Figure 5.2:

The hypothetical polarization curve shown in Figure 5.2 illustrates a near-realistic industrial condition since most corroding solutions contain more than one oxidizing agent. Normally, ferric-ferrous salts and other ionic impurities are contained in acid solutions due to contamination from corrosion products and existing oxidizers [4]. Nevertheless, the electrochemical situation shown in Figure 5.2 implies that

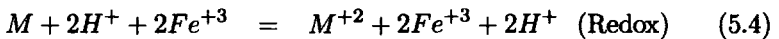
- The $E_{corr} - i_{corr}$ point is shifted as compared with Figure 5.1 due to addition of Fe^{+3} ions to M/H^+ system. Consequently, both E_{corr} and i_{corr} are increased.
- The rate of metal dissolution is increased as well as corrosion rate.

- Reduction of Fe^{+3}/Fe^{+2} and H^+/H oxidizers causes a mixed potential shift known as corrosion potential E_{corr} . This upward potential shift means that the metal becomes more noble (more positive).
- Redox reactions occur simultaneously on the metal surface. The exchange current densities (i_o) and their corresponding potentials open-circuit potentials (E_o) are indicated in Figure 5.2 according to the following reduction reactions



Recall that the potential for the redox reaction is $E^o = E_{Fe^{+3}/Fe^{+2}}^o + E_{H_2/H^+}^o$ and that the potentials for the anodic and cathodic reactions are given in Table 2.1.

- The principle of charge conservation at the point of intersection between requires Fe^{+3}/Fe^{+2} reduction line and H_2/H^+ oxidation line requires an addition of current density for reducing H^+/H_2 . Then, H^+/H_2 follows the dashed line above the Fe^{+3}/Fe^{+2} line until it intersects the M/M^{+z} line. The dashed line represents the total rate of reduction.
- For one metal oxidation reaction, two reduction reactions are needed. Therefore, the addition of Fe^{+3} ions reduce the hydrogen evolution.
- The possible reactions that can occur due to the electrochemical system shown in Figure 5.2 are



Addition of an oxidizer to an electrolyte not necessarily increases the corrosion potential. It is the exchange current density that dictates such a situation. For instance, if $i_{o,Fe^{+3}/Fe^{+2}} \ll i_{o,M/M^{+2}}$, then Fe^{+3} ions does not have a strong effects on E_{corr} and i_{corr} . The opposite is clearly understood since $i_{o,oxidizer}$ must be high enough to have an effect on E_{corr} and i_{corr} . Furthermore, if the applied potential is $E = 0$, then the current does not flow and metal oxidation and oxidizer reduction occur simultaneously at the metal/electrolyte interface. Therefore, the oxidation and reduction current densities are equal and $i = i_{ox} - i_{red} = 0$. On the other hand, if $E \neq 0$, then polarization takes place due to developed anodic and cathodic overpotentials

$$\eta_a = (E - E_{corr}) > 0 \quad (5.5)$$

$$\eta_c = (E - E_{corr}) < 0 \quad (5.6)$$

5.3 INTERPRETATION OF POLARIZATION

Anodic reactions represent metal deterioration since a corroding metal loses electrons. This is a surface electrochemical phenomenon that may cause drastic effects on metallic structures. Therefore, the driving force for corrosion is the overpotential (η) defined by

$$\eta = E_a - E_c \quad (5.7)$$

The subscript "a" and "c" stand for anodic and cathodic. With regard to Figure 5.1, assume that current does not flow, then the local potentials become the open-circuit potentials of the corroding system. Thus,

$$E_o = \begin{cases} E_{o,c} = E_{H^+/H_2} \\ E_{o,a} = E_{Z^n/Z^{n+2}} \end{cases} \quad (5.8)$$

On the other hand, if current flows, irreversible effects occur at the electrode surface due to electrochemical polarization effects. In this case, the corrosion potential and corrosion current density are compared with the cathodic and anodic terms. Thus,

$$E_c < E_{corr}, E_a \quad (5.9)$$

$$i_{corr} > i_{o,a} > i_{o,c} \quad (5.10)$$

$$i_{o,a} = i_{o,Z^n/Z^{n+2}} \quad (5.11)$$

$$i_{o,c} = i_{o,H^+/H_2} \quad (5.12)$$

Additionally, electrochemical polarization is a measure of the overpotential and represents a deviation of the electrochemical state of half-cell electrodes induced by an applied external potential. Therefore, the driving force for electrochemical polarization is the overpotential.

Consequently, the electrochemical polarization is divided into two classifications, such as anodic polarization and cathodic polarization. The corresponding overpotentials are defined by eqs. (3.35a) and (3.35b). Recall that the overpotentials for the anodic and cathodic parts of a polarization curve represent deviation from equilibrium anodically or cathodically. For convenience,

$$\eta_a = \beta_a \log \left(\frac{i_a}{i_{corr}} \right) > 0 \quad (5.13)$$

$$\eta_c = -\beta_c \log \left(\frac{i_c}{i_{corr}} \right) < 0 \quad (5.14)$$

In general, the higher the current density the higher the overpotential and the faster the electrochemical rate of reaction. Furthermore, other aspects of the polarization must be considered as a beneficial phenomenon for electrometallurgical operation, such as electrowinning, electrorefining, electroplating, and

cathodic protection against corrosion or a detrimental process for material surface deterioration known as corrosion. Therefore, continuous polarization causes local potentials to change until a steady state is reached and the observed mixed potential is the corrosion potential (E_{corr}) of the corroding electrochemical system. Thus far it has been assumed that the temperature and pressure are remain constant; otherwise, temperature and pressure gradients must included in the analysis of the electrochemical system.

A polarization diagram predicts the type of half-cell controlling the electrochemical system. Figure 5.3 depicts two schematic case for determining the controlling type of polarization.

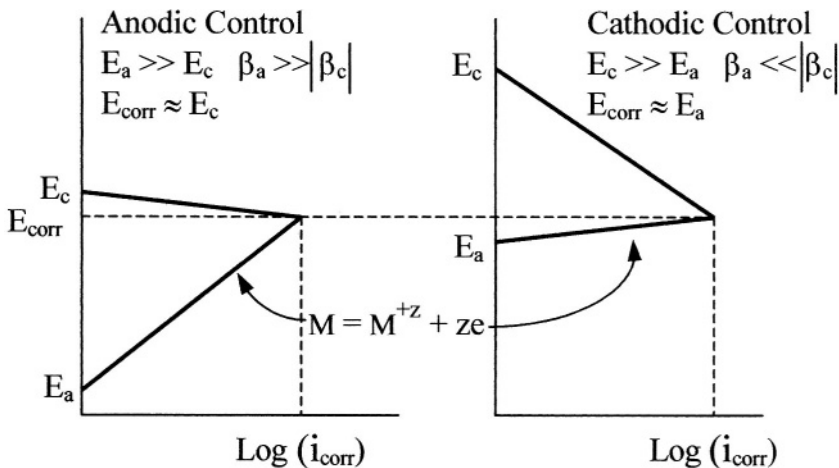


Figure 5.3 Schematic Evans diagrams showing controlling polarization.

Consider the electrochemical cells illustrated in Figure 5.4. When the circuit is disconnected current does not flow and the cell is at thermodynamics equilibrium. However, when current flows the cell is polarized and the forward (cathodic) and reverse (anodic) currents and potential at the electrodes have the following conditions

$$\begin{array}{ll}
 I_c > I_a & \text{for } M^{+z} + ze \rightarrow M \text{ at the cathode electrode} \\
 I_a > I_c & \text{for } M \rightarrow M^{+z} + ze \text{ at the anode electrode} \\
 I = (I_c - I_a)_c = (I_a - I_c)_a & \text{at the anode electrode} \\
 E_c < E < E_a & \text{at the voltmeter } V
 \end{array}$$

Subsequently, the rates of charge transfer processes are not equal and the equilibrium state is disturbed. Therefore, the electrodes are polarized. The

corresponding overpotentials for this polarized cell are given by eqs. (5.13) and (5.14).

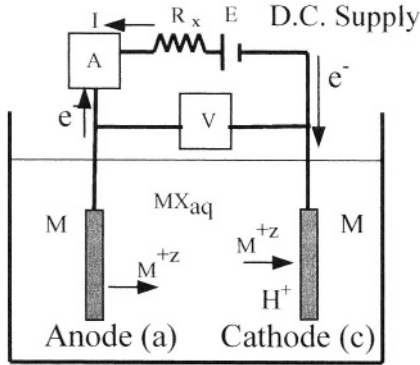


Figure 5.4 Polarization cell for metal M.

5.4 PREDETERMINED CORROSION RATE

Consider the cell shown in Figure 5.5 for measuring corrosion rate of zinc (Zn) at a predetermined rate through a resistor in the circuit [12].

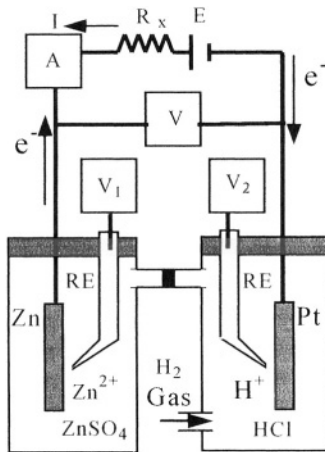
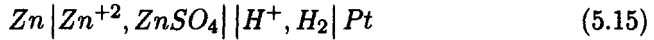
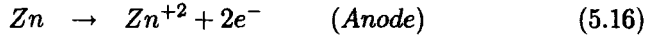


Figure 5.5 Reversible cell for measuring corrosion rate of zinc.

RESISTANCE-OFF. The reversible cell shown in Figure 5.5 can be represented by the following notation



According to this cell with the resistance R_x being disconnected the following reactions occur



According to eq. (5.17), hydrogen evolution occurs on the **Zn** surface electrode not on the **Pt** electrode [12]. This is far way from the real electrochemical interaction and therefore, the current cannot be measured. This implies that the potential of each electrode can be measured by connecting high-impedance voltmeters, V_1 and V_2 , as shown in Figure 5.5. At equilibrium, the currents and potentials are $I_c = I_a = 0$ and $E = E_c - E_a$. The free energy change (ΔG) and the electric potential difference (E) of the cell for the redox reaction can be determined using eqs. (2.31) and (2.32), respectively. For convenience, these equations

$$E = E^\circ - \frac{RT}{zF} \ln(K) \quad (5.19)$$

$$\Delta G = -zFE \quad (5.20)$$

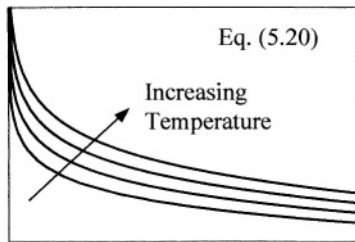
RESISTANCE-ON. Adjusting the resistance in the external circuit develops an overpotential and corrosion of **Zn** proceeds at a finite rate. This suggests that the cell is polarized. This polarization process implies that the anode becomes more positive for the oxidation of zinc (Zn/Zn^{+2}) and the cathode becomes more negative for the reduction of hydrogen ions or hydrogen evolution ($2\text{H}^+/\text{H}_2$). The measurable cell electric potential is defined in terms of open-circuit electric potential, anodic and cathodic electric overpotentials and by Ohm's law. Hence, $E = E_o - (\eta_a + \eta_c + IR_s)$ and according to Ohm's law the potential is $E = IR_x$. Therefore, $E_o - (\eta_a + \eta_c + IR_s)/R_x$, which suggests that the current I is strongly dependent on the external resistance R_x , but the corrosion of zinc can proceed at a finite rate when R_x is constant. If $R_x = 0$, then the cell becomes short-circuited and the current becomes a measure of rate of charge transfer [12]. Thus,

According to Shreir [12], a well-defined electrochemical cell containing an electrolyte of high conductivity dictates that Ohm's law for the external circuit and for the solution must give $IR_x \approx 0$ and $IR_s \approx 0$. Thus, the cell reversible open-circuit potential becomes $E_o = \eta_a + \eta_c$. This expression clearly shows that there is a mixed potential relationship, which implies that the measured potential is a mixed-potential in nature. This mixed potential is shown in Figure 3.2 as the Stern diagram or the polarization diagram.

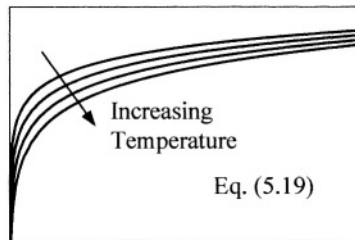
Example 5.1 Determine the overpotential and free energy change profiles as functions of the reaction constant at varying temperature. Explain the electrochemical behavior.

Solution:

The figures below show the required profiles for $E = f(K, T)$ and $\eta = F(K, T)$ in two dimensions Succinctly, both overpotential and free energy change are very sensitive to variations of both the reaction constant and temperature.



K



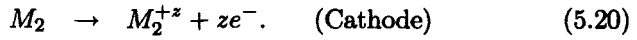
K

Example 5.1

5.5 POLARIZATION OF A GALVANIC CELL

This is the case for polarizing a galvanic coupling. Particular hypothetical galvanic polarization curves for metals M_1 and M_2 are shown in Figure 5.6. These curves imply that metals M_1 and M_2 are connected (coupled) and electron flow occurs from M_1 to M_2 since $i_{corr,M1} < i_{corr,M2}$. For convenience, assume that the metals have the same valence z . The main reactions that take

place in the coupling are



Thus, the coupling corrosion current density is depicted from Figure 5.6 at the crossover (intersect) of the anodic and cathodic polarization curves. This couple current density has a value between the corrosion current density for metal M_1 and M_2 , respectively

$$i_{corr,M1} < i_{couple} = i_{corr} < i_{corr,M2} \quad (5.24)$$

When steady-state is reached the current densities and potentials become equal; that is,

$$i_{couple} = i_a = -i_c \quad @ \text{ Equilibrium} \quad (5.25)$$

$$E_{couple} = E_{corr} \quad @ \text{ Equilibrium} \quad (5.26)$$

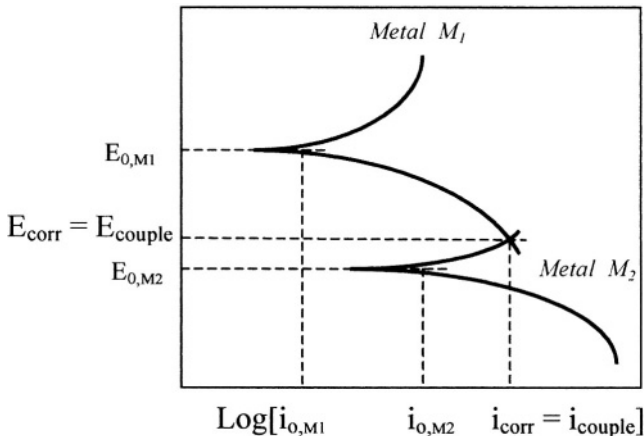


Figure 5.6 Schematic Galvanic couple polarization.

It should be pointed out that the corrosion potential in the galvanic series (Table 2.3) and that in the emf series (Table 2.4) are not the same. The former may be measured as a coupled potential at different temperatures and ionic concentrations used in the latter series. Therefore, the galvanic series must be used with caution since it is temperature and concentration dependent kinetic parameter.

5.6 EFFECT OF SURFACE AREA

The surface area of the electrode in the corrosive medium is known as the relative area, which influences the rate of galvanic corrosion. For instance, the experimental data on brass/steel couple in 20%NaCl at room temperature reported by Jones [19] can be used to determine that increasing the surface area ratio increases the the galvanic corrosion potential. Therefore, the corrosion potential of galvanic couplings is strongly dependent on the cathode-to-anode surface area ratio.

5.7 SUMMARY

The mixed-potential theory includes both anodic and cathodic polarization, in which diffusion of species is related to the current flowing in the electrolyte. The principles of mixed-potential allows the characterization of electrochemical corrosion systems by developing an Evan's diagram if the Tafel slopes and exchange current densities and at least one oxidizer agent are known. The kinetic parameters that are determined from an Evan's diagram are the corrosion potential and the corrosion current densities. Potentiodynamic polarization curves also know as Stern diagrams are obtainable very easily and exhibit different features that are useful in characterizing the electrochemical behavior of electrodes.

In addition, a departure from electrochemical equilibrium leads to a polarization scheme due to a developed overpotential $\eta > 0$ for anodic polarization and $\eta < 0$ for cathodic polarization. If current flows and $\eta \neq 0$, irreversible effects occur on the electrodes surfaces during polarization, which in turn, causes changes in local potentials until a steady-state is reached.

Characterizing galvanic corrosion in a particular environment simulating the service atmosphere must be done with caution. As previously mentioned, the galvanic corrosion potential is sensity to changes in temperature, ionic concentration and cathode-toanode surface area ratio.

5.8 REFERENCES

- [1] M.G. Fontana, "*Corrosion Engineering*," third edition, McGraw-Hill Book Company, New York, (1986).
- [2] T.N. Andersen and H. Eyring, "*Principles of Electrode Kinetics*," Chapter 3 in *Physical Chemistry: An Advanced Treatise*, Vol. IXA/Electrochemistry, edited by Henry Eyring, Academic Press, Inc., (1970).
- [3] D. W. Shoesmith, "*Kinetics of Aqueous Corrosion*," in *Corrosion*, ASM Handbook, Vol 13, American Society for Metals, Ninth edition, (1987).
- [4] D.A. Jones, "*Principles and Prevention of Corrosion*," Macmillan Publishing Company, New York, (1992).
- [5] I.N. Levine, "*Physical Chemistry*" McGraw-Hill Book Company, New York, (1978) 454-459, 498-500.
- [6] M. Stern, *J. Corrosion*, 13 (1957) 755.

- [7] L.L. Shreir, "*Outline of Electrochemistry*," in Corrosion, Vol. 2, Corrosion Control, Edited by L.L. Shreir, R.A. Jarman, and G.T. Burstein, Butterworth-Heinemann, Boston, (1994).
- [8] U.R. Evans, J. Franklin Institute, 208 (52) (1929).
- [9] U.R. Evans, "*The Corrosion and Oxidation of Metals*," Arnold, London, (1961).
- [10] M. Stern, J. Electrochem. Soc., 104 (1957) 56.
- [11] M. Stern, Corrosion, 13 (1957) 755.
- [12] L.L. Shreir, "*Corrosion in Aqueous Solutions*" in Corrosion, Vol. 1, Metal/Environment Reactions, Edited by L.L. Shreir, R.A. Jarman, and G.T. Burstein, Butterworth-Heinemann, Boston, (1994).
- [13] J.R. Scully, "*Electrochemical Methods of Corrosion Testing*," in Corrosion, Vol. 13, Laboratory Testing, ninth edition, ASM Inter. (1987) 213.
- [14] H.P. Hack, "*Evaluation of Galvanic Corrosion*" in Corrosion, Vol. 13, Ninth edition, ASM Inter., (1987) 236.
- [15] J.R. Maloy, J. Chem. Educ., 60 (1983) 285.
- [16] J. Wang, "*Analytical Electrochemistry*," Second edition, Wiley-VCH, Inc., (2000) 4-7.
- [17] J.W. Evans and L.C. De Jonghe, "*The Production of Inorganic Materials*," Macmillan Publishing Company, New York, (1991) 149.
- [18] T. Erdey-Cruz, "*Kinetics of Electrode Processes*," Wiley-Interscience, New York, (1972) 442.
- [19] D.A. Jones, Corrosion, Vol. 4, (1984) 181

Chapter 6

CORROSIVITY AND PASSIVITY

6.1 INTRODUCTION

The electrochemical corrosion behavior of metals and alloys can be studied by generating polarization curves, which provide several electrochemical regions of diverse physical meaning. A material exposed to severe environments can be characterized by analyzing a complete polarization curve, which includes electrochemical processes such as concentration polarization, activation polarization, and passivation. A material, specifically metallic solids, may exhibit some degree of corrosivity; that is, the tendency of an aggressive electrolyte (environment) to cause metal dissolution (corrosion through oxidation reaction). However, the same material may undergo passivation in the same environment at relatively high potentials independent of the current. Thus, passivity may be manifested due to electrodeposition of an impervious metal oxide film compound on the material surface, protecting it from deterioration. Further, increments in potential, the film usually breakdown leaving localized bare metal experiencing corrosion at relatively high potential.

6.2 INSTRUMENTATION

Electrochemical corrosion (*EC*) can be characterized using a proper electrochemical instrumentation. A custom design device is shown in Figure 6.1. The power supply is a potentiostat for controlling the potential or a galvanostat for current control flow. This electrochemical cell design gives satisfactory results for thin or brittle working electrodes (*WE*). The *WE* is embedded in epoxy resin along with a spot-weld wire. Actually, this type of *WE*-epoxy resin is just a metallographic sample, which is well polished prior to immersion in a working electrolyte. All parts immersed in the electrolyte must be inert to the

electrolyte in order to avoid electrochemical complications. Other custom design cells can be found elsewhere [5]. Figure 6.2 shows a commercially available ASTM G-5 standard electrochemical cell designed by EG&G Princeton Applied Research as Model K47. This cell has two auxiliary graphite electrodes for providing a uniform current distribution to the *WE* surface and it is known as a three-electrode cell.

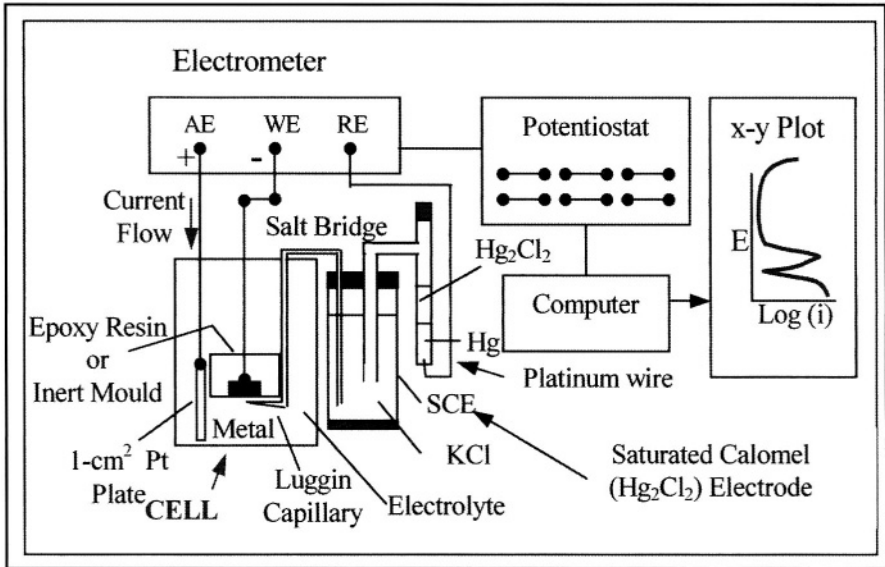


Figure 6.1 Schematic polarization device [4].

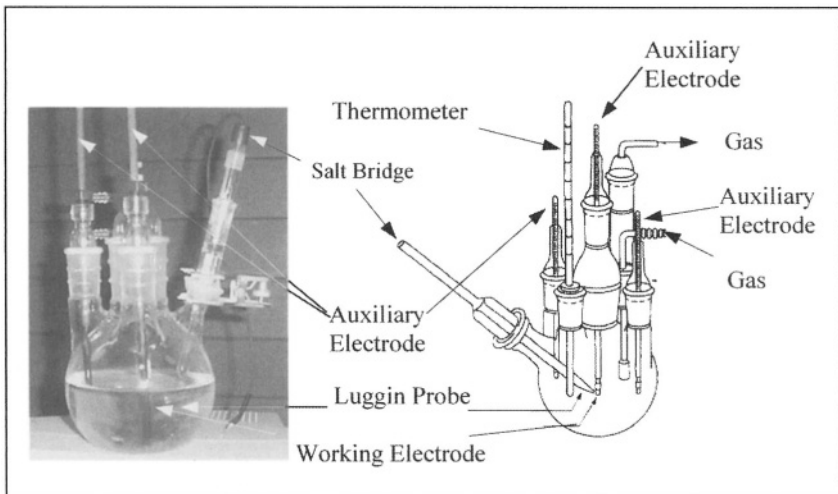


Figure 6.2 Commercially available electrochemical cell.

Furthermore, corrosion and electrochemical studies can be performed using a well-calibrated electrochemical instrumentation/equipment. Figure 6.3 illustrates an automated modern experimental instrumentation, which includes the commercially available device known as the Princeton Applied Research (PAR) EG&G Potentiostat/Galvanostat Model 273A and the electrochemical or polarization cell model K47. This particular cell known as a three-electrode electrochemical cell for characterizing the kinetics of the working electrode (*WE*) in a suitable environment at a desirable temperature.



Figure 6.3 Modern electrochemical instrumentation.

For instance, common corrosion studies using the above instrumentation can include the determination of the corrosion potential and the corrosion current density, linear polarization resistance, Tafel plot, potentiodynamic polarization at scan rates and cyclic polarization. The most common electrochemical techniques are potentiostatic, potentiodynamic, galvanostatic and galvanodynamic polarization. In addition, this device can be used as a potentiostat for measuring the current response due to an applied potential or as a galvanostat to measure the potential response at an applied current. This device is very popular among researchers and can also be used for studying the microstructural evolution of oxide and nitride coatings during electrodeposition.

Later in this chapter, the reader will be provided with experimental potentiodynamic polarization curves obtained using the 273A potentiostat/galvanostat device and the experimental set up shown in Figure 6.1.

The schematic electrical circuit for a basic potentiostat can be found elsewhere [6,30]. Nevertheless, the potentiostat uses R_s as the electrolyte resistance between the auxiliary electrode (*AE*) or counter electrode (*CE*) and the reference electrode (*RE*), R_c as the resistance developed due to current flow between the working electrode (*WE*) and *RE*, E as an adjustable potential for keeping the *WE* potential at a constant value [6].

The adjustable potential E is measured with a zero-resistance ammeter (*ZRA*) and an analog-to-digital converter (*ADC*). The main objective of the potentiostat is to control the potential difference between *WE* and *RE* by supplying a current flow through the *AE*.

Recall from Chapter 3 that the open-circuit potential is the corrosion potential (E_{corr}) in the absence of an externally applied potential and the corrosion current density (i_{corr}) cannot be measured or determined in this case. However, electrochemical techniques can be used for determining i_{corr} from a polarization curve generated by sweeping the *WE* surface with an applied potential and for measuring the response current or current density. This means that i_{corr} cannot be measured but graphically estimated. Also, polarization is a measure of the overpotential and the electrochemical process on the *WE* is basically a combination of kinetics and diffusion processes.

If the applied potential is at or very near E_{corr} , which can be defined as the electrochemical open-circuit potential in the presence of an applied potential for current to flow, the potential noise and the current noise can be monitored for evaluating the corrosion behavior of the *WE*. A particular potentiostat block used for analyzing electrochemical noise is shown in Figure 6.3c. This implies that the potential difference becomes the overpotential (η), which represents the degree of polarization, and it is very small ($\eta \rightarrow 0$). If inhomogeneous (nonuniform) corrosion occurs when the anodic overpotential is $\eta_a \rightarrow 0$, the corrosion behavior can be characterized using an **electrochemical noise (ECN)** technique, in which measurements of the noisy signals quantify the discrete electrochemical events that perturb the steady-state of the *WE* surface. Electrochemical noise represents fluctuations in potential and current. Thus, potential noise occurs between the *WE* and *RE* due to changes in the thermodynamic state of the *WE*, and current noise occurs between the *WE* and *AE* due to changes in the kinetic state of the corrosion process on the *WE* [31]. Instrumentation for electrochemical noise analysis can be found elsewhere [31-34].

6.2.1 TREE-ELECTRODE SYSTEM

This system is shown in Figure 6.2. The working electrode (*WE*) potential is measured against the reference electrode, provided that an ohmic resistance gradient is significantly reduced and current flows only between the auxiliary electrode and the working electrode [1-2]. The electrochemical cell components and their functions are described below.

- **Platinum (*Pt*) Auxiliary Electrode:** It passes current to the working electrode (specimen) to be studied.
- **Luggin Capillary:** It is a probe or tube filled with an electrolyte to provide an ionic conductive path through the soluble ionic salt (*KCl*). The Luggin capillary and salt bridge connecting the cell and the reference electrode (*RE*) do not carry the polarizing current, and it serves the purpose of reducing the ohmic resistance gradient through the electrolyte between the *WE* and *AE*. In fact, some of the ohmic potential ($E = IR$) is included in the polarized potential [1].

- Working Electrode (WE):** It must be carefully prepared with a known exposed or contact area. In fact, a 1-cm^2 surface (exposed) area is desirable. The distance between the WE surface and the tip of the Luggin capillary should be in the range of $1\text{ mm} \leq x \leq 2\text{ mm}$. In the case of metal-resin interface is not properly prepared, crevice corrosion may lead to erroneous results. Another important factor in carrying out electrochemical corrosion experiments is that the specimen immersion time must be constant in order to stabilize the electrode in the electrolyte prior to start the polarization test.
- Potentiostat:** A manually operated potentiostat is a stepwise instrument for measuring potential (E) and current density (i), and develop E vs. $\log(i)$ plots. A commercially programmable potentiostat, together with an electrometer, logarithmic converter, and data acquisition device is an automated instrument that provides variability of continuous sweep (scan) over a desired potential range, normally in the order of $-2\text{ V} < E < 2\text{ V}$ for obtaining an entire polarization curve, including the cathodic and anodic regions. This automated procedure is called potentiodynamic polarization technique, which provides a polarization curve at desire scan rates. Furthermore, a time factor is very important in steady-state polarization runs since the mechanism of the electrochemical reactions may be altered otherwise [6].

Figure 6.4 shows a schematic polarization curve illustrating details of the ideal parameters that can be determined from this type of curve.

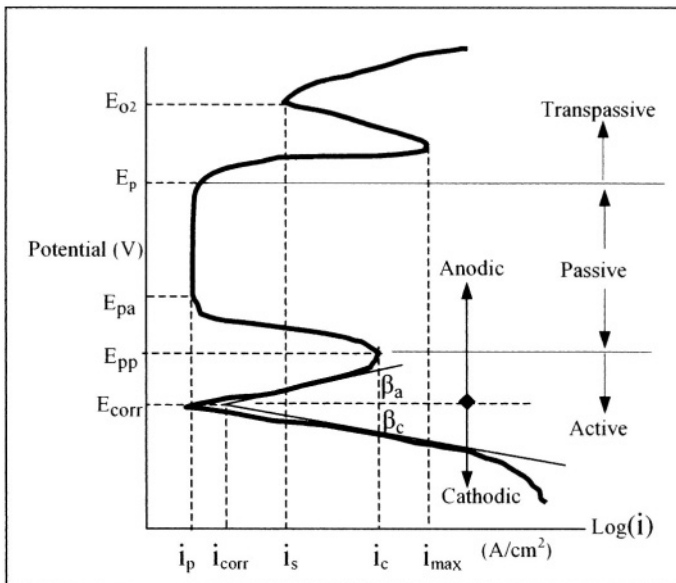


Figure 6.4 Hypothetical polarization curve.

Nomenclature for Figure 6.4: i_p = Passive current density E_{pa} = Passive potential i_{corr} = Corrosion current density E_{corr} = Corrosion potential i_s = Secondary current density E_{O_2} = Oxygen evolution potential i_c = Critical current density E_{pp} = Primary passive potential i_{max} = Maximum current density E_p = Pitting potential

6.3 POLARIZATION CURVES

Figure 6.5 shows a stepwise (potentiostatic) polarization curve for a eutectoid steel in deaerated sulfuric acid solution [11]. This polarization curve is clearly divided into anodic and cathodic regions. The Tafel slopes for these regions and the corrosion current density can be determined very easily. The pertinent experimental data extracted from this figure are included as legend. Notice that the polarization curve covers data near the corrosion potential ($-0.51 V_{SCE}$) only. It is clearly indicated in Figure 6.5 that gathering a large amount of data for plotting the polarization curve at potentials far from the corrosion potential is a time consuming process. Therefore, an automated potentiostat seems to alleviate the prolong experimental procedure for this type of characterization.

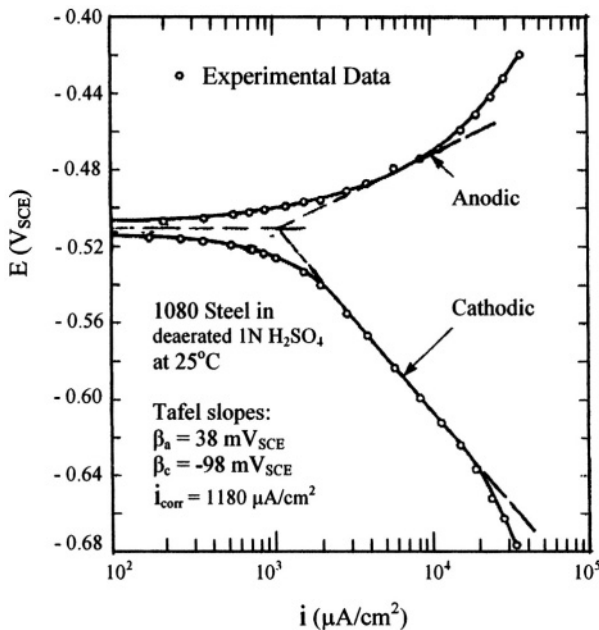


Figure 6.5 Experimental stepwise polarization curve for 1080 eutectoid steel in deaerated 1N sulfuric acid [11].

A polarization curve can provide evidence on whether or not a material is active, passive or active-passive. Hence, the corrosion behavior of an electrode can be characterized in a particular environment. For instance, potentiostatic and potentiodynamic testing methods can give fairly similar results; however, the latter method requires a slow scan rate (mV/s) in order to maintain a stable corrosion potential and a steady-state behavior [1]. Kinetic studies using potentiodynamic polarization curves may involve deficiencies in characterizing the corrosion behavior of a metal or alloy since service conditions are susceptible to changes in corrosion potential. Nevertheless, both potentiostatic and potentiodynamic procedures are useful in determining the electrochemical corrosion behavior of an active-passive material. Hence, the **passivity** of a metal and the **corrosivity** of an electrolyte can be characterized as functions of temperature, concentration of an ionic specie, scan rate, convection, and even pressure. For example, Figure 6.6 shows the effect of concentration of sulfuric acid (H_2SO_4) exposed to still air at room temperature and Figure 6.7 illustrates the effect of scan rate on the electrochemical behavior of a stainless steel type AISI 304. This stainless steel was prepared by rapid solidification and conventional ingot metallurgy solidification technologies. The former alloy is called RSA 304 and the latter IM 304.

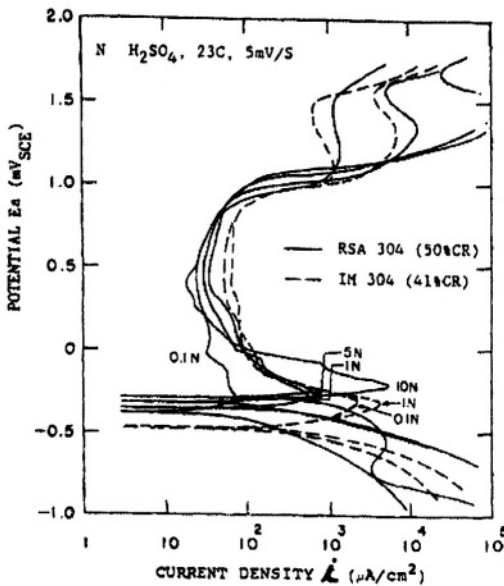


Figure 6.6 Experimental potentiodynamic polarization curves for cold rolled RSA 304 and IM 304 in sulfuric acid concentrations at room temperature [4].

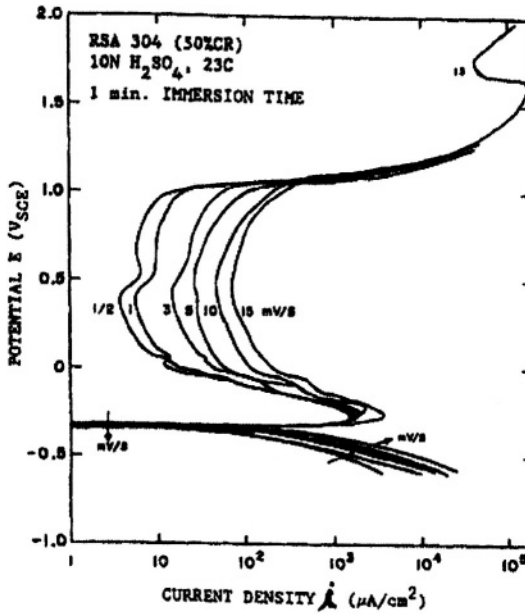


Figure 6.7 Experimental potentiodynamic polarization curves for (50%CR) RSA 304 as functions scan rate in 10N sulfuric acid solution at pH = -1.2 [4]

Initially, RSA 304 was 50% cold rolled (CR) and IM304 was 41%CR. These cold rolled percentages were performed in order to have the same yield strength on both stainless steels. Observe from Figure 6.6 that the 304's have slightly different electrochemical behavior. The variable shapes of polarization curves can be attributed to the irreversible reactions which represents dissipation of electrical energy into heat [4]. Both 304's are active-passive stainless steels and both show a fairly good passive potential range.

On the other hand, it is clearly shown in Figure 6.7 that the electrochemical corrosion behavior of 50%CR RSA 304 is significantly affected by scan rate. The passive current density i_p is not well defined, but the passive potential range is displaced to the right as scan rate increases. This passive potential range is approximately $1 V_{SCE}$. Other polarization parameters are not significantly affected by scan rate. For instance, the pitting and critical potentials are approximately $1 V_{SCE}$ and $-0.25 V_{SCE}$, respectively, at all scan rates used in Figure 6.7. It is apparent from Figure 6.6 and 6.7 that the polarization runs are adequate to evaluate in great details the electrochemical behavior of the stainless steels RSA 304 and IM 304. Conclusively, the RSA 304 is slightly more corrosion resistant than its counterpart IM 304.

Furthermore, the effect of annealed microstructural conditions on the electrochemical behavior on both RSA 304 and IM 304 is shown in Figure 6.8.

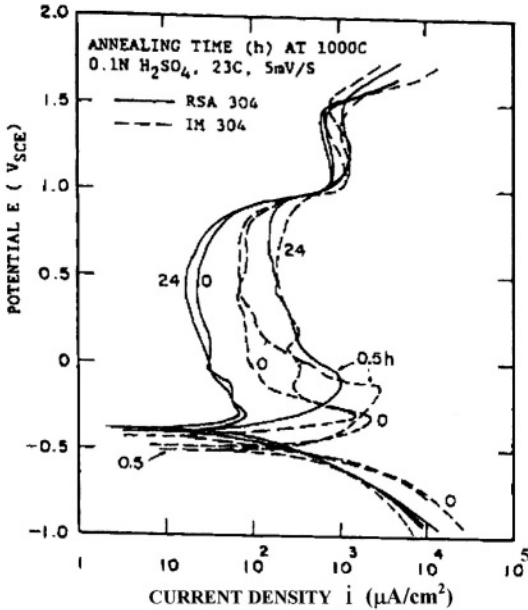


Figure 6.8 Experimental potentiodynamic polarization curves for annealed 304 stainless steels [4].

The varying metallurgical parameter is the heat treatment time at 1000°C . Basically, the *RSA 304* is more corrosion resistant than *IM 304* due to the attributable inherent properties induced by the rapid solidification processing (*RSP*) and to the formation of an oxide surface film of higher quality. This passive film has been reported [7] to be an amorphous oxide compound. With respect to the corrosion rate (C_R) in familiar units, the *RSA 304* exhibited

$$\begin{aligned} C_R &= 5.47 \text{ mm/y} && @ i_c \\ C_R &= 0.89 \text{ mm/y} && @ i_p \\ C_R &= 0.098 \text{ mm/y} && @ i_{corr} \end{aligned}$$

for the 0.5 h annealed condition. The most interesting case is the corrosion rate at the corrosion current density. Thus, $C_R = 0.098 \text{ mm/y} @ i_{corr}$ is very low in magnitude. In fact, both *RSA 304* and *IM 304* show high corrosion resistance in sulfuric acid solutions which can be attributed to the high chromium (Cr) content for passivation due to the formation of a hydrated chromium oxyhydroxide, $CrO_x(OH)_{3-2x} \cdot nH_2O$, protective film [8].

Not all metals and alloys show active-passive behavior as 304 stainless steel in a particular environment. Aluminum and its alloys have the tendency to be active in most environments. Advanced alloys such as a *Ni/Mo*-base rapidly

solidified alloy (RSA), $Ni_{53}Mo_{35}Fe_9B_2$, tested in sulfuric acid solution passivates very briefly as indicated in Figure 6.9. This rapidly solidified alloy was annealed for prolonged times at $1100^\circ C$ and characterized potentiodynamically in $0.10 N$ ($pH = 1.5$) sulfuric acid (H_2SO_4) solution at $25^\circ C$. As a result, this RSA acts as an active material, despite that its corrosion current density is very low in the order of $11 \mu A/cm^2$. The electrochemical behavior of this alloy in H_2SO_4 may be attributed to galvanic effects due to several boride particles embedded in the $Ni-Mo$ matrix [4]. These borides were revealed by x-rays as

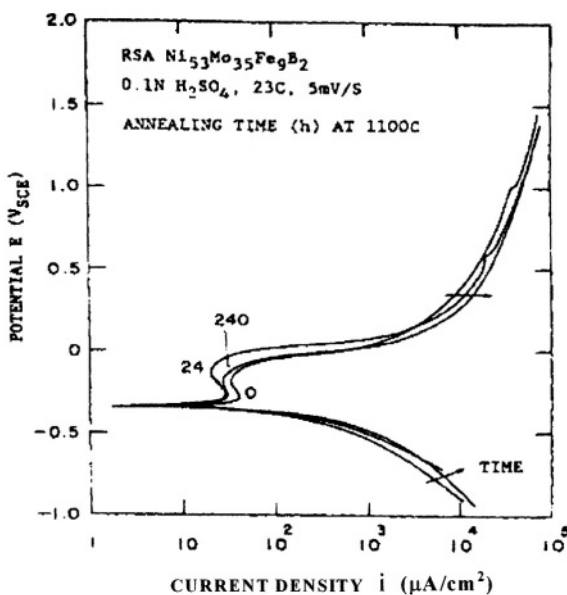
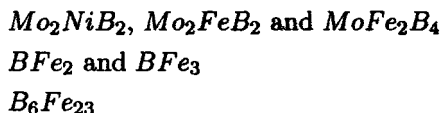


Figure 6.9 Experimental potentiodynamic polarization curves for RSA Ni-Mo base alloy [4].

In addition, **anodizing** is a process in which aluminum and aluminum alloys are readily oxidized by an adherent and protective oxide film on the surface and further oxidation of the film is by solid state diffusion. However, these materials are active in an electrochemical environment containing sodium chloride.

For instance, Figure 6.10 shows experimental potentiodynamic polarization curves for 2195 $Al - Li$ alloy being aged at $190^\circ C$ and tested in deaerated $3.5\% NaCl$ solution. All polarization curves show active electrochemical behavior since the formation of an oxide protective film does not occur on all aged

conditions. Despite that this alloy passivates in air due to the anodizing process, it becomes active electrochemically since a critical current density does not develop in the tested solution. Therefore, the alloy does not passivate, instead it oxidizes potentiodynamically when the applied potential is above the corrosion potential.

Furthermore, both corrosion potential and corrosion current density for the aged alloy are affected by the aging time (heat treatment time). This experimental observations may be attributed to the precipitation of secondary phases, which may form localized galvanic cells on the surface of the 2195 *Al-Li* alloy.

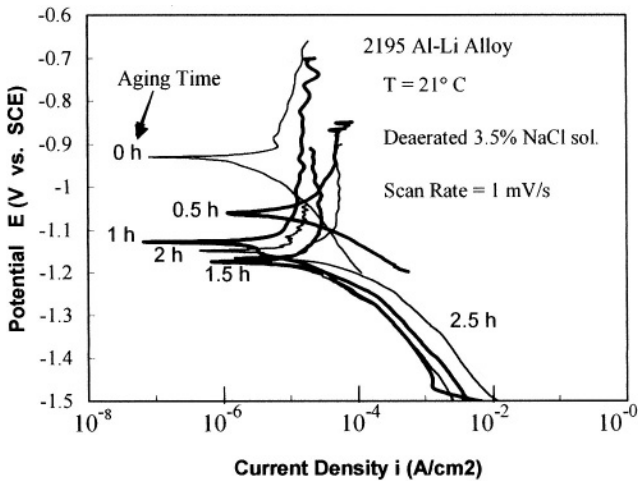


Figure 6.10 Effect of aging time on polarization of 2195 Al-Li alloy in deaerated 3.5 % sodium chloride solution [40].

6.4 CYCLIC POLARIZATION CURVES

Essentially, it is a mixed potential phenomenon in which the anodic and cathodic polarization processes are carried out using a reverse scan rate. The scan rate is reversed at a predetermined potential, leading to a cathodic polarization in the passive region until both anodic and cathodic curves intersect. The output of this technique is schematically shown in Figure 6.11.

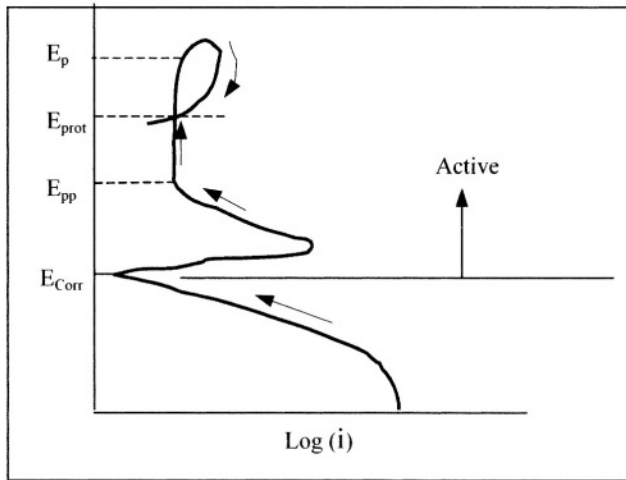


Figure 6.11 Schematic cyclic polarization curve showing the protected potential.

This cyclic curve shows the protective potential against localized or pitting corrosion. This potential is below the pitting (breakdown) corrosion potential (E_p). The area of the hysteresis loop is virtually the power supplied to the electrode surface [39]. The more active both E_{prot} and E_p are the more resistant the metal is to crevice corrosion [36]. Among all suitable applications of the cyclic polarization technique, the biological field can benefit since the pitting potential can be used as a measure of the resistance of metallic implants exposed to human body fluids. According to Fontana [35] a body fluid is an aerated physiological saline solution containing approximately 1% $NaCl$, other salts and some organic compounds at $37^\circ C$ and the corrosivity of the human body fluid is similar to that of aerated warm water. The Tyrode's [37] and Hank's [38] physiological saline solutions are nowadays commercially available. The former solution is given below as reported by Sedriks [36]. **Tyrode's solution** [37] in g/l : $NaCl = 8.00$, $CaCl_2 = 0.20$, $KCl = 0.20$, $NaHCO_3 = 1.00$, $MgCl_2 = 0.10$, and $Na_2HPO_4 = 0.50$.

6.5 PASSIVE OXIDE FILM

Passivity is an electrochemical reduction mechanism that occurs on a metal-electrolyte interface. The resultant reduction product is a solid film of a metal oxide compound having a stoichiometric reaction (a reaction that goes to completion) based on the corroding metal. Thus, passivity occurs on metals that are active-passive by **natural passivation** without the influence of external potentials or **artificial passivation** due an applied external anodic potential.

Herein, artificial passivation will be referred though out the context of this chapter, unless stated otherwise. The passive oxide film is a solid interfacial

oxide compound that protects the metal against further oxidation and ranges from **1 nm** to **10 nm** in thickness [12]. Apparently, thin films in the order of **1-2 nm** in thickness are of higher quality than thick films due to lesser atomic defects. A metal that exhibits passivity is thermodynamically unstable within a potential range independent or nearly independent of current or current density. This means that the metal is unstable in the passive state since a slight disturbance may increase the passive potential to or above the pitting potential causing film breakdown. Furthermore, chemical passivity is a state related to cathodic reactions on the metal surface, while electrochemical passivity depends on an external anodic potential to force cathodic reactions to occur [13]. According to Figure 6.4, the i_c - i_p region defines the active/passive transition. Passivation starts at i_c and ends at i_p . Thus, film thickness increases from from the E_{pa} potential at i_p , but ionic conductance of the oxide film controls its thickness. Moreover, high ionic conductivity of metal cations promotes a thick film. The opposite occurs for a low ionic conductivity [14-15].

Most metals and alloys do not show a well-defined passive potential range as indicated schematically in Figure 6.4. For instance, the *RSA 304* and *IM 304* data shown in Figures 6.6 through 6.8 is more realistic since these polycrystalline alloys have numerous defects, such as voids, dislocations, grain boundaries, and the like, contributing to the passive behavior. This implies that the inherent formation of passive oxide films have a complex mechanism due to these defects. The passive oxide film and passive behavior are strongly dependent on the scan rate (dE/dt) as shown in Figure 6.7. This experimental data was obtained [4] using the electrochemical device (Figure 6.1) containing deaerated H_2SO_4 solutions at 23°C. Despite the need for simulating service conditions to conduct accelerated corrosion test; one has to be very careful in surgical implant materials since toxicity must be avoidable.

Passivity of metals and alloys is important in anodic protection schemes. This will be dealt with in a later chapter. The former, however, depends on the metal/electrolyte system, in which the current density to maintain passivity is $i_p \ll i_c$ at high oxide film resistance. The stability of passivity can be achieved if the potential is kept low within the passivation region $E_{pp} \leq E < E_p$ (Figure 6.4). Apparently, i_c must exist as an essential kinetic parameter for passivation to occur. This is clearly shown in Figures 6.6 through 6.8. Also, The *Ni/Mo* base alloy in Figure 6.9 shows passivity, but it cannot be maintained due to boride/matrix galvanic effects in H_2SO_4 solutions.

6.6 KINETICS OF PASSIVATION

Assume a defect-free single crystal and a mechanism of oxide film growth by vacancy migration. Thus, the rate of film formation for a single crystal, related to Faraday's law, can be approximated as [13]

$$\frac{dx}{dt} = \frac{i_p A_w}{zF\rho} \quad (6.1)$$

where x = Film thickness (cm)
 dx/dt = Rate of film formation (cm/s)
 i_p = Passive current density (A/cm^2)
 z = Valence
 F = 96,500 C/mol ($= A.s/mol$)
 ρ = Density of metal (g/cm^3)

Note that eq. (6.1) mathematically resembles eq. (3.48), but both have different meanings. In addition, eq. (6.1) is related to several factors shown in Figure 6.12.

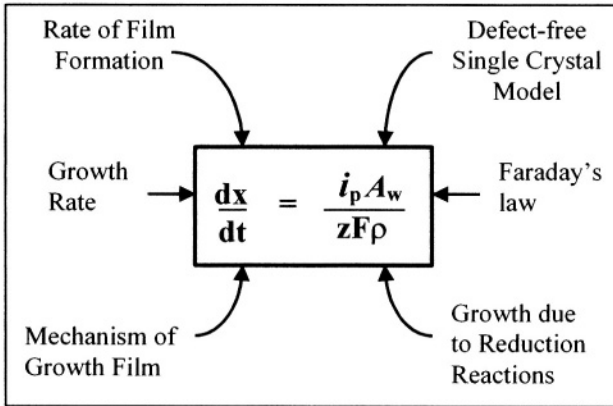


Figure 6.12 Significance of the rate of film formation.

In addition, if the Arrhenius equation applies, then the rate of film growth is described by the forward/reverse current densities at equilibrium

$$i_f = i_r = \alpha z F \exp\left(-\frac{Q}{RT}\right) \quad (6.2)$$

where α = Rate constant (mol/s)
 Q = Activation energy ((J/mol))
 R = Gas constant = 8.314 $J/mol.^{\circ}K$
 T = Absolute temperature ($^{\circ}K$)

Now, apply an anodic overpotential for film growth to take place and consequently, an electric field potential gradient (η/x) develops. If there exists a linear electric field across the film, then the forward (f) and reverse (r) cases become [13], respectively

$$i_f = \alpha z F \exp\left(\frac{-Q - zFL\eta/x}{RT}\right) \quad (6.3)$$

$$i_r = \alpha z F \exp\left(\frac{-Q + zFL\eta/x}{RT}\right) \quad (6.4)$$

where L = Distance from the electrode surface at which a potential drop exist in the electrolyte

$zFL\eta/x$ = Energy barrier due to an overpotential.

If the net current density at a distance x is $i_x = i_f - i_r$, then

$$i_x = i_o \left[\exp\left(\frac{B\eta}{x}\right) - \exp\left(-\frac{B\eta}{x}\right) \right] \quad (6.5)$$

$$i_x = 2i_o \sinh\left(\frac{B\eta}{x}\right) \quad (6.6)$$

where

$$i_o = \alpha z F \exp\left(-\frac{Q}{RT}\right) = \text{constant} \quad (6.6a)$$

$$B = \frac{zFL}{RT} \quad (6.6b)$$

If $B\eta/x \rightarrow \infty$, then eq. (6.5) yields the high field equation

$$i_x = i_o \exp\left(\frac{B\eta}{x}\right) \quad (6.7)$$

If $B\eta/x \rightarrow 0$, then eq. (6.6) yields

$$i_x = 2i_o \left(\frac{B\eta}{x}\right) = \frac{\eta}{R_x} \quad (6.8)$$

since the film resistance due to Ohmic effect can be defined as

$$R_x = \frac{x}{2i_o B} \quad (6.9)$$

For an anodic current density $i_x < i_c$, eq. (6.1) can be redefined as

$$\frac{dx}{dt} = \frac{i_x A_w}{zF\rho} \quad (6.10)$$

Substituting eq. (6.6) into (6.10) yields

$$\frac{dx}{dt} = \frac{2i_o A_w}{zF\rho} \sinh\left(\frac{B\eta}{x}\right) \quad (6.11)$$

Letting

$$\lambda = \frac{2i_o A_w}{zF\rho} \quad (6.12)$$

$$\theta = \frac{B\eta}{x} \quad (6.13)$$

eq. (6.11) becomes

$$\frac{dx}{dt} = \lambda \sinh(\theta) \quad (6.14)$$

where $-1 \leq \theta \leq +1$ radians. Since the overpotential $\eta \geq 0$ for anodic polarization, the profile for the rate of oxide film formation, eq. (6.14), is theoretically shown in Figure 6.13.

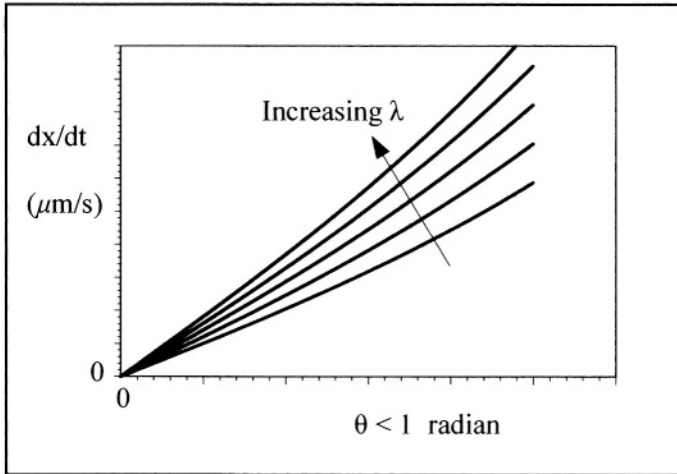
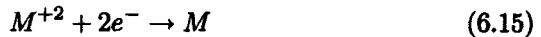


Figure 6.13 Theoretical profile for the rate of oxide film formation.

The thermodynamics of passivity together with the **Nernst equation** can be generalized in simple reaction steps for the formation of an oxide film (MO). Hence,

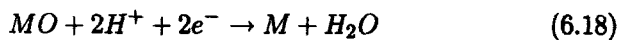
- Metal reduction



$$E_{M^{+2}/M} = E_M^{\circ} - \frac{RT}{zF} \ln \frac{[M]}{[M^{+2}]} \quad (6.16)$$

$$E_{M^{+2}/M} = E_M^{\circ} + \frac{RT}{zF} \ln [M^{+2}] \quad (6.17)$$

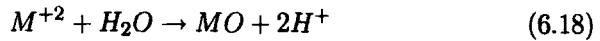
- Metal oxide reduction



$$E_{MO/M} = E_{MO/M}^{\circ} - \frac{RT}{zF} \ln \left[\frac{[M][H_2O]C_M C_{H_2O}}{[MO][H^{+}]^2} \right] \quad (6.19)$$

$$E_{MO/M} = E_{MO/M}^{\circ} + \frac{2RT}{zF} \ln [H^{+}] \quad (6.20)$$

- Formation of metal oxide



$$E_{M^{+2}/MO} = E_{M^{+2}/MO}^{\circ} - \frac{RT}{zF} \ln \left[\frac{[MO][H^+]^2}{[M^{+2}][H_2O]} \right] \quad (6.19)$$

$$E_{M^{+2}/MO} = E_{M^{+2}/MO}^{\circ} - \frac{2RT}{zF} \ln \left[\frac{[H^+]}{[M^{+2}]} \right] \quad (6.20)$$

$$E_{M^{+2}/MO} = E_{M^{+2}/MO}^{\circ} - \frac{4.606RT}{zF} [\log [M^{+2}] - pH] \quad (6.21)$$

where $[M] = [MO] = [H_2O] = 1 \text{ mol/l}$ and

$$pH = -\log [H^+] \quad (6.22)$$

In addition, the structure, composition, and thickness of a passive oxide film may be determined using **ex-situ** techniques, such as [27-28]

- Electron Spectroscopy (AES)
- Ion Mass Spectroscopy (IMS)
- X-Ray Diffraction (XRD)
- X-Ray Photoelectron Spectroscopy (XPS)

Further characterization of oxide films can be done using **in-situ** techniques, such [27-29] as

- Ellipsometry
- Frequency Response Analysis (FRA)
- Photocurrent Spectroscopy (OS)

Passive oxide films are extremely difficult to characterize due to their thin thickness and strong adhesion on the metal surface. Some schematic passive oxide films are shown in Figure 6.14 for some metals and alloys.

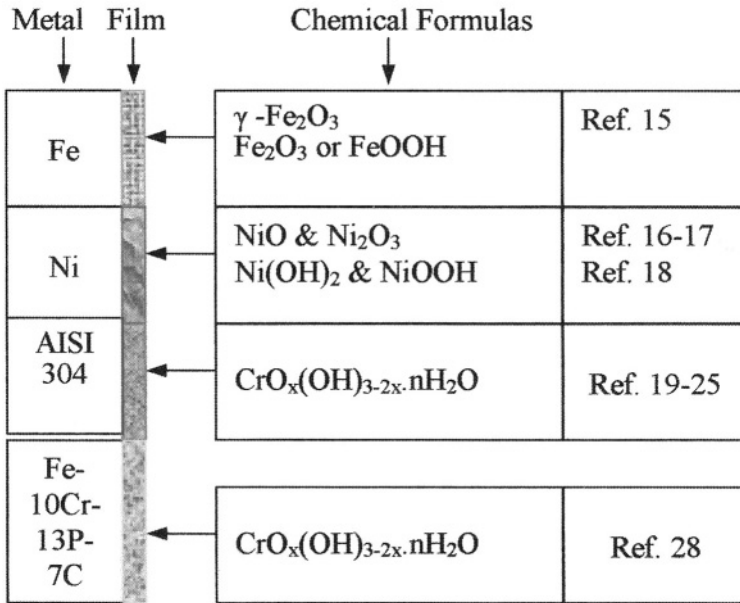


Figure 6.14 Schematic oxide passive films.

One particular application of passive film is through the Electrogaining technique in which metal surface is roughen by pitting corrosion for printer's lithographic aluminum sheets in HCl or H_2NO_3 acid [17].

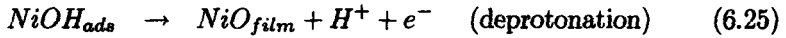
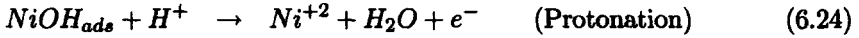
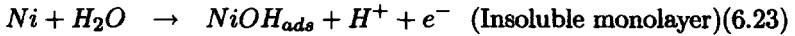
Apparently, metals and alloys that readily passivate may be due to rapid formation of the passive oxide film. If the film forms, then the metal is easily protected. This may be an indication of the higher quality of passive films, which induce higher pitting potentials and lower corrosion rates.

6.7 MECHANISM OF PASSIVATION

A distinction between surface layers and passive oxide films should be made. If a metal is insoluble in an environment, it may form an insoluble oxide corrosion product on the metal surface as a crystalline and poorly adherent surface layer (non-passive thick layer), such as the blue/green layer on corroded copper plumbing and well-known brown "Rust" layer on iron and iron alloys. On the other hand, if a metal is soluble in a solution, it oxidizes and dissolves in the solution as cations. These cations react with dissolved oxygen and are deposited back on the metal as oxides, forming a passive oxide film under the influence of an electric field. Also, the metal may be oxidized readily on the metal/solution interface forming a spontaneous passive oxide film, protecting the base metal from corrosion [13].

An example of reaction steps for a passive film formation is given below. According to Burstein [13], a passive nickel (*Ni*) oxide film may form through

An example of reaction steps for a passive film formation is given below. According to Burstein [13], a passive nickel (*Ni*) oxide film may form through several reaction steps on the metal surface. One possible mechanism is as follows:



The subscript “ads” stands for adsorption, which means that the product $NiOH_{ads}$ is in contact with the metal surface and it is said to be adsorbed, whilst $NiOH_{film}$ is a thin and coherent film on the metal surface forming a metallic couple, and it may be crystalline having its own atomic structure.

Despite that the protective action of a passive oxide film, it is thermodynamically unstable in a particular electrolyte. However, the film may be amorphous in a specific environmental condition. Suppose that nickel oxide (NiO) film has a crystalline structure and for comparison, $CrO_x(OH)_{3-2x} \cdot nH_2O$ is amorphous, then it can be deduced that the latter is of higher film quality than the former due to the lack of crystal defects, such as grain boundaries. In fact, it is apparent that passive oxide films are amorphous and insoluble, and they isolate the metal surface from solution. However, if a passive oxide film has defects, thin films from **1-nm** to **2 nm** in thickness are preferred over thicker ones due to fewer defects [13].

The passive film thickness at time t can be predicted using eq. (6.1), provided that the passive current density (i_p) remains constant in the passive potential range, $E_{pp} \leq E \leq E_p$, shown in Figure 6. 11. Hence,

$$\int_0^x dx = \int_0^t \frac{i_p A_w}{zF\rho} dt \quad (6.26)$$

$$x = \frac{i_p A_w t}{zF\rho} \quad (6.27)$$

6.8 SUMMARY

Corrosivity and passivity can be characterized using polarization curves, which have significant electrochemical regions of diverse physical meaning. The degree of corrosivity can be assessed quantitatively based on the aggressiveness of an electrolyte to cause continuous metal dissolution. On the other hand, if a metal oxidizes with increasing applied current until reverses its direction; that is, it decreases, it is assumed that there exists sufficient cations in solution to react with dissolved oxygen to form an oxide film on the electrode surface. This electrochemical phenomenon is known as passivation and passivity is also qualitatively defined by how easy or fast an electrode passivates.

Control of electrochemical corrosion rely on principles of electrochemistry and the type of test to be performed. Thus, practical control of corrosion is more realistic when conducted simulating service conditions. However, laboratory tests provide an insight on the corrosion behavior of a metal in service because the experimental conditions are controlled as desired. Despite that the degree of corrosivity of an electrolyte on a metal is influenced by its electrical conductivity at a temperature T , corrosion induced by galvanic effects can be very complex. It suffices to say that galvanic corrosion can be classified as corrosion caused by dissimilar metals, corrosion by plastics and even corrosion by wood in a particular corrosive environment. Nevertheless, electrical measurements of potential and current are used for characterizing corrosion on a metal surface. Thus, electrochemical techniques can be based on direct current (*d.c.*) for obtaining polarization curves shown in Figures 6.5 through 6.10 or alternating current (*a.c.*) for obtaining transient kinetics plots for characterizing electrochemical noise, which is related to corrosion. The former is used in potentiostatic or potentiodynamic polarization, linear polarization (known a polarization resistance), Tafel extrapolation, cyclic polarization. The latter is for electrochemical noise and electrochemical impedance measurements.

Metals and alloys, specifically many stainless steels are known to passivate in acid solutions having a wide enough passive potential range determined from polarization curves. Nonetheless, there are two potential-control techniques used to develop polarization curves. These are potentiostatic and potentiodynamic techniques. The former is a stepwise technique and the latter is a dynamic technique, in which a polarization curve is obtainable in a few minutes at low potential scan rates. If the scan rate is reversed at a potential slightly above the pitting potential (E_p), the result is a cyclic polarization curve used for determining the protective potential (E_{prot}) against pitting corrosion as schematically shown in Figure 6.11.

The kinetics of passivation is normally characterized through Faraday's law for determining the rate of film formation in terms of growth of film thickness according to eq. (6.1). As a crude approximation, the rate of film formation (dx/dt) is related to vacancy diffusion and it is assumed to obey the Arrhenius equation (6.2). In fact, dx/dt increases provided that there exists a net anodic current density i_x and an overpotential η_x at a distance x from the electrode surface.

6.9 PROBLEMS

6.1 Determine a) the electric potential E in millivolts, b) the time in seconds, and c) the growth rate in $\mu\text{m/s}$ for electroplating a $3\text{-}\mu\text{m}$ thick Cr film on a Ni -undercoated steel part, provided that the electrolyte contains 10^{-4} mol/l of Cr^{+3} cations at 25°C , the Ni -steel part has a 10-cm^2 surface area, and the cell operates at 50% current efficiency and at a passive current of 0.8 amperes.

6.10 REFERENCES

- [1] D.A. Jones, "*Principles and Prevention of Corrosion*," Macmillan Publishing Company, New York, (1992).
- [2] D.L. Piron, "*Potential Measurements with Reference Electrodes*," in Corrosion, Vol. 13, ASM Inter., ASM Handbook, Ninth edition, (1987) 21.
- [3] R.W. Staehle, "*Stress Corrosion Cracking and Hydrogen Embrittlement of Iron Base Alloys*," Edited by R.W. Staehle et al., NACE-5, Houston, (1977).
- [4] N.L. Perez, Ph.D. Dissertation, (1989).
- [5] D.A. Jones and J.P. Paul, "*Hydrometallurgical Reactor Design and Kinetics*," Edited by R.G. Bautista, R.J. Wesley, and G.W. Warren, THS-AIME, Warrandale, PA, (1987) 293.
- [6] D. van Rooyen, "*The Potentiostat and its Application to Corrosion Studies*" in Corrosion, Vol. 2, Corrosion Control, third edition, Edited by L.L. Shreir, R.A. Jarman, and G.T. Burstein, Butterworth-Heinemann, New York, USA, (1994) 19:134.
- [7] T.K.G. Namboodhiri, "*Metallic Glass Production, Properties and Applications*" Edited by T.R. Anantharaman, Trans. Tech. Publications, Varanasi, India, (1984) 203-218.
- [8] T.R. Anthony and H.E. Cline, J. Appl. Phys., 49 (1978) 1248.
- [9] K. Hashimoto, M. Kasaya, K. Asami, and T. Masumoto, Corrosion Eng., 26 (1977) 445.
- [10] K. Hashimoto, K. Asami, and K. Teramoto, Corrosion Sci., 19 (1979) 43.
- [11] R. Bandy and D.A. Jones, Corrosion, Vol. 32, (1976) 126.
- [12] J.R. Scully, "*Electrochemical Methods of Corrosion Testing*" in Corrosion, Vol. 13, Laboratory Testing, ASM Inter., ASM Handbook, Ninth edition, (1987) 213.
- [13] G.T. Burstein, "*Passivity and Localized Corrosion*," in Corrosion, Vol. 1, Metal/Environment Reactions, third edition, Edited by L.L. Shreir, R.A. Jarman, and G.T. Burstein, Butterworth-Heinemann, New York, USA, (1994) 1:119-1:147.
- [14] T.P. Hoar, in Modern Aspects of Electrochemistry, Edited by J.O'M Bobricks, Butterworth, London, 2 (1959) 262.
- [15] L. Young, "*Anodic Oxide Films*," Academic Press, London, (1961).
- [16] F. Zucchi and G. TrabANELLI, Electrochem. Metals, 4 (1969) 313.
- [17] I.A. Maier, Corrosion, Vol. 40, 10 (1984) 533.
- [18] M. Yasuda, F. Takeya, and F. Hine, Corrosion, Vol. 39, 10 (1983) 400.
- [19] K. Hashimoto, M. Kasaya, K. Asami, and T. Masumoto, Corrosion Eng., (Boshoku Gijutsy), 26 (1977) 445.
- [20] K. Asami, K. Hashimoto, T. Masumoto, and S. Schimodaira, Corrosion Sci., 16 (1976) 909.
- [21] K. Hashimoto, K. Asami, M. Naka, and T. Masumoto, Corrosion Eng., (Boshoku Gijutsy), 28 (1979) 271.
- [22] K. Hashimoto and K. Asami, "*Passivity of Metals*" Corrosion Monograph Series, Edited by R.P. Frankenthal and J. Kruger, Electrochem. Soc.,

Princeton, New Jersey, (1978) 749.

- [23] K. Asami and K. Hashimoto, and S. Shimodaira, *Corrosion Sci.*, 18 (1978)151.
- [24] K. Hashimoto, K. Asami, and K. Teramoto, *Corrosion Sci.*, 19(1979)3.
- [25] K. Hashimoto and K. Asami, *Corrosion Sci.*, 19 (1979) 251.
- [26] K. Hashimoto, “*Amorphous Ferrous and Non-Ferrous Alloys*,” in *Corrosion*, Vol. 1, Metal/Environment Reactions, third edition, Edited by L.L. Shreir, R.A. Jarman, and G.T. Burstein, Butterworth-Heinemann, New York, USA, (1994) 3:152.
- [27] M. Froment (editor), “*Passivity of Metals and Semiconductors*” Elsevier, Amsterdam, (1983).
- [28] B.R. MacDougall, R.S. Alwitt, and T.A. Ramanarayanan (editors), “*Oxide Films on Metals and Alloys*” Proc. Electrochem. Soc. 92-22, Pennington, New Jersey, (1992).
- [29] P. Laevers, H. Terryn, and J. Vereeken, *J. Trans. Inst. Met Finish*, 70 (1992) 105.
- [30] J.A. von Fraunhofer and C.H. Banks, “*Potentiostat and its Applications*,” Butterworth-Heinemann, New York, USA, (1972).
- [31] S. Campbell, V. Jovancevic, M. Law, and S. Ramachandran, NACE inter., Sponsored by Baker Petrolite Corporation (a Baker Hughes Company), www.bakerhughes.com/bakerpetrolite/newsbytes/NACE/New.htm, (2002).
- [32] Zahner[®] Messsysteme, www.zahner.de/noise/noise.htm, (2002).
- [33] KH Design & Development, Electrochemical Corrosion Measurement and Control Consultancy, “*Circuits for Electrochemical Corrosion Measurement Hardware*,” www.khdesign.demon.co.uk/hardwareindex.htm, (2002)
- [34] EG&G Instruments Princeton Applied Research, Technical Note 101, www.prodigital.com.au/86.html.
- [35] M.G. Fontana, “*Corrosion Engineering*,” Third edition, McGraw-Hill Book Company, New York, (1986). 398.
- [36] A. J. Sedriks, “*Corrosion of Stainless Steels*,” Second edition, A Wiley-Interscience Publication, John Wiley & Sons, Inc., New York, (1996) 162.
- [37] B.C. Syrett and S.S. Wing, *Corrosion*, Vol. 34, (1978) 138-142.
- [38] T.P. Chen, W.T. Tsai, and J.T. Lee, *J. Materials Sci.*, Vol. 25, (1990) 936-939.
- [39] M.S. Walker and L.C. Rowe, “*The Use of Electrochemical Techniques for Corrosion Research in the Automobile Industry*,” Electrochemical Techniques for Corrosion, A Symposium sponsored by the NACE Technical Committee T-3L, Edited by R. Baboian, AN Official NACE Publication, (1977) 89.
- [40] L. Baca, M.S. Thesis, Figure 4.3, (2002) 43.

Chapter 7

ELECTROMETALLURGY

7.1 INTRODUCTION

The objective of this chapter is to illustrate the application of electrochemical principles to electrolytically produce or win pure metals or refine electrodeposited metals containing impurities, which codeposit during production. Before describing details related to electrowinning and electrorefining a metal, it is adequate to schematically show (Figure 7.1) a simplified block diagram of engineering fields involved in metal production.

The engineering field of extractive metallurgy is divided into different areas, which are shown in Figure 7.2 and described below [1-6,11].

- Pyrometallurgy is used for melting metals at high temperatures. Subsequently, molten metals are cast into several shapes using slow (conventional) solidification or into ribbons or powders by rapid solidification.
- Hydrometallurgy is for extracting metals from their ores using solvent extraction (*SX*) and ion exchange (*IE*). Thus, the result is a leaching solution containing a desired metal cations (M^{+z}) and some impurities.
- Electrometallurgy is used for recovering or winning some metals from leaching solutions using an aqueous electrolysis and molten salt electrolysis for recovering aluminum, magnesium and uranium.

Furthermore, electrometallurgy is also divided into subfields shown in Figure 7.2. Each subfield has its own unique cell characteristics, but they operate under similar electrolysis. Hence,

- Electrowinning for recovering a metal *M*, such as *Cu*, *Ni*, *Zn*, *Ti*, *Pb*, etc. from their low-grade ores. The metal is recovered by electrodeposition in the form of cathodes, which are normally rectangular shapes (plates). If rotating cylinders and disks are used, the final electrodeposition product can be in the form of ribbons and powders, respectively.

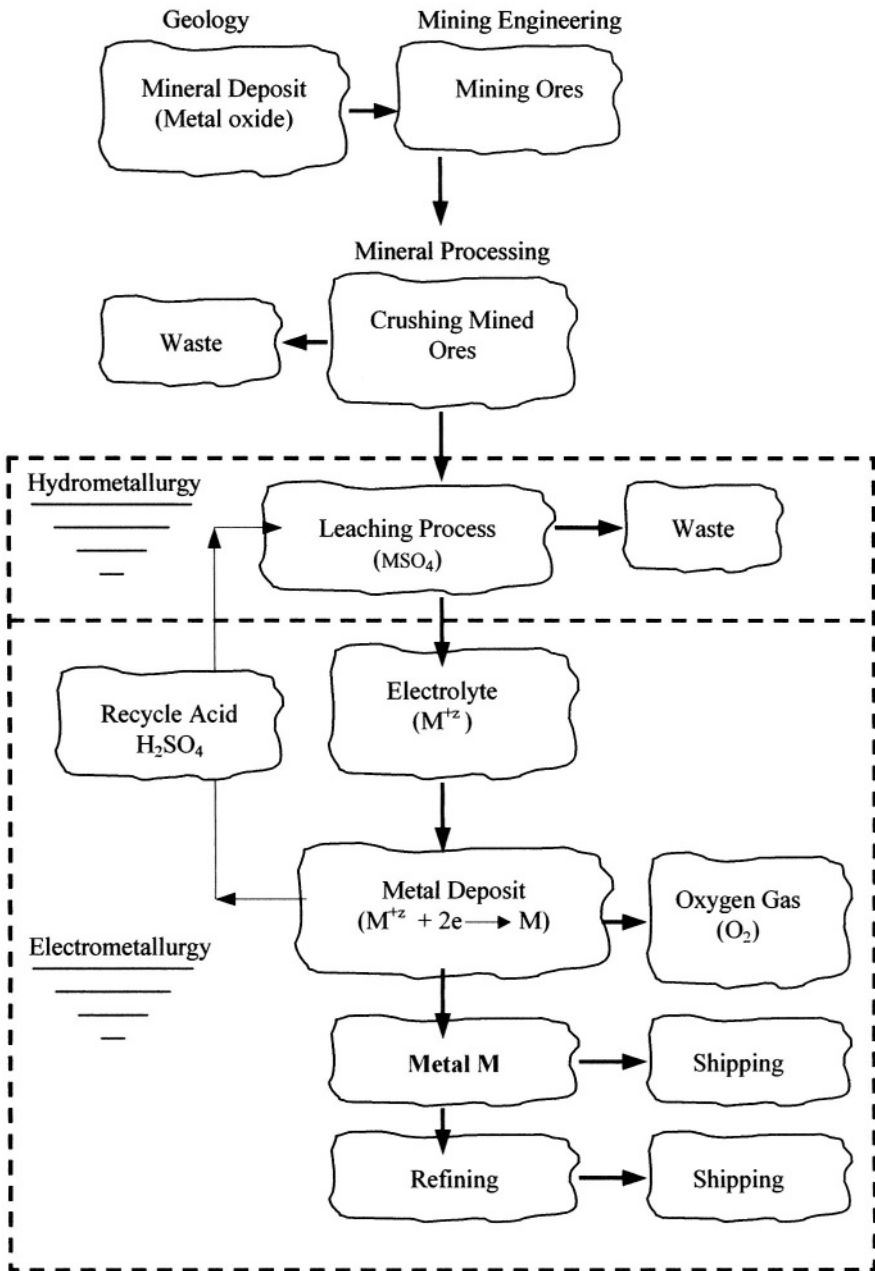


Figure 7.1 Block diagram for electrowinning of a metal M.

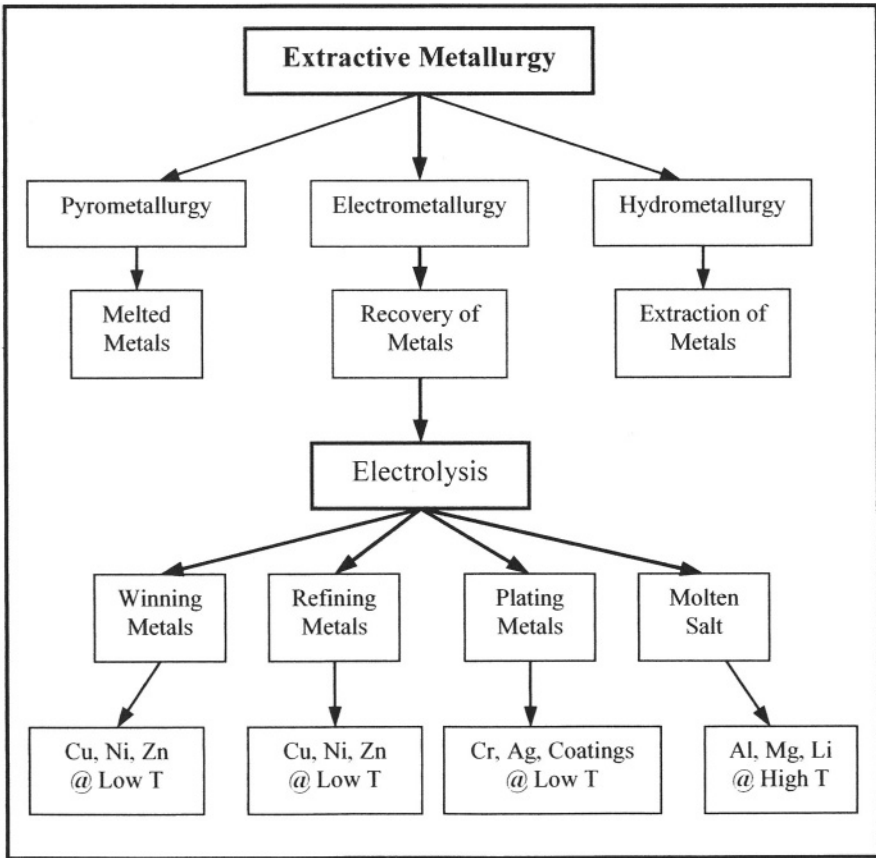


Figure 7.2 Block diagram for the extractive metallurgical field.

- Electrowinning (EW) is used for producing metals from their ores by dissolving the metal ions in solution and subsequently, deposited on new cathodes.
- Electrorefining (ER) is used for refining electrowon metals to their purest form by dissolving the electrowon cathodes into solution and subsequently, deposited on new cathodes.
- Electroplating (EP) is employed for electrodeposition of metal coatings onto another metal or alloy.
- Molten salt electrolysis (MSE) is a high temperature electrowinning operation for producing metals that cannot be electrowon due to water decomposition, which promotes hydrogen evolution at the cathode before metal deposition occurs. Metals produced or recovered using this technique are *Al, Mg, Be, Ce, Na, K, Li, U, Pu*, etc..

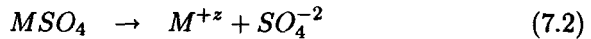
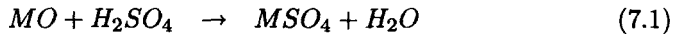
7.2 ELECTROWINNING

Conventional electrowinning (*EW*), as well as electrorefining, utilizes rectangular electrodes (planar starter sheets) having surface areas that occupy the space $1m \times 1m$ approximately. The anodic and cathodic electrodes are suspended vertically and alternatively at a distance $3\text{ cm} \leq x \leq 10\text{ cm}$ in the cells. The electrodes in one cell are connected in parallel and the cells are connected in series as shown in Figure 7.3. This is a classical electrode-cell arrangement for reducing the net cell potential drop and ohmic resistance [27,34].

Electrowinning is an electrochemical process used to reduce (win or deposit) metal cations on the surface of a cathode sheet from an aqueous solution prepared by a leaching chemical process, which is mainly based on metal cations M^{+z} , sulfuric acid H_2SO_4 and H_2O . This type of solution is widely used as an electrolyte containing dissolved metal ions in low concentrations. Recent advances in research have uncovered the usefulness of organic substances as part of the electrolyte. One of these substances is the Di-Ethylene Tri-Amine (**DETA**), which is used to extract or leach *Zn*, *Ni*, and *Cu* from their hydroxide form (sludge) and reacts to reject *Fe* and *Ca*, but it forms specifically *Cu:DETA* complexes [16,23-24]. Usually, a small amount of salt, such as *NaCl* or *NaSO₄*, is added to the electrolyte to enhance ionic conductivity, increase pH values, and reduce the electrolyte resistance, which in turn, reduces the cell operating potential and energy consumption [16].

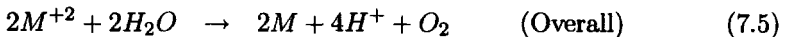
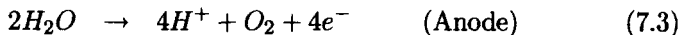
In general, electrowinning (*EW*) is commonly used to produce atomic *Zn*, *Ni*, and *Cu* from their ionic solutions. The common reactions involved in producing metals by electrolytic deposition (reduction), provided that impurities codeposition is absent and that the electrochemical cell walls and anodes do not dissolve, are

1) Leaching steps:



Here, *MO* stands for metal oxide and the most common metal sulfates are *CuSO₄*, *ZnSO₄* and *NiSO₄*.

2) Electrowinning (*EW*) reaction steps:



Note that water molecules decompose to promote oxygen evolution as O_2 gas. Thus far it has been assumed that the electrolytically deposit metal *M* has suitable characteristics for easy removal from the starter cathode sheets and that hydrogen evolution does not occur; otherwise, metal deposition is obstructed.

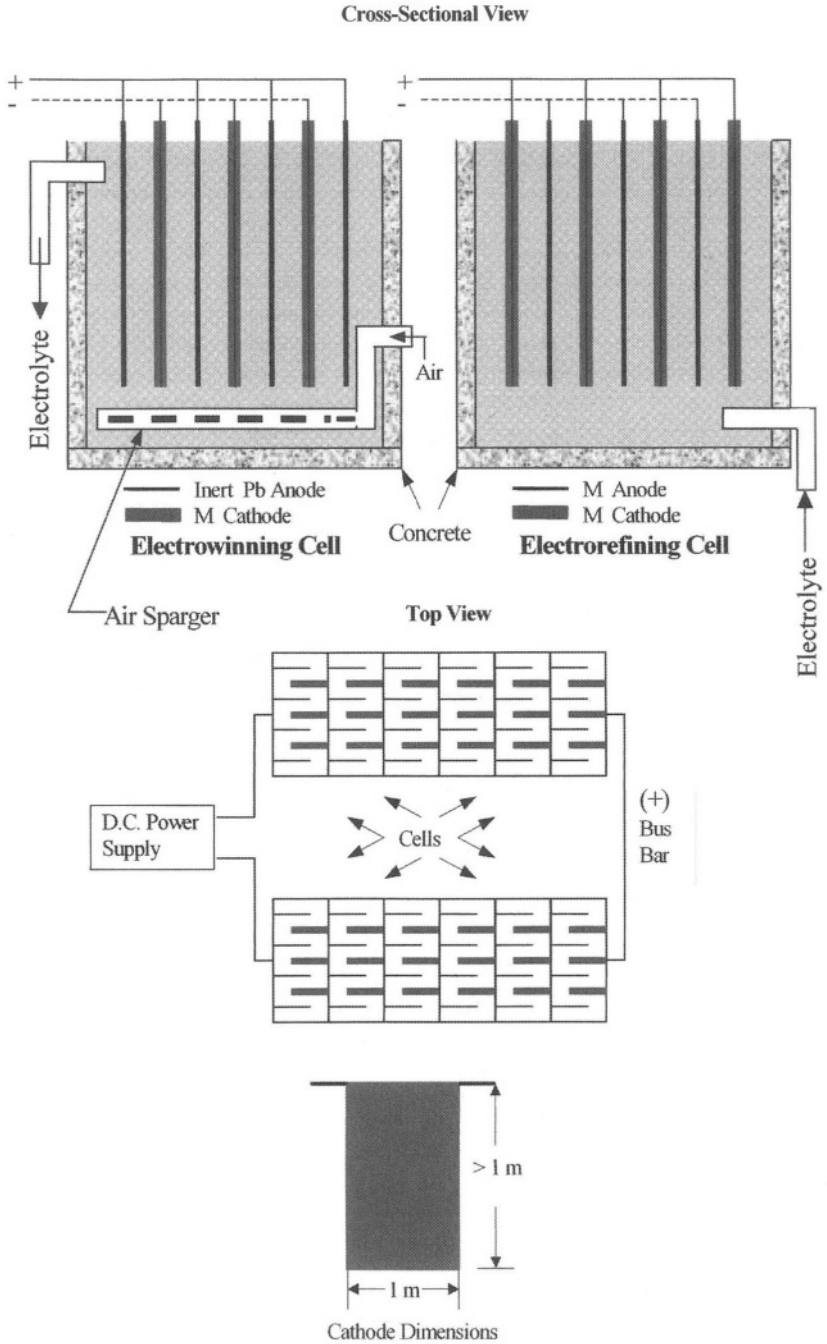


Figure 7.3 Schematic electrowinning cell layout.

3) Recycling step:

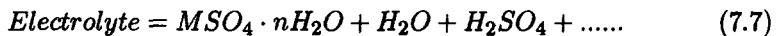


The electrochemistry of electrodeposition is influenced by several factors that must be controlled for producing a metal very efficiently. These factors are

- Electrolyte composition. Impurities may codeposit.
- Electrolyte conductivity, which can be enhanced by adding a small amount of a salt (*NaCl*, *KCl*).
- pH which determines the degree of acidity. In fact, control of pH is desired since the rate of hydrogen evolution may be faster than the rate of metal deposition, and therefore, metal deposition is impaired and current density for deposition is reduced [16].
- Temperature, which is usually less than 70°C.
- Applied current and potential. These variables determine the cell power, which in turn, is linearly proportional to energy consumption.
- Mass transfer by diffusion, migration and convection.
- Electrode surface roughness, which must be reduced for better electrolytic deposition.

Conventional electrochemical and electrorefining plant cell layouts are schematically shown in Figure 7.3. It is convenient to describe the events that occur in these electrochemical cells in a outline manner. Hence,

- The electrolyte in these cells are normally composed of at least three components



- Conventionally, lead (*Pb*) is used as the starter anodic electrode sheets connected to the power supply positive terminal. The cathode sheets can be made out of metal *M*, stainless steel or titanium electrode sheets.
- Anodic reactions occur on the anode-electrolyte interface according to eq. (7.3) having a standard potential of $E_a^0 = -1.23 \text{ V}$ (Table 2.2) for the oxidation reaction to proceed. The electrons produced by eq. (7.3) are driven through the external circuit by the D.C. power and are consumed by the cathodic reactions at the cathode-electrolyte interfaces and proceeds according to the reaction defined by eq. (7.5)
- Electrolyte direct flow or air-sparging agitation system enhances the current density.

- The electrolyte is kept replenished as electrolysis proceeds; otherwise, the concentration of the metal cations M^{+z} drops very significantly and the potential vanishes, $E \rightarrow 0$ [2].
- For metal deposition to occur, the applied potential must be greater than the sum of the anode and cathode standard potentials. For example, in copper electrowinning (EW) the applied potential must be

$$E > (E_{a,H_2O}^{\circ} + E_{Cu}^{\circ}) = -1.229 V + 0.337 V \quad (a)$$

$$E > -0.892 V \quad (b)$$

- Usually, the potential is in the range of $1.5 V < E < 4.00 V$. This is a practical potential range used in conventional *Pb*-anodes and gas diffusion anodes in electrochemical operations [2,14-17].
- Using gas diffusion anodes [16] and dimensionally stable anodes (DSA[®]) [14-15] in electrowinning (EW) of zinc yields high current efficiency in the range of $90\% \leq \epsilon \leq 100\%$, but the current densities are higher than most conventional planar *Pb*-anode practices. The common current efficiency range for conventional practices is $80\% \leq \epsilon \leq 90\%$.
- During the electrolytic process, current flows at a fine rate, but overpotential drop emerges due to connectors and wiring system, and electrolyte electrical resistance at the cathode-electrolyte interface. Also, overpotential may occur when concentration polarization is due to mass transfer by diffusion [1].
- In EW and ER, an aggregation of acid drops suspended above the electrolytic cells is a phenomenon known as “acid mist,” which comes from bursting bubbles of hydrogen and even oxygen in acid solutions. Therefore, spraying acid drops into the atmosphere are detrimental to health and equipment. One can alleviate the hazardous of acid mist by implementing a ventilation system [1,13] or using close-ended cylindrical cells [40].
- Heat generation occurs as current flows due to electrolyte resistance and electrical connection resistance. Therefore, a heat exchanger is required to overcome overheating the electrolyte, avoid cathode deterioration and oxidation of anodes. Thus, a temperature range of $30^{\circ}C \leq T \leq 45^{\circ}C$ is adequate for most EW operations [1].
- Once enough metal deposition is obtained, the cathodes are mechanically removed from the cells and peeled off (stripped off), provided that a weak atomic bonding exists at the sheet-deposit interface. Then, the cathode starter sheets are recycled [1-3,34]. Figure 7.4 shows an electrowinning cells as part of a class project and Figure 7.5 illustrates ASARCO industrial cells for producing copper [33].

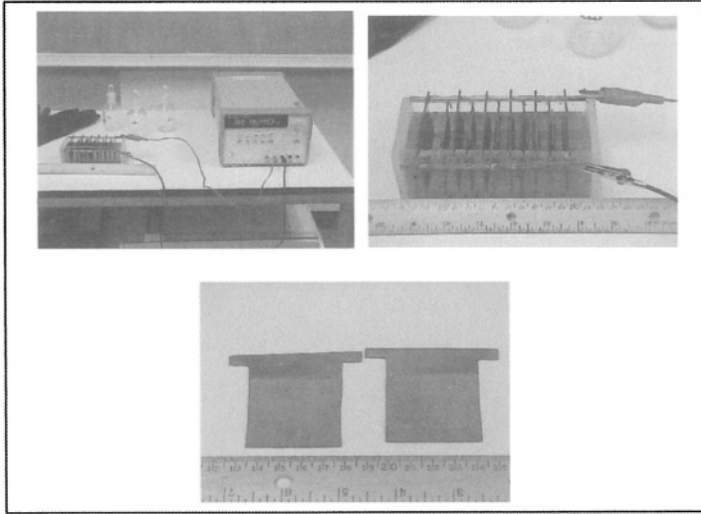


Figure 7.4 Laboratory electrowinning cell for producing copper.

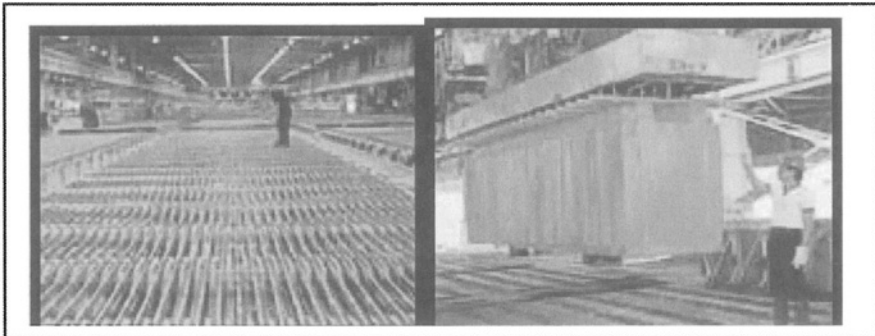


Figure 7.5 ASARCO a) Copper electrowinning cells and b) Cathodes [33].

Figure 7.6 shows schematic and oversimplified electrowinning cells containing non-planar electrodes. Cylindrical and disk cathodes have been used for over two decades. The *EMEW*[®] cell has recently been developed by Electrometals Technologies Limited [40] for electrowinning metals such as *Cu*, *Zn*, *Ni*, *Ag*, *Au* and *Pt* from a variety of concentrations at current densities in the range of $400 \text{ A/m}^2 < i < 700 \text{ A/m}^2$, potential at $E < 4.00 \text{ V}$, and current efficiency at $\epsilon > 85\%$. The *EMEW*[®] cell consists of concentric cylindrical electrodes enclosed by a PVC pipe and it has several advantages over the conventional planar-electrode cells. For instance, the cell is inexpensive, the “acid mist” problem is eliminated since the cell has closed ends, and metal recovery from alkaline and chloride-containing solutions is suitable at low energy consumption.

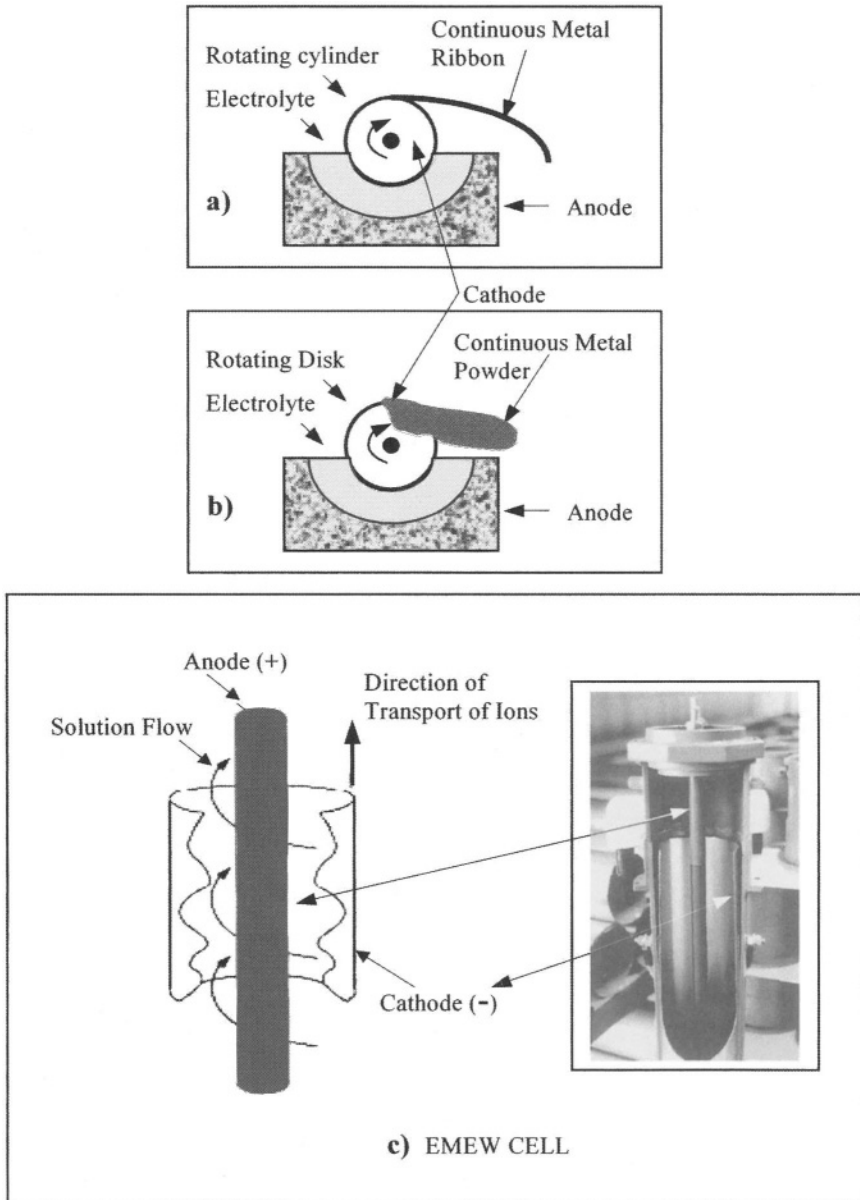


Figure 7.6 Non-conventional electrowinning cells. a) Rotating cylinder for producing a continuous ribbon, b) rotating disk for producing powder, and c) *EMEW*[®] cylindrical cell for a variety of metal recovery [40].

7.3 MATHEMATICS OF ELECTROWINNING

This section is mainly concerned with simple formulas based on Faraday's law of electrolysis and energy consumption for producing high purity metals from electrolytes through an aqueous electrolysis. The mathematics is simple to understand and easy to use in basic engineering calculations. However, complications may arise when diffusion and migration of solute are coupled. Diffusion itself is rather a complex subject that depends on the type of diffusion process to be analyzed. The economics of electrowinning is introduced very briefly since this is not the main subject in this section.

7.3.1 FARADAY'S LAW OF ELECTROLYSIS

The law of electrolysis states that the amount of a species j that is gained or liberated on the electrode surface during the electrochemical process is directly proportional to the quantity of electric charge (Q) that passes through the aqueous electrolyte. The electric charge is defined as the electric current per unit time as previously defined by eq. (3.81). For a constant current flowing through the electrolyte, the electric charge is

$$\int dQ = I \int dt \quad (7.8a)$$

$$Q = It \quad (7.8b)$$

Thus, the amount of a species j is defined as the Faraday's weight gained or liberated due to the flowing electric current during a period of time

$$W = \lambda_e Q \quad (7.8c)$$

$$W = \lambda_e It \quad (7.8d)$$

where λ_e = Electrochemical constant (g/A)

Q = Electric charge ($C = A.s = J/V$)

In addition, λ_e is defined by

$$\lambda_e = \frac{A_w}{zq_e N_A} \quad (7.8e)$$

$$\lambda_e = \frac{A_w}{zF} \quad (7.8f)$$

where F = Faraday's constant

$F = q_e N_A = 96,500$ ($C/mol = A.s/mol = J/mol.V$)

q_e = Electron charge = 1.6022×10^{-19} ($C/electrons$)

N_A = Avogadro's number = 6.02213×10^{23} ions/mol

A_w = Atomic weight (g/mol)

Combining eqs. (7.8d) and (7.8f) yields the theoretical weight gain

$$W_{th} = \frac{ItA_w}{zF} \quad (7.8g)$$

$$W_{th} = \frac{QA_w}{zF} \quad (7.8i)$$

Example 7.1 Calculate a) the number of electrons and b) the weight of electrodeposited nickel on a cathode electrode when a current of 1 A flows through a nickel sulfate ($NiSO_4$) electrolyte for one hour at a temperature $T > 25^\circ C$. Assume an ideal electrolysis process for recovering nickel cations from solution at 100% current efficiency.

Solution:

a) The reduction reaction for the electrodeposition is $Ni^{+2} + 2e = Ni$. Using the given data yields

$$\begin{aligned} Q &= It = (1 \text{ A})(3,600 \text{ s}) = 3,600 \text{ C} \\ N_e &= \frac{Q}{q_e} = \frac{3,600 \text{ C}}{1.6022 \times 10^{-19} \text{ C/electrons}} \\ N_e &= 2.25 \times 10^{22} \text{ electrons} \\ N_{Ni} &= \frac{N_e}{z} = \frac{2.25 \times 10^{22} \text{ electrons}}{2 \text{ electrons/atoms}} \\ N_{Ni} &= 1.125 \times 10^{22} \text{ atoms} \end{aligned}$$

b) The weight gained is

$$\begin{aligned} W_{th} &= \frac{QA_w}{zF} = \frac{(3,600 \text{ C})(58.71 \text{ g/mol})}{(2)(96,500 \text{ C/mol})} \\ W_{th} &\approx 1.10 \text{ grams} \end{aligned}$$

Furthermore, the electric current evolved during electrolysis has been derived in section 3.8. Recall that the electrical conduction is a mass transfer phenomenon within which electrons and ions carry the electric charge through their mobilities. Both positively charged ions (cations) negatively charged ions (anions) flow in the opposite direction. Thus, cations and electrons move to the negatively charged cathodic electrode surface (-) and the anions move toward the positively charge anodic electrode surface (+).

7.3.2 PRODUCTION RATE

Actual electrochemical cells do not operate at 100% efficiency because of imperfections in the wiring system and possible contaminants or impurities in the electrolyte. Therefore, Faraday's law of electrolysis, eq. (7.8g), must include the cathodic current efficiency parameter for determining the amount of electrolytic metal deposit or weight gain on cathodes. Normally, the current efficiency at the cathodes is less than 100% due to hydrogen evolution or codeposition of impurities. Hence, the actual weight gain together with the current efficiency and total cathode surface area becomes

$$W = \frac{\epsilon I A_w t}{zF} = \frac{\epsilon i A_s A_w t}{zF} \quad (7.9)$$

$$\epsilon = \frac{W}{W_{th}} = \frac{i}{i_{th}} < 1 \quad (7.10)$$

$$A_s = 2N A_c \quad (7.11)$$

where ϵ = Current efficiency

I = Current (A)

A_w = Atomic weight or molar mass (g/mol)

t = Time (s)

z = Valence

$F = 96,500$ C/mol (= A.s/mol = J/mol.V)

A_s = Total cathode surface area (cm²)

N = Number of cathodes

A_c = Cathode surface area (cm²)

Conventional electrowinning cells utilize planar *Pb*-base anodes at current densities in the range of $200 \text{ A/m}^2 < i < 500 \text{ A/m}^2$ [2,14]. On the other hand, advanced electrowinning cells use hydrogen gas diffusion (*HGD*) anodes at $2 \text{ kA/m}^2 < i < 8 \text{ kA/m}^2$ [15-18]. Normally, the current density and energy efficiency (ϵ^*) are less than 100% due to drawbacks mainly caused by ohmic potential drop and oxygen evolution reaction. The energy efficiency can be defined by

$$\epsilon^* = \frac{\epsilon E_{cell}}{E} < 1 \quad (7.12)$$

where E is the applied potential. The potential E is the sum of electrode potentials and overpotentials, including the ohmic effect [2,23]. Hence,

$$E = E_a + E_c + \eta_a + \eta_c + IR_s \quad (7.13)$$

Also, E can be defined as [4]

$$E = \frac{IL\rho_x}{A_s} = iL\rho_x \quad (7.14)$$

where ρ_x = Solution resistivity (*ohm.cm*)
 $\rho_x = 5 \text{ ohm.cm}$ resistivity for Cu^{+2} in solution [2]
 L = Anode to cathode distance (*cm*)

According to Ohm's law, the distribution of the solution resistance can be deduced from eq. (7.14) as

$$R_s = \frac{E}{I} = \frac{L\rho_x}{A_s} \tag{7.15}$$

Another important parameter for assessing the performance of an electrowinning cell is the production rate, which is defined by

$$P_R = \frac{dW}{dt} = \frac{\epsilon i A_s A_w}{zF} \tag{7.16}$$

In order to analyze an electrowinning cells from economical point of view, the power and the energy consumption needed to operate the cell are, respectively

$$P = EI \tag{7.17}$$

$$\gamma = P/P_R = \frac{zF E}{A_w \epsilon} \tag{7.18}$$

The power P is converted to kW and γ to kWh/Kg . Eq. (7.18) is a simple and yet, essential in analyzing electrowinning processes. One can observe that this is one expression that depends on two independent variables. Thus, the behavior of this equation is best understood by plotting a surface (mesh) in a three-dimensional space as shown in Figure 7.7.

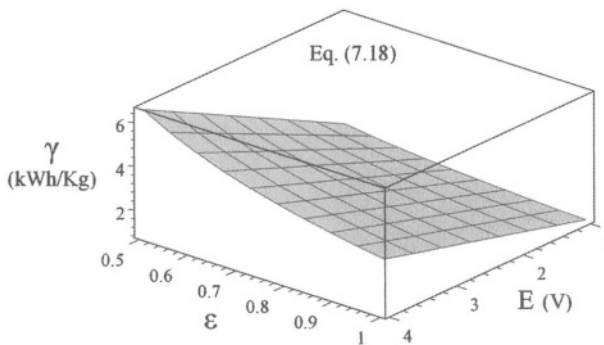


Figure 7.7 Theoretical energy consumption surface for electrowinning zinc.

The surface indicates that γ decreases with decreasing E and increasing ϵ . The optimum metal recovery can be achieved when $\epsilon = 1$ and $E = 1$ V so that the energy consumption becomes $\gamma = 0.82$ kWh/Kg for Zn, $\gamma = 0.84$ kWh/Kg for Cu and $\gamma = 0.91$ kWh/Kg for Ni. However, real electrowinning operations are seldom at 100% efficiency due to many design factors, such as electrical contacts, electrolyte resistance, and the like. Nevertheless, an idealized electrowinning cell must operate at very low energy consumption so that production cost is kept as low as possible.

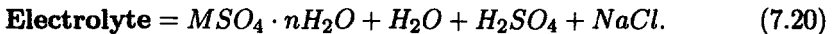
Since electrometallurgical processes operate on a continuous schedule, a continuous supply of fresh electrolyte from a leaching plant to the cells places a very important roll in producing metals from solutions. Therefore, the volume flow rate (F_r) of the electrolyte entering the cells based on Faraday's law must be controlled mechanically. A pump in the order of F_r is needed for circulating the electrolyte through the electrodes to the leaching plant for recycling purposes and for avoiding an increase in the electrolyte acidity.

The electrolyte volume flow rate (F_r) is another parameter that must be controlled during the electrolysis of a particular metal under forced laminar flow. Thus,

$$F_r = \frac{P_R}{C_{o,M}} = \frac{P_R}{C_o A_w} \quad (7.19)$$

where $C_{o,M}$ = Bulk concentration of metal cations M^{+z} (g/l)
 C_o = Bulk activity of metal cations M^{+z} (mol/cm³)
 F_r is normally in units of l/min

Common electrolyte constituents are metal sulfate, water, sulfuric acid, and a small amount of salt for enhancing the electrolyte electric conductivity (K_c). Hence,



For a fixed total volume of the electrolyte, the weight of hydrated metal sulfate, sodium chloride, and volume of sulfuric acid can be determined, respectively, using the following formulas

$$W_{MSO_4 \cdot nH_2O} = (VC_{o,M}) \frac{A_{w,MSO_4 \cdot nH_2O}}{A_{w,M}} \quad (7.21)$$

$$W_{NaCl} = VC_{NaCl} \quad (7.22)$$

$$V_{H_2SO_4} = (VC_{H_2SO_4}) / \rho_{H_2SO_4} \quad (7.23)$$

where V = Total volume of electrolyte (l)

$\rho_{H_2SO_4}$ = Density of sulfuric acid (g/cm³ or g/l)

$C_{H_2SO_4}$ = Concentration of sulfuric acid (g/l)

$A_{w,MSO_4 \cdot nH_2O}$ = Molecular weight of metal sulfate (g/mol)

$A_{w,M}$ = Atomic weight of metal M (g/mol)

Example 7.2 Calculate the weight of hydrated copper sulfate ($\text{CuSO}_4 \cdot 5\text{H}_2\text{O}$) to prepare a 10-liter electrolyte containing 35 g/l of Cu^{+2} and 180 g/l of H_2SO_4 . The density of H_2SO_4 is 1.80 g/cm^3 (1,800 g/l). Ignore additions of NaCl .

Solution:

$$\begin{aligned}
 M &= \text{Cu} \quad \text{MSO}_4 \cdot n\text{H}_2\text{O} = \text{CuSO}_4 \cdot 5\text{H}_2\text{O} \\
 C_{o,\text{Cu}} &= 35 \text{ g/l} = 5.51 \times 10^{-4} \text{ mol/cm}^3 & A_{w,M} &= 63.55 \text{ g/mol} \\
 C_{\text{H}_2\text{SO}_4} &= 180 \text{ g/l} & A_{w,\text{MSO}_4 \cdot n\text{H}_2\text{O}} &= 249.55 \text{ g/l} \\
 \rho_{\text{H}_2\text{SO}_4} &= 1,800 \text{ g/l} & V &= 10 \text{ g/l}
 \end{aligned}$$

Using eqs. (7.21) and (7.23) yields

$$\begin{aligned}
 W_{\text{MSO}_4 \cdot n\text{H}_2\text{O}} &= (VC_{o,M}) (A_{w,\text{MSO}_4 \cdot n\text{H}_2\text{O}}) / (A_{w,\text{Cu}}) = 1,374.39 \text{ g} \\
 V_{\text{H}_2\text{SO}_4} &= (VC_{\text{H}_2\text{SO}_4}) / \rho_{\text{H}_2\text{SO}_4} = 1.00 \text{ l} \\
 V_{\text{H}_2\text{O}} &= 10.00 \text{ l} - 1.00 \text{ l} = 9.00 \text{ l}
 \end{aligned}$$

Mix the components and stir until a homogeneous solution is obtained.

Example 7.3 A circulating acid system is important in electrowinning copper in order to have a continuous deposition process. However, if the cell is not replenished with fresh solution, the cathode potential vanishes. Based on this information, determine a) the minimum concentration of Cu^{+2} in g/l that can be recovered at 35°C and 101 kPa. b) When will hydrogen evolution occur?

Solution:

$$\text{a) } \text{Cu}^{+2} + 2e = \text{Cu} \quad @ \quad E^\circ = 0.337 \text{ V}$$

Solving the Nernst equation, eq. (2.32), for the concentration yields

$$\begin{aligned}
 E &= E^\circ - (RT/zF) \ln K \\
 K &= a_{\text{Cu}} / a_{\text{Cu}^{+2}} = \\
 0 &= 0.337 \text{ V} + (0.0133) \ln a_{\text{Cu}^{+2}} \\
 a_{\text{Cu}^{+2}} &= 9.31 \times 10^{-12} \text{ mol/l}
 \end{aligned}$$

Then,

$$\begin{aligned}
 C_{\text{Cu}^{+2}} &= (9.31 \times 10^{-12} \text{ mol/l}) (63.55 \text{ g/mol}) \\
 C_{\text{Cu}^{+2}} &= 5.92 \times 10^{-10} \text{ g/l}
 \end{aligned}$$

b) Hydrogen evolution will start when $a_{\text{Cu}^{+2}} = 9.31 \times 10^{-12} \text{ mol/l}$.

Example 7.4 An electrowinning cell produces 10 Kg/h of nickel (Ni) at a current efficiency (ϵ) of 80%. The cell contains 20 cathodes and operates at a current of 215 A/m^2 and a potential of 2 V. Determine a) the energy consumption, b) flow rate of the electrolyte and c) the cathode length for a width of 1 m. The concentration of nickel cations is 35 g/l. d) Plot eq. (7.18) and explain the result.

Solution:

$$Ni^{+2} + 2e = Ni \quad @ \quad E = 2 \text{ V and } i = 215 \text{ A/m}^2 \text{ with } z = 2$$

$$P_R = 10 \text{ Kg/h} = 10^4 \text{ g/h}, \quad N = 20, \quad A_{w,Ni} = 58.71 \text{ g/mol}$$

$$C_o = 35 \text{ g/l} = 5.96 \times 10^{-4} \text{ mol/cm}^3$$

a) From, eq. (7.16),

$$A_s = zFP_R / (\epsilon i A_w) = 53.10 \text{ m}^2$$

$$I = i A_s = 11,416.20 \text{ A}$$

$$P = EI = 22.83 \text{ kW}$$

$$\gamma = P/P_R = 2.28 \text{ kW.h/Kg}$$

b) $F_r = P_r/C_o = 4.76 \text{ l/min}$

c) $A_c = A_s / (2N) = 1.3275 \text{ m}^2$

$$L = A_c/w = 1.3275 \text{ m}$$

d) From eq. (7.18), the simplified energy consumption equation becomes

$$\gamma = 1.83/\epsilon \quad (\text{in kW.h/Kg})$$

which is plotted in Figure 7.8 below indicating that the energy consumption is strongly dependent on the current efficiency since γ is inversely proportional to ϵ . However, this strong dependency begins to have a lesser effect when $\epsilon \geq 0.25$ and when $\epsilon > 0.80$ the energy consumption is significantly reduced.

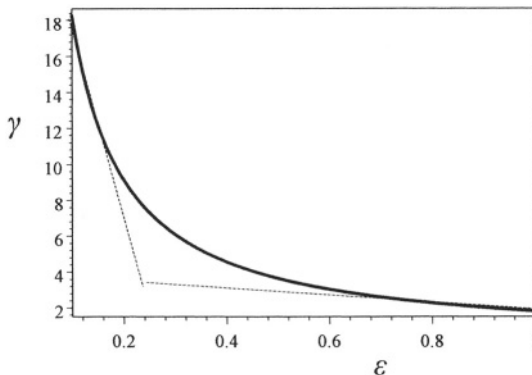


Figure 7.8 Influence of current efficiency on the energy consumption.

7.3.3 ECONOMY

Cost analysis is essential in electrowinning a metal M in order to determine the total cost of production, in which the energy consumption is one of the most important parameters that must be reduced [14-15]. Nevertheless, the fixed (F_c) and variable (V_c) cost per unit mass expression are, respectively

$$F_c = \frac{X_s I_r}{P_r} = \frac{z F S_a I_r}{\epsilon i A_w} \quad (7.24)$$

$$V_c = \frac{z F \gamma_c E}{\epsilon A_w} \quad (7.25)$$

$$S_a = \frac{X_s}{A_s} \quad (7.26)$$

- where X_s = Specific equipment cost (\$)
 I_r = Interest rate of return (fraction/year)
 t = Time (y)
 S_a = Specific surface cost (\$/cm²)
 i = Current density (A/cm²)
 γ_c = Specific energy cost (\$/kWh)
 ϵ = Current efficiency (fraction)
 A_w = Atomic weight of metal M (g/mol)
 A_s = Total cathode area (cm²)
 F = 96,500 A.s/mol
 z = Valence of cation M^{+z}

The total cost per unit mass, including maintenance cost (M_c) is

$$T_c = F_c + V_c + M_c \quad (7.27)$$

$$T_c = \frac{zF}{\epsilon A_w} \left(\frac{S_a I_r}{i} + z F \gamma_c E \right) + M_c \quad (7.28)$$

Using eq. (7.28) for optimizing the total cost per unit mass requires that $dT_c/di = 0$. Thus, the optimal current density is derived as [14]

$$i = \sqrt{\frac{S_a I_r}{\gamma_c (dE/di)}} \quad (7.29)$$

where dE/di = slope of a $E = f(i)$ relationship. Inserting eq. (7.29) into (7.28) yields

$$T_{c,\max} = \frac{zF}{\epsilon A_w} \left[\sqrt{S_a I_r \gamma_c (dE/di)} + z F \gamma_c E \right] + M_c \quad (7.30)$$

which is the maximum total production cost per unit mass equation.

7.3.4 ELECTROWINNING OF ZINC

A typical industrial production of zinc metal is accomplished by electrolysis of highly purified zinc sulfate ($ZnSO_4$). The energy consumption is in the order of 3.3 kW.h/Kg for a current efficiency of 90% at 500 A/m^2 [14]. Since the energy consumption is an economical factor that dictates the feasibility of an electrowinning cell, substantial energy savings can be accomplished by reducing the irreversible energy dissipation due to oxygen evolution on the anodes. In fact, reducing ohmic potential drop induces energy savings. A reduction in energy consumption can be achieved by using catalytic oxygen evolution anodes, such as dimensionally stable anodes ($DSA^{\text{®}}$) [14] and hydrogen gas diffusion (HGD) anodes [38,44]. The latter type of anode reduces production cost [15,19-21]. Thus, HGD anodes require a low potential range, $1.5 \text{ V} < E < 4 \text{ V}$, and high current densities, $2 \text{ kA/m}^2 \leq i \leq 8 \text{ kA/m}^2$, as compared with the conventional range of $400 \text{ A/m}^2 \leq i \leq 800 \text{ A/m}^2$. Moreover, the structure of a gas diffusion anode can be found elsewhere [15,22]. Some relevant data for electrowinning zinc is displayed in Table 7.1.

Table 7.1 Relevant parameters used in electrowinning of Zn.

i (A/m^2)	E (V)	ϵ (%)	γ (kWh/Kg)	Anode	T $^{\circ}C$	Ref.
500	3.3	90	3.30	Pb-alloy	> 25	[14]
5,000	4.0	91	3.60	$DSA^{\text{®}}$	> 25	[15]
5,000	1.8	90	1.64	$DSA^{\text{®}}$	> 21	[17]
5,000	4.0	90	3.10	$DSA^{\text{®}}$	50	[18]
5,000	4.0	95	3.50	$DSA^{\text{®}}$	50	[18]

According to these data, the main difference between the electrowinning cells containing conventional Pb -alloy and non-conventional DSA anodes is the current density. However, E , ϵ , and γ are similar, except for one reported DSA cell [17]. These observations suggest that conventional cells are still promising in metal recovery of zinc from solutions. Despite that catalytic oxygen anodes promote substantial savings, impurities in the zinc electrolyte limit their service life, but purification of the electrolyte can reduce this detrimental effect [14]. According to a literature review of HGD anodes conducted by Bestetti et al. [15] suggests that these type of anodes offer a feasible technological approach and have the advantage over the conventional Pb -alloy anodes to resist higher concentrations of sulfuric acid containing lower concentrations of zinc. Thus, energy consumption is reduced as well as the cell potential.

Figure 7.9 shows a 3-D surface plot of Bestetti et al. [14] reported data on electrowinning of zinc. This 3-D plot indicates that energy consumption (γ) decreases with increasing efficiency ϵ at fixed values of potential E . On the other hand, keeping ϵ constant, γ increases with increasing E . Therefore, the

ideal operating conditions can be achieved by keeping a low E and a high ϵ for low γ . This surface is in accord with eq. (7.18).

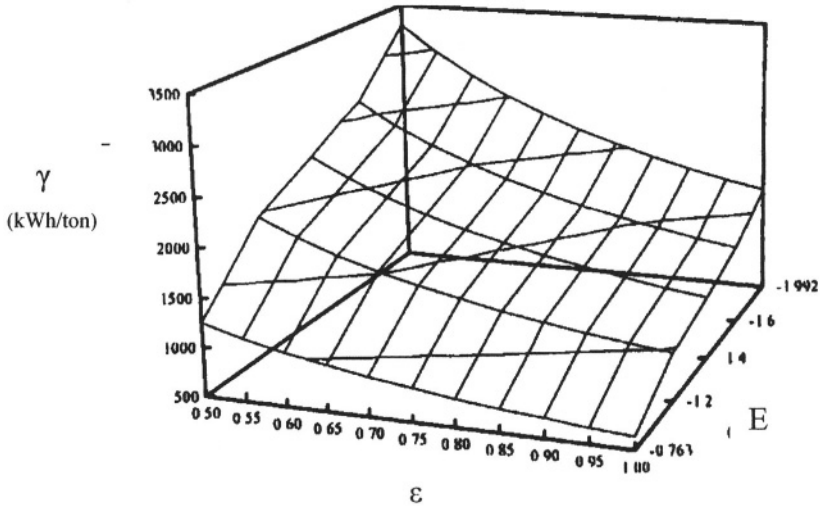


Figure 7.9 Experimental energy consumption surface for electrowinning zinc using hydrogen gas diffusion (HGD) anodes [21].

Table 7.2 lists available experimental data from the literature. Observe that the applied cell potential for both conventional anode and hydrogen gas diffusion (HGD) anode is in accord with eq. (7.13). The HGD anode yields lower cell potential than the conventional electrodes at a constant current density flowing through a strong acid solution. This suggests that HGD is very promising in electrowinning operations since the energy consumption is lower than its counterpart.

Table 7.2 Components of cell potentials.
at $i = 450 \text{ A/m}^2$ and $pH = 1$ [38]

Variable	Conventional (V)	HGD (V)
$E_a + E_c$	2.04	0.81
η_a	0.86	0.14
η_c	0.06	0.06
IR_s	0.54	0.54
E	3.50	1.55

7.4 ELECTROREFINING

Electrorefining (*ER*) is an electrochemical technique suitable for refining metals produced by electrowinning or smelter. The final metal product from a smelter and an electrowinning (*EW*) processes contains impurities, but further refinement can be accomplished by electrorefining cells, which deliver high purity metal M , such as copper, and a secondary recovery of precious metals may follow. A plant layout for electrorefining is shown in Figure 7.3. The impurities are more noble than the metal being produced. For instance, the nearly pure cathodes are used as anodes in order to force metal dissolution to approximately 85% and the remaining is used as scrap for producing started sheet. Subsequently, metal reduction follows for depositing pure metal at a current density in the range of $200 \text{ A/m}^2 \leq i \leq 215 \text{ A/m}^2$ and at a potential $E_{ER} < E_{EW}$. During electrorefining (*ER*), the impurities fall to the bottom of the cells and are collected as “anode slime,” rich in precious metals, such as *Au*, *Ag*, *Pt* [1-2]. Furthermore, the reason for using starter sheets made out of a different alloy is to compensate for a weak atomic bonding at the sheet-deposit interface for easy removal by mechanical means.

Electrorefining has its fundamentals based on the principles of electrochemical kinetics. The anodes are artificially oxidized by losing electrons and freeing cations, which migrate towards the cathode surfaces through the solution under the influence of an applied current in opposite direction. As a result, the cations M^{+z} combine with electrons to form reduction reactions. This is the source of electrolytic metal deposition, which in turn, becomes adhered as a layer on the cathode surfaces. This layer increases in thickness as electrolysis proceeds up to an extend determined by experimentation or industrial practice. The refining process can be represented by a reversible electrochemical reactions of the form



which implies that the metal M loses ze^{-} electrons at the anode surface and regains them at the cathode surface by a reverse electrochemical reaction. The electrolysis involves exchange of electrons rather than chemical reactions. Some impurities M_1 less noble than metal M can oxidize at the anode surface forming cations dissolved in the electrolyte. Thus far the electrorefining process has been described as a idealized electrochemical process for purifying metals at a macroscopic production. Macroscale operating parameters, such as temperature, electrolyte flow, electrolyte concentration and constituents, applied potential and current density have a strong influence on the quality of the electrolytic deposition [28]. Smoothed, adhered and defect-free (cracks) electrodeposition can be obtained by using adequate amounts of organic additives (inhibitors) in the electrolyte, casting anodes being free of impurity segregation and oxidized surfaces, and keeping a uniform distribution of the current density among the electrodes. Otherwise, the anodes polarize leading to a low rate of dissolution and a reduced rate of metal deposition, and consequently, the plating process yields a rough and nodular surface deposition [2,28,44].

7.5 ELECTROPLATING

Electroplating (EP) is an electrochemical process similar to electrowinning of zinc in which metal deposition is accomplished as a metal coating having a very thin thickness, and it is based on the principles of electrochemical reactions caused by exchange of electrons, instead of chemical reactions. Also, electroplating can be defined as an electrolytic metal deposition due to reduction reactions on the cathode electrode, where a film (thin layer) of metal is adhered as a surface finishing process. Thus, thin metal films are plated on metals and alloys surfaces to enhance their appearance, corrosion resistance, wear resistance, and aesthetic for jewelry and tableware. Such films must be adherent and uniform on regular or irregular metal surfaces, which must be cleaned prior to electrodeposition; otherwise, poor film adhesion and incomplete deposition will not protect the base metal and appearance will not be so appealing. In general, cleaning the surface of a base metal (object) is achieved by using organic, alkaline or acid solutions. The cleaning details depend on the type of solvent, but the main objective is to remove all foreign substances, such as oils, grease, dirt, oxides, and the like.

The most common metal coatings are based on plated *Cr*, *Ni*, *Cd*, *Co*, *Ag*, and *Au*. A metal coating may be electronegative or electropositive to the base metal with respect to the potential difference in a particular environment due to galvanic effects [2]. In general, a metallic or plastic object can be coated with a different plating metal from an aqueous solution, which is the electric conductor, by passing a current from the anode (-) through the solution to the cathode (+). In this electrochemical event the positively charged ions (cations) are the charge carriers that move in parallel with the current direction towards the cathode.

Many factors are controlled for plating a thin film on a particular solid surface. Thus, the following should be considered [2]

- Low current density and relatively low temperature promote coherent deposits with fine grains; otherwise a loose and coarse grained film is produced.
- Small amounts of organic solutes, such as ureas and glues, may enhance the electrodeposition since they hinder metal ion discharge, and increase the cathodic polarization
- The electroplating process must be uniform on the surface object. The geometry of the base metal may cause uneven plating distribution and electric field.

The most common industrial applications of electroplating can be summarized as follows:

- Tin (*Sn*) coating on steel cans for food storage.

- Chromium (*Cr*) coating of less than $2\ \mu\text{m}$ thick on steel parts, such as automobile bumpers and household towel holders, serve as decorative and protective film. *Cr-coating* is hard, wear and corrosion resistance. In certain decorative applications, a *Cr-coating* is plated over a *Ni-undercoating* on steel.
- Silver (*Ag*) and gold (*Au*) coatings are individually used as decorative films on jewelry and electric conductive parts. *Ag-coatings* are also used on utensils.

It should be mentioned that electroplating is considered as one type of finishing process. Other finishing processes include coating on an object for protecting or decorating purposes, but these processes are not electroplating at all since electricity is not used to accomplish a practical industrial procedure. Some of these non-electrolytic finishing processes are briefly cited below [41-42]. Hence,

- Paint coating, which does not need a detailed explanation at all since it is a familiar technique used to decorate or protect an object or structure.
- Hot dipping is a technique used to coat steel parts with zinc (*Zn*) for protection against corrosion. Thus, the *Zn-coated* part is known as galvanized steel.
- Chemical vapor deposition (*CVD*), which requires vapor condensation on a solid surface in a vacuum chamber or inside of a tube furnace at relatively high temperatures. Nowadays, this technique is used for coating metal and optical components,. Also, *CVD* is used for producing carbon nanotubes of a few nanometers in diameter on a variety of substrates at relatively low temperatures, but their alignment and direction on a substrate apparently are difficult to achieve. This may be attributable to the graphite sheet size and morphology.
- Aluminum anodizing consists of a chemical reaction between aluminum and oxygen to form a thin aluminum oxide film on an aluminum-base metal. This process occurs as a natural phenomenon in air. Therefore, this process is an electroless plating process based on chemical reactions.
- Chemical Mechanical Planarization (*CMP*) process is used to prepare silicon wafer surfaces for multi-layer integrated circuits containing copper interconnections [42].
- Powder coating in which a metal powder is melted on the surface of a base material in a furnace at relatively high temperatures. The molten metal is used to coat sport and playground equipment, washing and drying machines, etc..
- Plasma consists of a cloud of ionized gas for coating a metal substrate at high temperature. This technique is classified as a low-pressure or high-pressure plasma according to a particular application.

7.6 MOLTEN SALT ELECTROLYSIS

Conventionally, molten salt electrolysis (MSE) is used for producing molten aluminum and magnesium. Metals less electropositive in the *emf* series than *Al* and *Mg* cannot be electrowon [1-3,11,27]. Conveniently, the Soderberg[32] and Hall-Heroult (*HH*) cells[35] are the classical cells design for producing molten aluminum from bauxite mineral in a molten salt at high temperatures. A schematic Soderberg cell is shown in Figure 7.10. The electrodes are made out of carbon (graphite). The carbon anodes are immersed in the electrolyte, but above the molten *Al* layer, while the carbon cathodes are placed below the molten *Al*. The current is applied through the anode busbar and it passes through the electrolyte and molten *Al* and drained through the carbon cathodes. Consequently, an electromagnetic field (*EMF*) is generated due to the applied current, which interacts with magnetic forces, leading to a possible reduction in current efficiency of the cell.

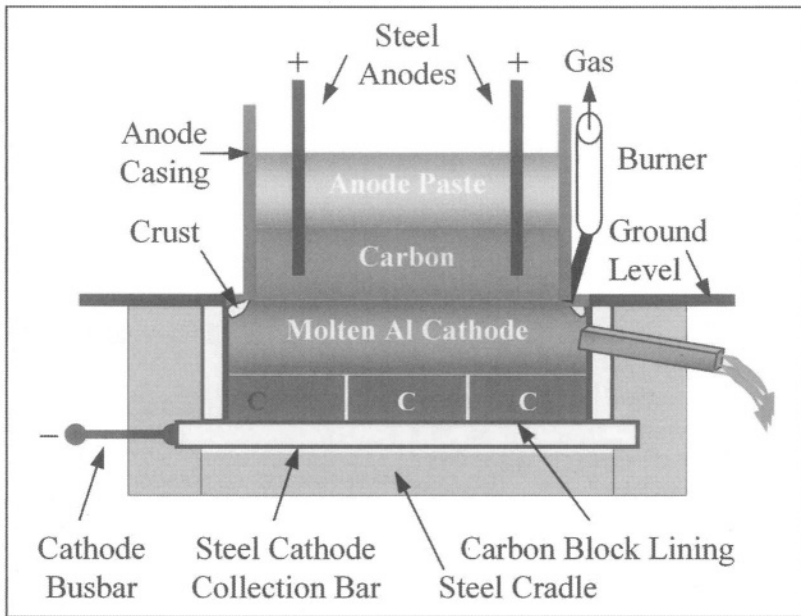


Figure 7.10 Schematic Soderberg cell.

The conventional *HH* cell [$\approx (10m) \times (4m) \times (1m)$] operates at [3]

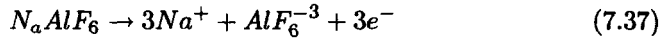
$$4 \text{ V} \leq E \leq 4.5 \text{ V} \quad (7.33)$$

$$5 \text{ kA/m}^2 \leq i \leq 10 \text{ kA/m}^2 \quad (7.34)$$

$$960 \text{ }^\circ\text{C} \leq T \leq 1000 \text{ }^\circ\text{C} \quad (7.35)$$

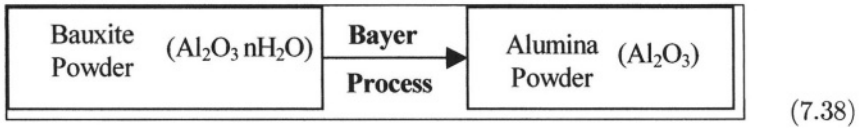
$$90\% \leq \epsilon < 100\% \quad (7.36)$$

The electrolyte is a molten cryolite salt (N_aAlF_6) which melts at 940 °C and decomposes into sodium and hexafluoroaluminate ions (AlF_6^{-3}) [1,69]

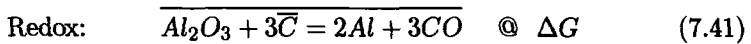
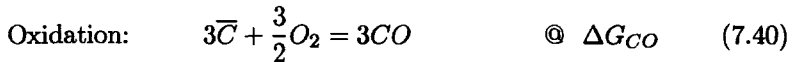
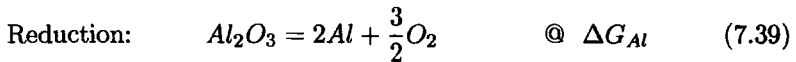


This electrolyte has a high electrical conductivity, which is a requisite in producing molten aluminum from alumina mineral (Al_2O_3) mixed with N_aAlF_6 at high temperatures and high current densities, which in turn, cause high energy consumption. In fact, this high energy consumption may be reduced by using recently developed titanium diboride and carbon ($TiB_2 - C$) cathodes containing an adhered thin film of aluminum (Al) [30,32-33]. High purity of molten Al is produced and subsequently, cast into molds of characteristic shapes.

The production of molten Al can be summarized by the following mineral processing step [31] and main reactions [11]



When Al_2O_3 is added to the molten N_aAlF_6 the following simplified reactions take place



where \bar{C} is graphite (crystalline carbon).

The free energies for these reactions in the written directions are [11]

$$\Delta G_{Al} = -1.68 \times 10^6 + 322.17T \quad (7.42)$$

$$\Delta G_{CO} = 0.354 \times 10^6 + 253.05T \quad (7.43)$$

$$\Delta G = \Delta G_{Al} + \Delta G_{CO} = -1.33 \times 10^6 + 575.22T \quad (7.44)$$

and from eq. (3.25),

$$\Delta G = -zFE \quad (7.45)$$

Combining eqs. (7.44) and (7.45) with $z = 3$ and $F = 96,500 \text{ A.s/mol}$ yields the theoretical cell potential as

$$E = 4.59 - 2 \times 10^{-3}T \quad (7.46)$$

where $\Delta G's$ = Gibbs free energies (J/mol)
 T = Absolute temperature ($^{\circ}K$)

Molten Al ($\rho = 2.3 \text{ g/cm}^3$, $K_c = 2.20 \pm 0.2 \text{ ohm}^{-1}\text{cm}^{-1}$) settles on the bottom of the cell since it is more denser than molten N_aAlF_6 ($\rho < 2 \text{ g/cm}^3$). During electrolysis, the current flows through the molten N_aAlF_6 , breaking down the dissolved Al_2O_3 according to eq. (7.39). Consequently, molten Al and carbon oxide CO gas are produced at the cathode and anode surfaces, respectively. This gas arises due to carbon consumption of the anode. For a continuous electrolysis, the amount of alumina consumed is compensated by additions of fresh alumina powder. Figure 7.11 shows an oversimplified version of the HH cell shown in Figure 7.10 for illustrating the above details [35].

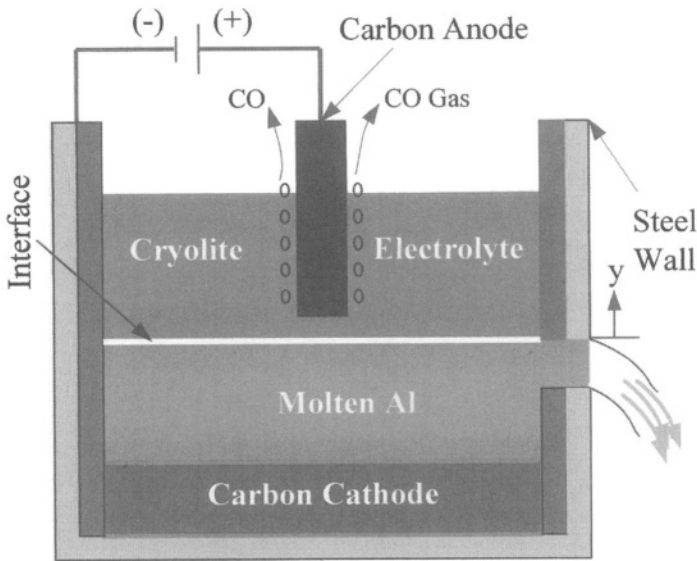


Figure 7.11 Oversimplified HH cell for producing molten aluminum.

7.6.1 CURRENT EFFICIENCY MODEL

The current efficiency of an actual Hall-Heroult (HH) cell depends on internal interactions in the magnetohydrodynamic (MHD) flow, reactions in different zones of the cell, electrical contact system, operating parameters, and anode-to-cathode distance. In principle, Haupin and Frank [65] developed a model of relevant zones within the HH cell. This model is shown in Figure 7.12 and it suggests that the possible interactions that are related to current efficiency and energy consumption may be attributable to diverse potentials in the these zones

and gas evolution during the high temperature electrolysis. These interactions leads to high energy consumption.

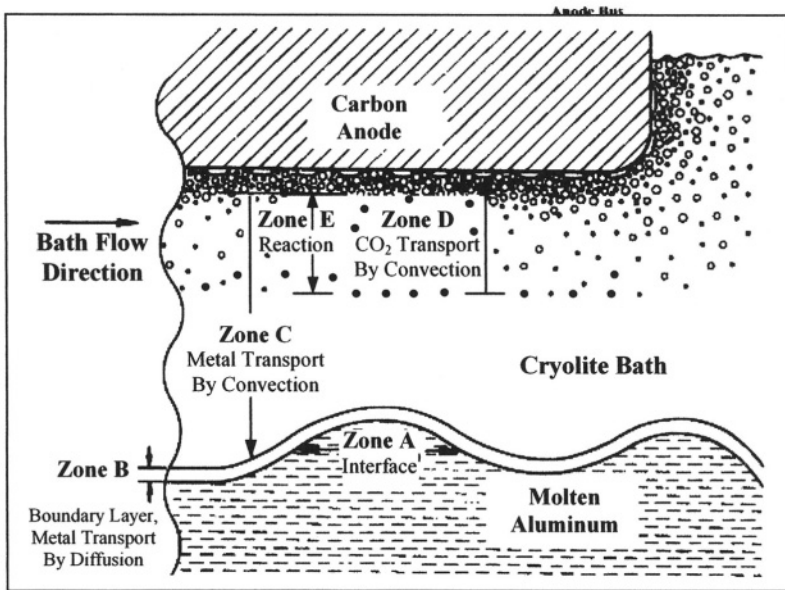


Figure 7.12 Mechanism of current efficiency [69].

The zones in the model are briefly identified as

- **Zone A:** This particular zone is defined as the metal-electrolyte interface and it is very sensitive to the magnetohydrodynamic (*MHD*) instability that may develop due to oscillations of the molten metal. Therefore, the *MHD* instability decreases the current efficiency and increases the energy consumption.
- **Zone B:** It is the diffusion layer containing reactants and reduced ions. According to the model in Figure 7.12, the metal mass transfer is mainly by ionic diffusion, which is a physical phenomenon described by the Fick's laws of diffusion.
- **Zone C:** It is the convective mass transfer of the reduced ions towards the anode. Thus, the motion direction of this mass transfer phenomenon is perpendicular to the bath flow direction as shown in Figure 7.12.
- **Zone D:** It is the convective mass transfer of carbon dioxide (CO_2) gas away from the anode and that of carbon oxide (CO) gas towards the anode.
- **Zone E:** It is a region of mixing ions.

7.6.2 MAGNETOHYDRODYNAMIC FLOW

The theory of magnetohydrodynamic (*MHD*) deals with the interactions induced by a magnetic field in the electrically conducting fluid (molten aluminum). For incompressible fluids, the *MHD* flow stability is principally governed by the Maxwell and Navier-Stokes equations which are coupled through the Lorentz force and Ohm's law. In particular, the Lorentz forces may affect or disturb the flow stabilization of the fluid, but the principal sources of *MHD* instabilities are current flow perturbations that cause distortion of the molten metal-electrolyte interface and discontinuities of the flow velocity at this interface [68]. In general, the electrometallurgy of molten aluminum depends on the *MHD* fluid flow, which in turn, is affected by the inner and outer magnetic fields. The former is generated in the fluid and the latter is applied through the electrically connected busbars of the *HH* cells. In general, among many excellent scientific and theoretical sources on *MHD*, the theory of *MHD* is clearly covered in Hughes and Young book [64] and the Electrometallurgy of Aluminum is adequately written by Haupin and Frank in the Treatise of Electrochemistry edited by J. O'M Bobricks et al. [65].

The thermo-electric design of the *HH* cell requires a careful analysis of the electromagnetic field because of a complicated interaction in the molten $N_aAlF_6 - Al$ interface caused by a magnetohydrodynamic (*MHD*) instability, which leads to high energy consumption and low current efficiency [36-37]. The *MHD* instability arises by the presence of electromagnetic and hydrodynamic waves at the interface, where a thermo-magnetic turbulence (fluctuations of the molten aluminum height) may generate due to magnetic forces and the magnetic energy is converted to kinetic energy [33,36]. Therefore, this interface becomes unstable, leading to short-circuiting the cell, and consequently the cell potential and energy consumption increase. The reader should be aware of the fact that designing an external busbar system as part of the *HH* cell requires an analysis of the current fluctuations induced by a magnetic field within the cell. Therefore, a mathematical analysis, if required, can be very complicated due to the effect of coupled magnetic and electric fields [36].

Figure 7.13 shows a volume element as the geometry model of the *HH* cell (Figure 7.10). The vectors illustrated in Figure 7.13 are the current density (\mathbf{J}), fluid velocity (\mathbf{v}), magnetic flux (\mathbf{B}), Lorentz force (\mathbf{F}), and the vector product ($\mathbf{v} \times \mathbf{B}$), which represents the magnitude of the electric field.

This model can be used to predict both *MHD* and magnetic field characteristics, provided that magnetization of the *HH* steel shell and the current-carrying steel busbar (positive terminal) are included in the numerical simulation. Application of a *d.c.* magnetic field generates a Lorentz force distribution in the opposite direction of the fluid velocity (\mathbf{v}_z). Thus, an electromagnetic force field generates in the *HH* cell. If this force field is strong enough, it can cause unfavorable physical conditions leading to *MHD* instabilities since the force field drives the fluid flow to oscillate harmonically. This unfavorable condition is referred to as perturbation at the molten metal upper face (metal pad) and as a result, the potential fluctuates and energy consumption increases. An example

of potential fluctuation in an unstable HH cell is shown in Figure 7.14 [36].

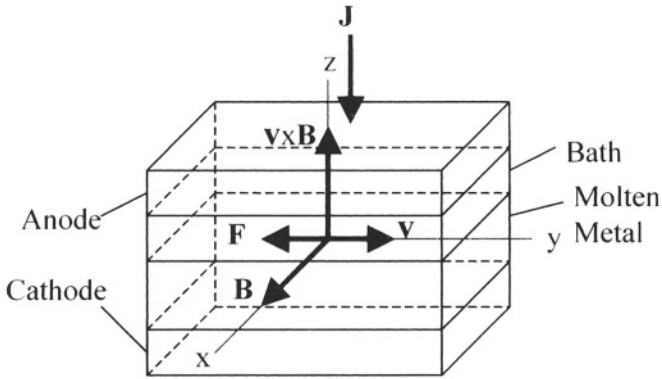


Figure 7.13 Volume element of an HH cell under d.c. field [36].

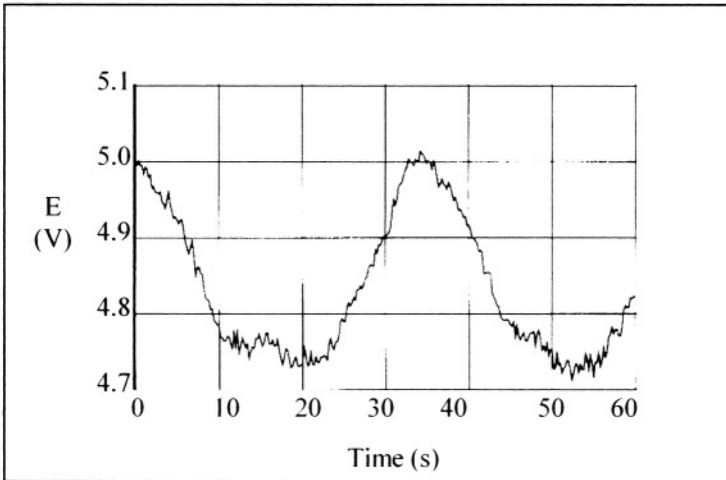


Figure 7.14 Potential fluctuation in an HH unstable cell [36].

Furthermore, the key factor in successful HH cells (pot operations) is to predict and maintain MHD stability. This leads to the characterization of the internal MHD flow using Navier-Stokes equation of motion and Maxwell's equations, including of charge distribution, Faraday's law of induction, Ohm's law, Lorentz force law, Poisson's equation, and even Laplace's equation. The set of these laws and equations constitute the MHD expressions.

For isotropic and homogeneous fluids the Navier-Stokes equation of motion in terms of fluid velocity is

$$\rho \frac{\partial \mathbf{v}}{\partial t} + \rho (\mathbf{v} \cdot \nabla) \mathbf{v} + \nabla P - \eta_v \nabla^2 \mathbf{v} - \mathbf{J} \times \mathbf{B} = 0 \quad (7.47)$$

and the *MHD* expressions are defined below in general vector notation (bold-faced letters)

$$\nabla \cdot \mathbf{D} = q \quad (\text{Coulomb's Law}) \quad (7.48)$$

$$\nabla \times \mathbf{E} = -\frac{\partial \mathbf{B}}{\partial t} \quad (\text{Faraday's Law}) \quad (7.49)$$

$$\mathbf{F} = \mathbf{J} \times \mathbf{B} \quad (\text{Lorentz Law}) \quad (7.50)$$

$$\mathbf{J} = -\sigma \nabla \cdot \phi \quad (\text{Ohm's Law}) \quad (7.51)$$

$$\Delta P = \nabla \cdot \mathbf{F} \quad (\text{Poisson's Equation}) \quad (7.52)$$

$$\nabla \cdot \phi = 0 \quad (\text{LaPlace's Equation}) \quad (7.53)$$

$$\nabla \cdot \mathbf{v} = 0 \quad (\text{Continuity Equation}) \quad (7.54)$$

$$\nabla \cdot \mathbf{J} = 0 \quad (\text{Continuity Equation}) \quad (7.55)$$

$$\nabla \cdot \mathbf{B} = 0 \quad (\text{in the exterior}) \quad (7.56)$$

$$\nabla \cdot \mathbf{B} = \mu \mathbf{J} \quad (\text{in the fluid}) \quad (7.57)$$

$$\mathbf{B} = \mu \mathbf{H} \quad (7.58)$$

where $\mathbf{D} = \epsilon \mathbf{E}$ = Electric current displacement (C/cm^2)

ρ = Charge density (C/cm^3)

η_v = Fluid viscosity ($g/cm.s$)

\mathbf{E} = Electric intensity (gradient) (V/cm)

\mathbf{B} = Magnetic flux density ($V.s/cm^2 = \text{weber}/cm^2$)

\mathbf{H} = Magnetic field intensity ($A/cm = C/cm.s$)

\mathbf{J} = Current density (A/cm^2)

\mathbf{F} = Lorentz force (N)

ϕ = Electric potential (V)

\mathbf{v} = Fluid velocity (cm/s)

P = Scalar hydrodynamic pressure (N/cm^2)

σ = Electric conductivity

ϵ = Dielectric constant

μ = Permeability of the medium ($V.s/A.cm = \text{henry}/cm$)

Details on mathematical modeling an electromagnetic problem in molten salt electrolysis can be found elsewhere [36-37,45-61]. In fact, $\nabla \cdot \mathbf{B} = 0$ implies that the magnetic lines are path-independent since they close on themselves. Also, $\nabla \cdot \mathbf{B} = \text{div } \mathbf{B} = 0$ is the divergence of the vector \mathbf{B} , $\nabla \times \mathbf{E} = \text{curl } \mathbf{E}$ is the curl of the vector \mathbf{E} , and $\mathbf{J} \times \mathbf{B}$ is a vector product.

According to Hughes and Young [64], the most general form of the electromagnetic body forces (\mathbf{F}_e) in a control volume filled with a fluid that includes the effects of charge and current interactions can be determined by

$$\mathbf{F}_e = \rho\mathbf{E} + \mathbf{J}\times\mathbf{B} \quad (7.59)$$

where $\rho\mathbf{E}$ is the electric force and $\mathbf{F} = \mathbf{J}\times\mathbf{B}$ is the interaction force between the current and the magnetic field known as Lorentz force. In metallic conductors $\mathbf{J}\times\mathbf{B}$ is the predominant force in *MHD* flow.

The electromagnetic field generates due to electricity, but the magnetic and electric strengths decrease very rapidly at an infinite distance from the source. Therefore, the strength is distance-dependent. A short distance between the electrodes is essential for keeping a low cell potential. This may be achieved using $TiB_2 - C$ cathodes, which are stable and thermal resistant [33]. Characterizing the electromagnetic field requires an analysis of Maxwell's equations. Hence, the electromagnetic field in a medium is defined by field quantities under steady and transient states. Thus, the *MHD* instabilities may rise due to oscillations of the fluid (molten metal) caused by interactions of the magnetic field and current distribution [36].

Furthermore, molten salt electrolysis of nuclear waste (spent fuel) is an innovative electrometallurgical process essentially developed by *CMT* Division at Argonne National Laboratory [29]. Figure 7.15 shows a schematic cell for treating nuclear waste, specifically for recovering uranium (*U*) and plutonium (*Pu*), and collecting fission products, such as rare earth *Cs*, *Sr*, and *Ce*, at the bottom of the molten *LiCl - KCl* eutectic electrolyte at $500^\circ C$. This high efficiency electrolytic cell consists of a stationary solid cathode where pure *U* is deposited, a stationary liquid cadmium (*Cd*) cathode (*LCC*) for collecting *U* and *Pu* due to their chemical stability in liquid *Cd*, which reacts with plutonium to form $PuCd_6$ intermetallics, and a rotating-anode basket containing chopped nuclear solids. Details on operating parameters and cell conditions, and cell design features can be found elsewhere [29].

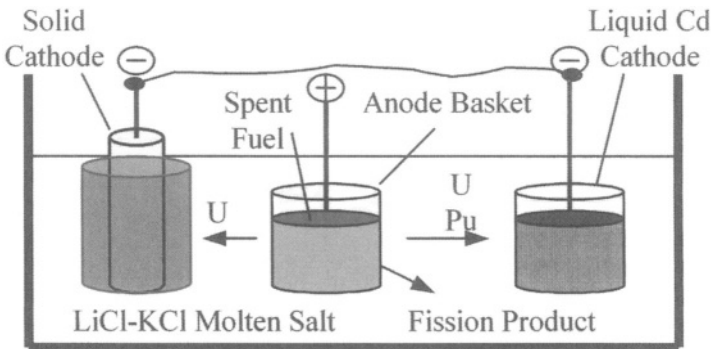


Figure 7.15 Rotating basket anode in molten salt electrorefining [29].

7.7 MOVING BOUNDARY DIFFUSION

It is known that diffusion in liquids is usually faster than in solids of the same solute at the same temperature. However, the liquid geometry is not well understood because of the imperfect atomic arrangement. Despite of this problem, Einstein derived the diffusivity based on Brownian motion of fine particles in liquid water by assuming random direction and jump length of particles [43]. The main objective of a diffusion problem is to understand the problem and subsequently, determine the proper boundary conditions needed for developing a suitable mathematical solution of Fick's second law equation. The boundary conditions, however, depend on the electrochemical system and the type of diffusion taking place.

In this section, surface boundary motion is considered as an essential feature for solving such an equation. Thus, diffusion accompanied by an electrode thickness increment due to diffusion of metal cations (solute) and immobile species is considered to be a particular diffusion problem that resembles mass transfer diffusion toward the faces of cathode sheets in an electrowinning (*EW*) cell.

Figure 7.16 shows Crank's idealized model [25] for moving boundaries towards an aqueous bulk of solution and schematic concentration distribution. This diffusion problem requires that the medium be free of convective mass transfer and that boundary motion occurs along stationary x_1 and x_2 axes. In this case, the boundary motion occurs perpendicular to x_1 and x_2 .

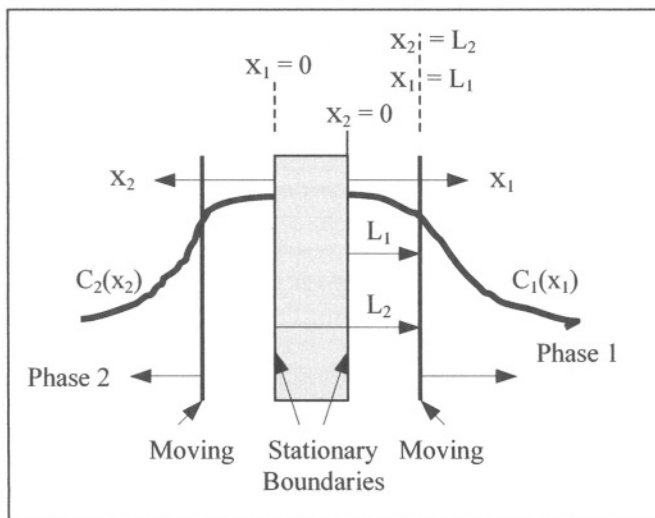


Figure 7.16 Model for moving boundary diffusion in infinite media.

Metal diffusion can be simulated by letting a stationary electrode sheet be the cathode and be immersed in an electrolyte at temperature T and pressure

P. A film of cationic solute M^{+z} in phase 1 (Figure 7.16) deposits on the sheet by diffusion on the outer surfaces and the film is constantly saturated with the electrolyte. Film thickness growth occurs in the x_1 and x_2 directions having a thickness L_1 in phase 1 and L_2 in phase 2, respectively. Thus, the spaces occupied by the deposited film on each side of the sheet are $0 \leq x_1 \leq L_1$ and $-L_2 \leq x_2 \leq 0$. Thus, motion of one or two phases relative to the boundary is caused by the mass transfer diffusion across the interface. This diffusion problem resembles the tarnishing reactions forming an oxide film on a metal surface [25].

Assuming that Fick's second law is obeyed in the media along the interfaces of the moving film boundaries (Figure 7.16) yields

$$\frac{\partial C_1}{\partial t} = D \frac{\partial^2 C_1}{\partial x^2} \quad (7.60)$$

$$\frac{\partial C_2}{\partial t} = D \frac{\partial^2 C_2}{\partial x^2} \quad (7.61)$$

According to the following boundary conditions

$$\begin{array}{l} \underline{x_1 - direction} \\ C_1 = C_{o,1} \quad @ \quad x_1 = 0, \quad t = 0 \end{array} \quad (7.62)$$

$$C_1 = 0 \quad @ \quad x_1 = \infty, \quad t > 0$$

$$\begin{array}{l} \underline{x_2 - direction} \\ C_2 = C_{o,2} \quad @ \quad x_2 = 0, \quad t = 0 \end{array} \quad (7.63)$$

$$C_2 = 0 \quad @ \quad x_2 = -\infty, \quad t > 0$$

and assuming symmetry during diffusion on both sides of the moving boundaries so that $C_o = C_{o,1} = C_{o,2}$, $x = x_1 = x_2$, and $D = D_1 = D_2$, the solution of eq. (7.60) for infinite media are easily obtainable using the analytical procedure included in Appendix A. Hence,

$$\frac{C}{C_o} = \text{erf } c \left(\frac{x}{\sqrt{4Dt}} \right) \quad (7.64)$$

Thus,

$$C = -\frac{C_o}{\sqrt{\pi Dt}} \int_{\infty}^y \exp\left(-\frac{x^2}{4Dt}\right) dx \quad (7.65)$$

$$\frac{\partial C}{\partial x} = -\frac{C_o}{\sqrt{\pi Dt}} \exp\left(-\frac{x^2}{4Dt}\right) \quad (7.66)$$

where $y = x/\sqrt{4Dt}$.

Now, the diffusion molar flux (Fick's first law of diffusion) is

$$J_x = -D \frac{\partial C}{\partial x} \quad (7.67)$$

$$J_x = \frac{DC_o}{\sqrt{\pi Dt}} \exp\left(-\frac{x^2}{4Dt}\right) \quad (7.68)$$

from which the rate of mass transfer is deduced as

$$\frac{dM}{dt} = A_s A_w J_x \quad (7.69)$$

$$\frac{dM}{dt} = A_s A_w \frac{DC_o}{\sqrt{\pi Dt}} \exp\left(-\frac{x^2}{4Dt}\right) \quad (7.70)$$

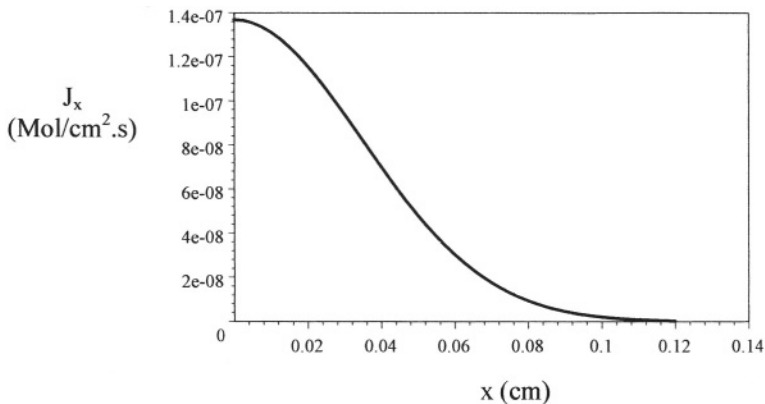
Example 7.5 Use the data given in Example 7.3 and a diffusivity of $10^{-5} \text{ cm}^2/\text{s}$ and $0 \leq x \leq 0.12 \text{ cm}$ and $t = 1 \text{ hour}$ to determine the diffusion molar flux profile.

Solution:

$$\begin{aligned} A_s &= 53.10 \times 10^4 \text{ cm}^2, & A_w &= 58.71 \text{ g/mol} \\ C_o = C_b &= 5.96 \times 10^{-4} \text{ mol/cm}^3, & D &= 10^{-5} \text{ cm}^2/\text{s}, & t &= 3,600 \text{ s} \\ z &= 2, & E &= 2 \text{ V}, & t &= 1 \text{ h} = 3,600 \text{ sec} \end{aligned}$$

a) From eq. (7.68),

$$\begin{aligned} J_x &= C_o \sqrt{D/\pi t} \exp\left(-\frac{x^2}{4Dt}\right) \\ J_x &= [1.37 \times 10^{-7} \text{ mol}/(\text{cm}^2 \cdot \text{s})] \exp(-416.67x^2) \\ J_{x=0} &= 1.37 \times 10^{-7} \text{ mol}/(\text{cm}^2 \cdot \text{s}) \end{aligned}$$



Example 7.4

7.8 DIFFUSION AND MIGRATION

Since electrowinning requires current flow, assume a coupled diffusion and migration mass transfer and neglect any reaction rate controlling the chemical process. The coupled current density has been derived in Chapter 4. Letting $D = D_1 = D_2$ due to the assumed symmetry in section 7.7 gives

$$i = zFD \left[\left| \frac{\partial C}{\partial x} \right| + \frac{zFC_o}{RT} \frac{\partial \phi}{\partial x} \right] \quad (7.71)$$

Substituting eq. (4.63) and (7.66) into (7.71) yields [66]

$$i = 2zFD \frac{\partial C}{\partial x} = \frac{2zFDC_o}{\delta} \exp\left(-\frac{x^2}{4Dt}\right) \quad (7.72)$$

If $x = 0$, then eq. (7.72) becomes

$$i = \left(\frac{2zFDC_o}{\delta} \right) \Big|_{x=0} \quad \text{for } t > 0 \quad (7.73)$$

Recall that $\delta = \sqrt{\pi Dt}$ is the electric double-layer defined in Chapter 3. Experimentally, $0.3 \text{ mm} \leq \delta \leq 0.5 \text{ mm}$ for most practical electrochemical cells under diffusion and natural convection [2]. The latter topic will be dealt with in a later section. In this section, δ is due to diffusion and migration and its value is normally $\delta < 1 \text{ mm}$.

For $x = \sqrt{4Dt} > 0$, eq. (7.72) becomes

$$i \simeq \left(\frac{3zFDC_o}{4\sqrt{\pi Dt}} \right) \Big|_{x>0} \quad \text{for } t > 0 \quad (7.74)$$

Therefore, the current density is higher on the electrode surface than that at in the solution at $x > 0$. The current density, as predicted by eq. (7.73) or (7.74), strongly depends on the inverse square root of time (\sqrt{t}) as theoretically given by eq. (4.52).

Example 7.6 Determine the diffusion double-layer on the surface of a cathode if $C_o = 1.82 \times 10^{-4} \text{ mol/cm}^3$, $D = 1.25 \times 10^{-5} \text{ cm}^2/\text{s}$, $i = 2.20 \times 10^{-2} \text{ A/cm}^2$, and $z = 2$ for zinc reduction.

Solution:

From eq. (7.73),

$$\delta = 2zFDC_o/i$$

$$\delta = \frac{2(2)(96500 \text{ A}\cdot\text{s/mol})(1.25 \times 10^{-5} \text{ cm}^2/\text{s})(1.82 \times 10^{-4} \text{ mol/cm}^3)}{2.20 \times 10^{-2} \text{ A/cm}^2}$$

$$\delta = 0.40 \text{ mm}$$

7.9 MASS TRANSFER BY CONVECTION

7.9.1 STATIONARY PLANAR ELECTRODES

Consider the electrolyte hydrodynamic flow condition shown in Figure 7.17. This is a mass transfer found in electrowinning and electrorefining cells, in which the electrolyte motion is upwards on the anode surface due to the generation of oxygen bubbles, which enhances the mass transfer. The reader can observe in this model that the electrolyte motion is more intense at the top than at the bottom of the electrode as indicated by the arrows. If the current flows, then the electrolyte motion increases and descends to the bottom of the cathode. This is the case in which a significant convective molar flux is superimposed on the Fick's diffusion molar flux. The concentration gradient in the fluid adjacent to the vertical electrode (plate) surface causes a variation in the fluid density and the boundary layer (δ_u) develops upwards from laminar to turbulent conditions [2,7].

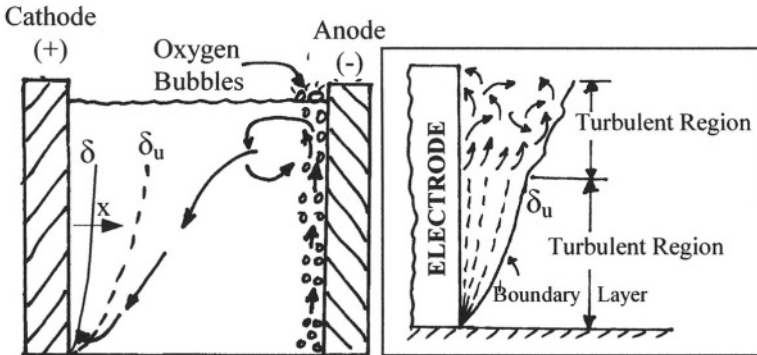


Figure 7.17 a) Natural convective mass transfer between two vertical plates and b) formation of boundary layer [2, 6-7].

The forced convective mass transfer emerges provided that $C_s \neq C_b$, where $C_s \ll C_b$ at $x = 0$ on the cathode surface. According to Geiger and Poirier [5] many forced-convection mass transfer solutions are analogous to heat-transfer cases. This suggests that changes in notations from the latter to the former can be made as given in Table 7.3. The mass transfer phenomenon is a well documented engineering field. Thus, books by Evans [3], Geiger and Poirier [5], Hagen [6], Gaskell [7] and Incropera and DeWitt [8], among many excellent sources, can be consulted on the current topic for laminar and turbulent conditions. In general, the mass transfer by convection for the case shown in Figure 7.17 may be further described by the Sherwood Number. Hence,

Table 7.3 Changes in dimensionless numbers and temperature[5]

Nusselt Number (N_u)	\Rightarrow	Sherwood Number (S_h)
Prandtl Number (P_r)	\Rightarrow	Schmidt Number (S_c)
Thermal Diffusivity (α)	\Rightarrow	Atomic Diffusivity (D)
Reynolds Number (R_e)	\Rightarrow	Reynolds Number (R_e)
Temperature (T)	\Rightarrow	Concentration (C_x)

$$S_h = \lambda_f (S_c)^\alpha (R_e)^\beta \quad (\text{Forced Convection}) \quad (7.75)$$

$$S_h = \lambda_n (S_c)^\gamma (R_e)^\mu \quad (\text{Natural Convection}) \quad (7.76)$$

where $\lambda_f, \lambda_n = \text{Constants}$
 $\alpha, \beta, \gamma, \mu = \text{Exponents}$

In addition, the Reynold, Schmidt, Rayleigh (R_a), and Grashof (G_r) numbers are empirically defined by

$$R_e = \frac{\text{Inertia Force}}{\text{Viscous Force}} = \frac{\rho v_x^2 / d}{\eta_v v_x / d^2} \quad (7.77)$$

$$R_e = \frac{\rho v_x d}{\eta_v} = \frac{v_x d}{K_v} \quad (7.78)$$

$$S_c = \frac{K_v}{D} = \frac{\eta_v}{\rho D} \quad (7.79)$$

$$R_a = G_r S_c \quad (7.80)$$

$$K_v = \frac{\eta_v}{\rho} \quad (7.81)$$

where $v_x = \text{Fluid flow velocity in the x-direction (cm/s)}$
 $d = \text{Characteristic length of a channel (cm)}$
 $K_v = \text{Kinematic viscosity (cm}^2/\text{s)}$
 $\eta_v = \text{Fluid viscosity (g/cm.s)}$
 $\rho = \text{Fluid density (g/cm}^3\text{)}$
 $D = \text{Diffusivity or diffusion coefficient (cm}^2/\text{s)}$

An electrowinning cell can be treated as an open channel (open top) with an equivalent diameter as the characteristic length, which depends on the geometry of the cross-sectional area. This diameter is needed for determining the Reynolds Number. In general, this diameter is also known as hydraulic diameter defined as

$$d = \frac{4A}{p} \quad (7.82)$$

where A is the cross-sectional area of the channel and p is the wetted perimeter of the channel that is in contact with the flowing fluid.

For square cross-sectional and rectangular cross-sectional areas, d becomes

$$d = \frac{4a^2}{3a} \quad (\text{Square}) \quad (7.83)$$

$$d = \frac{4ab}{2a + b} \quad (\text{Rectangular}) \quad (7.84)$$

where a = Height of the channel (cm)

b = Width of the channel

According to Twidwell [2], in most electrowinning cells $d = 2x$ where x is the distance between electrodes. In addition, the fluid velocity is defined as

$$v_x = \frac{F_r}{A} \quad (7.85)$$

Recall that F_r is the volume flow rate and it is defined in terms of mass flow rate and density

$$F_r = \frac{\dot{m}}{\rho} \quad (7.86)$$

If an electrochemical cell is treated as a pipe, then the conditions for the type of flow may be characterized by the Reynolds and Rayleigh Numbers as listed in Table 7.4 [6].

Table 7.4 Characterizing fluid flow by convection

Flow	Forced Flow	Natural Flow
Laminar	$Re \leq 2,300$	$Ra < 10^9$
Transient	$2,300 < Re < 10^4$	$Ra \approx 10^9$
Turbulent	$Re \geq 10^4$	$Ra > 10^9$

Physically, the Sherwood Number is defined as the ratio of convection to diffusion mass transfer through the concentration boundary layer at the cathode surface [2,5,7]. Thus, S_h can be derived by using eqs. (4.3) and (4.5)

$$S_h = \frac{i}{zFJ_x} \quad (7.87a)$$

$$S_h = \frac{i\delta}{zFD\Delta C} = \frac{i}{zFh\Delta C} \quad (7.87b)$$

where δ = Nernst diffusion layer (cm),

L = Cathode length or characteristic distance (cm)

$\Delta C = C_o - C_b$ = Change in concentration (mol/cm³),

h = Mass transfer coefficient (cm/s).

Considering diffusion of a specie j through the diffusion layer of thickness δ , the mass flux according to Fick's modified first law of diffusion and that for convection are defined by the following expression

$$J_{x,m} = \frac{D(\rho_s - \rho_\infty)}{x} \quad (7.87c)$$

$$J_{c,m} = h(\rho_s - \rho_\infty) \quad (7.87d)$$

The local Sherwood Number for $0 < x \leq \delta$ is [7]

$$S_h = \frac{J_{c,m}}{J_{x,m}} = \frac{hx}{D} \quad (7.87e)$$

In addition, the forced convection mass transfer coefficient for transfer of the specie j to or from the electrode interface can also be defined by [5]

$$h = \frac{J_x}{\Delta C} = \frac{D}{\delta} \quad (7.88)$$

Assuming mass transfer by laminar electrolyte flow in electrodeposition between two relatively large plate electrodes and combining eqs. (7.87e) and (7.88), and letting $x = d$ be the characteristic distance between the electrodes yields a simplified Sherwood Number [2]

$$S_h = \frac{d}{\delta} \quad (7.88a)$$

where $d = 2w$ and w is the channel width in the order of 3 cm [2].

In addition, the Sherwood Number S_h can be semi-empirically defined for natural (free) and forced convection for the case shown in Figure 7.17.

A) From Twidwell's work [2].

1) Natural convection flow:

$$S_h = \frac{2}{3} (S_c G_r)^{1/4} \quad (\text{Laminar}) \quad (7.89)$$

$$S_h = \frac{13}{42} (S_c G_r)^{7/25} \quad (\text{Turbulent}) \quad (7.90)$$

2) Forced convection flow:

$$S_h = \frac{9}{5} \left[\frac{d}{L} (S_c R_e) \right]^{1/3} \quad (\text{Laminar}) \quad (7.91)$$

$$S_h = \frac{1}{65} (S_c)^{1/3} (R_e)^{1/2} \quad (\text{Turbulent}) \quad (7.92)$$

where d is defined in eq. (7.88a) and L is the cathode length [2]

B) From Geiger and Poirier [5] and Gaskell [7] books.

1) Natural convection flow:

$$S_h = \frac{3}{2\pi} \left(\frac{S_c^2 G_r}{S_c + 5/9} \right)^{1/4} \quad (\text{Laminar}) \quad (7.93)$$

2) Forced convection flow:

$$S_h = \frac{2}{3} (S_c)^{1/3} (R_e)^{1/2} \quad (7.94)$$

where $10^2 \leq S_c \leq 10^3$ for most fluids.

Particularly, assume that the electrochemical deposition (Figure 7.17) is under laminar flow. For this practical condition, the Sherwood Number can be redefined by inserting eqs. (7.78) and (7.79) into (7.91). Hence,

$$S_h = \frac{9}{5} \left(\frac{v_x d^2}{LD} \right)^{1/3} \quad (\text{Forced laminar flow}) \quad (7.95)$$

Combining eqs. (7.87) and (7.95) yields an expression for predicting the current density as

$$i = \frac{9}{5} zF (C_x - C_s) \left(\frac{v_x d^2 D^2}{L^4} \right)^{1/3} \quad (\text{Forced laminar flow}) \quad (7.96)$$

If $C_s = 0$ at $x = 0$, then i is the limiting current density [2]. However, eq. (7.96) is more conveniently used if $C_x = C_o$ at $x = \infty$ from the cathode surface since the bulk concentration is normally known prior to operating an electrolytic cell. Hence, the current density in this case becomes the limiting current density as defined by

$$i_L = \frac{9}{5} zFC_o \left(\frac{v_x d^2 D^2}{L^4} \right)^{1/3} \quad (\text{Forced laminar flow}) \quad (7.97)$$

This limiting current density arises due to a high rate of metal reduction at the cathode surface since ion depletion occurs in the bulk solution unless the electrochemical cell is replenished with fresh solution for a continuous operation. The application of eq. (7.97) is essential for determining the fluid velocity when the limiting current density is known.

Example 7.7 A hypothetical copper electrowinning cell operates at 35°C and 101 kPa under forced laminar flow. If the electrolyte/cell has the following conditions

$$\begin{aligned}
 C_o &= 7.10 \times 10^{-4} \text{ mol/cm}^3 \text{ (concentration of } \text{Cu}^{+2} \text{ ions)} \\
 x &= L = 100 \text{ cm (cathode length)} \\
 d &= 5 \text{ cm (cell equivalent diameter)} \\
 D &= 10^{-5} \text{ cm}^2/\text{s (diffusivity of } \text{Cu}^{+2} \text{ ions)} \\
 K_v &= 0.80 \text{ cm}^2/\text{s (kinematic viscosity)} \\
 v_x &= 0.50 \text{ cm/s (electrolyte flow velocity)} \\
 \rho_x &= 5 \text{ ohm.cm (resistivity for } \text{Cu}^{+2} \text{ in solution)} \\
 \rho &= 8.96 \text{ g/cm}^3 \text{ (density)}
 \end{aligned}$$

calculate a) the Sherwood Number, b) the mass transfer coefficient, c) the molar flux, d) the current density, e) the rate of electrolytic deposition (R^*), and f) Is it practical to recover Cu^{+2} ions if the electrolyte flow velocity is at its transitional flow condition in a conventional electrowinning cell?

Solution:

a) From eq. (7.95),

$$S_h = (9/5) [v_x d^2 / (LD)]^{1/3}$$

$$S_h = (9/5) \left\{ \left[(0.50 \text{ cm/s}) (5 \text{ cm})^2 \right] / \left[(100 \text{ cm}) (10^{-5} \text{ cm}^2/\text{s}) \right] \right\}^{1/3}$$

$$S_h = 41.77$$

b) From eq. (7.87c),

$$h = DS_h/x = (10^{-5} \text{ cm}^2/\text{s}) (41.77) / (100 \text{ cm})$$

$$h = 4.18 \times 10^{-6} \text{ cm/s}$$

c) From eq. (7.88), the convective molar mass is

$$J_x = h\Delta C = hC_o = (4.18 \times 10^{-6} \text{ cm/s}) (7.10 \times 10^{-4} \text{ mol/cm}^3)$$

$$J_x = 2.97 \times 10^{-9} \text{ mol/cm}^2 \cdot \text{s}$$

d) From eq. (7.87a),

$$i = zFJ_x S_h = (2) (96,500 \text{ A.s/mol}) (2.97 \times 10^{-9} \text{ mol/cm}^2 \cdot \text{s}) (41.77)$$

$$i = 2.39 \times 10^{-2} \text{ A/cm}^2 = 239 \text{ A/m}^2$$

which is within the practical potential range in electrowinning cells.

e) From eq. (3.13a),

$$R^* = iA_w/zF = (2.39 \times 10^{-2} \text{ A/cm}^2) (63.54 \text{ g/mol}) / (2) (96,500 \text{ A.s/mol})$$

$$R^* = 7.87 \text{ } \mu\text{g/cm}^2 \cdot \text{s}$$

f) Using $Re = 2,300$ from Table 7.4 as the transitional number, eq. (7.78) gives the transitional fluid velocity

$$v_x = Re K_v / d$$

$$v_x = (2,300) (0.80 \text{ cm}^2/\text{s}) / (5 \text{ cm}) = 368 \text{ cm/s (too high)}$$

Using this transitional fluid velocity calculate the Sherwood Number, the mass transfer coefficient, the molar flux, and the current density. Hence,

$$S_h = (9/5) [v_x d^2 / (LD)]^{1/3}$$

$$S_h = (9/5) \left\{ [(368 \text{ cm/s}) (5 \text{ cm})^2] / [(100 \text{ cm}) (10^{-5} \text{ cm}^2/\text{s})] \right\}^{1/3}$$

$$S_h = 377.17$$

$$h = DS_h/x = (10^{-5} \text{ cm}^2/\text{s}) (377.17) / (100 \text{ cm})$$

$$h = (10^{-5}) (377.17) / (100) = 3.7717 \times 10^{-5}$$

$$h = 3.77 \times 10^{-5} \text{ cm/s}$$

$$J_x = h\Delta C = hC_o = (3.77 \times 10^{-5} \text{ cm/s}) (7.10 \times 10^{-4} \text{ mol/cm}^3)$$

$$J_x = (3.77 \times 10^{-5}) (7.10 \times 10^{-4}) = 2.6767 \times 10^{-8}$$

$$J_x = 2.68 \times 10^{-8} \text{ mol/cm}^2 \cdot \text{s}$$

$$i = zFJ_x S_h = (2) (96,500 \text{ A}\cdot\text{s/mol}) (2.68 \times 10^{-8} \text{ mol/cm}^2 \cdot \text{s}) (377.17)$$

$$i = 1.95 \text{ A/cm}^2 = 19,500 \text{ A/m}^2$$

Therefore, $i = 19,500 \text{ A/m}^2$ is too high and it is not a practical current density in conventional electrowinning cells containing planar electrodes. This implies that an electrolyte motion at the chosen transition forced laminar flow, Reynolds Number of $Re = 2,300$, is not practical.

Example 7.8 A hypothetical chemical vapor deposition of a gas is carried out at 600°C and 101 kPa on a metal substrate. If the gas has the following properties

$$D = 0.40 \text{ cm}^2/\text{s} (\text{diffusivity})$$

$$\rho = 3 \times 10^{-3} \text{ g/cm}^3 (\text{density})$$

$$\eta_v = 2.5 \times 10^{-4} \text{ g/cm}\cdot\text{s} (\text{viscosity})$$

$$v_x = 97 \text{ cm/s} (\text{gas flow velocity})$$

$$A_w = 95 \text{ g/mol} (\text{molecular weight})$$

at $x = 100 \text{ mm}$ from the origin of the gas stream to the metal substrate surface. Determine a) the Sherwood Number, b) the mass transfer coefficient, c) the molar flux and d) the rate of vapor deposition (R^*). Use a change of concentration equals to $2 \times 10^{-4} \text{ mol/cm}^3$ of the gas.

Solution:

a) From eqs. (7.78) and (7.79),

$$R_e = \rho x v_x / \eta_v = (3 \times 10^{-3} \text{ g/cm}^3) (10 \text{ cm}) (97 \text{ cm/s}) / (2.5 \times 10^{-4} \text{ g/cm.s})$$

$$R_e = 11,640$$

$$S_c = \eta_v / D \rho = (2.5 \times 10^{-4} \text{ g/cm.s}) / [(0.40 \text{ cm}^2/\text{s}) (3 \times 10^{-3} \text{ g/cm}^3)]$$

$$S_c = 0.21$$

From eq. (7.94),

$$S_h = (2/3) (S_c)^{1/3} (R_e)^{1/2} = (2/3) (0.21)^{1/3} (11640)^{1/2}$$

$$S_h = 42.75$$

b) From eq. (7.87),

$$h = D S_h / x = (0.40 \text{ cm}^2/\text{s}) (42.75) / (10 \text{ cm}) = 1.71 \text{ cm/s}$$

c) From eq. (7.87)

$$J = h \Delta C = (1.71 \text{ cm/s}) (2 \times 10^{-4} \text{ mol/cm}^3) = 3.42 \times 10^{-4} \text{ mol/cm}^3$$

d) From eqs. (3.13b) and (4.8),

$$R^* = J A_w / \rho = (3.42 \times 10^{-4} \text{ mol/cm}^3) (95 \text{ g/mol}) / (3 \times 10^{-3} \text{ g/cm}^3)$$

$$R^* = 10.83 \text{ cm/s} = 30 \text{ } \mu\text{m/s}$$

This vapor deposition seems adequate for most practical applications.

Moreover, mass transfer by convection is a well documented topic in the literature in which a hydrodynamic viscous convective layer develops due to fluid flow. This convective layer is known as Prandtl boundary layer, which depends on the fluid velocity. According to Erdey-Gruz [66] and Probstein [67] among other excellent authors, the convective layer is defined as

$$\delta_u = x R_e^{-1/2} = \sqrt{\frac{x K_v}{v_o}} \quad (7.98)$$

where x = Distance from the electrode surface (cm)

v_o = Fluid velocity in the bulk of solution (cm/s)

The correlation of the diffusion and convective layers is graphically shown in Figure 7.17 and mathematically defined as [5,7,66,68]

$$\delta = \delta_u \left(\frac{D}{K_v} \right)^{1/3} \quad (7.99)$$

The profile of the layer ratio is shown in Figure 7.18.

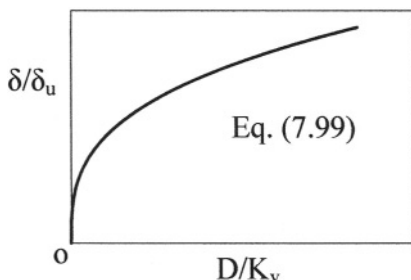


Figure 7.18 Layer ratio profile.

Substituting eq. (7.98) into (7.99) yields the diffusion layer dependent on the fluid velocity

$$\delta = D^{1/3} K_v^{1/6} x^{1/2} v_o^{-1/2} \quad (7.100)$$

Inserting eq. (7.100) into (7.87) gives the current density for $x > 0$

$$i = zF(C_o - C_s) D^{2/3} K_v^{-1/6} \left(\frac{v_o}{x}\right)^{1/2} \quad (7.101)$$

$$i_L = zFC_o D^{2/3} K_v^{-1/6} \left(\frac{v_o}{x}\right)^{1/2} \quad (7.102)$$

7.9.2 ROTATING-DISK ELECTRODE

In characterizing the effects of solution on corrosion, a rotating-disk electrode is convenient for such an assessment since the angular velocity (ω) must influence the limiting current density. For forced convection under laminar flow, the Sherwood Number is applicable in the following form [9,62-63]

$$S_h = \lambda_f (S_c)^{1/3} (R_e)^{1/2} \quad (7.103)$$

where

$$R_e = \frac{r^2 \omega}{K_v} < 10^5 \quad \text{For laminar flow} \quad (7.104)$$

$$\lambda_f = 0.62 \quad \text{(Factor)} \quad (7.105)$$

Substituting eqs. (7.79), (7.104) and (7.105) into (7.103) and inserting the resultant expression into (7.87) along with $\delta = r$ yields the current density, eq. (4.90), for kinetic studies

$$i = 0.62zF(C_o - C_s) D^{2/3} K_v^{-1/6} \sqrt{\omega} \quad (7.106)$$

where r = Disk radius

$\omega = v_x/d = 2\pi N$ = Angular velocity (*rad/s*)

N = Revolutions per second

d = Disk diameter

If $C_s = 0$ at the electrode surface, eq. (7.106) becomes Levich limiting current density [9]

$$i_L = 0.62zFC_o D^{2/3} K_v^{-1/6} \sqrt{\omega} \quad (7.107)$$

This expression, eq. (7.106) or (7.107), takes into account the effect of fluid motion on the diffusion layer δ , which is an adherent thin film on the electrode surface. Therefore, diffusion coupled with convection contributes to the total mass transfer process to or from the electrode surface and it is known as convective diffusion in which δ is considered immobile at the electrode surface [66]. Recall that the limiting thickness of the diffusion layer is illustrated in Figure 4.5. Also, Levich equation describes the effect of rotation rate, concentration, kinetic viscosity on the current at a rotating-disk electrode.

In addition, Levich [9] derived an expression for the diffusion layer as a function angular velocity or rotating speed as

$$\delta = 1.62 D^{1/3} K_v^{1/6} \sqrt{\omega} \quad (7.108)$$

$$\delta = \left(\frac{\pi}{4}\right)^2 D^{1/3} K_v^{1/6} \sqrt{\omega} \quad (7.109)$$

Other hydrodynamic cases for corrosion studies can be found elsewhere [10]. On the other hand, for a continuous metal removal from solution in electrowinning, rotating cylinders and disks are used as cathodes (Figure 7.6). The classical rotating-disk cathode is known as Weber's disk [25-26] having a diameter of $2a$. The corresponding differential equation in cylindrical coordinates is free of the diffusivity and it is given by

$$\frac{\partial C}{\partial r^2} + \frac{1}{r} \frac{\partial C}{\partial r} + \frac{\partial^2 C}{\partial r^2} = 0 \quad (7.110)$$

Using the following boundary conditions

$$C = 0 \quad @ \quad x = 0, \quad r \leq a \quad (7.111)$$

$$\frac{\partial C}{\partial r} = 0 \quad @ \quad x = 0, \quad r > a \quad (7.112)$$

$$C = C_o \quad @ \quad x = \infty, \quad r \geq 0 \quad (7.113)$$

$$C = C_o \quad @ \quad x \geq 0, \quad r = \infty \quad (7.114)$$

the solution of eq. (7.110) using the Modified Bessel function is [25]

$$\frac{C}{C_o} = 1 - \frac{2}{\pi} \tan^{-1} \left\{ \left(\frac{a^2}{2} \left[+ \left([r^2 + x^2 - a^2]^2 + 4a^2r^2 \right)^{1/2} \right] \right)^{-1/2} \right\} \quad (7.115)$$

where C_o is the concentration in the bulk of solution.

The concentration gradient at $x = 0$ is determined from eq. (7.115) as

$$\frac{\partial C}{\partial x} \Big|_{x=0} = \frac{2C_o}{\pi} (a^2 - r^2)^{-1/2} \quad (0 \leq r \leq a) \quad (7.116)$$

Moreover, the concentration ratio given by eq. (7.115) can be simplified very significantly by setting a constraint on the disk radius. Thus, if $0 < r < a$ the concentration ratio is approximated as [25]

$$\frac{C}{C_o} = \begin{cases} \pi \left[1 + (2/a) \sqrt{Dt/(2\pi)} \right] & \text{For } t \rightarrow 0 \\ Dt/(\pi a^2) & \text{For } t \rightarrow \infty \end{cases} \quad (7.117)$$

This simplified concentration ratio is now very easier to manipulate. For instance, the concentration rate can now be determined as

$$\frac{\partial C}{\partial t} = C_o \begin{cases} (\pi/a) \sqrt{D/(2\pi t)} & \text{For } t \rightarrow 0 \\ D/(\pi a^2) & \text{For } t \rightarrow \infty \end{cases} \quad (7.118)$$

7.10 LIMITING CURRENT DENSITY

The cathodic overpotential equation derived in Chapter 4 for concentration polarization is very useful in electrowinning operation. In analyzing the electrodeposition of metal M_1^{+z} cations from aqueous solution, the cathodic overpotential and current density for stationary and rotating-disk electrodes are related by

$$\eta_c = \frac{RT}{zF} \ln \left(1 - \frac{i_c}{i_L} \right) \quad \text{For } i_c < i_L \quad (7.119)$$

For an electrode containing no metallic impurities under concentration polarization, the applied current density must be a fraction of the limiting current density; that is, $i_c < i_L$ for optimizing the electrolytic deposition of M_1^{+z} cations on the cathode surface electrodes. This current density constraint is the basis for deriving eq. (7.119), which dictates that $\eta_c \rightarrow -\infty$ when $i_c \rightarrow i_L$ since $\ln(1 - i_c/i_L) \rightarrow -\infty$. Therefore, if $i_c < i_L$ yields $\eta_c \gg -\infty$ and a regular and uniform (smooth) layer of M_1 atoms is ideally deposited at a relatively high current efficiency ϵ as predicted by eq. (7.21).

According to eq. (7.119) the optimum overpotential depends on both i_c and T ; $\eta_c = f(T, i_c)$. It is known that i_L increases with increasing temperature.

This, then, requires that $\eta_c = f(T, i_c, i_L)$, and the optimization scheme is more complex. However, fixing i_L at a temperature T leaves eq. (7.119) be i_c dependent only. On the other hand, if $i_c \geq i_L$ an irregular and porous (powdery) metal deposition and anode passivity result [2].

Since i_L is usually known, a current density factor can be defined as

$$\lambda = \frac{i_c}{i_L} \quad (7.120)$$

Thus, eq. (7.119) becomes

$$\eta_c = \frac{RT}{zF} \ln(1 - \lambda) < 0 \quad \text{For } 0 < \lambda < 1 \quad (7.121)$$

which dictates that $\eta_c \rightarrow 0$ as $\lambda \rightarrow 0$ and electrochemical equilibrium is nearly achieved and polarization is then nearly lost under these conditions. Therefore, the cathodic overpotential range is $-\infty < \eta_c < 0$ for electrodeposition of metal M_1^{+z} cations. Thus, η_c is now dependent on two variables, instead of three. Figure 7.19 shows the theoretical trend for η_c as per eq. (7.121). Notice that the drawn straight line from 0 to P serves as a crude approximation scheme for predicting $\lambda = 0.50$, which gives $i_c = 0.50i_L$. This is remarkably in agreement with most practical electrowinning operations [2]. Using $\lambda = 0.50$ in eq. (7.121) yields

$$\eta_c|_{\lambda=0.50} = -\frac{0.69zF}{RT} \quad (7.122)$$

$$\frac{d}{d\lambda} \left(\frac{zF\eta_c}{RT} \right)_{\lambda=0.50} = \frac{1}{\lambda - 1} = -0.50 \quad (7.123)$$

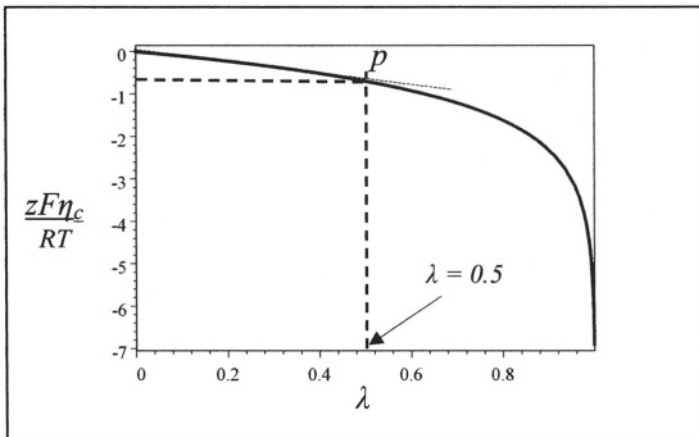


Figure 7.19 Theoretical trend of the cathodic overpotential showing the idealized point P .

Furthermore, if an electrolyte contains M_2^{+z} cations as impurities, the electrodeposition of the principal cation M_1^{+z} can be achieved, provided that the cathodic current density is defined by the following inequality

$$i_L(M_2^{+z}) < i_c < i_L(M_1^{+z}) \tag{7.124}$$

otherwise, M_1^{+z} and traces of other impurities will codeposit [2,11]. There can be a situation in which codeposition of impurities is required for obtaining an alloyed electrode layer [12], but this is an unusual case in electroplating of pure metals from aqueous solutions. If codeposition occurs, electrorefining is used for purifying or refining the electrode metal M_1 . The above current density inequality, eq. (7.124), is schematically shown in Figure 7.20 for the principal metal M_1 and impurity metal M_2 .

If codeposition is inevitable, a low concentration of impurities must be maintained in solution so that the mass transfer of the impurity M_2^{+z} is minimal and that of M_1^{+z} is maximal since the diffusivity $D_{M_1^{+z}}$ will increase. Also, increasing the electrolyte temperature ($T < 70^\circ\text{C}$) reduces its viscosity, and therefore, increases the mass transfer of M_1^{+z} cations. For instance, the application of eq. (7.124) in electroplating copper provides the constraints of the applied current density for controlling the mass transfer of copper and impurity iron. Hence,

$$i_{L,Fe} < i_c < i_{L,Cu} \tag{7.125}$$

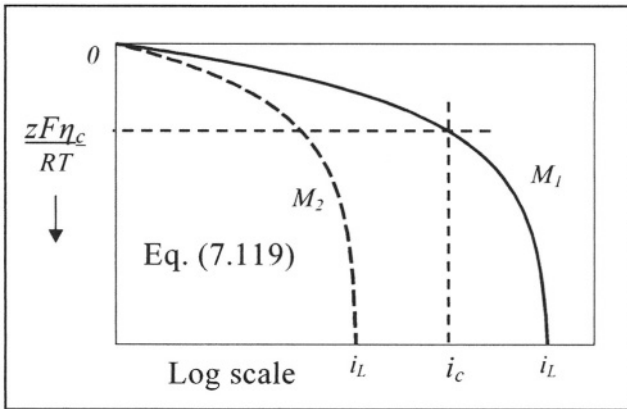


Figure 7.20 Schematic polarization curves showing limiting current densities.

Apparently, very little $Fe^{+3} + e^- \rightarrow Fe^{+2}$ mass transfer occurs [2]. In addition, the limiting current density due to diffusion mass transfer can be determined using eq. (4.29) as

$$i_L = \frac{zFDC_o}{\delta} \tag{7.126}$$

If mass transfer is aided by convection, which is the case for most practical purposes, then i_L can be predicted from eq. (7.96). However, both diffusion, migration and convection mass transfer influence the electrolytic deposition in electrowinning, electrorefining and electroplating. In this case, the total molar flux is predicted by eq. (4.2) and the current density by eq. (4.9).

In the above expression, eq. (7.126), the diffusivity is the only temperature dependent variable which can be assumed to obey the Arrhenius equation. Thus,

$$D = D_o \exp\left(-\frac{Q}{RT}\right) \quad (7.127)$$

where $D_o = \text{Constant } (cm^2/s)$

$Q = \text{Activation energy } (J/mol)$

Consequently, the limiting current density becomes temperature dependent through the diffusion coefficient. In this case, eq. (7.126) becomes

$$i_L = \frac{zFD_oC_o}{\delta} \exp\left(-\frac{Q}{RT}\right) \quad (7.128)$$

Hence,

$$\frac{di_L}{dT} = \frac{zFC_o}{\delta} \frac{dD}{dT} \quad (7.129)$$

$$\frac{di_L}{dT} = \frac{i_L}{D} \frac{dD}{dT} \quad (7.130)$$

This expression clearly shows the temperature dependence of the limiting current density in diffusion control processes [66].

Assume a hypothetical case in which the limiting current density, eq. (7.128), depends on the temperature only. Thus, Figure 7.21. shows the hypothetical limiting current density profile for increasing concentration of a type of cations in solution.

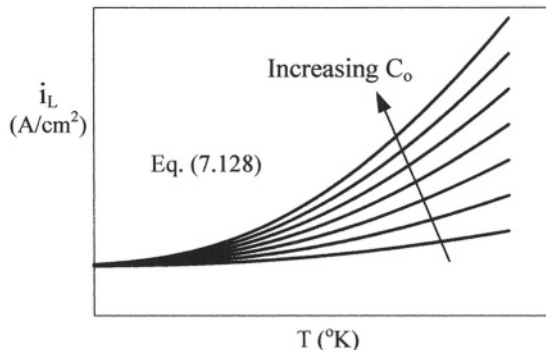


Figure 7.21 Limiting current density as a function of temperature.

In addition, eq. (7.119) is plotted in Figure 7.22 for showing the effects of temperature on both overpotential and limiting current density of a hypothetical electrochemical system.

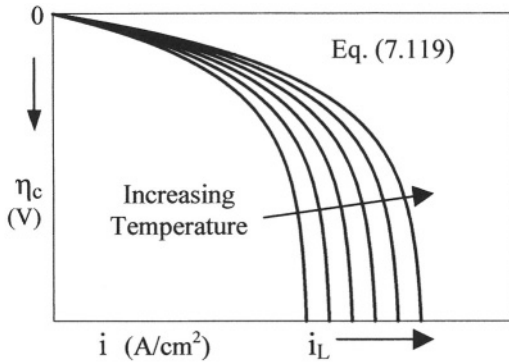


Figure 7.22 Schematic cathodic overpotential profile showing increasing limiting current density with increasing temperature.

7.11 SUMMARY

The beneficial application of electrochemical principles is to electrolytically recover and refine metals from aqueous solutions. Thus, the engineering science that deals with metallic ions is electrometallurgy, which is subdivided into electrowinning for recovering or winning metallic cations, and electrorefining for refining or purifying electrowon metals containing codeposit. impurities, and electroplating for applying metal coats onto another metal or substrate for corrosion protection or decorative purposes. The distinctive difference between a galvanic cell and an electrolytic cell is that the former discharges electricity, such as a flashlight, and latter is externally charged in order to force a reduction reaction to occur, provided that the externally applied potential (voltage) is greater than the cell electrode. This is accomplished if the starter sheet cathodes are connected to the negative terminal of the power supply. Apparently, those metals having potentials above the hydrogen potential in Table 2.1 are most easily electrolytically deposited or reduced from their ionic state in solution and those that listed below are more difficult to reduce. For instance, copper ions are easily reduced since copper standard potential is positive. On the other hand, aluminum and magnesium cannot be reduced from aqueous solutions due to hydrogen evolution at the cathode surface. Therefore, metals like *Al*, *Mg*, *Ti*, *Li*, *Na*, and the like are recovered using molten salt electrolysis at high temperatures.

Electroplating and electrowinning require an external potential through the electrodes for electrolytic deposition. Thus, electrical energy is supplied through an external circuit which is converted to chemical energy. This energy conversion causes reduction reactions to occur on a cathode surface (negative terminal). This implies that positively charged ions (cations) are attracted by the negatively charged cathode surface and positively charged anode attracts the negatively charged ions (anions). Therefore, the anode oxidizes by losing electrons and the cathode reduces by gaining these electrons. This series of electrochemical events is known as electrolysis or electrolytic deposition, which is simply an electron-exchange phenomena between half-cell reactions.

Since deviation from electrochemical equilibrium requires an excess potential (voltage) over the theoretical quantity, this process is known as polarization due to the imposed overpotential, which is needed to force an electrolytic deposition of cations. Thus, an electrochemical cell must be polarized for electrodeposition to occur. This polarization process is maintained due to depletion of cations in the vicinity of the cathode surface. However, the overpotential for polarization should not be too high; otherwise, hydrogen evolution emerges and hydrogen absorption (pickup) by the metal cathode may result during electrodeposition causing a decrease in current efficiency and an increase in energy consumption. In addition, if hydrogen evolution transpire in electroplating, hydrogen absorption occurs as atomic hydrogen leading to an undesirable form of corrosion known as Hydrogen Embrittlement (*HE*), which causes cracking or internal blistering due to a buildup of hydrogen pressure in the electroplated metal. Therefore, *HE* arises due to the lack of plastic slip of the metal being electroplated.

7.12 PROBLEMS

7.1 Copper cations are reduced on a cathode for 8 *hours* at a current of 10 *amps.* and 25°C. Calculate a) the theoretical weight of copper deposited on the cathode and b) the number of coulombs of electricity in this electrodeposition process. Data: $A_{w,Cu} = 63.55 \text{ g/mol}$ and $F = 96,500 \text{ C}$. [Solution: a) $W = 94.83 \text{ g}$ and b) $Q = 288,000 \text{ C}$ ($= A.s$)].

7.2 An electrochemical cell operates at 6 A, 25°C and 85% current efficiency in order to electrolytically deposit copper ions (Cu^{+2}) from a leaching solution in a 8 – *hour* shift. Calculate a) the amount of electrolytically deposited Cu and b) the thickness of the deposit layer of copper. Data: $A_g = 100 \text{ cm}^2$ (total cathode surface area), $A_{w,Cu} = 63.55 \text{ g/mol}$, $\rho = 8.96 \text{ g/cm}^3$ and $F = 96,500 \text{ C/mol}$. [Solution: a) $W = 94.83 \text{ g}$ and b) $x = 0.54 \text{ mm}$].

7.3 It is desired to electroplate chromium (Cr) onto a ferritic-martensitic carbon steel automobile bumper for an attractive appearance and corrosion resistance. An electroplating cell is operated at $I = 6.68 \text{ A}$ and 25°C. The

Cr^{+3} cations are reduced on the bumper (cathode) to form a thin film of $1.5 \mu\text{m}$ thick. How long will it take to produce a $1.5 \mu\text{m}$ thick electroplated chromium film on the bumper if the total surface area is 100 cm^2 and $\epsilon = 60\%$? [Solution: $t = 100 \text{ sec.}$].

7.4 An electrowinning cell contains $2 \times 10^{-4} \text{ mol/cm}^3$ of Cu^{+2} ions and operates for 10 minutes at 40°C and 1 atm. . Assume an ionic copper diffusivity equals to $2.34 \times 10^{-5} \text{ cm}^2/\text{s}$. Calculate the current density due to diffusion mass transfer. Compare your result with a typical industrial current density value of 200 A/m^2 . Explain any discrepancy. [Solution: $i = 43 \text{ A/m}^2$].

7.5 Calculate the amount of silver that can be electroplated in an electrochemical cell containing Ag^+ ions and operates at 7 A , 25°C and 101 kPa for 10 minutes. Assume a current efficiency of 95% . [Solution: $W = 4.46 \text{ g}$].

7.6 What are the differences between galvanic and electrolytic cells? Recall that both are electrochemical cells.

7.7 Consider the bipolar electrode for electrorefining metal M . Thus, the rate of formation (reduction) and dissolution (oxidation) are treated as steady-state quantities. Despite that the initial formation of a thin film at the cathode face and dissolution rates are controlled by reactions at the electrode-electrolyte interfaces, assume a steady-state diffusion mechanism. Derive expressions for the weight gain at the cathode side and the weight loss at the anode side.

7.8 An electrowinning cell contains 75 g/l of Cu^{+2} ions at 35°C . Calculate a) the applied potential and b) the actual production rate in Kg/h if the current efficiency is 85% and [Solution: a) 2 volts and b) 16.12 Kg/h]

d	Characteristic distance	$= 12 \text{ cm}$.
$L = x$	Cathode height	$= 100 \text{ cm}$.
w	Cathode width	$= 80 \text{ cm}$.
N	Number of cathodes	$= 50$.
K_v	Kinematic viscosity	$= 0.80 \text{ cm}^2/\text{s}$.
D	diffusivity	$= 1.24 \times 10^{-5} \text{ cm}^2/\text{s}$.
v_x	Flow velocity	$= 46.90 \text{ cm/s}$.
P	Power	$= 32 \text{ kW}$.

7.9 a) Determine the amount of copper that can be electrowon in a 8-hour shift using the actual production rate of problem 7.8. Assume a steady-state production rate and a finite current density, b) Plot W vs. t if $0 \text{ h} \leq t \leq 8 \text{ h}$. What does the slope of this plot mean?

7.10 A steel plate is Ni-plated for corrosion protection, but its appearance is not so appealing. Therefore, a chromium electroplating process is carried out for

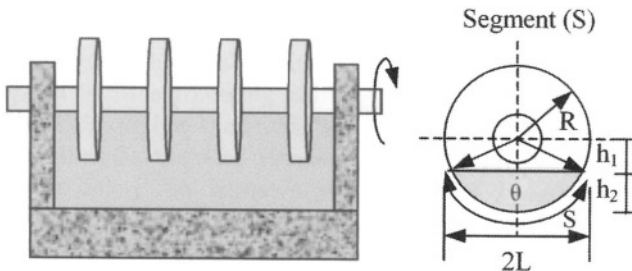
decorative purposes. Eventually, 0.25 g of Cr^{+6} cations are electroplated for a period of 15 minutes at 8 amps. If the density and atomic weight of chromium are 7.19 g/cm^3 and 52 g/mol , respectively, calculate a) the thickness of the electroplated film of chromium and b) the deposition rate. Data: $A_c = 100 \text{ cm}^2$ (cathode area). [Solution: a) $3.48 \text{ }\mu\text{m}$, b) 1 g/h , c) 39%].

7.11 It is desired to produce a $20 \text{ }\mu\text{m}$ thick film of chromium on a Ni-plated steel part, which has a surface area of 65 cm^2 . This can be accomplished by setting up an electroplating cell to operate at 7 amps and current efficiency of 70%. The density and atomic weight of chromium are 7.19 g/cm^3 and 52 g/mol , respectively. Calculate a) the amount of Cr being plated and b) the time it takes to plate the $20 \text{ }\mu\text{m}$ thick film of chromium from a solution containing Cr^{+6} cations at 30°C . [Solution: a) 0.94 g and b) 35.40 min].

7.12 An electrolyte containing Pb^{+2} ions at 35°C is used in an electrowinning cell. The electrolyte is under steady laminar force convection. Use the data given below to determine a) the applied current and b) the lead production rate. [Solution: a) $I = 4.91 \text{ kA}$ and b) 16.15 Kg/h].

C_b	Bulk concentration	= 75 g/l
D	diffusivity	= $1.24 \times 10^{-5} \text{ cm}^2/\text{s}$
$L = x$	Cathode length	= 100 cm
S_c	Schmidt Number	= 64, 516.13
R_e	Reynolds Number	= 703.50
A_s	Total cathode area	= 800, 000 cm^2
ϵ	Current efficiency	= 85%

7.13 A hypothetical rotating-disk cell is shown below for electrowinning copper cations from a solution containing $C_o = 65 \text{ g/l}$ at 40°C and 101 kPa . Assume that the diffusivity and the electrolyte kinematic viscosity are $10^{-5} \text{ cm}^2/\text{s}$ and $0.60 \text{ cm}^2/\text{s}$, respectively. Each disk has a radius of 50 cm, a width of 6 cm, and only a 160° segment is immersed in the electrolyte. Assume a cell current efficiency range of $0.50 \leq \epsilon \leq 1$.

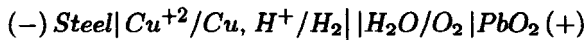


Theoretically, analyze the effect of a) the angular velocity ω on the current density and b) the angular velocity (ω) and the current density (ϵ) on the production rate of metal powder, and c) the potential (E) and the current density (ϵ) on the energy consumption γ .

7.14 Use the hypothetical rotated disk voltammetry data given in the table below for determining the diffusivity D of a metal cation M^{+2} in solution at room temperature. [Solution: $D = 3.97 \times 10^{-5} \text{ cm}^2/\text{s}$].

ω (1/sec)	100	225	400	625	900	1,225
$\omega^{1/2}$ ($\text{s}^{1/2}$)	10	15	20	25	30	35
i (mA/cm^2)	4.81	7.22	9.58	12.10	14.38	16.80
$C_o = 2.21 \times 10^{-6} \text{ mol}/\text{cm}^3$						
$K_v = 0.056 \text{ cm}^2/\text{s}$						
$z = 2$						

7.15 It is desired to produce copper according to the electrolytic cell diagram

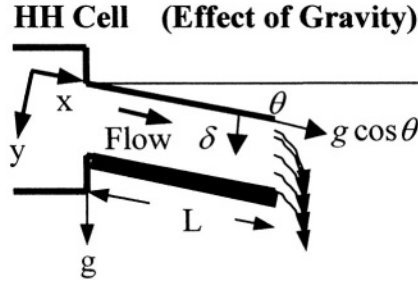


for 24 hours at which time the cathodes are mechanically stripped (removed). Copper is reduced from an aqueous copper sulfate (CuSO_4) and sulfuric acid (H_2SO_4) solution at 35°C . The anodes operate at 100% current efficiency with respect to oxygen evolution and that for the cathodes is $\epsilon = 90\%$ due to hydrogen evolution. These type of electrodes are connected in parallel within 100 tanks that operate at 2.4 volts each and the electrodes have an specific submerged area A_e . Use the following relevant data to perform some calculations sited below.

$P = 7.2 \text{ MW}$	$A_w = 63.54 \text{ g/mol}$
$E = 2.4 \text{ V}$	$D_{\text{Cu}^{+2}} = 1.24 \times 10^{-5} \text{ cm}^2/\text{s}$
$N_T = 100 \text{ Tanks}$	$K_v = 0.80 \text{ cm}^2/\text{s}$
$N_a = 3,000 \text{ Anodes}$	$v_x = 0.312 \text{ cm/s}$
$N_c = 2,900 \text{ Cathodes}$	$d = 6 \text{ cm}$ (electrode distance)
$A_e = 0.80 \text{ m}^2$	$P_e = 0.30 \text{ \$/Kg}$

a) Write down all the reactions and the standard half-cell potential involved in this electrowinning process. What should the applied potential be? b) Calculate the total current and current density, c) calculate the bulk concentration in g/l per tank. The Sherwood number ($S_h < 100$) and the Reynolds number ($Re = 2,300$) will assure force laminar flow and d) calculate the total gross income (GI) for a 24-hour run if the cost of energy is $C_{\text{energy}} = 0.10 \text{ \$/kW.h}$ and the market price is $C_{\text{market}} = \$0.70/\text{Kg}$ (sales). [Solution: b) $i_c = 0.1293 \text{ A}/\text{cm}^2$, c) $C_b = 75 \text{ g/l}$, and d) $GI = \$37,039.29$].

7.16 A Hall-Heroult (HH) cell is used to produce molten aluminum containing hydrogen. The hydrogen content can be removed by allowing a thin film of molten aluminum flow down on an inclined plane during pouring in vacuum. The incline plane is shown below and it is in the L - w - δ space, where δ is the film thickness and w is the width.



The weight-induced and gravity-induced free fluid flow occurs in the x -direction. Using Newton's law of viscosity yields the force acting on the fluid in the direction of the flow, together with the moment balance. Thus, this phenomenon is described by an ordinary differential equation.

$$\eta_v \frac{d^2 v_x}{dy^2} = -\rho g \cos(\theta) \quad \text{with BC's} \quad \left\{ \begin{array}{l} v_x = 0 \quad @ \quad y = \delta \\ v_x > 0 \quad @ \quad y > 0 \end{array} \right\}$$

where η_v = Fluid viscosity, v_x = Fluid velocity and ρ = Density of the fluid. Solve this differential equation and calculate the average a) value of the boundary layer, b) velocity \bar{v}_x , c) molar flux of hydrogen due to both diffusion and convection effects, d) time it takes to remove the dissolved hydrogen along the channel length L and the amount of hydrogen being removed, and e) the Reynolds number. The cross-sectional of the flowing fluid is $A = \delta w$. Given data:

$\rho = \rho_{Al} = 2.5 \text{ g/cm}^3$	$w = 50 \text{ cm}$
$\eta_v = 40 \text{ g.cm}^{-1}\text{s}^{-1}$	$L = 100 \text{ cm}$
$D_{H,b} = 5 \times 10^{-3} \text{ cm}^2/\text{s}$	$\theta = 2^\circ$
$C_{H,b} = 30 \text{ mol/cm}^3$	$m = \bar{v}_x \rho A = 100 \text{ g/s}$
$C_H = 0 \quad @ \quad y = 0$	$g = 981 \text{ cm/s}^2$

[Solution: a) $\delta = 0.46 \text{ cm}$, b) $\bar{v}_x = 4.34 \text{ cm/s}$, c) $J_x = 130.53 \text{ mol.cm}^{-2}.\text{s}^{-1}$, d) $t = \frac{L}{\bar{v}_x} = 23.04 \text{ sec}$, and $m = 2.30 \text{ Kg}$, e) $Re_e = 0.13$].

7.17 Predict a) the electric potential E , b) the time in minutes, and c) the film growth rate in $\mu\text{m}/\text{min}$ for electroplating a $10 \mu\text{m}$ -thick Cr film on a Ni -undercoated steel part when the electrolyte contains 10^{-4} mol/l of Cr^{+3} cations at 25°C . The Ni -plated steel part has a 10 cm^2 surface area, the cell

operates at 50% current efficiency and at a passive current density of $5.12 \times 10^{-3} \text{ A/cm}^2$. [Solution: a) $E > E_o = -0.82 \text{ V}$, b) $t = 26 \text{ min}$, and c) $dx/dt = 0.38 \text{ } \mu\text{m/min}$.

7.13 REFERENCES

[1] "Electrolytic and Electrothermal Reduction and Refining," in *Metals Handbook*, Desk edition, Edited by H.E. Boyer and T.L. Gall, ASM Metals, Metals Park, Ohio 44073, (1985) 21.20 – 21.22.

[2] L.G. Twidwell, "Electrometallurgy," Unit Process in Extractive Metallurgy, NSF Project SED 75-04821, (1978).

[3] J.W. Evans and L.C. De Jonghe, "The Production of Inorganic Materials," Macmillan Publishing Company, New York, (1991).

[4] J.B. Mohler, "Electroplating and Related Processes," Chemical Publishing Company, Inc., New York, (1969) 119,225-228.

[5] G.H. Geiger and D.R. Poirier, "Transport Phenomena in Metallurgy," Addison-Wesley Publishing Company, Readings, Massachusetts, (1973) 514-541.

[7] D.R. Gaskell, "An Introduction to Transport Phenomena in Materials Engineering" Macmillan Publishing Company, New York, (1992).

[8] F.P. Incropera and D.R. DeWitt, "Introduction to Heat Transfer," John Wiley & Sons, New York, (1985).

[9] V.G. Levich, "Physicochemistry Hydrodynamics," Prentice-Hall Inc., (1962).

[10] P.J. Boden, "Effect of Concentration, Velocity and Temperature," in *Corrosion: Metal/Environment Reactions*, Third edition, edited by L.L. Shreir, R.A. Jarman, and G.T. Burstein, Butterworth-Heinemann, (1998) 2:3-2:30.

[11] R.D. Pehlke, "Unit Processes of Extractive Metallurgy," Elsevier North-Holland Publishing Company, Inc., (1973) 201-225.

[12] J.W. Graydon and D.W. Kirks, *Canadian J. Chem. Eng.*, Vol. 69, No. 2, (1991) 564-570.

[13] C. Hughes, AJ Parker Cooperative Research Center for Hydrometallurgy, www.parkercentre.crc.org, (2000).

[14] M. Bestetti, U. Ducati, G.H. Kelsall, G. Li, and E. Guerra, *Canadian Metallurgical Quarterly*, Vol. 40, No. 4, (2001) 451-458.

[15] M. Bestetti, U. Ducati, G.H. Kelsall, G. Li, E. Guerra, and R. Allen, *Canadian Metallurgical Quarterly*, Vol. 40, No. 4, (2001) 459-469.

[16] D. Felsher, J.A. Finch, and P.A. Distin, *Canadian Metallurgical Quarterly*, Vol. 39, No. 3, (2000) 291-296.

[17] N. Furuya and Y.T. Sakakibara, *J. Appl. Electrochem.*, Vol. 2., No. 1, (1996) 58-62.

[18] P. Ardelan, K.J. Cathro, E.J. Frazer, J.F. Kubachi, T. Lwin, R.H. Newham, and L.J. Rogers, *Electrometallurgical Plant Practice*, Edited by P.L. Claessens and G.B. Harris, Pergamon Press, (1990) 115-127.

- [19] N. Furuya and N. Mineo, *J. Appl. Electrochem.*, Vol. 20, No. 3, (1990) 475-478.
- [20] N. Furuya and S. Motoo, *J. Electroanal. Chem.*, Vol. 179, (1984) 297-301.
- [21] S. Motoo, M. Watanabe and N. Furuya, *J. Electroanal. Chem.*, Vol. 160 (1984) 351-357.
- [22] C.H. Hamann, A. Hamnett and W. Vielstich, "*Electrochemistry*," Wiley-VCH, New York, (1998).
- [23] S.R. Rao, X. Zu, and J.A. Finch, *Second Inter. Simp. on Waste Processing and Recycling in Mineral and Metallurgical Industries*, (1995).
- [24] M. Sheedy, *Proc. 1997 TMS Ann. Meet.*, Orlando, FL, USA, (Feb. 9-13, 1997) 433-441.
- [25] J. Crank, "*The Mathematics of Diffusion*," Oxford University Press, (1975) 31, 42-43.
- [26] Y. Saito, *Rev. Polarogr.*, Kyoto 15, (1968) 177.
- [27] T. Rosenquist, "*Principles of Extractive Metallurgy*," McGraw-Hill Book Company, New York, (1983).
- [28] B. Veileux, A.M. Lafront, and E. Ghali, *Canadian Metallurgical Quarterly*, Vol. 40, No. 3, (2001) 343-354.
- [29] J.L. Willitt, R.J. Blaskovitz and G.A. Fletcher, Argonne National Laboratory, CMT, www.cmt.anl.gov
- [30] Great Lakes Research Corporation (GLRC). www.es.epa.gov, (2000)
- [31] EPA Office of Compliance Sector Notebook Project, Profile of the Non-ferrous Metals Industry, SIC Codes 333-334, EPA/310-R-95-010, (Sept. 1995).
- [32] X.J. Xue, *Proc. 121st TMS Annu. Meet.*, Light Metals 1992, San Diego, CA, (March 1-5, 1992) 773-778.
- [33] "New Materials Improve Energy Efficiency and Reduce Electricity Use in Aluminum Production," DOE/CH-10093-140, www.es.epa.gov, (Sept. 1992).
- [34] ASARCO Incorporated, Commercial Department, Denver, CO, USA, www.asarco.com [2001].
- [35] www.elmhurst.edu, (2001).
- [36] H.D. Peters, VAW Aluminium Technologic GmbH, Bonn, Germany, www.vaw-atg.de, (2001).
- [37] A. Moraru, I. Panaitescu, A. Panaitescu, D. Mocanu, and A.M. Morega, *Rev. Roum. Sci. Techn.-Electrotechn. et Energ.*, 43 (4)(1998) 473-484.
- [38] Cook, G.M. *Energy Reduction Techniques in Metal Electrochemical Processes*, Edited by G.R. Bautista and R.J. Wesley, The Metallurgical Society, PA, (1985) 285-296.
- [39] ASARCO Incorporated, Commercial Department, Denver, CO, www.asarcotechnologies.com (2001).
- [40] Electrometals Technologies Limited, www.electrometals.com (2001).
- [41] The American Electroplaters and Surface Finishers Society, Inc., www.aesf.org, (2001)
- [42] www.mse.berkeley.edu, (2001)
- [43] C.A. Wert and R.M. Thompson, "*Physics of Solids*" McGraw-Hill Book Company, New York, (1970) 71-72.

[44] Ch. Droste, M. Segatz, D. Vogelsang, *Light Metals: Proc. 127th TMS Ann. Meet.*, San Antonio, TX, USA, (Feb. 15-19, 1998) 419-428.

[45] D. Vogelsang, I. Eick, M. Segatz, and Ch. Droste, *Light Metals: Proc. 126th TMS Ann. Meet.*, Orlando, FL, USA, (Feb 9-13, 1997) 233-238.

[46] M. Segatz, Ch. Droste, and D. Vogelsang, *Light Metals: Proc. 126th TMS Ann. Meet.*, Orlando, FL, USA, (Feb 9-13, 1997) 429-435.

[47] M. Segatz, M. and C. Droste, *Light Metals: Proc. 123rd TMS Ann. Meet. on Light Metals*, San Francisco, CA, USA, (Feb 27-Mar 3, 1994) 313-322.

[48] D. Vogelsang, M. Segatz, C. Droste, P. Baekler, and R. Stucher, *Light Metals: Proc. 123rd TMS Ann. Meet. on Light Metals*, San Francisco, CA, USA, (Feb 27-Mar 3, 1994) 245-251.

[49] M. Segatz, D. Vogelsang, C. Droste, and P. Baekler, *Light Metals: Proc. 122nd Ann. Meet.*, Denver, CO, USA, (Feb 21-25, 1993), 361-368.

[50] D. Vogelsang, and M. Segatz, *Light Metals: Proc. 120th TMS Ann. Meet.*, New Orleans, LA, USA, (Feb 17-21, 1991) 375-379

[51] M. Segatz, and D. Vogelsang, *Light Metals: Proc. 120th TMS Ann. Meet.*, New Orleans, LA, USA, (Feb 17-21, 1991,) 393-398.

[52] V. Potocnik, *Light Metals: Proc. 21st TMS Ann. Meet.*, San Diego CA, USA, (March 1-5, 1992) 1187-1193.

[53] I. Panaitesco, Repetto, Maurizio, Leboucher, Laurent, Pericleous, and Kyriacos, *IEEE Trans. on Magnetics*, Vol. 36, No. 41, (July 2000) 1305-1308.

[54] H.Q. Tang, N. Urata, C.M. Read, and S.L. Stejer, *Light Metals: Proceedings of Sessions, TMS Annual Meeting, Proceedings of the 1997 127th TMS Annual Meeting*, San Antonio, TX, USA, (Feb 15-19, 1998) 349-357.

[55] H.Q. Tang and N. Urata, *Light Metals: Proceedings of Sessions, TMS Annual Meeting, Proceedings of the 1997 126th TMS Annual Meeting*, Orlando, FL, USA, (Feb 9-13, 1997) 387-394.

[56] P.A. Davidson and R.I. Lindsay, *Light Metals: Proceedings of Sessions, TMS Annual Meeting, Proceedings of the 1997 126th TMS Annual Meeting*, Orlando, FL, USA, (Feb 9-13, 1997) 437-442.

[57] N. Urata, *Light Metals: Proc. of the Technical Sessions at the 114th Ann. Meet. of the Metallurgical Society of AIME*, New York, NY, USA, (1985) 581-591.

[58] N. Yanagi, S. Morimoto, K. Ichiguchi, S. Besshou, M. Sato, S. Kobayashi, M. Iima, H. ;Nakamura, M. Wakatani, and T. Obiki, *Nuclear Fusion*, Vol. 32, No. 7, (July, 1992) 1264-1269.

[59] T.X. Hou, Q. ;Jiao, W. Chin, W. Crowell, and C. Celik, *Light Metals: Proc. 124th TMS Ann. Meet.*, Las Vegas, NV, USA, (Feb 12-16, 1995) 755-761.

[60] V. Potocnik, *Light Metals 1992, Light Met 92, Proc. 121st TMS Ann. Meet.*, San Diego, CA, USA, (Mar 1-5, 1992) 1187-1193.

[61] J.T. Hogan and N.A. Uckan, *Fusion Technology*, Vol. 21, No. 3 pt 2A, *Proc. 10th Topical Meet. on the Technology of Fusion Energy*, Boston, MA, USA, (Jun 7-12, 1992) 1397-1405.

[62] A.J. Bard and L.R. Faulkner, "Electrochemical Methods," John Wiley Inc., (1980) 283.

[63] Z. Zembura, *Corrosion Sci.*, 8 (1968) 703.

[64] W.F. Hughes and F.J. Young, “*The Electromagnetodynamics of Fluids*,” John Wiley & Sons, Inc., New York, (1966).

[65] W.E. Haupin and W.B. Frank, “*Electrometallurgy of Aluminum*,” in *Comprehensive Treatise of Electrochemistry Vol. 2: Electrochemical Processing*, edited by J. O’M. Bobricks, B.E. Conway, E. Yeager, and R.E. White, Plenum Press, New York, (1981) 301-324.

[66] T. Erdey-Gruz, “*Kinetics of Electrode Process*,” Wiley-Interscience, a Division of John Wiley & Sons Inc., New York, (1972) 104-106, 115–118.

[67] R.F. Probst, “*Physicochemical Hydrodynamics: An Introduction*,” Butterworth Publisher, A Division of Reed Publishing Inc., USA, Boston, (1989) 59-61.

[68] A.D. Sneyd and A. Wang, *Magnitnaya Gidrodinamika*, Vol. 32, No. 4, (1996) 487-493, www.mhd.sal.lv/contents/1996/4/mg.32.4.r.html

Chapter 8

CATHODIC PROTECTION

8.1 INTRODUCTION

The mechanism of corrosion involves metal dissolution due to an electrochemical phenomenon. Thus, corrosion is associated with current flow over finite distances from the corroding metal and the amount of corrosion that can be accounted for is quantitatively determined by the amount of current passing through the metal. The electrochemical phenomenon occurs because of differences in potential between areas of the corroding metal surface. Therefore, the **driving force of corrosion** is the decrease in free energy associated with the formation of corrosion product on the metal surface. In contrast, preventing corrosion leads to cathodic protection under steady-state conditions.

Simple engineering structures, such as a spherical steel tank for storing water in hospital, need to be protected against corrosion. A thin coating of paint can protect the tank. However, complex structures, such as buried steel pipelines near steel tanks, steel bridges, multiple storage tanks in a refinery, offshore oil-drilling rigs, seagoing ships, and many more metallic structures have to be protected against corrosion.

Cathodic protection methods are useful for designing against corrosion, but these methods require knowledge of electrochemical polarization. The main objective in protecting a metallic structure is to eliminate or reduce corrosion rate by supplying an electron flow to a structure to reduce or eliminate metal dissolution (oxidation). This implies that the anodic reactions is suppressed on the surface of the structure. This can be accomplished using secondary materials and appropriate instrumentation to supply electrons to the structure.

Cathodic protection is an electrochemical technique in which a cathodic potential is applied to a structure in order to prevent corrosion from taking place. This implies that Ohm's law, $E = IR_{\text{p}}$, can be used to control the potential so that $E < E_{\text{corr}}$ and implicitly the current must be $I < I_{\text{corr}}$.

8.2 ELECTROCHEMICAL PRINCIPLES

Cathodic protection is an electrochemical technique in which a cathodic (protective) potential is applied to an engineering structure in order to prevent corrosion from taking place. This implies that Ohm's law, $E = IR$, can be used to control the potential, as well as the current. Hence, metal oxidation is prevented since the potential must be below the corrosion potential ($E < E_{corr}$). This is the main reason for this potential-control technique. In principle, all structures can be protected cathodically, but structural steels being the most common ferrous materials used to build large structures are cathodically protected by an external potential (impressed potential).

Figure 8.1 shows the general diagram for protecting a structure from corrosion. The useful techniques for protecting metallic structures can be solely applied or coupled with other technique, such as coating supplemented with impressed current cathodic protection (ICCP).

According to the electrochemical principles, the formation of a solid oxide corrosion product on a metal M immersed in an electrolyte depends on the constituents in solution. For instance, consider the presence and absence of oxygen in solution. The following reactions for a hypothetical oxidizing metal M are used to classify the type of solution.

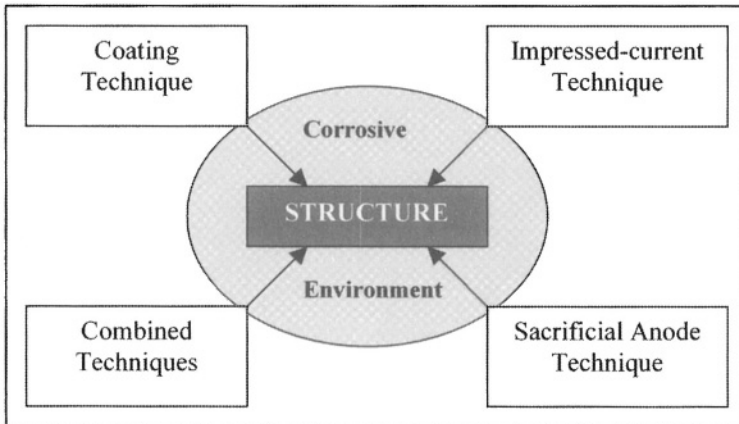
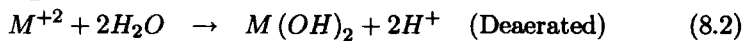
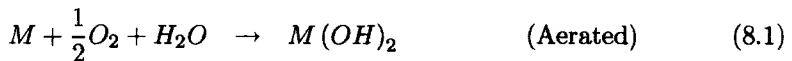
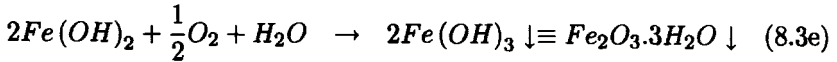
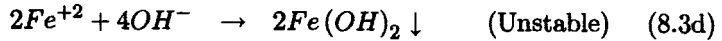
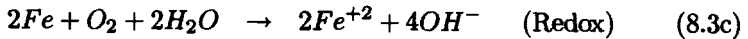
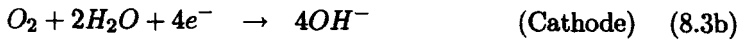
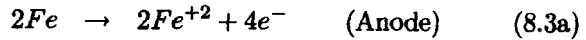


Figure 8.1 Diagram illustrating protective techniques against corrosion.

Thus, an aerated solution contains oxygen and its deaerated counterpart lacks of dissolved oxygen. The former is the most common reaction encounter in industrial schemes. For corroding iron or steel, the coupled anodic and cathodic reactions in the presence of oxygen generate an overall (redox) reaction similar to eq. (8.2), which is formed as follows [see eq. (1.6)]



In general, cathodic protection can be applied to any material susceptible to corrode, but this method is commonly used to protect carbon steel structures in diluted or alkaline electrolytes, such as seawater and soil. The corrosion mechanism of iron or carbon steel was introduced in Section 1.3, Chapter one and Chapter four. Nevertheless, the corrosion product may be an unstable ferrous hydroxide [$Fe(OH)_2$] solid compound, which reacts in the environment to form ferric hydroxide compound [$Fe(OH)_3$] or hydrated ferric oxide ($Fe_2O_3 \cdot 3H_2O$) known as “rust.” The formation of this corrosion product is avoidable using cathodic protection. However, careful application of an external potential to a structure must be considered because hydrogen evolution may be induced leading to destruction of any coating and Hydrogen Embrittlement [1].

The principles for corrosion and cathodic protection is illustrated in Figure 8.2 for an iron or carbon steel structure. Corrosion occurs at a slow or fast rate of iron dissolution in the aerated electrolyte since it is the iron atoms that release electrons, which are needed for the reduction of water to form hydroxyl ions in the electrolyte, such as air or soil. On the other hand, cathodic protection is achieved by supplying external electrons to the structure. Thus, the amount of external electrons reduce significantly or prevent the rate of dissolution of iron, but hydroxyl ions still form on the structure surface.

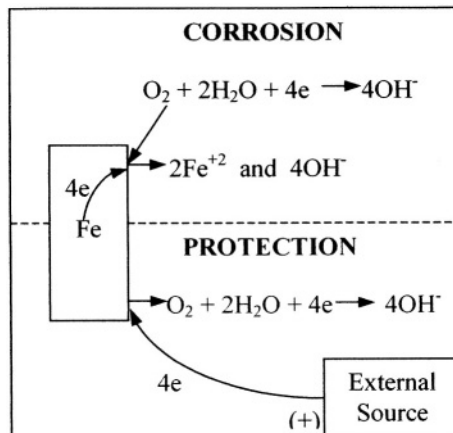


Figure 8.2 Schematic illustration for corrosion and protection of iron.

Cathodic protection can also be illustrated using the polarization diagram shown in Figure 8.3. The principles of electrochemical reactions using polarization curves has been introduced in great details in Chapter 3 and 4, but it is convenient to include a schematic diagram for exhibiting the methodology for evaluating the cathodic kinetics of a metal in an aerated electrolyte.

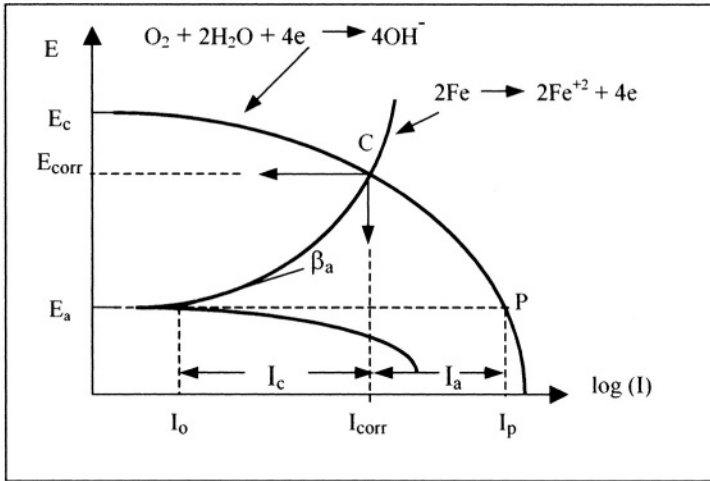


Figure 8.3 Schematic polarization diagram showing the corrosion point "C" and the protective point "P" for a hypothetical metal.

Assume that oxygen reduction occurs and no other oxidizing agents are present. This is then an ideal case for protecting a buried or underground structure. Recall that oxygen is an uncharged species which implies that its mass transfer depends on its concentration gradient [2]. Use of Figure 8.3 is subjected to the following interpretation

- The schematic electrochemical polarization curve suggests that metal dissolution occurs along the E_a -C curve if the applied potential and the applied current are $E > E_a$ and $I > I_a$, respectively.
- If $E_a < E < E_{corr}$ and $I_a < I < I_{corr}$, then an external supply of electrons must be provided to the system for reducing metal dissolution.
- The ideal protection can be achieved if $E \lesssim E_a$ and $I \lesssim I_p$, which means that the applied potential is the open-circuit (no current flows at this potential) of the metal and the applied current is purely cathodic. Consequently, the metal is ideally protected cathodically. However, if $E < E_a$ the structure is also protected at a higher current, but hydrogen evolution evolves leading to Hydrogen Embrittlement.

Coating Technique (CT): It is cost effective and provide the major part of the protection, but they are susceptible to have surface defects called **holidays**, which promote current drainage points causing localized corrosion sites. However, the coating defects must be cathodically protected against corrosion. Apparently, the combination of coating and cathodic protection techniques are adequate to protect a metallic structure, commonly made out of steel.

Coal tar pitch is a black resin used for coating underground structures. The type of coating has a good water, acid and mineral resistance, and can be applied on structures as a hot melt using a spray method or mops, rollers or any other manual method.

Coating defects develop due to chemical reactions and mechanical damage, leading to an increase in defect density and current requirements for protection. An increase in the protective current due to low resistance defects can be determined using Ohm's law, $I = E/R_x$. Nonetheless, cathodic protection is applied to the coated structure through an impressed current.

Sacrificial Anode Technique (SAT): It can also be used to protect an uncoated (bare) structures, seagoing vessels, offshore tanks, offshore platforms, water heater, and the like. In fact, a cathodic protection design using sacrificial anodes requires several anodes. These anodes must be monitored frequently because they dissolve sacrificially (purposely) and eventually are reduced in size and become incapable of delivering the necessary current to the structure.

The main requirement for using this technique is that the structure must be polarized, while the sacrificial anodes are oxidized to provide the source of electron flow needed to protect a structure. In fact, these anodes are coupled to a structure forming a closed-circuit, which must be properly designed in order to avoid anode passivation. Sacrificial anodes are characterized by their capacity to electrochemically dissolve in a particular environment. The anode capacity (C_a) is a measure of the electric energy per weight provided by an anode and it can be determined using Faraday's law

$$C_a = \frac{\epsilon z F}{A_w} \quad (8.4)$$

where ϵ = Anode current efficiency: $\epsilon_{Mg} = 0.50$, $\epsilon_{Al} = 0.60$, $\epsilon_{Zn} = 0.90$ [42]

A_w = Atomic weight (g/mol)

z = Valence

$F = 96,500 \text{ A.s/mol} = 26.81 \text{ A.h/mol}$

C_a = Anode capacity (A.h/Kg)

In addition, anodes are classified as sacrificial anodes and impressed-current anodes. The former must be anodic to the structure and must dissolve at a low rate, providing electrons to the cathode. On the other hand, the latter must have low consumption rates in cathodic protection designs. Specifically, sacrificial magnesium (**Mg**) anodes are widely used in buried pipelines and domestic or industrial water heater applications. For instance, a **Mg** anode may protect as much as 8 Km of a coated pipeline buried in the soil [3].

8.3 CATHODIC PROTECTION CRITERIA

The electrochemical foundation for cathodic protection is based on the criterion described by eq. (3.29), $i_a = -i_c = i_{corr}$ @ E_{corr} or $i_{corr} = i_a + i_c = 0$. This model states that the corrosion rate on a metal surface is zero when the forward and reverse current densities become exactly the same at equilibrium ($E = E_{corr}$). This criterion was recognized by Mears and Brown [36] in 1938 and it has become a common practice for protecting steel structures.

However, designing a cathodic protection system requires an initial current greater than the maintenance value for a specific design life and fortunately, the structure can be polarized cathodically during the lifetime. A particular design using an anode material containing a layer of magnesium (Mg) is very attractive in the early stages of cathodic protection. For soil structures, Mg strips can be used [37] and those in marine environments, Al-alloy plus a layer of Mg have been reported [18] to be effective in polarizing the structures by allowing Mg dissolution at the initial current density prior to steady state conditions at the maintenance current density. Therefore, Mg is the starter material that is consumed in the early stages of protection and eventually, the polarized structure reaches steady state.

Half-Cell Potential Criterion: For steel structures, cathodic protection is achieved when polarized at the iron (Fe) equilibrium half-cell potential [3]. In neutral environments (soil and seawater), the half-cell potential is based on the following reactions and it is determined by the Nernst equation

$$Fe^{+2} + 2e = Fe \text{ with } K_{Fe} = \frac{[Fe]}{[Fe^{+2}]} \text{ and } z = 2 \quad (8.5a)$$

$$Fe(OH)_2 = Fe^{+2} + 2(OH^-) \text{ with } K = 1.8 \times 10^{-15} \quad (8.5b)$$

$$E_{Fe} = E_{Fe}^{\circ} - \frac{RT}{zF} \ln(K_{Fe}) \quad (8.5c)$$

$$E_{Fe} = -0.44 V_{SHE} + \frac{2.303RT}{zF} \log [Fe^{+2}] \quad (8.5d)$$

$$E_{Fe(OH)_2} = E_{Fe(OH)_2}^{\circ} - \frac{RT}{zF} \ln(K_{Fe(OH)_2}) \quad (8.5e)$$

The activity of ferrous iron Fe^{+2} and hydroxyl OH^- ions are related as $[Fe^{+2}] = 2[OH^-]$ in eq. (8.5b). Consequently, the solubility constant $K_{Fe(OH)_2}$ and $[Fe^{+2}]$ become $K_{Fe(OH)_2} = [Fe^{+2}][OH^-]^2 = \frac{1}{4}[Fe^{+2}]^3$ and $[Fe^{+2}] = 1.931 \times 10^{-5} \text{ mol/l}$. Hence, theoretical potential for polarizing iron and carbon steel at $T = 25^\circ C = 298 \text{ K}$ becomes

$$E = E_{Fe} \approx -0.60 V_{SHE} = -0.92 V_{Cu/CuSO_4} \quad (8.5f)$$

which is close to the National Association of Corrosion Engineers (NACE) recommended potential of $-0.85 V_{Cu/CuSO_4}$. Consult Table 2.7 for conversions. In fact, a potential lower than $-0.92 V_{Cu/CuSO_4}$ enhances hydrogen evolution.

pH Criterion: The above theoretical potential for polarizing a steel structure can be determined using a different approach. If pH is defined as given in Table 2.6, then

$$pH = 14 + \log a(OH^-) = 14 + \frac{1}{2.303} \ln [OH^-] \quad (8.6a)$$

Thus, the hydroxyl activity becomes

$$[OH^-] = \exp [2.303 (pH - 14)] \quad (8.6b)$$

Combining eqs. (8.5f) and (8.6b) yields

$$\ln (K_{Fe(OH)_2}) \approx 7pH - 96 \quad (8.6c)$$

Once more, the Nernst equation gives the theoretical potential for polarizing iron and steel

$$E = E_{corr} + \frac{RT}{zF} \ln (K_{Fe(OH)_2}) \quad (8.6d)$$

Ideally, cathodic protection is achieved when $E_{corr} = 0$. Thus, eq. (8.6d) becomes

$$E \approx \frac{RT}{zF} \ln (K_{Fe(OH)_2}) \quad (8.6e)$$

Substituting eq. (8.6c) into (8.6e) yields the potential as a function of both temperature T and pH

$$E \approx \frac{RT}{zF} (7pH - 96) \quad (8.7)$$

For iron or steel in a neutral solution at $pH = 7$ and $T = 25^\circ C = 298^\circ K$, eq. (8.7) gives the same result as predicted by eq. (8.5f)

$$E \approx -0.60 V_{SHE} = -0.92 V_{Cu/CuSO_4} \quad (8.5f)$$

Cathodic protection is unusually performed in acid environments, but it is possible, at least, theoretically. Normally, protection of a metal in acid solutions is done anodically, provided that the metal is active-passive and shows a significant passive region. Thus, the anodic protection technique would prevail in such a case. This topic is dealt with in Chapter 9.

With regard to eq. (8.7), if $T = 35^\circ C = 308^\circ K$ and $pH = 7$, then the cathodic potential becomes slightly more negative; that is, $E \approx -0.62 V_{SHE} = -0.94 V_{Cu/CuSO_4}$.

β_a -Criterion: This is a criterion that requires known Tafel anodic constant (slope) β_a of the metal to be protected cathodically. According to Jones [1,38] and the overpotential required to reduce corrosion rate can be graphically determined as shown in Figure 8.4. However, the same results can be mathematically estimated using eq. (3.20a).

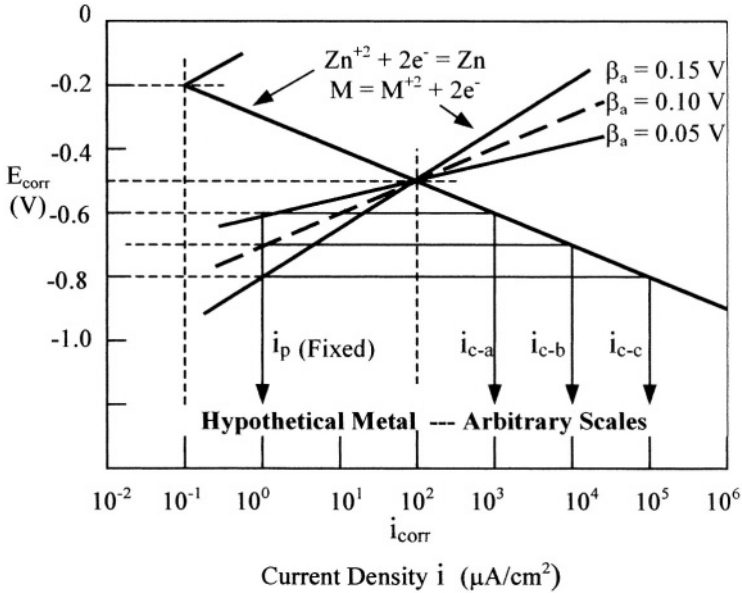


Figure 8.4 Effect of Tafel anodic constant on overpotential for cathodic polarization [1,38].

For a fixed polarization current density (i_p), the only changing variable is the Tafel anodic slope β_a . In this case, the overpotential becomes

$$\eta = \beta_a \log \left(\frac{i_{corr}}{i_c} \right) \quad (8.7b)$$

The effect of Tafel anodic constant for the hypothetical case shown in Figure 8.4 is calculated below as well as the half-cell potential, $E = E_{corr} - \eta$. Thus,

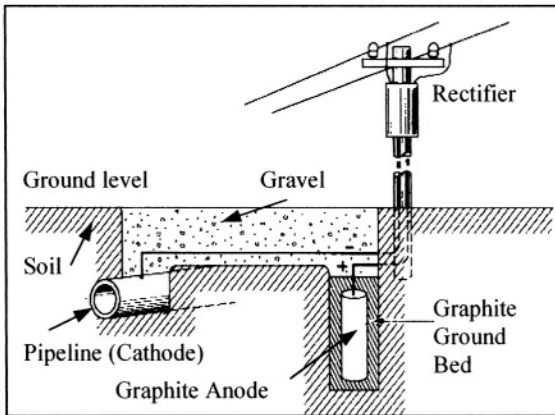
$$\eta = \beta_a \log \left(\frac{100}{i_c} \right) = \begin{cases} 0.10 \text{ V} & \text{for } \beta_a = 0.05 \text{ V} \\ 0.20 \text{ V} & \text{for } \beta_a = 0.10 \text{ V} \\ 0.30 \text{ V} & \text{for } \beta_a = 0.15 \text{ V} \end{cases} \quad (8.7c)$$

$$E = -0.50 - \eta = \begin{cases} -0.60 \text{ V} & \text{for } \eta = 0.10 \text{ V} \\ -0.70 \text{ V} & \text{for } \eta = 0.20 \text{ V} \\ -0.80 \text{ V} & \text{for } \eta = 0.30 \text{ V} \end{cases} \quad (8.7d)$$

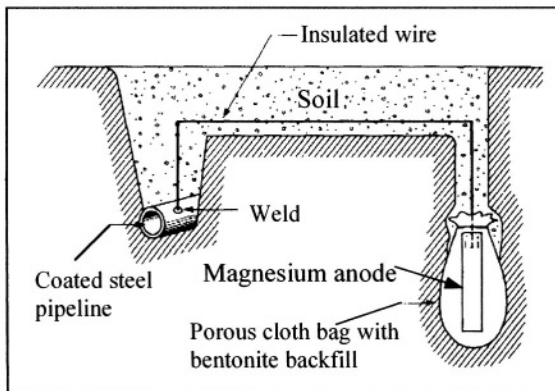
Other criteria can be found elsewhere [1].

8.4 IMPRESSED CURRENT TECHNIQUE

The impressed current technique is a simple and yet, significant form of cathodic protection of underground steel pipelines as shown in Figure 8.5a. A buried pipeline is connected to the positive terminal of a rectifier (power supply) and the anode to the negative terminal. Both terminals must be well insulated; otherwise, current leakage (stray-current) occurs and the structure may not be protected adequately. The significance of the cathodic protection setups shown in Figure 8.5 is that the current flows from the rectifier to the inert anode or sacrificial anode (graphite) through the soil (electrolyte) to the cathode. For structures immersed in seawater, the anodes may be platinum-coated titanium or high-silicon cast iron [1]. The purpose of the rectifier is to convert alternating current (ac) to uniform direct current (dc).



a) Impressed current



b) Sacrificial anode

Figure 8.5 Schematic cathodic protection technique [3,9].

Other cathodic protection systems are schematically shown in Figures 8.6 and 8.7. For instance, Figure 8.7 illustrates the three-electrode technique to conduct measurements of the potential difference between the working electrode (WE) and the reference electrode (RE) using a voltmeter V, and the current flowing to the anodic auxiliary electrode (AE) using an ammeter A.

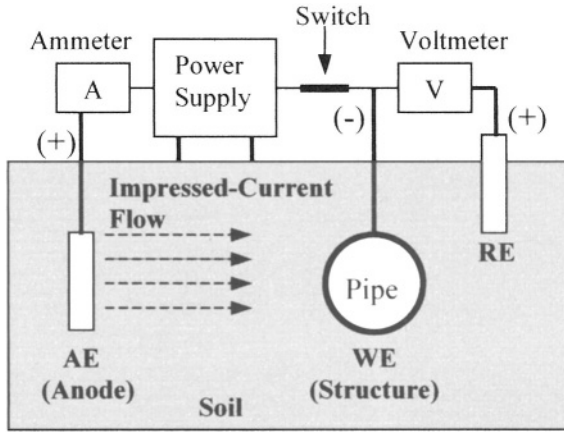


Figure 8.6 Three-electrode technique

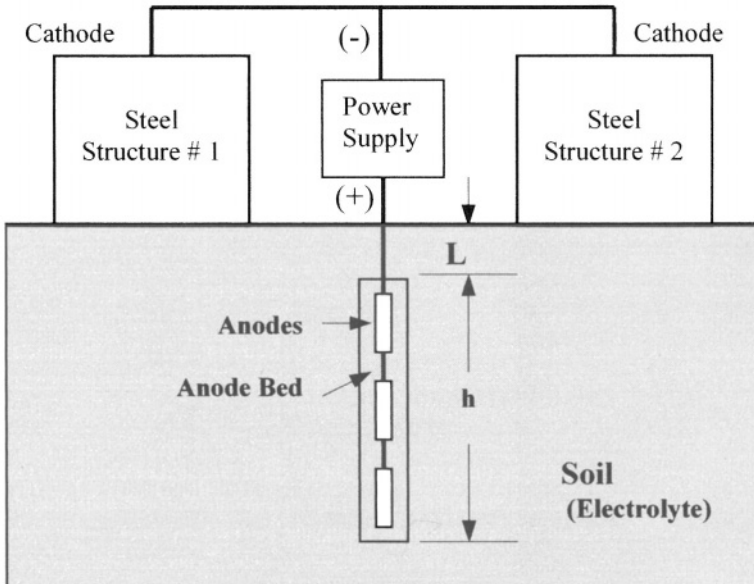


Figure 8.7 Cathodic protection system of two steel structures using an embedded anode bed.

The design and installation method for a buried structure using magnesium or any other suitable anode material as the source of current requires that the wiring system be well insulated with a good electrical resistance material; otherwise, the insulation may be destroyed by the anodic reaction products once the anode is energized by a power supply. Also, moisture must exist at the backfill-soil interface to provide a path for uniform current flow toward the active anode bed.

Potential measurements of structures buried in soil are carried out along the soil surface directly above the pipeline at discrete intervals. Similarly, for immersed structures, a submersible RE is placed near and moved along the pipeline. The outcome of these measurements is to determine if a structure is maintained polarized at the design potential.

Furthermore, the length of the anode-backfill column, known as active anode bed, must not be chosen arbitrarily because it is related to the current density entering the anode bed. Hence, the backfill current density is simply defined by the ground current divided by the column surface area

$$i_b = \frac{I}{\pi Dh} \quad (8.8)$$

where I = Ground current

D = Diameter of the column

h = Length of the column

Example 8.1 Suppose that a buried steel structure is to be cathodically protected using a rectifier capable of delivering 1 volt and 5 amperes through the wiring system. Assume that the soil resistance is 80% of the external resistance. Calculate a) the soil resistance when the anode bed is 4-meter long, and 0.10-meter in diameter and b) the current density.

Solution:

a) Using Ohm's law yields the external resistance as

$$R_x = \frac{E}{I} = \frac{1 \text{ V}}{5 \text{ A}} = 0.20 \text{ ohm}$$

Thus, the soil resistance is

$$R_s = 0.80R_x = 0.16 \text{ ohm}$$

b) From eq. (8.8),

$$i_b = \frac{I}{\pi Dh} = \frac{5 \text{ A}}{\pi (0.10 \text{ m}) (4 \text{ m})}$$

$$i_b \approx 4 \text{ A/m}^2 \quad @ \quad h = 4 \text{ m}$$

Despite that designing a cathodic protection system using sacrificial anodes requires suitable data prior to starting the protection scheme, the generalized picture of a pipeline being cathodically protected is schematically shown in Figure 8.5b. Pipelines and other steel structures may be cathodically protected using aluminum, zinc, and magnesium sacrificial anodes, which can be welded on the structure. These buried sacrificial anodes are usually backfilled with a high conductive material, such as granulated coke or graphite flakes, for preventing anode consumption and spreading the current in a relatively large area [1,9].

In summary, the impressed current technique requires the following

- A power supply (rectifier) that converts ac to dc in order to cathodically polarize the structure if and when the applied potential and current are $E \ll E_{corr}$ and $I \ll I_{corr}$, respectively.
- Despite that $I \ll I_{corr}$ is required, this current should not be large in magnitude; otherwise, hydrogen evolution may cause embrittlement of the structure. This is a well known fact being studied and reported in the literature for decades.

Table 8.1 illustrates a list of impressed-current anodes used in known corrosive environments. These anodes are high corrosion resistant solid materials. For instance, platinum (*Pt*) is used as the primary anode material due to its excellent corrosion resistance leading to low consumption.

Table 8.1 Impressed-current anodes [8-9].

Anode	Application
Platinized <i>Ag</i>	Chloride-containing tanks
Platinized <i>Ti</i>	Surface pipelines
Platinized <i>Ta</i>	Pipelines
<i>Ti₄O₇</i> and <i>Ti₅O₉</i> Base Ceramics	Steel-reinforced concrete, buried steel structures, Chloride-containing steel tanks,
Polymers	Electrowinning electrodes, batteries Steel-reinforced concrete roof Bridge decks, Parking garages Steel-reinforce bars
<i>Fe - 14Si - 4Cr</i>	Offshore structures
Graphite	Buried pipelines Onshore pipelines

Graphite anodes are made by mixing calcined petroleum coke particles and coal tar pitch binder. The desired shape is heated at 2800°C in order to convert amorphous carbon to crystalline carbon (graphite), which is immune to chloride solutions [10-11]. These anodes are normally impregnated with linseed oil or synthetic resins for reducing porosity and spalling. In addition, the anodes are buried in the soil and backfilled with coke breeze for a uniform distribution

of the electrical conductivity. The coke breeze surrounding the graphite anodes increase the surface area and disperse the anode reactions forming CO_2 and O_2 gases, which are vented through the soil porosity [8].

In measuring the potential of the a cathodically protected structure, the National Association of Corrosion Engineers (NACE) recommends a potential of $E = -0.85$ V vs. $Cu/CuSO_4$ reference electrode for steel and iron buried in the soil [8] and $E = -0.81$ V vs. $Ag/AgCl$ reference electrode for **Mg-alloy** anodes buried in the soil and in domestic water heater [12]. For submerged structures, the polarizing potential is normally within the range -1.05 V < $E < -0.80$ V $_{Ag/AgCl}$ as reported in the literature using dual anodes made out of **Al - Zn - Hg** alloys having an outer layer of **Mg** [19-21]. Recent papers describing experimental procedures using laboratory cells for testing specimens in seawater can be found elsewhere [19-23].

With regard to sacrificial anode cathodic protection (*SACP*), this technique uses the natural potential difference between the cathodic structure and the anode as the driving force for protection against corrosion of the structure. Therefore, the anode is sacrificed for a long period of time since it becomes the source of electrons.

The advantage of this technique over the impressed current is that it does not require a power supply since the structure and the anode are coupled through a wiring system or by mounting the anode on the structure forming a galvanic cell. Table 8.2 lists relevant data for common sacrificial anode materials used for protecting steel structures. In fact, a sacrificial anode has to be more electronegative than the structure and be sufficiently corrosion resistance; otherwise, anode dissolution would be too fast and the design life time would be shorten significantly. Therefore, **Al**, **Zn**, and **Mg** alloys are commonly used in order to comply with these requirements. Also, the electrons released by the anodes must be transferred to the steel structure to support the cathodic reactions on the structure and maintain cathodic polarization [6].

Table 8.2 Sacrificial anode materials and operating parameters for protecting steel structures [2,6].

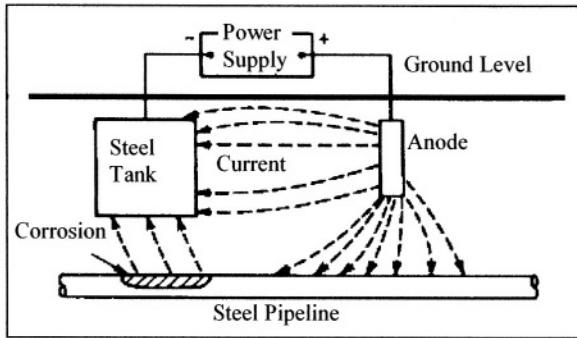
Alloy	Potential (V) vs. $Ag/AgCl$ in Seawater	Bare Steel Potential (V)	Anode Capacity C_a (A.h/Kg)
Al-Zn-In	-0.95 to -1.10	0.15 - 0.3	1300 - 2650
Al-Zn-Hg	-1.00 to -1.05	0.20 - 0.25	2600 - 2850
Al-Zn-Sn	-1.00 to -1.05	0.20 - 0.25	925 - 2600
Zn-Al-Cd	-1.05	0.20	780
Mg-Al-Zn	-1.50	0.70	1230
Mg-Mn	-1.70	0.90	1230
Zn	-0.95 to -1.03	0.15 - 0.23	750 - 780

8.5 STRAY CURRENT TECHNIQUE

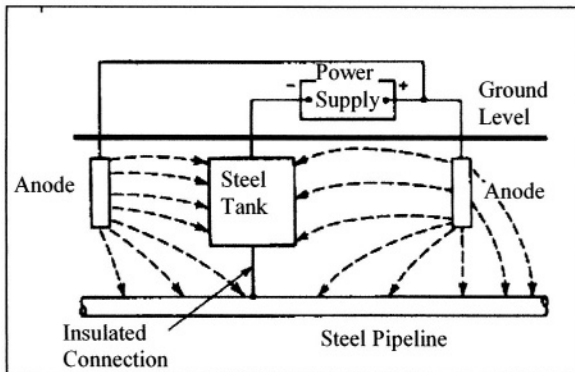
Let's use Fontana's cases [5] for protecting a pipeline against corrosion near a buried steel tank using the stray-current technique. Firstly, Figure 8.8a shows the detrimental effect of stray current (leakage current), which has the following path (dashed lines) in the cathodic circuit

$$\text{Power Supply} \rightarrow \text{Anode} \rightarrow \left\{ \begin{array}{l} \text{Soil} \\ \text{Pipeline} \end{array} \right. \rightarrow \text{Steel Tank} \rightarrow \text{Power Supply}$$

As a result, the pipeline corrodes near the steel tank. Secondly, the solution to this problem relies on placing and connecting another anode to the circuit as shown in Figure 8.8b. Thus, current flows from both anodes toward the tank and pipeline and consequently, both structures are cathodically protected by this uniform stray current flow.



a) Stray-current corrosion



b) Prevention of Stray-current corrosion

Figure 8.8 Stray-current technique [5].

In the above cathodic protection design, the current being discharged from the anodes is picked up by the tank and pipeline in the directions shown as dashed lines. In treating the tank and the pipeline as a whole structure, the total cathodic potential (E) can be measured with respect to a reference electrode (RE), excluding any ohmic potential drop (IR_x). This can be accomplished by using the recommended switch-off technique, in which the rectifier is switched off for interrupting the current flow and eliminating IR_x , and measure the potential immediately with a high-impedance voltmeter. Consequently, the Ohmic potential drop is dissipated immediately, while polarization of the structure decays at a low rate [2]. With regard to Figure 8.8a, the stray currents flow through the soil to the tank and to the pipeline, and corrosion occurs where the stray currents leave the pipeline in a confined area. This is the reason for the shown localized corrosion. Stray-current corrosion is an unusual metal deterioration of buried or submerged structures.

In general, the source of stray currents is an electric generator, such as an electric welding machine, a grounded dc power supply, a cathodic protection system, an electroplating cell [3-5]. Some structures are more vulnerable than others due to localization, design, and surrounding electric generators. Nevertheless, the principal remedy for stray-current corrosion is to eliminate the current leakage source whenever possible. Otherwise, an undesirable metal deterioration or even catastrophic failure may occur.

Stray currents flow through paths other than the designed circuit and the effect of this flow can render designs very ineffectively. In fact, stray-current corrosion is different from natural corrosion since it is induced by an external electric current. Corrosion may be accelerated when other corrosion mechanisms induced by environmental factors are coupled with stray currents. For instance, both stray-current corrosion and galvanic corrosion have cathodic and anodic sites on a structure, but the former may vary with time and metal dissolution is induced by the current flow, while the latter is a continuous electrochemical process independent of an external current and proceeds at a constant rate. These sites may be meters apart and corrosion damage occurs on the metal surface since the structure has a higher electric conductivity than a particular internal fluid. However, if the stray-current flow reaches the internal fluid, corrosion damage may occur on the inside of the a pipeline, making matters worse because undetected corrosion may be ignored and consequently, a disastrous and regrettable problem may occur.

Additionally, stray-current corrosion is common on seagoing vessels, such as boats. For example, powered battery chargers generate dc stray currents, which may flow indefinitely if proper precautions are ignored or overlooked. This type of corrosion can manifest as pitting in confined areas, metal surface discoloration, rust formation on steel parts or weakening of batteries.

The magnitude of the current leaving or entering a buried pipeline in the soil may be determined by measuring the potential difference between two points on the soil surface as illustrated in Figure 8.9. This type of potential measurement yields the electric potential difference that can be mathematically predicted by eq. (8.28), which requires a known depth of the buried structure.

8.6 POTENTIAL ATTENUATION

The potential attenuation (fluctuation of potential) in an impressed-current system has a detrimental effect on corrosion prevention of a metallic structure containing defects. For instance, a coated pipeline buried in soil is subjected to experience current leakage due to coating defects known as holidays.

Consider the schematic buried pipeline in soil shown in Figure 8.9 containing a current drain point at a holiday. The pipeline is buried in the soil at a remote distance from an sacrificial anode. This setup creates an impressed-current field induced by the anode in the soil of constant electrical resistivity. As Ashworth pointed out [2], this is just an approximation technique used for deriving an expression for an infinite pipeline.

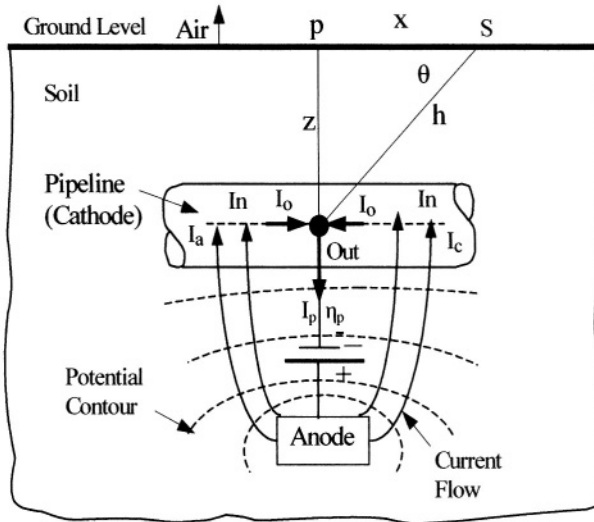


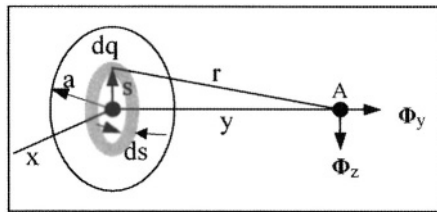
Figure 8.9 Schematic pipeline showing the impressed-current and potential fields, and a current drainpoint [1].

In this case, the following concrete assumptions are considered

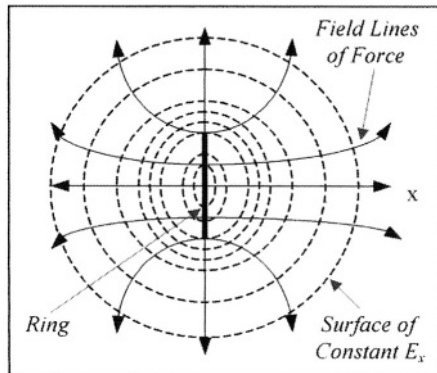
- There is a uniform soil resistivity. The reader should be aware of the fact that the resistivity is not exactly uniform due to soil heterogeneity.
- There is a uniform defect density in the pipeline coating. Detachment of the coating and crevice formation must be considered.
- There is a positive current field for inducing an electric field gradient in the soil (electrolyte), specifically between the anode and the cathodic structure. In fact, the electric field gradient approaches zero in magnitude near the pipeline outer wall.

- Any electrode potential change at the pipeline-soil interface is assumed to be equals to the pipeline cathodic overpotential.
- The current and potential fields are uniform around the buried pipeline. Thus, the potential and current field gradients are quantitatively determined in either impressed-current or sacrificial anode techniques. This assumption is not realistic since the complexity of real engineering structures and heterogeneity of the soil or seawater electrolytes preclude exact theoretical calculations. The margin of error between the theoretical and experimental results depends on the assumptions considered to develop a particular mathematical model.

Charged Disk Model: Assume that the holiday of radius a is a uniform charged flat disk shown in Figure 8.10a and that point A is located at a distance from the drainage point in the soil. Also, assume that all charge elements in the ring-shaped annular segment of the disk lie at the same distance from point A and that the amount of charge on the disk is $dp = \sigma dA_s$, where σ is the charge density, $dA_s = 2\pi s ds$ is the area of the segment, s is the radius of the segment, and ds is the width of the segment. Figure 8.10b shows the electric field for a holiday standing alone. This a typical model used in physics [34].



a)



b)

Figure 8.10 Holiday as a current drainage point on a pipeline. a) Model for finding the potential along the y-direction and b) electric field.

Thus, the potential along the y -direction (perpendicular to the disk flat surface) is defined as

$$\phi = \int \frac{dp}{r} = \int_0^a \frac{2\pi\sigma s ds}{\sqrt{s^2 + y^2}} \tag{8.9}$$

$$\phi = 2\pi\sigma \left[\sqrt{a^2 + y^2} - y \right] \quad \text{For } y > 0 \tag{8.10}$$

$$\phi = 2\pi\sigma \left[\sqrt{a^2 + y^2} + y \right] \quad \text{For } y < 0 \tag{8.11}$$

The electric field around the disk is shown in Figure 8.10b. The electric field in the y -direction can be defined as

$$E_y = -\frac{\partial\phi}{\partial y} = 2\pi\sigma \left[1 - \frac{y}{\sqrt{a^2 + y^2}} \right] \quad \text{For } y > 0 \tag{8.12}$$

The potential attenuation (profile) based on this model is shown in Figure 8.11 along with the ideal protective area for cathodic protection. The protective points are located at a distance y between the anode and the pipeline structure. This potential attenuation indicates that the potential falls off from the center of the disk implying that the electric field has an outward component in the plane of the disk. The solid line is for the coated steel pipeline, while the dashed line is for possible nonlinear potential distribution of a bare steel pipeline.

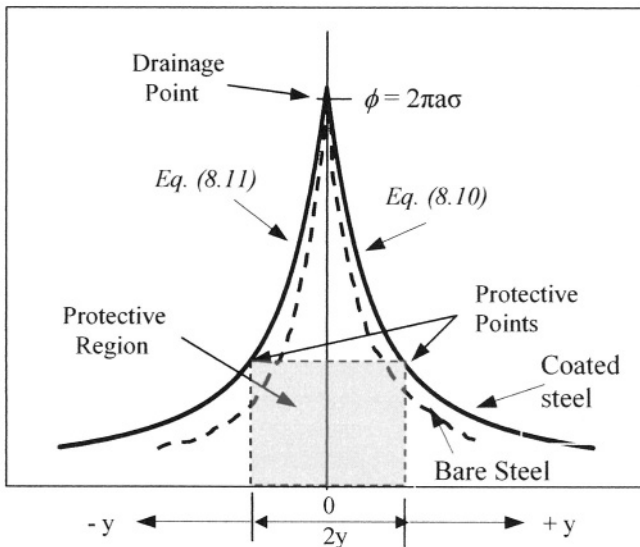


Figure 8.11 Schematic potential attenuation (potential profile) along the y -direction for one drainage point.

Uhlig's Model: It is instructive to include Uhlig's model for deriving the potential change along a cathodically protected pipeline. Thus, the potential and current attenuations of a buried pipeline (Figure 8.9) can be approximated by using the free-body diagram depicted in Figure 8.12.

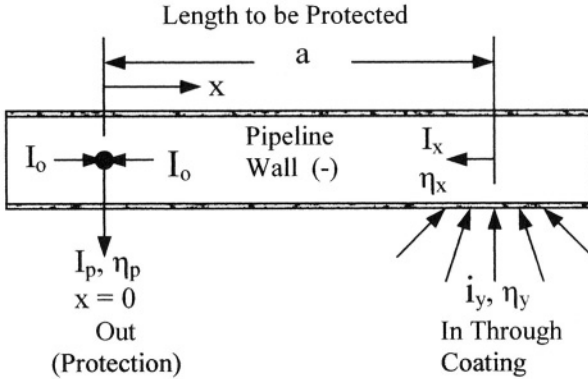


Figure 8.12 Free-body diagram of a pipeline wall.

In pursuing the mathematical details peculiar to Uhlig's model, when the current is defined as $I_x = Ai_x$, while the cross sectional area of the pipe is $A = 2\pi rx$, the current gradient in the x-direction is

$$\frac{dI_x}{dx} = -2\pi ri_x \tag{8.13}$$

The overpotential at a distance x is $\eta_x = E - E_{corr}$, where E is the applied cathodic potential and the corrosion potential, E_{corr} , is zero in the cathodic protection system. Thus, the overpotential gradient becomes [2]

$$\frac{d\eta_x}{dx} = -R_c I_x \tag{8.14}$$

$$\frac{d^2\eta_x}{dx^2} = (2\pi ri_x) R_c \tag{8.15}$$

At small values of the current density i_x , the polarization of the pipeline is assumed to be linear and the potential becomes [3]

$$\eta_x = \lambda R_L i_x \tag{8.16}$$

- where R_c = Coating resistance per unit length (*ohm/cm*)
- R_L = Leakage resistance of the structure (*ohm.cm*)
- λ = Constant

Combining eqs. (8.15) into (8.16) to eliminate the current density i_x yields the second order partial differential equation for the overpotential at a distance x . Thus,

$$\frac{d^2\eta_x}{dx^2} - \left(\frac{2\pi r R_c}{R_L}\right)\eta_x = 0 \quad (8.17)$$

$$\frac{d^2\eta_x}{dx^2} - \left(\frac{R_s}{R_L}\right)\eta_x = 0 \quad (8.18)$$

Using the following boundary conditions

$$\eta_x = 0 \quad \text{at} \quad x = \infty \quad (8.19a)$$

$$\eta_x = \eta_o \quad \text{at} \quad x = 0 \quad (8.19b)$$

the solution of eq. (8.18) is

$$\eta_x = \eta_o \exp(-\alpha x) \quad (8.20)$$

where $\alpha = (R_s/R_L)^{1/2} = R_s/R_k =$ Attenuation coefficient (cm^{-1})

$\eta_o =$ Overpotential coefficient or drainage overpotential (V)

$R_s =$ Longitudinal resistance of the structure (ohm/cm)

$R_k =$ Characteristic resistance between the structure and earth (ohm)

Example 8.2 A pipeline is buried in humid soil has an outer diameter of 30.48 cm (12 inches). If the longitudinal resistance (R_s) and the leakage resistance (R_L) of the structure are $1.31 \times 10^{-7} \text{ ohm/cm}$ and $3,048 \text{ ohm.cm}$, respectively, calculate a) the characteristic resistance, b) attenuation coefficient, c) the overpotential ratio at 1 Km from a drainage point, and the potential gradient at 1 Km.

Solution:

$$a) R_k = \sqrt{R_s R_L} = \sqrt{(1.31 \times 10^{-7} \text{ ohm/cm})(3,048 \text{ ohm.cm})}$$

$$R_k = 0.02 \text{ ohm}$$

$$b) \alpha = R_s/R_k = 6.55 \times 10^{-6} \text{ cm}^{-1}$$

c) From eq. (8.20),

$$\eta_x/\eta_o = \exp(-\alpha x) = \exp[(-6.55 \times 10^{-6} \text{ cm}^{-1})(10^5 \text{ cm})]$$

$$\eta_x/\eta_o = 0.52$$

d) From eq. (8.20),

$$d\eta_x/dx = -(\eta_o/\alpha) \exp(-\alpha x)$$

$$d\eta_x/dx = -218.34 \eta_o$$

Now, the overpotentials are approximated as $\eta_x = \phi_x - E_{corr} \approx \phi_x$ and $\eta_o = \phi_o - E_{corr} \approx \phi_o$ due to $E_{corr} \approx 0$ since the pipeline is designed against corrosion. Thus, these assumptions lead to the cathodic protection attenuation equation known as Uhlig's equation for an infinite pipeline which is compared with the disk model equation in mathematical and graphical form (Figure 8.13)

$$\phi_x = \phi_o \exp(-\alpha x) \quad \text{(Uhlig's Model)} \quad (8.21)$$

$$\phi_x = 2\pi\sigma \left[\sqrt{a^2 + x^2} - x \right] \quad \text{(Disk Model)} \quad (8.22)$$

Observe that Uhlig and Disk models give similar potential trends as shown in Figure 8.13.

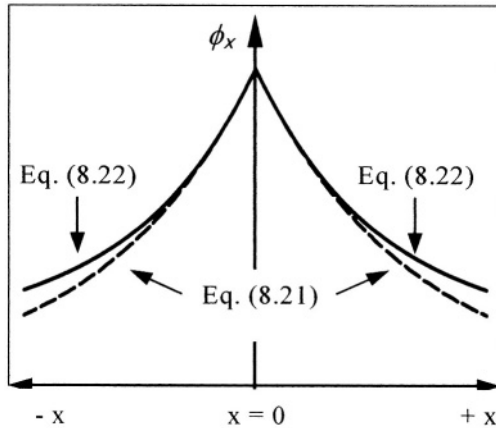


Figure 8.13 Comparing potential attenuation trends.

On the other hand, the current attenuation is derived by differentiating eq. (8.20) with respect to x . The resultant expression leads to the current density attenuation. Thus,

$$I_x = I_o \exp(-\alpha x) \quad (8.23)$$

$$i_x = \frac{I_x}{\pi d L} \quad (8.23a)$$

where $I_o = \alpha \eta_o / R_L =$ Drainage current (A)

$d =$ Pipe diameter (cm)

$L =$ Pipe length at a distance x from a drainage point (cm)

$\pi d =$ Circumference of the pipe

The protective parameters are $I_x = I_o$ and $E_x = \phi_x = \phi_o$ when $x = 0$ [3]. According to Ohm's law, the leakage resistance is equals to the potential drop from the leakage point divided by the polarization current difference at the coating-metal interface. Thus,

$$R_L = \frac{\phi_x - \phi_o}{I_x - I_o} \quad (8.24)$$

The preceding analytical approach for determining the potential and current distribution of a simple pipeline has been based on a uniform current attenuations and uniform soil resistance. However, real structures being cathodically protected require more complex analyses due to either inherently imperfect coatings, nonuniform structure potential, complexity of the structure, and the like.

The potential distribution along the soil surface (ground level) for a buried pipeline shown in Figure 8.9 is easy to determine. Consider the schematic side view of the pipeline shown in Figure 8.14 illustrating two locations on the soil surface denoted as point P just above the pipeline and point S at a distance x from point P . Thus, the configuration forming a triangle is used to determine the potential difference. The dashed curves in Figure 8.14 are current and potential profiles around a buried pipeline [33].

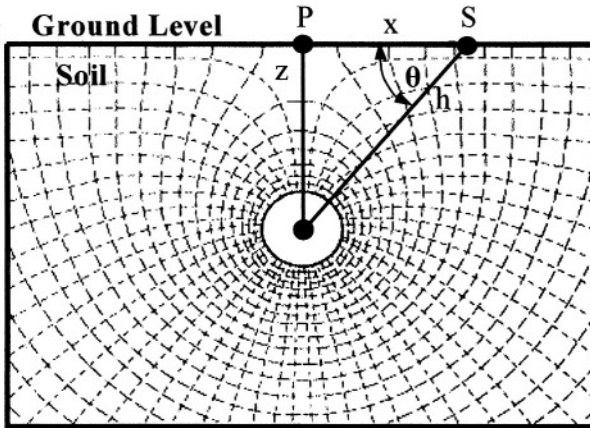


Figure 8.14 Schematic buried pipeline in an electric field [33].

According to the triangle in Figure 8.14, the component of the current density along the x -direction is defined as [3]

$$i_x = \frac{2I}{2\pi rh} \cos \theta = \frac{I}{\pi rh} \frac{x}{h} = \frac{xI}{\pi rh^2} \quad (8.25)$$

where $2\pi rh$ is the surface area.

Using Ohm's law the potential gradient along the soil surface in the x -direction is

$$\frac{d\phi}{dx} = \rho_s i_x = \frac{x \rho_s I}{\pi r h^2} \tag{8.26}$$

$$\frac{d\phi}{dx} = \frac{\rho_s I}{\pi r} \frac{x}{x^2 + z^2} \tag{8.27}$$

Integrating eq. (8.27) yields the potential along the x-direction at a depth z

$$\phi = \frac{\rho_s I}{2\pi r} \ln \left[\frac{x^2 + z^2}{z^2} \right] \tag{8.28}$$

- where ρ_s = Soil resistivity (ohm.cm)
- z = Depth directly above the pipeline (cm)
- r = Radius of the pipeline (cm)

Figure 8.15 shows the potential profile given by eq. (8.28) as a function of both x and varying depth z . Observe that the potential on the soil surface along the x-direction approaches zero as the depth goes to infinity. This implies that the boundary conditions for x and z are $0 < x < \infty$ and $0 < z < \infty$. Also, if $x \rightarrow 0$, then $\phi \rightarrow 0$. The current I in eq. (8.28) is either leaving or entering the buried pipeline.

Furthermore, the model predicts that the potential is not strongly dependent on depth z at a short distance x (Figure 8.15). The opposite trend is remarkably indicated in Figure 8.15 at large distance x . The potential gradient, eq. (8.27), is included in this figure for comparison purposes. Observe that this gradient has increases with increasing x and has a maximum. Subsequently, $d\phi/dx$ begins to decrease as the potential increases.

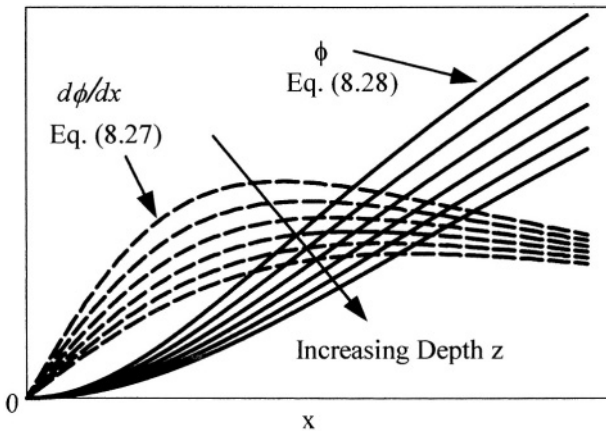


Figure 8.15 Potential profile along the x-direction and depth z.

8.7 EQUIVALENT CIRCUIT

Figure 8.16 shows an equivalent electrical circuit that simulates the pipeline cathodic protection depicted in Figure 8.9. Both pipeline and sacrificial anode (galvanic anode or inert anode) are buried in the soil of uniform resistivity. The pipeline is connected to the negative terminal and the anode to the positive terminal of an external power source (battery). The arrows in Figure 8.16 indicates the direction of the current flow from the anode to the pipeline. The electron flow is also toward the pipeline to support local cathodic reactions and the protective current (I_p) flows from the pipeline to the power supply. The soil becomes the electrolyte for completing the protective electrochemical system or cathodic protection circuit [24].

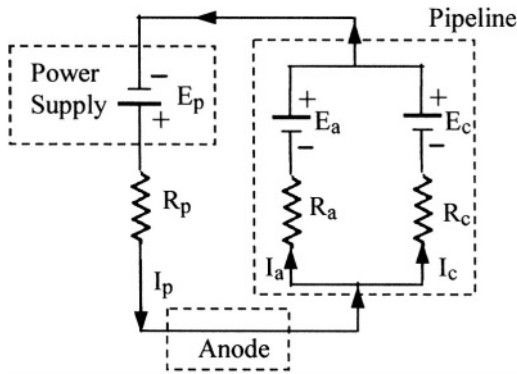


Figure 8.16 Equivalent circuit for cathodic protection of a buried pipeline [24].

Nomenclature for Figure 8.16:

I_p = Protective current	E_p = Protective potential
I_a = Local anodic current	E_a = Anodic potential
I_c = Local cathodic current	E_c = Cathodic potential
R_p = Protective resistance	R_s = Soil resistance
R_a = Anodic resistance	R'_c = Coating resistance
R_c = Cathodic resistance	R_x = External resistance

According to Jastrzebski [24] the protective current, the protective potential and the total resistance for the equivalent circuit in Figure 8.16 are defined as

$$I_p = I_a + I_c \quad (8.29)$$

$$E_p = E_c - E_a \quad (8.30)$$

$$\sum R = R_a + R_c + R_s + R_x + R'_c \quad (8.31)$$

If $(R_a + R_c) \gg (R_s + R_x)$, then eq. (8.31) becomes

$$\sum R = R_a + R_c + R'_c \quad (8.32)$$

Ohm's law predicts the corrosion current for the coated and bare steel pipelines before a cathodic current is applied to the cathodic protection system [24]. Hence, at equilibrium

$$I_{corr} = I_a = I_c = \frac{E_p}{\sum R} \quad (8.33)$$

$$I_{corr} = \frac{E_p}{R_a + R_c + R'_c} \quad (\text{Coated steel}) \quad (8.34)$$

$$I_{corr} = \frac{E_p}{R_a + R_c} \quad (\text{Bare steel}) \quad (8.35)$$

If the protective anodic and cathodic potentials are equal, then Ohm's law yields $E_a = E_c$ and

$$I_a R_a = I_c R_c \quad (8.36)$$

Now, the application of a protective current yields

$$I_a^* = I_{corr} - I_a \quad (8.37)$$

Combining eqs. (8.29) and (8.36) and solving for I_a , and inserting the resultant expression into (8.37) yields

$$I_a^* = I_{corr} - I_p \left(\frac{R_c}{R_a + R_c} \right) \quad (8.38)$$

Thus, cathodic protection is achieved when $I_a^* = 0$ and eq. (8.38) gives the protective or applied current as [24]

$$I_p = I_{corr} \left(\frac{R_a + R_c}{R_c} \right) \quad (8.39)$$

Substituting eq. (8.34) and (8.35) into (8.39) gives

$$I_p = \frac{E_p}{R_a + R_c + R'_c} \frac{R_a + R_c}{R_c} \quad (\text{Coated steel}) \quad (8.40)$$

$$I_p = \frac{E_p}{R_c} \quad (\text{Bare steel}) \quad (8.41)$$

The protective current is schematically predicted in Figure 8.3 at point P . If $I_p = I_{corr}$ the cathode (pipeline) and anode are polarized according to the potential at point C . This is an undesirable condition since the anode polarizes and eventually, the pipeline corrodes. Therefore, $I_p > I_{corr}$ for polarizing (protecting) the cathode and keeping the anode unpolarized (active).

8.8 MASS TRANSFER IN A CREVICE

Underground steel pipelines are normally protected to a large extent by external coatings, which are susceptible to mechanical or chemical damage in the form of holidays (coating flaws). A holiday is known as a pinhole with a radius of a few millimeters (mm). If the coating is partially detached beneath the holiday, the base metal undergoes crevice corrosion in an aggressive environment. Recall that a simple mechanistic model for crevice corrosion is shown in Figure 1.11. Crevice corrosion beneath holidays is common on buried pipelines in low conductivity soils. In order to prevent crevice corrosion the cathodic current has to flow to the pipeline surface.

The molar flux in this type of corrosion is mainly due to the mass transfer of Na^+ , Cl^- , and OH^- ions and dissolved molecular oxygen (O_2) in the soil. According to the stoichiometry in eq. (8.4), the hydroxyl ions (OH^-) form in the presence of water and oxygen and react with ferrous ions (Fe^{+2}) to form ferrous hydroxide, $Fe(OH)_2$, as the crevice corrosion product, eq. (8.6). However, crevice corrosion can be avoided by cathodic protection of holidays by controlling current leakage and related local potentials.

The mass transfer phenomena and current distribution can be modeled using an ideal circular crevice beneath a holiday as indicated in Figure 8.17. Some relevant parameters are in the order of $R_H = 0.80\text{ mm}$, $6\text{ mm} < R_o < 80\text{ mm}$, and $\delta = 0.8\text{ mm}$ [25].

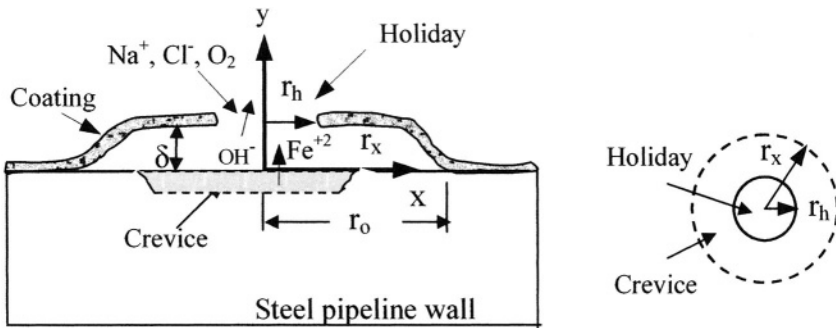


Figure 8.17 Schematic circular crevice and holiday [25].

This model has been successfully used by Chin and Sabde [25] for crevice cathodic protection using numerical analysis based on the dilute solution theory and reduction reaction of dissolved oxygen and Na^+ , Cl^- , and OH^- ions at the crevice surface. Hence, the Nernst-Planck equation, eq. (4.2), can be generalized as a differentiable and continuous scalar diffusion molar flux function

$$J_j = -D_j \nabla \cdot C_j - Z_j \left(\frac{F}{RT} \right) D_j \nabla \cdot \phi + C_j V_j \quad (8.42)$$

where $j = 1, 2, 3$, and 4 for the species Na^+ , Cl^- , OH^- and O_2 , respectively

∇ = Laplacian differential operator

r = Radius of the circular crevice

Z_j = Valence of the species Na^+ , Cl^- , OH^- and O_2

C_j = Concentration of the species Na^+ , Cl^- , OH^- and O_2

D_j = Diffusivity of species Na^+ , Cl^- , OH^- and O_2

The ferrous Fe^{+2} ions are not included in the analysis since the crevice cathodic protection is for preventing the formation of this type ion. For a coupled diffusion and migration molar flux under steady-state conditions, $\partial C_j / \partial t = 0$, the molar flux becomes the continuity equation for mass transfer under steady state conditions

$$\nabla J_j = 0 \quad (8.43)$$

Thus, eq. (8.42) yields

$$\nabla^2 C_j + Z_j \left(\frac{F}{RT} \right) \nabla \cdot [C_j \nabla \phi] = 0 \quad (8.44)$$

where

$$\nabla^2 = \frac{\partial^2}{\partial r^2} + \frac{1}{r} \frac{\partial}{\partial r} + \frac{\partial^2}{\partial y^2} \quad (8.45)$$

Expanding eq. (8.44) into two-dimensional cylindrical coordinates gives a generalized expression that is solved numerically for particular species involved in the electrochemical process of crevice cathodic protection

$$0 = \left[\frac{\partial C_j^2}{\partial r^2} + \frac{1}{r} \frac{\partial C_j}{\partial r} + \frac{\partial C_j^2}{\partial y^2} \right] + Z_j \left(\frac{F}{RT} \right) \left[\frac{C_j}{r} \frac{\partial \phi}{\partial r} + C_j \frac{\partial \phi^2}{\partial r^2} \right. \\ \left. + \frac{\partial C_j}{\partial r} \frac{\partial \phi}{\partial r} + C_j \frac{\partial \phi^2}{\partial y^2} + \frac{\partial C_j}{\partial y} \frac{\partial \phi}{\partial y} \right] \quad (8.46)$$

Electric neutrality of the electrolyte dictates that $\nabla \phi = 0$ and eq. (8.42) along with $y = 0$ gives

$$\sum Z_j C_j = 0 \quad (8.47)$$

Also, the concentration of OH^- ions is related to pH as

$$pH = 14 + \log(C_3) \quad (8.48)$$

Furthermore, the electrolyte conductivity, eq. (3.93), ionic mobility, eq. (3.97), and the current density, eq. (4.9), expressions are generalized as follows

$$K_c = Z_j F B_j C_j \quad (8.49)$$

$$B_j = \frac{D_j}{RT} \quad (8.50)$$

$$i = Z_j F J_j \quad (8.51)$$

Thus, eqs. (8.46) through (8.51) are useful expressions in modeling the crevice cathodic protection shown in Figure 8.17. On the other hand, the potential can be simulated using the following boundary conditions [25]

$$\frac{\partial \phi}{\partial r} = 0 \quad \text{and} \quad \frac{\partial C_j}{\partial r} = 0 \quad \text{for } y \geq 0, \quad r = 0 \quad (8.52)$$

$$\frac{\partial \phi}{\partial y} = 0 \quad \text{and} \quad \frac{\partial C_j}{\partial y} = 0 \quad \text{for } y = \delta, \quad r_h < r < r_o \quad (8.53)$$

The reader should consult references [18-19,25] for insight details on numerical simulations of cathodic protection. From the work of Chin and Sabde [25], Figure 8.18 is included in this section in order to illustrate typical numerical simulation results, such as potential as a function of dimensionless radius of the holiday/crevice shown in Figure 8.17. These results indicate that the potential strongly depends on the concentration of sodium chloride ($NaCl$) in the soil.

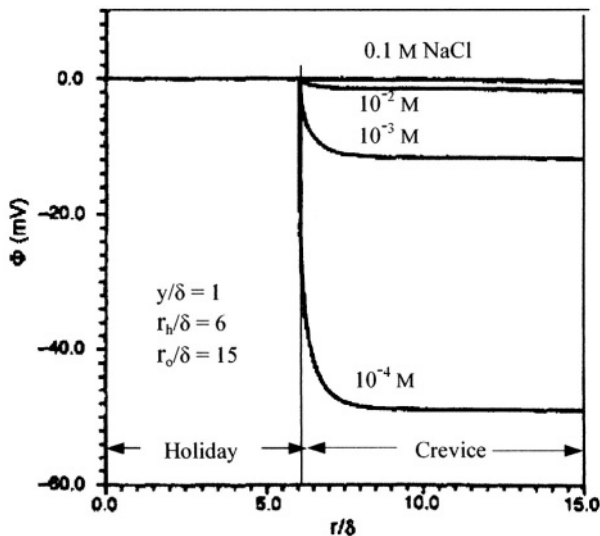


Figure 8.18 Potential of crevice as a function of dimensionless radius [25].

8.9 CREVICE GROWTH RATE

The inward crevice growth rate (dy/dt) may be predicted using Faraday's law. Letting $dy/dt = r^*$ in eq. (3.13b) yields

$$\frac{dy}{dt} = \lambda I \quad (8.54)$$

$$\lambda = \frac{A_w}{ZF\rho A_c} \quad (8.55)$$

where λ = Rate constant ($cm/A.s$)
 I = Current (A)
 Z = Valence
 F = 96,500 $A.s/mol$
 ρ = Density of steel (g/cm^3)
 $A_c = \pi r^2$ = Crevice area (cm^2)
 r = Radius of crevice

Integrating eq. (8.54) yields the crevice depth

$$\int_{y_o}^{y_c} dy = \lambda I \int_0^t dt \quad (\text{Theoretical}) \quad (8.56)$$

$$y_c = y_o + \lambda I t \quad (8.57)$$

which implies that the crevice depth y_c increases with increasing current and time. The term y_o is the initial depth.

Previous work by MacDonald et al. [29-30] and Liu et al. [31] suggest that pit growth data can be fitted to an empirical relationship of the form

$$\frac{dy}{dt} = \beta t^n \quad (\text{Empirical}) \quad (8.58)$$

$$y_c = y_o + \frac{\beta}{1+n} t^{1+n} \quad (8.59)$$

where $0.40 \leq n \leq 0.70$ for different materials under different corrosive conditions.

Despite the several mathematical models being developed for describing corrosion problems and their solutions, each model has its own degree of accuracy, which depends on the chosen variables and conditions, and numerical method for determining relevant parameters that describe a particular corrosion phenomenon. Comprehensive reviews of models for describing a particular problem, such as crevice cathodic protection, pitting growth rate, current and potential attenuation are available in the literature [2,3,18, 25-32].

8.10 DESIGN FORMULAE

The given design guidelines included in this section are for cathodic protection of onshore, offshore, underground, and hybrid structures. The practical application of cathodic protection is inherently complex since an optimum design requires theoretical knowledge of electrochemical principles, an imaginary engineering mind for proper judgement on engineering decision, and a sense of artistic approach. Thus, a cathodic protection designer must consider the following

- The size and lifetime of the structure
- Environmental diversity and economical impact
- Impressed-current, sacrificial anode or hybrid systems.
- Coating material and coating decay that leads to current drainage
- The applied current, potential, electrolyte-to-anode resistance, and wiring resistance.
- The instrumentation capacity
- Experience

For cathodically protecting an offshore structure, use the current densities given in Table 8.3. Valuable formulae are given in Table 8.4 for coatings and anodes. The reader should consult the cited references for additional details.

Table 8.3 Required current density for steel surfaces in seawater [9].

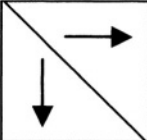
	Current Density i ($\mu\text{A}/\text{cm}^2$)			
	Uncoated Steel		Coated Steel	
	To Polarize	After Polarization	To Polarize	After Polarization
Moving Seawater	32 – 37	7 – 11	3 – 5	1 – 2
Stagnant Seawater	16 – 27	4 – 7	1 – 3	0.5 – 1
Soil Zone	4 – 5	1 – 2	0.5 – 1	0.1 – 0.5

Table 8.4 Formulae for coating and anode design life.

Parameter	Formula	Ref.																		
Total Required	$A_T = \sum \alpha' A_s \quad A_s = \pi N d L$																			
Surface Area	<table border="1"> <thead> <tr> <th>Coating life</th> <th colspan="2">α'</th> </tr> <tr> <th>L_c (years)</th> <th>Initial</th> <th>Final</th> </tr> </thead> <tbody> <tr> <td>10</td> <td>0.02</td> <td>0.10</td> </tr> <tr> <td>20</td> <td>0.02</td> <td>0.30</td> </tr> <tr> <td>30</td> <td>0.02</td> <td>0.60</td> </tr> <tr> <td>40</td> <td>0.02</td> <td>0.90</td> </tr> </tbody> </table>	Coating life	α'		L_c (years)	Initial	Final	10	0.02	0.10	20	0.02	0.30	30	0.02	0.60	40	0.02	0.90	[6-7]
	Coating life	α'																		
	L_c (years)	Initial	Final																	
	10	0.02	0.10																	
	20	0.02	0.30																	
30	0.02	0.60																		
40	0.02	0.90																		
Total Weight of Anodes	$W = (i A_T L_d) / (F_e F_u C_a) = (I L_d) / (F_e F_u C_a)$ $W = (3\pi I L_d) / (7 C_a)$ (Average)	[9]																		
Anode Life	$L_d = (M F_e F_u C_a) / (I)$ $L_d = (7 M C_a) / (3\pi I)$ (Average)	[6]																		
Number of Anodes	$N = A i / I$ $N M \geq W$	[6]																		
Where α' = Coating break down factor M = Mass of a single anode F_e = Efficiency Factor = 0.85 – 0.95 $F_e = 0.90$ (Average) F_u = Utilization factor = 0.75 – 0.85 $F_u = 0.80$ (Average) i = Current density (A/cm^2) I = Current (A/cm^2)																				

The coating damage during installation and service are important factors to be considered in calculating the average applied current. For instance the following coating damage is suggested in order to adjust the coated and uncoated surface areas per structural zones [9]

- Zone → Installation**
- Tidal Zone (TZ) → 10% coating damage**
- Immersed Zone (IZ) → 15% coating damage** (8.60)
- Soil Zone (SZ) → 50% coating damage**

Figure 8.19 illustrates particular zones as well as suitable locations of anodes on a offshore structure. Figure 8.20 shows some schematic fixed-bottom offshore structures available on the world wide web sites. After a structure is cathodically protected, the coatings deteriorate during service. Therefore, cathodic protection (CP) is maintained, provided that the total applied current is adjusted in order to compensate for coating damage. It is suggested that $\epsilon = 2\%$ coating damage per year is appropriate for a particular prolong life (L_d). Hence, the applied current for polarization and the final current can be defined as, respectively [9]

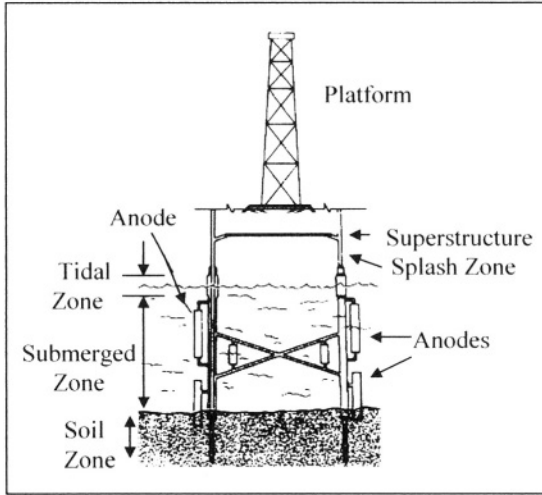


Figure 8.19 Schematic submerged structure [9].

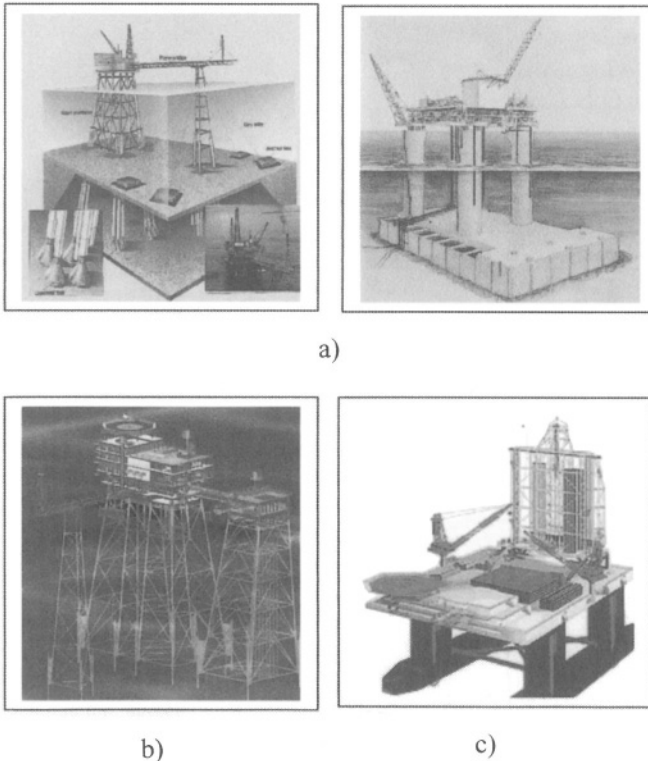


Figure 8.20 Offshore platforms available online. a) www.oil-gas.uwa.edu.au, b) www.dcintl.com, and c) www.titanprojects.com

$$I_p = \sum I_{zone} \quad (8.61)$$

and the final current is defined as

$$I_f = (1 - \lambda_i - \lambda_c L_d) (Ai)_{zone} \quad (8.62)$$

where λ_i = Fraction of installation damage

λ_c = Fraction of coating damage per year

A_{zone} = Surface area per zone per uncoated or coated steel

i_{zone} = Current density from Table 8.3 or predicted ($\mu A/cm$)

The average current is

$$I = \frac{I_p + I_f}{2} \quad (8.63)$$

Anode Resistance. The impressed-current system permits variability of the current out and monitor-control instrumentation. However, interactions with nearby structures may cause detrimental results. On the other hand, sacrificial anode systems do not require a power source and are easily installed, but large numbers of anodes are needed to protect structures. In addition, offshore structures are cathodically protected by hybrid systems [13].

The following formulae are compiled from Currer and Gerrard [13] and Heidersbach [9]. Other formulas for specific cathodic protection design can be found elsewhere [14-16]. The electrolyte-to-anode resistance equations are given in Table 8.5.

Table 8.5 Resistance Formulae for underground anodes.

Anode	Formula	Ref.
Single Horizontal Rod or pipe	$R_h = \rho_x / (2\pi L) [\ln(4L/d) - 1]$	[13]
Single Vertical Rod or pipe	$R_v = \rho_x / (2\pi L) [\ln(8L/d) - 1]$	[13,17]
N Vertical Parallel Rods	$R_v = \rho_x / (2\pi NL) \{ [\ln(8L/d) - 1] + (2L/S) \ln(2N/\pi) \}$	[13]
Flush Mounted Plate or Bracelet	$R_f = \pi \rho_x / (10\sqrt{A})$	[7]
Where R_h, R_v, R_f = Resistances (ohm) ρ_x = Soil resistivity (ohm.cm) L = Length of anode (cm) N = Number of anodes S = Anode spacing (cm) d = Rod diameter (cm) $d = \sqrt{A_a/\pi}$ = For non-cylindrical shapes A_a = Cross-sectional area of anodes (cm ²)		

Example 8.3 a) Determine the power supply output for cathodically protecting several onshore steel storage tanks using 15 sacrificial anodes. Use (4cm) \times (4cm) \times (150cm) Al – Zn – Sn cast anodes, which are to be installed vertically in coke breeze backfill for a uniform current distribution. The anode spacing is 500 cm and the soil resistivity is 5,000 ohm.cm. In addition, the anode-backfill couples are buried in the soil and the backfill bags are large enough. The initial applied current is 4 amperes. Calculate b) the total weight of the anodes for a lifetime of 20 years and c) the individual anode weight (M).

Solution:

$$N = 15 \text{ anodes}$$

$$\rho_x = 5,000 \text{ ohm.cm}$$

$$S = 500 \text{ cm}$$

$$I = 4 \text{ A}$$

$$A_a = (4\text{cm}) (4\text{cm}) = 16 \text{ cm}^2$$

$$d = \sqrt{A_a/\pi} = \sqrt{(16 \text{ cm}^2)/\pi}$$

$$d = 2.26 \text{ cm}$$

$$L = 150 \text{ cm}$$

From Table 8.5,

$$R_w = \rho_x / (2\pi N L) \{ [\ln(8L/d) - 1] + (2L/S) \ln(2N/\pi) \}$$

$$R_w = 2.34 \text{ ohm}$$

From Ohm's law,

$$E = IR_w = 9.36 \text{ V}$$

The power supply should have a capacity greater than 9.36 V. That is, $E_{ext} > 9.36 \text{ V}$. (If 4 – cm diameter rods are used, then $R_w = 2.14 \text{ ohm}$, $E = 8.56 \text{ V}$ with a difference of 8.5%).

From Table 8.4, the total exposed area is

$$A_T = \pi N d L = 35,979.09 \text{ cm}^2 = 3.60 \text{ m}^2$$

$$i = I/A_T = 1.11 \times 10^{-4} \text{ A/cm}^2 \quad (\text{Initial current density})$$

From Table 8.2, the average Al-Zn-Sn anode capacity is

$$C_a = (925 + 2600) / 2 = 1,762.50 \text{ A.h/Kg}$$

From Table 8.4, the total average and individual weight of the anodes are

$$W = (3\pi I L d) / (7C_a)$$

$$W = [(3\pi) (4 \text{ A}) (20 \times 365 \times 24 \text{ h})] / [(7) (1,762.50 \text{ A.h/Kg})]$$

$$W \simeq 535 \text{ Kg} \quad (\text{Initial weight})$$

$$M = W/N \simeq 36 \text{ Kg} \quad (\text{Initial weight of an anode})$$

So far the tank coating is intact since the tanks are coated after installation. Assume a 2% ($\lambda_c = 0.02$) deterioration of the coating per year so that the total damage in 20 years is 40%. From eq. (8.62), the final current along with zero installation damage ($\lambda_i = 0$) is

$$I_f = (1 - 0.40)(A_T)(i) = 2.40 \text{ A}$$

From Table 8.3, the current density for polarizing the steel is $i_p = 1 \mu\text{A}/\text{cm}^2$. Then, the polarizing and maintenance (average) currents are, respectively

$$I_p = i_p A_T = (10^{-6} \text{ A}/\text{cm}^2)(35,979.09 \text{ cm}^2) \simeq 0.04 \text{ A}$$

$$I = (I_f + I_p)/2 = 1.22 \text{ A} \quad (\text{For maintenance})$$

Now, the estimated cathodic potential and the rectifier or power supply potential are, respectively

$$E = IR_w = (1.22 \text{ A})(2.34 \text{ ohm}) = 2.51 \text{ V}$$

$$E_{\text{rect}} > 2.51 \text{ V, say 5 volts!}$$

Thus, the final and individual weight of the anodes in 20 years are

$$W = (3\pi IL_d) / (7C_a)$$

$$W = [(3\pi)(1.22 \text{ A})(20 \times 365 \times 24 \text{ h})] / [(7)(1,762.50 \text{ A.h}/\text{Kg})]$$

$$W \simeq 163 \text{ Kg} \quad (\text{Final total weight})$$

$$M = W/N \simeq 11 \text{ Kg} \quad (\text{Final weight of an anode})$$

These results represent (100%) (36 Kg – 11 Kg) / (36 Kg) \simeq 69% reduction in anode weight at the end of the 20-year design life.

Example 8.4 Cathodically protect an offshore steel platform in moving seawater. The platform has to be polarized using **Al-Zn-In** anodes. Use the data given below to determine the applied potential and applied current for maintenance. The procedure below is similar to Heidersbach, Baxter, Smart III, and Haroun example [35].

Design life	$L_d = 20 \text{ years}$
Single anode volume	$V = (0.25\text{m}) \times (0.25\text{m}) \times (2.50\text{m})$
Anode density	$\rho = 2.315 \text{ g}/\text{cm}^3 = 2,315 \text{ Kg}/\text{m}^3$
Anode cross-sectional area	$A_a = 0.0625 \text{ m}^2 = 625 \text{ cm}^2$
Platform surface area	$A_w = 50\text{m} \times 60\text{m} = 3.0 \times 10^7 \text{ cm}^2$ (Water) $A_s = (55\text{m}) \times (80\text{m}) = 4,400 \text{ m}^2$ (Soil) $A_T = A_w + A_s = 7,700 \text{ m}^2$
Water resistivity	$\rho_x = 25 \text{ ohm.cm}$
Polarized current density	$i_p = 5 \mu\text{A}/\text{cm}^2$ (From Table 8.3)
Anode capacity	$C_a = 2,650 \text{ A.h}/\text{Kg}$ (Average, Table 8.2)
Steel potential	$E_s = 0.25 \text{ V}$ (From Table 8.2)
Anode potential	$E_a = -1.00 \text{ V}_{\text{Ag}/\text{AgCl}}$ (From Table 8.2)

Solution:

Total current in the water and soil zones is needed to calculate the number of anodes for protecting the steel structure. Thus,

$$I_w = i_p A_w = (5 \mu\text{A}/\text{cm}^2) (3.0 \times 10^7 \text{ cm}^2) = 150 \text{ A (Water)}$$

$$I_s = i_p A_s = (5 \mu\text{A}/\text{cm}^2) (4.4 \times 10^7 \text{ cm}^2) = 220 \text{ A (Soil)}$$

$$I = i_p A_T = (5 \mu\text{A}/\text{cm}^2) (7.7 \times 10^7 \text{ cm}^2) = 385 \text{ A (Total)}$$

From Table 8.4, the average weights are

$$W = (3\pi I L_d) / (7C_a) = (3\pi/7) (385 \text{ A}) (20 \text{ y}) / (2,650 \text{ A.h/Kg})$$

$$W = 34,270.63 \text{ Kg (Total)}$$

$$W_w = (3\pi I_w L_d) / (7C_a) = (3\pi/7) (150 \text{ A}) (20 \text{ y}) / (2,650 \text{ A.h/Kg})$$

$$W_w = 13,352.19 \text{ Kg (Total in the water zone)}$$

$$W_s = W - W_w = 34,270.63 \text{ Kg} - 13,352.19 \text{ Kg}$$

$$W_s = 20,918.44 \text{ Kg (Total in the soil zone)}$$

$$M = \rho V = (2,315 \text{ Kg/m}^3) (0.15625 \text{ m}^3)$$

$$M = 361.72 \text{ Kg (Each anode)}$$

Number of anodes:

$$N = W/M = (34,270.63 \text{ Kg}) / (361.72 \text{ Kg}) = 95 \text{ Total anodes}$$

$$N_w = W_w/M = (13,352.19 \text{ Kg}) / (361.72 \text{ Kg}) = 37 \text{ Anodes in water zone}$$

$$N_s = N - N_w = 95 - 37 = 58 \text{ anodes in the soil zone}$$

From Table 8.5, the vertical anode resistance is

$$d = \sqrt{A_a/\pi} = \sqrt{(625 \text{ cm}^2)/\pi} = 14.10 \text{ cm}$$

$$R_v = \rho_x / (2\pi L) [\ln(8L/d) - 1]$$

$$R_v = \frac{(25 \text{ ohm.cm})}{(2\pi)(2.5 \times 10^2 \text{ cm})} \{ \ln [(8)(2.5 \times 10^2 \text{ cm}) / (14.10 \text{ cm})] - 1 \}$$

$$R_v = 0.06294 \text{ ohm}$$

From ohm's law, the initial current and current density, and rectifier output are determined as follows:

$$I_i = \Delta E / R_v = (E_a - E_s) / R_v = (1.00 \text{ V} - 0.25 \text{ V}) / (0.06294 \text{ V/A})$$

$$I_i = 11.92 \text{ A}$$

$$i = N I_i / A_T = (95)(11.92 \text{ A}) / (625 \text{ cm}^2) = 1.81 \text{ A/cm}^2$$

$$E_{\text{rect}} > E = E_s - E_a = 1.00 \text{ V} - 0.25 \text{ V} = 0.75 \text{ V}$$

Maintenance current and potential:

$$I_m = I_i / N = (385 \text{ A}) / 95 = 4.05 \text{ A}$$

$$E_m = I_m R_v = (4.05 \text{ A}) (0.06294 \text{ V/A}) = 0.25 \text{ V}$$

Therefore, the current $I_m = 4.05 \text{ A}$ is adequate for the design life because the calculated the design life must be $L_{\text{new}} \geq L_d$. Thus,

$$L_{\text{new}} \geq (7MC_a) / (3\pi I_m) = 20 \text{ years}$$

8.11 DESIGNING PRESSURE VESSELS

The objective of this section is to provide the reader with some insights of pressure vessels used nowadays in our daily life and subsequently derive expressions for predicting the current and potential developed during cathodic protection of pressure vessels using sacrificial anodes. Among many type of pressure vessel designs the domestic electric water heater schematically depicted in Figure 8.21 is of interest in this section. There are also gas water heaters available in the market. According to the ASME Code Sections IV and VIII, electric water heaters operate at 125 or 150 *psi* working pressure. The pressure vessel is a cylinder normally made of a carbon steel, which is commonly coated internally with vitreous silica compound known as porcelain enamel linings (glass coating) for protecting the steel walls against the corrosive action of portable water and possibly dissolved minerals, which in turn may enhance the electric conductivity of the water. The thickness of the glass coating is in the order of **254 μm** (10 *mils*), which serves as the primary protection against corrosion. During the manufacturing process of the vessel, the glass coating is accomplished by spraying a uniform layer of slurry silicate on the steel inner surface and subsequently, the layer is fired at approximately 900°C. As result, the glass coating protects the steel due to its highly corrosion resistance. With respect to the electric water heater components, the TPR valve stands for **temperature-pressure relief (TPR) valve**, which is a safety device that releases pressure when the temperature or pressure reaches an unsafe level.

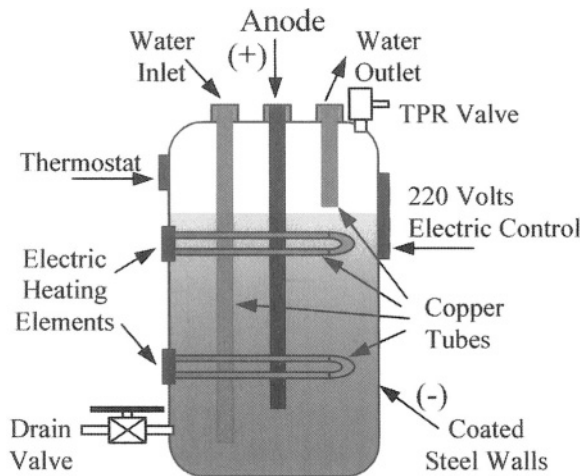


Figure 8.21 Schematic electric water heater.

Further protection of the steel vessel against corrosion is achieved by placing one or two magnesium (Mg) or Mg-alloy anode rods in a vertical position as

shown in Figure 8.21. This, then, is a secondary or supplemental corrosion protection to mitigate localized galvanic cells in the interior of the vessel. For convenience, the chemical composition and the average anode capacity (C_a) of two commercially available extruded Mg-alloy anode rods are given in Table 8.6. According to the electromotive (emf) series given in Table 2.2, Mg is anodic to Fe and consequently, the Mg anode is sacrificed during cathodic protection. This means that the electron flow due to the electrochemical reaction $Mg \rightarrow Mg^{+2} + 2e$ is a measure of current flow inside the pressure vessel. The electron flow is directed to bare steel inner areas, such as sharp corners and fittings. In addition, the oxidation potential range for Galvorod and Galvomag are 1.4-1.5 volts and 1.6-1.7 volts vs. $Cu/CuSO_4$ reference electrode [39].

Table 8.6 Chemical composition (%) of anode rods and average anode capacity (C_a) of 1,125 A.h/Kg [39]								
Alloy	Mg	Al	Mn	Zn	Si	Cu	Fe	Ni
						(Maximum)		
Galvorod	Bal.	2.5-3.5	≥ 0.20	0.7-1.3	0.05	0.01	0.002	0.001
Galvomag	Bal.	≤ 0.01	0.5-1.3	-	-	0.02	0.03	0.001

Despite that the glass coating and the sacrificial anode cathodically protect the pressure vessel, a through the thickness crack, which is an imperfection, in the glass coating is detrimental to steel because it would eventually corrode in hot water. In fact, galvanic corrosion may occur in the interior of the pressure vessel due to presence of impurities in the water, oxygen, and dissimilar metallic materials, such as brass (Cu-Zn alloy) electric heating elements, brass fittings and drain, inlet and outlet nipples. This implies that localized electrochemical galvanic cells may develop, proceed readily at relatively high temperatures, and consequently, the vessel lifetime is reduced due to high corrosion rates. For instance, the usefulness of the sacrificial anode for corrosion protection is clearly shown in Figure 8.22, which depicts sound, partially sacrificed, and depleted Mg anodes rods. This figure also indicates the galvanic corrosion of the Mg anode rods. In fact, each anode has a steel core wire placed lengthwise through its center. The threaded upper part is for easy installation or replacement. In addition, the corrosion rate the depleted Mg anode rod is usually low and therefore, its lifetime is long enough in terms of years, provided that the water heater works efficiently.

Eventually, the cathodic protection may fail and consequently, the inner steel surface corrodes. One particular case is shown in Figure 8.23 for an old gas water heater and its pertinent sediment. The lifetime of the anode depends on the water temperature, the glass coating quality, and the water chemistry. Therefore, inspection of the anode must be done according to the manufacturer recommendations or experience in order to avoid corrosion in the interior of the vessel. Apparently, a 5-year period after anode installation may be a good practice, but it depends on the water heater efficiency. If a water heater operates very efficiently, then the anode can last 10 or more years.

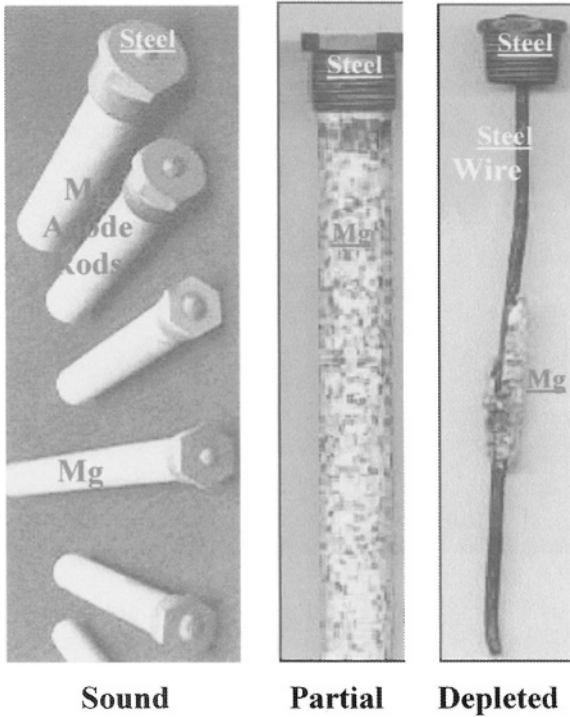


Figure 8.22 Photos of Mg anode rods. The photo for the sound rod was taken from Ref. [39] and the other two photos were taken from Ref. [40].

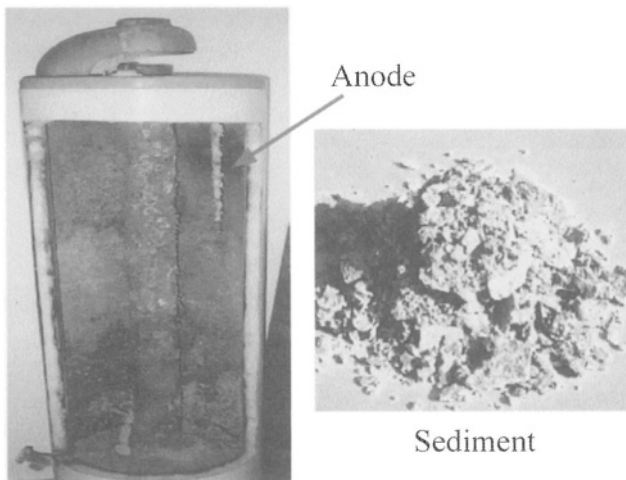


Figure 8.23 Corroded gas water heater and sediment [41]

The second part of this section is based on Faraday's law, which states that the rate of thickness reduction is a measure of corrosion rate, which in turn, is a direct representation of structural damage. Let's start with the rate of weight loss equation given by eq. (3.10e)

$$\frac{W}{t} = \frac{iAA_w}{zF} \quad (8.64)$$

Divide eq. (8.64) by the product $A\rho = AW/V = W/B$, where A is the vessel exposed area, ρ is the density of the metal. Solving for the thickness B yields

$$B = \frac{iA_w t}{zF\rho} \quad (8.65)$$

For a cylindrical pressure vessel, the thickness B in eq. (8.65) must satisfy the average hoop stress (average tangential stress) equation defined by

$$\sigma = \frac{PD}{2B} \quad (8.66)$$

where P = Internal pressure (MPa)

D = Internal diameter

Combining eqs. (8.65) and (8.66) yields the current density

$$i = \frac{zF\rho PD}{2\sigma t A_w} \quad (8.67)$$

and the corrosion rate becomes

$$C_R = \frac{iA_w}{zF\rho} = \frac{PD}{2\sigma t} \quad (8.68)$$

For coated structures, wisely assume or determine the coating efficiency in order to compute the bare surface and the corresponding current that must protect the bare surface from corrosion. The bare area and the current are easily determined as

$$A_s = A_o(1 - \lambda_s) \quad (8.69)$$

$$I = i_{corr} A_o(1 - \lambda_s) \quad (8.70)$$

where λ_s = Fraction of the protected surface area

A_o = Total surface area

In addition, cathodic protection based on sacrificial anodes requires a cell potential as the driving force for a self-imposed spontaneous protective current imparted by sacrificial anodes liberating electrons at a specific rate [42]. The driving force for this current is the potential difference (overpotential) between the sacrificial anode and cathode; that is, $E = E_c + E_a$. In fact, the resultant

electrochemical system is a naturally polarized galvanic cell, in which the anode is oxidized or sacrificed to provide electrons to the cathodic structure. In general, an alloy, instead of a pure element, with known standard potential and being anodic to the a structure is normally used as a sacrificial anode (Table 8.6).

For carbon steel structures, the NACE recommended protective potential, $E_c = -0.85 V_{Cu/CuSO_4}$, and the standard potential or emf series (Table 2.2) of an element, which is anodic to iron, can be used to determine the cell potential and the free energy change. Thus, $E = -0.85 V_{Cu/CuSO_4} + E_a$ where E_a from Table 2.2 is for a reduction process and therefore, its sign must be changed and the its magnitude be changed from V_{SHE} to $V_{Cu/CuSO_4}$.

Example 8.5 A vertical cylindrical steel pressure vessel containing oxygenated water is subjected to 15 MPa internal pressure and it is to be cathodically protected using one **Mg-alloy** (Galvorod) anode rod and the NACE recommended potential of $-0.85 V_{Cu/CuSO_4}$. The hoop stress is limited to half the yield strength of the steel; that is, $\sigma = 300 \text{ MPa}$. The tank inside diameter is $D = 40 \text{ cm}$. If the design life (L_d) is 10 years and if the bare inner surface area is 98% coating-protected, calculate a) the corrosion rate as a measure of the rate of thickness reduction and the vessel thickness at the end of its lifetime, b) the cell potential, c) the effective mass of the **Mg-alloy** anode rod, which has 50% current efficiency due to hydrogen evolution, d) the system current density, the anode and the system electric resistances, e) the net current density and the reduction in anode diameter, and f) Will the tank burst at the end of 10 years? Data for steel: $i_{corr} = 65 \mu\text{A}/\text{cm}^2$ (uniform), $A_w = 55.85 \text{ g/mol}$, $\rho = 7.70 \text{ g/cm}^3$, $H = 80 \text{ cm}$ (height of tank) and for the sacrificial **Mg** anode rod: $L = 30 \text{ cm}$, $d = 12 \text{ cm}$, $B = 1.30 \text{ cm}$, $A_w = 24.31 \text{ g/mol}$ and $\rho = 1.74 \text{ g/cm}^3$. The water resistivity is $\rho_w = 1,000 \text{ ohm.cm}$.

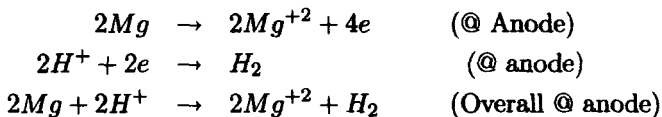
Solution:

a) In fact, corrosion of the steel tank is manifested through the anodic reaction $Fe \rightarrow Fe^{+2} + 2e$. Thus, eq. (8.68) gives the uniform corrosion rate of the bare steel vessel without cathodic protection

$$C_R = \frac{i_{corr} A_w}{zF\rho}$$

$$C_R = \frac{(6.50 \times 10^{-5} \text{ A/cm}^2) (55.85 \text{ g/mol})}{(2) (96,500 \text{ A.s/mol}) (7.70 \text{ g/cm}^3)} = 0.77 \text{ mm/y}$$

This corrosion rate is to be eliminated by sacrificing a **Mg** anode. Thus, the main electrochemical reactions during the cathodic protection process are



The thickness reduction of the steel vessel is

$$B_x = tC_R = (10 \text{ y})(0.77 \text{ mm/y})$$

$$B_x \simeq 7.70 \text{ mm} \quad (\text{Lost thickness})$$

b) The average anodic potential for the chosen **Mg-alloy** anode rod (Table 8.6) is $E_a = 1.45 \text{ V}_{\text{Cu/CuSO}_4}$ and that recommended by NACE is $E_c = -0.85 \text{ V}_{\text{Cu/CuSO}_4}$. Thus, the cell potential is

$$E = E_c + E_a = -0.85 \text{ V} + 1.45 \text{ V}$$

$$E = 0.60 \text{ V}$$

c) The anode volume and its useful mass based on 50% anode current efficiency ($\epsilon = 0.50$) are, respectively

$$V = \frac{\pi d^2 L}{4} = \frac{\pi (12 \text{ cm})^2 (30 \text{ cm})}{4} = 3,392.92 \text{ cm}^3$$

$$m = \epsilon \rho V = (0.5) (1.74 \text{ g/cm}^3) (3,392.92 \text{ cm}^3)$$

$$m = 2.95 \text{ Kg}$$

d) The inner bare area of the vessel is

$$A_s = A_o (1 - \lambda_s) = \pi DH (1 - \lambda_s)$$

$$A_s = \pi (40 \text{ cm}) (80 \text{ cm}) (1 - 0.98)$$

$$A_s = 201.06 \text{ cm}^2$$

This is the area to be protected by the anode for 10 years. Thus, the average self-imposed spontaneous protective current (Table 8.4) and current density imparted by the sacrificial **Mg-alloy** anode are, respectively

$$I = \frac{7mC_a}{3\pi L_d} = \frac{(7) (2.95 \text{ Kg}) (1,125 \text{ A.h/Kg})}{(3\pi) (87,600 \text{ h})}$$

$$I = 28.14 \text{ mA}$$

$$i = \frac{I}{A_s} = \frac{28.14 \text{ mA}}{201.06 \text{ cm}^2} = 0.14 \text{ mA/cm}^2$$

Then, the anode and the system resistances are

$$R_a = \frac{E_a}{I} = \frac{1.45 \text{ V}}{28.14 \times 10^{-3} \text{ A}} = 51.53 \text{ ohm}$$

$$R_s = \frac{E}{I} = \frac{0.60 \text{ V}}{28.14 \times 10^{-3} \text{ A}} = 21.32 \text{ ohm}$$

e) The net current density is controlled by the cathodic current density of the steel structure. That is,

$$i_{net} = i_c - i_a \simeq i_{corr}$$

The corrosion rate of the **Mg-alloy** is

$$\begin{aligned} C_R &= \frac{iA_w}{zF\rho} \\ C_R &= \frac{(0.14 \times 10^{-3} \text{ A/cm}^2) (24.31 \text{ g/mol})}{(2) (96,500 \text{ A.s/mol}) (1.74 \text{ g/cm}^3)} \\ C_R &= 0.32 \text{ mm/y} \quad (\text{Anode}) \end{aligned}$$

Assuming a uniform anode corrosion, one can predict the diameter reduction or lost as

$$d_x = tC_R = (8.76 \text{ y}) (2.74 \text{ mm/y}) = 24 \text{ mm} = 2.4 \text{ cm}$$

f) In this part of the example, the minimum vessel thickness (B_m) is calculated using the theory of thin-walled vessels and the average hoop stress (average tangential stress). Thus,

$$\begin{aligned} B_m &= \frac{PD}{2\sigma} \\ B_m &= \frac{(15 \text{ MPa}) (40 \text{ cm})}{(2) (300 \text{ MPa})} \\ B_m &= 1 \text{ cm} = 10 \text{ mm} \end{aligned}$$

Now, the final thickness (B_f) due to corrosion at the end of 10 years is

$$\begin{aligned} B_f &= B - B_x \\ B_f &= 13 \text{ mm} - 7.7 \text{ mm} \\ B_f &= 5.30 \text{ mm} \end{aligned}$$

Therefore, the vessel will burst because $B_f < B_m$. This particular design can be enhanced by using a thicker steel vessel so that

$$\begin{aligned} B &> B_m + B_x = 10 \text{ mm} + 7.7 \text{ mm} \\ B &> 17.70 \text{ mm} \end{aligned}$$

The actual design thickness is subjected to the designer's experience or a particular design code, such as the ASME code for pressure vessels.

8.12 SUMMARY

Cathodic protection is nowadays an electrochemical technique well understood from an engineering point of view. The theoretical aspects of the electrochemical mechanisms need to be further investigated in order to develop new mathematical models that will provide more accurate results. However, cathodic protection is a design approach for preventing corrosion on metallic structures, such as steel tanks, buried pipelines and offshore systems. Either impressed-current or sacrificial anode techniques are widely used to protect large structures. The choice of technique to design against corrosion depends on the type of structure and degree of corrosiveness of the environment. This technique requires a dc input for controlling the applied potential and current density.

Among several cathodic protection criteria recommended by NACE, the most common criterion is the half-cell potential, which predicts the theoretical potential to be $-0.59 V_{SHE} = -0.90 V_{Cu/CSO_4}$ for iron in neutral environments. This theoretical value is close to NACE potential ($-0.85 V_{Cu/CSO_4}$). On the other hand, overprotection at $E < E_{corr}$ can be harmful because of hydrogen evolution and diffusion of atomic hydrogen into the structure causing hydrogen embrittlement.

In addition, the phenomenon of potential attenuation has been theoretically included as a crude approximation as predicted by the Charge Disk and Uhlig models. Both models exhibit similar potential profiles. Finally, sets of formulae used in cathodic protection are given as mathematical recipes for practical purposes in the field of corrosion prevention.

Structure integrity can be achieved using well established cathodic protection (CP) criteria, but potential measurements must be carried out at discrete time interval to assure that the structure is maintained polarized at the design potential. In general, CP criteria are based on external potential and current, but the former is the parameter that requires close control. Absolute CP is based on the theory of electrochemistry since it predicts zero corrosion rate when the forward and reverse reaction rates are exactly the same. This implies that reliable CP systems are required to be kept polarized at the equilibrium potential so that $i_{corr} = 0$.

A reliable CP design strongly depends on the environment and anode materials, which are characterized by their anode capacity. The most common anodes are AL-alloys, Mg-alloys, and Zn-alloys.

8.13 PROBLEMS/QUESTIONS

8.1 Why cathodic protection is not generally recommended for stress corrosion problems on high-strength ferritic steels?

8.2 A steel structure exposed to seawater is to be cathodically protected using the sacrificial anode technique. calculate a) the number of **Zn** anodes (N) that will be consumed in a *year* if the **Zn** anode capacity is **770 A.h/Kg** (average value as per Table 8.2) and the current is **0.70 amps.**, and b) the individual weight (M) of anodes so that $NM \geq W$, where W is the total theoretical weight of the anodes. [Solution: a) $N \simeq 1$ and b) $m = 7.48 \text{ Kg}$].

8.3 Cathodically protect the pressurized steel tank in **Example 8.3** using one flush mounted **Mg-Al-Zn** bracelet. Assume 2% tank coating damage per year and neglect any installation damage if the tank is coated after installation. Use a bracelet with dimensions equal to $(0.50\text{cm}) \times (3\text{cm}) \times (6\text{cm})$. a) What can you conclude from the calculated maintenance current and current density? Will it be convenient to protect the tank? b) Will the tank explode at the end of the anode life time? Assume that $\rho = 1.74 \text{ g/cm}^3$ and $A_w = 24.31 \text{ g/mol}$ for the anode Mg-alloy and $\rho_x = 5,000 \text{ ohm.cm}$ for the soil. [Solution: $I_i = 7.74 \mu\text{A}$, $E_i = 2.87 \text{ mV}$, $W_i = 1.86 \text{ g}$ of anode, $I_f = \bar{I} = 6.64 \mu\text{A}$, $E_f = 2.38 \text{ mV}$].

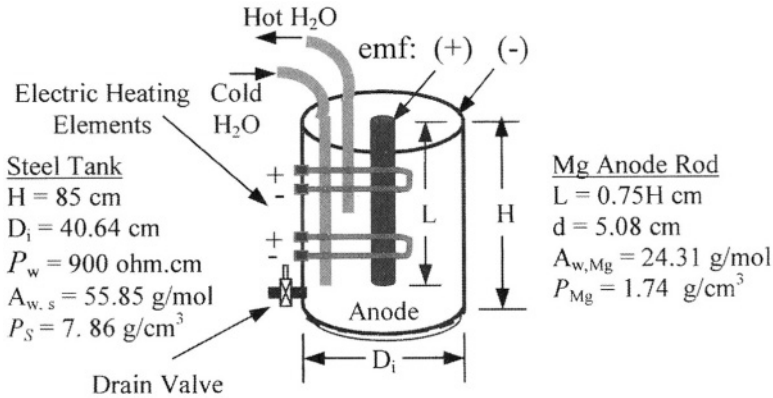
8.4 A 2-m diameter steel tank containing water is pressurized at 200 kPa. The hoop stress, thickness, and height are 420 MPa, 2 cm, and 8 cm, respectively. If the measured corrosion rate is 0.051 mm/y, determine a) the tank life and b) the developed current. Data: $\rho = 7.86 \text{ g/cm}^3$ and $A_w = 55.86 \text{ g/mol}$. [Solution: a) $t = 9.34 \text{ years}$ and b) $I = 92.49 \text{ A}$].

8.5 a) Derive eq. (8.4) and b) calculate the theoretical anode capacity for magnesium and zinc. [Solution: b) $C_a(\text{Mg}) = 2,969 \text{ A.h/Kg}$ and $C_a(\text{Zn}) = 1,104 \text{ A.h/Kg}$].

8.6 Show that $\alpha = \sqrt{R_s/R_L}$.

8.7 Use an annealed (@ 792°C) 1040 steel plate of $B = 0.635 \text{ cm}$ thickness to design a cylindrical pressurized vessel using a safety factor (SF) of 2. The annealed steel has a yield strength of 355 MPa. Calculate a) the average allowable pressure according to the theory for thin-walled vessels. Will the vessel fail when tested at 2 MPa for 10 minutes? If it does not fail, then proceed to cathodically protect the cylindrical pressure vessel as a domestic or home water heater having a cylindrical magnesium (**Mg**) anode rod. All dimensions shown below. Calculate b) the applied hoop stress, the current, the potential for polarizing the heater and the resistance of the system, c) the theoretical anode capacity and the anode lifetime of the anode in years and d) how much electric energy will delivery the Mg anode rod? The steel vessel has a 98% internal glass coating (vitreous porcelain enamel lining) for protecting the steel inner

wall against the corrosive action of portable water. Assume a water column of 76.20 cm and an internal pressure of 1 MPa. Assume that the exterior surface of the steel vessel is coated with an appropriate paint for protecting it against atmospheric corrosion and that the anode delivers $1.5 V_{Cu/CuSO_4}$. The NACE recommended potential for steels is $-85 V_{Cu/CuSO_4}$.



8.14 REFERENCES

[1] D.A. Jones, "Principles and Prevention of Corrosion" Macmillan Publishing Company, New York, (1992) 442.

[2] V. Ashworth, "Principles of Cathodic Protection," in Corrosion Control, Third edition, edited by L.L. Shreir, R.A. Jarman, and G.T. Burstein, Butterworth-Heinemann, (1994) 10:24.

[3] H.H. Uhlig and R.W. Revie, "Corrosion and Corrosion Control" John Wiley, New York, (1985) 217-223.

[4] S.L. Pohlman, "Stray-Current Corrosion" in Corrosion Vol 13, Ninth edition, ASM Handbook, ASM International, (1987) 87.

[5] M.G. Fontana, "Corrosion Engineering," third edition, McGraw-Hill Book Company, New York, (1986).

[6] L. Sherwood, "Sacrificial Anodes," in Corrosion Control Vol. 2, third edition, Edited by L.L. Sheir, R.A. Jarman, and G.T. Burstein, Butterworth-Heinemann, Boston, (1994) 10:29-10:54.

[7] Det Norske Veritas Recommended Practice, "Cathodic Protection Design," RP B401, March (1993).

- [8] J.W.L.F. Brand and P. Lydon, “*Impressed-current Anodes*” in Corrosion Control Vol. 2, third edition, Edited by L.L. Sheir, R.A. Jarman, and G.T. Burstein, Butterworth-Heinemann, Boston, (1994) 10:56-10:87
- [9] R.H. Heidersbach, “*Cathodic Protection*,” Corrosion, Vol. 13, Handbook, ASM International, (1987) 466-477.
- [10] G.D. Brady, Materials Performance, Vol. 10, No. 10, (1971) 20.
- [11] H. Heink, Ind. Eng. Chem., 47 (1955) 684.
- [12] “Corrosion Control on Steel, Fixed Offshore Platforms Associated with Petroleum Production,” NACE EP-01-76, (1976).
- [13] G.W. Curren and J.S. Gerrard, “*Practical Application of Cathodic Protection*,” in Corrosion Control Vol. 2, third edition, Edited by L.L. Sheir, R.A. Jarman, and G.T. Burstein, Butterworth-Heinemann, Boston, (1994) 10:93.
- [14] M.E. Parker, “*Pipeline Corrosion in Cathodic Protection*,” Gulf Publishing Co., (1962).
- [15] A.W. Peabody, “*Control of Pipeline Corrosion*,” NACE, (1967).
- [16] L. West and T. Lewicki, “*Corrosion Control: General*,” Vol. I and II, Civil Engineering Corrosion Control, NTIS AD/A-004 082 and 083, Air Force Civil Engineering Center, TR 74-6, (Jan. 1975).
- [17] W.T. Bryan, editor, “*Designing Impressed-Current Cathodic Protection Systems with Durco Anodes*” 2nd. edition, The Duriron Company Inc., (1970).
- [18] P. Pierson, K.P. Bethude, W.H. Hartt, and P. Anathakrishnan, Corrosion, Vol. 56, 4 (2000) 350.
- [19] W.H. Hartt and S. Chen, Corrosion, Vol. 56, 1 (2000) 3.
- [20] S. Rossi, P.L. Bonora, R. Pasinetti, L. Benedetti, M. Draghetti, and E. Sacco, Corrosion, 54 (1998) 1018.
- [21] J.D. Burk, “*Dual Anode Field Performance Evaluation-Cathodic Protection for Offshore Structures*” Corrosion/91, Paper No. 309, NACE, Houston, TX, (1991).
- [22] W. Wang, W.H. Hartt, and S. Chen, Corrosion, 52 (1996) 419.
- [23] W.H. Hartt, S. Chen, and D.W. Townley, Corrosion, 54 (1998) 317.
- [24] Z.D. Jastrzebski, “*The Nature and Properties of Engineering Materials*,” John Wiley & sons, New York, (1987) 600-603.
- [25] D.T. Chin and G.M. Sabde, Corrosion, Vol. 56, 8 (2000) 783-793.
- [26] J.S. Newman, “*Electrochemical Systems*,” Prentice-Hall, New Jersey, (1991) 241.
- [27] K. Grasshoff, “*The Electrochemical Determination of Oxygen*,” in Marine Electrochemistry, edited by M. Whitefield and D. Jagner, John Wiley & sons, New York, (1981) 327.
- [28] E.C. Potter and G.E. Everitt, J. Appl. Chem., 9 (1957) 642.
- [29] D.D. McDonald, C. Liu, M. Urquidi-Macdonald, G.H. Stickford, B. Hindin, A.K. Agrawal, and K. Krist, Corrosion, Vol. 50, 10 (1994) 761-780.
- [30] D.D. McDonald et al., SRI Inter. Report to Gas Research Inst. (GRI) No. 5090-260-1969, (Jan. 1992).
- [31] C. Liu, D.D. McDonald, and M. Urquidi-Macdonald, Pennsylvania State University Report to Gas Inst., GRI Contract No. 5092-260-2353, NTIS GRI 93/0365, CAM 9311, (Sept. 1993).

- [32] F. Brichau and J. Deconinck, *Corrosion*, Vol. 50, 1 (1994) 39-49.
- [33] M.E. Parker, "*Pipeline Corrosion and Cathodic Protection*," Gulf Publication Co., Houston, Texas, 1962.
- [34] E.M. Purcell, "*Electricity and Magnetism*" Berkeley Physics Course, Vol 2., McGraw-Hill Book Co., (1965) 43-48.
- [35] R.H. Heidersbach, R. Baxter, John S. Smart III, and M. Haroun, "*Cathodic Protection*," *Corrosion*, Vol. 13, Handbook, ASM International, (1987) 919-924.
- [36] R.B. Mears and R.H. Brown, *Trans. Electrochem. Soc.*, Vol. 74, (1938) 519.
- [37] R.P. Howell, *Corrosion*, Vol. 8, 9 (1952) 300-304.
- [38] D.A. Jones, *Corrosion Science*, Vol. 11, (1971) 439.
- [39] www.farwst.com, 2003
- [40] www.rheem.com, 2003
- [41] www.waterheaterrescue.com
- [42] D.L. Piron, "*The Electrochemistry of Corrosion*," NACE, (1991) 231,

Chapter 9

ANODIC PROTECTION

9.1 INTRODUCTION

Use of anodic protection (*AP*) can be considered when coating and cathodic protection techniques are not suitable for protecting a structure against corrosion. The *AP* technique is normally used very successfully in aggressive environments, such as sulfuric acid (H_2SO_4), and mild solutions [1-4]. The main requirement for *AP* is that the material to be protected must exhibit an active-passive behavior, but the passive potential range must be wide enough and the passive current must be sufficiently low as compared with the corrosion current. Thus, a potentiostat can be used to supply a potential in the passive region of a polarization diagram, but potential monitoring is necessary; otherwise, a potential deviation can make the material to become active and anodic protection is lost.

In anodic protection the structure to be protected is the anode by connecting it to the positive terminal of an electrochemical circuit, whereas the negative cathode is made of steel or graphite. On the other hand, in cathodic protection, the structure to be protected is made the cathode (positive).

9.2 DESIGN CRITERIA

Anodic protection, like cathodic protection, is an electrochemical technique in which the metal or structure is polarized from the critical current density (i_c) as schematically shown in Figure 9.1. In order to anodically protect a structure, such as sulfuric acid (H_2SO_4) storage steel tanks, heat exchangers, and transportation vessels [2,5], the critical current density i_c is high in the active state, but the goal is to force the active state change to a passive state at a potential E_x as shown in Figure 9.1. Thus, the protective parameters are

$$E_{pa} < E_x < E_p \quad (9.1)$$

$$i_x = i_p < i_{corr} \quad (9.2)$$

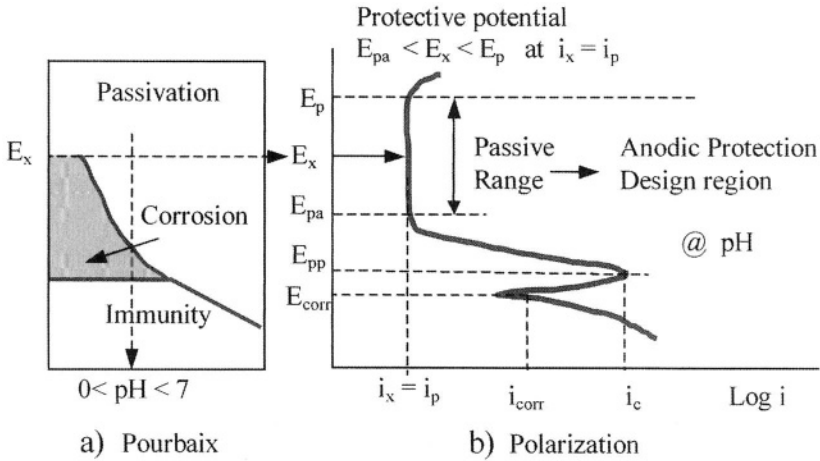


Figure 9.1 Schematic Pourbaix diagram and active-passive polarization curve showing the passive region for anodic protection at E_x .

Also included in Figure 9.1 is an schematic Pourbaix diagram (potential-pH diagram) showing the electrochemical regions needed for characterizing the electrochemical behavior of a metal immersed in an electrolyte. This diagram is related to the polarization diagram (Figure 9.1b). Observe the correspondence of potential in both diagrams. As indicated in Chapter 3, the Pourbaix diagram does not give an indication of the rate of reaction, but the polarization curve does at a pH value indicated by a downward arrow in Figure 9.1a.

Hence, a structure is anodically protected if the metal is active-passive and shows a sufficiently large passive potential range, eq. (9.1), due to the formation of a dynamic oxide film. This implies that the current density depends on time and therefore, the power supply must provide the required potential E_x so that $i_x < i_{corr}$ [1]. Thus, anodic polarization results due to the formation of an insoluble oxide film of a few μm in thickness. The effectiveness of anodic protection depends on the quality of the oxide film in a particular environment and the applied potential. For instance, if the applied potential is $E_x \geq E_p$, then the film corrodes by pitting, which is a localized electrochemical process. On the other hand, if $E_x \leq E_{pa}$ the metal corrodes by general and uniform process.

Passivation may be accomplished due to the accumulation of reacting ions forming an oxide film (metallic coating) on the anode surface. Consequently, the current flowing from the anode to the electrolyte reduces since the metallic coating has a high electric resistance. This can be defined by Ohm's law

$$E_x = I_x R_x \quad (9.3)$$

Figure 9.2 shows a schematic set up for AP of a steel tank for storing an acid solution. Normally, sufficiently large cathodes are needed in order to compensate

for the large structure surface area and the highly conductive electrolyte (acid). This indicates that AP is achieved if the circuit resistance (R_x) due to Ohmic potential drop is controlled and maintained. This phenomenon known as the Ohmic effect.

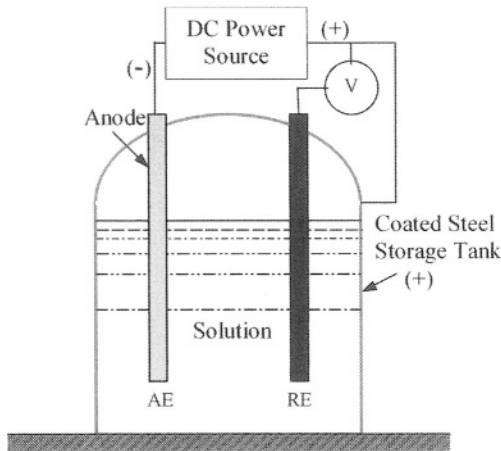


Figure 9.2 Schematic anodic protection system.

The potential E_x is assumed to be constant since anodic protection (AP) is a potential-control technique, in which the power supply is a potentiostat capable of supplying a constant potential; otherwise, a significant change in potential causes a change in the current and the structure may become unprotected due to film breakdown.

A successful anodic protection design, not only requires a controlled potential/current, but a high quality passive film which must be insoluble in the aggressive solution. In fact, the very low anodic corrosion rate in terms of the current density i_p as shown in Figure 9.1 is apparently due to the limited ionic mobility in the passive film [1].

Since the anodic protection technique is restricted to materials that exhibit active-passive transitions, it is important to determine the sensitiveness of the polarization behavior of metallic material exposed to solutions containing contaminants, such as chloride ions, and temperature.

Figure 9.3 schematically illustrates the possible polarization trends based on the above variables. For instance, the protective potential E_x being a measure of anodic protection and the passive potential range, $\Delta E = E_p - E_{pa}$, decreases and the protective current density i_x increases as either chloride concentration in solution and temperature increase. In fact, anodic protection of a material such as stainless steel becomes a complex task if the magnitude of the passive potential range is not sufficiently large. Furthermore, E_x is inversely proportional to i_x as the metallic coating resistance decreases due to the effects of chloride concentration and temperature. Nevertheless, a high critical current

density is required to cause passivation and a low current density is needed for maintaining passivation.

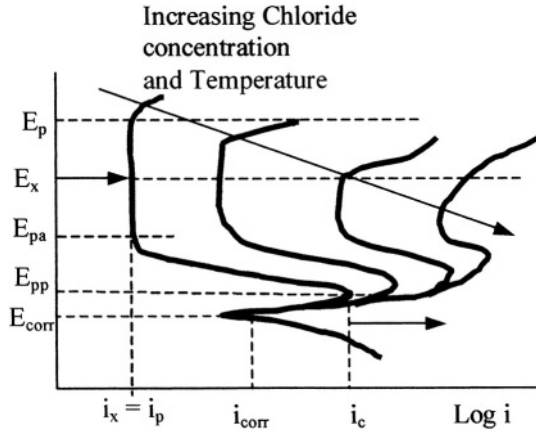


Figure 9.3 Detrimental effects of chloride concentration and temperature on the passive region and critical current density.

9.3 RELEVANT DATA

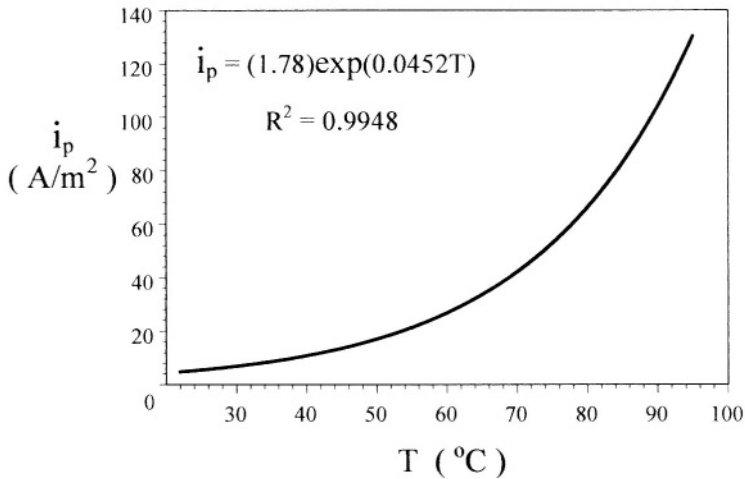
The intend in this section is to provide that reader some experimental data available in the literature. In practice, cathode materials and reference (*RE*) electrodes used in anodic protection are given in Tables 9.1 and 9.2, respectively.

Table 9.1 Cathode materials for anodic protection [2]

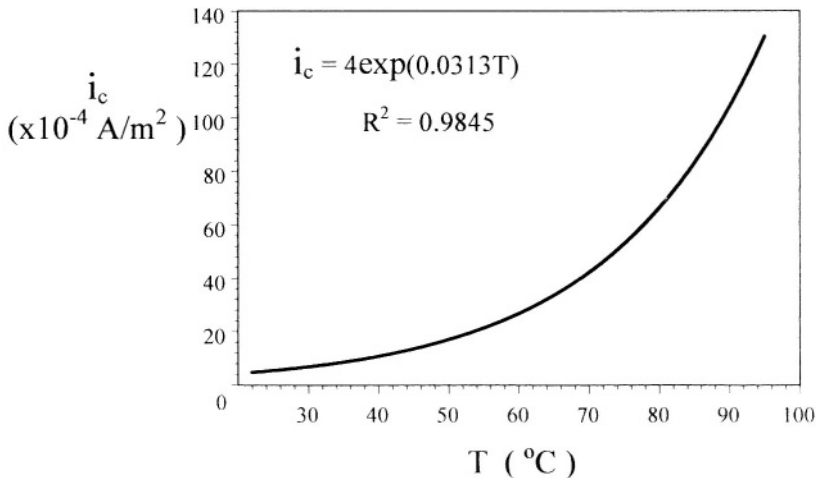
Electrode	Environment
Calomel	Sulfuric Acid
Silicon Cast Iron	Sulfuric Acid
Silver-Silver Chloride	Sulfuric Acid, Kraft Digester Liquid
Copper	Hydroxylamine Sulfate
Stainless Steel	Liquid Fertilizers (Nitrate Solutions)
Nickel-Plate Steel	Chemical Nickel Plating Solutions
Hastelloy	Liquid Fertilizers, Sulfuric Acid

Figure 9.4 shows temperature dependency current density curves for 316 stainless steel exposed to sulphuric acid solution. These curves are the results of nonlinear regression analysis on experimental data found elsewhere [4]. Clearly, both passive (i_p) and critical (i_c) current densities are strongly affected

by temperature. Specifically, both i_p and i_c increase very rapidly at temperatures greater than 60°C. The current density trend illustrated in Figure 9.4 can be considered very unique for 316 stainless steel in sulphuric acid solution.



a) Passive current density



b) Critical current density

Figure 9.4 Effect of temperature on the current density of 316 stainless steel in 67% H_2SO_4 solution [4].

9.4 SUMMARY

Anodic protection (AP) is a potential-control electrochemical technique suitable for preventing corrosion of a metal in aggressive environments, such as sulfuric acid (H_2SO_4). In this technique, the metal to be protected must exhibit passivity at relatively low current density so that the passive current density (i_p) is at least one order of magnitude lower than the corrosion current density (i_{corr}). Care must be exercised in selecting a material that shows a wide enough passive potential range. Thus, the protective potential is $E_{pa} > E_x < E_p$.

Furthermore, AP is normally used when coatings and cathodic protection methods do not provide adequate protection against corrosion.

9.5 REFERENCES

- [1] D.A. Jones, “*Principles and Prevention of Corrosion*,” Macmillan Publishing Company, New York, (1992).
- [2] C.E. Locke, “*Anodic Protection*,” in *Corrosion*, Vol. 13, ASM International, Ninth edition, Metals Handbook, (1987) 463.
- [3] D.A. Shock, O.L. Riggs, and J.G. Sudbury, *Corrosion*, Vol. 16, 2 (1960) 99.
- [4] R. Walker, “*Anodic Protection*” in *Corrosion*, Vol. 2, Corrosion Control, Edited by L.L. Shreir, R.A. Jarman, and G.T. Burstein, Butterworth-Heinemann, Boston, (1994).
- [5] O.L. Riggs and C.E. Locke, “*Anodic Protection: Theory and Practice in the Prevention of Corrosion*” Plenum Press, New York, (1981).
- [6] J.R. Myers, F.H. Beck, and M.G. Fontana, *Corrosion*, Vol. 9, 21 (1965) 277.

Chapter 10

HIGH-TEMPERATURE CORROSION

10.1 INTRODUCTION

High-temperature corrosion (HTC) of metals and alloys is a scale-forming oxidation process in gaseous environments. HTC is influenced by metal temperature, gas composition, exposure time, and pressure and it may be characterized by , thickness reduction (penetration) and rate of oxide thickness growth, which is a measure of the rate of oxidation in oxidizing (O_2), sulfidizing (H_2S), carburizing (CH_4 or CO), and nitriding (N_2) conditions. HTC is also referred to as high-temperature oxidation, tarnishing and scaling, and the rate of attack is significantly increased with increasing temperature.

In characterizing HTC, X-Ray Diffraction is a very useful and reliable technique for indexing patterns of phases leading to phase identification in the corrosion product known as surface scale. In fact, this high temperature phenomenon is different from the rust layer formation (in the presence of moisture) since it virtually occurs in dry gaseous environments or molten salts. In certain cases, HTC may be an internal oxidation process when oxygen diffusion is faster than the surface oxidation rate.

Most experimental data available in the literature is based on weight gain per unit surface area. However, weight gain and thickness reduction or penetration are adequate parameters for assessing HTC. For instance, measurements of metal thickness reduction and oxide layer thickness increments are very important because the former is related to structure strength.

The protectiveness of an oxide layer is significantly dependent on the temperature and corrosive environments. In high-temperature oxygen media, the Pilling-Bedworth law can be used for assessing quantitatively the protectiveness of oxide layers. These layers are also known as scales, but they can be treated as oxide coatings as well. These coatings may protect the surface of equipment components from thermal deterioration.

10.2 THERMODYNAMICS OF OXIDES

Thermodynamically, the driving force for the oxidation of a metal in gaseous environments is the Gibbs free energy of formation (ΔG) and consequently, the occurrence of an oxidation chemical reaction depends on the magnitude of ΔG . Mathematically, ΔG at a constant pressure is defined by

$$\Delta G^\circ = -RT \ln(K) \quad (10.1)$$

$$\Delta G^\circ = \Delta H^\circ - T\Delta S^\circ \quad (10.2)$$

where K is the equilibrium constant, ΔH° is the enthalpy change, which is a measure of the heat absorbed or released at constant gas pressure. The term ΔS° is the entropy change and it is a measure of atomic disorder. The variations of both ΔH° and ΔS° with temperature are given by

$$\Delta H^\circ(T) = \Delta H^\circ(T_o) + \int_{T_o}^T C_p(T) dT \quad (10.3)$$

$$\Delta S^\circ(T) = \Delta S^\circ(T_o) + \int_{T_o}^T \frac{C_p(T)}{T} dT \quad (10.4)$$

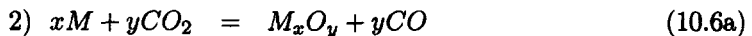
where $\Delta H^\circ(T_o)$ = Standard enthalpy change (kJ/mol) at $T_o = 298^\circ\text{K}$
 $\Delta S^\circ(T_o)$ = Standard entropy change ($\text{kJ/mol}\cdot^\circ\text{K}$) at $T_o = 298^\circ\text{K}$
 C_p = Heat capacity ($\text{kJ/mol}\cdot^\circ\text{K}$) at constant pressure

In addition, a plot of the function given by eq. (10.2) with constant ΔH° and ΔS° gives a straight line, for which ΔH° is the intercept at $T = 0$ and $\Delta S = (\partial\Delta G/\partial T)_p < 0$ is the slope. Thus, a thermodynamic linear behavior of the metal-gas oxidizing system is obtained (Figure 10.1).

Oxidation of a metal caused by oxygen (O_2), carbon dioxide (CO_2), and/or water vapor (H_2O) at relatively high temperatures is briefly described in this section. According to the generalized reactions given below, the standard Gibbs free energy (ΔG°) of oxide formation for varying temperature and gas partial pressure at equilibrium are



$$\Delta G^\circ = -RT \ln \left(\frac{[M_xO_y]^{2x/y}}{[M]^{2x/y} [O_2]} \right) = RT \ln(P_{O_2}) \quad (10.5b)$$



$$\Delta G^\circ = -RT \ln \left(\frac{[M_xO_y][CO]^y}{[M]^x [CO_2]^y} \right) \quad (10.1)$$

$$\Delta G^\circ = -yRT \ln \left(\frac{P_{CO}}{P_{CO_2}} \right) \quad (10.6c)$$

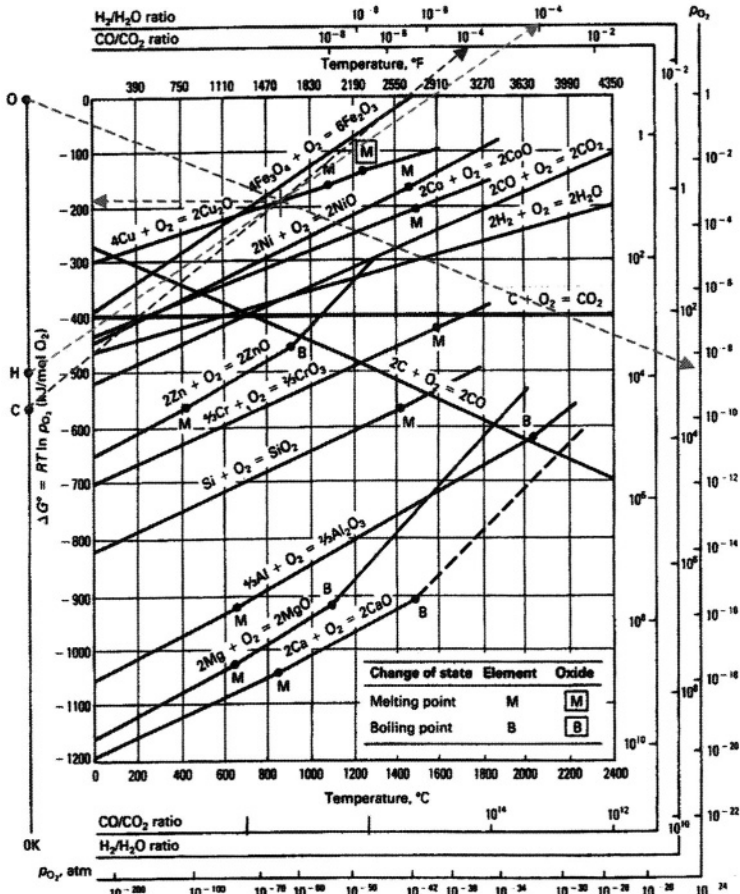


Figure 10.1 Ellingham standard energy change diagram [4].

$$3) \quad xM + yH_2O = M_xO_y + yH_2 \quad (10.7a)$$

$$\Delta G^\circ = -RT \ln \left(\frac{[M_xO_y][H_2]^y}{[M]^x [H_2O]^y} \right) \quad (10.7b)$$

$$\Delta G^\circ = -yRT \ln \left(\frac{P_{H_2}}{P_{H_2O}} \right) \quad (10.7c)$$

where $[j] = a_j =$ Activity of species j (mol/l or mol/cm^3)
 $P =$ Pressure (kPa)

Notice that M_xO_y is the common composition of an oxide scale. P_{O_2} , P_{CO} , P_{CO_2} , P_{H_2} , and P_{H_2O} are partial pressures. However, if $\Delta G < 0$, then it is a measure of negative deviation from equilibrium and the reaction proceeds from

left to right as written. On the contrary, if $\Delta G^\circ > 0$, then a positive deviation from equilibrium implies that a reaction occurs in the reverse direction from right to left. Figure 10.1 shows the standard Gibbs energy of formation as a function of temperature for oxides under oxygen partial pressure (P_{O_2}), carbon oxide/dioxide pressure ratio (P_{CO}/P_{CO_2}), and hydrogen /water pressure ratio (P_{H_2}/P_{H_2O}).

Figure 10.2 illustrates the model for oxide scale formation in gaseous environments at high temperatures.

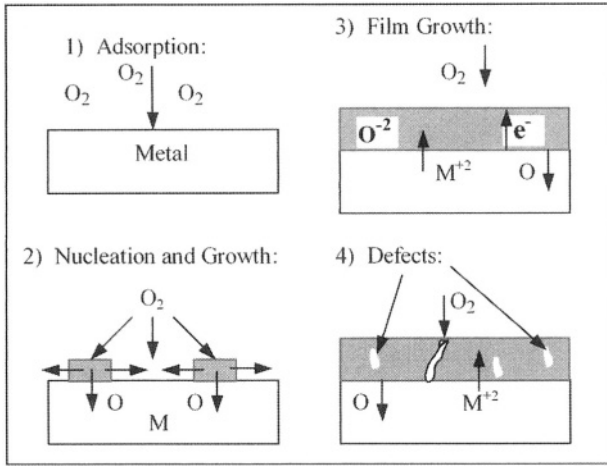
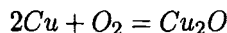


Figure 10.2 Model for scale formation [3].

The schematic sequence of events for scale formation indicates that the mechanism involves adsorption of atomic oxygen on the metal surface at stage 1. Then, nucleation and growth occurs at favorable sites until a thin oxide film forms covering the metal surface at stage 2. If the film lacks of macro and micro defects, it protects the metal from oxidizing any further. When scale growth occurs as shown in stage 3, metal oxidation occurs, $M \rightarrow M^{+2} + 2e^-$, releasing electrons which migrate through the oxide film to react with atomic oxygen. At stage 4, the oxide scale thickens and the growth stresses cause defects such as porosity, cavities, and microcracks. Consequently, the oxide scale is not protective and the metal is oxidized by a different mechanism [5].

Example 10.1 This example can make it clear on how to use Figure 10.1. a) Suppose that one is interested in forming copper oxide (Cu_2O) scale at $887^\circ C$. Then, using the left-hand side vertical pressure line with points “O” for oxygen, “H” for P_{H_2}/P_{H_2O} ratio, and “C” for P_{CO}/P_{CO_2} ratio, draw straight lines from these points through the aluminum and oxygen reaction line



at 887°C until they intercept the pertinent outer lines for the oxygen and pressure ratios. This is done in Figure 10.1 with dashed color lines. The read-off pressures and the corresponding standard Gibbs free energy change are

$$\begin{aligned} P_{O_2} &= 2.78 \times 10^{-9} \text{ atm} \\ P_{CO}/P_{CO_2} &= 10^4 \\ P_{H_2}/P_{H_2O} &= 10^{-4} \\ \Delta G^\circ &= -190 \text{ kJ/mol of } O_2 \end{aligned}$$

b) Furthermore, metals below $\Delta G^\circ = -190 \text{ kJ/mol}$ at 887°C can be oxidized and those above can be reduced. However, **Cu** can be reduced by **Ni** because its line is below the aluminum free-energy line. A similar reasoning may be used at different free energy values at a specific temperature. Finally, metals with the free-energy lines above the $2C + O_2 = CO$ line can be reduced by carbon C as the affinity of metals for oxygen increases.

c) Despite that Figure 10.1 is normally used for reducing mineral compounds, such as oxides, it provides a basis for evaluating the possibility of chemical separation by oxidation.

Furthermore, Figure 10.3 shows oxide layers on iron and a titanium alloy exposed to oxygen-rich environments at high temperatures. Observe how multi-phase scales form at the expense of material thickness reduction, which is actually related to . For example, Figure 10.3a shows that *FeO* oxide has a substantial amount of defects next to the metal substrate, but it may be sound at the extreme end. Also, the **Fe₃O₄** oxide exhibits defects, including an inclined crack.

The scales in Figure 10.3 indicate that those metals and alloys which oxidize to more than one valence can form a series of oxide layers. The inner layer is the most metal-rich compound and has the lowest valence, such as **Fe⁺²** in Figure 10.3a. This implies that cation vacancies and electron holes are the dominant defects as in p-type *FeO* oxide. On the other had, the outer layer, such as **Fe₂O₃**, is oxygen-rich and may be n-type oxide because of anion vacancies diffusing inward.

Figure 10.4a shows an oxide layer of less than 1 μm thick on a cast **Fe – 7.5Al – 2Cr** alloy exposed to a complex gas mixture containing sulfur. Despite-fully the oxide has a complex structure, mostly **Al₂O₃** phase, the layer breaks down due to formation of cracks, which act as fast diffusion sites for sulfur-containing nodules growth as indicate in Figures 10.4b and 10.4c. Eventually, the layer becomes nonprotective since these nodules collapse after a prolonged exposure time. The final oxide surface morphology is shown in Figure 10.4d which represents a nonprotective single-phase oxide scale mostly composed of aluminum oxide (**Al₂O₃**) [15].

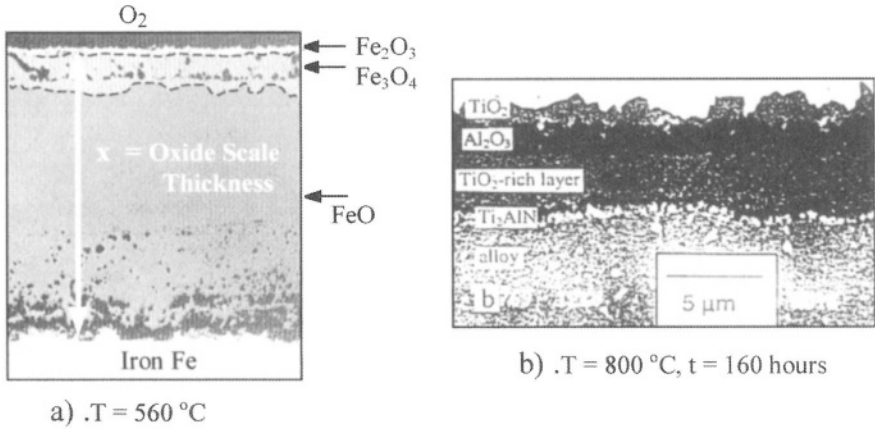


Figure 10.3 SEM photomicrographs of protective oxide scales on a) iron at high temperatures [6] and b) Extruded Ti-46.8Al-1Mo-0.19Si alloy heated in an oxygen environment at 800C for 160 hours [12].

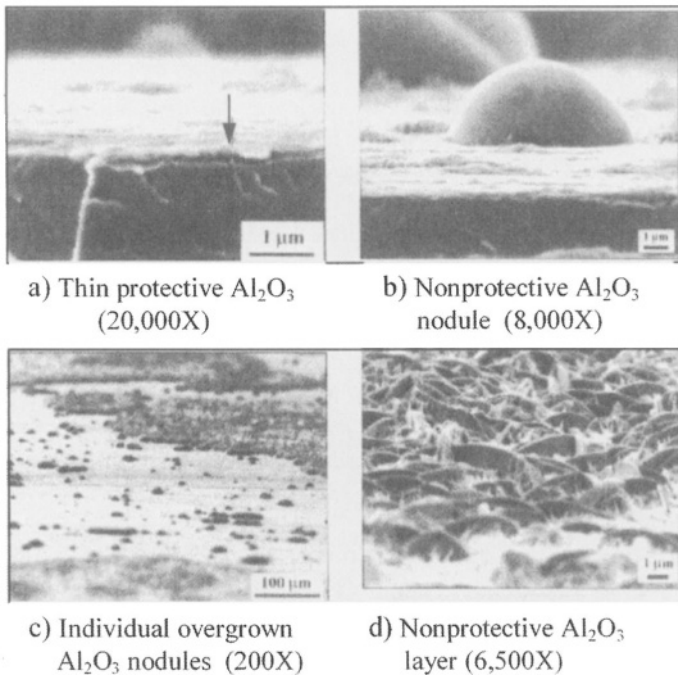
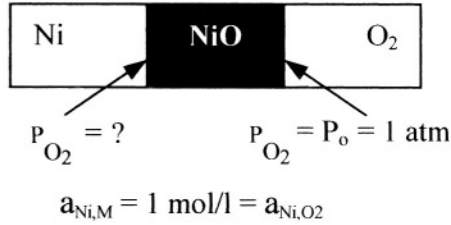


Figure 10.4 SEM photomicrographs showing the sequence of mostly passive alumina Al_2O_3 scale breakdown. The arrow in part a) indicates the initial oxide scale of $< 1 \mu m$ thick on a cast $Fe - 7.5Al - 2Cr$ alloy in a complex gas mixture composed of oxygen, carbon dioxide, water, nitrogen and sulfur at $500^\circ C$. The prolonged exposure time was 100 hours.[15].

Example 10.2 The application of thermodynamics in metal oxidation is succinctly presented in this example. One of the simplest method for characterizing metal oxide formation is to use a thin plate exposed to an oxidizing environment such as oxygen. The Experimental output may be oxide thickness and weight measurements for a given oxygen partial pressure and time at temperatures. However, thermodynamical parameters are significant in this type of work. Suppose that a thin nickel plate is exposed to oxygen for a fixed time at relatively high temperatures and the Gibbs free energy is measured in such an environment. Only the standard free energy (ΔG°) data is illustrate in the Table given below along with the overall reaction.

T ($^\circ\text{C}$)	ΔG° (kJ/mol)
100	-431
300	-390
500	-348
1000	-252
1400	-170
$2\text{Ni} + \text{O}_2 = 2\text{NiO}$	
$\Delta G^\circ = -RT \ln K$	



- a) Plot ΔG° vs. T ($^\circ\text{C}$) and determine the standard enthalpy change (ΔH°) and entropy change (ΔS° in kJ/ $^\circ\text{C}$) by regression analysis, b) Plot the reaction equilibrium constant K_{NiO} vs. T ($^\circ\text{C}$), c) Plot the oxygen partial pressure P_{O_2} vs. T ($^\circ\text{C}$), and d) calculate the activity at 100°C and 1400°C

Solution:

a) Linear regression equation (curve fitting):

$$\Delta G^\circ = \Delta H^\circ - T\Delta S^\circ \tag{a}$$

$$\Delta G^\circ = -450 \text{ kJ/mol} + (0.20 \text{ kJ/mol}\cdot^\circ\text{C})T \tag{b}$$

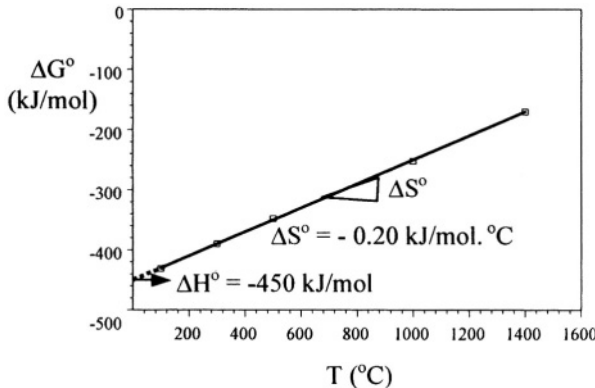


Figure E101.a

b) The equilibrium constant profile:

$$\Delta G^\circ = -RT \ln(K_{NiO}) \quad (c)$$

$$K_{NiO} = \exp\left(-\frac{\Delta G^\circ}{RT}\right) \quad (d)$$

$$K_{NiO} = \exp\left(-\left(\frac{-450 + 0.20T}{8.314(T + 273)}\right) \times 10^3\right) \quad (e)$$

$$K_{NiO} = 1.66 \times 10^{60} \quad @ \quad T = 100^\circ C$$

$$K_{NiO} = 4.01 \times 10^3 \quad @ \quad T = 1400^\circ C$$

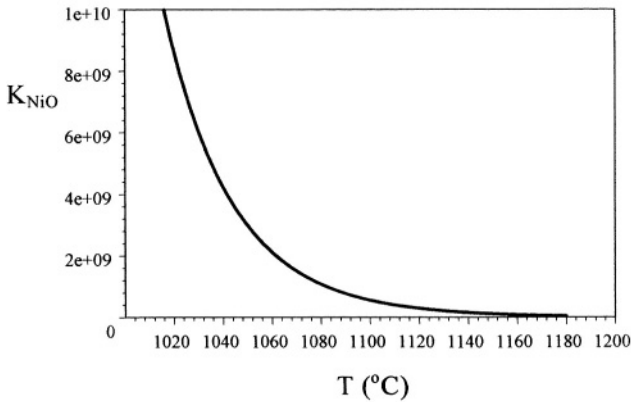


Figure E10.2b

c) Oxygen partial pressure at the Ni – NiO₂ interface:

$$K_{NiO} = \frac{[NiO]^2}{[Ni]^2 [O_2]} = \frac{1}{[O_2]} \quad (f)$$

$$[O_2] = \frac{P_{O_2}}{P_o} \quad (g)$$

Combining eqs. (e) through (g) yields the oxygen pressure profile in the Ni-NiO₂ interface

$$P_{O_2} = \frac{P_o}{K_{NiO}} = P_o \exp\left[\left(\frac{-450 + 0.20T}{8.314(T + 273)}\right) \times 10^3\right] \quad (h)$$

$$P_{O_2} = 6.04 \times 10^{-61} \quad @ \quad T = 100^\circ C$$

$$P_{O_2} = 2.49 \times 10^{-4} \quad @ \quad T = 1400^\circ C$$

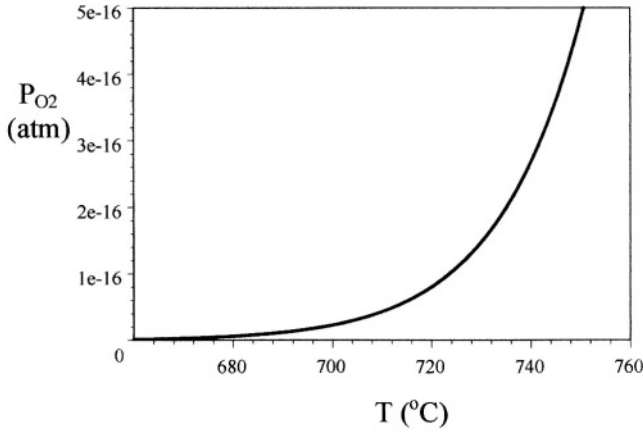


Figure E10.c

d) The activity of nickel cations at Ni – O₂ interface:

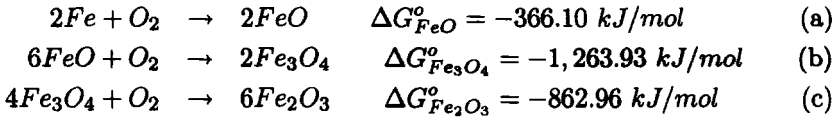
$$\begin{aligned}
 \Delta G_{Ni-face}^o &= \Delta G_{O_2-face}^o & (i) \\
 -RT \ln (K_{NiO})_{Ni-face} &= -RT \ln (K_{NiO})_{O_2-face} \\
 \ln \left(\frac{[NiO]^2}{[Ni]^2 [O_2]} \right)_{Ni-face} &= \ln \left(\frac{[NiO]^2}{[Ni]^2 [O_2]} \right)_{O_2-face} \\
 \ln \left(\frac{1}{[O_2]} \right)_{Ni-face} &= \ln \left(\frac{1}{[Ni]^2 [O_2]} \right)_{O_2-face} \\
 \left(\frac{P_o}{P_{O_2}} \right)_{Ni-face} &= \left(\frac{P_o}{[Ni]^2 (P_{O_2} = P_o)} \right)_{O_2-face} \\
 a_{O_2-face} &= [Ni]_{O_2-face} = \left(\sqrt{\frac{P_{O_2}}{P_o}} \right)_{Ni-face} & (j)
 \end{aligned}$$

Substituting eq. (h) into (j) gives

$$\begin{aligned}
 [Ni]_{O_2-face} &= \sqrt{\exp \left(\left(\frac{-450 + 0.20T}{8.314 (T + 273)} \right) x 10^3 \right)} & (k) \\
 [Ni]_{O_2-face} &= 7.77 x 10^{-31} \quad @ \quad T = 100^\circ C \\
 a_{O_2-face} &= [Ni]_{O_2-face} = 2.22 x 10^{-3} \quad @ \quad T = 1400^\circ C
 \end{aligned}$$

In addition, **variations in gas pressure** at constant temperatures limit the stability of oxide compounds. This implies that there must exist a chemical stability domain in terms of pressure [8]. For instance, the oxide phases in Figure 10.3a is a particular case in which FeO and Fe_3O_4 phases are stable layers at a specific gaseous partial pressure range. Beyond the maximum partial pressure limit, FeO becomes unstable and therefore, FeO changes to Fe_3O_4 . The following example illustrates how the oxygen partial pressure stability domain is determined.

Example 10.3 *This example is adapted from Barsoum [8] in order to determine the oxygen partial pressure stability domain for the iron oxide phases shown in Figure 10.3a. Use the data given below at 1000°C.*



Solution:

Applying eqs. (10.5a) and (10.5b) to reactions (a) through (b) yields the equilibrium constants and activities

$$\begin{aligned}
 K_{FeO} &= \frac{[FeO]}{[Fe][O_2]} = \frac{1}{[O_2]} \\
 a_{FeO} &= [O_2]_{FeO} = \left(\frac{P_{O_2}}{P_o} \right)_{FeO} \quad \text{with } P_o = 1 \text{ atm}
 \end{aligned}$$

Thus, the free energy and oxygen partial pressure equations for the FeO phase (wustite) are

$$\begin{aligned}
 \Delta G_{FeO}^{\circ} &= -RT \ln(K_{FeO}) = RT \ln(P_{O_2})_{FeO} \\
 (P_{O_2})_{FeO} &= \exp\left(\frac{\Delta G^{\circ}}{RT}\right)_{FeO}
 \end{aligned}$$

For the $FeO-Fe_3O_4$ and Fe_3O_4-FeO systems, the free energy of formation for reactions (b) and (c) are determined by the oxides energy balance. According to these reactions, the free energy of formation is given by

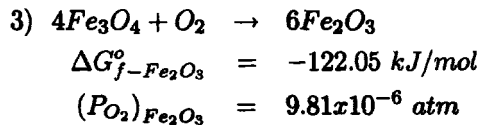
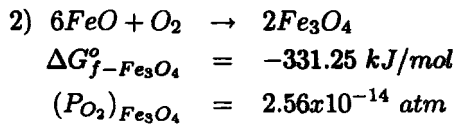
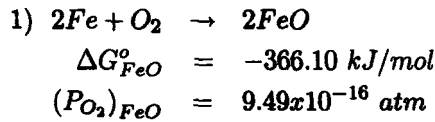
$$\begin{aligned}
 \Delta G_{f-Fe_3O_4}^{\circ} &= \Delta 2G_{Fe_3O_4}^{\circ} - 6\Delta G_{FeO}^{\circ} \\
 \Delta G_{f-Fe_2O_3}^{\circ} &= 6\Delta G_{Fe_2O_3}^{\circ} - 4\Delta G_{Fe_3O_4}^{\circ}
 \end{aligned}$$

Thus, the reaction oxygen partial pressure equations become dependent on the free energy of formation of the $\text{FeO} - \text{Fe}_3\text{O}_4$ and $\text{Fe}_3\text{O}_4 - \text{FeO}$ systems. Hence,

$$(P_{\text{O}_2})_{\text{Fe}_3\text{O}_4} = \exp\left(\frac{\Delta G_{f-\text{Fe}_3\text{O}_4}^\circ}{RT}\right)_{\text{Fe}_3\text{O}_4}$$

$$(P_{\text{O}_2})_{\text{Fe}_2\text{O}_3} = \exp\left(\frac{\Delta G_{f-\text{Fe}_2\text{O}_3}^\circ}{RT}\right)_{\text{Fe}_2\text{O}_3}$$

Now, the calculated free energy of formation and oxygen partial pressure for each reaction are given below



Therefore, the stability pressure domain for each phase is

Fe	is stable at	$P_{\text{O}_2} < (P_{\text{O}_2})_{\text{FeO}}$
FeO	is stable at	$(P_{\text{O}_2})_{\text{FeO}} \leq P_{\text{O}_2} < (P_{\text{O}_2})_{\text{Fe}_3\text{O}_4}$
Fe ₃ O ₄	is stable at	$(P_{\text{O}_2})_{\text{Fe}_3\text{O}_4} \leq P_{\text{O}_2} < (P_{\text{O}_2})_{\text{Fe}_2\text{O}_3}$
Fe ₂ O ₃	is stable at	$(P_{\text{O}_2})_{\text{Fe}_2\text{O}_3} \leq P_{\text{O}_2} \leq P_o = 1 \text{ atm}$

For the sake of clarity, the reader should verify the calculated values of $\Delta G_{f-\text{Fe}_3\text{O}_4}^\circ$ and $\Delta G_{f-\text{Fe}_2\text{O}_3}^\circ$ from the free-energy chart at 1000°C. A similar procedure can be carried out for oxide formation in $\text{Fe} - \text{CO}/\text{CO}_2$ and $\text{Fe} - \text{H}_2/\text{H}_2\text{O}$ systems.

In the light of present knowledge, this example is simple and yet, significant for understanding the relevant information a free-energy chart possesses. This chart is used for both oxidation and reduction of common metal oxide compound, which are usually nonstoichiometric. With respect to the example, FeO should have been written as Fe_xO since its stoichiometric number $0.80 < x < 1$ may have different values in the $\text{FeO} - \text{Fe}_3\text{O}_4$ and $\text{Fe}_3\text{O}_4 - \text{FeO}$ systems.

10.3 POINT DEFECTS IN OXIDES

In this section, the phenomenon of point defects, such as vacancies and interstitial, in crystals is briefly introduced. The oxide entropy change (ΔS) increases when more points defects, also known a imperfections, generate within a crystal. Metal oxides at equilibrium may contain nearly equal numbers of cations and anion vacancies. Thus, the number of point defects (n) producing a minimum free energy change, $\Delta G = \Delta H_f - T\Delta S$, can be modeled by the Arrhenius law [21-23]

$$n = N \exp\left(-\frac{\Delta G}{2kT}\right) = N \exp\left(\frac{\Delta S}{2k} - \frac{\Delta H_f}{2kT}\right) \tag{10.8}$$

$$\frac{n}{N} \simeq \exp\left(-\frac{\Delta H_f}{2kT}\right) \quad \text{For } \Delta S \rightarrow 0 \tag{10.9}$$

where N = Number of atoms

ΔG = Gibbs free energy (J/mol)

ΔS = Entropy change ($J/mol \cdot ^\circ K$)

ΔH_f = Enthalpy change of formation ($eV = 1.602 \times 10^{-19} J/mol$)

k = Boltzmann constant = $1.38 \times 10^{-23} J/(mol \cdot ^\circ K)$

$k = 8.62 \times 10^{-5} eV/^\circ K = 8.82 \times 10^{-5} eV/^\circ C$

T = Absolute temperature ($^\circ K$)

Equation (10.9) predicts that the equilibrium defect fraction (n/N) increases exponentially with increasing temperature. The defect fraction profile given by eq. (10.9) is shown in Figure 10.4 for several values of the enthalpy change. Observe that n/N is strongly dependent on the temperature above $800^\circ C$ for selected values of the enthalpy change (ΔH_f).

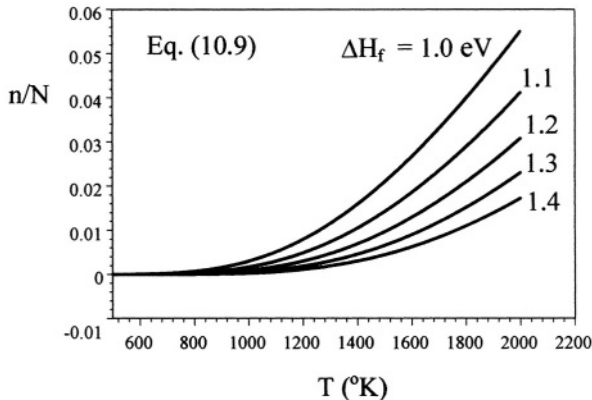


Figure 10.5 Theoretical profiles for the defect fraction in solid crystals.

Furthermore, point defects are mobile imperfections at high temperatures, and eventually, their rate of diffusion may obey the Arrhenius law [22]

$$R_x = R_o \exp\left(-\frac{\Delta H_d}{kT}\right) \tag{10.10}$$

where $\Delta H_d < \Delta H_f$
 R_o = Rate constant

It is known that ionic compounds have appreciable electrical conductivity, which is inseparable from diffusion, due to atomic defects, such as Schottky and Frenkel defects to an extent, and ionic migration and diffusion. For instance, **Schottky defects** are combinations of cation and anion vacancies necessary to maintain ionic electrical neutrality and stoichiometric ionic structure. In general, ions (cations and anions) diffuse into adjacent sites.

On the other hand, **Frenkel defects** are combinations of interstitial cations and cation vacancies. Electrical neutrality and stoichiometry are also maintained. Thus, combinations of the type of defects provide the ionic diffusion mechanism for oxide growth, but stoichiometry may not be maintained due to the electrical nature of oxides having either metal-excess or metal-deficit conditions.

Figure 10.6 schematically shows idealized lattice structures for continuous **n-type** and **p-type** oxide semiconductors containing point defects, such as interstitial cations, cation vacancies, and electron holes. For convenience, the metal is treated as a divalent element. The electron hole is a positive mobile electronic carrier in the valence band in an oxide crystal structure.

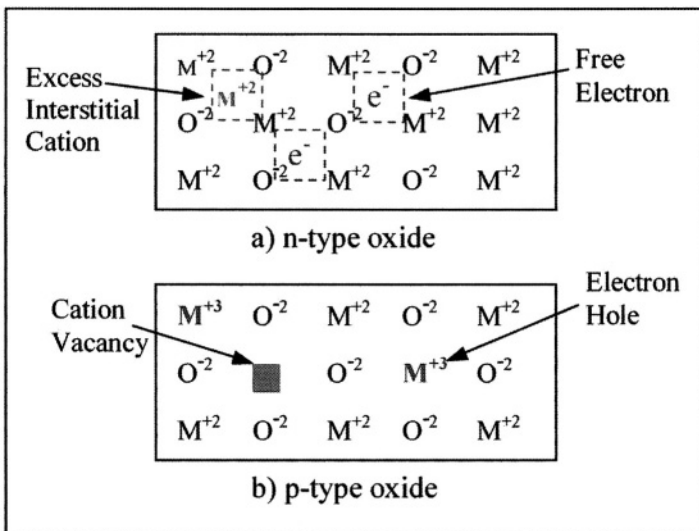
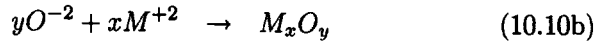
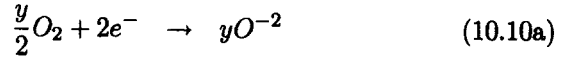


Figure 10.6 Schematic diagrams for oxide semiconductors.

Analysis of Figure 10.6 indicates that

- **n-type oxides** have metal-excess and oxygen-deficit conditions. Also, interstitial cations (M^{+2}) and electrons are free to move within the oxide lattice toward the oxide-gas interface, where the following reactions occur



Thus, the nonstoichiometric, M_xO_y oxide has its own lattice defects such as vacancies. In this process, both M^{+2} and electrons e^- diffuse through the oxide lattice until the oxide is thick enough. Consequently, the formation of n-type oxides is due to diffusion mechanism of interstitial M^{+2} cations and oxygen O^{-2} anions in the opposite direction. Eventually, M_xO_y grows at the metal-oxide inner interface. Oxides such as ZnO , ZrO_2 , MgO , BeO , Fe_2O_3 , Al_2O_3 , TiO_2 and others fall into this category.

p-type oxides are metal-deficit and oxygen-excess compounds in which M^{+2} cations are provided at the metal-oxide interface and diffuse toward the oxide-gas interface through cation vacancies. Consequently, M_xO_y oxide forms at the oxide-gas interface. The electron holes have positive charge and migrate through their conduction band. Therefore, ionic mass transfer occurs by metal vacancy diffusion [6]. Oxides such as NiO , CoO , Cr_2O_3 , FeO , Cu_2O , Cu_2S , and others fall into this category. Also, the presence of ionic impurities in the oxide lattice is referred to as the “**doping effect**”, which affects the concentration of ionic defects.

In addition, there are highly n-type stoichiometric, oxides such as Al_2O_3 , MgO , and ZrO_2 , since the Gibbs free energy change of formation is large and the cation valence is fixed [22]. On the other hand, for common multivalent cations, nonstoichiometry is pronounced in TiO_{2-x} , $Fe_{1-x}O$ and $Ni_{1-x}O$. For instance, FeO oxide is a face-centered cubic (FCC) structure that may contain a high concentration of cations and its nonstoichiometry arises due to the unequal number of cations and anions, resulting in $n_{cation}(Fe_xO) > n_{anion}(FeO)$. Consequently, Fe_xO forms since this oxide departs from its ideal stoichiometric composition FeO . In this case, the cation vacancy concentration can be determined as $(1 - x)$ since $0.80 < x < 1$ [5,22].

With regard to the case in which $n_{cation}(Fe_xO) > n_{anion}(FeO)$, the Schottky and Frenkel defects do not prevail as the dominant mechanisms for oxide formation. Instead, cation diffusion and electron migration toward the oxide surface are the dominant mechanisms. Also, some ferric iron (Fe^{+3}) cations can be present in the oxide structure and can associate with oxygen O^{-2} anions generating some cation vacancies. This implies that a fraction of ferrous iron Fe^{+2} cations oxidize to Fe^{+3} cations, resulting in a cation deficiency [21].

10.4 KINETICS OF CORROSION IN GASES

Application of metals and alloys in high-temperature environments is of technological importance since the rate of oxide layer formation, mechanism, and degree of protectiveness are the subject matter to be evaluated. Consider the model of oxide formation shown in Figure 10.7, in which a metal is exposed to an oxygen-rich environment at high temperatures [7-9].

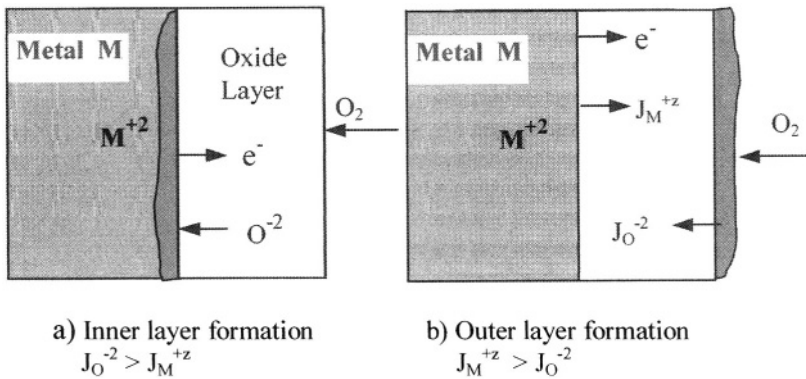


Figure 10.7 Model for oxidation by diffusion-control mechanism showing the dominant diffusion molar flux.

The model in Figure 10.7 predicts that

- The initial rate of oxide formation is determined by the reactions at the metal/oxygen interface. Thus, M_xO_y forms as a thin layer.
- Once the thin layer is formed, it serves as a barrier separating or insulating the metal substrate. The subsequent oxidation steps are controlled by the diffusion of the species M^{+2} and O^{-2} through the layer.
- If O^{-2} anions diffuse faster than M^{+2} cations, the diffusion molar flux is $J_{O^{-2}} > J_{M^{+2}}$, then an oxide inner layer forms as shown in Figure 10.6a. In order for O^{-2} anions to diffuse into the metal, there must be metal vacancies in the lattice. As oxide growth proceeds, the volume of the oxide is $V_{M_xO_y} > V_M$ causing a high stress concentration and consequently, the oxide layer may rupture, exposing the metal substrate to oxygen for further oxidation. Titanium falls into this category due to $J_{O^{-2}} > J_{Ti^{+2}}$.
- If M^{+2} cations diffuse faster than O^{-2} anions, then $J_{M^{+2}} > J_{O^{-2}}$ and an outer oxide layer forms and proceeds through the concentration gradient as shown in Figure 10.6b. In this situation, the stress concentration is reduced or relieved. Thus, the oxide layer adheres to the metal surface and protects the metal from further oxidation. Nickel falls into the category since $J_{Ni^{+2}} > J_{O^{-2}}$.

Consider the oxidation case in Figure 10.6b for divalent metal cations (M^{+2}) and oxygen anions (O^{-2}). If the ionic radius relationship is $R_{O^{-2}} > R_{M^{+2}}$ and O^{-2} anions diffuse at a negligible rate, then M^{+2} cations diffuse through the oxide layer. Consequently, the diffusion-control process dictates that the diffusion molar fluxes become $J_{O^{-2}} \simeq 0$ and $J_{M^{+2}} > 0$ and metal oxidation reactions proceed until the rate of diffusion slows down reaching steady-state conditions.

Also, the mechanism of high-temperature oxidation may be a combination of metal cations flowing outward and oxygen anions flowing inward due to diffusion and migration mass transfer. This dual mass transfer action leads to beneficial condensation of vacancies and prevention of voids for the formation of a uniformly adhered oxide layer for continuous and nonporous scales. Thus, the ionic mass transfer through the scale is the rate-controlling process. Initially, a thin and protective film forms until the reaction rate decreases. Consequently, film growth forms a scale, which may be attributed to the concentration and potential gradients. In a macroscale, the mechanism involved in scale formation is assessed below for different rate laws, which do not consider the nonstoichiometry of n-type or p-type oxides or sulfides or a combination of these, including carbides and hydrogen effects.

10.4.1 PILLING-BEDWORTH RATIO

Metal oxide scales can be defined as protective and nonprotective using the classical Pilling-Bedworth law as the ratio given by [1]

$$PB = \frac{V_o}{V_m} = PB = \frac{[\rho^{-1}A_w]_o}{[z\rho^{-1}A_w]_m} \quad (10.11)$$

where V_o = Volume of the oxide scale (cm^3)
 V_m = Volume of the solid metal (cm^3)
 ρ = Density (g/cm^3)
 A_w = Atomic or molecular weight (g/mol)
 z = Valence

The PB ratio is used to characterize several oxidation conditions. Thus,

- If $PB < 1$ or $PB > 2$, the oxide scale is nonprotective (NP) and noncontinuous due to insufficient volume to cover the metal surface uniformly. Thus, weight gain is usually linear.
- If $1 \leq PB \leq 2$, the oxide scale is protective (P), adherent and strong due to compressive stress, refractory due to high melting temperature, low electrical conductor, and nonporous. Because of these factors, diffusion proceeds in the solid state at low rates. Some oxides may not develop compressive stresses, invalidating PB law [2].
- If $PB = 1$, then the oxide scale is ideally protective.

Table 10.1 lists several metal/oxide PB ratios and quality. Observe that most metals have $PB > 1$. However, it is possible that some oxide scales may be plastically deformed at high temperatures, leading to a porosity-healing and crack-filling processes for $PB < 1$. Other oxide scales, such as WO_3 at $T \geq 800^\circ C$, may become unstable and volatile for $PB > 1$. This indicates that the protectiveness is lost [2]. Crystallographic structures and properties of many metal oxide scales can be found elsewhere [5].

In general, thermal degradation of metals and alloys, and oxide scales is a major concern in practical applications, such as furnace parts, heaters, tubes and the like. Degradation at high temperatures may occur isothermally or cyclically under operating conditions. Therefore, metallic parts must be protected using a lesser aggressive environments if possible; otherwise, applying a protective thin film prior to high temperature applications can be beneficial. Protective oxide films or coatings have been studied for over two decades using rare-earth elements to protect chromia (Cr_2O_3) and alumina (Al_2O_3) oxide scales from oxidizing beyond suitable thickness. A particular paper by Seal et al. [16] addresses the influence of superficially applied CeO_2 coatings ($\approx 2 \mu m$) on the isothermal and cyclic-oxidation behavior of austenitic stainless steel, such as AISI 316, 321, and 304, in dry air.

Table 10.1 PB ratios for common metals [2].

Metal	Oxide	PB	Protectiveness
Aluminum	Al_2O_3	1.28	P
Calcium	CaO	0.64	NP
Cadmium	CdO	1.42	P
Cobalt	Co_2O_3	2.40	NP
Copper	Cu_2O	1.67	P
Chromium	Cr_2O_3	2.02	NP
Iron	FeO	1.78	P
Magnesium	MgO	0.81	NP
Manganese	MnO_2	2.37	NP
Molybdenum	MoO_3	3.27	NP
Nickel	NiO	1.70	P
Lead	PbO	1.28	P
Silicon	SiO_2	2.15	NP
Tantalum	Ta_2O_3	2.47	NP
Titanium	Ti_2O_3	1.76	P
Tungsten	WO_3	1.87	P
Uranium	UO_2	1.97	P
Zinc	ZnO	1.58	P
Zirconium	ZrO_2	1.57	P

10.4.2 MATHEMATICS OF OXIDATION

The mathematics of oxidation kinetics involves diffusion and migration mass transfer. According to Fick's first law of diffusion, the molar flux is related to the rate of oxide thickness growth (dx/dt) is given by

$$J = -D \frac{dC}{dx} \quad (10.12)$$

$$J = -C \frac{dx}{dt} \quad (10.13)$$

from which the rate of thickness growth (also known as drift velocity) is

$$\frac{dx}{dt} = \frac{D}{C_x} \frac{\Delta C}{x} \quad (10.14)$$

where D = Diffusivity (Diffusion coefficient) (cm^2/s)

C_x = Concentration of the diffusing species ($ions/cm^3$)

x = Thickness of the oxide scale (cm or μm)

Integrating eq. (10.14) yields what is known as the parabolic equation for the oxide thickness

$$x = \sqrt{K_x t} \quad (10.15)$$

$$K_x = \frac{2D\Delta C}{C_x} \approx 2D \quad (10.16)$$

where K_x = Parabolic rate constant (cm^2/s)

In oxidation at high temperatures, most variables are temperature dependent. Thus, it is reasonable to assume that both diffusivity and parabolic rate constant obey the Arrhenius relationship (see Chapter 3)

$$D = D_o \exp\left(-\frac{Q_d}{RT}\right) \quad (10.17)$$

$$K_x = K_o \exp\left(-\frac{Q_x}{RT}\right) \quad (10.18)$$

Hence, the oxide thickness becomes $x = f(T)$. It is known that the oxide kinetics of many metals and alloys show parabolic behavior. However, other type of behavior is possible and eq. (10.12) is generalized and modeled as an empirical relationship given by

$$x = (K_x t)^n \quad (10.19)$$

where n is an exponent and K_x becomes the rate constant for the scale thickness growth in gaseous environments.

In fact, x in eq. (10.19) represents an external thickness in most cases. Now, the generalized equation for the rate of oxide thickness growth takes the form

$$\frac{dx}{dt} = n (K_x)^n t^{n-1} \quad (10.20)$$

Furthermore, mass gain is another parameter that can be employed in characterizing oxide kinetic behavior. Using the definition of density and eq. (10.19) yields the mass gain (M) and the rate of mass gain (dM/dt) during surface oxidation at high temperatures

$$M = \rho A_s (K_x t)^n = \lambda t^n \quad (10.21)$$

$$\frac{dM}{dt} = n \lambda t^{n-1} \quad (10.22)$$

$$\lambda = \rho A_s (K_x)^n \quad (10.23)$$

where $\rho =$ Density (g/cm^3)
 $A_s =$ Surface area (cm^2)
 $\lambda =$ Constant (g/s^n)

Since it is customary to represent weight gain in units of weight/area [10], eq. (10.21) is rearranged so that the weight gain and its rate become as

$$W = \frac{M}{A_s} = (K_w t)^n \quad (10.24)$$

$$\frac{dW}{dt} = n K_w^n t^{n-1} \quad (10.25)$$

$$K_w = \rho^{1/n} K_x \quad (10.26)$$

where $K_w =$ Rate constant ($g.cm^{-2}.time^{-n}$) for weight gain.

The above equations are analyzed based on the exponent n for most observable kinetic behavior. Thus, the physical interpretation of n is given below.

- If $n = 1$, a linear behavior is achieved for a noncontinuous, porous and cracked oxide scale with $PB < 1$ or $PB > 2$. In this case, the scale is nonprotective and diffusion of oxygen occurs through the pores, cracks, and vacancies.
- If $n = 1/2$, a parabolic behavior of nonporous, adherent, and protective scale develops by diffusion mechanism. Thus, $1 \leq PB \leq 2$ and the mechanism of scale growth is related to metal cations (M^{+z}) diffusing through the oxide scale to react with oxygen at the oxide-gas interface.
- If $n = 1/3$, a cubic behavior develops for a nonporous, adherent and protective oxide scale. Thus, $1 \leq PB \leq 2$.

In general, the kinetic behavior of a specific oxide scale may be different from the most observable ones cited above and therefore, the exponent n may take a different value, which must be determined experimentally. Also, a logarithmic behavior is possible for thin layers at relatively low temperatures [2]. For a logarithmic behavior, the weight gain may be defined by

$$W = K_a \log(a_2 + a_3 t) \quad (10.27)$$

where $K_a =$ Rate constant ($g.cm^{-2}$)
 $a_2 =$ Dimensionless constant
 $a_3 =$ Constant ($time^{-1}$)

Figures 10.8 and 10.9 illustrate the kinetic behavior cases describe above and their corresponding rates, respectively.

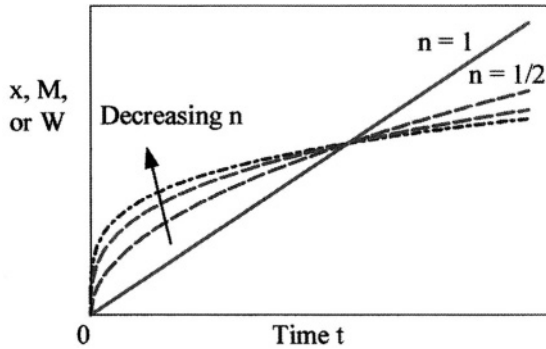


Figure 10.8 Schematic kinetic behavior cases.

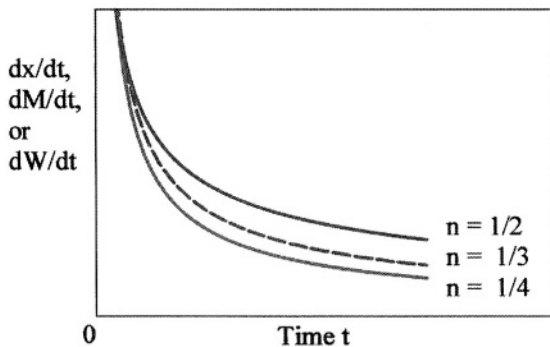
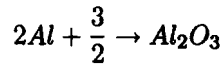


Figure 10.9 Schematic kinetic rates.

Example 10.4 Calculate the PB ratio for the oxidation of aluminum in hot oxygen. Data: $\rho_{Al} = 2.70 \text{ g/cm}^3$, $\rho_{Al_2O_3} = 3.80 \text{ g/cm}^3$. Will Al_2O_3 be protective?

Solution:

Assume that oxidation of aluminum in oxygen occurs by the reaction



and the pertinent atomic and molecular weights are, respectively

$$A_{w,Al} = 26.98 \text{ g/mol}$$

$$A_{w,Al_2O_3} = 2(26.98 \text{ g/mol}) + 3(16 \text{ g/mol}) = 101.96 \text{ g/mol}$$

From eq. (10.11),

$$PB = \frac{[\rho^{-1} A_w]_o}{[z\rho^{-1} A_w]_m}$$

$$PB = \frac{[(101.98) / (3.8)]_o}{[(2)(26.98) / (2.70)]_m}$$

$$PB = 1.34$$

Therefore, Al_2O_3 is theoretically protective as predicted by the Pilling-Bedworth ratio range $1 \leq PB \leq 2$.

Example 10.5 Calculate the thickness of the NiO oxide at a temperature T for 5 hours. Assume a $0.10 \mu\text{m}$ thick film after 1 minute treatment. Use the information given in Table 10.1.

Solution:

From Table 10.1, NiO oxide is protective and parabolic behavior is assumed. Thus, from eq. (10.15) at $t = 1 \text{ min} = 60 \text{ sec}$,

$$K_x = \frac{x^2}{t} = \frac{(0.10 \mu\text{m})^2}{60 \text{ sec}} = 1.67 \times 10^{-4} \frac{\mu\text{m}^2}{\text{s}}$$

At $t = 5 \text{ min} = 18,000 \text{ sec}$

$$x = \sqrt{K_x t} = \sqrt{\left(1.67 \times 10^{-4} \frac{\mu\text{m}^2}{\text{s}}\right) (18,000 \text{ s})}$$

$$x = 1.73 \mu\text{m}$$

10.5 IONIC CONDUCTIVITY

The ionic or electrical conductivity included in this section is due to ionic motion of species i within metal oxide compounds. These oxides may consist of one or more phases making up an oxide scale, which in turn, is the corrosion product to be analyzed with regard to its protectiveness, conductivity, mobility, diffusivity, and concentration of the species i .

For ionic or atomic transport, the force gradient acting on a diffusing species i along the x-direction can be defined by [21]

$$F'_i = -(z_i e) \frac{d\phi}{dx} \quad (\text{Electrical}) \quad (10.28)$$

$$F_i = -\frac{1}{N_A} \frac{d\mu_i}{dx} \quad (\text{Chemical}) \quad (10.29)$$

where $d\phi/dx$ = Electric potential gradient (V/cm)

$d\mu_i/dx$ = Chemical potential gradient ($J/mol.cm$)

These expressions indicate that the ionic force may be due to $d\phi/dx$ or $d\mu_i/dx$. If both force are present during an oxide formation and if they become equal in magnitude, then one can find a relationship between these gradients. Hence,

$$\frac{d\mu_i}{dx} = (z_i e) N_A \frac{d\phi}{dx} \quad (10.30)$$

But, the chemical potential gradient can also be defined in terms of ionic concentration gradient given by

$$\frac{d\mu_i}{dx} = \frac{RT}{C_i} \frac{dC_i}{dx} = \frac{kTN_A}{C_i} \frac{dC_i}{dx} \quad (10.31)$$

where z_i = Valence

$k = R/N_A$ = Boltzmann constant

$k = 1.38 \times 10^{-23} \text{ J}/^\circ\text{K} = 8.61 \times 10^{-5} \text{ eV}$

R = Gas Constant = $8.314 \text{ J}/^\circ\text{K} = 5.19 \times 10^{19} \text{ eV}$

N_A = Avogadro number = 6.022×10^{23}

e = Electronic charge = $1.602 \times 10^{-19} \text{ C}$ ($= A.s = J/V$)

T = Absolute temperature ($^\circ\text{K}$)

C_i = Atomic concentration ($ions/cm^3$ or $vacancy/cm^3$)

For ionic motion, the ionic velocity (drift velocity) and the force gradient acting on a species i are related to the mobilities

$$B'_i = \frac{v_i}{F'_i} \quad \text{and} \quad B_i = \frac{v_i}{F_i} \quad (10.32)$$

where B'_i = Electrical mobility ($cm^2/V.s$)

B_i = Ionic mobility ($cm^2/J.s$)

In addition, the intrinsic diffusivity D_i of a species i is related to the ionic mobility. This relationship is given in Chapter 4 as the Nernst-Einstein equation defined by

$$D_i = B_i kT \quad (10.33)$$

The relationship between the electrical mobility (B'_i) and the ionic mobility (B_i) is easily shown as

$$B'_i = (z_i e) B_i \quad (10.34)$$

where

$$B'_i = \frac{(z_i e) D_i}{kT} \quad (cm^2/V.s) \quad (10.35)$$

$$B_i = \frac{D_i}{kT} \quad (cm^2/J.s) \quad (10.36)$$

Also, the ionic flux is associated with the ionic velocity and concentration as

$$J_i = C_i v_i \quad (10.37)$$

Substituting eq. (10.28), (10.32), (10.35) and (10.37) yields the ionic migration flux as the partial component of the total flux involved in the oxide formation. Hence,

$$J_{i,m} = -\frac{(z_i e) C_i D_i}{kT} \frac{d\phi}{dx} \quad (10.38)$$

However, if diffusion and migration are coupled during oxide formation, then the diffusion ionic flux is given by the Fick's first law introduced in Chapter 4 or combine eqs. (10.29), (10.31), (10.32) and (10.37) to get this flux component

$$J_{i,d} = -D_i \frac{dC_i}{dx} \quad (10.39)$$

Thus, the total flux is

$$J_x = J_{i,d} + J_{i,m} \quad (10.40)$$

$$J_x = -D_i \frac{dC_i}{dx} - \frac{(z_i e) C_i D_i}{kT} \frac{d\phi}{dx} \quad (10.41)$$

Combining eqs. (4.8) and (10.38) yields the current density due to migration

$$i = -(z_i e) J_{i,m} \quad (10.42)$$

$$i = \frac{(z_i e)^2 C_i D_i}{kT} \frac{d\phi}{dx} \quad (10.43)$$

From Ohm's law, the ionic conductivity due to migration is given by

$$\sigma_i = -\frac{i}{d\phi/dx} \quad (10.44)$$

$$\sigma_i = \frac{(z_i e)^2 C_i D_i}{kT} > 0 \quad (10.45)$$

$$\sigma_i = (z_i e)^2 C_i B'_i > 0 \quad (10.46)$$

Notice from eqs. (10.45) and (10.46) that the electric conductivity principally depends on the ionic concentration, but $\sigma_i = f(C_i, D_i, T)$ and $\sigma_i = f(C_i, B'_i)$. Also, σ_i is a macroscopically measurable in terms of microscopic parameters [8]. Assume that the conductivity obeys the Arrhenius relationship so that

$$\sigma_i = \sigma_o \exp\left(-\frac{Q_\sigma}{kT}\right) \quad (10.47)$$

The electrical conductivity arises due to the electrical nature of the diffusing species and inherent defects since the ionic electrical conduction and diffusion are inseparable processes [8]. The major contribution to the electrical conduction is due to the presence of ionic species in the oxidation process of a metal in a gaseous environment [7]. In general, if the drift velocity (v_i) is primarily carried by cations, the ionic current density may be given by [8,21]

$$i_i = (z_i e) v_i C_i \quad (10.48)$$

where the concentration of the gas may be estimated by [8]

$$C_i = \frac{N_A S_o \rho_{oxide}}{A_{w,M} + A_{w,O_2}} \quad (10.49)$$

where S_o = Stoichiometry number of the oxygen in the oxide formula
 ρ_{oxide} = Density of the oxide compound (g/cm^3)

The total conductivity is simple the sum of the cation conductivity (σ_c), anion conductivity (σ_a) and electron conductivity (σ_e) or electron holes conductivity (σ_h) given by

$$\sigma_t = \sigma_c + \sigma_a + \sigma_e + \sigma_h = \sum \sigma_i > 0 \quad (10.50)$$

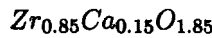
The notation for the electrical conductivity can be for defining the fraction of the total conductivity carried by each ionic species i . The fraction is a quantity called the transfer number (t_i) defined by

$$t_i = \frac{\sigma_i}{\sigma_t} < 1 \quad (10.51)$$

$$\sum t_i = 1 \quad (10.52)$$

This expression, eq. (10.52), suggests that $t_e \approx 1$ for electronic conductors and $t_e \approx 1$ for ionic conductors. In fact, this quantity is simply a conductivity ratio which represents that fraction of the specie i embodied in the oxide formation. Whatever its initial state is, the oxide evolves until it achieves a specific atomic arrangement and thickness at its equilibrium state.

Example 10.6 a) Derive expressions for the oxygen anion diffusivity and the mobility in



semiconductor oxide and b) plot its profile as a function of temperature, and c) calculate σ_i , D_i , B'_i , and B_i for oxygen anions. Use the Kingery et al. [24] oxygen conductivity expression given in Barsom's book, page 231, and the oxygen ionic concentration of 5.52×10^{28} ions/m³ [8]

$$\sigma_i = (1.50 \times 10^5 \text{ ohm}^{-1} \cdot \text{m}^{-1}) \exp\left(-\frac{1.26 \text{ eV}}{kT}\right) \quad (\text{a})$$

Solution:

$$\begin{aligned} \text{a) } C_i &= 5.52 \times 10^{28} \text{ m}^{-3} & e &= 1.602 \times 10^{-19} \text{ C (= A.s)} & z &= 2 \\ k &= 1.38 \times 10^{-23} \text{ J/}^\circ\text{K} & &= 8.61 \times 10^{-5} \text{ eV} & & \end{aligned}$$

From eq. (10.45), the O^{-2} anion diffusivity is

$$D_i = \frac{kT\sigma_i}{(ze)^2 C_i} \quad (\text{b})$$

$$D_i = \left(2.44 \times 10^{-15} \frac{\text{ohm} \cdot \text{m}^3}{\text{s} \cdot \text{K}}\right) T \sigma_i \quad (\text{c})$$

Substituting eq. (a) into (c) gives $D_i = f(T)$

$$D_i = \left(3.65 \times 10^{-10} \frac{\text{m}^2}{\text{s} \cdot ^\circ\text{K}}\right) T \exp\left(-\frac{1.46 \times 10^4 \text{ }^\circ\text{K}}{T}\right) \quad (\text{d})$$

Now, combining eq. (10.35) and (10.36) and (d) yields the sought ionic mobility expressions

$$B'_i = \left(8.46 \times 10^{-6} \frac{\text{m}^2}{\text{V} \cdot \text{s}}\right) \exp\left(-\frac{1.46 \times 10^4 \text{ }^\circ\text{K}}{T}\right) \quad (\text{e})$$

$$B_i = \left(2.64 \times 10^{13} \frac{\text{m}^2}{\text{J} \cdot \text{s}}\right) \exp\left(-\frac{1.46 \times 10^4 \text{ }^\circ\text{K}}{T}\right) \quad (\text{f})$$

Both B'_i and B_i profiles for oxygen are shown in the plots $E - 10.3B'_i$ and $E - 10.3B_i$ below.

b) Plots

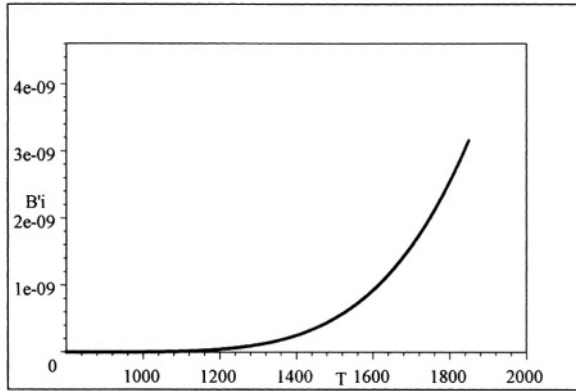


Figure E-10.6B'i

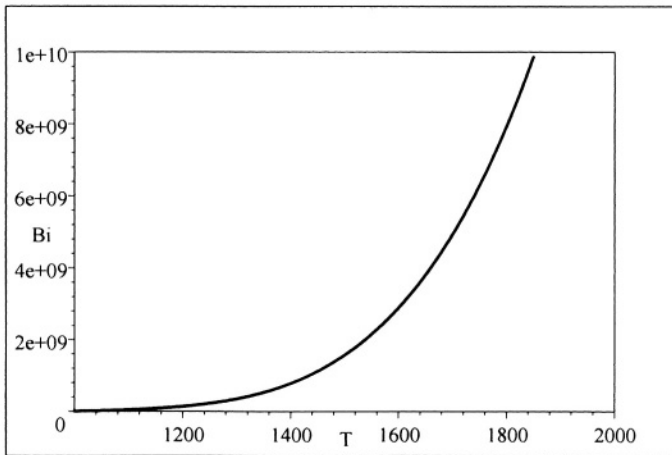


Figure E-10.6Bi

c) At $T = 1200^\circ\text{C}$

$$\sigma_i = 0.76 \text{ ohm}^{-1} \cdot \text{m}^{-1}$$

$$D_i = 2.28 \times 10^{-12} \text{ m}^2/\text{s}$$

$$B'_i = 4.40 \times 10^{-11} \text{ m}^2/\text{V} \cdot \text{s}$$

$$B_i = 1.37 \times 10^{-11} \text{ m}^2/\text{V} \cdot \text{s}$$

10.6 WAGNER THEORY OF OXIDATION

The Wagner theory [10] for a coupled diffusion and migration (also known as ambipolar diffusion) mass transfer during oxidation of metals and alloys is briefly described. This theory treats the parabolic kinetic behavior of high temperature oxides given by eq. (10.19) with $n = 1/2$.

First of all, combining eqs. (10.31) and (10.41) yields the total ionic flux in the x -direction

$$J_{x,i} = -\frac{\sigma_i}{(z_i e)^2} \left[\frac{d\mu_i}{dx} + (z_i e) \frac{d\phi}{dx} \right] \quad (10.52)$$

This expression represents the condition of the quantity of particles in motion of a reacting metal-oxygen system through the chemical and electrical potential gradients, $d\mu_i/dx$ and $d\phi/dx$, respectively. Thus, the relationship between these gradients illustrates the connection embodied in the ionic flux for a reacting system in which all moving species are charged particles. Therefore, both $d\mu_i/dx$ and $d\phi/dx$ are the driving forces of the ionic flux $J_{x,i}$. The oxidizing system under consideration consists of a pure metal exposed to a gaseous environment at relatively high temperature. Particularly, a pure metal and a single gas phase, such as oxygen, define an univariant system since the metal and gas react to form one single phase.

However, if the material is an alloy containing at least two elements, then the more active element oxidizes first and its cations react with the gas-phase anions to form the initial oxide, sulfide, carbide, nitride, and so on. Other elements in the alloy may react afterward to form other surface compounds. Consequently, the surface scale may be a combination of phases, which may be identified by X-Ray diffraction and revealed by scanning electron microscopy (SEM).

Assume that a pure metal is oxidizing and that a single-phase oxide forms by diffusion of cations and anions, and migration of electrons. This ideal atomic mass transfer for oxide growth requires that the positively charged cations and electrons flow outward and the negatively charged anions flow inward. Thus, the ionic flux balance for outward cations ($z_c J_c$), inward anions ($z_a J_a$) and electrons ($z_e J_e$) along with $z_e = 1$ is [10]

$$z_c J_c = z_a J_a + z_e J_e \quad (10.53)$$

This relationship derives directly from the conservation of mass that accompanies the mass transfer and it is succinctly represented in the treatment of ionic flux balance. For ionic electroneutrality, this notation, eq. (10.53), can be further simplified by letting $J_a \approx 0$ and using eq. (10.52) for both cations and electrons together with (10.53) yields the electrical potential gradient

$$\frac{d\phi}{dx} = \frac{\sigma_e}{e(\sigma_c + \sigma_e)} \left[\frac{d\mu_e}{dx} - \frac{\sigma_c}{z_c \sigma_e} \frac{d\mu_c}{dx} \right] \quad (10.54)$$

$$\frac{d\phi}{dx} = \left(\frac{t_e}{e} \right) \frac{d\mu_e}{dx} - \left(\frac{t_c}{z_c e} \right) \frac{d\mu_c}{dx} \quad (10.55)$$

Inserting eq. (10.54) into (10.52) and letting $J_{x,i} = J_{x,c}$ yields the cation vacancy flux in terms of more easily measurable electrical conductivity

$$J_{x,c} = -\frac{\sigma_c \sigma_e}{(z_c e)^2 (\sigma_c + \sigma_e)} \frac{d\mu}{dx} \quad (10.56)$$

$$J_{x,c} = -\frac{\sigma_c t_e}{(z_c e)^2} \frac{d\mu}{dx} \quad (10.57)$$

and the chemical potential gradient across the scale is described by

$$\frac{d\mu}{dx} = \frac{d\mu_c}{dx} + z_c \frac{d\mu_e}{dx} \quad (10.58)$$

where $d\mu_c/dx$ = Chemical potential gradient for M^{+z} cations

$d\mu_e/dx$ = Chemical potential gradient for electrons

$d\mu_c/dx < 0$

$d\mu_e/dx < 0$

The expression given by eq. (10.56) or (10.57) indicates that

- An oxide scale conducts both ions and electrons
- The chemical potential gradient $d\mu/dx$ of the neutral species is the driving force for growth of the oxide scale
- Cations, anions, and electrons diffuse together to maintain charge neutrality
- The rate-limiting is controlled by the slowest diffusion species
- If $\sigma_c = 0$ or $\sigma_e = 0$, then $J_{x,c} = 0$ (vanishes)
- If $\sigma_e \gg \sigma_c$ and $t_e \approx 1$, then $J_{x,c}$ may be determined by the rate electrons move through the oxide scale, which is the electronic conductor.
- If $\sigma_c \gg \sigma_e$ and $t_c \approx 1$, then $J_{x,c}$ may be determined by the rate cations (M^{+z}) move through the oxide scale (ionic conductor).

For a simple oxidation reaction ($M = M^{+z} + 2e^-$), $\sigma_e \gg \sigma_c$ and $\sigma_e \approx 1$. Consequently, eq. (10.56) becomes upon integration

$$J_{x,c} = -\frac{1}{x} \frac{\sigma_c}{(z_c e)^2} \int_{\mu_i}^{\mu_o} d\mu \quad (10.59)$$

where μ_i = Inside metal/oxide chemical potential (J/mol)

μ_o = Outside oxide-gas chemical potential (J/mol)

Additionally, the flow of cations in the x-direction occurs through the growing oxide layer, the cation flux $J_{x,c}$ becomes dependent on the thickness growth

rate (dx/dt) of the oxide layer. Hence, $J_{x,c}$ and dx/dt , eq. (10.20), are related as indicated below

$$J_{x,c} = C_c \frac{dx}{dt} \tag{10.60a}$$

$$J_{x,c} = nC_c K_x^n t^{n-1} \tag{10.60b}$$

where C_c = Concentration of cations ($mol.cm^{-3}$)
 K_x = Fundamental parameter

Combining eqs. (10.59) and (10.60) gives

$$\frac{dx}{dt} = -\frac{1}{x} \left[\frac{\sigma_c}{(z_c e)^2 C_c} \int_{\mu_i}^{\mu_o} d\mu \right] \tag{10.61}$$

For variations in oxygen pressure (P_{O_2}), the chemical potential gradient is given by Gibbs-Duhem equation [5,8]

$$\frac{d\mu}{dx} = -\frac{kT}{2} d \ln(P_{O_2}) \tag{10.62}$$

Substituting eq. (10.62) into (10.61) yields

$$\frac{dx}{dt} = \frac{1}{x} \left[\frac{kT\sigma_c}{2(z_c e)^2 C_c} \int_{P_i}^{P_o} d \ln(P_{O_2}) \right] \tag{10.63}$$

where P_i = Outer oxygen pressure
 P_o = Inner oxygen pressure

But, the term in brackets is defined as

$$K_r = \frac{kT\sigma_c}{2(z_c e)^2 C_c} \int_{P_i}^{P_o} d \ln(P_{O_2}) \tag{10.64}$$

Combining eqs. (10.45) and (10.64) along with $\sigma_i = \sigma_c$ gives

$$K_r = \frac{D_c}{2} \int_{P_i}^{P_o} d \ln(P_{O_2}) = \frac{D_c}{2} \ln \left(\frac{P_o}{P_i} \right) \tag{10.65}$$

and inserting eq. (10.65) into (10.63) yields

$$\frac{dx}{dt} = \frac{K_r}{x} \tag{10.66}$$

Integrating eq. (10.66) yields the parabolic equation for the oxide thickness

$$x = \sqrt{K_x t} \tag{10.67}$$

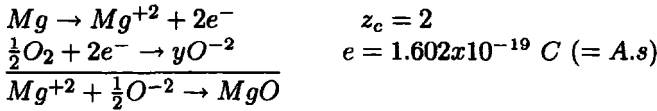
where $K_x = 2K_r$.

Example 10.7 Let's use some published data for magnesium oxide [21]. a) Determine if MgO containing aluminum ($2 \times 10^{19} \text{ cm}^{-3}$) is a mixed oxide conductor, provided that the conduction is by electrons and Mg^{+2} cation vacancies at $1600^\circ\text{C} = 1873^\circ\text{K}$. b) Calculate the species diffusivity. Given data:

Electron Holes	Cation Vacancies
$C_e = 5 \times 10^{13} \text{ cm}^{-3}$	$C_c = 5 \times 10^{13} \text{ cm}^{-3}$
$B'_e = 7.00 \text{ cm}^2/\text{V.s}$	$B'_c = 7.60 \times 10^{-6} \text{ cm}^2/\text{V.s}$

Solution:

a) Reactions involved in the magnesium oxide formation:



From eq. (10.46),

$$\begin{aligned} \sigma_e &= (z_e e)^2 C_e B'_e = (1) (1.602 \times 10^{-19} \text{ A.s}) (5 \times 10^{13} \text{ cm}^3) (7 \text{ cm}^2/\text{V.s}) \\ \sigma_e &= 5.61 \times 10^{-5} \text{ ohm}^{-1} \text{ cm}^{-1} \end{aligned}$$

$$\begin{aligned} \sigma_c &= (z_c e)^2 C_c B'_c = (2) (1.602 \times 10^{-19} \text{ A.s}) (2 \times 10^{19} \text{ cm}^3) (7.6 \times 10^{-6} \text{ cm}^2/\text{V.s}) \\ \sigma_c &= 4.85 \times 10^{-5} \text{ ohm}^{-1} \text{ cm}^{-1} \end{aligned}$$

Thus, the total conductivity and transfer numbers are

$$\sigma_t = \sigma_c + \sigma_e = 10.46 \times 10^{-5} \text{ ohm}^{-1} \text{ cm}^{-1}$$

$$t_e = \sigma_e / \sigma_t = 0.54 \text{ for electronic conduction}$$

$$t_c = \sigma_c / \sigma_t = 0.46 \text{ for ionic conduction}$$

$$\sum t_i = t_e + t_c = 1$$

Therefore, MgO is a mixed conductor since $t_e > 0$ and $t_c > 0$ and it is an n-type oxide since $0 < t_e < 1$ and $0 < t_c < 1$.

b) From eq. (10.35),

$$D_e = kTB'_e / (z_e e)$$

$$D_e = (1.38 \times 10^{-23} \text{ A.s.V/K}) (1873 \text{ K}) (7 \text{ cm}^2/\text{V.s}) / [(1) (1.602 \times 10^{-19} \text{ A.s})]$$

$$D_e = 1.13 \text{ cm}^2/\text{s}$$

$$D_c = kTB'_c / (z_c e)$$

$$D_c = (1.38 \times 10^{-23}) (1873) (7.6 \times 10^{-6}) / [(2) (1.602 \times 10^{-19})]$$

$$D_c = 6.13 \times 10^{-7} \text{ cm}^2/\text{s}$$

Therefore, the diffusion rate-limiting is due to the cations because of the differences in diffusion coefficient, $D_c < D_e$.

10.7 EXPERIMENTAL DATA

In general, the thermogravimetric technique (TGT) can be used to measure the amount and rate of change of sample mass as a function of time or temperature in gaseous environments. The thermogravimetric analyzer (TGA) is an instrument that can be used to characterize the thermal kinetic behavior of solid-gas reactions. As a result, a thermogravimetric analysis allows one to continuously measure weight changes, which depends on the instrument sensitivity.

The parabolic weight gain is a typical oxidation analysis of high-temperature corrosion, which is better known as oxidation kinetics. Figure 10.10 shows the influence of time and temperature on the linearized weight gain (W^2). This plot is a convenient way for determining the parabolic rate constant K_w as the slope of a straight line. Thus, the kinetic model given by eq. (10.21) is obeyed. Notice the parabolic rate constant in the literature is K_p , but here $K_w = K_p$.

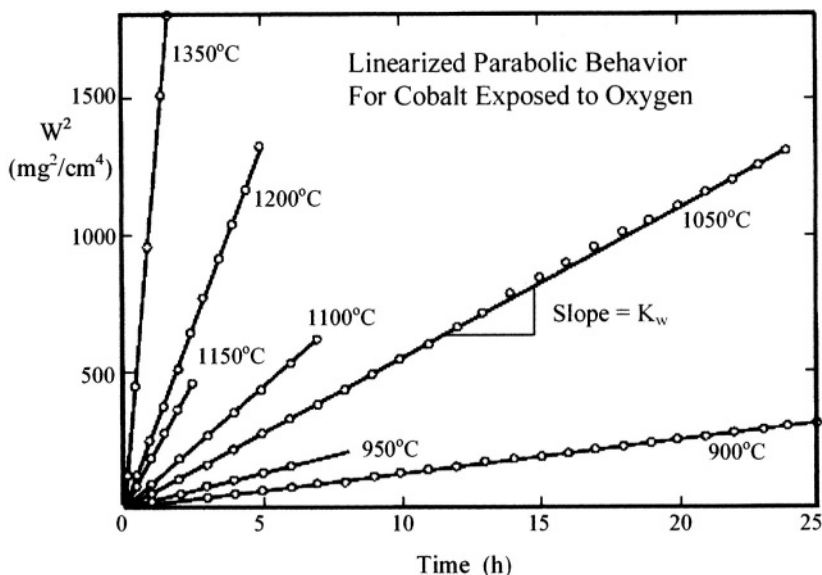


Figure 10.10 Linearized weight gain for Cobalt (Co) in oxygen environment [11].

The slopes of the lines in Figure 10.10 are plotted in Figure 10.11. Despite that there is a slight data scatter, the parabolic rate constant obeys the Arrhenius relationship as predicted by eq. (10.15). The curve fitting equation is given in Figure 10.11. Notice that the slope of the straight line and the activation

energy are, respectively

$$\frac{Q}{R} = 1.176^\circ C = 274.176^\circ K$$

$$Q \simeq 2,280 \frac{J}{mol}$$

Thus, Q is high which means that diffusion occurs at a high rate for oxide growth at the high temperature range $900^\circ C \leq T \leq 1350^\circ C$.

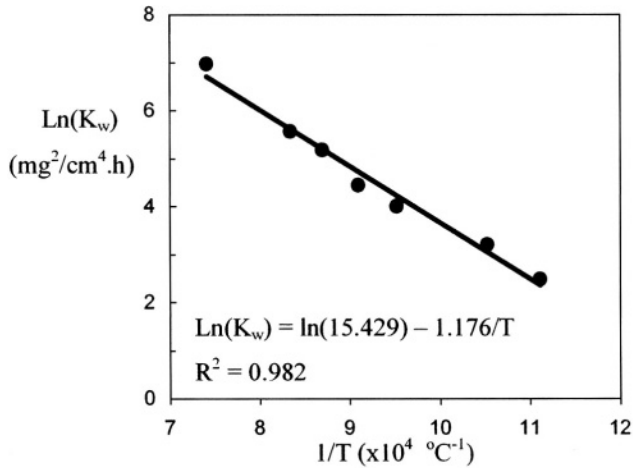


Figure 10.11 Arrhenius plot for the parabolic rate constant in Figure 10.10.

Table 10.2 lists some experimental parabolic rate constant values for common oxides. Using the K_w data for selected oxides at $T = 1000^\circ C$ and $P_{O_2} = 1.00 atm$ and eq. (10.24) yields the parabolic profiles shown in Figure 10.12.

Table 10.2 Parabolic rate constant values obtained in oxygen [5,7].

Metal	Oxide	K_w		T °C	P_{O_2} (atm)
		$(g^2/cm^4.s)$	$(\mu g^2/cm^4.h)$		
Co	CoO	2.10×10^{-10}	0.76	1000	1.00
Cu	Cu ₂ O	6.30×10^{-9}	22.68	1000	0.08
Ni	NiO	2.90×10^{-8}	104.40	1000	1.00
Fe	FeO	4.80×10^{-7}	1,728	1000	1.00
Fe	Fe ₃ O ₄	1.40×10^{-6}	5,040	1000	1.00
Cr	Cr ₂ O ₃	1.00×10^{-10}	0.36	1000	1.00
Cr	Cr ₂ O ₃	1.30×10^{-11}	0.0468	900	0.10
Si	SiO ₂	1.20×10^{-12}	0.0043	1000	1.00
Al	Al ₂ O ₃	8.50×10^{-16}		600	1.00

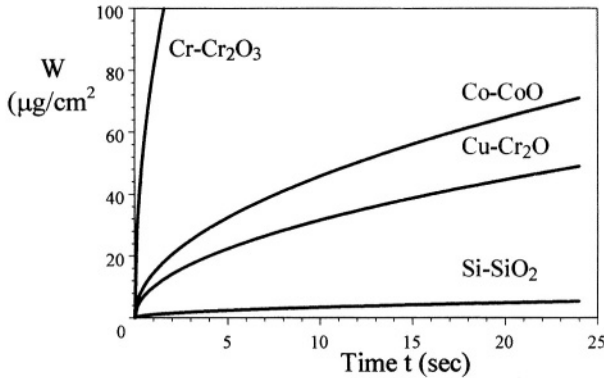


Figure 10.12 Parabolic behavior due to weight gain of some oxides listed in Table 10.2. Conditions: $T = 1000^\circ\text{C}$ and $P_{\text{O}_2} = 1.0 \text{ atm}$.

These results indicate that is very sensitive to diffusion of cations since the parabolic rate constant K_w depends on the diffusivity. For instance, chromium and silicon in Figure 10.12 are the fastest and the slowest elements that oxidize in oxygen, respectively. Therefore, $D_{\text{Cr}} \gg D_{\text{Si}}$ from Figure 10.12. Since weight gain and oxide thickness are related through eq. (10.26) with $n = 1/2$, it is convenient to combine eqs. (10.26) and 10.19) or (10.67) to get

$$x = \frac{1}{\rho} \sqrt{K_w t} \tag{10.68}$$

which is an alternative expression for characterizing oxide thickness growth.

Example 10.8 Calculate the thickness of Al_2O_3 oxide when pure aluminum is exposed to oxygen environment at 600°C and 1 atm for one day. Use the K_w value from Table 10.2 and $\rho_{\text{Al}_2\text{O}_3} = 3.80 \text{ g}/\text{cm}^3$.

Solution:

From Table 10.2 $K_w = 8.50 \times 10^{-16} \text{ g}^2/\text{cm}^4 \cdot \text{s}$ from eqs. (10.16) and (10.26)

$$K_x = \frac{K_w}{\rho^2} = \frac{8.50 \times 10^{-16} \text{ g}^2/\text{cm}^4 \cdot \text{s}}{(3.80 \text{ g}/\text{cm}^3)^2} = 5.89 \times 10^{-19} \text{ cm}^2/\text{s}$$

From eq. (10.68) or (10.67),

$$\begin{aligned} x &= \sqrt{K_x t} = \sqrt{(5.89 \times 10^{-19} \text{ cm}^2/\text{s})(86,400 \text{ s})} \\ x &= 0.23 \text{ }\mu\text{m} \end{aligned}$$

Furthermore, the effects of microstructure on stainless steels is of particular interest despite that chromium enhances oxidation resistance. Grain boundaries can provide suitable sites for accelerated oxidation, but chromium depletion at these boundaries aids the formation of chromium dioxide (chromia) Cr_2O_3 scale. Thus, the oxidation of stainless steels in high-temperature oxygen-rich environments strongly depends on composition and temperature, rather than on microstructure. For instance, the common service temperatures for wrought stainless steels in air varies according to the following inequalities

$$\begin{aligned} 800^{\circ}C &< T_{austenitic} < 1200^{\circ}C \\ 600^{\circ}C &< T_{martensitic} < 780^{\circ}C \\ 700^{\circ}C &< T_{ferritic} < 1100^{\circ}C \end{aligned}$$

and for cast stainless steels in air

$$600^{\circ}C < T_{cast} < 1200^{\circ}C$$

The service temperature of a particular stainless steel can be found elsewhere [17]. Recently published stainless steel, carbon steel and nickel data on oxidation clearly exhibit increasing oxide thickness growth with increasing temperature as summarized in Figure 10.13 after one year of exposure in air [18].

Both carburizing and nitriding are also oxidizing processes, which are important in industrial applications for enhancing the hardness and strength of steels. Therefore, these methods are out of the scope of this chapter.

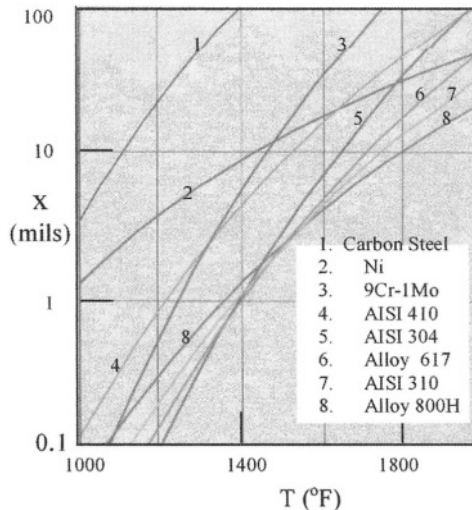


Figure 10.13 Effect of temperature on metal oxide growth of some materials exposed to air (21% O_2) for one year. 1 mil = 0.25 mm [18].

In general, it is known that stainless steels exhibit high oxidation resistance in gaseous environments. Using Rohrig et al. data [19], which can be found elsewhere [20], yields the kinetic behavior illustrated in Figure 10.14. Thus, the data clearly shows the beneficial effect of chromium content in steels exposed to steam. Therefore, the corrosion resistance of steel increases with increasing chromium content. The data indicates that penetration is significantly reduced as chromium content increases. For instance, at 2,000 – hour exposure time, the oxide thickness is

$$x = \begin{cases} 0.180 \text{ mm} & \text{for SAE 1010} \\ 0.130 \text{ mm} & \text{for SAE 1035} \\ 0.090 \text{ mm} & \text{for 1.25Cr,Mo,Si} \\ 0.060 \text{ mm} & \text{for 2.5Cr,Mo,Si} \\ 0.038 \text{ mm} & \text{for 5Cr-0.5Mo} \\ 0.012 \text{ mm} & \text{for 12Cr-2Mo} \\ 0.005 \text{ mm} & \text{for 18-8 alloy} \end{cases}$$

These remarkable differences dictate that carbon and chromium contents control the thickness growth for carbon and stainless steels.

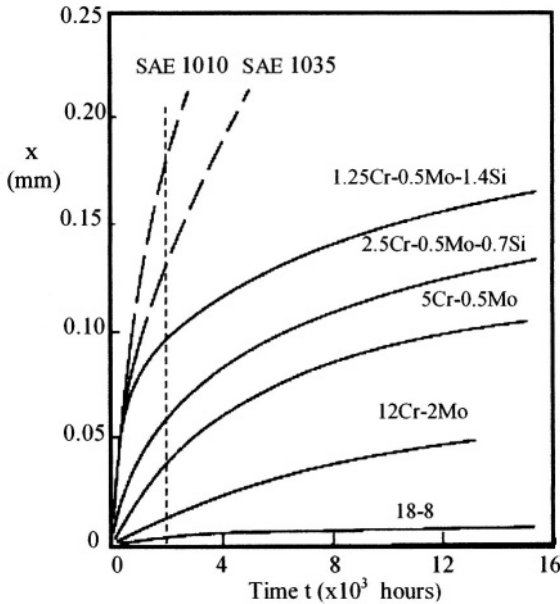


Figure 10.14 Effect of chromium content and exposure time to steam at 595°C on carbon and stainless steel bars [19].

10.8 SUMMARY

The oxidation of metals and alloys in gaseous environments at high temperatures form porous scales and consequently, the materials gain weight. Metals experiencing high-temperature oxidation (HTO) in gaseous environments gain weight and those in aqueous solutions lose weight. Therefore, HTO in hot gases opposes HTO in aqueous solutions. With regard to the former oxidation process, the oxide scale serves as the electrolyte and oxygen-containing gases are the most common oxidizing environments. The process of oxidation in electrolytes.

Also, HTO in hot gases may occur internally or externally, and it is characterized by its quality through the Pilling-Bedworth ratio. Thermodynamically, the occurrence of an oxidation reaction at high temperatures may be predicted by the Gibbs free energy of formation if $\Delta G < 0$, which dictates that a M_xO_y product forms by diffusion.

The characterization of the oxide scale formation is through the oxidation kinetics, from which the weight gain as a function of heating time may exhibit a linear behavior if the scale is porous and nonprotective ($PB < 1$), parabolic or logarithmic behavior for protective and adhered scale ($1 \leq PB \leq 2$). For instance, Wagner theory of oxidation predicts a parabolic behavior for the weight gain (W) and the oxide thickness growth (x). On the other hand, Fick's theory of diffusion predicts that the driving force for parabolic oxidation is the concentration gradient (dC_i/dx) of the diffusing species i . In the latter theory diffusivity is the measurable kinetic parameter related to the ionic mobility through the Nernst-Einstein equation.

Most metal oxides are nonstoichiometric., such as $Fe_{0.95}O$ instead of the ideal molecular formula FeO . This characteristic may be due to the different concentration of cations (C_c) and anions (C_a). If $C_c > C_a$, the metal oxide is an n-type semiconductor since there is metal-excess. On the other hand, if $C_c < C_a$, then a p-type semiconductor occurs due to metal-deficit condition.

Despite that the vacancy mechanism prevails as the atomic defect in oxide semiconductors, diffusion is strongly related to electrical conductivity. This implies that both diffusion and migration ionic fluxes of cations and anions may be defined by the simplified Nernst-Planck equation, which includes the Fick's steady-state diffusion equation or Fick's first law of diffusion. If oxide formation occurs by this dual mechanism, known as Ambipolar diffusion, then both concentration gradient and potential gradient together are the driving force for this ionic process at high temperatures. However, the thermal expansion coefficient of the metal substrate and that of the oxide may be different and consequently, spalling (separation) of the oxide scale may occur leading to more metal oxidation, which may jeopardize .

10.9 PROBLEMS

10.1 A silicon oxide crucible is used to melt pure aluminum in the presence of oxygen at 1300°C . a) Will the silicon oxide (SiO_2) corrode? b) What's the oxygen pressure? [Hint: Use Figure 10.1]. [Solution: b) $P_{\text{O}_2} = 5.71 \times 10^{-7} \text{ atm} = 5.77 \times 10^{-5} \text{ kPa}$].

10.2 An Alumina (Al_2O_3) crucible contains molten copper and oxygen (O_2) at 600°C . Determine a) if the crucible will corrode, if so, calculate the oxygen pressure.

10.3 In the case of thick oxide formation at high temperature, the Pilling-Bedworth theory may have a limited applicability. Explain why this may be the case.

10.4 If the protective nature of an oxide film at room temperature is lost at relatively high temperatures, explain the sequence of the oxide thickening process.

10.5 Determine the values of K_w from Figure 10.10 and plot K_w vs. T . What can you conclude from this plot?

10.6 Use the data given below to plot oxide molecular weight vs. K_p for $T = 1000^{\circ}\text{C}$ and $P_{\text{O}_2} = 1 \text{ atm}$. What can you conclude from the plot?

Element	Atomic Weight (g/mol)	Molecular Weight (g/mol)	K_w [$(\text{g}^2\text{O}_2)/\text{cm}^4 \cdot \text{s}$]
Co	58.93	CoO \rightarrow 74.93	2.10×10^{-10}
Cu	63.54	Cu ₂ O \rightarrow 143	6.30×10^{-9}
Fe	55.85	FeO \rightarrow 71.85	4.80×10^{-10}
Si	28.10	SiO ₂ \rightarrow 60.10	1.20×10^{-12}

10.7 Calculate a) the equilibrium constant K and b) the dissociation oxygen pressure P_{O_2} for the oxidation of aluminum at 1100°C . [Solution: a) $K = 1.58 \times 10^{31}$ and b) $P_{\text{O}_2} = 6.35 \times 10^{-32}$].

10.8 If 100 grams of pure aluminum (Al) oxidizes according to the reaction $4\text{Al} + 3\text{O}_2 = 2\text{Al}_2\text{O}_3$, calculate the PB ratio defined by

$$PB = V_{\text{Al}_2\text{O}_3}/V_{\text{Al}}$$

where V 's are volumes. Data: $\rho_{\text{Al}} = 2.70 \text{ g/cm}^3$ and $\rho_{\text{Al}_2\text{O}_3} = 2.70 \text{ g/cm}^3$ [Solution: $PB = 1.34$].

10.9 A chromium bar is exposed to oxygen gas at 900°C . Calculate a) the oxygen partial pressure and b) the oxygen activity. [Solution: a) $6.92 \times 10^{-7} \text{ kPa}$ and b) $6.85 \times 10^{-12} \text{ mol/cm}^3$].

10.10 REFERENCES

- [1] N.B. Pilling and R.E. Bedworth, *J. Inst. Met.*, 29 (1923) 529
- [2] D.A. Jones, "*Principles and Prevention of Corrosion*," Macmillan Publishing Company, New York, (1992)
- [3] P. Kofstad, in *High Temperature Corrosion*, edited by R.A. Rapp, NACE, Houston, (1983)
- [4] D.R. Gaskell, "*An Introduction to Transport Phenomena in Materials Engineering*" Macmillan Publishing Company, New York, (1992)
- [5] S.A. Bradford, *Corrosion*, Vol. 13, ASM Handbook, (1992) 64
- [6] M.G. Fontana, "*Corrosion Engineering*," third edition, McGraw-Hill Book Company, New York, (1986)
- [7] G.H. Geiger and D.R. Poirier, "*Transport Phenomena in Metallurgy*," Addison-Wesley Publishing Company, Reading, Massachusetts, (1973)
- [8] M.W. Barsoum, "*Fundamentals of Ceramics*," The McGraw-Hill Companies, Inc., New York, (1997)
- [9] "*Materials Principles and Practice*," edited by C. Newey and G. Weaver, Butterworth, The Open University, Boston, (1990) 356
- [10] C. Wagner, *Z. Physik Chem.*, Vol. B21, (1933)
- [11] F.R. Billman, *J. Electrochem. Soc.*, 119 (1972) 1198
- [12] P. Perez, J.A. Jimenez, G. Frommeyer, and P. Adeva, *Mat. Sci., Eng.*, A284 (2000) 138
- [13] S.Y. Liu, C.L. Lee, C.H. Kao, and T.P. Perng, *Corrosion*, Vol. 56, 4 (2000) 339
- [14] C. Wagner, *Atom Movements*, ASTM, (1951) 153
- [15] J. Regina, *Adv. Materials & Processes*, Vol. 160, 3 (March 2002) 47
- [16] S. Seal, S.K. Bose and S.K. Roy, *Oxidation of Metals*, Vol. 41, Number 1-2, (Feb. 1994) 139-178
- [17] A.J. Sedriks, "*Corrosion of Stainless Steels*," Second ed., John Wiley & Sons Inc., New York, (1996) 388-400
- [18] R.C. John, A.D. Pelton, A.L. Young, W.T. Thompson, I.G. Wright, and T.M. Nesmann, *Adv. Mat. & Processes*, Vol. 160, 3 (2002) 27-31
- [19] I.A. Rohrig, R.M. Van Duzer, and C.H. Fellows, "*High Temperature Steam Corrosion Studies at Detroit*," *Trans. ASME*, 66 (May 1944) 277-290
- [20] "The Making, Shaping, and Treating of Steel," Ninth ed., edited by H.E. McGannon, United States Steel Corporation (USS), Pittsburgh, PA, (1971) 1197
- [21] Y-M. Chiang, D.P. Bernie, III, and W.D. Kingery, "*Physical Ceramics: Principles for Ceramic Science and Engineering*," John Wiley & Sons, Inc., New York, (1997) 101-184
- [22] A. Kelly, G.W. Groves, and P. Kidd, "*Crystallography and Crystal Defects*," Revised edition, John Wiley and Sons, LTD, New York, (2000) 298-290
- [23] S.M. Allen and E.L. Thomas, "*The Structure of Materials*," John Wiley & Sons, Inc., New York, (1999) 251-260
- [24] W.D. Kingery, J. Pappis, M.E. Doty, and D.C. Hill, *J. Amer. Cer. Soc.*, 42 (8) (1959) 393-398

Appendix A

SOLUTION OF FICK'S SECOND LAW

The general diffusion equation for one-dimensional analysis under non-steady state condition is defined by Fick's second law, eq. (4.19). Hence,

$$\frac{\partial C}{\partial t} = D \frac{\partial^2 C}{\partial x^2} \quad (\text{A1})$$

Let D be a constant and use the function $y = f(x, t)$ be defined by

$$y = \frac{x}{2\sqrt{Dt}} \quad (\text{A2})$$

Thus, the partial derivatives of eq. A2 are

$$\frac{\partial y}{\partial x} = \frac{1}{2\sqrt{Dt}} \quad \text{and} \quad \frac{\partial y}{\partial t} = -\frac{x}{4\sqrt{Dt^3}} \quad (\text{a})$$

By definition,

$$\frac{\partial C}{\partial t} = \frac{dC}{dy} \frac{\partial y}{\partial t} = -\frac{x}{4\sqrt{Dt^3}} \frac{dC}{dy} \quad (\text{b})$$

$$\frac{\partial^2 C}{\partial x^2} = \frac{\partial}{\partial x} \left[\frac{dC}{dy} \left(\frac{\partial y}{\partial x} \right) \right] = \frac{1}{4Dt} \frac{d^2 C}{dy^2} \quad (\text{c})$$

Substituting eqs. (b) and (c) into A1 yields

$$\frac{dC}{dy} = -\frac{\sqrt{Dt}}{x} \frac{d^2 C}{dy^2} \quad (\text{A.3})$$

Combining eq. (A2) and (A3) gives

$$\frac{dC}{dy} = -\frac{1}{2y} \frac{d^2 C}{dy^2} \quad (\text{A4})$$

Now, let $z = dC/dy$ so that eq. (A4) becomes

$$z = -\frac{1}{2y} \frac{dz}{dy} \quad (\text{a})$$

$$-2 \int y dy = \int \frac{dz}{z} \quad (\text{b})$$

Then,

$$-y^2 = \ln z - \ln B \quad (\text{c})$$

where B is an integration constant. Rearranging eq. (c) yields

$$z = B \exp(-y^2) \quad (\text{A5})$$

and

$$\int dC = B \int \exp(-y^2) dy \quad (\text{A6})$$

The function $f = \exp(-y^2)$ represents the so-called "Bell-Shaped Curves". The solution of the integrals are based on a set of boundary conditions.

A.1 FIRST BOUNDARY CONDITIONS

In order to solve integrals given by eq. (A6) a set of boundary conditions the concentration and the parameter y are necessary. This boundary conditions are just the integral limits. Thus,

$$C = \begin{cases} C_x = C_o & \text{for } y = 0 \text{ at } t > 0 \text{ and } x = 0 \\ C_x = C_b & \text{for } y = \infty \text{ at } t = 0 \text{ and } x > 0 \end{cases} \quad (\text{a})$$

$$\int_{C_o}^{C_b} dC = B \int_0^{\infty} \exp(-y^2) dy \quad (\text{c})$$

$$C_b - C_o = B \int_0^{\infty} \exp(-y^2) dy \quad (\text{A7})$$

Use the following integral definitions and properties of the error function $\text{erf}(y)$

$$\int_0^\infty \exp(-y^2) dy = \frac{\sqrt{\pi}}{2} \tag{a}$$

$$\int_{-\infty}^\infty \exp(-y^2) dy = \sqrt{\pi} \tag{b}$$

$$\operatorname{erf}(y) = \frac{2}{\sqrt{\pi}} \int_0^y \exp(-y^2) dy \tag{c}$$

$$\operatorname{erf} c(y) = \frac{2}{\sqrt{\pi}} \int_y^\infty \exp(-y^2) dy \tag{d}$$

$$\operatorname{erf}(y) + \operatorname{erf} c(y) = 1 \quad \text{and} \quad \operatorname{erf}(-y) = -\operatorname{erf}(y) \tag{e}$$

$$\operatorname{erf}(0) = 0 \quad \text{and} \quad \operatorname{erf}(\infty) = 1 \tag{f}$$

By definition, the function $\operatorname{erf} c(y)$ is the complement of $\operatorname{erf}(y)$. Inserting eq. (a) into (A7) yields the constant B defined by

$$B = \frac{2}{\sqrt{\pi}} (C_b - C_o) \tag{A8}$$

A.2 SECOND BOUNDARY CONDITIONS

The second set of boundary conditions are given below

$$C = \begin{cases} C_x = C_x \text{ at } y < \infty \\ C_x = C_b \text{ at } y = \infty \end{cases} \tag{a}$$

Setting the limits of the integral given by eq. (A6) and using eq. (A8) yields the solution of Fick's second law of diffusion when the bulk concentration ($C_b = C_x$ at $x = \infty$) is greater than the surface concentration ($C_o = C_x$ at $x = 0$). Hence, the solution of eq. (A1) for **concentration polarization** ($C_b > C_o$) becomes

$$\int_{C_b}^{C_x} dC = B \int_\infty^y \exp(-y^2) dy = -B \int_y^\infty \exp(-y^2) dy \tag{b}$$

$$C_x - C_o = -\frac{2}{\sqrt{\pi}} (C_b - C_o) \frac{\sqrt{\pi}}{2} \operatorname{erf} c(y) \tag{c}$$

$$\frac{C_x - C_b}{C_o - C_b} = 1 - \operatorname{erf} \left(\frac{x}{2\sqrt{Dt}} \right) \quad \text{for } C_b > C_o \tag{A9}$$

A.3 THIRD BOUNDARY CONDITIONS

Similarly, the solution of eq. (A1) for **activation polarization** ($C_o < C_b$) upon using the boundary conditions given below as well as eqs. (A6) and (A8) yields the normalized concentration expression

$$C = \begin{cases} C_x = C_x \text{ at } y > 0 \\ C_x = C_o \text{ at } y = 0 \end{cases} \quad (\text{a})$$

$$\int_{C_o}^{C_x} dC = B \int_0^y \exp(-y^2) dy \quad (\text{b})$$

$$C_x - C_o = \frac{2}{\sqrt{\pi}} (C_b - C_o) \frac{\sqrt{\pi}}{2} \operatorname{erf}(y) \quad (\text{c})$$

$$\frac{C_x - C_o}{C_b - C_o} = \operatorname{erf}\left(\frac{x}{2\sqrt{Dt}}\right) \quad \text{For } C_o < C_b \quad (\text{A10})$$

This concludes the analytical procedure for solving Fick's second law of diffusion for concentration and activation polarization cases.

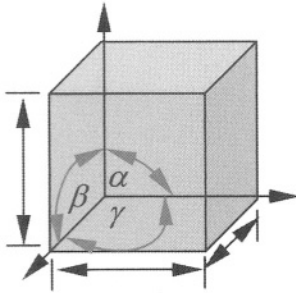
Appendix B

CRYSTAL STRUCTURES

Table B.1 Properties of Some Elements

Name	Symbol	Structure	Ion	Ionic Radius (nm)	Density @ 20C (g/cm ³)	Atomic Weight (g/mol)
Aluminum	Al	FCC	Al ⁺³	0.053	2.70	26.98
Beryllium	B	HCP	Be ⁺²	0.035	1.85	9.01
Boron	B	Rhomb.	B ⁺³	0.023	2.34	10.81
Cadmium	Cd	HCP	Cd ⁺²	0.095	8.65	112.40
Calcium	Ca	FCC	Ca ⁺²	0.100	1.55	40.08
Carbon	C	HCP	C ⁺⁴	0.016	2.25	12.00
Chromium	Cr	BCC	Cr ⁺²	0.084	7.19	52.00
		BCC	Cr ⁺³	0.063	7.19	52.00
Cobalt	Co	HCP	Co ⁺²	0.072	8.90	58.93
Copper	Cu	FCC	Cu ⁺²	0.096	8.96	63.54
Gold	Au	FCC	Au ⁺¹	0.137	19.32	196.97
Iron	Fe	BCC	Fe ⁺²	0.077	7.86	55.85
			Fe ⁺³	0.064	7.86	55.85
Lithium	Li	BCC	Li ⁺¹	0.068	0.53	6.94
Magnesium	Mg	HCP	Mg ⁺²	0.072	1.74	24.31
Manganese	Mn	SC	Mn ⁺²	0.067	7.43	54.94
Nickel	Ni	FCC	Ni ⁺²	0.069	8.90	58.71
Palladium	Pd	FCC	Pd ⁺²	0.064	12.02	106.40
Platinum	Pt	FCC	Pt ⁺²	0.080	21.45	195.08
Potassium	K	BCC	K ⁺¹	0.133	0.862	39.10
Silver	Ag	FCC	Ag ⁺	0.126	10.50	107.87
Silicon	Si	Cubic	Si ⁺⁴	0.041	2.33	28.09
Titanium	Ti	HCP	Ti ⁺³	0.076	4.51	47.90
Vanadium	V	BCC	V ⁺²	0.088	6.10	50.94
Zinc	Zn	HCP	Zn ⁺²	0.074	7.14	65.37

Table B.2 Lattice Parameters For Crystal Structures



Crystal	Axes	Angles	Element
Cubic	$a = b = c$	$\alpha = \beta = \gamma = 90^\circ$	Copper
Hexagonal	$a = b \neq c$	$\alpha = \beta = 90^\circ, \gamma = 120^\circ$	Cadmium
Tetragonal	$a = b \neq c$	$\alpha = \beta = \gamma = 90^\circ$	Tin
Rhombohedral	$a = b = c$	$\alpha = \beta = \gamma \neq 90^\circ$	Boron
Orthorhombic	$a \neq b \neq c$	$\alpha = \beta = \gamma = 90^\circ$	Sulfur
Monoclinic	$a \neq b \neq c$	$\alpha = \gamma = 90^\circ \neq \beta$	
Triclinic	$a \neq b \neq c$	$\alpha \neq \beta \neq \gamma \neq 90^\circ$	

Appendix C

CONVERSION TABLES

PREFIXES

Prefix	Symbol	Factor	Prefix	Symbol	Factor
exa	E	10^{18}	milli	10^{-3}	
peta	P	10^{15}	micro	10^{-6}	
tera	T	10^{12}	nano	10^{-9}	
giga	G	10^9	pico	10^{-12}	
mega	M	10^6	femto	10^{-15}	
kilo	k	10^3	atto	10^{-18}	

ABBREVIATIONS

atm = atmosphere	gal = gallon	MPa = megapascal
A = ampere	hp = horsepower	N = Newton
Å = angstrom	h = hour	nm = nanometer
Btu = British energy	in. = inch	Pa = pascal
C = coulomb	J = joule	psi = pounds/square inch
°C = degrees celsius	°K = degrees Kelvin	s = second
cal = calorie	Kg = kilogram	T = temperature
cm = centimeter	L = liter	W = watt or weight
eV = electron volt	min = minute	μ = micron
°F = degrees Fahrenheit	mm = millimeter	μm = micrometer
g = gram	mol = mole	Ω = ohm = V/A

GREEK ALPHABET

Alpha	α	Α	Iota	ι	Ι	Rho	ρ	Ρ
Beta	β	Β	Kappa	κ	Κ	Sigma	σ	Σ
Gamma	γ	Γ	Lambda	λ	Λ	Tau	τ	Υ
Delta	δ	Δ	Mu	μ	Μ	Upsilon	υ	Υ
Epsilon	ε	Ε	Nu	ν	Ν	Phi	φ	Φ
Zeta	ζ	Ζ	Xi	ξ	Ξ	Chi	χ	Χ
Eta	η	Η	Omicron	ο	Ο	Psi	ψ	Ψ
Theta	θ	Θ	Pi	π	Π	Omega	ω	Ω

AREA

1 m ² = 10 ⁴ cm ²	1 cm ² = 10 ⁻⁴ m ²
1 m ² = 10.76 ft ²	1 ft ² = 0.0929 m ²
1 cm ² = 0.155 in. ²	1 in. ² = 0.4516 cm ²
1 cm ² = 10 ² mm. ²	1 mm ² = 10 ⁻² cm ²

CORROSION RATE

1 mm/y = 39.37 mils/y (mpy)	1 mil/y = 2.54x10 ⁻² mm/y
1 μm/y = 3.937x10 ⁻² mils/y	1 μm/y = 25.40 mils/y

CURRENT RATE

1 A/m ² = 9.29x10 ⁻² A/ft ²	1 A/ft ² = 10.764 A/m ²
1 A/cm ² = 6.452 A/in ²	1 A/in ² = 0.155 A/cm ²
1 A/mm ² = 6.452x10 ² A/in ²	1 A/in ² = 1.55x10 ⁻³ A/mm ²
1 μA/cm ² = 6.452 μA/in ²	1 μA/in ² = 0.155 μA/cm ²

DENSITY

1 Kg/m ³ = 10 ⁻³ g/cm ³	1 g/cm ³ = 10 ³ Kg/m ³
1 Kg/m ³ = 0.0624 lb _m /ft ³	1 ft ³ = 16.02 Kg/m ³
1 g/cm ³ = 62.40 lb _m /ft ³	1 lb _m /ft ³ = 0.016 g/cm ³
1 g/cm ³ = 0.0361 lb _m /in ³	1 lb _m /in ³ = 27.70 g/cm ³

ELECTRICITY AND MAGNETISM

$d\phi/dx = V/cm$	V = volts
1 mho = 1 S	1 S = 1 mho
1 S = ohm ⁻¹ = Ω ⁻¹	1 ohm = 1 S ⁻¹
1 Ω.cm = 1.00x10 ⁻² Ω.m	1 Ω.m = 100 Ω.cm
1 Ω.cm = 1 ohm.cm	1 ohm = V/A
1 maxwell = 10 ⁻² μweber	1 μweber = 100 maxwell

ENERGY

1 J = 2.778x10 ⁻⁷ kW.h	1 kW.h = 3.60x10 ⁶ J
1 J = 0.239 cal	1 cal = 4.184 J
1 J = 9.48x10 ⁻⁴ Btu	1 Btu = 1.05x10 ³ J
1 J = 0.7376 ft.lb _f	1 ft.lb _f = 1.3558 J

FLOW RATE

1 L/min = 2.1189 ft ³ /h	1 ft ³ /h = 0.4719 L/min
1 L/min = 3.53x10 ⁻² ft ³ /min	1 ft ³ /min = 28.31
1 L/min = 15.85 gal/h	1 gal/h = 6.31x10 ⁻² L/min
1 L/min = 0.2642 gal/min	1 gal/min = 3.7854 L/min
1 m ³ /s = 2.1189x10 ³ ft ³ /min	1 ft ³ /min = 4.7195x10 ⁻⁴ m ³ /s
1 m ³ /s = 35.315 ft ³ /s	1 ft ³ /s = 2.8317x10 ⁻² m ³ /s
1 m ³ /s = 3.66x10 ⁶ in ³ /min	1 in ³ /min = 2.73x10 ⁻⁷ m ³ /s

FORCE

1 N = 10^5 dynes	1 dyne = 10^{-5} N
1 N = 0.2248 lb _f	1 lb _f = 4.448 N
1 N = 2.248×10^{-4} kips	1 kip = 4.448×10^3 N
1 N = 0.1019 Kg _f	1 Kg _f = 9.81 N

LENGTH

1 m = 10 A	1 A = 10^{-10} m	1 mil = 25.40 μm
1 m = 10^9 nm	1 nm = 10^{-9} m	1 yd = 0.9144 m
1 m = 10^6 μ	1 μ = 10^{-6} m	1 mile = 1.61 Km
1 m = 10^3 mm	1 mm = 10^{-3} m	
1 m = 10^2 cm	1 cm = 10 mm	
1 m = 39.36 in.	1 in. = 25.4 mm	
1 m = 3.28 ft	1 ft. = 12 in.	

MASS

1 Kg = 10^3 g	1 g = 10^{-3} Kg
1 Kg = 2.205 lb _m	1 lb _m = 0.4536 Kg
1 g = 2.205×10^{-3} lb _m	1 lb _m = 45.36 g
1 Kg = 10^{-3} metric ton	1 metric ton = 10^3 Kg
1 Kg = 1.1023×10^{-3} short ton	1 short ton = 2×10^3 lb _m
1 Kg = 9.8421×10^{-4} long ton	1 long ton = 1.016×10^3 Kg
1 metric ton = 1.1023 short ton	1 lb _m = 5×10^{-4} short ton
1 metric ton = 0.98421 long ton	1 long ton = 1.106 metric ton
1 Kg = 6.85×10^{-2} slug	1 slug = 14.59 kg

PHYSICAL CONSTANTS

Quantity	Symbol	Value
Acceleration of Gravity	g	= 9.81 m ² /s
		= 32.2 ft/s ²
Avogadro's number	N_A	= 6.022×10^{23} particle/mol
Boltzmann's constant	$k = R/N_A$	= 1.38×10^{-23} J/°K
		= 8.62×10^{-5} eV/°K
Electronic charge	q_e	= 1.602×10^{-19} C
Faraday's constant	$F = q_e N_A$	= 96,500 C/mol
		= 96,500 A.s/mol
		= 96,500 J/mol.V
Gas constant	$R = k N_A$	= 8.314 J/mol.°K
		= 1.987 cal/mol.°K
Plank's constant	h	= 6.626×10^{-34} J.s
		= 4.136×10^{-15} eV.s
Mass of electron	m_e	= 9.11×10^{-31} Kg
Velocity of light	c	= 3×10^8 m/s

POWER

1 W = 1 J/s	1 Btu/s = 1 ft.lbf/s
1 kW = 0.9478 Btu/s	1 Btu/s = 1.0551 kW
1 kW = 56.869 Btu/min	1 Btu/min = 1.758x10 ⁻² kW
1 kW = 3.4121x10 ³ Btu/h	1 Btu/h = 2.9307x10 ⁻⁴ kW
1 kW = 1.3405x10 ⁻³ hp	1 hp = 746 kW

PRESSURE (FLUID)

1 Pa = 1 N/m ²	1 atm = 760 mm.Hg, °C
1 Pa = 9.87x10 ⁻⁶ atm	1 atm = 1.0133x10 ⁵ Pa
1 MPa = 9.87x10 ⁻³ atm	1 atm = 101.33 MPa
1 Pa = 1.00x10 ⁻⁵ bar	1 bar = 1.00x10 ⁵ Pa
1 Pa = 1.45x10 ⁻⁴ psi	1 psi = 6.895x10 ³ Pa
1 MPa = 0.145 ksi	1 ksi = 6.895 MPa
1 Pa = 7.501x10 ⁻³ torr (mm Hg, °C)	1 torr = 1.333x10 ² Pa
1 Pa = 2.953x10 ⁻⁴ in. Hg, 32°F	1 in. Hg, 32°F = 3.386x10 ³ Pa
1 Pa = 2.0886x10 ⁻² lb _g /ft ²	1 atm = 14.7 psi

TEMPERATURE

T(K) = T(°C) + 273.15	T(R) = T(°F) + 459.67
ΔT(K) = ΔT(°C)	T(R) = (9/5)T(°K) + 459.67
	T(°F) = (9/5)T(°C) + 32
	T(°C) = (5/9)[T(°F) - 32]

VELOCITY

1 m/s = 1.1811x10 ⁴ ft/h	1 ft/h = 8.4667x10 ⁻⁵ m/s
1 m/s = 1.9685x10 ² ft/min	1 ft/min = 5.08x10 ⁻³ m/s
1 m/s = 3.281 ft/s	1 ft/s = 0.305 m/s
1 m/s = 39.37 in/s	1 in/s = 2.54x10 ⁻² in/s

VOLUME

1 m ³ = 10 ⁶ cm ³	1 cm ³ = 10 ⁻⁶
1 cm ³ = 10 ³ mm ³	1 mm ³ = 10 ⁻³ cm ³
1 m ³ = 35.32 ft ³	1 ft ³ = 0.0283 m ³
1 cm ³ = 0.061 in ³	1 in ³ = 16.39 in ³
1 L = 10 ³ cm ³ (cc)	1 cm ³ = 10 ⁻³
1 US gal = 3.785 L	1 L = 0.264 gal

Appendix D

GLOSSARY

A

Activation Energy: The energy required for to initiate a reaction or process.

Activation Polarization: An electrochemical condition controlled by the slowest step in a series of reaction steps.

Active Material: A metal or alloy susceptible to corrode.

Active-Passive Material: A metal or alloy that corrodes to an extent and then passivates due to an oxide film formation on its surface.

Anion: A negatively charged ion such as SO_4^{-2}

Anode: An electrode that oxidizes by liberating electrons or an electrode at which oxidation proceeds on its surface.

Anodic Dissolution: A corrosion process caused by an anodic overpotential, which depends on the exchange current density.

Auxiliary Electrode: An electrode used to provide a uniform current flow through the working electrode.

B

Battery: A galvanic cell that converts chemical energy into electric energy.

C

Calomel Reference Electrode: An electrode that has a potential dependent on chlorine anions.

Cathode: An electrode at which reduction proceeds by gaining electrons.

Cation: A positively charged ion such as Cu^{+2}

Corrosion: Surface deterioration or destruction due to metal loss caused by chemical or electrochemical reactions

Corrosion Current Density: The rate of electron exchange between cathodic and anodic electrodes at equilibrium.

Corrosion Potential: The potential difference between the cathodic and the anodic electrodes at their corrosion current density.

Crevice: A no-visible narrow area, such as a gap, crack, fissure.

Crevice Corrosion: A form of corrosion that occurs in crevices due to oxygen depletion and dirt.

Crystal Structure: A three-dimensional array of unit cells.

Cu/CuSO₄ Reference Electrode: An electrode that has a potential dependent on copper cations.

D

Daniel Cell: A galvanic cell used as battery to convert chemical energy into electric energy.

Degradation: A deteriorative process that may represent permanent damage, such as metal dissolution in metals and swelling in polymers.

Diffusion: Mass transport by atomic motion.

Dislocation: A linear defect in crystalline materials that represents atomic misalignment.

Diffusion Flux: The quantity of mass diffusing through a perpendicular unit cross-sectional area per time.

Driving Force: A term used to represent the parameter that causes a process to occur.

E

Electrochemical Cell: A system consisting of a cathode and an anode immersed in the electrolyte.

Electrolysis: A reduction process caused by an external current flow.

Electrolyte: A solution through which an electric current is carried by the motion of ions.

Electrolytic Cell An electrochemical cell with forced reactions to promote electrolysis.

Electromotive Force (emf) Series: The ranking of the standard electrochemical cell potential of metallic elements.

Electrometallurgy: The field of engineering that uses science and technology of electrolytic processes for recovering metals from solutions.

Electroplating: A metallurgical process used for reducing metal cations on an electrode surface by electrolysis. The resultant product is a metallic coating.

Electrorefining: A metallurgical process used for purifying metals from solutions by electrolysis.

Electrowinning: A metallurgical process used for extracting or recovering metals from solutions by electrolysis.

Equivalent Weight: A quantity determined by dividing the atomic weight by the valence of a metal.

Erosion Corrosion: Surface deterioration caused by the combined action of chemical attack and mechanical wear.

Exchange Current Density: The rate of electron exchange between cathodic and anodic reactions on an electrode at equilibrium.

F

Faraday: A quantity of electric charge equals to $96,500 \text{ C} = 26.81 \text{ Ah}$ required to oxidize or reduce one equivalent weight.

Free Energy: A thermodynamic quantity that is a function of internal energy and entropy of a system

G

Galvanic Cell: An electrochemical cell with spontaneous reactions.

Galvanic Corrosion: Surface deterioration due to localized galvanic cells imparted by dissimilar microstructural phases or materials.

Galvanic Series: The ranking of metallic materials to form galvanic couplings.

I

Imperfection: A deviation from atomic order in crystalline materials.

Inhibitors: Organic compounds or inorganic anions that form a protective coating *in situ* by reactions of the electrolyte and the corroding surface.

Intergranular Corrosion: Localized metal dissolution along grain boundaries in polycrystalline materials.

Ion: An electrically charged species j in an electrolyte.

L

Limiting Current Density: The maximum rate of reduction possible for a given electrochemical system.

Liquid Junction Potential: A potential difference between two ionic solutions.

M

Metallic Coating: An electroplated or melted coating that acts as a corrosion resistant coating or sacrificial coating for cathodic protection.

Mixed Potential: A potential caused by anodic and cathodic electrochemical and simultaneous reactions on an electrode surface.

Molarity: Concentration in moles per liter (or moles per cubic centimeters) of a species j in solution.

Mole: The quantity of a substance related to Avogadro's number.

O

Open-Circuit Potential: The reversible equilibrium potential of an electrode at its exchange current density value.

Oxidation: The removal of electrons from an atom, ions or molecule.

Overpotential: A potential difference between a working electrode and its open-circuit potential.

P

Passivity: Loss of chemical reactivity of an electrode in an environment due to the formation of an oxide film its surface.

Penetration Rate: The corrosion rate for thickness reduction per time in a corrosive environment.

pH: A quantity used as a measure of acidity or alkalinity of an aqueous electrolyte.

Pipeline Coatings: Thermoplastic coatings based on bituminous coal tar enamels or asphalt mastics.

Pitting Corrosion: A very localized metal dissolution forming pits or holes on the surface.

Polarization: Deviation of the electrode potential from its equilibrium caused by current flow.

Porcelain Enamel: A fused or melted glass powder and subsequently, cooled on a metal surface that acts as an inert vitreous-glass coating to water.

Potential: A parameter used as a measure of voltage.

R

Reduction: Addition of electrons to cations for recovering a metal in its atomic state.

Reference Electrode: An electrode of known electrochemical characteristics used for measuring the potential difference between the of the working electrode against it.

S

Sacrificial Anode: A metallic material that corrodes and cathodically protects a structure by liberating electrons.

Stress Corrosion Cracking: A form of failure due to the combined action of a tensile stress and a corrosive environment on a metallic material.

U

Unit Cell: A three dimensional atomic arrangement forming a specific geometry.

W

Working Electrode: An electrode exposed to an electrolyte at a finite current.

Index

- AC circuit theory, 97
- Acid mist, 195, 196
- Activation energy, 73
- Activation polarization, 81, 82, 113, 129, 132, 142, 144, 149, 167, 341
- Activation state, 72
- Active-passive, 173
 - behavior, 175, 295
 - materials, 173
 - stainless steels, 174
 - transition, 297
- Activity, 34, 47, 48, 54, 303, 307
- Admittance, 97, 98
- Aerated solution, 248
- Alternating current, 83
- Alumina, 24, 212, 213, 317
- Alumina powder, 212
- Aluminum, 41, 184, 211, 237, 258
 - alloys, 175, 176
 - molten, 212, 215
- Aluminum anodizing, 210
- Aluminum hydroxide, 17
- Aluminum oxide film, 210
- Ambipolar diffusion, 124, 327
- Amorphous structure, 175, 185
- Analog-to-digital converter, 169
- Angular frequency, 98
- Angular velocity, 146, 232
- Anion vacancies, 312
- Anions, 38, 41, 63, 238
- Anode, 7, 13, 192, 208, 209
 - backfill, 257
 - bed, 257
 - busbar, 211
 - carbon, 211
 - catalytic, 206
 - consumption, 258
 - conventional, 195, 206, 207
 - cylindrical, 196
 - dimensionally stable, 195, 206
 - dissolution, 259
 - electrode, 32
 - electrode current, 160
 - gas diffusion, 195, 206, 207
 - hydrogen gas diffusion, 200
 - impressed-current, 251, 258
 - localized, 12
 - non-conventional, 206
 - passivation, 251
 - passivity, 234
 - positively charged, 162, 238
 - sacrificial, 251
 - surface, 223
- Mg, 284
- rods, 284
- Anode capacity, 251, 259, 284, 290
- Anode resistance, 279
- Anode-electrolyte interface, 194
- Anode-to-cathode distance, 213
- Anodic overpotential, 81, 84, 86, 142
- Anodic polarization, 81, 83, 86, 159, 165, 179, 296
- Anodic protection, 27, 296–298, 300
- Anodic reaction, 1, 2, 16, 18, 25, 32, 194
- Anodizing, 176
- Aqua regia, 14
- Arrhenius equation, 73, 75, 127, 180, 186, 236, 313, 318, 324, 331
- Arrhenius law, 312
- Artificial passivation, 178
- ASME Code, 283
- Atmospheric corrosion, 3, 4

- Atomic mismatch, 12, 14
- Auxiliary electrode, 169, 170, 256
- Avogadro's number, 28

- Bauxite powder, 212
- Bayer process, 212
- BCC crystal structure, 14
- Bell-shaped curve, 340
- Bell-shaped function, 149
- Bi-metallic electrodes, 33
- Biological corrosion, 3
- Blistering, 23
- Bode plots, 102
- Boltzmann constant, 312
- Boltzmann distribution law, 72
- Boride particles, 176
- Boundary layer, 223
- Brass, 284
- Brittle materials, 21
- Bulk concentration, 130, 134
- Butler-Volmer equation, 72, 74, 90

- Capacitor, 98
- Carbon oxide, 213
- Carburizing, 334
- Cathode, 13, 209
 - carbon, 211
 - negatively charged, 162
- Cathode electrode, 32
- Cathodic current density, 142
- Cathodic overpotential, 81, 86, 141, 143
- Cathodic polarization, 81, 86, 159
- Cathodic protection, 6, 8, 27, 160, 247–253, 255, 256, 276, 277, 290, 295
 - design, 252, 279
 - Formulae, 276
 - guidelines, 276
- Cathodic protection criteria, 290
- Cathodic protection, crevice, 272, 273
- Cathodic reaction, 1, 4, 16
- Cation vacancies, 312
- Cations, 38, 41, 63
- Cations, definition, 238
- Cell potential, 200
- Cell potential, standard, 55
- Cementite, 13
- Ceramics, 24
- Characteristic distance, 225
 - between electrodes, 226
- Characteristic length, 224
- Charge carriers, 209
- Charge-transfer control, 98
 - mechanism, 81
- Charged disk model, 263
- Chemical Mechanical Planarization, 210
- Chemical potential gradient, 125, 322, 329
- Chemical rate constant, 73
- Chemical vapor deposition, 210
- Chromia, 317
- Chromium hydroxide, 17
- Coating damage, 277
- Coating flaws, 272, 284
- Coke breeze (graphite), 258
- Cole-Cole impedance formula, 105
- Complex transfer function, 97
- Concentration cell, 33, 96
- Concentration gradient, 124, 132, 134, 148, 233, 322
- Concentration polarization, 104, 129, 132, 133, 137, 141, 143, 145, 149, 155, 167, 195, 233, 341
- Concentration rate, 126, 128, 129
- Concentration ratio, 141
- Conductivity, 1, 87, 108, 109, 162, 179, 186, 192, 194, 202, 212, 217, 259, 261, 272, 273, 322, 324, 325, 328, 336
- Conductivity data, 115
- Constant load, 20
- Continuity equation, 217, 273
- Corrosion, 3, 31
 - aqueous, 4
 - atmospheric, 3, 4
 - biological
 - general, 3
 - localized, 3
 - crevice, 3, 18, 272
 - driving force, 159

- electrochemical, 7
 - filiform, 3
 - galvanic, 3, 7, 8, 261
 - general, 27
 - grain boundary, 12
 - high-temperature, 3, 301, 331
 - liquid-metal, 3
 - localized, 27
 - molten-salt, 3
 - oral, 3
 - pitting, 3, 16
 - principles, 249
 - product, 17, 142, 248, 249, 301, 322
 - resistance, 7
 - selective leaching, 3
 - steel pipeline, 6
 - stray-current, 3, 261
 - surface deterioration, 160
 - uniform, 4, 6
- Corrosion behavior, 71, 81, 170, 173
- Corrosion current, 271
- Corrosion current density, 71, 83, 85, 90, 100, 156, 164, 170, 172, 175, 176, 300
- Corrosion damage, 261
- Corrosion mechanism, 247, 249, 261
- Corrosion of aluminum, 5
- Corrosion potential, 71, 85, 86, 90, 113, 144, 156, 158, 160, 172, 173, 248, 265
- Corrosion prevention, 262
- Corrosion process, 2, 25, 97, 170
- Corrosion product, 272
- Corrosion protection, 237
- Corrosion rate, 1, 6, 7, 13, 71, 83, 85, 89, 90, 92, 97, 102, 157, 161, 175, 247, 249, 252, 253, 286, 297
- Corrosion rate equation, 92
- Corrosion resistance, 209, 210, 258, 259, 335
- Corrosion-fatigue cracking, 20
- Corrosion-induced spalling, 19, 25
- Corrosivity, 173
- Cottrell equation, 132
- Coulomb's law, 216
- Counter electrode, 169
- Crank's model, 127
- Crevice cathodic protection, 272–275
- Crevice corrosion, 3, 18, 171, 272
- Crevice depth, 275
- Crevice formation, 262
- Crevice growth rate, 275
- Crevice, circular model, 272
- Cryolite salt, 212
- Crystal lattice, 23
- Crystal lattices, 14
- Crystalline structure, 185
- Current control technique, 87
- Current density, 123, 124, 141, 164, 215, 231, 273, 286, 324
- Current density factor, 234
- Current density for steel, 276
- Current density function, 81
- Current density, coupled, 222
- Current density, net, 74
- Current efficiency, 195, 200, 206, 211, 213
- Current fluctuations, 215
- Current response, 97–99
- Cyclic polarization, 186
- Cyclic-oxidation behavior, 317
- Cylindrical cathode, 196
- Deaerated solution, 248
- Degree of dissociation, 63
- Deterioration, 1
- Dezincification, 3
- Diffusion, 23
- Diffusion impedance, 98, 104
- Diffusion in solids, 138
- Diffusion layer, 62, 131, 226
- diffusion layer, 133
- Diffusion molar flux, 133
- Diffusion of gases, 138
- Diffusion of liquids, 138
- Diffusion-convective layers, 230
- Diffusivity, 109, 123, 127, 138, 139, 224, 235, 318
- Dipole, 30
- Disk cathode

- disk, 196
- Dislocation network, 15
- Dislocations, 12
- Dissociation of water, 48
- Dissociation parameter, 63
- DNA, 24
- Doping effect, 314
- Drift velocity, 318, 322
- Driving force of corrosion, 247
- Dual anodes, 259
- Ductility, 21

- Ectrowinning of zinc, 206
- Electric double-layer, 222
- Electric field strength, 28
- Electric potential gradient, 322
- Electrical charge, 134
- Electrical double layer, 61
- Electrical double-layer, 100
- Electrical field, 140
- Electrical force field, 108
- Electrical potential, 108
- Electrochemical behavior, 87, 176
- electrochemical cell, ASTM G-5, 168
- Electrochemical cells, 32, 72, 124, 162, 192
- Electrochemical circuit, 98, 100
- Electrochemical corrosion, 7, 155, 165, 167, 171, 173, 174, 186
- Electrochemical deposition, 227
- Electrochemical noise, 170
- Electrochemical polarization, 159
- Electrochemical potential, 86
- Electrochemical rate constant, 73
- Electrochemical reactions, 1, 208
- Electrochemical system, 98, 140
- Electrochemistry, 27
- Electrode lattice, 55
- Electrode potential, 200
- Electrode surface roughness, 194
- Electrodeposition, 194, 235
- Electrogaining technique, 184
- Electrolysis, 33, 56, 206, 211, 213
- Electrolyte, 1, 3, 8, 9, 16, 18, 61, 63, 194
 - agitated, 13
 - stagnant, 13
- Electrolyte constituents, 202
- Electrolytes, 32
- Electrolytic cell, 33
- Electrolytic deposition, 192
- Electromagnetic body forces, 217
- Electromagnetic field, 211, 215, 218
- Electrometallurgy
 - of aluminum, 215
- Electromotive force, 7, 34, 35, 53
- Electroplating, 56, 209, 236, 238
- Electrorefining, 194, 208, 223, 236
- Electrowinning, 28, 56, 192, 195, 196, 198, 201, 202, 208, 209, 222, 223, 233–238, 258
 - of zinc, 195
 - step reactions, 192
- Electrowinning cells, 195, 196, 200–202, 206, 219, 224, 225
- Electrowinning economics, 205
- Electrowinning of copper, 235
- Electrowinning of zinc, 206
- Electrowinning, rotating cylinders, 232
- Electrowinning, rotating disks, 232
- Elongation, 20
- Energy consumption, 201, 206, 212, 215
- Energy dissipation, 91
- Energy distribution, 72
- Energy efficiency, 200
- Energy-producing system, 91
- Enthalpy change, 302, 312
- Entropy change, 302
- Environmentally induced cracking, 20
- Equilibrium conditions, 75
- Equilibrium constant, 56, 64, 76
- Equilibrium potential, 89
- Equivalent circuit, 97
- Error function, 130, 340
- Error function, complement, 130
- Evans diagram, 86
- Evans diagrams, 156
- Ex-situ techniques, 183
- Exchange current density, 156

- Exchange current density, 74, 158
- Experimental procedures
 - ASTM G-106 for impedance, 83, 98, 99
 - ASTM G-5 for anodic polarization, 83
 - ASTM G-59 for polarization resistance, 83
- Extractive metallurgy
 - Electrometallurgy, 159, 189
 - Electrowinning, 189
 - Electroplating, 56, 159, 191
 - Electrorefining, 159, 191
 - Electrowinning, 56, 159, 189, 191
 - Molten salt electrolysis, 191
 - Hydrometallurgy, 56, 189
 - Pyrometallurgy, 189
- Faradaic corrosion rate, 71
- Faradaic current, 49
- Faraday's constant, 28, 42
- Faraday's equation, 123
- Faraday's law, 33, 49, 77, 100, 146, 179, 186, 198, 202, 216, 251, 275, 286
- Faraday's law of electrolysis, 198, 200
- Faraday's reaction rate, 73, 92
- Faraday's weight, 77
- FCC crystal structure, 14, 15
- Ferric hydroxide, 4
- Ferrite, 13
- Ferrous hydroxide, 4
- Fick's diffusion molar flux, 223
- Fick's first law of diffusion, 126, 133, 140, 142, 149, 220, 226, 318, 323, 336
- Fick's second law of diffusion, 126-128, 140, 147, 149, 219, 220
- Fick's theory of diffusion, 336
- Filiform corrosion, 3
- Film adhesion, 209
- Fluid velocity, 215
- Fluid viscosity, 146, 224
- Force gradient, 108, 322
- Forced convection, 224
- Forced convection flow
 - laminar, 225, 226
 - transient, 225
 - turbulent, 225, 226
- Formation of metal oxide, 183
- Fourier's law of thermal conduction, 126
- Fracture surface, 22
- Frenkel defects, 313
- Galvanic cell, 27, 32, 33, 40
- Galvanic corrosion, 3, 7, 12, 284
- Galvanic coupling, 27, 163
- Galvanic effect, 179
- Galvanic microcells, 12
- Galvanic polarization, 163
- Galvanic series, 41
- Galvanized steel, 13
- Galvanostatic technique, 147
- General attack, 4
- General corrosion, 3
- Gibbs free energy change, 42-44, 67, 212, 302, 312, 314, 336
- Gibbs-Duhem equation, 329
- Glass coating, 283
- Grain boundaries, 12, 14, 15, 334
- Grain boundary corrosion, 12
- Grains, 14
- Graphite, 212
- Graphite anodes, 258, 259
- Graphite flakes, 258
- Graphitization, 3
- Grashof number, 224
- Half-cell reactions, 155
- Hall-Heroult Cell, 213
- Hall-Heroult cell, 211, 213
- HCP crystal structure, 14
- Heat capacity, 51, 67, 302
- Heat generation, 195
- Helmholtz layer, 62
- Helmholtz plane, inner, 62
- Helmholtz plane, outer, 62
- Henry's law, 48
- Hexafluoroaluminate, 212

- High-energy areas, 14
High-temperature corrosion, 3, 301, 331
High-temperature oxidation, 301, 316, 336
Holidays, 272
Hoop stress, 286
Hydrodynamic flow, 223
Hydrodynamic velocity, 123
Hydrodynamic viscous, 230
Hydrogen bubbles, 13
Hydrogen embrittlement, 23
Hydrogen evolution, 191, 192, 194, 237, 238
Hydrogen-induced cracking, 20

Impedance, 97–100, 104, 186
Impedance by charge-control, 97, 102
Impedance by diffusion, 103, 105
Impedance spectroscopy, 83, 97, 99
Imperfection, 284
Impressed-current, 276, 279
In-situ techniques, 183
Incomplete deposition, 209
Inflation point, 91
Ingot metallurgy, 21
Interfacial capacitance, 100
Interstitial, 312
Ionic flux, 75
Ionic flux balance, 327
Ionic motion, 322
Isotropic medium, 128
IUPAC, 35

Jewelry, 210

Kinematic viscosity, 146, 224
Kinetic parameters, 74, 81, 87
Kinetics of charge transfer, 80
Kinetics of corrosion, 315
Kinetics of electrochemical corrosion, 90

Laminar flow, 223, 225
Laplace transform, 139
LaPlace's equation, 216

Leaching steps, 192
Levich equation, 146, 232
Limiting current, 146
Limiting current density, 86, 142, 143, 146, 227, 233, 236
Linear behavior, 302, 319, 336
Linear polarization, 83, 85, 90, 113
Liquid-metal corrosion, 3
Lithography, 184
Localized corrosion, 3
Lorentz force, 215, 216
Luggin capillary, 170

Magnesia, 24
Magnetic field, 215
Magnetic flux, 215
Magnetite, 24
Magnetohydrodynamic
 flow instability, 213–215
 interactions, 215, 216
Magnetohydrodynamic instability, 215
Marble's reagent, 14
Mass transfer, 137, 142
Mass transfer by convection, 223, 230
Mass transfer by diffusion and migration, 140, 273
Mass transfer coefficient, 225, 226
Mass transfer modes, 121, 123, 149, 194
Maxwell equation, 215
Maxwell's equations, 216
Maxwell-Boltzmann distribution law, 72
Metal deposition, 209
Metal corrosion, 92
Metal oxide reduction, 182
Metal reduction, 182
Microstructural effects, 12
Microstructure, 14
Migration, 324
Migration flux, 124
Mixed potential, 162
Mobility, 105, 106, 108–110, 113, 125, 273, 297, 322, 323, 336
Molar flux, 323, 327
Mole fraction, 28

- Molten aluminum, 212, 215
Molten salt electrolysis, 211
Molten-salt corrosion, 3
Mono-metallic electrodes, 33
Monopole, 29
- n-type oxide semiconductors, 313
NACE, 252, 259, 290
Natural convection, 222, 224
Natural convection flow
 laminar, 225, 226
 transient, 225
 turbulent, 225, 226
Natural passivation, 178
Navier-Stokes equation, 215, 216
Nernst diffusion layer, 225
Nernst equation, 40, 48, 49, 56, 59,
 60, 63, 67, 88, 141, 182,
 203, 252, 253
Nernst potential, 51, 63
Nernst-Einstein equation, 109, 113,
 125, 323, 336
Nernst-Planck equation, 123, 140, 149,
 272, 336
Nernst-Planck-Faraday (NPF) equa-
 tion, 124
Net current density, 88
Newton's law of viscosity, 126
Niobium carbide, 24
Nitriding, 334
Non-linear polarization curve, 86
Non-steady state condition, 128
Nonmetallic materials
 ceramics, 24
 concrete, 18
 polymers, 24
 refractories, 24
 woods, 24
Nonstoichiometry, 314
Nusselt number, 224
Nyquist impedance, 102
Nyquist plot, 83, 101, 102, 105, 113
Nyquist-Warburg plot, 103, 104, 113
- Ohm's law, 86, 98, 111, 126, 201,
 215, 216
- Ohmic effect, 200
Ohmic resistance gradient, 170
Open-circuit potential, 49, 86, 88
Open-ended capillary, 138
Oral corrosion, 3
Organic coating, 16
Overpotential, 85, 143, 147, 148, 159,
 200, 233
Oxidation kinetics, 318
Oxidation number, 28
Oxidation process, 5, 17, 18
Oxidation rate, 301
Oxidation state, 145
Oxide coating, 301
Oxide film growth, 179
Oxide formation, model, 315
Oxide thickness growth, 301, 318,
 333, 334, 336
Oxidizing, 301, 302
Oxygen evolution, 192
- p-type oxide semiconductors, 313
Paint coating, 210
Parabolic behavior, 318, 319, 321,
 336
Parabolic equation, 318, 329
Parabolic kinetic behavior, 327
Parabolic rate constant K_w , 331–
 333
Parabolic rate constant K_x , 318
Passive behavior, 179
Passive oxide film, 5, 16, 178, 179,
 183–185
Passive potential range, 179
Passivity, 173, 178, 179
Pearlite, 13
Penetration, 301, 335
Permittivity, 29
pH, definition, 48
Phase shift angle, 98–102
Physiological saline solutions, 178
Pilling-Bedworth law, 301, 316
Pits, 16
Pitting corrosion, 3, 16
Pitting mechanism, model, 16
Plasma, 210

- Plastics, 24
Point defects, 312
Poisson's equation, 216
Polarization, 80, 162
Polarization curve, 88, 89, 144, 171, 173
Polarization device, 167
Polarization resistance, 71, 83–85, 90, 91, 97, 98, 100, 102, 104, 111, 113, 186
Polarization, a.c., 148
Polarized metal, 86
Polymers, 24
Polyvinyl chloride, 24
Pot operations, 216
Potential attenuation, 264, 290
Potential control technique, 87
Potential excitation, 97, 99
Potential fluctuation, 216
Potential gradient, 124
Potential range, practical, 195
Potential waveform, 98
Potential-pH plots, 56
Potentiodynamic method, 173
Potentiodynamic polarization, 171
Potentiodynamic polarization curve, 86
Potentiodynamic polarization method, 83
Potentiodynamic polarization technique, 86
Potentiostat, 171
Potentiostatic method, 173
Pourbaix diagram, 5, 56, 89
 for a metal M, 59
 for water, 56
Power supply, 32
Prandtl boundary layer, 230
Prandtl number, 224
Pressure gradient, 124
Pressure vessel, 286
Pressure vessels, 283
Prevention of crevice corrosion, 272
Prevention of uniform corrosion, 6
Proportionality constant, 91
Radial diffusion, 129
Rapidly solidified alloy, 21, 176
Rate constant K_a , 320
Rate constant K_w , 319
Rate constant K_x , 318
Rate of diffusion, 127
Rate of film formation, 186
Rate of metal deposition, 208
Rate of oxide thickness growth, 318, 319, 329, 332
Rate of reactions, 72
Rate of thickness reduction, 286
Rate of weight gain, 319
Rate of weight loss, 286
Rayleigh number, 224, 225
Recovery of aluminum, 189
Recovery of magnesium, 189
Recovery of uranium, 189
Recycling step, 194
Redox reaction, 1, 8, 36
Reference electrode, 7, 54, 284
Reference electrodes, 169
Refractories, 24
Resistance
 electrolyte-to-anode, 276
Resistance Formulae, 279
Resistivity, 108
Reversible electrochemical cell, 141
Reversible potential, 86
Reynold number, 224
Reynolds number, 146, 224, 225
Rotating anode, 218
Rotating-cylinder electrode, 189, 196, 232
Rotating-disk electrode, 146, 147, 189, 196, 231–233, 240
Rust, 4, 5, 184, 249, 261, 301
Sacrificial anode, 8, 34, 251, 255, 258, 259, 262, 263, 270, 276, 279
Sacrificial anode materials, 259, 284
Sacrificial anode technique, 251, 290
Sacrificial magnesium anode, 251
Scale-forming oxidation, 301
SCC curve, 21

- SCC susceptibility, 20
Schmidt number, 224
Schottky defects, 313
Secondary cracks, 21, 22
Selective leaching corrosion, 3
Self-diffusion, 126
self-diffusion, 138
Separation of variables, 139
SHE cell diagram, 54
Sherwood number, 224–227, 231
Short-circuit cell, 91
Silicon carbide, 24
Single crystal, 179
Sinusoidal current perturbation, 98
Sinusoidal excitation, 99
Sinusoidal potential excitation, 99
Sinusoidal potential perturbation, 98, 99
Slow strain-rate, 20
Soderberg cell, 211
Sodium nitrate, 20
Solution of Fick's second law, 129, 339
Solution resistance, 98
Spalling, 19
Stable corrosion potential, 173
Stagnant water, 18
Stainless steels, 21, 334
Standard electrode potential, 35
Standard free energy change, 64
Standard hydrogen electrode, 7, 35
Steady-state behavior, 173, 273
Steady-state condition, 129
Stern diagram, 86
Stoichiometric reaction, 83
Stoichiometry, 33, 272
Stoke's drag force, 126
Strain rate, 20
Stray-current corrosion, 3
Stress-corrosion cracking, 20
Structural integrity, 305, 336
Sub-grains, 15
Sulfuric acid, 21, 104, 206
Supplemental corrosion protection, 284
Surface damage, 1
Surface roughness, 105
Symmetry coefficient, 74
Tafel anodic slope, 81
Tafel cathodic slope, 81
Tafel equation, 76
Tafel extrapolation technique, 83, 86, 90, 186
Tafel slopes, 71, 83–86, 113, 145, 155, 165, 172, 253, 254
Temperature gradient, 124
Theory of corrosion, 31
Thermal diffusivity, 224
Thermodynamics of
 galvanic cells, 41
 oxide formation, 302
Thermogravimetric technique, 331
Thickness reduction, 301, 305
Time-dependent current, 98
Time-dependent potential, 98
Titanium diboride, 212
Transfer function, 98
Transfer number, 324
Transient flow, 225
Turbulent flow, 223, 225
Tyrode's solution, 178
Uhlig's model, 265
Uniform corrosion, 4, 6
Unpolarized metal, 86
Vacancies, 312
Vacancy diffusion, 186
Vacancy migration, 179
Valence, 28
Volume flow rate, 225
Wagner theory of oxidation, 327
Warburg impedance by diffusion, 103
Warburg impedance coefficient, 104
Warburg line, 104
Water heater, 283
Weber's disk, 232
Weight gain, 301, 316, 319, 320, 331, 333, 336
Woods, 24

Working electrode, 167, 170, 171

Zero-resistance ammeter, 169

Zinc sulfate, 206

Zinc, corrosion rate, 13

Zirconia, 24